Geogenic nitrogen as a nutrient source to subglacial microbial ecosystems

Timothy John Dixon

Submitted in accordance with the requirements for the degree of Doctor of Philosophy

The University of Leeds

School of Earth and Environment

UNIS – The University Centre in Svalbard

December 2019

The candidate confirms that the work submitted is his own and that appropriate credit has been given where reference has been made to the work of others.

Acknowledgements

I would like to thank my supervisor Simon Bottrell for his continued support through this project in numerous meetings and his company during fieldwork in Svalbard. I would also like to thank Andrew Hodson for all of his help in identifying field sites in Svalbard and for his excellent guidance. Thanks also to Rob Newton who has always given me encouragement and sound advice throughout this project.

Thank you to the staff at UNIS, particularly to Malte Jochmann who provided access to the rock cores used in this study.

I would also like to thank the many kind field assistants that joined me on cold and wet walks to collect samples in Svalbard. A particular thank you to Max Holthuis, Eleanor and Gwilym Jones for their excellent company and to Molly Peek for collecting snow samples on my behalf. Also, to Mikkel Toft Hornum for hauling back rock samples from the hut in Janssondalen.

Many thanks to everyone I've shared an office with in 9.160 and to colleagues in the Cohen lab for their great company and sharing breaks over coffee, lunch and beers. A huge thank you to all of the technicians who have helped me out with laboratory work to no end, particularly Andy Connelly, Stephen Reid, Fiona Keay, Bob Jamieson, Andy Hobson and David Ashley. A big thanks also to Angela Lamb and Andi Smith at NIGL for all of their help with N isotope analysis.

I would like to thank all of my friends that have stood beside me along the way and for being wonderful people to climb, cycle and spend time with. A big thanks to all of the Dixons and Ruxtons who have always encouraged and supported me.

I am very grateful to have been funded by NERC which has allowed me the opportunity to work in Svalbard and I will cherish the memories of the beautiful landscape.

My biggest thanks go to Sarah who has always been there for me.

Abstract

Glacial runoff often contains nitrate far in excess of nitrogen (N) concentrations in snow. ‘Excess’ nitrate is likely produced by nitrifying bacteria in subglacial environments, yet the source of the additional N has not been identified. In this thesis, rocks are investigated as an N source to subglacial microbial ecosystems following their comminution by glacial erosion and leaching with meltwater. Weathering processes involving the release of N and micronutrients, iron (Fe) and manganese (Mn), from rock to glacial environments were evaluated using a combination of field studies in Adventdalen (Svalbard) and rock weathering experiments. Attempts were also made to constrain isotope fractionation during weathering to improve the use of stable isotopes to trace N provenance.

The sedimentary geological succession underlying glaciers in the study area contained significant N (up to 0.21 wt. %), particularly in organic rich, siltstones and shales. Fe and Mn were largely found within oxide and carbonate minerals while significant pyrite bound Fe (max. 5.2 wt. %) was present in organic rich sediments.

In simulated glacial weathering experiments, nitrogen was almost entirely liberated as ammonium with much of it absorbed to mineral surfaces rather than dissolved in solution. Pyrite oxidation liberated Fe and generated acidity which drove i) silicate dissolution releasing N and ii) carbonate dissolution yielding dissolved Mn. The largest N yields were associated with rocks containing abundant organic N which may have been liberated via oxidative weathering, protonation of amines and/or organic matter degradation by free radicals produced during crushing. Liberated ammonium was partly lost as ammonia gas when the solution pH exceeded 8 and also absorbed to sediment, particularly when clay minerals were abundant. Further experiments demonstrated an isotope enrichment in adsorbed ammonium of up to 10‰ $\delta^{15}N$ relative to bedrock N, caused by fractionation from a combination of adsorption and volatilisation processes.

In Svalbard, up to 89% of nitrate in glacial runoff was derived from non-snowpack sources. Solute was acquired into snowmelt via chemical weathering of rock talus in ice marginal moraines largely via coupled sulphide oxidation and silicate dissolution. When oxygen was available, ammonium released from rock was converted to nitrate via microbial nitrification. This assertion is supported by nitrate $\delta^{18}O$ values of close to 0‰, vastly different from atmospheric oxygen. However, when flowpaths were anoxic, nitrate was absent likely due to microbial denitrification. Geological variations may control the magnitude of

nutrient export by weathering in glacial catchments. For instance, N and Mn were particularly enriched in water from the Longyearbreen catchment which overlies shales enriched in these elements. Furthermore, clay minerals in bedrock significantly influences the distribution of N (as ammonium) between dissolved and particulate phases through ion exchange reactions.

Table of Contents

Table of Figures

Table of Tables

Chapter 1 Introduction and literature review

1.1 Introduction

1.1.1 Project rationale

Subglacial environments were long considered as abiotic, however they have recently been shown to harbour active microbial populations that mediate biogeochemical weathering reactions. Subglacial environments are typically isolated from energy and nutrient sources such as solar insolation, atmospheric gases and atmospheric deposition. Therefore, microbes are typically chemotrophic, deriving energy and nutrients from biogeochemical reactions of organic matter and minerals.

These ecosystems are severely limited with the macronutrient nitrogen (N), yet elevated concentrations of nitrate in glacial runoff are commonly reported in Svalbard (Ansari et al., 2013; Wynn et al., 2007; Yde et al., 2008; Rutter et al., 2011), Greenland (Wadham et al., 2016), the European Alps (Tockner et al., 2002), rock glaciers (Williams, M. W. et al., 2007) and cold based Antarctic glaciers (Caulkett and Ellis-Evans, 1997; Hodson, 2006). Glacier nutrient budgets report that nitrate in runoff often exceeds nutrient inputs to the glacial system, which suggests a source of nitrogen has not been accounted for in these environments (Wynn et al., 2007; Hodson et al., 2005; Hodson, 2006). Understanding the provenance of this “excess” nitrogen is imperative to understanding how these ecosystems function in both modern and ancient environments.

Rocks contain under-appreciated concentrations of nitrogen (geogenic nitrogen) incorporated within silicate minerals, as organic matter and as N salts. Geogenic nitrogen may become bioavailable through subglacial weathering and therefore account for excess nitrogen in glacial runoff. Geogenic N is becoming increasingly acknowledged as an ecologically significant nutrient source and recently bedrock N was shown to rival atmospheric N as an N source to the global terrestrial environment (Houlton, et al 2018).

Previous studies have attempted to use N-isotopes to demonstrate N provenance in glacial environments. However, the insight that can be gained in this way is limited by a lack of a clear understanding of nitrogen speciation and isotope effects during weathering. In order to validate N-isotopes as a tracer for geogenic nitrogen, clarity is required on the chemical transformation of nitrogen

between reduced ammonium in rock and oxidised nitrate in meltwater and any associated isotope fractionation(s).

Rock weathering also contributes micronutrients iron and manganese to glacial runoff. Iron in glacial water is comprised of dissolved iron (<0.02 μm) and colloidal iron/nanoparticulate and particulate iron (<1 μm). Since iron is very insoluble in oxygenated water, authigenic iron (hydr)oxides contribute the bulk of glacial iron flux which is deposited in proglacial/fjord/marine sediment (Raiswell et al., 2006). Studies of sediments in Svalbard fjords fed by glaciers eroding different bedrock have identified variations in iron and manganese content (Wehrmann et al., 2014). It is not clear whether this is due to bulk rock iron/manganese content or their distribution between minerals. Iron occurs within different minerals in rock such as sulphides, carbonates, silicates and oxides while manganese occurs principally in carbonates and oxides. The flux of iron and manganese into fjord/marine sediments could be controlled by glacial erosion and the partitioning of these metals within source rock minerals.

An improved understanding of the chemical reactions which take place during weathering particularly relating to nitrogen as well as iron and manganese is required to constrain their availability as nutrient and energy sources to subglacial microbial ecosystems.

1.1.2 Research Aim

The aim of this research is to explore the weathering processes involved in the supply of geogenic nitrogen as well as rock derived micronutrients (Fe and Mn) to subglacial environments. It is envisaged that this will improve methods to trace the provenance of N in glacial catchments and improve our understanding of the geological control on subglacial nutrient cycling.

1.1.3 Research Objectives

This project seeks to achieve this aim using a combination of field work and laboratory experiments. Field work was undertaken and involved bedrock and glacial meltwater sampling in Svalbard. Svalbard is an ideal place to undertake this research since numerous glaciers, which overlie different geological formations, are easily accessible. Geochemical characterisation of bedrock will provide an understanding of the parent material available during subglacial weathering reactions. Solute derived from weathering will be evaluated through geochemical analysis of glacial runoff. Laboratory based weathering experiments will be carried out using bedrock collected during fieldwork to simulate subglacial geochemical reactions, the results of which will inform the interpretation of field data. The objectives of this research are thus to:

- Characterise the geochemistry of a bedrock sequence that underlies glacial catchments in terms of carbon, nitrogen, sulphur, iron and manganese. In addition, isotope analysis of bedrock will constrain source values of rock weathering for nitrogen and sulphur.
- Determine the magnitude of N liberation and associated geochemical weathering reactions in laboratory leaching experiments of different geological formations and determine any nitrogen speciation and isotope fractionation processes inherent in nitrogen weathering.
- Use glacial meltwater chemistry and stable isotopes of sulphur, nitrogen and oxygen to identify processes of biogeochemical weathering and nutrient cycling in the subglacial environment.

N.B. In this project, the release of nitrogen species from rock is referred to as N liberation i.e. the conversion from rock-bound N to a combined pool of adsorbed and aqueous nitrogen species. Whereas N leaching refers specifically to the removal of soluble forms of N species i.e. aqueous nitrogen species.

1.1.4 Hypotheses

- Geological variation between different glacial catchments accounts for differing export of nutrients: nitrogen, iron and manganese.
- The dissolution of geogenic nitrogen imparts a fractionation on N isotopes which accounts for the $\delta^{15}N$ difference between bedrock and glacial runoff.
- Anoxic sulphide oxidation generates acidity in subglacial environments which facilitates geogenic N dissolution through silicate weathering.

1.1.5 Outline of thesis structure

This thesis has 8 chapters. In the remainder of this chapter, a background to relevant existing literature is provided, covering nutrient cycling, the subglacial environment and geologic nutrient sources. Chapter 2 outlines the study field area and provides an overview of the bedrock geology. It also details standard methodologies used in this project. Chapter 3 covers the method development of laboratory rock leaching experiments. Subsequent chapters detail the results of research undertaken. Chapter 4 contains the results of geochemical analyses of Cretaceous and Palaeogene bedrock which underlie glaciers in the Adventdalen area of Svalbard and a discussion of sedimentary depositional and diagenetic history. The results of leaching experiments using the same bedrock and their discussion are provided in Chapter 5. Meltwater geochemical analyses from glacial catchments in Svalbard and a discussion of nitrogen and REDOX cycling is presented in Chapter 6. Chapter 7 explores the research conducted on the effects of nitrogen isotopes during rock weathering. Chapter 8 contains a

synthesis of the project results, conclusions and suggestions for further research.

1.2 Nitrogen, iron and manganese as nutrients

1.2.1 Nutrients for life

Nutrients are essential compounds required for life and include major inorganic nutrients such as P and N as well as micronutrients, required in smaller quantities, such as Fe and Mn. Nutrients may be utilised by microorganisms by directly incorporating them into their cell structures (assimilation) or through metabolic processes, using them as an energy source via various dissimilatory redox reactions.

Nitrogen is an important element in many biological compounds and is required to manufacture proteins which are a component of all lifeforms. Nitrogen exists as many species from pure N_2, to other fixed organic and inorganic forms due to biological cycling under various redox conditions. Whilst Nitrogen (N_2) is the major atmospheric gas (78% by volume), it is inaccessible to most organisms in this form. This is due to the strong triple bond of dinitrogen. Dinitrogen must first be converted to a fixed form (reactive nitrogen) for most organisms to use. Reactive forms of nitrogen include reduced species such as ammonia (NH_3), ammonium (NH_4^+) and organic bound nitrogen as well as oxidised species including nitric oxide (NO), nitrogen dioxide (NO_2), nitrous oxide (N_2O), nitrate (NO_3^-) and nitrite (NO_2^-). Dinitrogen may be converted naturally to reactive forms naturally by lightning (5 Tg N/yr) or more significantly by biological nitrogen fixation (BNF; 198 Tg N/yr) (Fowler et al., 2013) (Figure 1.1). The latter is a biological process carried out by only a small number of organisms collectively termed diazotrophs. In many ecosystems, the demand for reactive nitrogen exceeds supply and for this reason nitrogen is often a limiting nutrient.

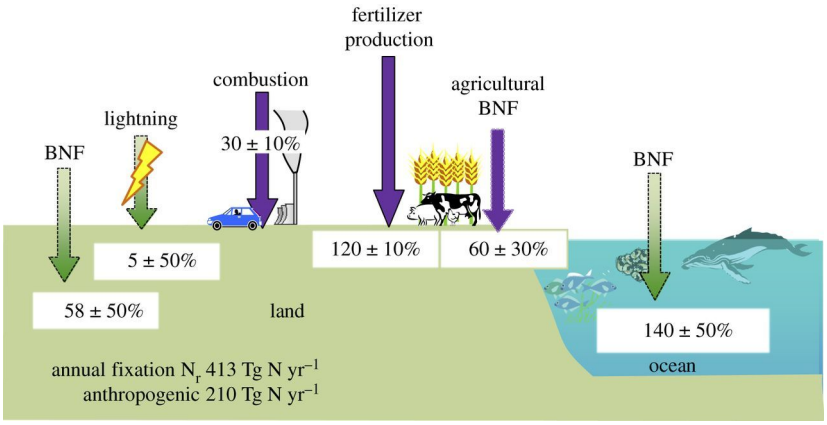

Figure 1.1 Global nitrogen fixation. Green arrows indicate natural sources, purple arrows represent anthropogenic sources (Fowler et al., 2013).

Iron is essential for enzymes and proteins required for processes such as chlorophyll synthesis, nitrate reduction, N_2 fixation and electron transfer (Martin, 1990; Crichton, 2016). Iron is highly abundant in the Earth's crust, (estimated 6.3 - 9.1 wt % of continental crust (Rudnick and Gao, 2003)), yet it is very insoluble in oxygenated water. Consequently iron can limit ecosystem productivity in environments such as the southern ocean (Martin, 1990).

Manganese is also a micronutrient which is a constituent of various enzymes and activator of other enzymes (Burnell, 1988; Morel and Price, 2003). It also plays a pivotal role in the evolution of oxygen from water molecules during photosynthesis (Burnell, 1988). Redox reactions involving manganese also play an important role in biogeochemical cycles within sediments and in marine surface waters (Morel and Price, 2003). In addition, manganese oxides are known to effectively scavenge other biologically important trace metals, such as cobalt, and therefore influence their distribution on continental margins (Knauer et al., 1982; Shaw et al., 1990).

1.2.2 Anthropogenic perturbation of nutrient cycling

Human activity has had a profound effect on global nutrient cycles, particularly since the advent of the Haber Bosch process (Figure 1.1). This technique, originally used to produce explosives, was later used to produce synthetic nitrogen fertilisers. It involves the industrial production of NH_3 by combining N_2 with hydrogen gas produced by fossil fuel combustion. Current fertiliser production accounts for an additional 120 Tg N/ yr to the natural nitrogen cycle (Fowler et al., 2013). Nitrogen fixing agricultural crops provide a further 60 Tg N/yr (Fowler et al., 2013) which is equivalent to estimates of pre-industrial BNF (Vitousek et al., 2013). The manner by which these nutrients enter Svalbard's glacial systems via long range atmospheric transport are described below.

1.2.3 Nutrient sources in glacial environments

Subglacial ecosystems and more broadly Arctic tundra ecosystems, which comprise much of the unglaciated land area in Svalbard, are believed to be nitrogen limited (Melle et al., 2015; Boyd, E.S. et al., 2011). Low nitrogen concentrations in soil/sediment are reinforced by low N mineralisation rates and rapid biological consumption of nitrogen which results in restricted primary productivity, microbial decomposition and biomass growth (Melle et al., 2015). Despite this, glacial runoff is frequently enriched in microbially derived nitrate, invoking biogeochemical nitrogen cycling to be a fundamental component of microbial glacial systems.

Polar glaciers receive fixed nitrogen principally from atmospheric and biological sources. Svalbard receives a large amount of precipitation due to its marine location. Anthropogenic pollutants from Eurasia such as nitrous oxides are deposited as precipitation in polar regions (Law and Stohl, 2007) providing the main source of fixed N to supraglacial environments on Svalbard glaciers (Telling et al., 2011). Firn ice cores in many parts of the Arctic have received a doubling of inorganic N concentrations from atmospheric deposition since the industrial revolution (Tye and Heaton, 2007). A further source of nitrogen is from N-fixing cyanobacteria on glacier surfaces which convert N_2 into NH_3 which further mineralises to NH_4^+ during decay (Telling et al., 2011). However, rates of N fixation on a glacial surface are over 2 orders of magnitude less than atmospheric deposition (Telling et al., 2011). During the early melt season, snowmelt provides the main source of nitrogen to the supraglacial environment, whereas later in the melt season, meltwater is mainly derived from low N ice melt, therefore N fixation becomes a more important source (Telling et al., 2011).

Nutrients within surface melt may be transported to the subglacial system via moulins and crevasses. However, some studies, using dual isotopes of N and O, report microbial production of nitrate within debris rich environments contributing to elevated nitrate in glacial runoff (Wynn et al., 2007; Ansari et al., 2013). This nitrate is associated with water derived from subglacial and ice marginal (moraine) environments rather than the glacier surface. Wynn et al. (2007) concluded that subglacial nitrification of snowpack ammonium and mineralised organic matter accounted for the nitrate in glacial runoff. However, in such environments ammonium may be sourced from the weathering of abundant crushed rock material. Yet, to date glacial studies have provided limited characterisation of rock nitrogen within glacial catchments.

Subglacial drainage also contains other nutrients derived from rock weathering such as iron and silica. Sulphide oxidation is a major weathering reaction in subglacial environments and provides a source of Fe and SO_4 which act as terminal electron acceptors in biogeochemical cycling (Sharp and Tranter, 2017). Iron produced from sulphide oxidation is present in meltwater in both dissolved and colloidal forms (Statham et al., 2008). The oxidation of this glacially liberated iron results in the precipitation of authigenic iron oxyhydroxides which may stimulate primary productivity in downstream iron limited environments (Raiswell et al., 2006; Raiswell et al., 2008; Raiswell et al., 2009). Iron reducing bacteria, which are known to colonise subglacial environments e.g. (Foght et al., 2004; Skidmore et al., 2005; Mikucki and

Priscu, 2007; Nixon et al., 2017), also make use of glacially derived iron in the oxidation of organic carbon.

Manganese may also be used as an electron acceptor in this reaction, however this has yet to be demonstrated in subglacial environments (Hodson et al., 2008). Minimal data was found in the literature regarding manganese concentrations in glacial runoff, however glacial runoff from Austre Brøggerbreen, a glacier in northern Svalbard, contains high dissolved Mn concentrations (153 – 296 nM) that persist for 4 km downstream of the glacier output (Zhang, R. et al., 2015). The potential role of manganese in redox reactions in subglacial environments is significant to understanding nitrogen cycling since it may provide a pathway for abiotic ammonium oxidation (Luther et al., 1997).

1.2.4 Stable isotopes in biogeochemistry

1.2.4.1 Isotopes as tracers

Stable isotopes have been used effectively as tracers in many environmental studies to better understand hydrologic processes. The stable isotope composition of a given compound is determined by the biogeochemical processes and the environment conditions in which it formed, so the compound will have a characteristic isotope signature. This signature can act as a tracer for the geochemical evolution of a water body, provide insights into recharge processes, water-rock interaction and contaminant processes (Clark and Fritz, 1997).

1.2.4.2 Fundamentals of stable isotopes

Isotopes are atoms of an element whose nuclei contain the same number of protons but a different number of neutrons. Isotopes are usually written in the form ^{m}E, where m represents the mass number of the isotope of an element, E. Isotopes may be stable or unstable (radioactive). Radioactive isotopes decay over time to form different isotopes while stable isotopes do not decay. Since most elements have one major isotope and low abundances of minor isotopes, measurements are generally given as the ratio of a minor isotopes to the major isotope. For example, nitrogen isotopes are reported as the ratio of the lesser abundant ^{15}N isotope relative to the abundant isotope ^{14}N. Since variations in isotope ratios are small, isotopes are reported in delta (δ) notation which are given in parts per 1000 or per mille (‰). Delta values represent the normalised deviation from a standard specific for each element (Equation 1.1), where R_A is the ratio of the numbers of any 2 isotopes in a chemical compound A and R_{st} is the ratio of the appropriate standard. The isotopes of elements relative to this project are detailed along with their relative natural abundances and standard reference materials in Table 1.1.

$$\delta_A(‰) = \left(\frac{R_A - R_{st}}{R_{st}}\right).1000 \qquad \textbf{Equation 1.1}$$

Table 1.1 Stable isotopes relevant to this project with their relative natural abundances (Rosman and Taylor, 1998) and standard reference materials

Element	Stable Isotopes	Natural abundance	Ratio measured	Standard
H	^{1}H ^{2}H (D)	99.9885% 0.0115%	D/^{1}H (δD)	Vienna Standard Mean Ocean Water (V-SMOW)
N	^{14}N ^{15}N	99.63% 0.37%	$^{15}N/^{14}N$ ($\delta^{15}N$)	Atmospheric N_2 (AIR)
O	^{16}O ^{17}O ^{18}O	99.757% 0.038% 0.205%	$^{18}O/^{16}O$ ($\delta^{18}O$)	Vienna Standard Mean Ocean Water (V-SMOW) or Vienna Pee Dee Belemnite (VPDB)
S	^{32}S ^{33}S ^{34}S ^{36}S	94.93% 0.76% 4.29% 0.02%	$^{34}S/^{32}S$ ($\delta^{34}S$)	Cañon Diablo Troilite (V-CDT)

1.2.4.3 Fractionation

Whilst isotopes share the same number of electrons and many physical and chemical properties, the mass difference between isotopes of an element can result in small differences in thermodynamic properties and thus influence the bonding strength of atoms in a compound. Greater dissociation energies are associated with isotopes of greater atomic mass, therefore bonds between lighter isotopes are more easily broken. Consequently, biological, physical and chemical processes may preferentially affect one isotope over another. Such processes can thus cause isotope fractionation, the partitioning of isotopes between different substances or phases. This phenomena makes it possible to identify biogeochemical processes and trace sources of nutrients through the analysis of stable isotopes. Nitrogen and sulphur compounds traverse a wide range of oxidation numbers (+5 (NO_3^-) to -3 (NH_4^+); +6 (SO_4^{2-}) to -2 (H_2S)) and the processing between these oxidation states results in a wide range of natural isotope compositions (Kendall, 1998).

There are 2 types of mass dependent isotope fractionation: equilibrium fractionation and kinetic fractionation.

Equilibrium isotope fractionation occurs in reversible reactions where forward and backward reaction rates are equal. Such reactions are restricted to well mixed closed systems at chemical equilibrium (Kendall and Caldwell, 1998). Heavier isotopes tend to accumulate in higher oxidation state compounds during equilibrium fractionation. At higher temperatures, reaction rates are greater and reactions are likely more complete, therefore the difference between isotope ratios in any 2 species is reduced. Consequently, low temperature equilibrium reactions can produce significant isotope fractionation effects.

For isotope exchange reactions (for example between compounds A and B), the fractionation factor (α) is used to define the ratio (R) of the numbers of any 2 isotopes in a chemical compound A divided by the ratio for another compound B (Equation 1.2).

$$\alpha_{A-B} = \frac{R_A}{R_B} \qquad \textbf{Equation 1.2}$$

Fractionation factors can be converted to enrichment factors (ε) which display the difference between isotope ratios on the per mille (‰) scale.

$$\varepsilon\ (‰) \cong (\alpha - 1).1000 \qquad \textbf{Equation 1.3}$$

Kinetic fractionation occurs in systems out of isotopic equilibrium where forward and backward reaction rates are not identical, and the reactions may be

unidirectional if the reaction products are physically removed from the reactants (Kendall and Caldwell, 1998). An identical equation is used to define the fractionation factor for kinetic reactions, however the terms product and reactant are used instead (Equation 1.4). Where α > 1, the product will have a heavier isotope composition than the reactant. Biochemical processes typically favour lighter isotopes due to their lower energy demands. As these reactions proceed, the fraction of reactant decreases and the heavier isotope becomes enriched in residual reactant. The instantaneous product also becomes enriched in the heavier isotope, but with a δ value less than the residual reactant. The cumulative product becomes enriched in the heavy isotope until all the reactant has been converted to product, at which point the product is isotopically identical to the original reactant.

$$\alpha_{Product-Reactant} = \frac{R_{Product}}{R_{Reactant}} \qquad \textbf{Equation 1.4}$$

Different biogeochemical processes can impart differing fractionation factors on stable isotopes, therefore an understanding of these isotope effects is required to interpret stable isotope data. In the following sections, an overview is provided of reactions which may cause such effects on nitrogen (Figure 1.2) and sulphur isotopes in natural systems. Stable isotope analysis of these elements are utilised in this study to further understand nutrient cycling and weathering processes in subglacial environments.

1.2.5 Biogeochemical processes and their effects on nitrogen isotope ratios

1.2.5.1 N_2 fixation

Nitrogen fixing organisms reduce N_2 to NH_3, using the enzyme nitrogenase, while oxidising organic carbon to produce energy (Denk et al., 2017). Diazotrophs include aquatic cyanobacteria and N_2 fixing bacteria which may live freely in soil, within plants or in symbiosis with plants (Denk et al., 2017). Atmospheric nitrogen has an isotopic composition of 0‰ and nitrogen isotope fractionation is limited during this reaction, producing organic N with $\delta^{15}N$ of -3 to +1‰ (Fogel and Cifuentes, 1993).

1.2.5.2 Mineralisation

Up until relatively recently, it was believed that organic nitrogen must be broken down first by microbes into forms which plants could effectively compete for (Schimel and Bennett, 2004). However, the current paradigm involves the breakdown of complex organic matter molecules into organic N monomers

(depolymerisation) by microbial extracellular enzymes which may be used by plants or microbes (Schimel and Bennett, 2004). Organic monomers are also further converted to inorganic NH_4^+ via microbes (mineralisation).

Organic N polymers → organic N monomers →
microbes → NH_4^+ **Equation 1.5**

This process likely imparts very minor fractionation, typically ±1‰ (Kendall, 1998), however, the literature is scarce with studies to quantify any isotope effects (Denk et al., 2017).

1.2.5.3 Nitrification

Nitrification involves the oxidation of ammonium to nitrate via multiple biological processes (Equation 1.6). Ammonium is initially oxidised to hydroxylamine (NH_2OH) by ammonium oxidisers possessing the enzyme ammonia monooxyenase (AMO). Hydroxylamine is then converted to nitrite with the enzyme hydroxylamine oxidoreductase (HAO). Finally, nitrite is oxidised to nitrate catalysed by the nitrite oxidoreductase (NOR) enzyme. The oxidation of nitrite to nitrate is relatively rapid, therefore most of the isotope fractionation is caused by slower oxidation of ammonium (Hoefs, 2009). In terrestrial soil ecosystems, this process may exert an isotope fractionation of -29.6 ± 4.9‰ (Denk et al., 2017), however in nutrient limited environments, efficient nitrogen cycling may result in negligible fractionation (Heaton, T. H. E., 1986; Fogel and Cifuentes, 1993). During nitrification, oxygen, incorporated into nitrate, is derived from water and oxygen in a 2:1 ratio. Since these oxygen sources have distinctive oxygen isotope ratios: atmospheric oxygen (+23.5‰ (Hoefs, 2009)) and water (typically negative), an estimate of microbial derived nitrate can be calculated using these values (Equation 1.7). This technique has been widely used in aqueous geochemical studies to identify microbial nitrification as a source of nitrate. However, several experimental studies found that microbial nitrate can have variable $\delta^{18}O$, perhaps due to isotope fractionation during oxygen incorporation, which cast doubt on this approach (Casciotti, Karen L. et al., 2010; Snider et al., 2010; Mayer et al., 2001; Spoelstra et al., 2007). An alternative isotope method ($\Delta^{17}O$) based on the ratio of $\delta^{17}O$ to $\delta^{18}O$ in nitrate is a useful way to discriminate between nitrate derived from atmospheric sources (which are enriched in ^{17}O) v microbial nitrification (Michalski et al., 2004). This method benefits from the fact that $\Delta^{17}O$ is unaltered by post-depositional processes such as denitrification.

$NH_4^+ \rightarrow NH_2OH \rightarrow NO_2^- \rightarrow NO_3^-$ **Equation 1.6**

$$\delta^{18}O_{NO3} = (0.33 \times \delta^{18}O_{Air}) + (0.66 \times \delta^{18}O_{Water})$$ **Equation 1.7**

1.2.5.4 Denitrification

In the absence of oxygen, such as poorly aerated soils or anaerobic water, nitrate is used as an electron acceptor during the process of denitrification, where it is reduced stepwise via NO_2^-, NO, N_2O to N_2. This process returns nitrogen to the atmosphere as N_2, accounting for nitrogen removed by N fixation. During each reduction step, isotopically light ^{14}N is preferentially utilised by microbes, leaving the residual nitrate enriched in ^{15}N by 5 to 40‰ (Kendall, 1998). Experimental studies have demonstrated that weaker isotope effects are evident under increased temperatures (Mariotti et al., 1982) since this determines the rate limiting step of substrate (NO_3^-) diffusion into the cell (Denk et al., 2017). Therefore, in cold climates such as the Arctic, isotope fractionation may be more pronounced, especially given the low natural abundance of nitrogen species in these environments.

1.2.5.5 Dissimilatory nitrate reduction to ammonium

Dissimilatory nitrate reduction to ammonium (DNRA) involves the initial reduction of nitrate to ammonium through fermentation (Equation 1.8) (Schlesinger, 2013). This process is particularly important in anoxic wetland ecosystems where nitrate availability is low and organic carbon is abundant (Schlesinger, 2013). Unlike denitrification, this reduction pathway retains fixed nitrogen within the environment as NH_4^+, therefore, this reaction may be favoured when nitrate concentrations are limited (Tiedje, 1988). Isotope fractionation effects associated with this process have yet to be investigated but may be on the order of ε = -30‰ (McCready et al., 1983).

$$½\ NO_3^- + (CH_2O) + H^+ \rightarrow ½\ NH_4^+ + CO_2 + ½\ H_2O$$ **Equation 1.8**

1.2.5.6 Anammox

Anammox, or anaerobic ammonium oxidation, produces N_2 from ammonium and nitrite under anoxic conditions. This process has been observed in sewage treatment works and in coastal/marine sediments (Dalsgaard et al., 2005) but limited research has been carried out in freshwater ecosystems (Schlesinger, 2013). Furthermore, investigations into isotope fractionation effects on ammonium during this reaction are limited to a single study which used an enrichment culture to demonstrate that ammonium becomes enriched with ^{15}N during anammox (ε = -23.5‰ to -29.1‰) (Brunner et al., 2013).

$$NH_4^+ + NO_2^- \rightarrow N_2 + 2H_2O$$

Equation 1.9

1.2.5.7 Adsorption

Electrochemically charged nitrogen species can interact with charged mineral surfaces of particulate matter in sorption/desorption reactions. 2:1 type clay minerals naturally have a net negative charge as a result of Al^{3+} ions substituting for Si^{4+} in silicate lattices. This negative charge is balanced by cations in interlayer sites between silica tetrahedral and hydroxyl octahedral sheets. When a clay particle interacts with water, interlayer cations can enter solution, creating a diffuse cloud of positively charged counterions next to the negatively charged surface, a phenomena known as a 'double layer' (Drever, 1997). As the concentration of protons at a mineral surface increases at low pH, the density of protons in the double layer causes the surface to obtain an apparent positive charge. This repels positively charged ions such as ammonium and attracts negatively charged ions such as nitrate. Oxide minerals may also become negatively charged at high pH during the deprotonation of surface hydroxyl groups, while protonation (and thus positively charged surfaces) is favoured at low pH (Drever, 1997). The pH at which the surface charge is balanced by deprotonated and protonated groups is termed the point of zero charge (PZC). Above the PZC, surfaces are negatively charged which encourages adsorption of ions such as ammonium and repulsion of nitrate. The PZC is variable for different minerals, with many oxides having PZCs at pH <9 (Kosmulski, 2011). In near neutral – slightly alkali pH water, characteristic of glacial runoff, oxides and clay minerals are therefore generally negatively charged. Therefore, adsorption is only a significant process for positively charged ions i.e. ammonium. Ammonium adsorbs to clay mineral surfaces principally via cation exchange processes, however other factors including negative surface charge, water absorption and surface morphology may also contribute (Alshameri et al., 2018).

Adsorption of ammonium onto surfaces has been shown experimentally to impart an isotopic fractionation on nitrogen, whereby heavy ^{15}N preferentially enters the adsorbed phase, leaving residual dissolved ammonium isotopically light. Isotope fractionation factors are typically +1 to +11‰ (Karamanos and Rennie, 1978; Delwiche and Steyn, 1970). However, no isotope fractionation was associated with ammonium adsorption in a study of a contaminated groundwater plume (Böhlke et al., 2006).

1.2.5.8 Volatilisation

Volatilisation involves the loss of dissolved ammonia gas from a liquid to the atmosphere. Isotope fractionation may take place during both equilibrium and kinetic reactions during this process. Equilibrium isotope fractionation occurs between dissolved ammonium and dissolved ammonia (Equation 1.10) as well as between aqueous and gaseous ammonia (Equation 1.11); while kinetic isotope fraction occurs during the diffusive loss of ^{15}N depleted ammonia (Kendall, 1998).

$$NH_{3\ (aq)} + H^{+} \leftrightarrow NH_4^{+}{}_{(aq)} \qquad \textbf{Equation 1.10}$$

$$NH_{3\ (aq)} \leftrightarrow NH_{3\ (g)} \qquad \textbf{Equation 1.11}$$

Consequently, ammonia gas produced during volatilisation is isotopically light while residual ammonium is isotopically heavy. Experimentally derived isotope fractionation factors of -29‰ have been derived for this reaction at 25°C (Kirshenbaum et al., 1947). While the degree of fractionation is pH dependent, other environmental factors such as temperature, wind speed and moisture affect the reaction rate (Kendall, 1998). Nitrogen isotope fractionation between ammonium and aqueous ammonia has been modelled to be inversely related to temperature with enrichment of 45.4‰ at 23°C, 37.7‰ at 50°C and 33.5‰ at 70°C (Li, L. et al., 2012). At lower temperatures, representative of glacial environments, isotope fractionation factors may therefore be greater than 45‰. Yet, since volatilisation is temperature dependent, rates of NH_3 loss may be lower, thus negating the overall isotope effect.

In natural systems, despite both equilibrium and kinetic reactions described above, the overall loss of ammonium is unidirectional with ultimate oxidation to nitrate. The isotopic signature of the product nitrate will therefore reflect kinetic isotope enrichment during volatilisation, becoming isotopically heavier than the source ammonium/organic N. The isotopic enrichment associated with this overall reaction was calculated as ~ -33‰ (Heaton, T. H. E. et al., 1997).

1.2.5.9 Assimilation

Assimilation is the incorporation of nitrogen compounds into organic biomass and may be referred to as immobilisation and uptake for microorganisms and plants respectively. Assimilation of nitrate by microbes and plants incurs isotope enrichment within the range of 0 to -19.2‰ with a mean of -5.9‰ (Denk et al., 2017). While average isotope fractionation associated with ammonium assimilation is -7.5‰ for plants and -10.2‰ for microbes (Denk et al., 2017).

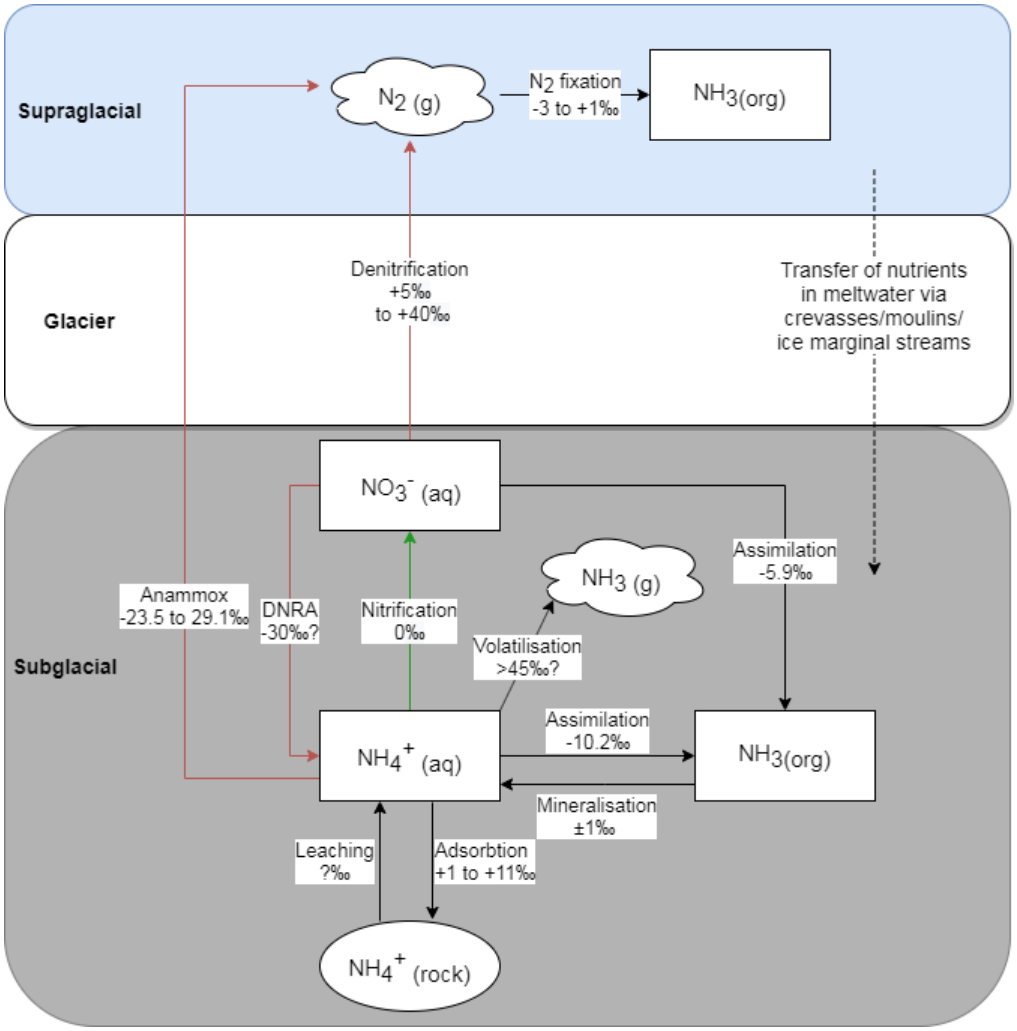

Figure 1.2 Biogeochemical reactions involving nitrogen which may occur in glacial environments and their associated isotope fractions. Red and green arrows indicate strictly anaerobic and aerobic processes respectively. Isotope enrichments are reported as ε (‰) and values are as given in text. Rectangles represent aqueous phases, ellipses represent solids and clouds represent gases.

1.2.6 Biogeochemical processes and their effects on sulphur and sulphate isotope ratios

1.2.6.1 Sulphide oxidation

Sulphur

Sulphide oxidation to sulphate occurs in both oxic (Equation 1.12) and anoxic (e.g. Equation 1.13) settings via abiotic and biotic pathways. Abiotic sulphide oxidation rates are slow while microbially mediated sulphide oxidation may be up to 2 orders of magnitude higher (Sharp et al., 1999). Negligible sulphur isotope fractionation is associated with sulphide oxidation, although $\delta^{34}S - SO_4$ may be marginally depleted relevant to the sulphide (Toran and Harris, 1989; Clark and Fritz, 1997).

$$FeS_2 + 3.5O_2 + H_2O \rightarrow 2SO_4^{2-} + Fe^{3+} + 2H^+ \quad \textbf{Equation 1.12}$$

$$FeS_2 + 14Fe^{3+} + 8H_2O \rightarrow 2SO_4^{2-} + 15Fe^{3+} + 16H^+ \quad \textbf{Equation 1.13}$$

Sulphate – oxygen

Sulphate produced by sulphide oxidation which occurs under oxic conditions incorporates 3.5 oxygen atoms out of 4 from atmospheric O_2 (Equation 1.12), whereas oxygen in sulphate produced under anoxic conditions is derived entirely from water, where iron is the usual electron acceptor (Equation 1.13). Therefore, the oxygen isotopic composition of sulphate is dependent on the $\delta^{18}O$ of water and/or oxygen. Upon incorporation of oxygen into sulphate molecules, kinetic isotope fractionation effects cause $\delta^{18}O\text{-}SO_4$ to differ from the original $\delta^{18}O\text{-}H_2O$ (ε_w) or $\delta^{18}O\text{-}O_2$ (ε_o). Experimental studies have constrained values of ε_w to between 0 and +4.1‰ (Balci et al., 2007; Taylor et al., 1984); while ε_o values are larger, ranging between -10.0‰ and -11.4‰ for biological experiments and -4.3 to -9.8‰ for abiotic experiments (Balci et al., 2007; Taylor et al., 1984; Lloyd, 1968).

Since the oxygen isotope composition of meteoric water and atmospheric oxygen are significantly different, $\delta^{18}O$ of sulphate has been used to determine oxygen sources during sulphide oxidation. For example, Bottrell, S. and Tranter (2002) used this approach to distinguish between aerobic and anaerobic weathering environments. Sulphide oxidation to sulphate proceeds in a stepwise manner involving intermediate S species. This process involves the loss of 8 electrons, with a maximum of 2 electrons donated at each reaction step. Sulphur intermediates are prone to exchange of oxygen atoms with water molecules, which can dilute the atmospheric oxygen isotope signal and

therefore complicate the interpretation of oxygen isotopic ratios to 'fingerprint' the oxygen source. Once the final oxygen atom is incorporated into the sulphate molecule, no further oxygen isotope exchange can occur. Therefore, at least 1 of the 4 oxygen atoms will represent an original oxygen source. Consequently, if at least 25% of oxygen is derived from atmospheric oxygen, sulphide oxidation must have occurred under oxygenated conditions. Some experimental studies, however, suggest that even when oxygen is present in solution, the majority of oxygen incorporated into sulphate is derived from water (Chandra and Gerson, 2011; Usher et al., 2004). Nevertheless, the oxygen isotope ratio of sulphate provides a qualitative assessment of the oxygen source in pyrite oxidation and thus is a useful tool to determine whether an environment is anoxic alongside other redox proxies.

1.2.6.2 Sulphate reduction

Sulphate may be reduced under anoxic conditions via microbial anaerobic respiration. From here on, this reaction will be referred to as bacterial sulphate reduction (BSR). Dissimilatory BSR produces hydrogen sulphide which may be recycled back to sulphate and/or other sulphur compounds via interaction with dissolved oxygen or Fe^{3+} or Mn^{4+} (Bottrell, S.H. and Newton, 2006). Alternatively, it may react with reduced iron to form sulphide minerals such as pyrite (FeS_2). This reaction is mediated by sulphate reducing bacteria which preferentially utilise isotopically light $^{32}SO_4$ during oxidation of an electron donor such as organic carbon or hydrogen (Equation 1.14). Pure culture experiments demonstrate that sulphide produced through this reaction exhibit a variable isotope depletion (ε) of between +3 to -66 ‰ (Sim et al., 2011). Repeated oxidation and reduction cycles can also result in strongly depleted sulphides (Canfield and Teske, 1996). BSR also causes isotope fractionation of oxygen as ^{18}O accumulates in residual sulphate as ^{16}O is preferentially incorporated into CO_2/HCO_3^- (Fritz et al., 1989; Mizutani and Rafter, 1973). Sulphate is initially reduced to intermediate S compounds (SO_3) whose oxygen atoms may exchange with water causing further isotope fractionation (Fritz et al., 1989). An oxygen isotope fractionation factor of -8‰ for this reaction has been determined by Strebel et al. (1990).

$$SO_4^{2-} + 2CH_2O \rightarrow 2HCO_3^- + H_2S$$

Equation 1.14

In contrast, assimilatory reduction involves the reduction of sulphate to organic sulphur compounds which are incorporated into organisms. Organic sulphur is generally more enriched in ^{34}S than pyrite sulphur. Under certain marine depositional/diagenetic conditions, organic sulphur may represent a significant proportion of sedimentary sulphur (Raiswell et al., 1993; Anderson, T.F. and

Pratt, 1995), however, this reaction is not generally considered a major component of the global sulphur cycle (Goldhaber, 2003).

1.3 The subglacial environment

Glaciers and ice sheets (and therefore subglacial environments) currently cover approximately 10% of the Earth's surface (Benn and Evans, 2010), however their geographic spread has varied over geological time as evidenced by the glacially influenced landscapes and rock formations present in currently unglaciated areas. Subglacial environments are dark, cold, dynamic environments featuring interactions between rock, ice and/or liquid water.

1.3.1 Glacier hydrology

Glacial meltwater exerts a significant control on glacier behaviour. It directly facilitates rock weathering, transports dissolved and particulate material and deposits eroded material, while the presence of subglacial meltwater lubricates ice masses which increases glacial motion causing physical abrasion. Water is also vital for life which enables biochemical processes, electrochemical gradients and the transfer of chemical substances (Yde et al., 2011). Therefore, the presence/absence of meltwater also exerts a control on the presence of life within glacial environments.

Water in glacial catchments may derive from snow or ice melt on the glacier surface, within the glacier or at the glacier bed. Water may also derive from rain, terrestrial runoff or groundwater. The presence/absence of liquid water at the glacier bed is determined by the glacier's thermal regime.

Ice may reach the pressure melting point (PMP) where the overburden mass causes a lowering of the melting point by 0.072°C per 100m (Benn and Evans, 2010) such that liquid water exists. Therefore, the melting point of subsurface ice in larger glaciers is depressed to a greater extent meaning that subglacial water is more likely to exist. Such glaciers, whose subglacial ice is above the PMP, are termed warm based. Thinner glaciers which do not reach the PMP and are cold based meaning they are frozen to their beds all year round limiting subglacial flow. Polythermal glaciers represent an intermediate category which have a warm based core surrounded by cold based margins. Glaciers in Svalbard vary in size from small valley glaciers to ice caps (König et al., 2014), many of which are polythermal with glacier beds frozen to the underlying permafrost (Björnsson et al., 1996).

Meltwater in glacial catchments may flow on the glacier surface (supraglacial), in channels/gaps within the ice (englacial) or beneath the ice (subglacial). The

connectivity between these discrete meltwater networks is restricted by the impermeable nature of glacial ice, however water may be routed vertically through crevasses and moulins. Crevasse formation is greater in warm based glaciers where subglacial meltwater facilitates basal motion (Benn and Evans, 2010), therefore in cold based glaciers, surface derived meltwater is generally unable to access the subglacial environment (Laybourn-Parry et al., 2012), hence water flow is generally confined to supraglacial and ice marginal environments. However supraglacial channels may incise glacial ice and eventually reach the glacier bed through cut and closure (Gulley et al., 2009).

1.3.2 Glacial erosion and weathering

Glaciers are effective at directly eroding landscapes through 2 principal mechanisms: abrasion and plucking.

Abrasion is the process of wearing rock down by striation (scouring of bedrock) and polishing of rock surfaces. Abrasion is typically more dominant in warm based subglacial environments where liquid water lubricates basal ice facilitating glacier motion (Benn and Evans, 2010). In cold based ice, sliding and therefore abrasion is limited, yet internal deformation and associated shearing may promote limited abrasion via clasts embedded in glacial ice (Benn and Evans, 2010). Glacial erosion rates in modern warm based glaciers are up to 100 mm/yr while cold based glaciers may have rates as low as 0.01 mm/yr (Hallet et al., 1996). Plucking is the process whereby rocks, removed from bedrock, become trapped or frozen into basal ice and transported downstream. In cold based ice, where sliding is limited, plucking is a more effective erosional mechanism (Benn and Evans, 2010).

These processes work together to effectively comminute bedrock to fine grained sediments (glacial rock flour). This creates an abundance of fine (typically silt size) grains with large surface area as well as ultrafine (< 1 μm) particles (Holdren and Berner, 1979). Crushing also results in the fracture and internal plastic deformation of silicate minerals (Petrovich, 1981) as well as exposing unweathered surfaces. These factors cause the crushed material to be highly reactive, therefore interaction with melt water can stimulate rapid initial dissolution rates as observed in laboratory experiments which may influence bulk glacial meltwater chemistry (Anderson, S.P. et al., 1997). Glaciated catchments usually have high specific runoff and the interaction of this water with crushed rock causes the weathering of base cations from exposed and abraded minerals through exchange with protons in solution. As a result, glaciers produce some of the highest cation denundation rates in the world (Anderson, S.P. et al., 1997).

The specific weathering rates of a glacier is largely controlled by the extent of rock-water interaction. Warm based and polythermal glaciers feature subglacial drainage through narrow conduits (channelised systems) as well as in distributed drainage systems (DDS), an interconnected network of cavities and thin films of water between ice and rock/sediment (Benn and Evans, 2010). Channelised systems route water efficiently through the glacier whereas DDS are less efficient which facilitates prolonged rock-water interaction. Furthermore, high rock – water ratios associated with DDS generally enhance solute acquisition. As the margins of ice masses freeze, they can act as a barrier to water flow, prolonging rock-water contact time and thus solute acquisition (Tranter, 2003). Cold based glaciers, in addition to having lower erosion rates, afford fewer opportunities for rock-water reaction due to the lack of liquid water at the glacier bed. Yet they still produce significant solute through sub-aerial chemical weathering in turbid channels and saturated lateral moraines (Hodgkins, 1997; Hodgkins et al., 1998).

1.3.3 Glacial hydrochemistry overview

Subglacial environments and ice marginal environments such as moraines are a focal point of crushed rock and water interaction. Numerous weathering reactions occur in such environments which are outlined in Table 1.2 and discussed below.

Early glacial studies considered ion exchange processes as major reactions that occur initially as dilute meltwater comes into contact with rock flour. These involve the preferential exchange of monovalent cations on sediment exchange surfaces with divalent cations from solution (Stumm and Morgan, 1996). However, this does not increase the net amount of solute acquisition, merely the distribution of base cations in meltwater (Tranter et al., 1993).

Later studies and models of subglacial weathering considered glacial environments as abiotic where solute acquisition was derived from the atmosphere and bedrock (Tranter et al., 1993). In such a model, protons required for acid hydrolysis reactions, that liberate base cations, are derived from the dissolution of atmospheric carbon dioxide into meltwater (carbonic acid) (Equation 1.15) and the oxidation of sulphide minerals (Equation 1.12) which produces sulphuric acid. The former reaction is limited by the slow dissolution rate of CO_2 while the latter is limited by the amount of dissolved oxygen in meltwater. Gases may also be sourced from regelation which is the process of melting under pressure and refreezing when the pressure is reduced i.e. as ice encounters obstacles on the glacier bed. Gases are excluded from ice during freezing (Hallet, 1976), however this flux of gas was considered negligible (Sharp and Tranter, 2017). As such according to this abiotic model, solute acquisition is directly controlled by atmospheric gas exchange (Tranter et al., 1993).

$$CO_2 + H_2O \rightleftharpoons H^+ + HCO_3^-$$

Equation 1.15

Initial weathering reactions are dominated by hydrolysis reactions owing to their rapid kinetics and requirement of only water and an exposed mineral surface (Equation 1.16, Equation 1.17). These reactions slow as the solution pH rises and the equilibrium shifts to the right. Acidity produced by CO_2 dissolution and sulphide oxidation reduce the pH which lowers the saturation index of carbonates driving carbonate weathering via carbonation (Equation 1.18) and coupled sulphide oxidation and carbonate weathering respectively (Equation 1.21). Carbonate minerals, whilst mainly occurring in limestone and dolomite rocks, are found dispersed in low concentrations in almost all rock types. Despite, their low concentrations, their rapid dissolution kinetics (Plummer and

Wigley, 1976) ensure that they are preferentially dissolved over silicates which have slower dissolution rates.

Table 1.2 Principal subglacial geochemical weathering reactions (Tranter et al., 2002)

Carbonate hydrolysis **Equation 1.16**

$Ca_{1-x}(Mg_x)CO_3\,(s) + H_2O\,(l) \rightleftharpoons (1-x)Ca^{2+}\,(aq) + xMg^{2+}\,(aq) + HCO_3^- + OH^-\,(aq)$

Feldspar hydrolysis e.g. **Equation 1.17**

$KAlSiO_8\,(s) + H_2O\,(l) \rightleftharpoons HAlSi_3O_8 + K^+ + OH^-$

Carbonation of carbonate **Equation 1.18**

$Ca_{1-x}(Mg_x)CO_3\,(s) + CO_2\,(aq) + H_2O\,(l) \rightleftharpoons (1-x)Ca^{2+}\,(aq) + xMg^{2+}\,(aq) + 2HCO_3^-\,(aq)$

Carbonation of feldspar e.g. **Equation 1.19**

$CaAl_2Si_2O_8\,(s) + CO_2\,(aq) + H_2O\,(l) \rightleftharpoons Ca^{2+}\,(aq) + 2HCO_3^-\,(aq) + H_2Al_2Si_2O_8\,(s)$

Sulphide oxidation coupled to silicate dissolution e.g. **Equation 1.20**

$4FeS_2 + 16Na_{1-x}(K_x)AlSi_3O_8\,(s) + 15O_2\,(aq) + 86H_2O\,(l) \rightleftharpoons$

$16(1-x)Na^+\,(aq) + 16xK^+\,(aq) + 8SO_4^{2-}\,(aq) + 4Al_4Si_4O_{10}(OH)_8(s) + 32H_4SiO_4\,(aq) + 4Fe(OH)_3\,(s)$

Sulphide oxidation coupled to carbonate dissolution **Equation 1.21**

$4FeS_2 + 16Ca_{1-x}(Mg_x)CO_3\,(s) + 15O_2\,(aq) + 14H_2O\,(l) \rightleftharpoons$

$16(1-x)Ca^{2+}\,(aq) + 16xMg^{2+}\,(aq) + 16HCO_3^-\,(aq) + 8SO_4^{2-}\,(aq) + 4Fe(OH)_3\,(s)$

Sulphide oxidation by Fe^{3+} **Equation 1.22**

$FeS_2 + 14Fe^{3+} + 8H_2O\,(l) + 16CaCO_3\,(s) \rightleftharpoons$

$15Fe^{2+}\,(aq) + 16Ca^{2+}\,(aq) + 2SO_4^{2-}\,(aq) + 16HCO_3^-\,(aq)$

Dissolution of gypsum **Equation 1.23**

$CaSO_4.2H_2O\,(s) \rightleftharpoons Ca^{2+}\,(aq) + SO_4^{2-}\,(aq) + 2H_2O\,(l)$

Oxidation of organic carbon **Equation 1.24**

$C_{org}\,(s) + O_{2\,(aq)} + H_2O\,(l) \rightleftharpoons CO_{2\,(aq)} + H_2O\,(l) \rightleftharpoons H^+ + HCO_3^-$

The rapid transit of sediment in glacial systems means that there is thought to be limited time for the formation of secondary weathering products such as clays (Tranter, 2003). As such silicates generally weather incongruently (Equation 1.19). Therefore, while glaciers are effective at weathering base cations, their overall chemical weathering is comparable with other terrestrial environments which more effectively dissolve silicate bedrock (Anderson, S.P. et al., 1997). Glacial weathering dissolves carbonate to silicate in a ratio of ~5:1 in contrast to the global average of ~1.3:1 (Tranter, 2003). However, as carbonate weathering proceeds and meltwaters become saturated, silicate weathering may become more of a significant process, coupling with sulphide oxidation (Equation 1.20). This is particularly the case under large ice sheets where water residence times are prolonged (Wadham et al., 2010). Fairly recent work has also emphasised that the precipitation of secondary clays cannot be overlooked in such environments (Crompton et al., 2015).

In glacial forefields and moraines, seasonal evaporation and freezing, in summer and winter respectively, concentrate solutes often resulting in the precipitation of secondary minerals such as gypsum and anhydrite (Wadham et al., 2001; Cooper et al., 2002). Re-dissolution of such minerals in dilute water can contribute to catchment solute export by run off (Equation 1.24).

1.3.3.1 Microbially mediated weathering and subglacial biogeochemical reactions

A paradigm shift in subglacial weathering occurred with the discovery of active microbial ecosystems in subglacial sediment (Sharp et al., 1999). Since then, microbes have been sampled in small valley glaciers e.g. (Sharp et al., 1999; Foght et al., 2004), polythermal glaciers e.g. (Bhatia et al., 2006; Skidmore et al., 2005), ice caps e.g. (Lanoil et al., 2009; Mikucki and Priscu, 2007; Sheridan et al., 2003), subglacial lakes e.g. (Christner et al., 2014) and outlet glaciers e.g. (Kivimaki, 2005).

Life in glaciers is dominated by microorganisms such as bacteria, protozoa and algae (Laybourn-Parry et al., 2012). In supraglacial environments, microbial ecosystems are found in meltwater pockets called cryoconite as well as algae which alter the colour of ice surfaces. Subglacial environments also feature microbes with higher cell abundances associated with debris rich ice (Sharp et al., 1999). Diverse microbial communities have adapted to living in dark, cold and oligotrophic environments through the exchange of electrons via reduction and oxidation (redox) reactions they mediate involving carbon (Boyd, E.S. et al., 2011; Stibal et al., 2012), nitrogen (Skidmore et al., 2000; Boyd, E.S. et al.,

2011), sulphur (Boyd, E.S. et al., 2014; Harrold et al., 2016) and iron (Nixon et al., 2017).

Following the discovery of active microbial ecosystems in glacial sediment, geochemical studies on the Haut d'Arolla glacier demonstrated that biologically mediated weathering exerts a dominant control on solute acquisition (Tranter et al., 2002). Sulphide oxidation is the dominant reaction in subglacial environments providing protons to solution (Tranter, 2003). Oxygen is the preferred terminal electron acceptor in this reaction since it is both abundant and energetically favourable (Patrick and Jugsujinda, 1992). Microbes amplify rates of sulphide oxidation, which depletes water of dissolved oxygen such that it may drive parts of the subglacial system to anoxia (Bottrell, S. and Tranter, 2002; Wadham et al., 2004; Wynn et al., 2006; Wadham et al., 2007). Under such conditions, sulphide oxidising bacteria mediate pyrite oxidation using alternative oxidising agents (Bottrell, S. and Tranter, 2002) generally in the sequence NO_3^-, Mn^{4+}, Fe^{3+}, SO_4^{2-}, CO_2. Sources of nitrate include snowmelt and microbial nitrification of ammonium. Mn^{4+} reduction has been shown to also pair with pyrite oxidation in anoxic marine sediment (Schippers and Jørgensen, 2002) as well as facilitate anoxic nitrification (Hulth et al., 1999). However, manganese reduction has not received much attention in subglacial weathering literature, likely because of its lower abundance in rock. Nonetheless, given that MnO_2 reduction is energetically more favourable than iron reduction, it is likely this process occurs in subglacial environments where bedrock contains MnO_2. Fe^{3+} may be sourced from the oxidation of Fe^{2+} derived from iron oxides and the weathering of pyrite and Fe^{2+} bearing silicates and carbonates in previously oxygenated environments. Furthermore, microbial activity can increase the rate of oxidation of ferrous iron to ferric iron by as much as 10^6 times (Singer and Stumm, 1970).

In addition, the microbial oxidation of organic matter (Equation 1.24) further reduces dissolved oxygen concentrations and produces CO_2, contributing extra acidity (Equation 1.15). In contrast to other environments, the supply of organic matter, may be limited to that which is delivered from the glacier surface (e.g. algae, insects and animal faeces), as well as microbial necromass and any soils overridden during past glacial advances (Tranter, 2003). However, ancient organic matter occurring as kerogen within bedrock is abundant particularly where bedrock contains sedimentary units such as shales. Microbial oxidation of kerogen can couple with bacterial sulphate reduction (Equation 1.14) in anoxic settings (Wadham et al., 2004). Under highly reducing conditions, as sulphate becomes depleted, methanogenesis may occur. Methanogenic microbial assemblages have been identified in subglacial sediments (Boyd, E.S.

et al., 2010; Stibal et al., 2012) and enrichment cultures of this material have been shown to produce methane (Boyd, E.S. et al., 2010) with higher rates associated with substrates of lacustrine organic carbon over soil organic carbon (Stibal et al., 2012).

The biogenic supply of protons from sulphide (Equation 1.12, Equation 1.13) and organic carbon oxidation (Equation 1.24) therefore facilitate carbonate and silicate weathering under both oxic and anoxic conditions, thereby increasing the acquisition of base cations (Montross, S.N. et al., 2012) and thus negating the need for atmospheric CO_2 for proton supply. This explains how weathering may occur in isolated parts of the glacier bed where water filled channels inhibit atmospheric CO_2 dissolution (Sharp and Tranter, 2017). Recent studies, however, have also demonstrated an alternative abiogenic source of energy to subglacial ecosystems. Glacial comminution of rocks can liberate gases such as CO_2, CH_4 and H_2 from pore spaces, fluid inclusions and crystal structures (Macdonald et al., 2018). In addition, subglacial abrasion of silicate rock shears surface mineral bonds producing silica free radicals which upon interaction with water, produce hydrogen (Telling et al., 2015). Crushing may also release potentially bioavailable hydrocarbons and acetate via degradation of organic matter (Gill Olivas, 2019). Therefore, crushing may represent an important energy source to subglacial environments particularly when organic matter is limited.

Cycles of C, N, S, Fe, Mn are intimately linked via redox reactions catalysed by microbial organisms. Subglacial ecosystems based on chemolithotrophic organisms are therefore able to derive energy and nutrients in cold, dark environments isolated from the atmosphere. Such environments may have acted as refugia for life during snowball earth events over geological timescales (Telling et al., 2015).

1.3.4 Glacial N cycling

Nitrate in glacial runoff has been previously assumed to derive entirely from snowmelt, however more recent advances in glacial biogeochemistry have transformed the way glaciers are considered from sterile weathering environments to microbial ecosystems. During early snow melt in the spring solute is quickly eluted, leaving residual snow solute poor e.g. (Tranter, 1991). Yet, numerous studies of valley glaciers and ice sheets now demonstrate enhanced nitrate concentrations in late summer glacial runoff (Ansari et al., 2013; Wynn et al., 2007; Yde et al., 2008; Rutter et al., 2011; Wadham et al., 2016; Tockner et al., 2002; Williams, M. W. et al., 2007; Caulkett and Ellis-Evans, 1997; Hodson, 2006). The magnitude of nitrate export generally

exceeds the nitrogen budget of snow and ice and together with widespread loss of ammonium in catchment scale mass balance calculations, imply nitrate production within glaciers (Wynn et al., 2007; Hodson et al., 2005; Hodson, 2006). Nitrification has been found to not occur within snowpacks (Wynn et al., 2007; Williams, Mark W. et al., 1996). The locus of nitrate production has instead been attributed to the subglacial environment from studies of valley glaciers, ice sheets and subglacial lakes e.g. (Wynn et al., 2007; Boyd, E.S. et al., 2011; Christner et al., 2014; Wadham et al., 2016). Multiple lines of evidence have been used to come to this conclusion, although there is still much uncertainty as to the ultimate source of nitrogen. Nitrate is often positively correlated with crustally derived elements such as silica (Hodson, 2006) which implies that nitrogen is acquired into water that has derived solute from rock weathering. Stable isotopes analysis of nitrate in glacial runoff have been used to demonstrate a microbial origin on the assumption that microbial nitrate incorporates 2 of 3 oxygen atoms from water (see section 1.2.5) (Ansari et al., 2013; Wynn et al., 2007; Hodson et al., 2010a). Furthermore, Christner et al. (2014) used Δ17O isotopes to infer that nitrification is a dominant biogeochemical reaction in subglacial Lake Whillans. Microbiological studies also support nitrate production in subglacial environments. Functional gene analysis and microcosm experiments of subglacial sediments show that these harbour diverse N cycling microbial taxa including nitrifiers, nitrate reducers and diazotrophs (Boyd, E.S. et al., 2011). In addition, in-situ soil incubations demonstrate nitrification in a glacial forefield with N cycling rates greatest near the glacier terminus (Doxsey-Whitfield, 2012).

The timing of nitrate enrichment during late summer has been attributed to enhanced nitrification rates in subglacial and ice marginal environments (Ansari et al., 2013; Hodson, 2006). Early summer meltwater contains nitrate largely from snowmelt and low proportions of microbial/non snowpack nitrate (Hodson, 2006). This suggests that microbial activity may be reduced or masked by other sources. During the early melt season, subglacial drainage is inefficient with long transit times through distributed drainage systems causing reducing conditions through extensive rock-water interaction (Wynn et al., 2006). It is therefore likely that early season nitrate dynamics reflect enhanced rates of denitrification (Hodson, 2006; Wynn et al., 2006). Periodic decreases of nitrate concentrations and increased $\delta^{15}O$ NO_3 in glacial runoff have been suggested to represent microbial denitrification of nitrate to N_2 (Hodson et al., 2005; Wynn et al., 2006; Wynn et al., 2007). The occurrence of nitrate reducing bacteria in subglacial sediment supports this assertion (Skidmore et al., 2000; Foght et al., 2004). In addition, rapid decreases of nitrate and ammonium following an

extreme nitrogen deposition event in Svalbard, imply biological nitrate assimilation and denitrification during water storage at the glacier bed (Hodson et al., 2010b).

N fixation has been shown to occur on glacier surfaces in Svalbard too, when other N sources are limited. However N fixation rates have been found to be two orders of magnitude less than precipitation inputs (Telling et al., 2011). N fixing bacteria have also been cultured from subglacial sediments, which suggests this process is not limited to the supraglacial environment (Foght et al., 2004).

This growing body of evidence suggests that N cycling plays a key role in subglacial microbial ecosystems. While nitrification in subglacial and ice marginal moraine/talus environments is now considered responsible for the bulk of late summer nitrate production in glacial runoff, the exact ammonium substrate is hitherto unknown. Snowpack ammonium and mineralised organic matter have generally been considered the major sources of nitrogen for subglacial nitrification (Wynn et al., 2007; Ansari et al., 2013). However another potential source is nitrogen derived from rock weathering, but few studies have assessed this contribution to glacial catchments in detail, and attempts have been confounded by a limited understanding of nitrogen stable isotope dynamics during weathering (Wynn et al., 2007).

1.4 Rock nutrients

1.4.1 A crustal nitrogen reservoir

Nitrogen is generally thought to enter terrestrial environments from the atmosphere, which contains 4×10^{18} Kg of N (Bebout et al., 2013), via N fixation or wet/dry deposition. Despite longstanding reports of a geologic source of N (Stevenson, 1959), low concentrations within rocks as well as a lack of routine N quantification analysis, have meant that geologic N has often been overlooked as a nutrient source (Holloway and Dahlgren, 2002). However, a growing body of evidence challenges this assumption and demonstrates that the huge mass of solid Earth contains a significant nitrogen reservoir. Estimates of the original composition of the silicate part of the Earth after accretion and separation of a core (Bulk Silicate Earth, BSE) suggest that Earth initially contained $9 - 10 \times 10^{18}$ Kg N (Galloway, 2003; Palya et al., 2011). However, a more recent study suggests that BSE may have been as high as $27 \pm 16 \times 10^{18}$ Kg N, equivalent to ~ 7 ± 4 times present atmospheric N (Johnson and Goldblatt, 2015).

Nitrogen has accumulated from the deposition and burial of organic matter over the course of Earth's history where it is incorporated in rock as organic N (e.g. Kerogen) or as ammonium (NH_4^+) within silicate lattices during diagenesis or low grade metamorphism. As organic matter is broken down to ammonium during burial and heating, adsorption of ammonium to clay minerals facilitates its substitution for potassium in interlayer sites of illite, which in sufficient quantities may form tobelite, an ammonium rich end-member (Drits et al., 1997). Nitrogen may also be present in igneous rocks such as granites, following partial melting of (meta)sedimentary rock through the emplacement of a magma body (anataxis) (Holloway and Dahlgren, 2002). Furthermore, hydrothermal fluids interacting with nitrogen rich rocks may enrich surrounding bedrock with ammonium (Bebout et al., 1999), which may partition into feldspar or mica minerals (Boyd, S.R. et al., 1993). Nitrogen is also found within nitride minerals (meteorites and mantle rocks) and evaporite minerals following atmospheric deposition of ammonium/nitrate salts which accumulate in arid regions (Holloway and Dahlgren, 2002). Studies to date have shown that the N content of rock is variable but can reach up to 243 mg kg^{-1} in igneous rocks and >10 000 mg kg^{-1} in coal bearing sedimentary formations (Holloway and Dahlgren, 2002). Nitrogen is therefore widespread, albeit variable in concentration, in sedimentary, igneous and metamorphic rocks.

1.4.2 The role of geogenic nitrogen in global biogeochemical cycling

Weathering processes may liberate nitrogen from rock during which organic nitrogen within sedimentary/meta-sedimentary rocks is mineralised forming ammonium, a more biologically labile form. Weathering of silicate minerals and ammonium salts are other geogenic N sources which together enter the near surface environment. Rock weathering contributes significant nitrogen during soil formation, for example Holloway and Dahlgren (1999) calculated that between 30 and 50% of soil nitrogen was derived from rock weathering. Such magnitudes of nitrogen release are ecologically significant and can contribute to enhanced carbon and nitrogen storage in forest soil and biomass (Morford et al., 2011). While, in barren landscapes, nitric acid produced from the nitrification of rock derived ammonium can produce acidic soils (Dahlgren, 2005; Dahlgren, 1994). Bedrock weathering also contributes to elevated nitrate concentrations in water bodies such as aquifers (Strathouse et al., 1980) and surface waters (Holloway et al., 1998). Global chemical weathering fluxes of geogenic nitrogen are modelled to be between 11 – 18 Tg N/yr (Houlton et al., 2018). A further 8 – 13 Tg N are removed by physical weathering to downslope environments where

weathering may release this N to ecosystems (Houlton et al., 2018). Geogenic N weathering fluxes vary according to bedrock N concentration, relief and climate. In this regard, mountainous environments in northern latitudes coincide with N rich rocks and generate some of the highest N weathering fluxes (Houlton et al., 2018). These fluxes may be particularly important in polar environments such as glaciated terrain where nitrogen sources are limited.

The geochemical processes involved in the weathering of nitrogen from rock are currently poorly understood, which hampers attempts to identify rock derived nitrogen in field studies. Abiotic laboratory weathering experiments have demonstrated the release of nitrogen from rock as nitrate and ammonium (Holloway et al., 2001; Montross, G.G. et al., 2013; Dixon et al., 2012). Approximately 65% of total global rock N denudation (chemical + physical weathering) is estimated to derive from organic N, likely due to its susceptibility to oxidative weathering cf. silicate weathering which is limited by acid hydrolysis reactions (Houlton et al., 2018). Yet, efficient ammonium liberation from rock has been found to exceed weathering rates of sodium and potassium (Morford et al., 2016a; Dixon et al., 2012). This has been inferred by Morford et al. (2016a) to imply biological mediation of nitrogen weathering.

Glacial studies which have attempted to identify sources of nitrogen to catchments have, to date, undertaken limited characterisation of bedrock nitrogen (Wynn et al., 2007; Ansari et al., 2013; Wadham et al., 2016). Where N content of bedrock is measured, sample sizes are generally small and are unlikely to accurately represent heterogeneities within each rock type. Stable isotopes of nitrogen have been used to constrain nitrogen sources in glacial catchments, however such studies have assumed that weathered nitrogen will have an identical isotopic signature to the parent bedrock. Isotope fractionation during chemical weathering is poorly understood and chemical transformations such as adsorption and volatilisation may affect weathered N $\delta^{15}N$. Montross, G.G. et al. (2013) measured N release during a laboratory weathering experiment alongside stable isotope measurements, however in such rock, N was derived largely from nitrate impurities which is not representative of most rock types. Furthermore, microbial nitrification is assumed to have negligible effect on $\delta^{15}N$, yet this has yet to be conclusively demonstrated. As a result, the use of stable isotopes as a tool to identify geogenic N in glacial environments must be used with caution. A more thorough investigation is required into the geochemical and isotopic transformations involved in the release of nitrogen from bedrock in order to better understand geogenic N as a nutrient source to glacial environments.

1.4.3 Iron, manganese and sulphur

Weathering of bedrock also provides an important source of other macro and micronutrients including iron, manganese and sulphur. Iron is one of the most abundant elements in the Earth's continental crust, representing between 6.3 and 9.1% by weight as FeO (Rudnick and Gao, 2003). It is found in a multitude of minerals including sulphides, carbonates, oxides and silicates. In oxygenated environments typical of much of the earth's surface, iron is rapidly oxidised forming a range of iron oxyhydroxide minerals such as magnetite and hematite. Iron is a key component of mafic igneous rocks occurring in minerals such as olivine and pyroxene as well as mica group sheet silicates including the iron end member glauconite. Iron carbonate, also known as siderite, forms in brackish water as well as in hydrothermal veins. Iron also forms pyrite, one of the most widely distributed sulphide minerals, occurring as an accessory mineral in igneous rocks; in many sedimentary rocks forming under anoxic conditions as well as metamorphic rocks such as slates.

In contrast to iron, manganese is a minor component of crustal rocks. According to 12 studies of the average composition of the upper continental crust compiled by Rudnick and Gao (2003), the average concentration of MnO is 0 - 0.12 wt.%. Marine sediments contain manganese in much greater concentrations than in the crust. This accumulation is particularly pronounced in deep distal parts of the ocean featuring pelagic red clays where calcite dissolution means that much of the sediment is derived from aeolian dust, riverine input from terrestrial weathering and hydrothermal vents (Edmond et al., 1979). Microbial oxidation of dissolved manganese to Mn^{4+} further concentrates manganese in marine sediments e.g. (Ehrlich, 1982). Mn oxides form extensive nodules on the sea bed containing 15 - 25% Mn (Schlesinger, 2013). Above the carbonate compensation depth, manganese is incorporated as a trace element into carbonate minerals such as calcite and siderite or as a major constituent of the Mn endmember rhodochrosite ($MnCO_3$).

Sulphur is incorporated into rocks as sulphate and sulphide minerals. Sulphate minerals such as gypsum ($CaSO_4 \cdot 2H_2O$) and barite ($BaSO_4$) form in a wide range of evaporitic environments. Sulphide forms from the interaction of reduced iron with hydrogen sulphide produced via bacterially mediated sulphate reduction. This typically occurs within anoxic marine sediments where there is an abundant source of marine sulphate and reduced iron from continental weathering. Sulphides represent a trace component of most rocks, however their instability under low temperature oxygenated conditions means that they are particularly reactive at the Earth's surface.

1.5 Summary

Subglacial environments are areas of intense erosion and chemical weathering which are colonised by active microbial ecosystems. Microbial nitrate production has been attributed to these environments yet our understanding of geological nitrogen sources to such nutrient limited environments is poorly constrained. Sulphide oxidation to sulphate is a key weathering reaction in glacial environments and the isotopic composition of sulphate can provide valuable insights into the redox potential of the weathering environment. Therefore, an understanding of sulphur isotope geochemistry provides the context of subglacial conditions in which to interpret the liberation of geogenic N through weathering. Furthermore, glacial runoff contains other redox sensitive elements such as iron and manganese which can provide further insights into the redox state of the weathering environment. These rock derived elements are also micronutrients which may stimulate subglacial microbial activity and/or primary productivity in downstream fjord/marine environments. However, the influence of geological variability (e.g. iron/manganese content, mineralogy) as a control on their supply has not been explored in great detail. Here the contributions of nitrogen and micronutrients (Fe, Mn, S) in glacial meltwater following rock-water interaction are examined through both field work and novel experimental research.

Chapter 2 Materials and methods

2.1 Field Site Location and Description

2.1.1 Svalbard

Svalbard is an archipelago of islands located in the Arctic (74-81°N, 10-35°E) in between Greenland and Novaya Zemlya. Approximately 60% of its land area is covered by glaciers (Hagen et al., 2003). The largest island, Spitsbergen, is the locus for fieldwork in this project.

2.1.2 Geology of Adventdalen

This section outlines the underlying geology of the study area, the Adventdalen valley, Spitsbergen (Figure 2.1). The rock sequence here is part of the Central Tertiary Basin (CTB), an accumulation of clastic sediments deposited in the Cretaceous and early Cenozoic following the rifting of Greenland from Eurasia (Hindshaw, R. S. et al., 2018; Dypvik et al., 2011; Helland-Hansen, 1990; Elling et al., 2016; Jones et al., 2016; Cui et al., 2011; Müller and Spielhagen, 1990). The CTB is an asymmetrical basin with sedimentary infill thickest in the west (Helland-Hansen, 1990). Since Adventdalen lies in the north east of the CTB, the geological units are generally at their thinnest extent. Consequently, a wide range of different formations are exposed in Adventdalen. The shallow dipping angle of multiple geological formations make Adventdalen an ideal study area. Whilst all formations are clastic sedimentary rocks, the lithological variations of each formation are exposed at different elevations across the study area. Therefore each glacier erodes and weathers different parts of the sedimentary sequence.

This section specifically focuses on the bedrock underlying the glaciers within the study area. This includes the Carolinefjellet Formation (Late Cretaceous) of the Adventdalen Group and the Van Mijenfjorden Group (VMG) (Paleocene to Eocene) (Figure 2.2). Cretaceous rocks below the Carolinefjellet Fm are not discussed here. The stratigraphic names adopted in this chapter follow those used by Dallman (1999). N.B. Formation is shortened to Fm and Member to Mb in the following text.

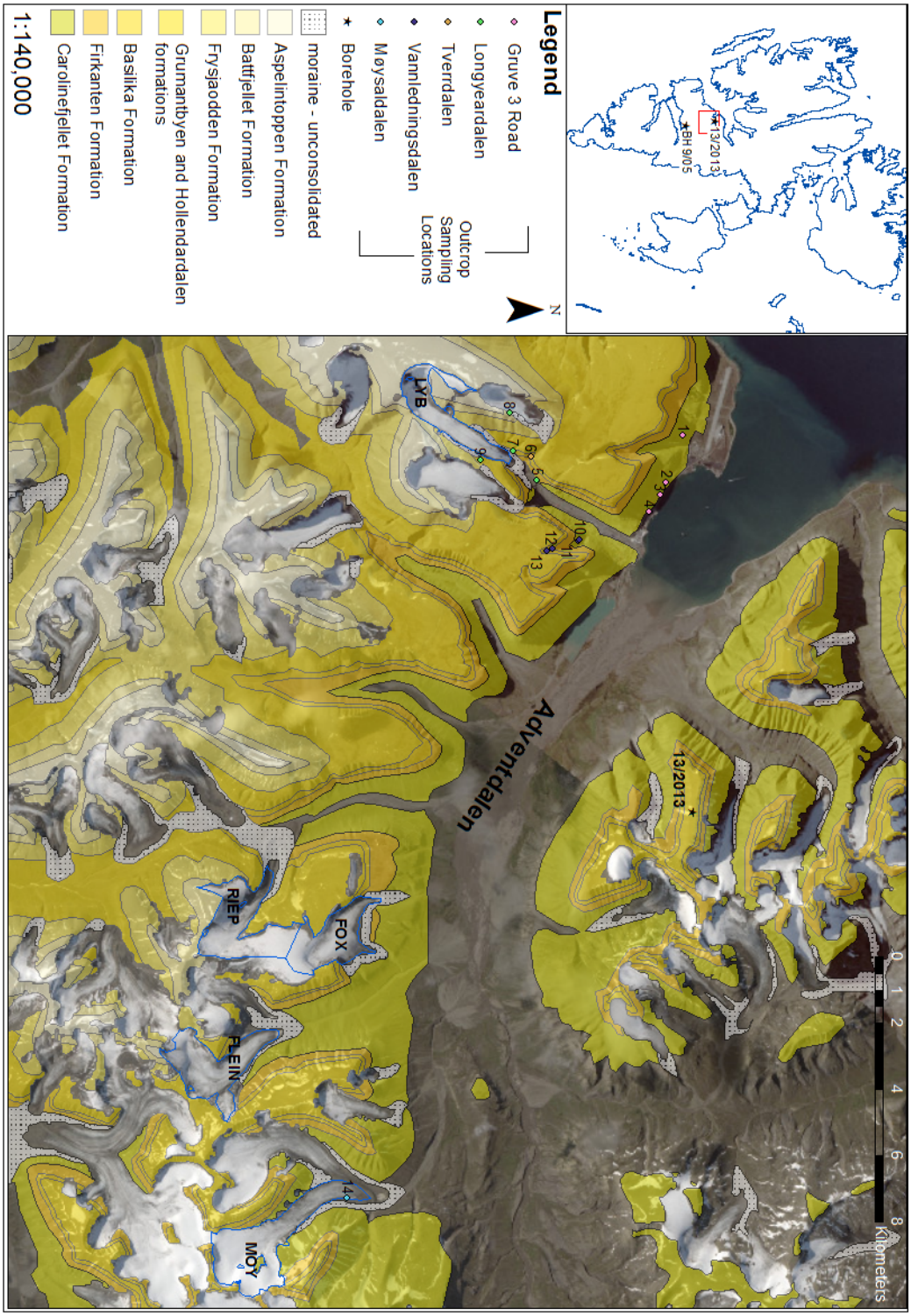

Figure 2.1 Satellite map of Adventdalen with geology superimposed. Red box on inset map represents spatial extent of satellite map. Glaciers included in the study are outlined in blue (König et al., 2014) and are labelled on the map: LYB = Longyearbeen, FOX = Foxfonna, RIEP = Rieperbreen, MØY = Møysalbreen, FLEIN = Fleinisen. Stars indicate locations of boreholes where bedrock core was extracted by Store Norsk. Outcrop sampling locations refer to tables in Appendix A. Base Map (NPI, not released), Geology (NPI, 2016)

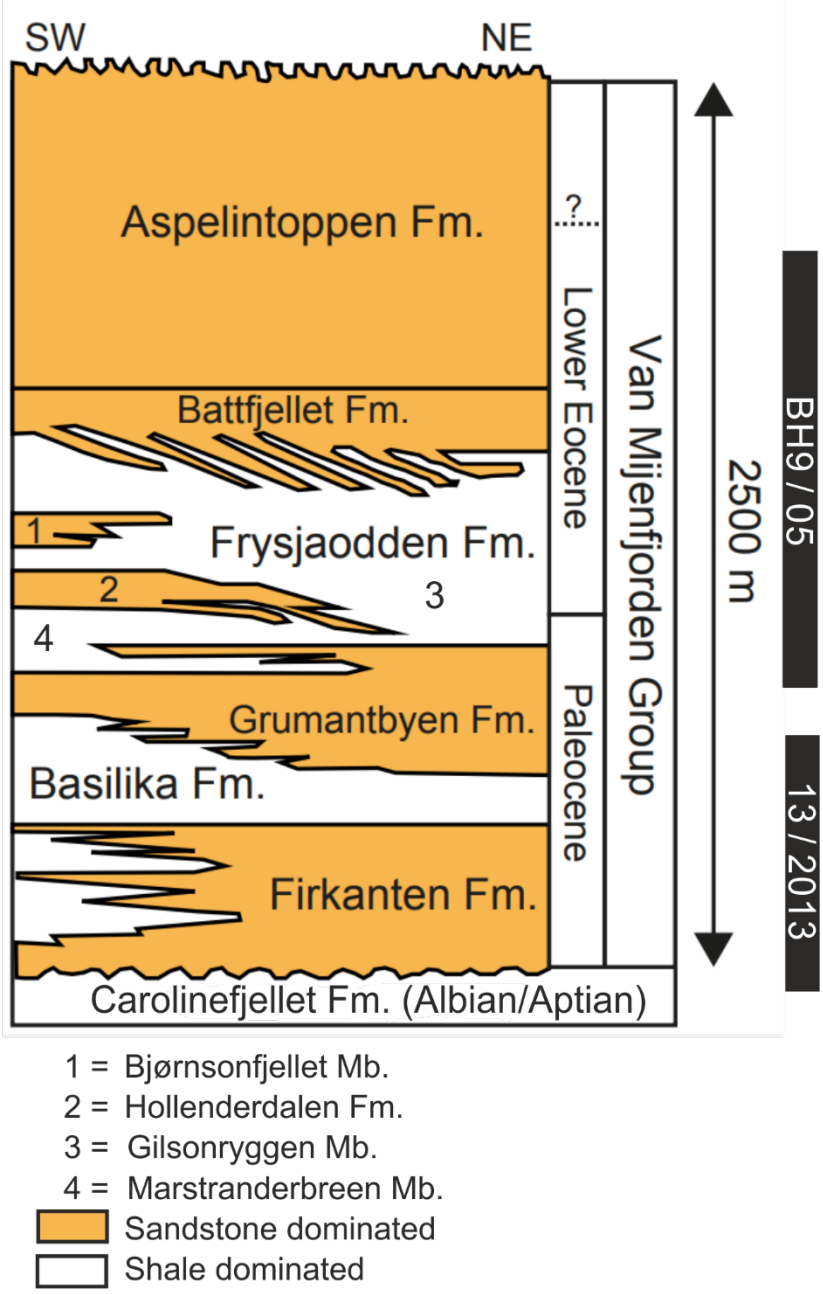

Figure 2.2 The stratigraphic sequence of the Van Mijenfjorden Group modified from Hindshaw, R. S. et al. (2018). Black rectangles indicate range of bedrock cores sampled in this study.

The sedimentary sequence was deposited during a greenhouse climate and sea level highstand. The lowermost Carolinefjellet Fm is a shale dominated unit that contains increasingly frequent sand bodies in its upper part. The lower formations of the Van Mijenfjorden Group (Firkanten, Basilka and Grumantbyen Fms) consist of alternating shales, siltstones and sandstones. These were deposited during the Palaeocene with an eastern sediment source, likely Siberian basalts (Helland-Hansen, 1990). Whereas in the later Paleocene/Eocene, there is a shift in sediment source to the west forming the Frysjaodden, Hollenderdalen, Battfjellet and Aspelintoppen Fms (Hindshaw, R.

S. et al., 2018; Helland-Hansen, 1990). This is likely associated with erosion of the uplifted West Spitsbergen fold and thrust belt. Rocks in this latter sequence show an upwards transition from shales to sandstones.

2.1.2.1 Carolinefjellet Formation

The Carolinefjellet Formation (Albian - Aptian) is the uppermost unit of the Adventdalen Group and Mesozoic strata (Dallman). It is the lowermost unit of the sequence in this study and crops out along Adventdalen but at increasing elevation towards the East due to the south-west dip of bedding. It is comprised of alternating sandstones and shales deposited in prodelta to distal marine conditions (Dallman). The interbedded sandstone units of up to 1m thick have fine-medium grains and feature cross bedding. Finer rippled sandstone layers occur above these coarser units which often contain drapes of siltstone and bivalve fossils. Large “cannon-ball” carbonate concretions were observed in exposed sections of Janssondalen (Figure 2.3). These were seen at stratigraphic levels below the elevation of glaciers in this study. However they have been observed by others within higher units of the VMG (Spielhagen and Tripati, 2009). A disconformity/slight angular unconformity marks the upper boundary with the overlying Firkanten Fm.

Figure 2.3 “Cannonball” concretion within shales of Carolinefjellet Fm, found in Janssondalen

2.1.2.2 Firkanten Formation

The Firkanten Formation is the lowermost unit of the Palaeogene Van Mijenfjorden Group. The formation varies in thickness from 80 m to 140 m (Major and Nagy, 1972), at borehole 13/2013, this unit measures 81 m thick. It is subdivided into 2 members – the lower Todalen Member (46m) and the upper Endalen Member (35 m). A third member, the Kolthoffberget Member, exists outside of the study area (Dallman, 1999) and is not considered in this discussion. The lower boundary of the Firkanten Fm is often identified by the presence of a conglomerate. Above this, the formation consists of a mixture of sandstones, siltstones, shales and several coal seams. Both marine and non-marine fossils are observed such as bivalves and both plant leaves (broadleaf and coniferous) and roots, indicative of a coastal environment (Major and Nagy, 1972).

2.1.2.2.1 Todalen Member

The Todalen Member is a coal bearing sequence of clastic sediments interpreted as having formed in a delta plain environment (Steel et al., 1981). Five economic coal seams in the Todalen Member were deposited in raised bog/fen environments, linked to rising sea levels (Marshall et al., 2015). Iron is present as both and siderite within sediment and coal seams (Marshall et al., 2015; Major and Nagy, 1972).

2.1.2.2.2 Endalen Member

The Endalen Member is dominated by buff coloured sandstones forming distinctive cliffs in the glacial valleys adjoining Adventdalen (Figure 2.14). Fragments of coalified plant material are frequently found within this member. Minor conglomerates and siltstones are interbedded within the sandstones (Dallman, 1999). This unit is interpreted as a delta front environment continuing a transgressive sequence into the overlying Basilka Fm (Steel et al., 1981).

2.1.2.3 Basilika Formation

The Basilika Fm is a dark grey to black unit of siltstones and shales measuring 59m thick in core 13/2013 but varies between 10 and 350 m within the CTB. These prodelta deposits, coarsen upwards from siltstones up to fine sandstones (SNSK, 2013; Steel et al., 1981). The Basilka Fm, being the most distal unit of the Firkanten-Basilka delta sequence, represents the end of this transgression period (Steel et al., 1981). The unit contains fossil gastropods and bivalves as well as small pyrite nodules and pebbles, the latter likely represent ice rafted debris (Steel et al., 1981; Müller and Spielhagen, 1990). The lack of bioturbation and presence of pyrite in the Basilka Fm suggest the depositional environment

suffered from hypoxia (Müller and Spielhagen, 1990). Beds of bentonite clay are also common in the Basilka Fm representing altered volcanic ash layers (Elling et al., 2016).

Cannon ball carbonate concretions were observed in the Baslika Fm (Figure 2.4). Spielhagen and Tripati (2009) identified glendonites associated with these concretions. Glendonite is a hydrated calcium carbonate mineral that forms from the degradation of the mineral ikaite. Ikaite forms at freezing temperatures and breaks down at temperatures greater than 4°C. The presence of glendonites in this unit and elsewhere in the VMG suggest that marine waters reached near freezing temperatures. This is consistent with the interpretation of erratic clasts deposited as ice rafted debris. Yet, such a climate is at odds with the warm/temperate climate inferred from conifer fossils (Schweitzer, 1980). Spielhagen and Tripati (2009) infer that climate varied in the Arctic during the Tertiary from warm/temperate conditions to intermittent cold climates.

Figure 2.4 “Cannonball” concretion in the Basilka Fm in Tverrdalen

2.1.2.4 Grumantbyen Formation

There is a transitional boundary between the Basilka Fm and the overlying Grumantbyen Fm. This is marked by an increase in grain size from shales to silt/sandstones. These sandstones form rock walls and plateaux capping many of the valley sides in the Adventdalen area (Major and Nagy, 1972). The Grumantbyen Fm is up to 450 m thick in the northern parts of the CTB and thins southwards. Neither of the boreholes used in this study capture the entire depth

of the Grumantbyen Fm, however we record 143 m from the base (13/2013) and the top 72 m of the formation (BH9/05). This unit becomes paler and green in colour up section due to the presence of glauconite (Dallman, 1999). The Fm is highly bioturbated and contains abundant trace fossils which suggests a transition to shallower, more oxygenated lower shoreface marine environment perhaps as a complex of offshore bars (Müller and Spielhagen, 1990; Steel et al., 1981). Individual sub-rounded chert clasts occurring as erratics were occasionally found within rocks of this formation (Figure 2.5).

Figure 2.5 Erratic pebble found in Grumantbyen Fm sandstone in Longyeardalen.

2.1.2.5 Frysjaodden Formation

A sharp lithological contact marks the boundary between the underlying sandstones of the Grumantbyen Fm and the shales of the Frysjaodden Fm. The Frysjaodden Fm is 200 m thick in the northern part of the basin but thickens to 400 m southwards (Dallman, 1999). This formation is almost entirely shale (Marstranderbreen Member and Gilsonriggen Member) but in the west it contains a significant sandstone unit near its base (Hollenderdalen Fm) as well as thin sandstone wedges (Bjørnsonfjellet Member) in the middle of the formation. These sediments are derived from the West Spitsbergen Mountain belt to the west. The Bjørnsonfjellet Member is neither found in the study area nor either core and is therefore not discussed further. The Frysjaodden Fm is present in borehole BH9/05 entirely as the Gilsonryggen Member. The

Marstranderbreen Member and Hollenderdalen Fms are only present in the western part of the basin and are absent from the boreholes in this study, however they do crop out in Longyeardalen as observed by the author and by Burcă (2008).

2.1.2.5.1 Marstranderbreen Member

The Marstranderbreen Member has only been observed where the Hollenderdalen Fm crops out. It has a maximum thickness of 60 m although in Longyeardalen it is only 10 m thick (Burcă, 2008). It is heavily bioturbated and consists of siltstones fining upwards to shales (Burcă, 2008; Dallman, 1999). During field work it was not possible to collect fresh samples from outcrop as all exposure was heavily weathered and friable.

2.1.2.5.2 Gilsonryggen Member

The Gilsonryggen Member consists of black marine silty shales containing thin bentonite beds and siderite laminations (Riber, 2009). Few fossils exist in this member and bioturbation is more common in the middle and upper shales (Nagy et al., 2013). A coarsening up sequence is observed in the top 90m with a greater proportion of sand size grains. It has been interpreted as a prodelta environment (Steel et al., 1981). Dypvik et al. (2011) identified the Paleocene-Eocene Thermal Maximum (PETM) interval within the Gilsonryggen Member from core BH9/05. During this event a short period of extreme global warming occurred due to a large flux of greenhouse gases to the ocean and atmosphere. It caused increased sea temperatures and drastically effected terrestrial and marine life (Zachos et al., 2001). Palaeontological evidence including limited bioturbation and reduced foraminiferal diversity are indicative of suboxic bethic conditions, likely generated by restricted thermohaline circulation in a warm, low salinity environment (Nagy et al., 2013).

In the field, the Gilsonryggen Member forms smooth slopes of heavily weathered rock fragments. As such it was not possible to collect any fresh outcrop samples so all samples presented here are from core BH9/05.

2.1.2.6 Hollenderdalen Formation

The Hollenderdalen Fm is a laterally discontinuous unit whose thickness varies from over 150 m in the west to non-existent in the east (Figure 2.2) (Steel et al., 1981). Where present, it appears within the lower half of the Frysjaodden Fm. In the study area of this project, it is only observed in the valley sides of Longyeardalen. This formation is not in either borehole sampled, however outcrop samples were collected from Longyeardalen. The lower section of this unit consists of fine grained, well laminated sandstones and siltstones parallel

lamination, cross bedding and soft sediment deformation (Burcă, 2008). Upper sections consist of both mudstone and sandstone, the former associated with a 20 cm thick coal seam and rootlets (Burcă, 2008). Finer mudstones, siltstones and siderite horizons are also present along with a 20 cm thick coal seam (Burcă, 2008). The Hollenderdalen Fm contains a greater proportion of rock fragments and a lower proportion of feldspar and matrix than the Grumantbyen sandstones (Müller and Spielhagen, 1990). These sandstones represent uplift of the western edge of the basin resulting in a shallowing environment to a more tidal influenced environment (Steel et al., 1981). In contrast to the underlying deposits, the sediment supply to the Hollenderdalen Fm and overlying units is thought to come from erosion associated with the concurrent West Spitsbergen Orogeny (Dallman, 1999).

2.1.2.7 Battfjellet Formation

The Battfjellet Fm thickens southwards with a maximum thickness of 300 m (Dallman, 1999) although in BH9/05 it measures 57 m. It consists of multiple coarsening upward sequences of very fine to medium grained sandstones and minor siltstones with cross stratification and wave ripple lamination (Helland-Hansen, 1990). The eastern part of the formation consists of flat tabular units which were deposited in a wave dominated shoreline environment (Helland-Hansen, 1990).

2.1.2.8 Aspelintoppen Formation

The Aspelintoppen Fm represents the end of the regressive megasequence from the marine Frysjoadden and Battfjellet Fms with a sandstone unit derived from terrestrial deposition (Helland-Hansen, 1990). It contains abundant plant fossils, thin coal seams and soft sediment deformation (Helland-Hansen, 1990). This formation was likely deposited in streams, crevasse splays or swamps on a depositional plain (Helland-Hansen, 1990; Dallman, 1999).

This formation records a depth of over 1000 m south of Van Mijenfjorden (Dallman, 1999) although little is preserved in the northern reaches of the basin. Only 37 m of Aspelintoppen Fm was measured from its base to the top of core BH9/05.

2.1.3 Glaciers

This section provides an overview of each glacier in the study. These glaciers, all within the Adventdalen area, are relatively small (Table 2.1) and likely cold based. They overlay different stratigraphic levels of the same bedrock sequence (Chapter 4).

Table 2.1 Glacier dimensions (König et al., 2014)

Glacier Name	Length (Km)	Area (Km^2)
Longyearbreen	4.42	2.93
Foxfonna	2.13	3.21
Rieperbreen	2.70	4.32
Møysalbreen	4.91	5.35
Fleinisen	3.29	3.9

2.1.3.1 Longyearbreen

Longyearbreen is narrow valley glacier located south of the main town of Longyearbyen. The subglacial topography consists of a V shaped valley (Etzelmüller et al., 2000) and the glacier has a maximum thickness of 110 m (Sevestre et al., 2015). The glacier is cold based (Sevestre et al., 2015) and a basal ice temperature of -4°C was recorded in 2001 - 2003 (Humlum et al., 2005). Limited basal motion is likely to have occurred in the last 11 000 years since in situ plant remains have been found at the ice-bed interface (Humlum et al., 2005). Because of strong negative mass balance during recent years, there is no remaining accumulation zone (Sevestre et al., 2015), therefore Longyearbreen is receding like many other small glaciers on Svalbard. The main body of ice is flanked and terminated by iced core moraines, it is in between these where the largest supraglacial meltwater channels form (Gulley et al., 2009). The largest drainage system is on the western flank of the glacier where a supraglacial channel has incised into glacier ice through cut and closure (Gulley et al., 2009). The water sampling points in this study are located on the western margin, where this drainage system emerges from the glacier. Water was sampled from a moraine spring which is likely ice cored due its hummocky morphology (Figure 2.6b). The spring feeds into an ice marginal channel which is fed by a subglacial source (ice seep) (Figure 2.6c). Combined subglacial and moraine water is diverted beneath glacier ice before re-emerging where it was sampled (LYB subglacial) (Figure 2.6a). An englacial stream combines with the subglacial water downstream of here. The englacial flow is

non-turbid and has low electrical conductivity (EC) unlike the moraine spring and ice seep which are turbid and have high EC. This suggests the latter flows have drained through debris rich environments while their highly similar conductivity values may imply a common source.

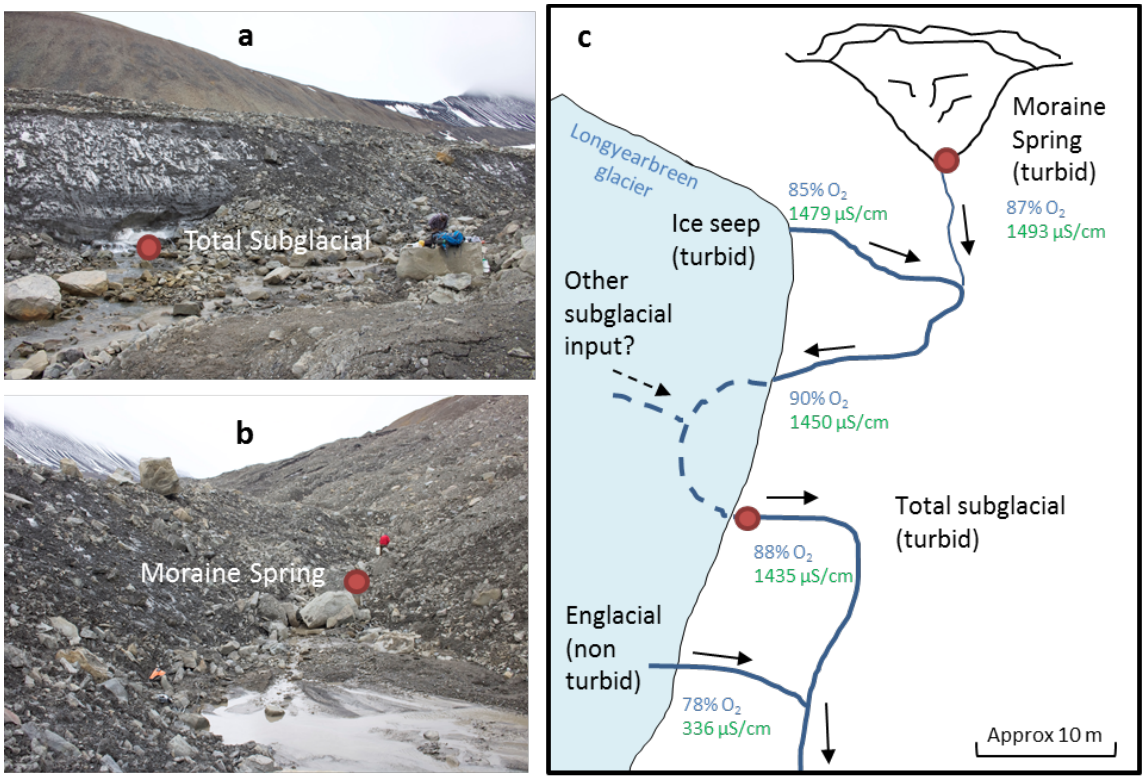

Figure 2.6 Meltwater sampling sites at Longyearbreen. Red dots indicate where a) bulk subglacial water and b) moraine spring water was collected. C) Sketch of the water sampling sites. Oxygen saturation (%) is given in blue and electrical conductivity in green. Measurements were recorded on 27/08/2017 at 11.30 am.

Coal mining was active at Gruve 4 in Longyeardalen in the 20th century (Dallman, 2015). Subsurface tunnels have been excavated beneath Longyearbreen near to the water sampling point (Figure 2.7). The sampling sites are located at a higher elevation than the mine workings, therefore any meltwater that may have entered the mine would have been diverted through lateral adits. Consequently, it is unlikely that meltwater chemistry has been influenced by the mine workings beneath Longyearbreen.

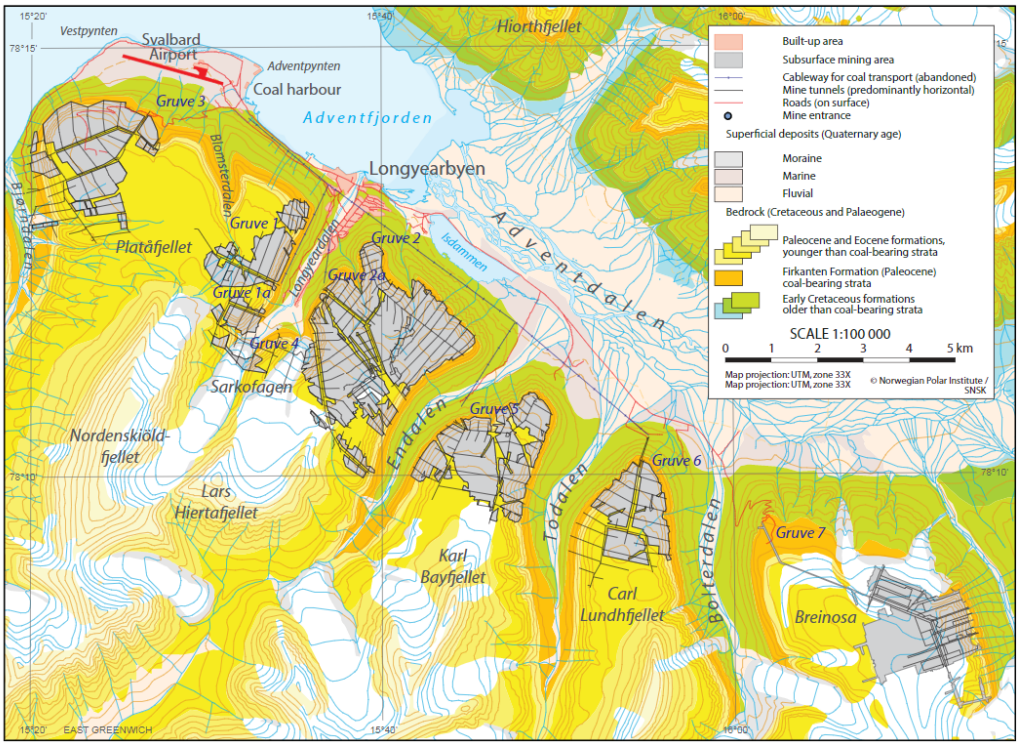

Figure 2.7 Map showing locations of mines in Adventdalen (Dallman, 2015)

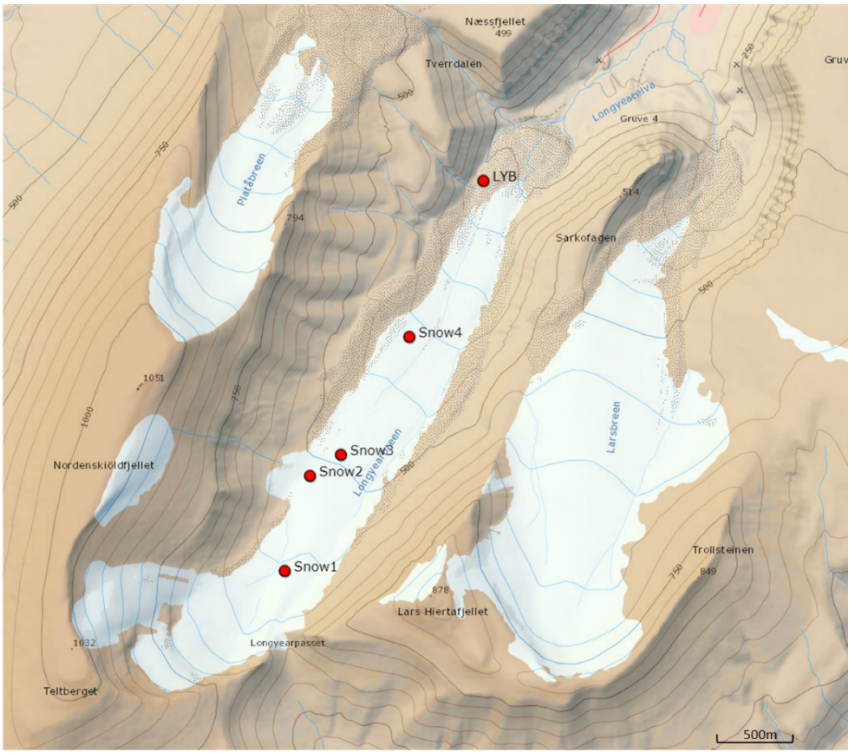

Figure 2.8 Map of Longyearbreen glacier. Meltwater sampled from 'LYB'. Snow sample locations marked on glacier surface. Map source: toposvalbard.npolar.no courtesy of Norwegian Polar Institute.

2.1.3.2 Foxfonna

The Foxfonna ice cap lies atop the Breinosa plateau and descends northwards towards Adventdalen and also feeds the outlet glacier, Rieperbreen. Glacier ice is < 80 m thick and completely cold based (Rutter et al., 2011). Active coal mining operations take place at Gruve 7 beneath Foxfonna glacier (Figure 2.7). Bedrock temperatures beneath glacier covered terrain are consistently below 0°C throughout the year (Christiansen et al., 2005), therefore meltwater ingress into the mine is unlikely. Water was sampled from a proglacial spring (Foxfonna Spring) and an ice marginal channel (Foxfonna Glacial). The spring may derive from a deep groundwater source and is characterised by ochre deposits and has a distinctive sulphurous smell. The glacial channel is a supraglacial channel that flows along the eastern margin of the glacier adjacent to a large moraine.

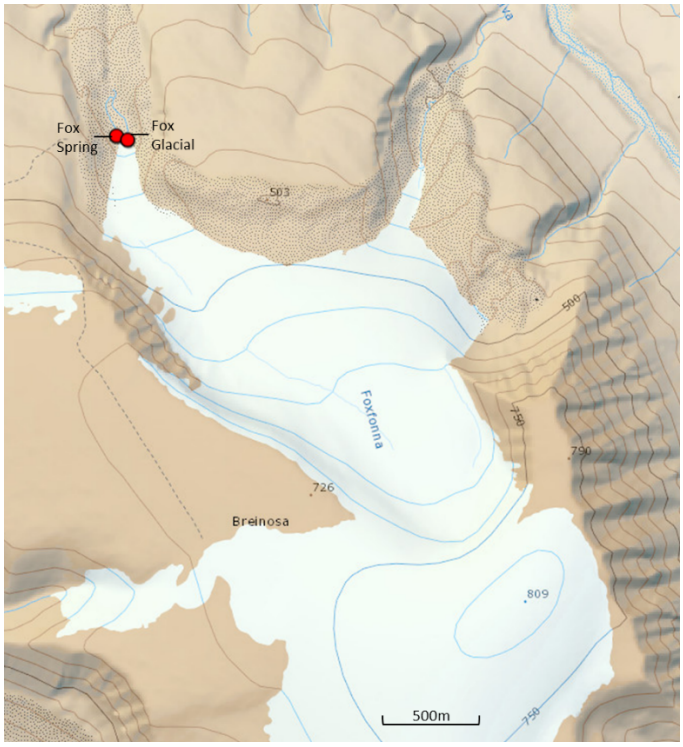

Figure 2.9 Map of Foxfonna glacier. Meltwater sampling points labelled. Map source: toposvalbard.npolar.no courtesy of Norwegian Polar Institute.

2.1.3.3 Rieperbreen

Rieperbreen is a small (~2 km x 400 m) valley glacier that forms an outlet of the Foxfonna ice cap into the Bolterdalen valley (Lysså and Lønne, 2001). The glacier is believed to be less than 40m thick and cold based (Lysså and Lønne, 2001; Rutter et al., 2011), however a subglacial conduit in frozen glacial till exists which has formed by cut and closure of a supraglacial channel (Gulley et al., 2012).

Glacial runoff drains from the north western terminus of the glacier which incorporates snow and glacial ice melt as well snowmelt fed springs draining moraines, where the majority of solute acquisition takes place (Rutter et al., 2011). Mining takes place beneath the Foxfonna ice cap however mine drainage does not enter the Rieperbreen catchment (Rutter et al., 2011).

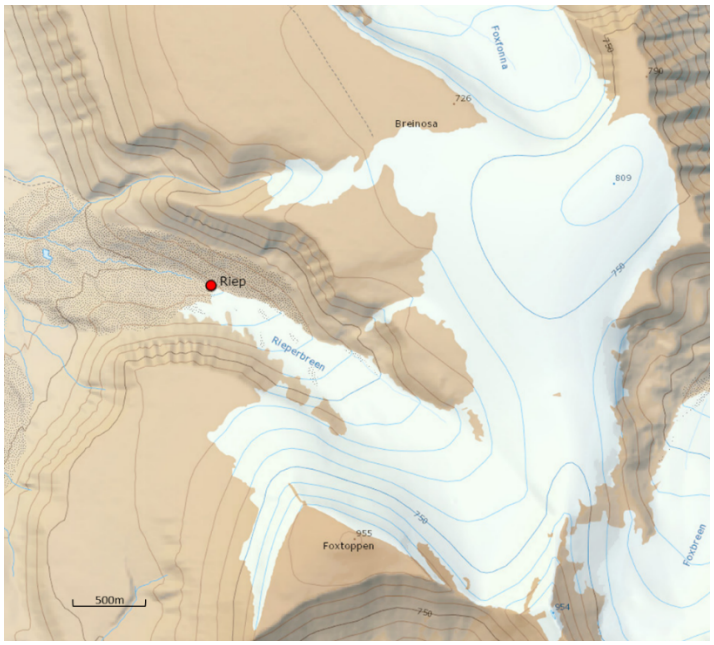

Figure 2.10 Map of Rieperbreen glacier. Meltwater sampling point labelled. Map source: toposvalbard.npolar.no courtesy of Norwegian Polar Institute.

2.1.3.4 Møysalbreen

Møysalbreen is the largest glacier in the study area. It is 4.9 km long with an area of 5.4 km^2. The glacier forms a moraine complex with the adjacent Gløttfjellbreen near the glaciers' termini. There is very little literature available on this glacier, likely due to its remote location at the eastern end of Adventdalen. Given that nearby glaciers of a similar size and elevation are known to be cold based, it is assumed that Møysalbreen is also cold based. Glacial runoff appears to be largely routed through an incised supraglacial channel on the north eastern margin of the glacier. This channel is also fed by springs in the moraine on the eastern glacial flank. In 2016, glacial runoff filled a large proglacial lake, however when revisited in 2017, the lake had drained via an incised channel below the lake.

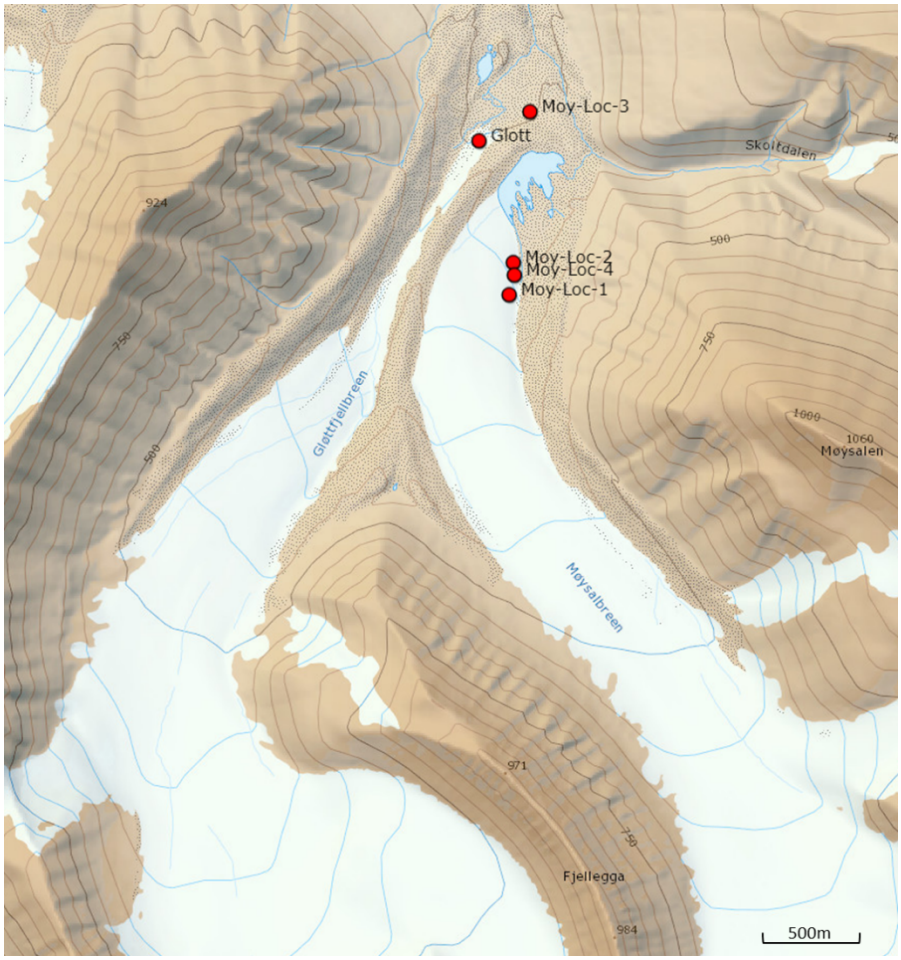

Figure 2.11 Map of Møysalbreen & Gløttfjellbreen glaciers. Meltwater sampling points labelled. Map source: toposvalbard.npolar.no courtesy of Norwegian Polar Institute.

2.1.3.5 Fleinisen

Fleinisen is a valley glacier situated at the top of the Foxdalen valley. There is very little mention of this glacier in the literature. It is of comparable size to the other glaciers in this study but little is known of its hydrology. Glacial runoff was sampled from a pressurised upwelling within the ice front. This stream of water is thought to be fed from a subglacial drainage system. Satellite imagery (Figure 2.13) reveals there are at least 2 other supraglacial channels, cut by upwelling water, which may suggest that the routing of subglacial water is dynamic. Ochrous deposits are also visible in the satellite imagery on snow surfaces close to the subglacial portal. This is indicative of fluid transport through an anoxic environment in which iron is reduced and then precipitated as (hydr)oxides as the water oxygenates on emergence.

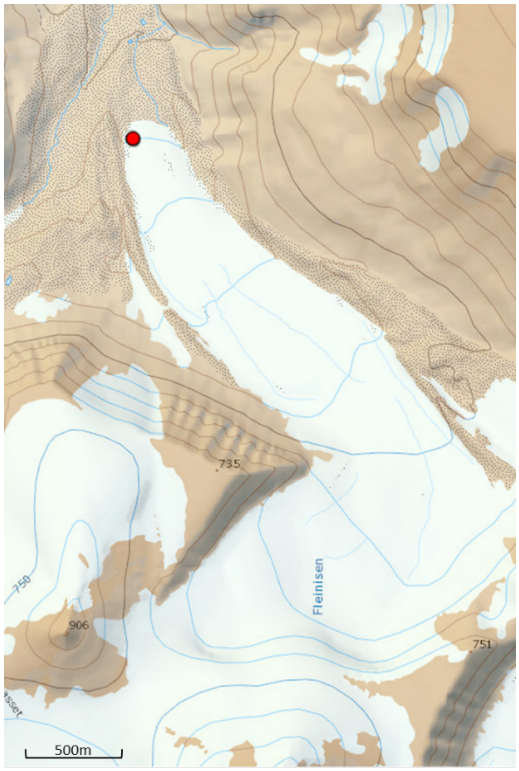

Figure 2.12 Map of Fleinisen glacier. Meltwater sampling point labelled. Map source: toposvalbard.npolar.no courtesy of Norwegian Polar Institute.

Figure 2.13 Satellite image of North West corner of Fleinisen. Imagery source: toposvalbard.npolar.no courtesy of Norwegian Polar Institute. 3 large supraglacial channels can be seen (2 are snowfilled) which have been cut by subglacial upwelling. Red circle highlights ochrous deposits in proglacial zone.

2.2 Bedrock Geochemical Analysis

2.2.1 Sampling and sample processing

Rock samples used in this study were collected from both outcrop and from bedrock cores drilled by Store Norsk. There is excellent exposure of coarser units in cliff sections around Adventdalen, however finer grained (shale) units are heavily weathered and difficult to sample (Figure 2.14). Furthermore, due to the difficult terrain and glacier cover, sampling a continuous sequence from outcrop was not possible. Outcrop samples were collected from Tverrdalen, Vannledningsdalen, Longyeardalen, Moysaldalen and at various roadside outcrops along the road to Gruve 3 between 2016 and 2018 (Chapter 4).

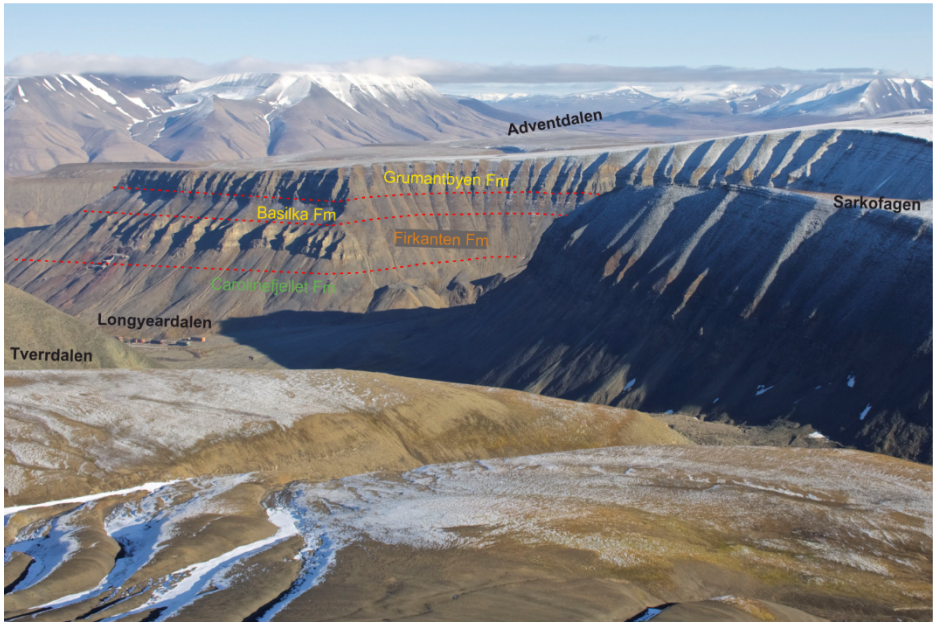

Figure 2.14 Annotated photograph of Longyeardalen to show geological formations of lower Van Mijenfjorden Group (Paleocene) and upper Cretaceous rocks. Photograph was taken on northern slopes of Nordskiöldfjellet facing NE. Place names are in black font, formation names are coloured, and geological boundaries are represented by dashed red lines.

Bedrock cores have been drilled by Store Norsk as part of coal mining operations on Svalbard. These cores target the coal bearing strata of the Tertiary bedrock. Sampling from these cores provided a near continuous sequence of the CTB. Cores 13/2013 and BH9/05 were chosen due to their proximity to the study area and broad coverage of rock formations.

Core 13/2013 was drilled in the mountain Dirgenten, on the north shore of Adventdalen. It measures 293 m and contains the lower part of the sequence from the Carolinefjellet Fm up to the Grumantbyen Fm. A summary sedimentary log of the sequence was prepared based on the original Store Norsk log

produced by Anna Stella Guðmundsdóttir. This core was sampled every 10 – 15 m.

The upper part of the bedrock geology (Grumantbyen to Aspelintoppen Fms) is captured in BH9/05 which was drilled on the northern flank of Urdkollbreen to a depth of 680 m. This core has been extensively studied (Nagy et al., 2013; Dypvik et al., 2011; Riber, 2009) since it includes the PETM. A summary sedimentary log was produced from the section logged by Riber (2009) supplemented with logged data by the author. This core was sampled approximately every 20 m.

Bedrock cores were sampled using a rock saw. Sections of core were cut vertically, keeping one half and leaving the other in the core box. Any weathered surfaces of core and bedrock samples were removed with either a lapidary trim saw (Lortone, USA) or grinding surface (Saphir 330, ATM, Germany). Samples were cut into small blocks and washed with deionised water in an ultrasonic bath before being dried in an oven at 50°C.

An investigation to determine optimum crushing methodology was carried out as described below (section 2.2.1.1). The findings of this led to the following methodology: dried rocks were pulverised, using a steel piston pestle and mortar, into small chips which were further comminuted to fine powder in an agate disc mill (Tema, UK). Crushed samples were inspected visually to crudely determine that grain size was fine sand/silt. All crushing equipment was washed with water, dried with compressed air and cleaned with ethanol between samples. Ground rock samples were stored in sealed 50 ml centrifuge tubes for geochemical analysis and weathering experiments.

2.2.1.1 Rock crushing test

Since this material was to be used for experiments designed to mimic subglacial weathering reactions, the final grain size distribution should reflect that of subglacial sediment. Glacial till tends to have polymodal grain size distributions of silt/fine sand and gravel. The finer grains of glacial till are more readily held in suspension and have a greater surface area. These grains are therefore likely to liberate the bulk of solute and represent realistic sorption surfaces as opposed to coarser gravels. A unimodal distribution is therefore adopted for the purposes of this study. Silt is composed of grains between 3.9 and 63 μm. Grains finer than this are classified as clays and grains between 63 and 125 μm are termed very fine sand (Wentworth, 1922). During crushing, it was aimed to comminute samples to < 100 μm size grains.

In order to evaluate the best method for crushing rock 2 methods were compared on both a granite and an amphibolite (from the University of Leeds rock collection):

- **Disc mill** – rock is pre-crushed to small pieces in a steel piston pestle and mortar, followed by crushing in a disc mill (30 s-1 min intervals). After each crush, the sample was sieved using an 80 µm sieve. Coarser material was crushed further in the disc mill. The final 30 g of grains were crushed in the pestle and mortar as this quantity was too small to go in the disc mill.
- **Hand Crush** – repetitions of crushing in steel piston pestle and mortar and filtering with 80 µm sieve.

An 80 µm sieve was chosen since this was the closest available sieve to the upper limit of silt sized grains (63 µm). Between crushing, the grains were sieved to remove any grains finer than 80 µm to avoid crushing below the lower bound of silt (3.9 µm). During sieving, grains were pressed with a handheld piece of agate to accelerate the process.

Grain sizes were measured using a laser diffraction particle size analyser (Malvern Mastersizer 2000E) which assumes all grains are spherical.

2.2.1.1.1 Results

Both crushing methods produce similar grain size distributions for both rock types (Figure 2.15). The distributions are almost identical distribution for amphibolite whereas, crushing the granite by disc mill produces rock powder slightly coarser (mean = 44.2 µm) than that crushed in pestle and mortar (mean = 36.5 µm).

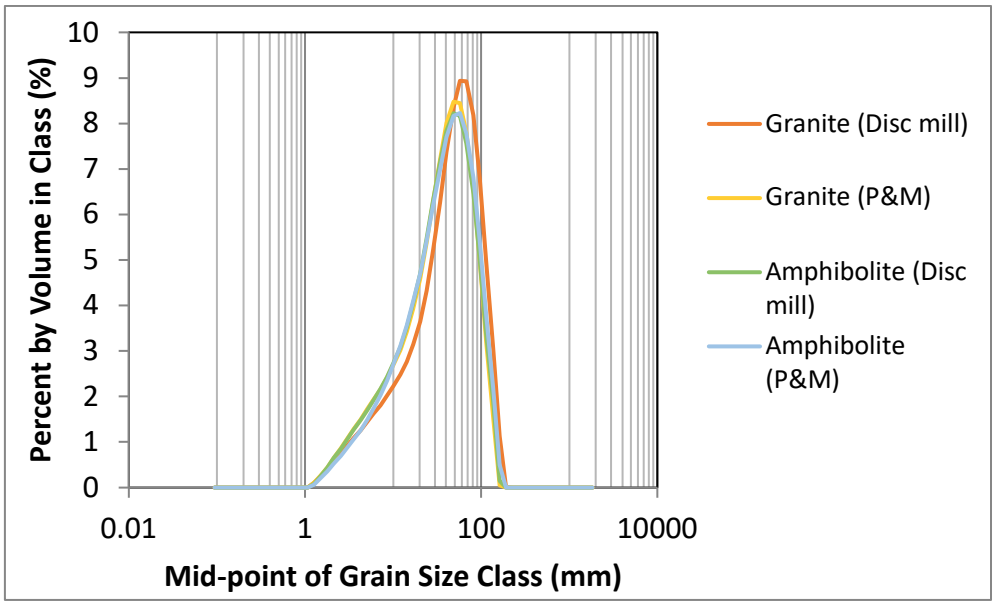

Figure 2.15 Grain size distributions of rocks crushed in test. P&M = (steel piston) pestle and mortar.

However, all crushed samples consisted of predominantly silt size grains (63 - 71%) (Figure 2.16). No more than 5% of grains were finer than silt size in any sample. The maximum grain size class measured had an upper bound of 176 μm, coarser than the mesh size of the sieve. Whilst the 80 μm sieve does allow some coarser grains through its mesh, the percentage of grains smaller than 80 μm that pass through the sieve ranges between 84 and 90%.

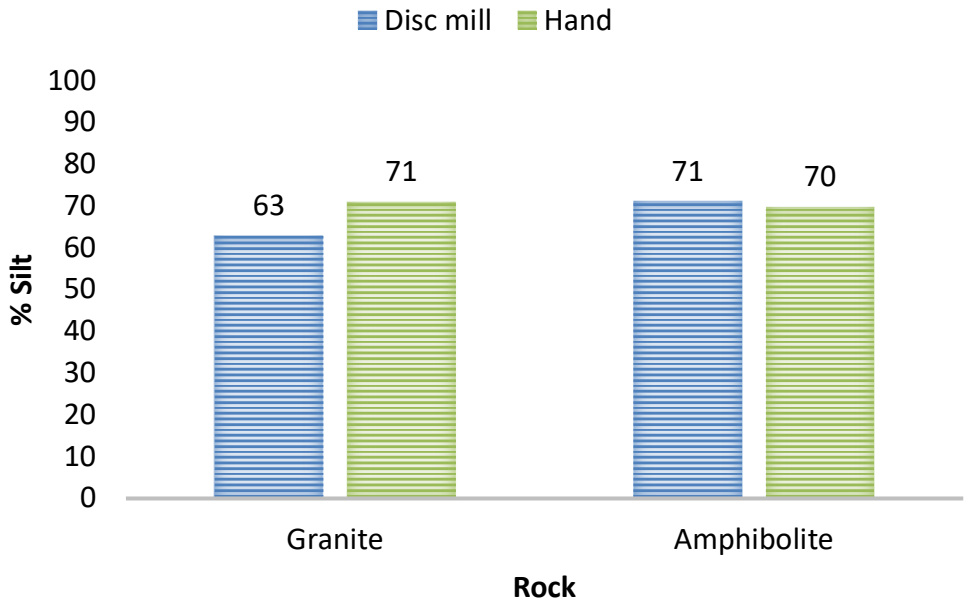

Figure 2.16 Proportion of silt in samples from crushing experiment.
Labels on bars are in %.

The similarity of grain size distribution between both methods of crushing amphibolite is most likely due to the mineralogy of the rock. With a composition dominated by the amphibole mineral edenite, the majority of the rock crushes uniformly.

The process of forcing grains through the sieve with agate may have expanded the mesh size allowing coarser grains to pass through. This may be particularly relevant for the granite which has a greater proportion of quartz. As a very tough mineral (7 on Mohs hardness scale), quartz is naturally more resistant to abrasion. Consequently, the granite took much longer to grind in the disc mill than the equivalent quantity amphibolite. Residual grains also required more abrasion with agate during sieving. This additional force on the sieve mesh, may have permitted a greater proportion of coarser grains through the sieve.

In order to reduce the bias in grain size between these different methods, forcing through a sieve with agate should be avoided. Instead, residual grains should be ground in the pestle and mortar.

The disc mill method is a less strenuous method to crush large volumes of rock and is therefore also a more sustainable technique. It is also potentially more consistent since the time left in the disc mill and the force can be kept constant. Whereas this cannot be so easily maintained with a pestle and mortar due to human fatigue.

This study has evaluated the suitability of two methods of comminuting rocks to silt size grains. Using a grain size analyser, the grain size distributions of each method of different rocks was measured. The results suggest that grinding with a disc mill produces results consistent with hand crushing (pestle and mortar) if done carefully. Since this is a consistent and less strenuous method, it is the preferred option for future comminution of rocks.

2.2.2 Nitrogen

2.2.2.1 Total N, total inorganic N and total organic N methods

2.2.2.1.1 Total N (TN)

Bulk rock samples were analysed for $\delta^{15}N$ and weight percent nitrogen (wt. % N) via combustion in an Elementar Pyrocube elemental analyser coupled to an Isoprime continuous flow mass spectrometer. Samples were combusted at 1150°C to N_2 in the presence of pure oxygen (N5.0) into a stream of helium (CP grade). The produced N_2 flowed through tungstic oxide packed into the combustion column to ensure quantitative conversion. Excess oxygen was removed by reaction with hot copper wires at 850°C and water was removed in a Sicapent trap. All solid reagents were sourced from Elemental Microanalysis, UK, and all gases were sourced from BOC, UK. 60 - 70 mg of rock powder was weighed into 8 x 5 mm tin cups.

Weight percent nitrogen was calculated by the Pyrocube software using a calibration based on repeat analysis of sulphanilamide samples with a range of weights. Relative standard deviations of wt. %N on check standard B2153 (low organic content soil, 0.133 wt. % N) were <2%.

Pilot work

Since rock samples have relatively low nitrogen concentrations, it is important to determine the mass of N required to achieve accurate sample values of wt % N and $\delta^{15}N$. A size test was carried out to see if measured values of wt % N and $\delta^{15}N$ vary with mass of sample. 5 aliquots of the standard B2153 were prepared at 5 different weights (1.9, 3.75, 7.5, 15, 30 mg) i.e. total 25 samples. These were weighed into 8 x 5mm tin cups and analysed on the pyrocube/mass spectrometer and gave peak heights of between 0.07 and 1.35 nA. This batch of B2153 had a reported value of 6.97‰ ± 0.13 and contained 0.133 wt % N. Sample $\delta^{15}N$ values were obtained from the integrated m/z 28 and 29 ions relative to those in a pulse of N_2 reference gas (N5.0). These ratios were calibrated to the international AIR scale using international standard USGS-25 (-30.4‰ AIR) and USGS-26 (+53.7‰ AIR). These standards had peak heights of 0.3 – 0.6 nA.

Pilot work - results

Larger masses of sample give higher peak heights and more accurate and precise measurements relative to the reported B2153 $\delta^{15}N$ and N wt % values (Figure 2.17, Figure 2.18). As sample mass decreases, measured wt % N decreases and $\delta^{15}N$ becomes more positive and variable. Samples with peak heights greater than 1 give the most accurate and precise $\delta^{15}N$ and N wt % values. However, uncertainty becomes significantly higher at peak heights less than 0.6 nA, where wt %N and $\delta^{15}N$ of standard B2153 diverge significantly from certified values. Therefore, most accurate values will be obtained when samples give peak heights of at least 0.6 nA.

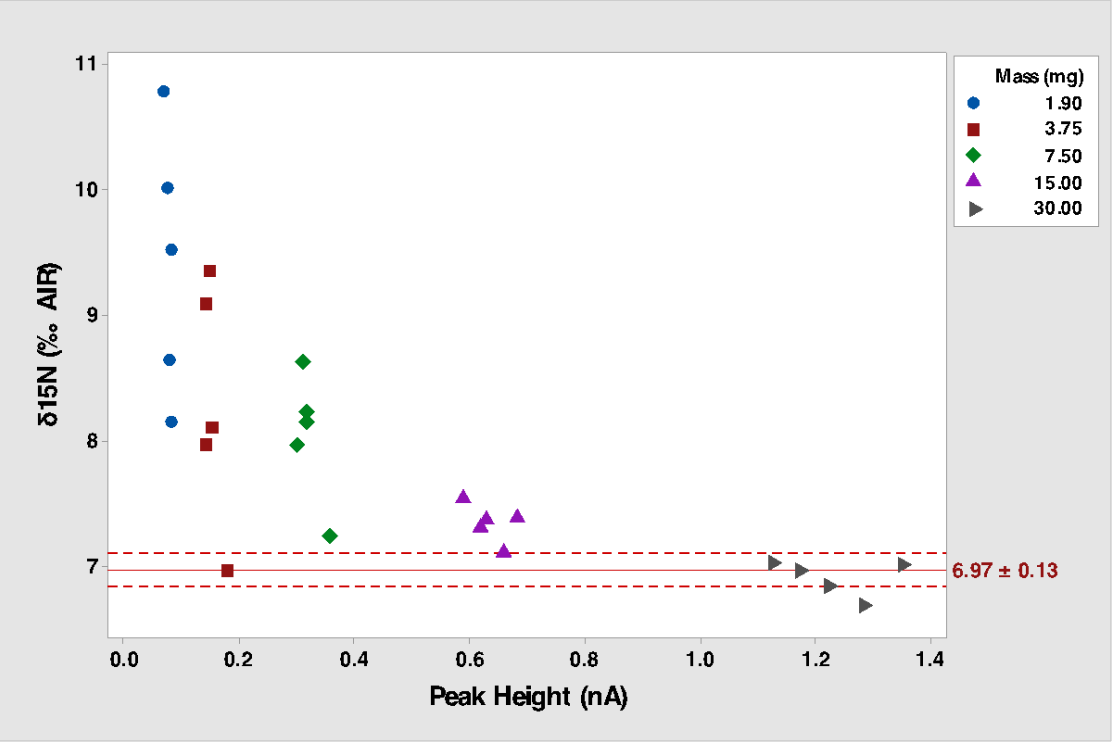

Figure 2.17 $\delta^{15}N$ of B2153 standard at different masses. All data points are calibrated with standards of peak height 0.3 - 0.6 nA. The red line represents the reported value of B2153, the dashed lines represent the upper and lower bounds.

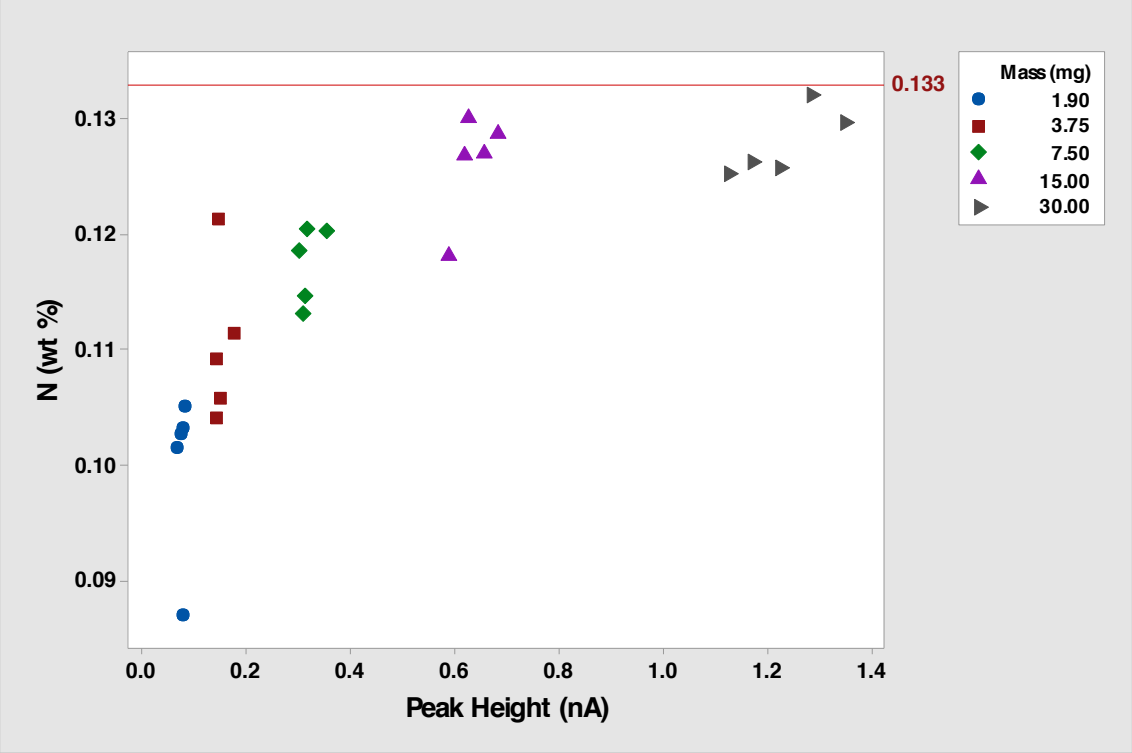

Figure 2.18 Reported wt % N of B2153 standards against peak height. Data categorised by approximate weight of standard. Red line indicates certified value.

2.2.2.1.2 Total inorganic N (TIN)

Inorganic N was measured in rock samples treated with potassium hypobromite (KOBr-KOH) to remove organic N (Silva, J.A. and Bremner, 1966). Potassium hypobromite was prepared by the addition of bromine to a 2N KOH solution. To prepare the KOH, 112 g KOH/l was dissolved in a beaker cooled in an ice bath. 5.4 ml bromine was added slowly (500 µl/minute) to 180 ml of cooled KOH with constant stirring.

0.5 g of crushed rock was weighed into a 250 ml glass beaker. 10 ml of prepared potassium hypobromite was added to each beaker and left to stand for 2 hours. 30 ml of deionised water was then added to each beaker and placed on a preheated hot plate until the mixture had reached a vigorous boil. Once the samples had boiled for 5 minutes, the hot plate was switched off and samples were allowed to cool overnight. The supernatant containing oxidised organic N was then discarded and the solid residue transferred to a pre-weighed 50 ml centrifuge tube using 0.5 M KCl. KCl is used to remove exchangeable ammonium. The tube was topped up to 30 ml with 0.5M KCl, capped and the contents suspended. Tubes were then centrifuged and the supernatant decanted. A further 2 KCl rinses were followed by 3 rinses with deionised water. Care was taken to avoid decanting any of the solid material during rinses. Open tubes were dried overnight in an oven at 50°C. Dried tubes were weighed and the mass of organic free sample calculated by mass balance. The sample was scraped into a clean pestle and mortar and homogenised. KOBr treated rock was weighed into tin cups and analysed as described in section 2.2.2.1.1.

Total inorganic nitrogen (wt % N) is calculated as follows

$$\mathrm{TIN\ (wt\ \%)} = \mathrm{P_{IN}} * \frac{(\mathrm{m_{final}} - \mathrm{m_{tube}})}{(\mathrm{m_{inital}} - \mathrm{m_{tube}})} \qquad \textbf{Equation 2.1}$$

Where P_{IN} is percent inorganic nitrogen in KOBr treated sample from the pyrocube.

2.2.2.1.3 Total organic N (TON)

Total organic nitrogen is calculated by difference of TN and TIN. $\delta^{15}N$ of organic N is calculated by

$$\mathrm{TON}\ (\delta^{15}\mathrm{N}) = \frac{\mathrm{TN\ (wt\ \%)} * \mathrm{TN}\ \delta^{15}\mathrm{N} - \mathrm{TIN\ (wt\ \%)} * \mathrm{TIN}\ \delta^{15}\mathrm{N}}{N_{bulk}(wt\ \%) - N_{inorg}(wt\ \%)} \qquad \textbf{Equation 2.2}$$

Since organic nitrogen is calculated by mass balance using bulk and inorganic N measurements (Equation 2.2), there is greater uncertainty in calculated $\delta^{15}N_{org}$ where organic N (wt. % N) is small. This is because only a small natural variation in measured $\delta^{15}N_{bulk}$ or $\delta^{15}N_{inorg}$ is required to create a large divergence in $\delta^{15}N$ of organic N. As a result, $\delta^{15}N_{org}$ values are very light where there is little organic N present in a sample.

2.2.2.2 Pilot study of the partitioning of N between inorganic and organic phases

One of the key objectives of this project is to better understand the distribution of nitrogen (N) within rock in terms of mass and stable isotopes ($\delta^{15}N$). In order to provide some context to nitrogen partitioning in different rock types, a pilot study was carried out prior to analysis of samples from Svalbard cores. Here nitrogen concentrations in bulk, inorganic and organic phases within different rock types, from the Svalbard region and the UK, are examined alongside stable isotope data of each fraction of N.

The rock samples include: a shale from Longyeardalen (Svalbard), a modern marine sediment from the Barents Sea and Ordovician metasediments (Hornfels) from Skiddaw, UK. Samples were treated with KOBr in triplicate with data of each replicate displayed in Figure 2.19. Uncertainty in the discussion below is 1 standard deviation based on triplicate samples.

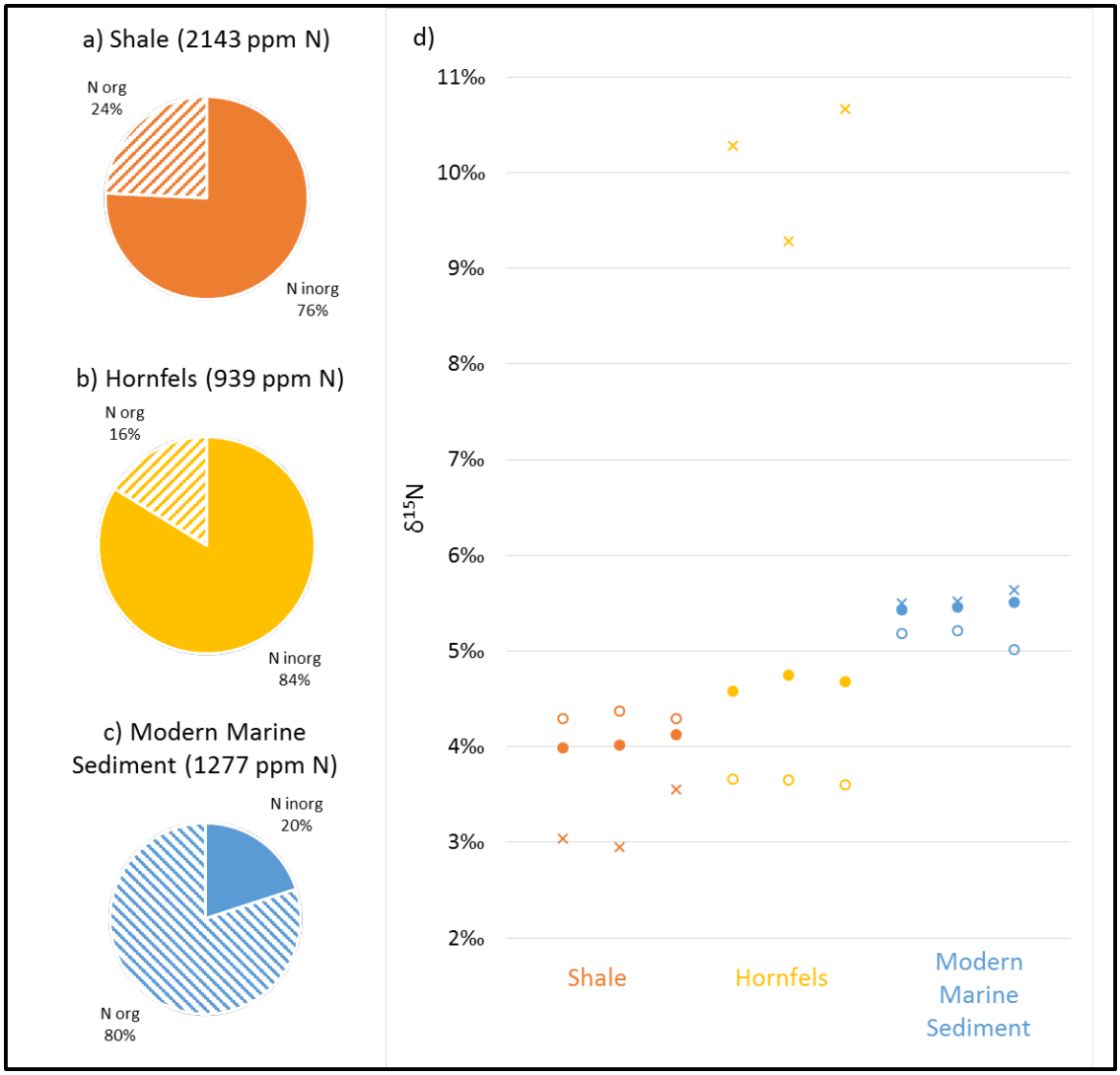

Figure 2.19 Partitioning of nitrogen between inorganic and organic phases in a) shale from Longyeardalen, Svalbard, b) Hornfels from Skiddaw, Lake District, UK and c) modern marine sediment from the Barents Sea. Pie Charts indicate proportion of N in each pool. d) Measured $\delta^{15}N$ values of bulk N (solid circles) and mineral N (open circles) as well as calculated organic N $\delta^{15}N$ values (crosses) from 3 replicates of each material.

2.2.2.2.1 Modern marine sediment

Organic N in modern marine sediment ($\delta^{15}N$ = 5.6‰ ± 0.07) is within error of bulk N $\delta^{15}N$ ($\delta^{15}N$ = 5.5‰ ± 0.035) as it represents the majority of N in sediment. This value is heavier than bulk $\delta^{15}N$ ratios for the shale and hornfels samples and is consistent with published data of modern marine sediment around Svalbard ($\delta^{15}N_{org}$ of 4.6 - 7.4‰ (Schubert and Calvert, 2001)). Conversely, terrestrially derived organic matter is thought to be isotopically lighter: the average $\delta^{15}N$ bulk of sediment from the Lena river, the largest discharge into Arctic sea, is 3.5‰ (Schubert and Calvert, 2001). Other estimates of terrestrial organic $\delta^{15}N$ from Japan (1.8‰) and California (0‰) are

lower still (Minoura et al., 1997; Peters et al., 1978). This divergence of $\delta^{15}N$ of marine and terrestrial organic matter may be explained by the fractionation process which occurs during nutrient uptake in marine settings (Schubert and Calvert, 2001). Conversely, limited fractionation is associated with nutrient utilisation by land plants such that terrestrial organic matter has $\delta^{15}N$ values of close to atmospheric N (0‰) (Schubert and Calvert, 2001; Wada et al., 1987)

2.2.2.2.2 Hornfels

The hornfels sample is a chiastolite cordierite biotite hornfels from Skiddaw, UK. Chiastolite is an andalusite mineral containing carbonaceous inclusions. This metasedimentary rock was formed due to contact metamorphism (high temperature) associated with the intrusion of the Skiddaw granite. It contains N almost entirely in an inorganic form with a bulk $\delta^{15}N$ value of +4.7‰ ± 0.08, yet the small proportion of organic N is significantly isotopically heavier (10.1‰ ± 0.7). The larger uncertainty on the calculated organic $\delta^{15}N$ of Hornfels than other samples is likely due to the lower organic N content. Whilst the wt.% of total and inorganic fractions are consistent, the organic N content in this sample is low enough that N isotopes may be significantly fractionated during metamorphism.

Due to the rock's high temperature thermal history, it is likely that organic N has been lost through devolatilisation. ^{14}N is preferentially lost from organic matter (to fluids/adsorbed to minerals) during this process since less energy is required to break ^{14}N-^{12}C than ^{15}N-^{12}C bonds (Williams, L.B. et al., 1995). In a closed system, where all thermally degraded organic N is incorporated into clay minerals, little isotope fractionation occurs (Williams, L.B. et al., 1995), however if the system is open or some refractory organics remain in the rock, the residual organic N will likely have a heavy ^{15}N signature. Therefore, the large divergence between inorganic and organic N isotope values in this rock is likely due to a small mass of highly fractionated refractory organic N.

2.2.2.2.3 Shale

The majority (76%) of nitrogen within the shale occurs as inorganic nitrogen. Bulk rock $\delta^{15}N$ therefore largely reflects the inorganic N signature. The smaller organic (3.2‰ ± 0.3) fraction is isotopically lighter than inorganic N (4.3‰ ± 0.04). Isotope ratios are unlikely to have been altered during diagenesis due to the low temperature thermal history of the rock compared to the high temperatures experienced by the Hornfels. The proximity of organic and inorganic $\delta^{15}N$ to terrestrial and marine organic matter end members makes it difficult to attribute their source environments based on stable isotopes alone. However, the minor difference in $\delta^{15}N$ between organic and inorganic fractions

may suggest a common source of N since only minimal fractionation is associated with the incorporation of organic nitrogen into clay minerals during burial and diagenesis (Scholten, 1991; Williams, L.B. et al., 1995).

2.2.2.3 Bedrock N $\delta^{15}N$ analysis

Bedrock samples were analysed in 2 batches on the pyrocube/mass spectrometer. Blanks were 0.004 nA or better and no blank correction was performed. Due to the variable amounts of N within samples, aliquots of standards were prepared at 2 different weights (referred to as high and low) to ensure standards and samples are closely matched in terms of peak height. High and low standard weights were 0.5 - 0.6 mg and 0.05 - 0.06 mg respectively which yielded peak heights of 4 - 6 nA and 0.4 - 0.6 nA. Sample peak heights varied between 0.1 and 3.4 nA. B2153 (low organic content soil) was run as a check standard.

Sample $\delta^{15}N$ values were obtained from the integrated m/z 28 and 29 ions relative to those in a pulse of N_2 reference gas (N5.0). These ratios are calibrated to the international AIR scale using international standard USGS-25 (ammonium sulphate; -30.4‰ AIR) and USGS-26 (ammonium sulphate; +53.7‰ AIR).

Calibration lines were produced for both high and low standards. All standards from each batch were used to create a bulk calibration however any standards that were more than 2 standard deviations from the mean were rejected. An extrapolated intermediate calibration line was derived at the average peak height of B2153 standards in each batch (1.8 & 2 nA) assuming a linear transition between calibrations. This composite calibration line is derived from 2 sets of standards, therefore the uncertainty on the line is less well defined. The average standard deviation on standards in the high calibrations for the 2 batches are 0.12 & 0.08 whereas for the low calibration they are 0.46 & 0.35.

Samples with peak heights lower than the low standards (0.4 nA) were rejected. In section 0, it was found that samples with peak height < 0.6 nA are liable to more positive $\delta^{15}N$ values. After removing samples with peak height < 0.4 nA, a negligible proportion of samples had peak height < 0.6 nA. Their $\delta^{15}N$ values were consistent with stratigraphically close samples and did not show $\delta^{15}N$ enrichment. Therefore these samples were not rejected.

Reproducibility was determined by repeat analysis of B2153. The vial of standard used had a certified value of 7.30‰ ± 0.13 (cf Pilot work). B2153 standards were calibrated using the intermediate calibration line. Repeat

analysis of B2153 throughout runs identified drift towards heavier values. A drift correction was applied therefore applied to data points as detailed below.

2.2.2.3.1 Drift Correction

In order to correct for drift in $\delta^{15}N$ through the run, a plot was constructed of sample number (a proxy for time point through run) and measured $\delta^{15}N$ value (

Figure 2.20). Measured values of B2153 fell in the range 6.7‰ to 7.7‰ AIR. Reported values of $\delta^{15}N$ for this batch of B2153 were 7.3‰ ± 0.13 AIR (N.B. different batch to that used in Section 0), therefore a transformation was required to shift the regression line of measured values to y = 7.3‰. This transformation was derived for B2153 values in each batch and then applied to samples within that batch to correct for drift. The drift correction formula is:

$$\delta^{15}N_{corr} = \delta^{15}N_{meas} + \text{Drift correction factor} \qquad \textbf{Equation 2.3}$$

Where $\delta^{15}N_{corr}$ = drift corrected isotope value of sample and $\delta^{15}N_{meas}$ = calibrated isotope value of sample and drift correction factor is defined by:

$$\text{Drift correction factor} = (m(x_0 - \text{sample number})) \qquad \textbf{Equation 2.4}$$

Where m = slope of regression line of calibrated B2153 standards, x_0 is the x value where the regression line intercepts with y=7.3‰ and sample number is the position of the sample in the run (Figure 2.20). x_0 is derived by rearranging the equation of the regression line:

$$x_0 = \frac{7.3 - c}{m} \qquad \textbf{Equation 2.5}$$

The drift corrected values for B2153 gave an average value of 7.29‰ ± 0.08 and 7.49‰ ± 0.10 (1 SD) in separate runs, both of which are within error of reported values.

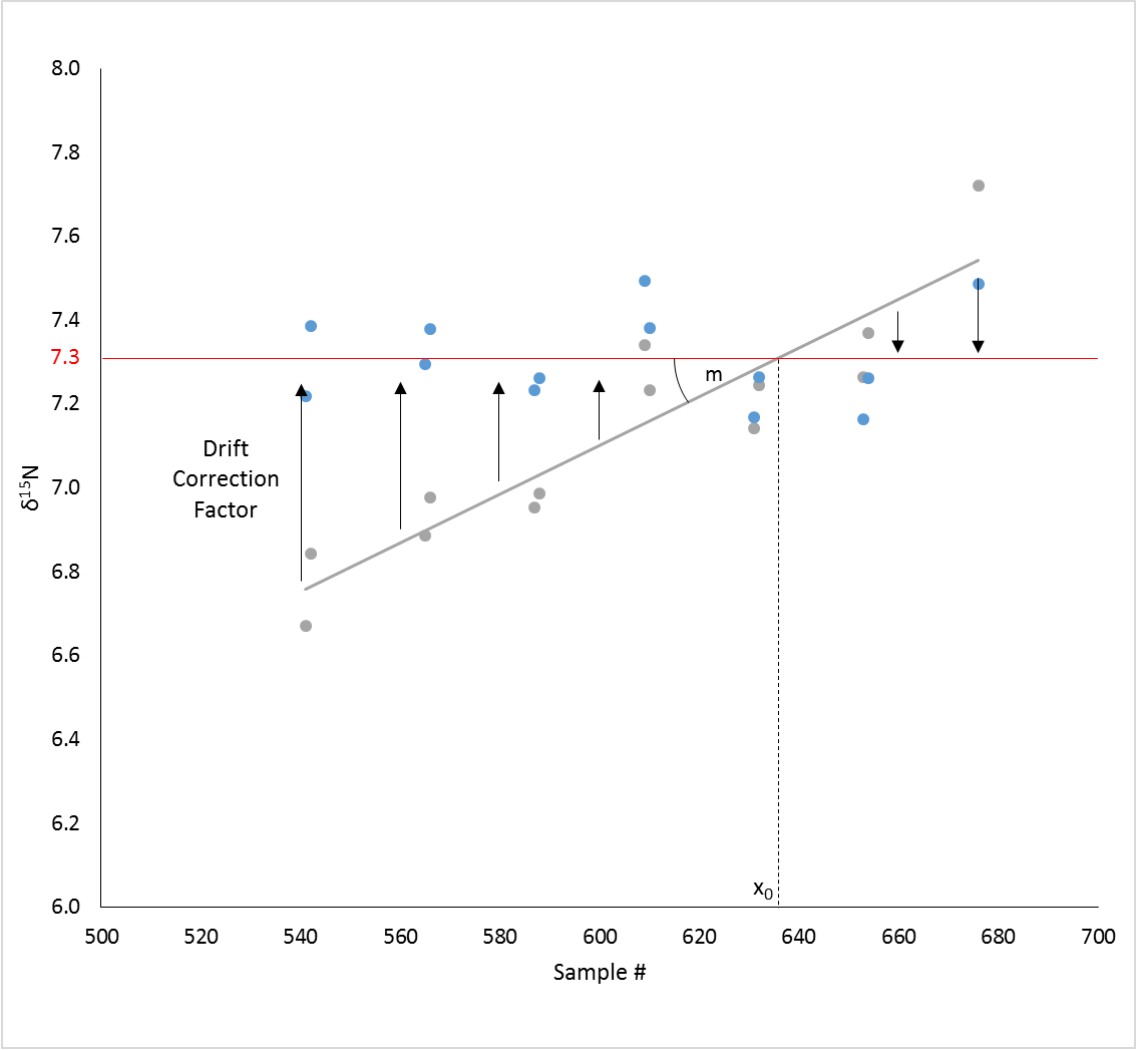

Figure 2.20 Graph displaying methodology for drift correction. Red line represents reference value of B2153. Grey dots are calibrated but uncorrected B2153 $\delta^{15}N$. Blue dots are calibrated and drift corrected B2153 $\delta^{15}N$. Arrows indicate the transformation of y values with the drift correction.

2.2.3 Iron and Manganese

2.2.3.1 Iron and Manganese speciation

Iron and manganese were extracted from rock samples using the iron speciation method developed by Poulton and Canfield (2005). This sequential extraction targets the following iron and manganese phases: carbonate associated (Fe/Mn_{carb}) e.g. siderite and ankerite; easily reducible oxides e.g. goethite, akaganeite and hematite (Fe/Mn_{ox}); and magnetite (Fe_{mag}). Iron pyrite (Fe_{py}) is extracted by a separate technique discussed in section 2.2.3.3.

70 - 90 mg of sediment was weighed into a 15 ml centrifuge tube. 10 ml of reagent was added to sediment as outlined in Figure 2.21. Tubes were then

tightly capped and placed on a shaking table at 100 RPM at the appropriate temperature for the extraction.

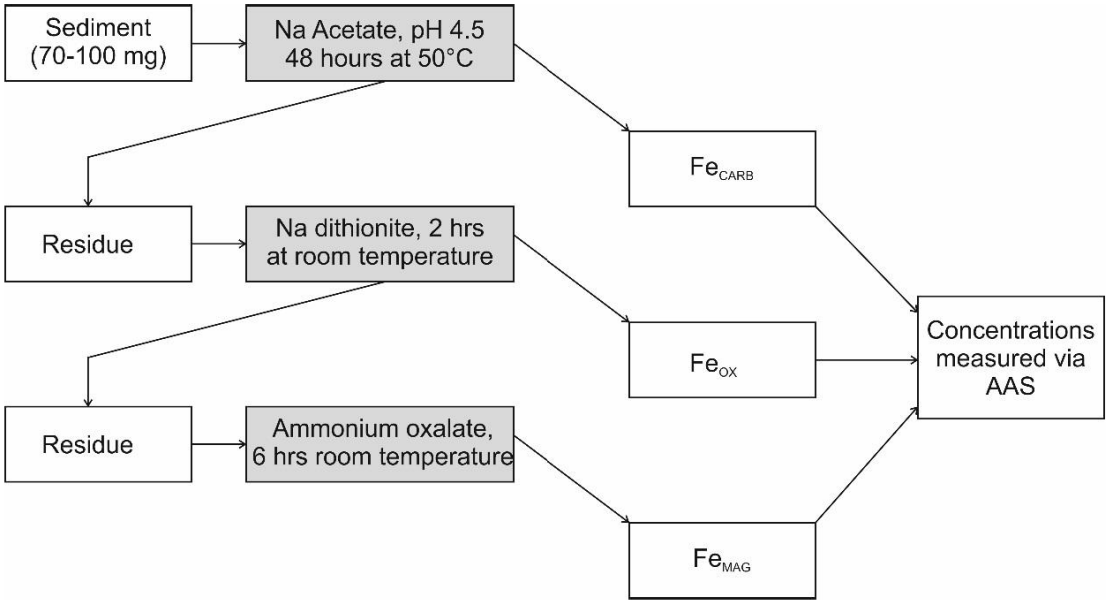

Figure 2.21 Flow chart showing the iron speciation method (Poulton and Canfield, 2005). Figure taken from (Doyle, 2018). Reagents are shown in grey boxes.

After the extraction has finished the tubes were centrifuged for 4 minutes at 4000 RPM. The supernatant was decanted into new centrifuge tubes, for analysis, taking care to not disturb the sediment. The next reagent was then added to the residual sediment and the procedure continued.

2.2.3.2 Analysis

Iron and manganese concentrations in the extractions were analysed using an Atomic Absorption Spectrometer (AAS) ThermoScientific iCE 3000 series. Samples are aspirated to an air-acetylene flame where the solvent evaporates and dissociates to free atoms. A hollow cathode lamp provides a radiation source which excites the atoms. The concentration of iron/manganese is determined by the difference in absorbance of radiation between a blank and the sample. Before each set of extractions was analysed, the instrument was calibrated by measuring standards of known concentration. Standards were prepared using reagent matrix and a stock standard at concentrations: 1, 3, 5, 7, 10 ppm (iron) and 0.1, 0.3, 0.5, 0.7, 1 ppm (manganese). A 0 ppm and 5 ppm Fe / 0.5 ppm Mn standard were analysed every 10 samples to ensure the instrument's precision did not drift. Samples were first diluted 20x with ultrapure (Type 1; 18.2 Ω) water. If samples concentrations were >10 ppm Fe or 1 ppm Mn, further dilutions were prepared. Iron/manganese wt. % of each phase was calculated using Equation 2.6.

$$Fe, Mn\ (\text{wt\%}) = \frac{\frac{[\text{Diluted conc (ppm)} \times \text{dilution factor}] \times \text{vol (L)}}{1000}}{\text{original sample weight (g)}} \text{ x } 100\% \quad \textbf{Equation 2.6}$$

2.2.3.3 Pyrite - iron

Iron was determined stoichiometrically by weight from an Ag_2S precipitate produced through a distillation method outlined in section 2.2.5.3. Iron pyrite is calculated by Equation 2.7.

$$Fe\ Py\ (wt\ \%) = \frac{\mathrm{Ag_2S}_{(g)} * \frac{A_r\ S}{m_r\ Ag_2S} * \frac{m_r\ FeS_2}{m_r\ S_2} * \frac{A_r\ Fe}{m_r\ FeS_2}}{Sample\ weight\ (g)} * 100\% \quad \textbf{Equation 2.7}$$

Where A_r and M_r represent the relative atomic mass and relative molecular mass of the given element/molecule.

2.2.4 Total Carbon, Total Organic Carbon and Total Inorganic Carbon

2.2.4.1 Total Carbon (TC)

Total carbon in rock samples was determined by dry combustion with an infrared carbon analyser (LECO). The LECO is kept at a constant 1350°C under a pure oxygen atmosphere. 0.3 g of sample is weighed into a ceramic sample boat and placed into the LECO.

A series of weights of the standard medium C soil (11.98% C ± 0.44, 0.136% S ± 0.009) were also weighed into sample boats to prepare a calibration line. At least 5 blank sample boats were analysed to calculate the limit of detection. Uncertainty was calculated using repeats of standards (1 standard deviation = 0.108, n = 20 combined from 3 separate analyses, RSD = 1%). Limit of detection (LOD) and Limit of quantification (LOQ) are calculated for each analysis, maximum values were 0.0841% and 0.1077% respectively.

2.2.4.2 Total Organic Carbon (TOC)

Total organic carbon is measured on acid treated samples which removes inorganic carbon (Ryba and Burgess, 2002). 4 – 5 g of rock was weighed into a pre-weighed 50 ml centrifuge tube. 10 ml of 10% HCl was added to each tube and mixed. After 1 hour, a further 10 ml of acid was added and samples were periodically shaken. After 48 hours, once the samples had stopped fizzing, tubes were centrifuged for 4 minutes at 4000 RPM. Supernatants were

decanted and disposed of and the sediment was washed with deionised water, centrifuged and decanted at least three times until the rinse water pH was greater than 4. This ensures any remaining chlorine is removed as it interferes with the LECO. Open tubes were placed in an oven at 40°C overnight after which tubes were re-weighed. 0.3g of acidified samples were weighed into ceramic sample boats and analysed on the LECO as per section 2.2.4.1. TOC is calculated using Equation 2.8 where POC is percent organic carbon of the treated aliquot from LECO, m_{tube} is the mass of empty tube, $m_{initial}$ is the starting mass of crushed rock and m_{final} is the mass of treated rock after acidification.

$$\mathrm{TOC\ (wt\ \%)} = \mathrm{P_{OC}} * \frac{(\mathrm{m_{final}} - \mathrm{m_{tube}})}{(\mathrm{m_{inital}} - \mathrm{m_{tube}})} \qquad \textbf{Equation 2.8}$$

2.2.4.3 Total Inorganic Carbon (TIC)

TIC was calculated by difference of measured total carbon and total organic carbon (Equation 2.9).

$$\mathrm{TIC\ (wt\ \%)} = \mathrm{TC\ -\ TOC} \qquad \textbf{Equation 2.9}$$

2.2.5 Sulphur

2.2.5.1 Total Sulphur

Total sulphur in rock samples was determined by dry combustion using the LECO at the same time as total carbon was measured (section 2.2.4.1). A series of weights of the standard medium C soil (0.136% S ± 0.009) were weighed into sample boats to prepare a calibration line. At least 5 blank sample boats were analysed to calculate limit of detection. Uncertainty was calculated using repeats of standards (1 standard deviation = 0.004, n = 20 combined from 3 separate analyses; RSD = 3%).

2.2.5.2 Sulphate and sulphide sequential extraction

In order to determine the partitioning of sulphur within bedrock, a method was required to measure different sulphur phases. Sulphur is known to occur in rocks as sulphide, sulfates and organosulfur complexes. If these pools can be extracted from rock separately, the partitioning of sulphur within rock can be derived. Once sulphur is extracted into solution, it can be precipitated as barium sulphate using barium chloride (section 2.5.3).

Sulfate minerals are often water soluble so a simple leach using ultrapure water will liberate these from crushed rock. Hydrogen peroxide is an oxidising agent which is able to oxidise sulphide minerals to sulphate (Fisher and Brown, 1994;

Jennings et al., 2000; Sobek et al., 1978). It is possible that peroxide may also oxidise organics too, resulting in an overestimate of inorganic sulphide sulphur. Therefore, this method is unsuitable for samples with appreciable organic C content.

A sequential extraction comprising an ultrapure water leach to release soluble sulfates followed by hydrogen peroxide leach to oxidise sulphides was trialled. Due to various problems with this method outlined below this method was not implemented beyond pilot testing.

During a trial rock-water leach, fine material floated on the water surface. These were either organic molecules or very fine sulphide minerals. If the latter they should not be decanted with the water. A surfactant was added to the water leach to break surface tension in order to help the floating material sink. However, during the subsequent peroxide leach, these samples foamed violently causing loss of sample. This was therefore not an appropriate method, instead separate (non-sequential) water and peroxide extractions were carried out on aliquots of samples using the following method:

Aliquots of 20 g and 10 g of powdered rock were weighed into separate 250 ml Nalgene bottle suitable for centrifugation. In a fume cupboard, 50 ml of hydrogen peroxide (30%, Fisher, certified AR for analysis) was added to one bottle and 50 ml of ultrapure water was added to the other. The peroxide filled bottles were placed in an ice bath and all bottles were agitated regularly over the course of 36 hours to ensure all powder was wetted and had reacted. The bottles were then centrifuged and the supernatants removed using syringes. A 0.45 μm and a 0.22 μm filter were placed on the end of each syringe in tandem and the liquid was filtered into a glass beaker. The peroxide treated sample was twice re-suspended in ultrapure water, centrifuged and filtered to remove any sulphate that may have adsorbed to sediment surfaces. The washings were added to the initial filtrate. Barium chloride was added to the solutions to precipitate barium sulphate following the procedure outlined in section 2.5.3.

Yields of total sulphur extracted from the combined water and peroxide leaches relative to total sulphur values derived from the LECO were < 46%. Therefore, there is either a large pool of another sulfur phase or this method is inefficient at extracting sulfur. TOC in these samples were fairly low (< 0.9 wt %), therefore it is unlikely that organosulfur compounds make up the bulk of rock sulfur. It seems that the efficiency of extracting sulphur from rock using water and peroxide leaches is inadequate using the methods employed here.

Of the sulphur extracted, no more than 10% of sulphur was extracted with water. This suggests that the vast majority of sulphur in rock is likely found in

non sulfate forms i.e. organics or sulphides. Given the above discussion, it is likely that most sulphur occurs as sulphide in these rock samples. Therefore, sulphide is extracted from samples for $\delta^{34}S$ analysis as discussed below.

2.2.5.3 Pyrite extraction

Pyrite was extracted from a subset of rock samples using a HCl and chromous chloride distillation method where sulphide is liberated as H_2S gas which is trapped in silver nitrate ($AgNO_3$) to precipitate silver sulphide (Canfield et al., 1986). The amount of sample used was determined by lithology and known total sulphur content (measured on LECO). Approximately 0.3 - 0.5 g was used for shale and up to 1 g for sandstones.

Chromous chloride reagent is prepared in advance of the extraction. 533 g/L of Chromous chloride ($CrCl_3$) is dissolved in 50% HCl. Zinc pellets are added to a 2L schott bottle forming a layer 2 – 3 cm thick. The chromous chloride solution is transferred to the schott bottle and gently swirled to ensure zinc pellets are wetted. The solution is purged with nitrogen gas for at least an hour before use to remove any dissolved oxygen. An airlock, partly filled with water, is fitted to the bottle cap to ensure the bottle interior remains anoxic (Figure 2.22b).

Test tubes are labelled for each sample into which is pipetted 0.5 ml 1M $AgNO_3$. Ultrapure water is added to each tube up to 2/3 full. The tip of the exit line from the condensing column is placed into the corresponding test tube trap. Nitrogen gas is pumped through to produce a steady stream of bubbles in the trap.

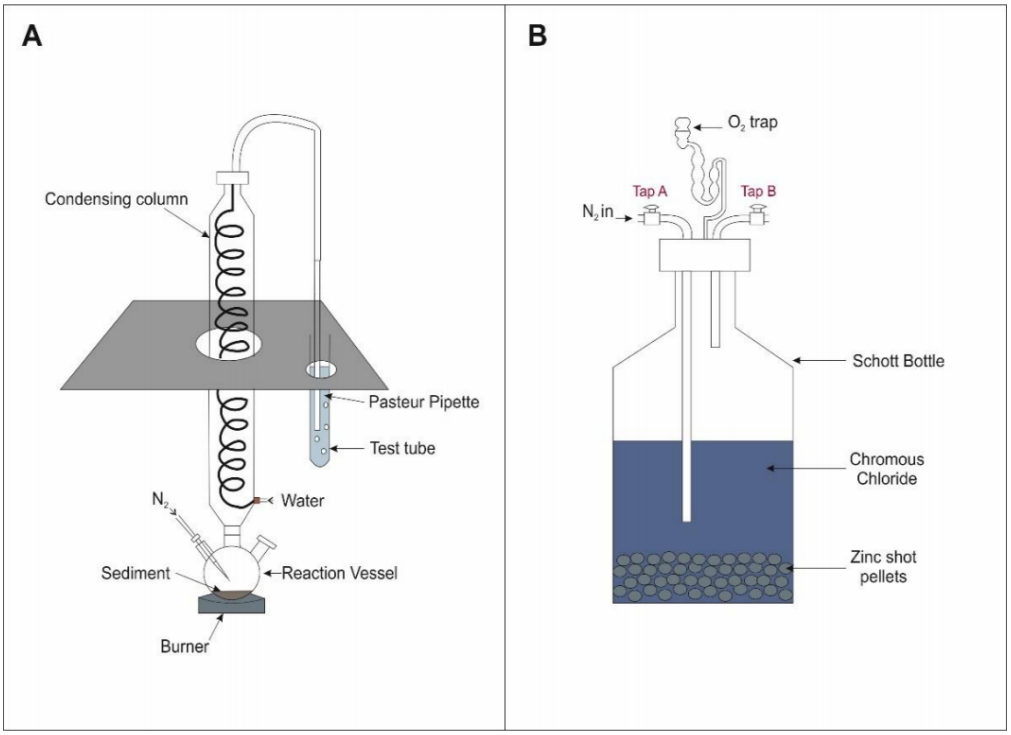

Figure 2.22 Setup of pyrite extraction taken from Doyle (2018)

Rock samples were weighed into reaction bulbs which are connected to a distillation tube and N_2 gas line. The sample bulb is placed on a hot plate and attached to the condensing column (Figure 2.22), 8 ml of 50% HCl is added to the reaction bulb and the bulb stoppered. This releases acid volatile sulfur (AVS) from samples. After 10 minutes, no precipitate had formed. Since the samples here are all ancient, AVS is not present and the next stage of the extraction began. 15 ml of chromous chloride is then added to each sample bulb to liberate sulphide from pyrite. H_2S enters the silver nitrate trap and forms a black silver sulphide precipitate. As the traps became increasingly brown, 0.5 ml aliquots of 1 M silver nitrate were added until the solution cleared. After an hour, the traps were removed from the condensing columns. The contents of the traps were vacuum filtered onto pre-weighed cellulose nitrate filter papers (0.45 µm pore size, 25 mm diameter). The traps were rinsed several times with ultrapure water to ensure quantitative transfer of silver sulphide to the filter paper. The papers are left to dry, covered, at room temperature. Once dry, filter papers and silver sulphide are weighed to derive the mass of silver sulphide by difference. Mass of sulphide is determined stoichiometrically by Equation 2.10.

$$Sulphide\ (wt\ \%) = \frac{\mathrm{Ag_2S}_{(g)} * \frac{A_r\ S}{m_r\ Ag_2S}}{Sample\ weight\ (g)} * 100\% \qquad \textbf{Equation 2.10}$$

As there is not currently an international rock standard with which to assess this method, an internal standard of Whitby Shale (1.999 ± 0.114 wt%) was used to determine reproducibility. An aliquot of Whitby Shale was processed with each batch of samples on the pyrite line. Average extracted sulphide sulphur was 2.137 ± 0.081 (n = 4) which is within uncertainty of the reported value.

2.2.5.3.1 Sulphide – $\delta^{34}S$ analysis

Silver sulphide precipitates were analysed for $\delta^{34}S$ via combustion in an Elementar Pyrocube elemental analyser coupled to an Isoprime continuous flow mass spectrometer. Samples were combusted at 1150°C to SO_2 in the presence of pure oxygen (N5.0) into a stream of helium (CP grade). The produced SO_2 flowed through tungstic oxide packed into the combustion column to ensure quantitative conversion. Excess oxygen was removed by reaction with hot copper wires at 850°C and water was removed in a Sicapent trap. All solid reagents were sourced from Elemental Microanalysis, UK, and all gases were sourced from BOC, UK. Duplicate aliquots (0.13 - 0.21 mg) of silver sulphide were weighed into 8 x 5 mm tin cups because of a small sulfur isotope memory effect incurred in SO_2 gas processing in the Pyrocube.

Peak heights of blanks were on average 0.02 nA and no blank correction was performed. Standards were run at the same peak height as samples (1.1 – 1.9 nA). Sample $\delta^{34}S$ values were obtained from the integrated m/z 64 and 66 ions relative to those in a pulse of SO_2 reference gas (N3.0). These ratios are calibrated to the international V-CDT scale using international standard IAEA S-3 (silver sulfide, -32.06‰ $_{V\text{-}CDT}$) and an inter-lab chalcopyrite standard CP-1 (-4.56‰ $_{V\text{-}CDT}$). Reproducibility of a check standard May & Baker ($BaSO_4$) gave an average value of 17.3‰ ± 0.24 (1 SD).

2.2.6 XRD

A selection of powdered rock samples from each formation were prepared for X-ray diffraction (XRD) to determine their mineral composition. Measurements were made using a Bruker D8 diffractometer. Cleaned sample holders were loaded with powders and set on a 1 hour scan between 2 - 86°. The Bruker Diffrac software was used to remove the background and fit XRD profiles. Minerals were identified using standard XRD traces from the Powder Diffraction File (PDF-2 1996).

2.2.7 Surface Area

Surface area of both crushed rocks, for leaching experiments, and glacial sediment were analysed on a Micromeritics Gemini VII 2390a BET (Brunauer, Emmett, Teller). Samples are weighed into pre-weighed test tubes and flushed with nitrogen gas overnight. Sample tubes were then reweighed and flushed with N_2 at the boiling point of nitrogen (-196°C). The volume of gas adsorbed to particle surfaces is correlated to the total surface area of the particles. The sample surface is calculated by the instrument software using BET theory. The correlation coefficient of each sample measurement was at least 0.9999.

2.3 Field Sampling

2.3.1 Sampling Approach

Glacial meltwater was collected from glaciers in the study area during fieldwork in August – September 2016 and August – September 2017. The aim of this field work was to collect glacial water representative of the subglacial environment. Subglacial water flows between overlying ice and underlying glacially comminuted rock, therefore the chemistry of the water reflects solute acquisition from bedrock. High conductivity and low dissolved oxygen are indicative of rock - water interaction in which the oxidation of organic carbon/sulphide minerals consume oxygen. Such processes are typical of

subglacial environments with limited oxygen sources. Therefore, meltwater emanating from subglacial portals was initially analysed for dissolved oxygen, pH and conductivity in the field (Section 2.3.2). These measurements were used to decide whether the water was likely subglacial in origin. Glaciers in this study are mainly cold based with drainage via ice marginal channels which are turbid and have high conductivity. Therefore, while meltwater samples may not be of true subglacial in origin, they are indicative of fluid pathways through crushed rock environments.

Supraglacial water samples were collected from above debris covered ice to provide an insight into nitrogen sources from meteoric/marine processes. Snow samples were collected prior to the main melt season in 2017 from Longyearbreen glacier.

2.3.2 In field measurements: pH, dissolved oxygen and electrical conductivity

In field measurements of pH, dissolved oxygen and electrical conductivity were made using an Orion Dual Star pH/ISE benchtop meter (ThermoScientific, USA) connected to probes for each analyte. The pH of the meltwater was measured using a Ross Ultra Combination pH electrode (ThermoScientific, USA) and the meter was calibrated weekly using low ionic strength pH buffer solutions (Thermoscientific Orion). An Orion 81010MD probe was used to determine dissolved oxygen concentrations. Conductivity was determined using an Orion conductivity probe.

2.3.3 Sample collection, filtration, storage

2.3.3.1 Meltwater

Meltwater was filtered at pressure using 0.45 µm high capacity groundwater filters into containers rinsed 3 times with filtered sample. Containers were sealed with no air bubble to reduce any oxidation/volatilisation of solute. A 15 ml centrifuge tube was filled with filtered sample and spiked with nitric acid to preserve cation/metal concentrations. The amount of acid used was sufficient to eliminate alkalinity and reduce pH to < 2. A 50 ml tube filled with filtered sample was stored for determination of anion concentrations. Two 15 ml glass vials were also filled with filtered sample and sealed with a crimp cap for oxygen isotope analysis and total dissolved inorganic carbon (TDIC) measurement. A 0.2 µm syringe filter was used to filter an aliquot of 0.45 µm filtered sample and stored in a 50 ml centrifuge tube which was spiked with sulfuric acid to preserve ammonium at pH < 2.

TDIC analysis was carried out in Svalbard but the remainder of the above samples were refrigerated and insulated in hold luggage on flights to UK before being returned to the fridge. Samples showed no signs of having frozen and are likely to have remained cool during transport. Small air bubbles formed in some bottles likely due to pressure changes during the flights.

2.3.3.2 Snow

Snow samples were collected from 4 sites in a linear transect on Longyearbreen in May 2017 (Figure 2.8). Snow 1 represents the highest sampling point, while samples 2-4 were collected progressively downslope. These were stored in plastic bags and frozen until September 2017 when they were melted in modified jerry cans and dripped onto anion/cation exchange resins immediately. Aliquots were also taken for anion and nutrient concentrations.

2.3.4 Suspended sediment

2.3.4.1 Sediment Collection

Suspended sediment was collected from subglacial streams in 2017 and 2018. 25 l of unfiltered water was left to settle in a large jerry can for over 24 hours. Approximately 24 l of supernatant were siphoned off without disturbing the settled sediment. The supernatant was drained to waste or filtered to collect clay sized grains that had not settled out of suspension. The remaining ~1 l of sediment rich water was filtered through cellulose filter papers. Samples collected in 2017 were dried for determination of suspended sediment concentration. Samples in 2018 were stored frozen to preserve adsorbed ammonium.

Recently deposited fine sediment from the same subglacial channels was identified by a shiny and smooth sheen of sediment on the channel banks just above the water level. Samples of this were collected using a trowel and drained of excess water using cellulose filter paper. Moist sediment was frozen in sample bags and transported to Leeds for further processing.

Sediment was carefully scraped from filter papers into pre-weighed medicine cups (bulk moist sediment). The filter paper was dried at 105°C over the weekend and weighed. An average filter paper weight (n = 10) was subtracted to calculate the residual sediment mass. An aliquot of the bulk sediment was weighed into a pre-weighed evaporating dish and dried at 105°C over the weekend. The dried sediment was re-weighed to calculate the sediment water

content. The mass of dried bulk sediment was determined using Equation 2.11. Suspended sediment concentrations were determined using Equation 2.12.

$$\text{Bulk dry sediment (g)} = \text{Bulk moist sediment (g)} \times \frac{\text{dry sediment (g)}}{\text{moist sediment (g)}} + \text{residual dry sediment (g)} \quad \textbf{Equation 2.11}$$

$$\text{Suspended sediment concentration (g/L)} = \frac{\text{bulk dry sediment (g)}}{25L} \quad \textbf{Equation 2.12}$$

2.3.4.2 Adsorbed ammonium extraction from sediment

An aliquot of frozen sediment was used to determine adsorbed/fixed ammonium ($NH_4^+{}_{(ad)}$) concentrations via a KCl extraction.

Ammonium adsorbed to sediment surfaces (exchangeable ammonium) was extracted using the procedure of Maynard et al. (2007). Sediment is washed and agitated with 2M KCl. The high concentration of potassium in solution displaces adsorbed cations including ammonium from mineral surfaces. The resultant salt solution can be analysed for ammonium using a colorimetric method on a continuous/segmented flow analyser.

A 2 molar solution of potassium chloride was prepared using Fisher (AR for Analysis) KCl. Merck (Emsure) KCl was used initially but this was found to contribute significant ammonium to blank samples.

The KCl solution was added to sediment in a 1:10 ratio i.e. 30 ml of solution added to 3 g of sediment. The sediment was suspended in the solution using a vortex shaker and then tubes were placed horizontally on a shaker table for 30 minutes at 160 RPM. The tubes were then centrifuged and the supernatant filtered using SFCA 0.45 and 0.2 µm syringe filters. Liquid samples were stored frozen in new centrifuge tubes until analysis on the AA3 (section 2.4.1.1). Prior to analysis samples were diluted by factor of 2. The wash solution for the AA3 was matrix matched to samples (1 M KCl). Higher concentration samples were diluted by factor of 10 and run with a 0.2 M KCl wash solution.

2.4 Aqueous Geochemical Analyses

These analytical methods apply to both experimental work and field samples.

All chemical and isotope analysis was performed at the University of Leeds within 3 months of sampling unless stated otherwise.

2.4.1.1 Nutrients

A Seal AA3 autoanalyzer was used to measure ammonium, nitrite and nitrate via a continuous flow analysis system. A continuous stream of sample, interspersed with air bubbles, is pumped through tubing using a peristaltic pump. The bubbles act as barriers creating segments in which chemical reactions occur. The sample is introduced to reagents which mix in glass coils causing colour producing reactions. The concentration of the analyte is proportional to the strength of colour produced. A light is shone through the coloured stream and the intensity of light is measured by a photometer. The difference between this measurement and the original light intensity is used to calculate the sample concentration. Three channels were used simultaneously on water samples: ammonium, nitrite and nitrite + nitrate. Nitrate is calculated by difference between nitrite and nitrite + nitrate. In the nitrite channel, nitrite reacts with sulphanilamide and N-1-naphthyl-ethylenediamine dihydrochloride under acidic conditions to produce a pink/purple dye (Seal Method G-062-92). In the nitrite + nitrate channel, nitrate is reduced to nitrite via a copper-cadmium column and nitrite measured as in the nitrite channel (Seal Method G-172-96). Ammonium is measured using the Berthelot reaction, in which ammonia reacts with salicylate and free chlorine in a heating bath to give a blue-green coloured complex (Seal Method G-320-05). KCl extracts were analysed for ammonium only.

Standards were prepared using stock solutions of ammonium sulphate, potassium nitrate and sodium nitrite. Certified standard VKI QC RW1 was run as a check standard for ammonium and nitrate (certified values: 101 µg/L ± 3.4 and 99 µg/L ± 2.6 respectively).

Table 2.2 LOD, LOQ and uncertainty (RSD %) for autoanalyzer analyses (µg/L). dashes indicate the analyte was not measured.

Samples	NH_4^+(aq)			NH_4^+(ad)			NO_3^-		
	LOD	LOQ	Uncertainty	LOD	LOQ	Uncertainty	LOD	LOQ	Uncertainty
Svalbard 2016	Not calculated		0.3%	-	-	-	9.6	11.7	0.9%
Svalbard 2017	6.6	11.8	1.3%	-	-	-	Not calculated		
Pilot Leach 1	1.8	3.8	2.5%	-	-	-	1.2	2.0	0.5%
Pilot Leach 2	0.7	2.1	0.4%	0.7	2.6	Not calculated	0.4	1.3	0.46%
Final Leach	1.4	5.2	0.8%	3.4	6.4	1.6%	Measured using ion chromatography		

2.4.1.2 Dissolved metals

Cation and metal concentrations were measured using a Thermo Fisher iCAP 7400 Radial inductively coupled plasma – optical emission spectroscopy (ICP-OES) analyser. This instrument works on a similar principle to AAS. Liquid samples are aspirated onto an argon flame which excites atoms such that they emit radiation at wavelengths specific to each element. The intensity of the emission is calibrated to the concentration of the element. Elements measured include: Na, Mg, K, Ca, Fe, Mn, Si, Al, S. LOD, LOQ and uncertainty are displayed for each analysis in Table 2.3, Table 2.4 and Table 2.5.

Iron and manganese in glacial meltwater collected in 2017 were analysed using a higher resolution Thermo Fisher iCAPQc inductively coupled plasma mass spectrometry analyser (ICP – MS). Samples are aspirated onto an argon flame where atoms are excited to form ions which are separated based on their mass to charge ratio. The intensity of the signal for each ion is proportional to their concentration. The iron in these samples represents that which passed through a 0.45 µm filter and will be termed ‘filterable’ iron from hereon.

Table 2.3 LOD, LOQ and % uncertainty for ICP-OES analyses of 2016 field work and pilot leach 1 samples

	Na	Mg	K	Ca	Fe	Mn	Si	Al	S
LOD / mg L-1	0.631	0.001	0.075	0.300	0.002	0.004	0.005	0.007	0.004
LOQ / mg L-1	2.10	0.004	0.249	1.000	0.005	0.012	0.015	0.022	0.012
% Uncertainty	1.13	1.15	1.18	0.90	1.16	1.18	1.07	1.12	0.623

Table 2.4 LOD, LOQ and % uncertainty for ICP-OES/MS analyses of 2017 field work samples

	ICP-OES (mg L-1)							ICP MS (µg L-1)	
	Na	Mg	K	Ca	Si	Al	S	Fe	Mn
LOD	0.09	0.01	0.04	0.02	0.01	0.01	0.06	0.70	0.27
LOQ	0.31	0.02	0.15	0.05	0.04	0.04	0.21	2.32	0.91
% Uncertainty	2.23	1.59	1.09	1.00	1.52	1.00	1.71	1.49	2.85

Table 2.5 LOD, LOQ and % uncertainty for ICP-OES analyses of final leach samples

	Na	Mg	K	Ca	Fe	Mn	Si	S
LOD / mg L-1	0.49	0.01	0.25	0.01	0.01	0.01	0.03	0.06
LOQ / mg L-1	1.65	0.03	0.84	0.04	0.04	0.03	0.08	0.20
% Uncertainty	1.61	2.11	3.70	5.34	3.69	2.54	3.82	2.52

2.4.1.3 Anions

Anions including sulfate, carbonate, chloride, nitrate and acetate were analysed using ion chromatography. A ThermoScientific Dionex ICS 5000 with column AS19 (2 x 250 mm) was used for analysis of the final leaching experiment (Chapter 5) while a ThermoScientific Dionex ICS 3000 with column AS11 (2 mm) was used to analyse meltwater samples collected in Svalbard (Chapter 7). Dionex DX 600 with column AS16 (2 x 250 mm) was used to measure pilot leach samples (Chapter 3).

Certified standards (Cranberry-05 and a multi element standard) were analysed as check standards with all samples. LOQ and uncertainty are reported in Table 2.6. LOQ is the lowermost standard used in the calibration of a run and uncertainty is the RSD of the calibration.

Table 2.6 LOQ (mg/L) and uncertainty (RSD %) of ion chromatography analyses. Dashes indicate that the analyte was not measured by ion chromatography.

Analyte	DX 600		ICS 5000		ICS 3000	
	LOQ	Uncertainty (RSD %)	LOQ	Uncertainty (RSD %)	LOQ	Uncertainty (RSD %)
Nitrate	-	-	0.1	3.7	-	-
Carbonate	10	< 4.4	2	3.5	-	-
Sulphate	0.8	< 6.0	0.3	1.4	0.6	1.4
Chloride	-	-	-	-	0.5	3.4
Acetate	-	-	0.3	0.8	-	-

2.4.1.4 Dissolved Inorganic Carbon

Total dissolved inorganic carbon analysis of glacial meltwater samples was conducted at UNIS using an Infra-Red Gas Analyser (IRGA PP Systems EGM 4). 15 ml of water sample is drawn into a syringe with a headspace of CO_2 free air. All forms of inorganic C are converted to CO_2 by addition of 1.5 ml of 5% HCl and agitation for 1 minute. Headspace in the syringe is then injected into the IRGA and CO_2 gas measured. A calibration was derived using sodium carbonate standards to determine TDIC. Bicarbonate and carbonate concentrations were derived from pH, TDIC values (µM) and dissociation constants for 0°C and 0% salinity: k_1 (2.67 x 10^{-7}; Equation 2.13) and k_2 (2.4 x 10^{-11}; Equation 2.14) (Millero and Roy, 1997). N.B. These calculations were also carried out for TDIC of weathering experiments determined via ion chromatography (see above) using dissociation constants for 5°C and 0% salinity: k_1 (3.069 x 10^{-7}) and k_2 (2.84 x 10^{-11}) (Millero and Roy, 1997).

$$CO_2 + H_2O \overset{K_1}{\leftrightarrow} H^+ + HCO_3^- \qquad \textbf{Equation 2.13}$$

$$HCO_3^- \overset{K_2}{\leftrightarrow} H^+ + CO_3^{2-} \qquad \textbf{Equation 2.14}$$

2.4.1.5 Charge Balance

Charge balance, ΔZ, of glacial water samples was calculated with the following equation, all units in meq/L.

$$\Delta Z = Na^+ + K^+ + Mg^{2+} + Ca^{2+} - Cl^- - SO_4^{2-} - NO_3^- \qquad \textbf{Equation 2.15}$$

Charge balance error (CBE) was also derived for each sample using Equation 2.16. All values of CBE from 2016 were between -2 and +5% while in 2017 CBE values were between -1 and -8%.

$$CBE = \frac{Total\ cations - total\ anions}{Total\ cations + total\ anions}$$ **Equation 2.16**

2.5 Isotope sample collection and analysis

Stable isotopes of nitrate and ammonium have been used in glacial hydrochemical studies to better understand biochemical processes involved in glacial nutrient cycling. However, low natural concentrations of nitrate and ammonium in glacial meltwater presents difficulties in stable isotope analysis of $\delta^{15}N$ and $\delta^{18}O$.

Different methods have been adopted over the years to isolate nitrate for isotope analysis. Such methods include the silver nitrate method (Chang, C.C.Y. et al., 1999; Silva, S.R. et al., 2000) and the denitrifier method (Casciotti, K. L. et al., 2002; Sigman et al., 2001). Whilst both methods have the advantage of high sensitivity, the former suffers with interferences from other anions and DOM e.g. Wynn et al. (2007) as we all as possible fractionation during processing of HNO_3 to $AgNO_3$. Furthermore, separate aliquots must be prepared for N and O analysis via a laborious and expensive process which uses silver oxide. The latter method is time consuming as it involves incubating bacteria over ~10 days prior to analysis using a less than simple lab setup. Two methods which have not been used in glacial studies are the cadmium method (McIlvin and Altabet, 2005) and the acetone method. The cadmium method benefits from using small volumes and works at concentrations as low as 0.5 µmol/L, however the main drawback is the use of highly toxic chemicals such as cadmium and sodium azide. The acetone method, developed by Huber et al. (2011), is simple to prepare and has a sensitivity equal to/better than the other methods. Whilst it avoids the usage of multiple toxic chemicals, it does require small volumes of n-hexane. 25 - 30 µmol NO_3^- are required for this technique so low concentration samples need to be pre-concentrated using a freeze dryer. Due to its simplicity and high sensitivity, the acetone method was adopted for this project (see 2.5.1.4). Unfortunately, a freeze dryer was not available in Svalbard to pre-concentrate meltwater. Instead water was loaded onto ion exchange columns from which it could be eluted in a more concentrated solution for us in the acetone method.

Ammonium is usually prepared for stable isotope analysis of nitrogen using the ammonium diffusion method (section 2.5.2.3.2). In a similar manner, ammonium

was pre-concentrated onto cation exchange columns prior to isotope sample preparation.

2.5.1 Anion columns

2.5.1.1 Column Methodology

Anion exchange columns were premade using 60 ml SPE tubes which were filled with 20 ml of BIO-RAD AG1-X8, 100-200 mesh, Chloride form. Resins were cleaned before use using 2 x bed volumes of 1 M HCl (Aristar) followed by 4 x bed volumes of ultrapure water following advice from BIO-RAD Tech Support.

During the 2016 field season, 10 l of 0.45 µm filtered glacial meltwater was dripped onto the anion column. The resins were continuously monitored to ensure a slow drip rate and that the head of water above the resin did not fall too low so as to disturb the resin. We found that a pragmatic approach was required when working with such volumes of water. Hence the drip rate was increased slightly by adding a long length of tubing to the column outflow which provided a driving force through the resin.

Analysis of nitrate concentrations from 2016 field samples revealed that nitrate concentrations were highly variable between sites. Consequently, the volume of sample required for isotope analysis varied significantly. Ion exchange resins have a limited exchange capacity, as these thresholds are approached, the resins can begin to self-elute. This is particularly problematic when the dominant anion in solution (sulfate) is not the ion of interest. In many of the samples as little as 0.2 l of sample was required to capture 25 – 30 µmol NO_3^- for the acetone method, therefore too much sample was collected and many of the resin columns became over saturated. Consequently, it is likely that the elevated sulfate concentration caused the displacement of nitrate ions, resulting in variable nitrate yields (39-100%) from the resin columns. To avoid this scenario in 2017, a calibration of EC and nitrate/ammonium concentrations was created based upon 2016 data. This calibration was used to determine a rough sample volume for isotope analysis.

2.5.1.2 Column processing

Ion adsorption onto exchange sites on resins is dependent on the concentration of the ion in solution and the relative selectivity of the resin for each ion. Ag 1-X8 has a relative selectivity of 65 for nitrate. Therefore the adopted eluant should contain an anion with a greater selectivity or the absolute amount of the anion in the eluant should greatly exceed the amount of nitrate on the resin.

Several different eluants were trialled using anions of different selectivities and concentrations (Table 2.7).

Table 2.7 Details of anions and eluants trialled during method development of anion exchange resins

Anion	Relative Selectivity for AG 1-X8	Eluant
Citrate	220	0.5M trisodium citrate
I^-	175	0.3M, 1.3M KI
Br^-	50	2M KBr
Cl^-	22	2M, 4M NaCl 3M HCl

Trial resin columns were prepared as above. Standard solutions containing nitrate and sulfate concentrations similar to samples collected in the field were prepared using nitrate and sulfate salts. A fixed volume of the solution was added to each resin column which was subsequently eluted using 3 bed volumes of the eluants listed in Table 2.7. HCl effluents were neutralised using MgO. An aliquot of the effluent was taken to determine nitrate concentration and the remainder was frozen at -20°C.

Frozen effluents were placed in the freeze dryer in preparation for the acetone extraction. However, during freeze drying the test samples melted. The samples were refrozen at -80°C and placed back in the freeze dryer, the 4 M NaCl sample melted but the remainder of the samples remained frozen and freeze dried successfully. The inability to remain frozen in the freeze dryer likely reflects the salinity of the solutions which raises the melting point of the solution. Freeze drying increases solute concentration and therefore continually raises the melting point causing the samples to melt.

Nitrate yields of the frozen samples were < 50% for the following eluants: 0.3 M KI (44%), KBr (nitrate < LD) and citrate (7%). However 1.3 M KI (97%) gave excellent nitrate yields. No data is available for NaCl as an eluant, however Li, W.-B. et al. (2015) found that Cl^- solutions are the most ideal eluants for nitrate on this resin.

The suitability of Cl^- and I^- were subsequently considered for the acetone method. Further nitrate/sulphate solutions were prepared in ultrapure water, 2 M NaCl and 1.3 M KI matrices in order to establish whether there are any interferences associated with the matrices. These samples were processed via

the acetone method to produce barium nitrate which was analysed for $\delta^{15}N$ and $\delta^{18}O$. KI samples featured low peak heights for N and elevated $\delta^{18}O$ relative to the water sample. NaCl samples reflect the true N and O isotope values of the nitrate salt. Low N peak heights in the KI samples suggest that limited barium nitrate was formed from the extraction. Inconsistent $\delta^{18}O$ values of KI samples may reflect some interference in the extraction process possibly from other oxygen sources such as formation of iodate ions. This trial demonstrates that chloride matrices are compatible with the acetone extraction method while concentrated iodine solutions are not. However, chloride effluents are incompatible with freeze drying.

An alternative approach was considered using an adaptation of the silver nitrate method (Silva, S.R. et al., 2000). Anion resins could be eluted using HCl with the subsequent effluent neutralised with silver oxide. This reaction, both lowers the salinity and acidity of the solution, making it suitable for freeze drying. Anion resins loaded with nitrate and sulphate solutions demonstrated good nitrate yields when eluted with 3 M HCl. The highest yielding elution method (101%) involved using 150 ml of acid applied to 20 ml of resin. The resin was stirred after each application and drained before beginning the next dose.

Anion resins from fieldwork in Svalbard were eluted and neutralised with silver oxide as per the method described in section 2.5.1.3 and the nitrate concentration of the effluent was analysed by ion chromatography. Unfortunately, the amount of nitrate derived from this method was inconsistent with the nitrate concentrations of meltwater samples. The samples were processed via the acetone method regardless and the product barium nitrate was analysed via mass spectrometry.

2.5.1.3 Anion resin effluent neutralisation using silver oxide

- Wash Ag_2O to remove any nitrate contaminant following the procedure of (Silva, 2000): 2 l of deionised water is added to 500 g of Ag_2O in a 4 l Erlenmeyer flask and stirred for several hours. The rinse water is decanted through a Whatman #1 filter. This process is repeated 7 times. The rinsed Ag_2O is oven dried at 50°C and stored in a dark container. The rinse water is collected and treated with an excess of NaCl to precipitate dissolved Ag as AgCl. The AgCl is filtered out through a 0.45 µm nylon filter before disposal of the rinse water. The AgCl can be regenerated to Ag_2O – see Silva (2000).
- Elute anion exchange resin with 3 x 50 ml aliquots of 3M HCl (150 ml) into a 250 ml glass beaker.

- Place glass beakers in cold water bath on magnetic stirrer. Restrict light to beaker where possible. Place a stir bar in each beaker.
- Add up to 52 g of Ag_2O slowly, ¼ teaspoon at a time, allowing heat to dissipate without producing vapour. Stir and crush Ag_2O with glass stirring rod to expose unreacted reagent until fully reacted. Product silver chloride is formed (purple colour), it should be a fine powder and any clumps must be broken up. Repeat, until HCl is neutralised – it will fizz and go cloudy in the final stages.
- Check final pH is 5.5 - 6 with pH paper
- Allow AgCl and $AgSO_4$ to precipitate and filter silver nitrate solution through Whatman # 1 papers (pre-rinsed with deionised water), retaining the liquid in a pre-weighed 250 ml nalgene bottle, wrapped in foil to prevent photo degradation of $AgNO_3$.
- Weigh the filled Nalgene bottle to calculate the volume of effluent.
- Analyse nitrate concentration of effluent via ion chromatography
- Using concentrations of original water and the concentration factor of resin, calculate the estimated volume of effluent required for 25 – 30 µmol of nitrate for the acetone extraction. Measure this volume of effluent into a Nalgene bottle (wrapped in tin foil) and freeze.
- Freeze dry the frozen effluent to powder.
- Using small amount of deionised water, dissolve $AgNO_3$ and transfer to a 50 ml centrifuge tube.
- Freeze the sample and freeze dry
- Begin the acetone extraction procedure to remove other oxygen sources e.g. residual sulphate

2.5.1.4 Nitrate $\delta^{15}N$, $\delta^{18}O$ sample preparation

Freeze dried water samples (containing 25 - 30 µmol nitrate) are prepared for isotope analysis of $\delta^{15}N$ and $\delta^{18}O$ of nitrate using the acetone method described by Huber et al. (2011). 350 µl of 1 M NaI solution are added to each sample in a 50 ml centrifuge tube and dissolved using a vortex shaker for one minute. In a fume cupboard, 20 ml of acetone is added to each tube followed by 10 ml of n-hexane. This step separates nitrates which are very soluble in acetone, from insoluble ions such as sulphate, phosphate and carbonate (Huber et al., 2011). The tubes are capped, refrigerated overnight and then centrifuged to separate solids. The nitrate bearing supernatants are pipetted into new 50 ml centrifuge tubes to which are added 750 µl if 0.1 M BaI_2 (in acetone). These are refrigerated overnight to precipitate barium nitrate and centrifuged. The supernatant is carefully decanted to waste avoiding losing any solid material and the tubes are dried open in an oven at 60°C overnight. The following day,

solids are dissolved in 240 µl of ultrapure water. 4 aliquots of this solution (60 µl) are pipetted into 4 x 6 mm silver capsules and dried in a desiccator containing silica gel for at least 4 - 5 days until completely dry. The capsules containing barium nitrate are then folded for dual isotope analysis. Samples are pyrolysed over glassy carbon at 1450°C in the pyrocube where oxygen from nitrate is converted to carbon monoxide and nitrogen is liberated as N_2 into a stream of helium which transfers gases to an Isoprime continuous flow mass spectrometer.

Samples are calibrated to international scales (AIR and VSMOW) using international standards IAEA-NO-3 ($\delta^{15}N$ = +4.7‰ $_{air\ N2}$, $\delta^{18}O$ = +25.6‰ $_{VSMOW}$) and USGS 34 ($\delta^{15}N$ = -1.8‰ $_{air\ N2}$, $\delta^{18}O$ = -27.9‰ $_{VSMOW}$). An internal standard $BaNO_3$–6 was used as a check standard. Weights of standards were adjusted to give similar peak heights of N and CO to samples.

2.5.2 Cation columns

2.5.2.1 Column Methodology

Cation exchange columns were premade using 20 ml SPE tubes which were filled with 10 ml of ion exchange resin (BIO-RAD AG 50W-X8 Resin: 100-200 mesh, hydrogen form). Resins were cleaned before use using 2 x bed volumes of 3 M HCl (Aristar) followed by 4 x bed volumes of ultrapure water as per the resin instruction manual.

During fieldwork in 2016, 10 l of 0.45 µm filtered water was filtered again through 0.2 µm cellulose nitrate filter papers. This was later dripped onto a cation resin to concentrate ammonium for isotope analysis. Ammonium concentrations are low in these meltwater samples (<20 µM), therefore the cation resins were also oversaturated. In 2017, cation columns were only prepared for Foxfonna spring and Longyearbreen meltwater where ammonium concentrations were known to be elevated, and snow samples of low ionic strength, therefore significant ammonium could be obtained without oversaturating the cation resin.

2.5.2.2 Column processing

Cation columns were eluted with 100 ml of 3 M HCl. Ammonium concentrations could not be determined using autoanalyser or ion chromatography due to the high ionic strength of the sample. Samples were instead analysed using flow injection analysis (Hall and Aller, 1992) to check the yield of ammonium from meltwater onto the resin columns and to quantify the mass of nitrogen for isotope processing. The flow injection method involves injecting a small volume

of sample into a basic stream of NaOH and Na citrate (to inhibit hydroxide precipitation) along a surface of PTFE tape. Ammonium in the sample is liberated as ammonia gas and diffuses across the PTFE membrane where it reaches a stream of HCl and dissolves as ammonium. The acidic stream passes through a conductivity meter and the ammonium concentration is calculated using the conductivity reading and ammonium standards.

Using these results it was determined that all of the effluent should be used for isotope processing. A significant amount of time was spent testing the hypobromite microdiffusion method (section 2.5.2.3.1) and the ammonia diffusion method (section 2.5.2.3.2) to prepare cation resin effluents for isotope analysis. After much testing, the latter was used to prepare these samples for isotope analysis.

2.5.2.3 Ammonium $\delta^{15}N$ sample preparation

2.5.2.3.1 Hypobromite Microdiffusion

Since ammonium concentrations in glacial meltwater are low, a method suitable for the isotope analysis of low NH_4^+ concentrations was sought. The hypobromite microdiffusion method (Risgaard-Petersen et al., 1995) requires only very small (nmol) amounts of ammonium. Ammonium is oxidised to N_2 in an exetainer with hypobromite and the isotope ratio of N_2 in the headspace is measured by mass spectrometry. This method has been used previously with ^{15}N enriched samples, however, here the method was tested for use with natural abundance samples. Ammonium sulphate standard solutions were prepared at various concentrations and put through the procedure. Unfortunately, after several trials, no signal above the background was detected during analysis on the mass spectrometer. This method was not considered further.

2.5.2.3.2 Ammonia Diffusion

The ammonium diffusion method converts aqueous ammonium into ammonium sulphate for isotope analysis. Several variations on this procedure have been published e.g. (Brooks et al., 1989; Holmes et al., 1998; Sebilo et al., 2004; Chen and Dittert, 2008; Heaton, T. H. E., 2001). In brief, the method involves volatilising ammonia in a sealed vessel by raising the solution pH. Ammonia gas is then trapped on a piece of acidified paper which is either suspended from the lid or floats on the liquid surface. The bottle may be heated or agitated to promote the diffusion of ammonia from solution onto the trap and when complete the acid trap is removed and dried for analysis via mass spectroscopy.

Initial tests in this project followed the procedure of Wynn (2004). Diffusion 'packets' were prepared by laying a strip (15 mm x 7 mm) of quartz filter (QMA) onto a 50 mm x 50 mm piece of parafilm. 40 µl of 10% H_2SO_4 is pipetted onto the paper and the packets sealed by folding the parafilm. The packets were suspended from ni-chrome wire hooks melted to the inside of schott bottle caps. An ammonium sulphate stock solution was prepared from which test solutions of varying amounts of N (1 µg – 1 mg) were made into schott bottles. Ammonium was volatilised by adding 3 ml of 9.4 N potassium hydroxide. The bottles were immediately capped and left on a heated shaker table (80°C) for up to 16 days. The diffusion packets were removed and dried in a desiccator containing an open jar of concentrated H_2SO_4 to remove any ambient ammonia from the atmosphere. The samples were then analysed using an Elementar Pyrocube elemental analyser coupled to an Isoprime continuous flow mass spectrometer.

Unfortunately, very limited N was measured. After many trials, experimenting with different temperatures, bases (MgO, KOH) packet design (including paper only), it was established that the parafilm used for the packets was likely inhibiting ammonia diffusion. Wide (47 mm) PTFE tape was found to be a much more effective casing for the acid traps. This design was used alongside the method of Sebilo et al. (2004) and resulted in the successful measurement of N.

Further tests in collaboration with NERC Isotope Geoscience Laboratory compared the effectiveness of packet position (suspended v floating), solution agitation (shaken v stirred) and mass of ammonium.

The results of these trials are displayed in the graphs below where offset is defined as the difference between the measured $\delta^{15}N$ of the diffusion sample and the true value of the ammonium sulphate. Diffusion samples were always isotopically lighter than the true value, since ^{14}N is preferentially volatilised. Floating diffusion packets gave far more precise $\delta^{15}N$ than suspended packets (Figure 2.23). All suspended packets were offset by > 2‰. Therefore only data pertaining to floating packets will be considered hereon. Stirred solutions show a slightly greater spread in offset than shaken ones, while offset is lowest when the starting mass of nitrogen > 150 µg (Figure 2.24). The standard error of the mean of $\delta^{15}N$ offset is also lowest at greater starting masses of N (Figure 2.25)

Therefore optimum parameters for the ammonium diffusion method based on these results are to ensure at least 150 µg N are in the sample, use a floating diffusion packet and place the bottles on a shaker table for the duration of the experiment. This method produces $\delta^{15}N$ values offset by -0.24 to -0.36‰ (Figure 2.26). The finalised ammonium diffusion procedure is outlined below.

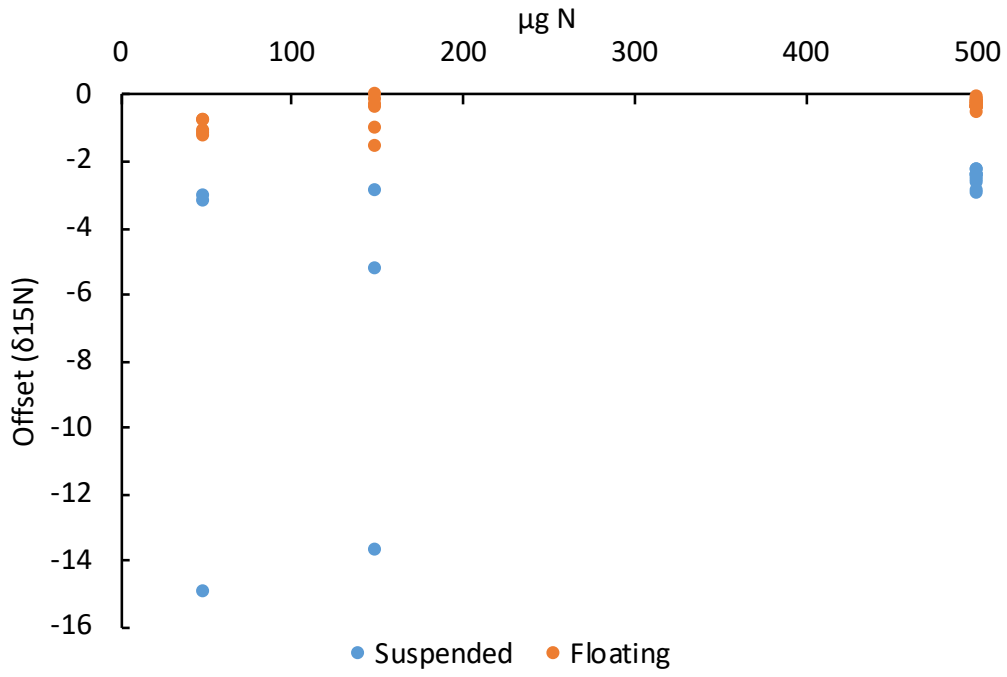

Figure 2.23 Comparison of offset between suspended and floating diffusion packets. The x axis represents the amount of N in the starting solution.

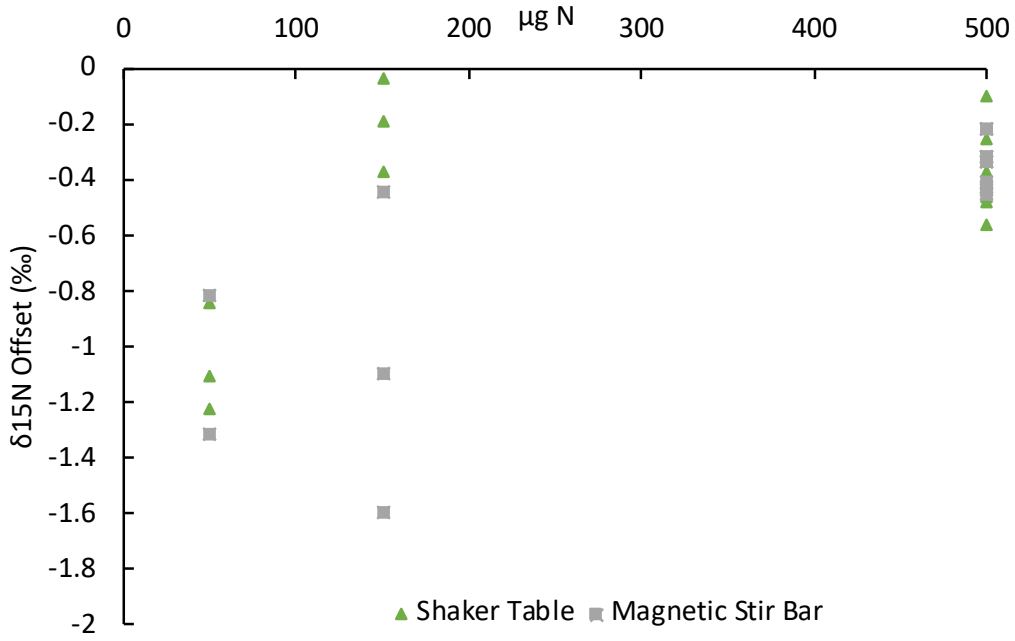

Figure 2.24 Comparison of offset between diffusion bottles that used a stir bar and those that were placed on a shaker table. The data here shows diffusion bottles using floating packets only. The x axis represents the amount of N in the starting solution.

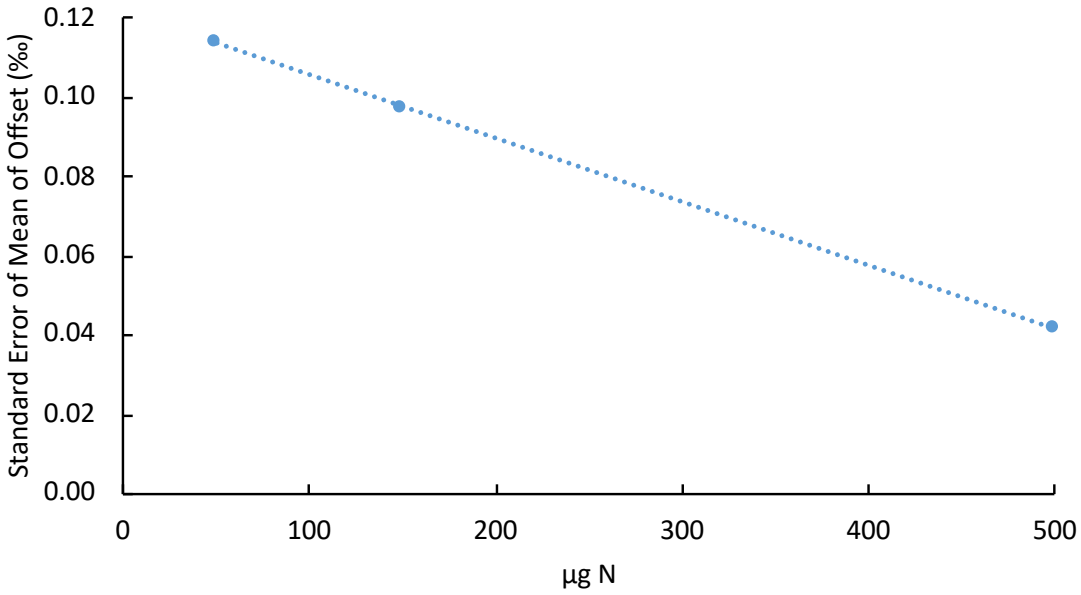

Figure 2.25 The standard error of the mean of offset of ammonia diffusion standards against starting mass of N.

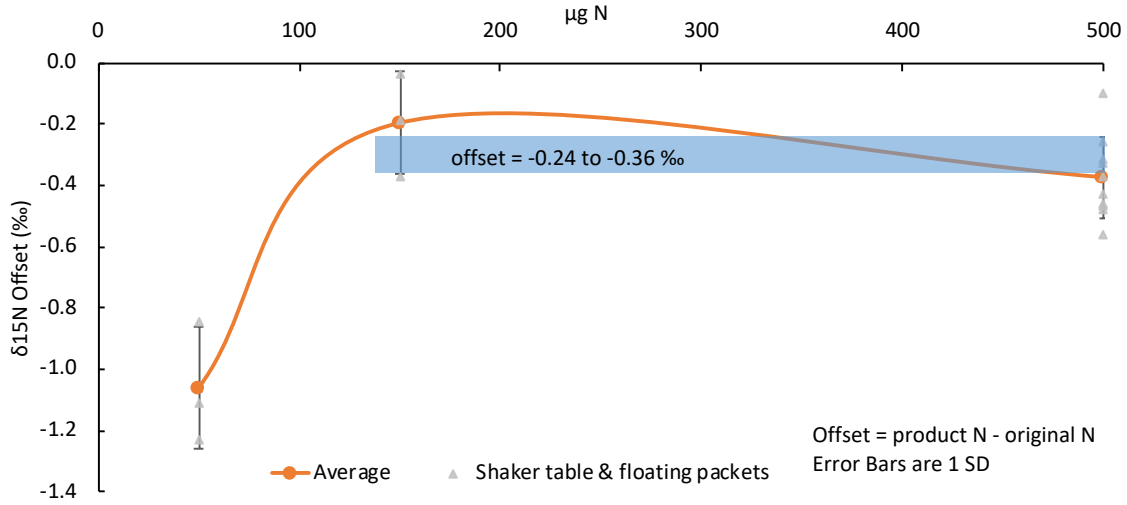

Figure 2.26 Offset of standards using finalised ammonium diffusion method (shaker table, floating packets). Repeats of standards were prepared at 3 different starting masses (50, 150, 500 µg N). The average of each starting mass is displayed in orange. The blue rectangle represents overlap of $\delta^{15}N$ offset of 150 and 500 µg standards.

Finalised ammonium diffusion method

- Cut quartz filter (QMA) paper into strips (15 mm x 5 mm). Combust at 400°C for 1h.
- Prepare working area: lay several paper towels covered with a sheet of aluminium foil cleaned with ethanol
- Take a strip of 47 mm PTFE tape and wipe with a Kim wipe tissue moistened with ultrapure water.
- Lay strip of filter paper onto cleaned PTFE tape and pipet 3 x 10 µl of 20% H_2SO_4 onto paper then create an envelope with the self-sealing tape to secure paper. Pressing down with an empty vial helps secure tape.
- Take aliquot of sample with volume sufficient to contain at least 150 µg N into wide mouth 100 ml Schott bottle.
- Add 3 g of pre baked (450°C for 4h) NaCl to solutions to avoid swelling of packets.
- Add diffusion packet to bottle so it floats on the surface of the liquid.
- Add 2 ml of 5N NaOH to the bottle, avoiding the packet.
- Immediately cap the bottle and leave on a shaking table at 110 RPM. Leave for 7 days.
- Remove bottle from shaker and retrieve packet.
- Using tweezers, remove one sheet of PTFE tape and carefully place the opened packet in a weighboat in a desiccator in the presence of concentrated H_2SO_4 to absorb any environmental ammonia until dry.
- Cut paper to appropriate size using a clean razor blade if necessary. ~100 - 150 µg N required for $\delta^{15}N$ isotope analysis.
- Fold paper using tweezers and put into silver capsules and crimp
- Place silver capsule inside tin capsule and crimp

The samples that would be processed using this method were: cation exchange resin effluents containing ammonium in glacial water from Svalbard (Chapter 7) and KCl extracts of leaching experiments (Chapter 5). A series of ammonium sulphate standards (same as used in previous tests) were processed alongside the samples. The $\delta^{15}N$ of the standards would be used to calculate any offset from true $\delta^{15}N$. The measured values of these standards are shown in Figure 2.27. Unfortunately, the offset of these is greater than in the test analysis which raises the uncertainty on sample $\delta^{15}N$. For standards containing between 80 and 160 µg N, there is an average offset of -0.71‰. Standards containing less than 80 µg N had significantly larger and more variable offsets. Therefore, data from any samples containing N < 80 µg N will be ignored while an offset of -0.71‰ will be applied to samples containing between 80 and 160 µg.

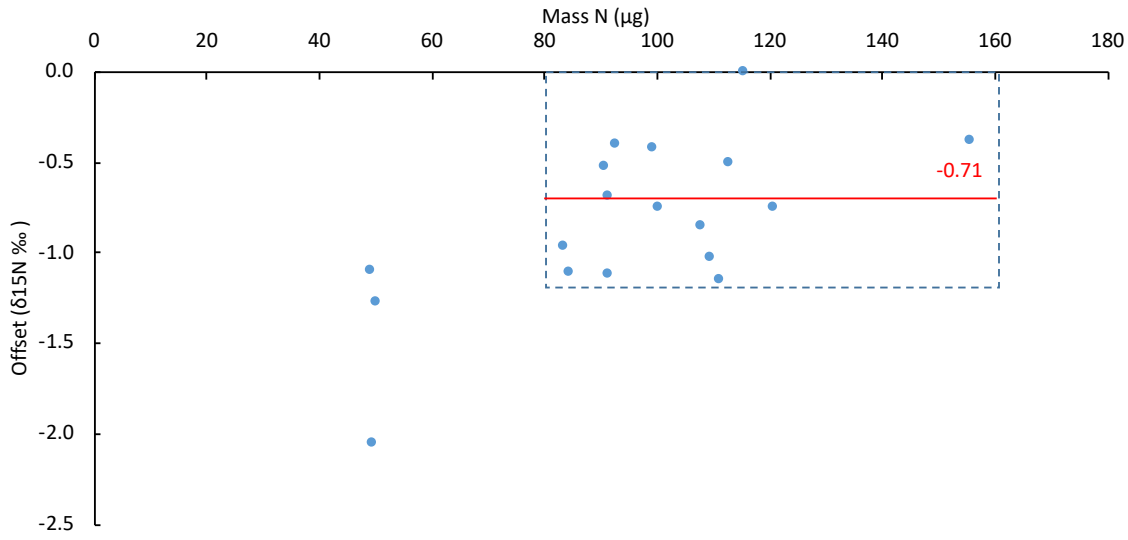

Figure 2.27 Offset of diffusion standards processed alongside samples. X axis represents N measured in standards.

2.5.3 Sulfate $\delta^{34}S$ and $\delta^{18}O$ sample preparation

Sulfate in glacial meltwater was prepared for isotope analysis of $\delta^{34}S$ and $\delta^{18}O$ through precipitation of barium sulfate ($BaSO_4$). Approximately 100 ml of filtered sample was poured into a glass beaker. The pH was adjusted to between 2.5 and 3 using HCl and the beaker placed on a hot plate at 70°C. At least 10 ml of 100 g/L $BaCl_2$ was added to each beaker and after an hour the hot plate was switched off. Beakers were left to cool slowly on the hot plate overnight. The precipitated barium sulfate was recovered on pre-weighed cellulose nitrate filter papers (0.45 µm) using vacuum filtration and dried at 110°C overnight. Dried papers were weighed and the mass of sulfur calculated by mass balance.

$\delta^{34}S$ of barium sulfate was analysed as per section 2.2.5.3.1. Duplicate aliquots (0.11 – 0.18 mg) of $BaSO_4$ weighed into 4 x 3.2 mm tin cups. Peak heights of blanks were on average 0.04 nA and no blank correction was performed. Standards were run at the same peak height as samples (1.2 – 1.7 nA). Sample $\delta^{34}S$ values were obtained from the integrated m/z 64 and 66 ions relative to those in a pulse of SO_2 reference gas (N3.0). These ratios are calibrated to the international V-CDT scale using inter-lab barium sulphate standard SWS-3B (20.3‰ $_{V\text{-}CDT}$) and chalcopyrite standard CP-1 (-4.56‰ $_{V\text{-}CDT}$).

2.5.4 H_2O $\delta^{18}O$ characterisation of meltwater

$\delta^{18}O$ H_2O isotopes of glacial meltwater samples collected in 2016 and 2017 were measured at NIGL, BGS and at the University of Liverpool respectively. Both facilities used the CO_2 equilibration method in which samples are loaded into exetainers which are evacuated to remove the atmosphere and then

flushed with CO_2 and left to equilibrate for at least 12 hours. Once the sample and headspace have achieved isotopic equilibrium, the headspace is admitted via a sample preparation module into the mass spectrometer. Samples were measured in duplicate in both facilities. At Liverpool, the samples were run against international standards USGS 46 and USGS 48. USGS 47 was also run in duplicate with each batch as a quality control with uncertainty of ± 0.056 (1 SD). At NIGL, $\delta^{18}O$ measurements were made using an Isoprime 100 mass spectrometer plus Aquaprep device. Isotope measurements used internal standards calibrated against the international standards VSMOW2 and VSLAP2. Errors are typically ± 0.05‰ for $\delta^{18}O$.

Chapter 3 Dissolution experiment technique and analysis development

3.1 Introduction

This chapter presents a chronological narrative of the method development of leaching experiments to determine nitrogen release from rocks during weathering. Experimental leaching of rocks with known nitrogen concentration will provide information on the effect of N speciation occurring during the weathering of N from rocks. This will enable a better understanding of the fate of nitrogen released from rocks by weathering, its bioavailability and its significance as a nutrient source. Numerous iterations of leaching experiments were carried out during the design and testing of the experimental setup. These pilot experiments tested variables such as the rock: water ratio, reaction time, the effect of the liquid matrix (ultrapure water v synthetic subglacial water), temperature, storage of rock samples before the experiment, oxygen availability and pre-sterilisation of rock samples. The findings of these experiments were used to design a novel weathering experiment using rocks from rock cores obtained in Svalbard to understand how geological variation can influence leachate chemistry (Chapter 5). In this chapter different nitrogen species are referred to, which are defined below:

N total = $NH_4^+{}_{(aq)}$ + $NH_4^+{}_{(ad)}$ + NO_3^-

$NH_4^+{}_{(aq)}$ = aqueous ammonium (present as the free hydrated ion in solution)

$NH_4^+{}_{(ad)}$ = adsorbed/exchangeable ammonium (adsorbed to mineral surfaces)

NO_3^- = aqueous nitrate (present as the free hydrated ion in solution)

3.2 Pilot Leach 1

An initial weathering experiment was designed to observe changes in water chemistry during rock weathering with a particular focus on nitrogen. The main aim of this experiment was to compare the effect of rock: water ratio on the solute concentration in order to scale future experiments. A balance in masses of rock and water to be used is required such that measurable N is released from rocks without requiring large, unworkable setups. Rock: water mixtures were prepared in 4 different ratios representing water-saturated sediment to turbid flows: 0.8, 0.27, 0.16 and 0.08 g/ml. Full experiment setup and methodology are explained below while experiment parameters are outlined in Table 3.1.

Table 3.1 Pilot leach 1 details

Year	2016
Temperature	4°C
Duration	16 days
Rock	Granite – quartz, albite, orthoclase, chlorite, biotite
Liquid	Synthetic subglacial water
Hypotheses	Concentration of liberated nutrients correlates with rock: water ratio

3.2.1 Method

A granite from Aberdeenshire was crushed to <100 µm (same rock and method as section 2.2.1.1).

A representative glacial water was prepared in lab (3 mmol/L $NaHCO_3$ and 125 µmol/L $CaCl_2$, 7.7 pH) and added to acid washed and autoclaved borosilicate glass schott bottles containing the crushed rock.

The bottles were sealed with silicon/PTFE septa through which a wide gauge needle was inserted to withdraw sample. An additional smaller needle was used to connect the bottle to a nitrogen gas line to maintain headspace when sample was removed. A stop tap was connected to each syringe to maintain a closed system during the experiment. Bottles were stored upright at 6°C in the dark and were shaken each day to mobilise the rock - water slurry. Samples were collected immediately at the start of the experiment, then on days 2, 5, 8 and 16. Prior to sample collection, the rock water mixture was remobilised with gentle shaking to ensure the rock: water ratio remained constant throughout the experiment (i.e. a rock-water slurry would be withdrawn). A 50ml syringe was connected to the sampling needle and the gas line connected to the small needle. Both stopcocks were opened and the syringe was filled with sample using a gentle stream of N_2 to replace the space occupied by the liquid sample (Figure 3.1).

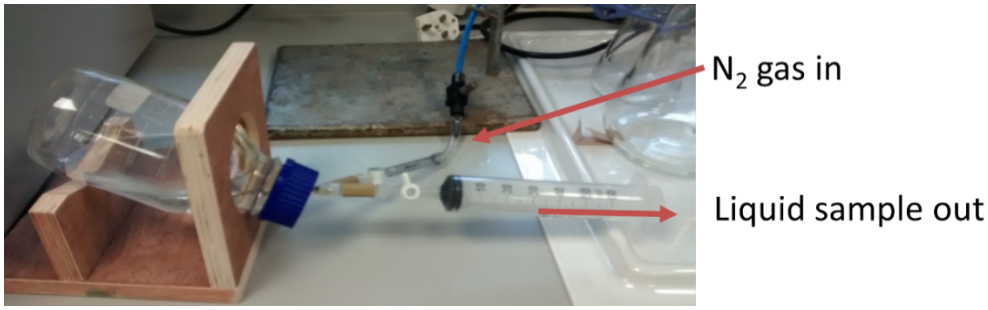

Figure 3.1 Sampling apparatus for pilot leaching experiment

Slurry samples were immediately centrifuged and filtered using 0.45 µm syringe filters (discarding the first few filtered drops to reduce the risk of any contamination from the filter entering the sample) into centrifuge tubes for aqueous chemical analysis. Nutrient analysis was carried out on an autoanalyzer; anion (carbonate, sulphate, chloride) concentrations were determined by ion chromatography; cation/metal concentrations were measured using ICP-OES. pH was measured using a Ross Ultra Combination pH electrode and a Dr Daq data logger (Pico Technology, UK).

Triplicate bottles of each slurry mix were prepared apart from 0.8g /ml samples which were prepared in duplicate. Relative standard deviation (RSD) of triplicate aliquots were < 15% (cations) and < 17% (ammonium).

3.2.2 Results

The results of the pilot leach are outlined below; data is blank corrected (sample concentration - synthetic glacial water concentration). The bulk of solute acquisition occurs immediately after rock and water are mixed which is accompanied by a coeval pH rise to 9 – 9.5. The dominant cations in all samples were sodium and potassium which have an order of magnitude higher concentrations than calcium and magnesium (Figure 3.2). Calcium concentrations decrease from the initial starting concentration throughout the experiment. Inorganic carbon is assumed to occur mostly as the carbonate anion at the experiment pH and this is the dominant anion (max 2311 µeq/L) with values remaining uniform until day 5 when they decrease. Limited sulphate was produced (< 150 µeq/L).

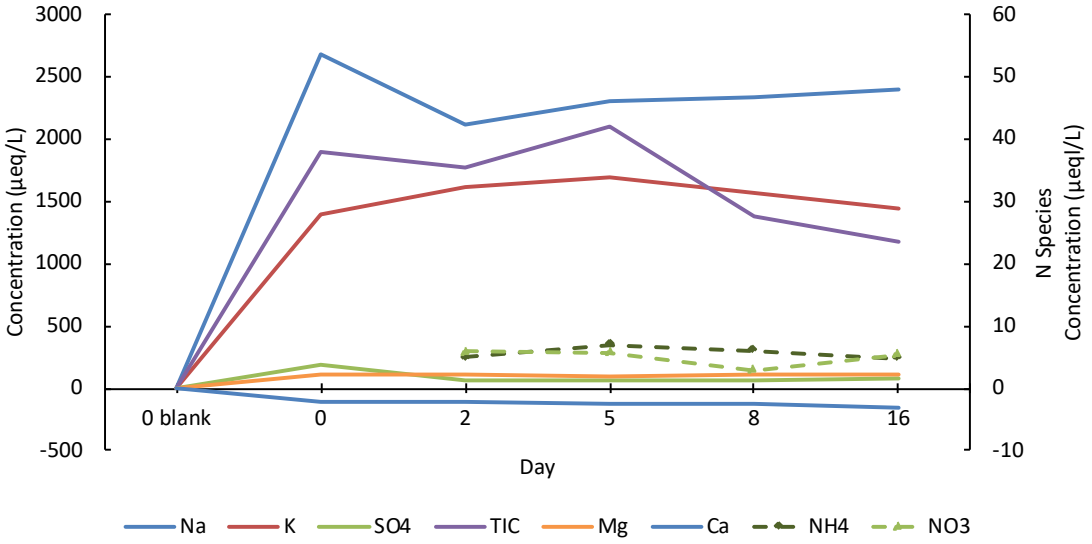

Figure 3.2 Time series of dissolved ions in the leachate of crushed granite and water solution (0.8 g/ml). Data is blank corrected i.e. 0 blank represents water before rock addition. Day 0 represents water immediately after rock addition. Nitrogen species are plotted on the secondary axis at a different scale. N.B. TIC = total inorganic carbon which is assumed to be entirely carbonate.

Nutrient concentrations are 3 orders of magnitude smaller than sodium and potassium. Ammonium concentrations are greater than nitrate in all samples except the most sediment-laden (0.8 g/ml) (Figure 3.3).

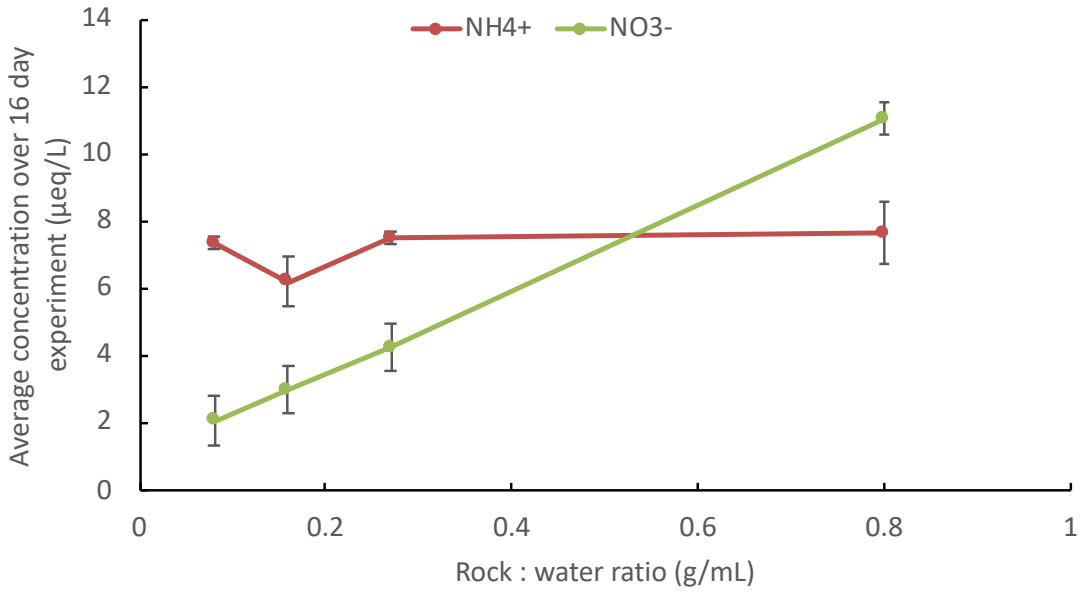

Figure 3.3 The effect of rock: water ratio on nutrient release. Vertical bars represent 1 standard deviation

3.2.3 Discussion

3.2.3.1 Weathering reactions

Solute chemistry dominated by sodium, potassium and carbonate (all > 1500 µeq/L) with other ions generally less than 200 µeq/L (values from 0.8 g/ml). Sodium is likely derived from albite weathering while potassium weathers from orthoclase and biotite. When water is added to rock, the pH immediately increases as sodium and potassium are liberated from the rock. Hydrolysis reactions, involving the interaction of silicate minerals and water dissociation, liberate cations from exposed mineral surfaces and hydroxide ions leading to elevated pH. Calcium and magnesium concentrations are low which may reflect a lack of carbonate minerals in the granite, however divalent cations such as Ca^{2+} and Mg^{2+} may exchange for monovalent cations on mineral surfaces through ion exchange reactions.

Day 0 samples showed elevated nitrate concentrations (data not shown). Such an effect has not been replicated in any subsequent experiments which suggests that this may be an artefact of experimental error. These samples were filtered using 5 µm cellulose nitrate filter papers compared with all samples on subsequent days, which were filtered using 0.45 µm PES syringe filtration which was a more time-efficient process. The cellulose nitrate filter papers used on Day 0 may have contaminated the samples with nitrate leached from the paper. Therefore Day 0 nutrient concentration data has been omitted from Figure 3.3. In light of this, ammonium is the dominant N compound leached from the granite sample in this experiment.

Nitrogen concentrations in leachate are very low (ppb) and are a minor component of dissolved species, occurring mainly as ammonium. Ammonium is likely sourced from potassium bearing minerals, where it occurs substituted for potassium. Ammonium partitions into feldspars more readily than biotite (Boyd, S.R. et al., 1993) therefore ammonium may more likely be sourced from orthoclase. In any case, the nitrogen liberated through weathering is limited by the low concentration in the rock. Nitrogen content was below the LOQ on the elemental analyser.

Nitrate is also present in solution which may represent natural low concentrations of nitrate in rock however, nitrate minerals are not thought to occur in granite. However, granites may contain nitrogen as ammonium within feldspars and micas. In addition, fluid inclusions within minerals may also contain nitrogen in various forms including N_2, NH_4^+ and NO_3^- e.g. (Voicu and Hallbauer, 2005). Nitrate has been identified in fluid inclusions in metamorphic

rocks in China (Zhang, G. et al., 2005), hydrothermal veins of the Omai gold deposit in Guyana (Voicu and Hallbauer, 2005) and the Witwatersrand Basin of South Africa (Frimmel and Hallbauer, 1999; Silver et al., 2012). Thus, the presence of nitrate in leachate from this experiment could result from the release of nitrate bearing fluid inclusions. In natural environments, ammonium is converted biologically to nitrate via nitrification. Since sterile conditions were maintained in this experiment, it is unlikely that nitrate is a product of nitrification of leached ammonium. Whether oxidation of ammonium could also occur by abiotic processes is something that was hypothesised almost 200 years ago (Graham, 1827) but has received little interest since then (Doane, 2017). Telling et al. (2015) demonstrated that glacial abrasion produces silica free radicals as mineral surfaces are sheared. As these interact with water, silica is hydrated and hydrogen gas produced. Here, we consider whether a similar process could occur through shearing of ammonium bearing minerals to produce N free radicals which could be oxidised through interaction with dissolved oxygen and/or water. Further experiments are required to determine whether this is a viable method of producing nitrate (See section 3.3).

Carbonate minerals are not present in this rock according to XRD analysis, yet carbonate is the dominant anion in solution. Inorganic C may derive from weathering of trace carbonates, however dissolution of CO_2 at the start of the experiment may provide much of the inorganic carbon in solution.

3.2.3.2 Rock: water ratio

Nitrate release increases linearly as the rock: water ratio increases. However, ammonium concentrations are uniform throughout the experiment at all ratios. Consequently, at the highest rock: water ratio (0.8 g/ml) nitrate concentrations exceed ammonium. At high pH, deprotonation of surface hydroxyl groups on oxide minerals occurs leaving surfaces negatively charged (Drever, 1997), whereas at low pH protonation occurs. The pH at which the surface charge is balanced by deprotonation and protonation is called the point of zero charge (PZC). Different minerals have different PZC values however they are commonly less than 9 (Kosmulski, 2011). Ammonium, being positively charged, can adsorb to mineral surfaces strongly when the pH of the solution is above the point of zero charge. The pH of these solutions was typically >9, hence mineral surfaces were negatively charged. Consequently, ammonium may be sequestered to mineral sites, producing the apparent ‘flat-lining’ of aqueous ammonium concentrations since aqueous ammonium concentrations are this controlled by equilibrium with surface sorbed ammonium. Conversely, negatively charged nitrate ions are repelled from mineral surfaces at pH ~9

where pH exceeds PZC. Therefore, as the ratio of rock to water increases, nitrate concentrations also increase. Future experiments will, therefore, include the measurement of adsorbed ammonium to ensure measurements are representative of nitrogen leaching processes.

3.2.4 Summary

This experiment tested the hypothesis that the concentration of liberated nutrients correlates with rock: water ratio. Here we see that this hypothesis was correct and smaller rock: water ratios produce measurable quantities of N (Figure 3.3) such that large quantities of rock and water are not necessary for these experiments. Scaled-down versions of these experiments can, therefore, be used to better understand nitrogen weathering from rocks. Future experiments will use a rock: water ratio of 0.2 g/ml in centrifuge tubes allowing larger numbers of samples to be more easily run with less sample preparation.

This experiment also highlighted that hydrolysis reactions occur immediately upon addition of water to crushed rock. Therefore, future pilot experiments can be run over short timescales.

An abiotic pathway of ammonium oxidation is also hypothesised. Shearing of minerals during glacial abrasion may produce N free radicals which may be subsequently oxidised by dissolved oxygen or reaction with water.

3.3 Pilot Leach 2

In this experiment, a revised rock leaching method is trialled where crushed rock samples are mixed with water in centrifuge tubes on a shaker table. This leach sought to refine the experiment design through:

- Better constraining the timing of nutrient release by comparing leachate immediately after water is added to rock to that sampled after an hour.
- Comparison of synthetic glacial water to ultrapure water which is a simpler matrix to prepare.
- Studying the effect of temperature on solute acquisition by comparing the results of this experiment (20°C) to pilot leach 1 (6°C).

This experiment also sought to provide insights into N cycling processes. Nitrogen adsorbed to mineral surfaces is quantified. Ammonium adsorption is significant where there is a large negatively charged surface area. The net negative charge on silica structures in clay minerals makes these particularly good absorbers of cations. Therefore, it is hypothesised that rocks containing abundant clay minerals will adsorb more ammonium than clay poor rocks.

As discussed earlier, an abiotic pathway of ammonium oxidation is considered. This will be directly tested through comparison of leachate from rock crushed under both oxic (air) and anoxic (argon) atmospheres, mixed with both oxic and deoxygenated water. It is hypothesised that shearing of minerals produces N free radicals which can react with dissolved oxygen or water to produce oxidised N compounds such as nitrate. Therefore, the degree of oxygenation of the crushing environment will influence N speciation when water interacts with the crushed rock. N free radicals produced during crushing may react with dissolved oxygen or water to produce nitrate as shown in the hypothetical chemical reactions below (Equation 3.1, Equation 3.2).

$$N\bullet + O_2 + H_2O \rightarrow NO_3^- + H^+ \; 0.5H_2$$ **Equation 3.1**

$$N\bullet + 3H_2O \rightarrow NO_3^- + 2.5H_2 + H^+$$ **Equation 3.2**

Experiment details and hypotheses are summarised in Table 3.2.

Table 3.2 Pilot leach 2 details

Year	2017
Temperature	20°C
Duration	1 hour
Rock	Granite – quartz, albite, orthoclase, chlorite, biotite Shale – quartz, albite, muscovite, chlorite, pyrite, siderite, organic macerals
Liquid	Synthetic subglacial water & ultrapure water
Hypotheses	The majority of solute is released from minerals immediately after the addition of water The effect of the water matrix is negligible upon solute release Warmer temperatures will enhance solute acquisition over the course of an experiment Adsorption of ammonium is greater in clay-rich rocks Crushing rocks creates N free radicals which react with oxygen and water in oxic environments to produce nitrate, therefore influencing nitrogen speciation in water

3.3.1 Method

Smaller scale batch weathering experiments were prepared using a rock: water ratio of 0.2 g/ml. These were carried out in 50 ml centrifuge tubes using 3g of sediment and 15 ml of water.

3 g sediment was weighed into a centrifuge tube and 15 ml of ultrapure water was added using a mechanical pipette. Capped tubes are placed on a shaker table at 110 RPM for the duration of the experiment. When sampling, tubes are removed from the shaker table and centrifuged. The plunger from a 50 ml syringe was removed and a 0.45 µm and a 0.2 µm syringe filter (SFCA) were added in tandem to the end of the syringe. The supernatant was poured into the syringe and the plunger reattached to filter the solution as aliquots into new centrifuge tube/vial for analyses. Samples were stored frozen until analysis of nutrient concentrations (autoanalyser). The pH of the filtered solution was measured using a Ross Ultra Combination pH electrode and an Orion Dual Star pH/ISE benchtop meter (both ThermoScientific, USA).

3.3.1.1 Anoxic rock crushing

In order to test the effect of anoxia on N weathering, a glove box was overfilled with argon at 10 l/min for 2 hours to generate inert and anoxic conditions. An atmospheric oxygen alarm was placed inside the chamber to monitor oxygen levels. Anoxic water was produced for the experiment by purging ultrapure water with argon for at least 1 hour. A set of weighing scales, centrifuge tubes, argon purged water, a pH meter and a shaking table were placed into the glove box prior to filling with argon.

30 g of sample, pre-crushed to mm size grains using a steel piston pestle and mortar, was transferred to the glove box along with an airtight tungsten carbide ball mill. The sediment was transferred to the ball mill under an inert atmosphere and sealed. The airtight mill was removed from the chamber and placed in a SPEX SamplePrep 8000M Mixer for 27.5 minutes. The ball mill was put back into the glove box where 3 g of anoxic crushed rock was weighed into 50 ml centrifuge tubes. 15 ml of water was added to each tube which were then capped and placed horizontally on a shaking table in the glove box at 75 RPM for 1 hour.

The tubes were then removed from the glove box and centrifuged before being returned to the glove box. The caps were removed and the supernatant was filtered and stored as above. pH was measured as described above and an exchangeable ammonium extraction was carried out on the residual sediment.

3.3.1.2 Exchangeable ammonium extraction

Ammonium adsorbed to the pre-leached sediment was extracted using the method described in Chapter 2. In this experiment 30 ml of KCl solution was added to 3 g of sediment in a 50 ml centrifuge tube.

3.3.2 Results and discussion

3.3.2.1 Reaction time

Section 3.2 suggests that most leaching occurs on the first day of rock - water interaction. Here, the chemistry of water immediately after a rock (granite) is added (time = 0) is compared to that of a 1 hour leach. Duplicate samples were prepared for time = 0, while 1 hour leach samples were prepared in triplicate. The results show highly similar values in both immediate and 1 hour samples (Figure 3.4). This implies that most of the leach occurs immediately after water is added to rock powder. The pH of ultrapure water added to crushed rock had an initial pH of 6.1 but at both t = 0 and t = 1 hour, pH had risen to 10.2 - 10.3. Rapid pH rise and solute acquisition reproduce the results of pilot leach 1 and are indicative of very rapid hydrolysis reactions.

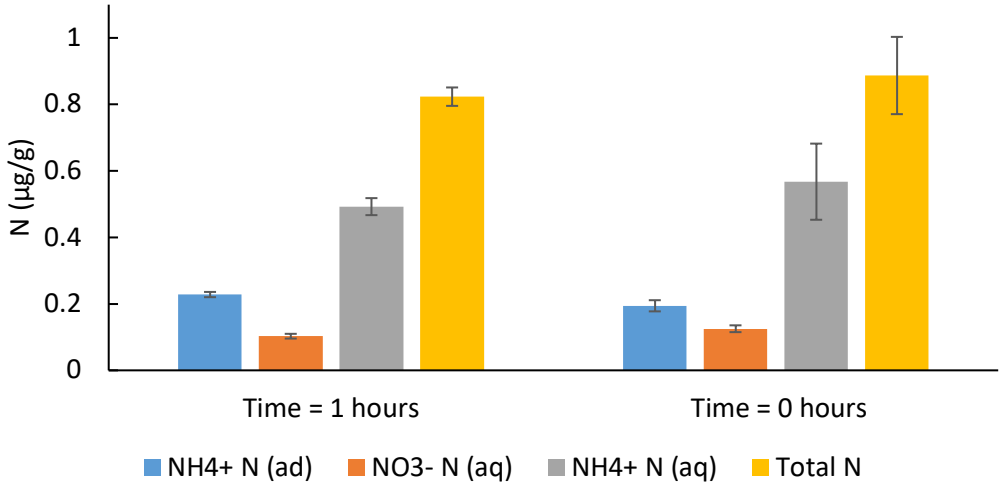

Figure 3.4 A comparison of leached N from experiments where samples are taken immediately after adding rock and after 1 hour of reaction.
Vertical bars are one standard deviation, n = 2 (t = 0 hours), n = 3 (t = 1 hours)

3.3.2.2 Liquid matrix

The effect of different liquid matrixes on leached N was also tested on crushed granite leached for one hour. There was no significant difference in nutrient concentrations between rock leached with ultrapure water and that of synthetic subglacial water (Figure 3.5). Therefore, experiment set up can be simplified to using ultrapure water with no effect on weathering.

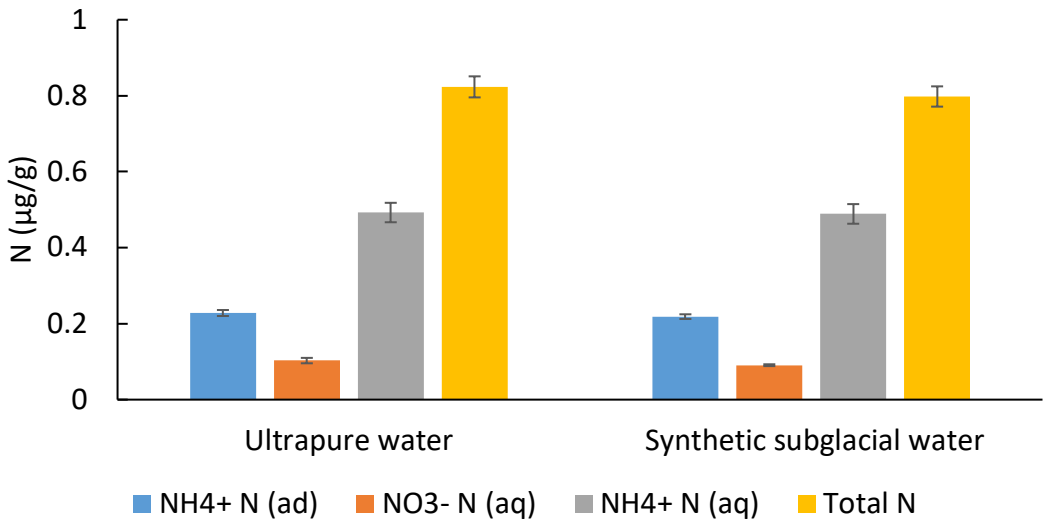

Figure 3.5 A comparison of N leached from granite with ultrapure water and synthetic subglacial water. Vertical bars represent 1 standard deviation, n = 3.

3.3.2.3 Temperature effect

Since this experiment involved weathering of rocks in an argon glove box, it was not possible to conduct this experiment in a cold room (cf pilot leach 1). Pilot leach 1 and pilot leach 2 both used the same granite sample but leaches were carried out at different temperatures. At comparable rock: water ratios and weathering duration, ammonium is the dominant N species with statistically similar NH_4^+ release at 6°C and 20°C (Figure 3.6). Therefore, warmer temperatures do not significantly increase the rate of ammonium release in these experiments.

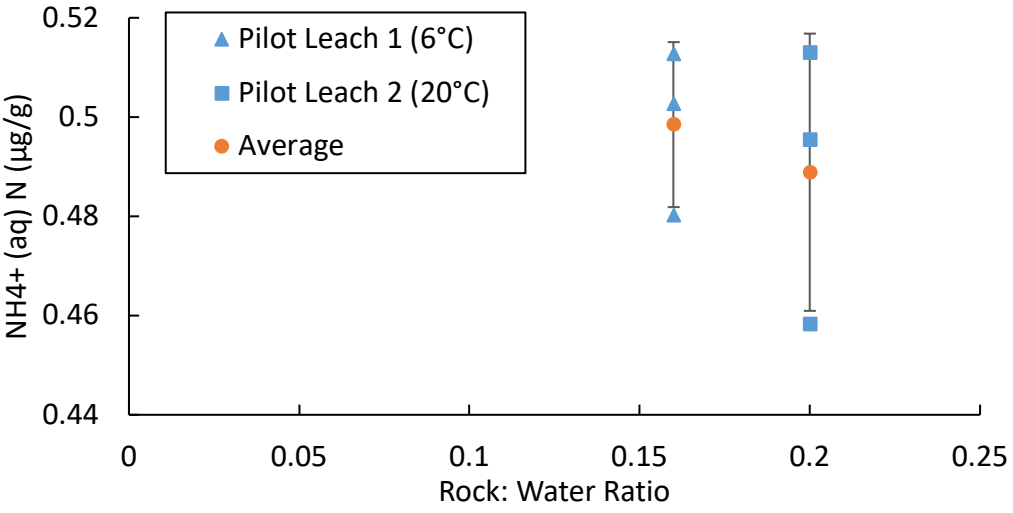

Figure 3.6 Comparison of ammonium yield from crushed granite and water leaching experiments carried out at 6°C and 20°C. Vertical bars are 1 standard deviation.

3.3.2.4 Oxygen availability

The results of the experiment to study the effect of oxygen availability on N speciation are outlined in Figure 3.7. This experiment leached 2 different rocks: a granite (as previously used) and an organic-rich shale. Rocks were subjected to an anoxic crush with anoxic water, oxic crush with anoxic water and oxic crush with oxic water.

Under all conditions, total N released from the shale is 30 times higher than the granite. In leachates of both rocks, the proportions of N species are largely unaffected by oxygen availability. N primarily occurs as adsorbed ammonium in the shale experiment, while aqueous ammonium is the dominant N species in the granite experiment. Concentrations of each N species at each degree of oxygenation are within error of each other in the shale samples. However, the oxic rock/oxic water variant of the granite experiment shows lower nitrate and aqueous ammonium concentrations than anoxic variants. Since the N released in these samples is so low this variation is hardly significant. Therefore, the availability of oxygen during crushing and leaching exerts no significant direct influence on the speciation of leached nitrogen. These results suggest that should crushing produce N free radicals, they do not react with dissolved oxygen to produce nitrate (i.e. Equation 3.1 does not proceed). However, it is not possible to say from these results whether nitrate is produced from the reaction of N free radicals with water (Equation 3.2). Nevertheless, for the purpose of experiment design, this experiment shows that the oxygenation of the crushing environment does not impact the speciation of nitrogen in water.

	Shale	Granite
Description	Sedimentary, organic rich rock	Crystalline, felsic, igneous rock
Mineralogy	Quartz, Muscovite, Chlorite, Albite, Pyrite, Siderite, Organic macerals	Quartz, Albite, Chlorite, K Feldspar, Biotite
N ppm	1336 (±36)	<LOD

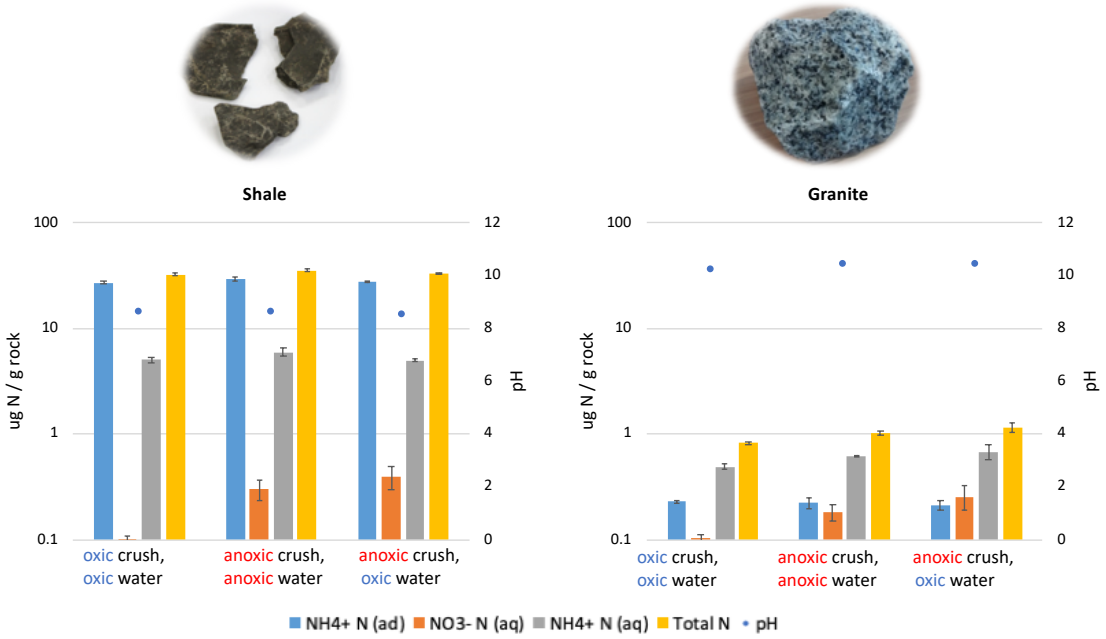

Figure 3.7 Results of a leaching experiment testing effect anoxic v oxic crushing on N speciation. Y axis (N µg/g) plotted in logarithmic scale to allow for comparison between shale and granite N yield.

3.3.2.5 Adsorption

Ammonium is the dominant N compound in both granite and shale experiments, although it is mainly adsorbed to sediment in the shale experiment whereas it occurs mainly in the aqueous form in the granite experiment (Figure 3.7). Partitioning of NH_4^+ between adsorbed and aqueous ammonium is represented by the partition coefficient, K_D, a ratio of adsorbed ammonium v mass of ammonium in solution.

$$K_D = \frac{Mass\ sorbed\ (mg/Kg)}{Mass\ in\ solution\ (mg/L)} \qquad \textbf{Equation 3.3}$$

Where K_D values are greater than 1, ammonium is mainly adsorbed to sediment, whereas values less than 1 indicate ammonium occurs mainly in the dissolved phase. K_D values derived from this experiment are displayed in Figure 3.8. When the shale was collected, it fragmented into multiple pieces. Two large pieces were crushed independently and both used in separate aliquots of this leaching experiment. Samples from these 2 pieces yield different K_D values (5.3 and 12.4), which may be accounted for by sample heterogeneity. The shale has a much higher K_D than the granite (K_D = 0.4) and can attract more ammonium to

mineral surfaces. Shales largely consist of clay minerals whereas granite mineralogy is dominated by quartz and feldspar minerals. Therefore, increased ammonium adsorption in the shale supports the hypothesis that ammonium is preferentially adsorbed to clay-rich rocks.

Abundant clay minerals in shale which have a net negative surface charge attract ammonium to mineral surfaces. With fewer clay minerals in granites, there is less electrostatic force to adsorb ammonium to sediment surfaces, therefore most ammonium remains in solution. This highlights the importance of particle-bound nitrogen measurement when assessing nutrient budgets in lab and field studies.

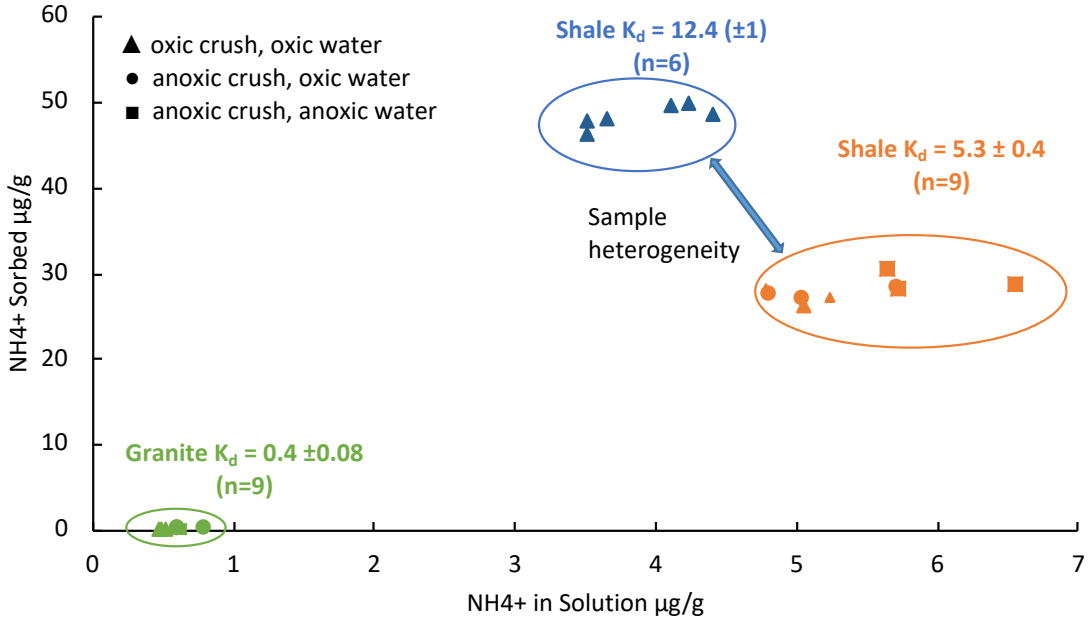

Figure 3.8 Ammonium distribution during leaching. K_D error is 1 standard deviation

pH is high in both sets of samples at 8.6 in shale and 10.4 in granite. Rapid hydrolysis reactions and a lack of acid production drive pH high, particularly in the granite experiment. As previously discussed, elevated pH associated with ion exchange reactions may also control ammonium adsorption where oxide minerals are present.

As well as influencing adsorption, pH also controls speciation of ammonium/ammonia. As pH increases, deprotonation of ammonium (aq) makes ammonia (aq) more stable and generates acidity (Figure 3.9, Equation 1.10). Ammonia (aq) forms an equilibrium with ammonia (g), therefore at higher pH, ammonia is increasingly lost from solution. At pH 10.4 in the granite experiment, assuming equilibrium is reached (temperature = 4°C), 74% of ammonium is deprotonated (Figure 3.9). Therefore, measured ammonium

liberated from the granite may only represent a small proportion of the total amount leached with the rest lost as gas from solution.

The lower pH of the shale suggests that the effect of hydrolysis reactions on pH is buffered by a source of acidity. Since the shale liberates an order of magnitude more ammonium than the granite, volatilisation of ammonia and generation of H^+ may contribute to the lower pH in the shale experiment. However, acidity may also be generated from the deprotonation of other amine groups and organic acids from sedimentary organic matter or the oxidation of sulphide minerals.

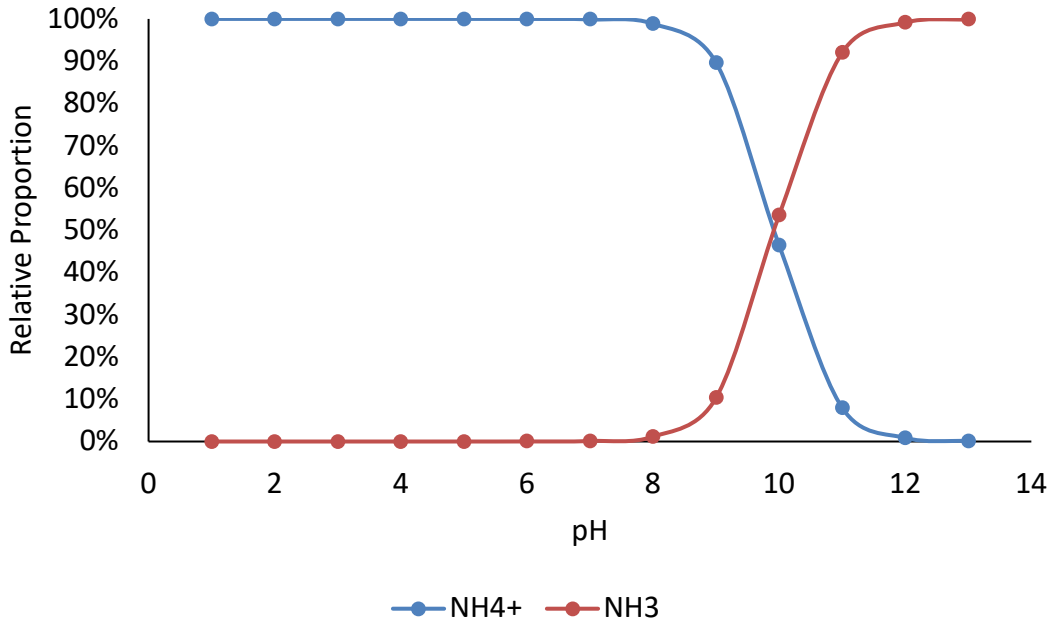

Figure 3.9 pH control on ammonium/ammonia speciation at 4°C

3.3.3 Summary

When crushed rock and water interact, ammonium is leached from rock via ion exchange reactions. Cations in solution exchange with exchangeable cations in minerals. The fate of ammonium is then controlled by sediment mineralogy and solution pH as it partitions from dissolved ammonium into adsorbed and gaseous phases.

In low ionic strength water, which has limited buffering capacity, protons in solution adsorb to mineral surfaces as cations including ammonium are liberated. The silicate framework of clay minerals has an overall negative charge and as a result ammonium is adsorbed to clay minerals, where present, by electrostatic forces. Ammonium may also be adsorbed by oxide minerals when pH exceeds their PZC. As pH increases, ammonium deprotonates to

ammonia which likely diffuses out of solution, lowering dissolved ammonium concentrations and lowering pH.

If there is a source of acidity that supplies protons faster than they can be consumed by weathering reactions, ammonium remains stable in solution. Under such conditions, pH may be close to or below the PZC of oxide minerals resulting in positive – near-neutral electrostatic surface charges. This surface charge would reduce the ammonium adsorption capacity of the sediment and thus the proportion of ammonium adsorbed.

Based on these findings, a conceptual abiotic model of nitrogen weathering is presented in Figure 3.10. As well as being easy to set up, this rock dissolution method was easy to set up, relatively quick to process, requires only a small amount of sample and allows many samples to be processed together. As such, this methodology will be adopted for all future leaching experiments including the experiment described in Chapter 5.

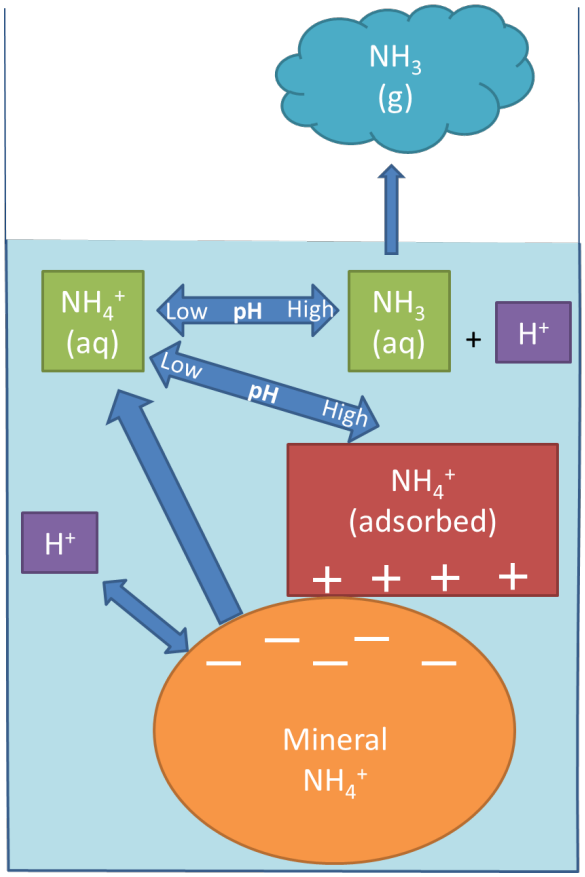

Figure 3.10 Conceptual diagram illustrating possible ammonium budget during rock dissolution. + and – indicate positive and negative net surface charge respectively

3.4 Sterilisation Test (Pilot Leach 3 and 4)

Abiotic conditions have tried to be maintained in the design of the pilot experiments discussed so far. For example, no microbes were introduced to the experiments and ultrapure water and new, sterile centrifuge tubes were used. However, the ubiquitous nature of microbes would suggest their presence on rock samples. Montross, S.N. et al. (2012) identified that microbes enhance mineral weathering rates in such experiments, therefore it is important to identify whether weathering in these experiments is affected by natural microbes on rock surfaces. Whilst all rocks in previous pilot leaches were cleaned with ultrapure water and dried, no sterilisation methods were undertaken before crushing. In this experiment, rocks subject to different sterilisation pre-treatments are leached to study any effect microbes inherent on sediment surfaces, have on nutrient release. Since ammonium is the dominant N species, aqueous ammonium is used as a proxy for nutrient release in this experiment. Rock samples collected from Svalbard bedrock cores were used in this experiment.

Table 3.3 Pilot leach 3 & 4 details

Year	2018
Temperature	20°C
Duration	1 day
Rock	Svalbard core samples
Liquid	Ultrapure water
Hypotheses	Sterilisation of rocks will reduce N release through inhibition of microbial enhancement of weathering

3.4.1 Method

Microbiota in natural sediment samples are known to accelerate weathering reactions e.g. (Montross, S.N. et al., 2012), however the biotic influence on weathering of cleaned, crushed bedrock is unknown. In order to test this, an experiment was devised to compare the leachate chemistry of sterilised abiotic sediment with a non-sterilised control. Numerous sterilisation methods are available including: wet heat, dry heat, radiation and chemical (Table 3.4). Dry and wet heating of rock samples was ruled out due to the potential for alteration of mineral surfaces. Irradiation is an effective sterilisation method, however it was not logistically possible for this project. Nitrogen free chemicals were therefore chosen as sterilising agents. The solvents ethanol and acetone were chosen to test the effect of sterilisation as these are safe to handle, accessible and inexpensive. Ethanol is more easily taken up by bacteria at a concentration of 70% and is often used in cleaning of laboratory equipment at this concentration. 70% ethanol was used in the first sterilisation experiment (pilot leach 3), however when applied to a rock sample the 30% of water in this mixture may pre-leach nutrients from the rock. Therefore, both 70% and concentrated ethanol were tested alongside acetone in Pilot Leach 4.

An experiment to test the effect of sterilisation upon the leaching of nutrients from rock was developed based on the methodology outlined in section 3.2. In this experiment however, multiple aliquots of each rock were weighed into 50 ml centrifuge tubes with each receiving a different pre-treatment followed by drying at 60°C overnight (Table 3.5). Aliquots are then leached with ultrapure water following the method in section 3.3 for 24 hours. Nitrogen in leachate was measured as aqueous ammonium on an autoanalyser.

Table 3.4 Sterilisation methods considered summarised from Sykes (1969) with additional notes from the author

Sterilisation method	Advantages	Disadvantages
Chemical sterilisation	Does not require heating which may affect rock mineralogy.	Many chemical sterilisation methods involve chemicals containing N compounds e.g. cyanide.
Gamma radiation	Does not require heating, doesn't affect mineralogy of rocks. No nitrogen compounds added.	Small penetration depth therefore very large surface area of rock flour would be required. A commercial company would need to be used; given amount of rock to be used this would be extremely costly.
Dry heat	Good for sterilising glassware.	High temperatures and longer heating times required to achieve sterilisation. Such temperatures would alter mineralogy of rocks.
Steam (Autoclave)	Moist heat is reliable and is usually the preferred method of sterilization. It uses lower temperatures than dry heat which may alter rock minerals.	Interaction of water and rock at high temperatures will likely cause weathering of the rock e.g. Kivimaki (2005)

Table 3.5 Pre-treatments used in sterilisation experiment

Aliquot	Pre-treatment	Heating
1	None	None
2	None	60°C overnight
3	Acetone	60°C overnight
4	70% ethanol	60°C overnight
5	99.8% ethanol	60°C overnight

3.4.2 Results and discussion

3.4.2.1 Pilot leach 3 - 70% ethanol

In the first leach to test sterilisation methods, it was found that rocks containing abundant TOC yielded higher N concentrations in leachate. A divergence in N yields between the control and 70% ethanol aliquots was observed, with the differences greater in higher TOC samples (Figure 3.11). The samples pre-treated with 70% ethanol show lower N yields. This may be due to inhibition of biological weathering, although the 30% of ultrapure water in the ethanol mixture may have leached N from the rock prior to the leaching experiment which was subsequently lost in vapour during drying. To clarify these results, a further experiment will compare 99% ethanol, 70% ethanol and acetone as sterilising agents.

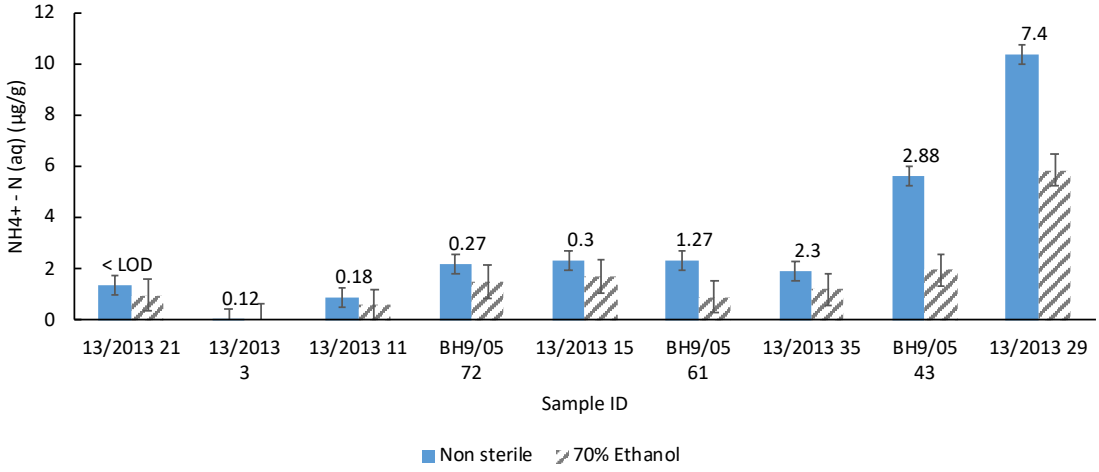

Figure 3.11 Results of pilot leach 3 using samples from Svalbard rock cores. Labels above bars indicate sample TOC (wt. %). Vertical bars are 1 standard deviation of repeat analyses of sample 13/2013 29.

3.4.2.2 Pilot leach 4 – ethanol and acetone

An additional leach experiment was carried out with acetone, 99.8% ethanol, 70% ethanol and no sterilisation as pre-treatments (Figure 3.12). Since, only a limited amount of each rock sample was originally crushed, rock samples in this experiment were a mixture of samples repeated from pilot leach 3 and some new samples. N yields of repeated samples are within error of pilot leach 3 except sample 13/2013 29. In samples with lower TOC (< 2 wt. %), N release is less than 3 µg/g. There is minimal difference in liberated nitrogen between control and sterilised aliquots, although in some cases treated aliquots liberate more N than untreated ones. These results are consistent with pilot leach 3. Samples with high TOC values (> 2 wt. %) liberated the greatest amount of

nitrogen and exhibited the greatest difference between sterilised and control samples (e.g. sample 43). Sample 29 does not reproduce the results of pilot leach 3. In this experiment, N release is ~18 µg/g and there is no significant difference between sterilised and non-sterilised experiments. This is in contrast to pilot leach 3 where sample 29 liberated 10.4 µg/g in an unsterilized experiment and 5.8 µg/g in a 70% ethanol experiment. The divergence in N release in control experiments suggests that the sample is heterogeneous. During crushing, sample 29 was split between 2 centrifuge tubes as the amount crushed would not fit in a single tube. It is possible that improper homogenisation of these samples may have led to the differences observed in this experiment. All other samples used in leaching experiments were stored in one tube only; therefore, this effect of sample heterogeneity is confined to sample 29.

Chemical pre-treatments seem to affect N release more in organic rich samples but the effect is not predictable and there is no systematic variation of N liberated with type of pre-treatment. Therefore, in these experiments, as weathering is dominated by non-microbial processes, such sterilisation is an unnecessary addition to these experiments.

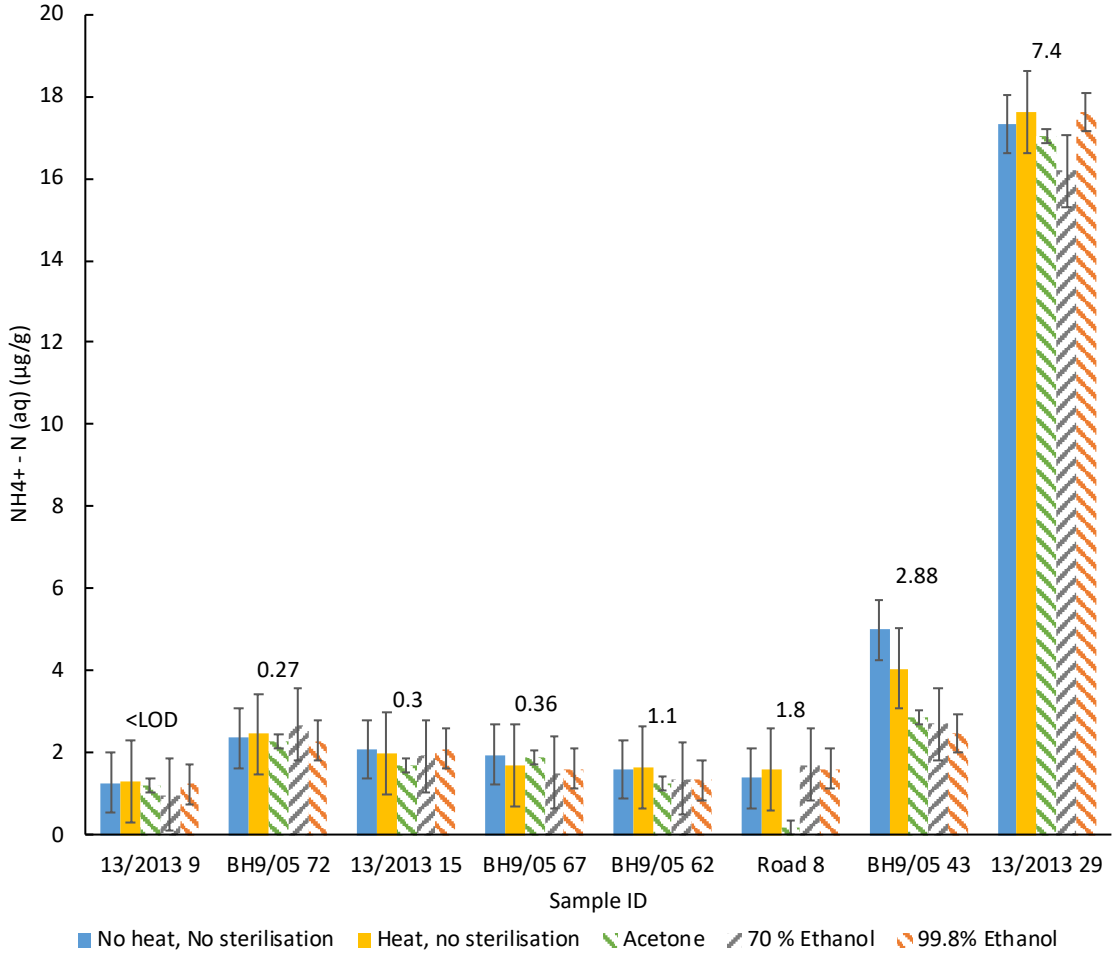

Figure 3.12 The effect of various sterilisation methods on leached ammonium (aq). Labels above bars indicate sample TOC (wt %). Vertical bars are 1 standard deviation of repeat analyses of sample BH9/05 72

3.4.3 Summary

These sterilisation experiments failed to identify a systematic relationship between N release and sterilisation method. The hypothesis that sterilisation would reduce liberated nitrogen through inhibition of microbial activity has therefore been shown to be false. As a result, sterilisation methods will not be used in the final leaching experiment.

3.5 Final Leach

Through testing numerous experiment variables, a finalised method for rock leaching experiments was devised. The method is described in 0 and is summarised in a flow diagram below (Figure 3.13). This method was used for the final leaching experiment, the results of which are detailed in Chapter 5. In that instance, the experiment was scaled up by a factor of 2 to ensure sufficient sample was available for $\delta^{15}N$ isotope analysis as described in Chapter 6. As a

result, after the water leach, weathered sediment was transferred from a 50 ml centrifuge tube to a 250 ml centrifuge tube for the KCl extraction since there was insufficient capacity in the smaller tube.

This experiment was carried out at as a time series at both 6°C and 20°C. Multiple tubes were prepared for each sample which were sacrificed, filtered and stored at each sampling interval prior to analysis. For ammonium analysis (autoanalyzer), samples were stored frozen; for anions (including nitrate) samples were stored in the fridge in 2 ml ion chromatography vials; for ICP-OES analysis of metals/cations, high purity nitric acid is added to the sample (1 % by volume) and refrigerated. N.B. nitrate was analysed by ion chromatography rather than autoanalyzer due to cadmium column degradation.

Several rock samples were leached from each geological formation to ensure the experiment was representative of variations within each unit. One sample (17A) was leached in triplicate at 20°C to evaluate reproducibility of each sample. The results of these repeats show poor reproducibility of cations with the exception of sodium (Table 3.6). Reproducibility of calcium and silica are particularly poor across replicates. Lower RSD in sodium data reflects the high concentrations of sodium (> 700 µg/g) relative to other ions. The RSD of ammonium is elevated on day 11 of the experiment (41% NH_4^+ (aq), 18% NH_4^+ (ad)) but lower on other days. These results contrast with repeat analyses of pilot leach 1 which had better reproducibility (cations RSD < 15%, ammonium RSD < 17%).

In these experiments where solute is largely controlled by ion exchange reactions, cation concentrations likely fluctuate until equilibrium between water and sediment has been reached. It is possible that these samples represent snapshots of solution chemistry before equilibrium has been reached. Variations in ion concentration may also reflect the availability or nature of ion exchange sites. This variation may be due to sample heterogeneity, if sample homogenisation was not thorough following rock crushing. However, cation concentrations from each sample show relatively consistent proportions on each day of the experiment, with overall cation (Ca^{2+}, Mg^{2+}, Na^+, K^+) concentration increasing with time through the experiment. This suggests that solute acquisition from samples is broadly predictable. Therefore, while individual sample solute concentrations may be lacking precision, comparisons between varying solute concentrations in different geological formations and at different time points can still be made.

Table 3.6 RSD of triplicate leachates of sample 17A during a 20°C leach (µg/g)

Day	Ca	Na	K	Mg	Mn	Fe	Si	NH_4^+ (aq)	NH_4^+ (ad)
1	57%	6%	14%	11%	n/a	n/a	51%	9%	4%
11	98%	3%	25%	51%	n/a	n/a	95%	41%	18%
49	60%	2%	11%	2%	2%	n/a	59%	17%	8%

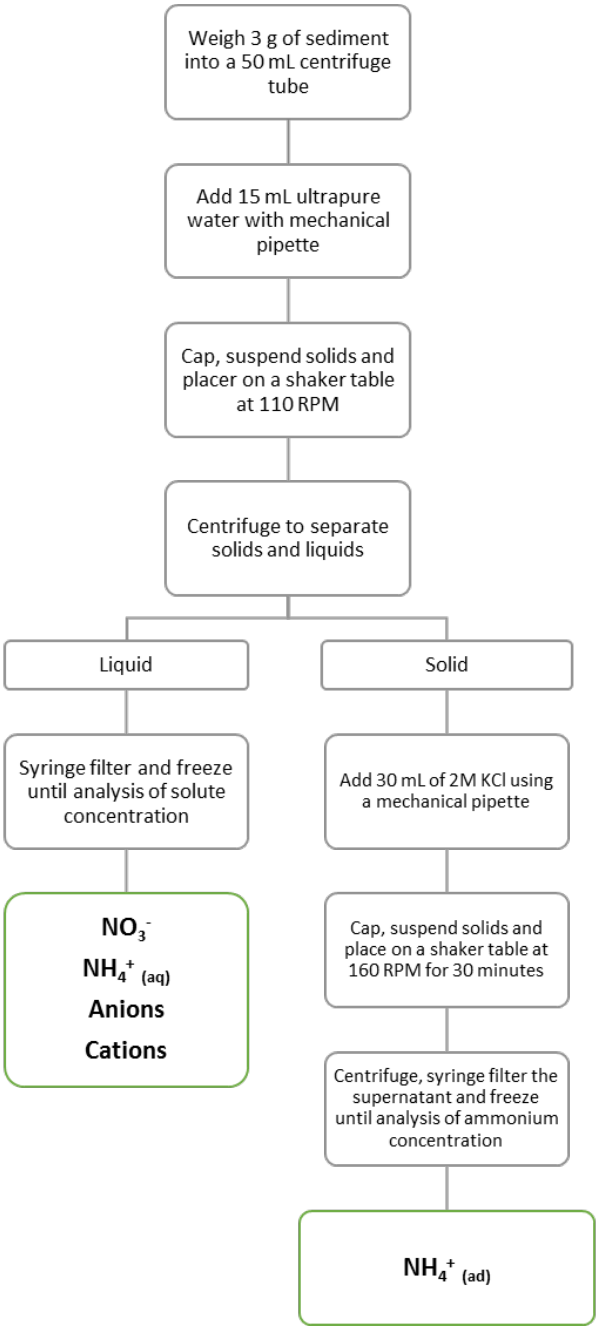

Figure 3.13 Flow diagram of finalised leaching experiment methodology. Green boxes indicate analysed ions.

Chapter 4 Characterisation of bedrock

4.1 Introduction

This chapter characterises the bedrock geology of the project study area, Adventdalen, Svalbard whose weathering processes are studied using both laboratory experiments (Chapter 4) and field work in modern glacial environments (Chapter 7). The aim of this chapter is to characterise bedrock as a solute/nutrient source and explore lithological and geochemical variations in the bedrock sequence. Geochemical analyses of rock samples were carried out to determine concentrations and partitioning of elements actively involved in biogeochemical cycles (N, C, S, Fe, Mn). Isotope analysis was also undertaken of rock nitrogen ($\delta^{15}N$) and sulphide-sulfur ($\delta^{34}S$).

4.2 Mineralogy

4.2.1 Results and Discussion

A summary of results from XRD analysis of powdered bedrock samples is provided in Table 4.1.

The bedrock sequence in the study area was found to consist of clastic sedimentary units comprised largely of quartz, potassium feldspar, plagioclase feldspar, mica and clay minerals (chlorite and kaolinite). Mica group minerals included, amongst others, muscovite, biotite, illite and glauconite. However, it was not possible to differentiate between mica group minerals on XRD traces. Quantitative XRD analysis undertaken by Schlegel et al. (2013) of bulk rock and clay mineral separates from VMG show micas are accompanied by illite and glauconite. This study also revealed that illite is the dominant clay mineral in VMG rocks, apart from in the Grumantbyen Fm, where chlorite is the major clay mineral. Results presented here show kaolinite in Firkanten Todalen Mb samples, which disagrees with Schlegel et al. (2013). Further, Dypvik et al. (2011) showed that kaolinite appears in Eocene age rocks with elevated kaolinite occurring in the PETM interval of the Frysjaodden Fm (due to enhanced continental weathering under a warmer climate). Rocks from the Grumantbyen Fm are often green in colour associated with the mineral glauconite. Glauconite was found in samples of all formations of the Van Mijenfjorden Group in thin section as an accessory mineral (Schlegel et al., 2013).

The carbonate content of almost all rocks was very low (average of both cores = 0.67 wt. %) hence the absence of calcite in most XRD traces. This is consistent with Nagy et al. (2013) who report that the deltaic/marine depositional environment had low salinity due to freshwater input. Some sedimentary layers have Total Inorganic Carbon (TIC) contents of up to 5.6 wt. % where diagenetic siderite is present. Siderite is associated with depositional environments containing brackish/fresh water where iron, derived from continental weathering, is enriched relative to calcium. Iron was also present as pyrite in the XRD traces of Firkanten (Todalen Mb) shales LG 4E and 13/2013 49.

Table 4.1 Mineralogy of bedrock samples collected in field and from cores (overleaf) Coloured squares indicate the presence of mineral in sample as identified in XRD traces

Sample ID	Formation	Rock Description	Minerals									
			Quartz	Feldspar		Oxides	Carbonates		Clays			Sulphide
				Microcline	Albite	Hematite	Siderite	Calcite	Mica Group	Kaolinite	Chlorite	Pyrite
			Si O2	K Al Si3 O8	Na Al Si3 O8	Fe2 O3	Fe C O3	Ca C O3		Al2 Si2 O5 (OH)4	(Mg,Fe)6 (Si, Al)4 O10 (OH)8	Fe S2
BH9/05 72	Aspelintoppen	Light coloured shale										
LG 3A	Battfjellet	Fine-medium grained laminated sandstone										
BH9/05 62	Frysjaodden	Silty shale containing siderite										
BH9/05 56		Siderite rich claystone										
LG 1a	Grumantbyen	Fine grained green, glauconite sandstone containing dropstones (small - large pebbles). Massive and bioturbated										
LG 2a	Basilika	Massive dark grey fine sandstone and concretions, bioturbated										
LG 1c	Firkanten - Endalen	Medium-coarse massive blue-grey sandstone with coal fragments. Weathers buff yellow colour and contains fine sand layers within unit (Longgeo1d)										
13/2013 23												
LG 4B	Firkanten - Todalen	wavy laminated grey siltsone with dark & light grey zonation. Sulphorous smell when broken apart - organic rich?										
13/2013 29		Dark grey parellel -sub parallel laminated siltstone containing visible pyrite and coalified plant remains.										
LG 4E		Shale containing sulphide minerals dispersed in matrix										
Moy 1	Carolinefjellet	Thin partings/mud drapes within ripples of fine sandstone, bioturbation, burrows										
Moy 3		Sandstone with siderite cemented layers parallel to wavy sed layers										
Moy 6-2		Black siltstone with thin bands of fine light sand. Coarser bands weather more extensively (Fe oxides). Heavily cemented in lenses and cementation also forms veins. Mud drapes and coalified pieces										

4.3 Chemical Analyses

Bedrock samples collected from outcrops in glacial valleys in the study area as well as core samples were analysed for various geochemical properties as outlined in chapter 2. Geochemical data of these analyses are presented in this section in diagrams against depth of core and in Appendix A. Equivalent core depths are estimated for samples collected from outcrop, these samples are plotted as a separate series in each diagram for clarity. A summary figure of bedrock geochemistry is provided in Appendix D.

4.3.1 Total Organic Carbon

4.3.1.1 Results

Total organic carbon (TOC) varied significantly throughout the rock sequence with maximum values (8 wt. %) occurring in the Todalen member of the Firkanten Fm (Appendix D). Prior to the Firkanten Fm, TOC levels were typically ~1 wt. %. Yet following this, TOC falls to <1 wt. % in the Basilka and Grumantbyen Fms before rising to a uniform value of ~1 wt. % in the Frysjaodden Fm. TOC was also elevated in the Aspelintoppen Fm (0.27 wt. % - 2.75 wt. %). Both core and outcrop samples have TOC values in agreement with one another. Yet TOC values were lower in outcrop Carolinefjellet samples. However, since there was only one Carolinefjellet Fm core sample, it is not possible to say whether there is a significant difference between core and outcrop samples.

4.3.1.2 Discussion

Very high TOC values in the Firkanten and Aspelintoppen Fms, are associated with coal seams, formed in terrestrial bogs. TOC values in these formations are ‘spiky’ since the coal seams are not evenly distributed throughout the rock unit. This is likely due to variations in global sea level controlling inundation of terrestrial surfaces.

Elevated TOC in the Frysjaodden Fm is not associated with coals but reflects the lithology of black shale which typically have higher organic carbon contents. The preservation of organic carbon in these rocks reflects the onset of anoxia in the depositional environment. The supply of dissolved oxygen could not keep up with the supply of organic material whose oxidation consumes oxygen. Maximum TOC in the Frysjaodden Fm is 2.88 wt. % (sample 43, 537 m). This stratigraphic depth is 3 m below a major faunal turnover during the PETM (Nagy et al., 2013). Decreasing faunal diversity, lack of bioturbation and lamination are observed in the sequence leading up to the PETM indicative of hypoxic conditions (Nagy et al., 2013).

Low values of TOC in the Grumantbyen and Battfjellet Fms likely reflect the shallower more oxygenated waters of their depositional environments which would have promoted organic matter degradation prior to lithification.

4.3.2 Nitrogen

4.3.2.1 Svalbard bedrock bulk N content

4.3.2.1.1 Results

Bedrock nitrogen varied throughout the samples collected from core and outcrop by 2 orders of magnitude from a minimum of 0.007 wt. % (68 ppm, Firkanten Endalen Mb) to a maximum of 0.21 wt. % (2061 ppm, Firkanten Todalen Mb). The variation of nitrogen through the sedimentary succession is described below, with average formation values calculated from core samples only unless specified.

In core 13/2013, there was only one sample from the lowermost Carolinefjellet formation, which contained 0.1 wt. % N. The average of all core and outcrop samples from this unit was 0.05 wt. %. N concentrations increase in the lower Todalen member (average 0.11 wt. %) of the Firkanten Fm before decreasing in the Endalen Mb (average 0.02 wt. %). Both the minimum and maximum N values of the entire sequence were found in the Firkanten Fm, revealing how variable nitrogen concentrations were in the lower part of the sequence. Above the Firkanten Fm, N concentrations initially increased in the Basilika Fm (average 0.4 wt. %) before decreasing upwards into the Grumantbyen Fm (average 0.02 wt. %). There was a sharp increase in N across the boundary of the Frysjaodden Fm (average 0.12 wt. %). N is fairly uniform within the Frysjaodden Fm although it decreased in the top 20% to 0.08 wt. %. Outcrop samples in the lower Frysjaodden Fm had less than half of the nitrogen content of equivalent depth core samples. These outcrop samples were a sandstone unit believed to be the Hollenderdalen Fm. N concentrations at all other stratigraphic levels were broadly consistent in both core and outcrop samples. The overlying sandstones of the Battfjellet Fm had a lower N average of 0.04 wt. %. The uppermost Aspelintoppen Fm had a slightly higher average of 0.05 wt. % but with a wider range of values (0.2 to 0.1 wt. %).

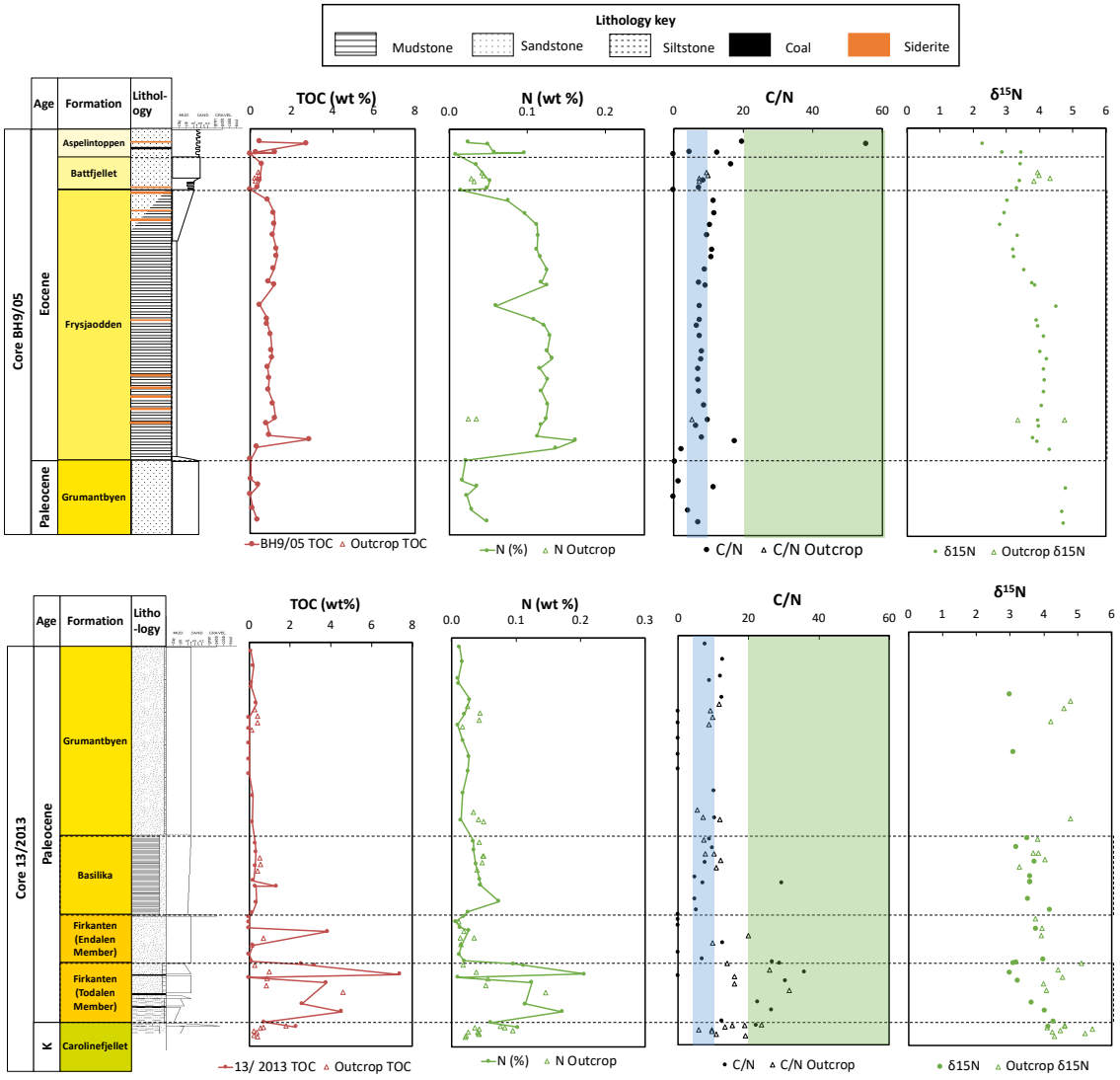

Figure 4.1 Bedrock carbon and nitrogen geochemistry. Blue rectangle on C/N plot represents C/N values of 4 - 10 (marine organic source) and green rectangle represents values > 20 (terrestrial organic source)

4.3.2.1.2 Discussion

N covaries with TOC in both cores 13/2013 and BH9/05. Rocks associated with coal seams in the Firkanten Fm and Aspelintoppen Fm exhibit elevated nitrogen concentrations > 0.1 wt. %. Whilst maximum nitrogen concentrations are measured in the heterogeneous Firkanten Fm Todalen Mb, average N concentrations are higher in the more uniform Frysjaodden Fm (0.12 wt. %). The Firkanten Fm has much more carbon relative to the Fryjaodden Fm as indicated by their C/N ratios (Figure 4.1).

Bedrock nitrogen is also dependent upon lithology since it is enriched in finer grained rocks containing abundant clay minerals such as the Todalen Member and Frysjaodden Fm. Since clays are able to fix ammonium within their mineral

lattice, an abundance of clay minerals will promote N retention within sediments during burial and diagenesis. Illite clay minerals are especially accommodating of ammonium since potassium occupies interlay sites within the clay. Ammonium easily substitutes for potassium in illites due to their similar ionic radius. Illite is the dominant clay found within rocks of the VMG (Schlegel et al., 2013) therefore where clay minerals are present, there is a greater retention of nitrogen in bedrock.

4.3.2.2 Svalbard bedrock $\delta^{15}N$

4.3.2.2.1 Results

A subset of rock samples collected in Svalbard was chosen to study the partitioning of nitrogen isotopes between organic and inorganic phases within the glacial catchments. High organic samples were targeted as differences in organic and inorganic $\delta^{15}N$ would be more easily observed. Therefore, samples containing elevated TOC were chosen as they likely had higher organic nitrogen.

The majority of nitrogen in these rocks was inorganic N (51 - 86% of bulk N), with organic N greatest in samples from the Firkanten Fm (up to 49% of bulk N). Inorganic N was proportional to organic N with most samples having a 3:1 ratio (Figure 4.2). Inorganic N was generally either within error of or isotopically heavier than organic N (Figure 4.3).

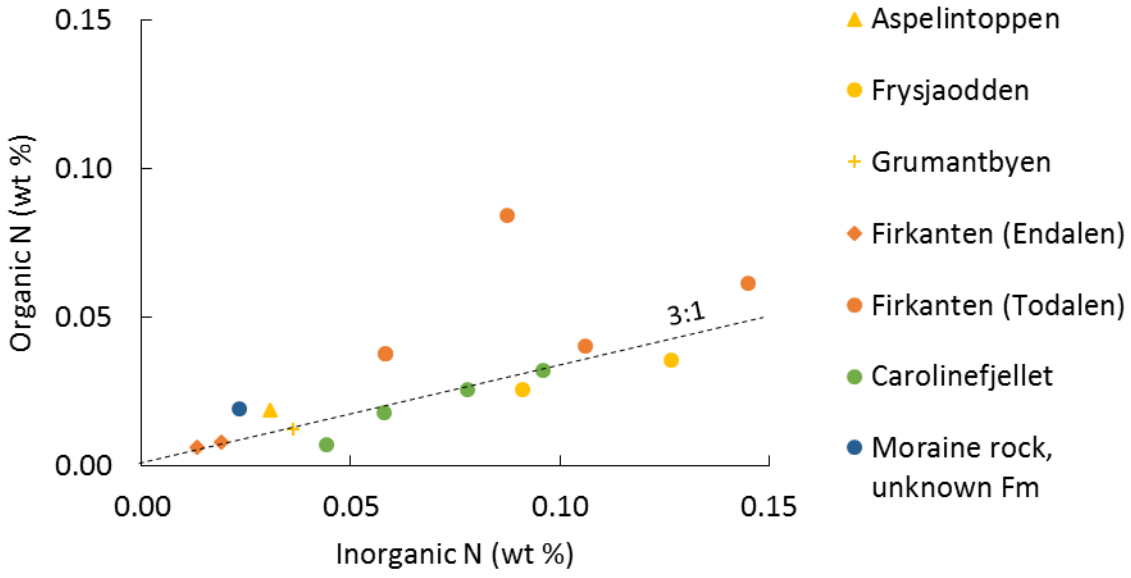

Figure 4.2 Inorganic N v Organic N in selected rocks Legend indicates geological formation of each sample

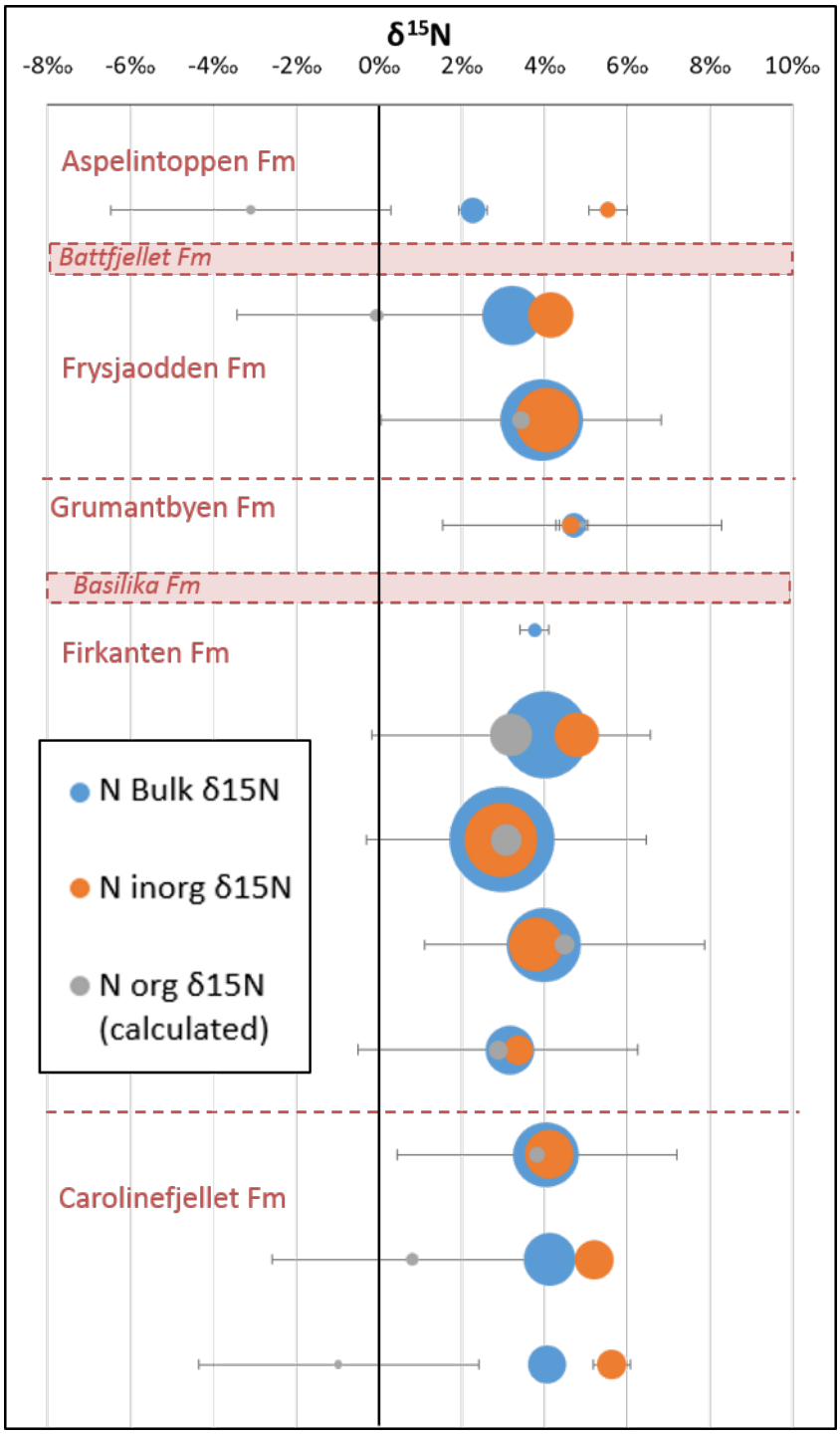

Figure 4.3 $\delta^{15}N$ Isotope values of bedrock samples from Van Mijenfjorden Group rocks. Vertical axis represents relative stratigraphic position (not to scale). Size of bubbles is relative to wt. % N. Horizontal bars represent one standard deviation and are not shown where smaller than bubbles. Organic N bars represent the propagated error (Eq 2.2) of 1 standard deviation on triplicate measurements of a representative sample. Dashed red lines indicate geological boundaries. Red boxes indicate geological formations not represented by data.

4.3.2.2.2 Discussion

Whilst inorganic N was the dominant form of N in the subsamples, bulk N correlated with TOC (Figure 4.1). This suggests that inorganic N may have been derived from an organic source which has been mineralised and incorporated into clay minerals via adsorption during diagenesis. N concentrations were elevated in geological units containing abundant clay minerals, whose adsorption capacities are able to scavenge ammonium and ultimately incorporate it into clay interlayers.

The similarity in isotope values of inorganic and organic N, supports an organic nitrogen source. Isotopic fractionation during adsorption of N may have caused a shift towards heavier values in the inorganic phase although this is reported to have a minimal effect (Williams, L.B. et al., 1995).

The average $\delta^{15}N$ value of bulk N in bedrock cores was 3.68‰ (Figure 4.1) which is consistent with other studies (Cui et al., 2011; Riber, 2009) and suggests a terrestrial nitrogen origin (see Section 2.2.2.2). $\delta^{15}N$ approaches 3‰ in the Todalen member of the Firkanten Fm, upper Frysjaodden Fm, and Aspelintoppen Fm, which may represent an increase of terrestrial derived nitrogen.

The C/N ratio is also diagnostic of organic nitrogen sources, such that values between 4 and 10 are typical of marine algae, whereas terrestrial vascular plants have C/N values greater than 20 (Meyers and Doose, 1999). The divergence in C/N values is due to a lack of cellulose (which has a high C/N ratio) in algae, which make up much of marine plant biomass, and it's abundance in vascular plants (Meyers and Doose, 1999). The C/N ratio in the Firkanten and Aspelintoppen formations was generally greater than 20, indicating a terrestrial source of nitrogen (Figure 4.1). This is consistent with the presence of coal seams in these units, which formed from the deposits of swampy terrestrial environments. Intermediate C/N values greater than 10 in the Battfjellet, Aspelintoppen and upper Frysjaodden Fm correspond with negative shifts in $\delta^{15}N$. These palaeoenvironments were all part of a marine regression sequence and therefore may represent a mixed marine/terrestrial source of organics. The C/N ratio could also be enhanced by mineralisation/degradation of organic nitrogen in a shallower, more oxygenated environment. The other formations have C/N values within the marine range which is consistent with sedimentological observations (Chapter 2). These units were deposited in more distal prodelta environments which is consistent with a marine nitrogen source.

4.3.3 Iron and Manganese

A sequential extraction for iron (Fe) and manganese (Mn) bound in different minerals was carried out on samples from cores 13/2013 and BH9/05 and bedrock from outcrop. The minerals extracted in this method include easily reduceable oxides and carbonates. A subset of samples was used to extract iron sulphide minerals (pyrite), the results of which are discussed separately (Section 4.3.4).

4.3.3.1 Results

Most of the rock samples contain iron principally associated with carbonate (NaAc extractable) (Figure 4.4). Easily reducible iron (NaD extractable) and ammonium oxalate extractable iron (e.g. magnetite) were the dominant form of iron in a smaller number of samples. Older rocks (Carolinefjellet – Basilika), showed heterogeneity in iron species with iron occurring in sulphide, carbonate and oxide minerals. A greater proportion of ammonium oxalate associated iron was found in Paleocene age rocks with greatest amounts in the uppermost Grumantbyen Fm, where on average 59% of Fe was extracted with ammonium oxalate. Non sulphide iron concentrations increased up sequence from < 1 wt.% in Carolinefjellet/Firkanten Member to ~ 2 - 3 wt. % in Frysjaodden - Aspelintoppen Fms. This steady rise in background iron was punctuated by iron rich units of up to 20 wt. % Fe often associated with siderite layers. Younger Eocene rocks (Frysjaodden - Aspelintoppen) were much more homogeneous, with most iron attributed to carbonate (Figure 4.5). For example, on average 81%, 79% and 75% of the Fe in Frysjaodden, Battfjellet and Aspelintoppen Fm samples, respectively, was extracted with sodium acetate.

Manganese concentrations were highest in the Frysjaodden Fm (maximum 0.5 wt. %), occurring almost entirely in carbonate phases (Figure 4.5). In younger Eocene rocks, Mn concentrations are generally > 0.02 wt. %, covary with Fe and show similar speciation. By contrast, in Palaeocene rocks, Mn concentrations did not show the same covariation with Fe, nor the same speciation. For example, Mn peaks occurred in samples with no associated peak in iron concentration. Therefore, there may be some Mn minerals or Mn rich endmembers of Fe/Mn minerals within these samples e.g. rhodocrosite ($MnCO_3$) and ankerite ($Ca(Fe,Mg,Mn)(CO_3)_2$.

Table 4.2 Oxidation states of Fe and Mn in different minerals

Mineral	Fe	Mn	Form of Fe/Mn
Carbonate	2+	2+	Reduced
Magnetite	2+/3+	2+/3+	Reduced/Oxidised
Oxide	3+	4+/3+	Oxidised

Different minerals contain iron and manganese in different REDOX states. Table 4.2 outlines the different REDOX states of Fe and Mn in the minerals relevant to the iron/manganese speciation method. Since iron and manganese in Eocene samples are predominantly associated with the sodium acetate extraction, the majority of non-sulphide iron and manganese occurs in reduced forms (Figure 4.4). Conversely, there are approximately equal proportions of reduced and oxidised forms of non-sulphide iron in Paleocene rocks.

4.3.3.2 Discussion

Iron/manganese mineralogy shifts from a mixture of carbonates and oxides found in Paleocene age rocks to dominantly carbonate minerals in Eocene age rocks. This is accompanied by an increase in TIC to 2.2 wt. % in the lower Frysjaodden Fm. The onset of more distal marine like conditions would have increased DIC availability while iron would have remained in its reduced form in deeper and more suboxic waters. The presence of siderite in these rocks indicates that a local source of continental weathering was still delivering iron to the ocean. Despite being deposited in a marine environment, TIC concentrations are low, yet the sea at that time is known to have had low salinity (Nagy et al., 2013).

After the initial increase in TIC in the Frysjaodden Fm, there is a sudden decrease of TIC and iron/manganese carbonates. The timing of this is coincident with the PETM. This global warming event was caused by a large release of carbon to the ocean/atmosphere, resulting in ocean acidification and the dissolution of deep sea carbonates (Zachos et al., 2005), thus inhibiting carbonate formation.

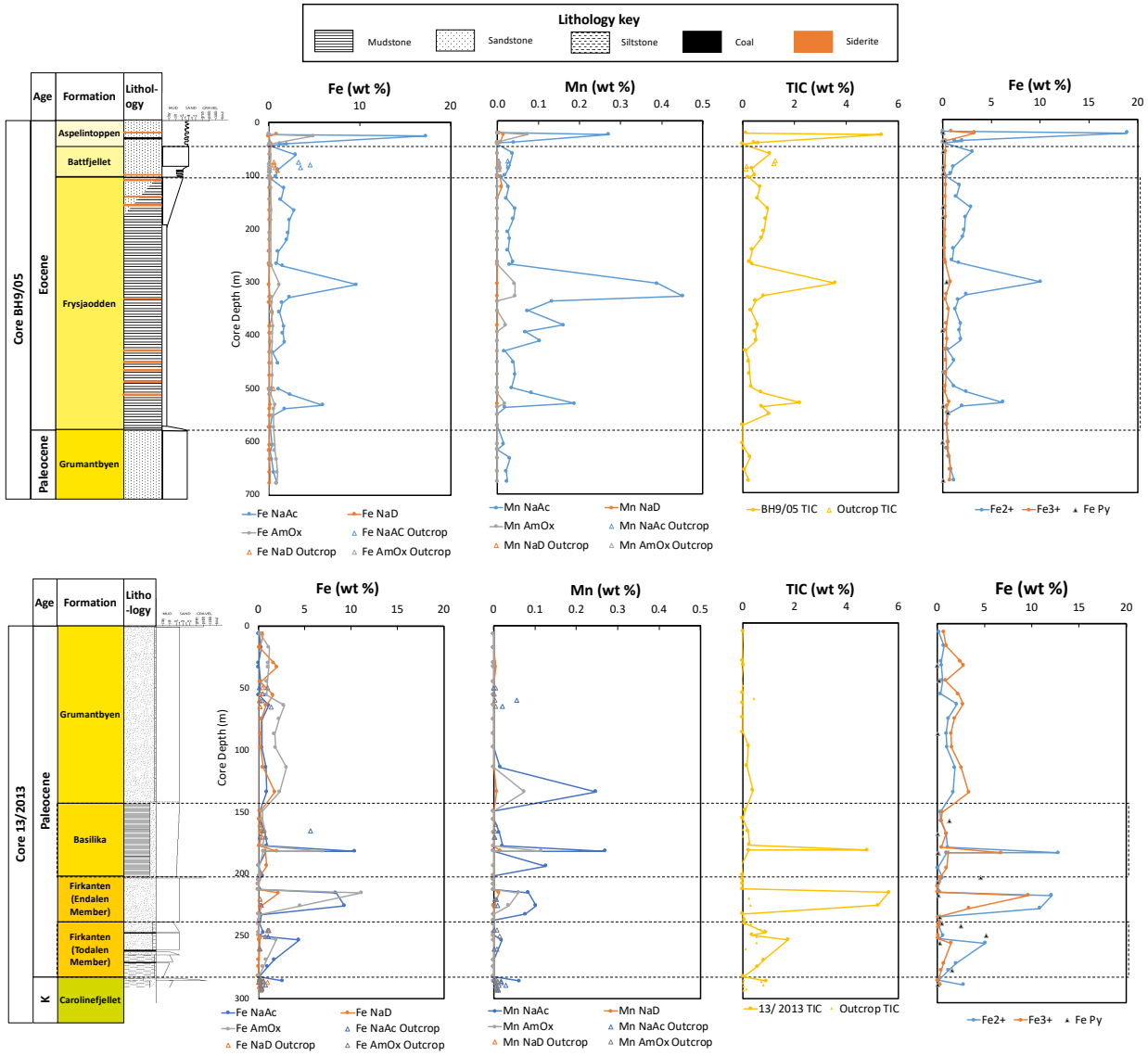

Figure 4.4 Fe and Mn geochemical data of core and outcrop samples. From left to right: iron speciation, manganese speciation, TIC, reduced v oxidised iron species excluding Fe (pyrite) which is plotted separately where data is available (black triangles)

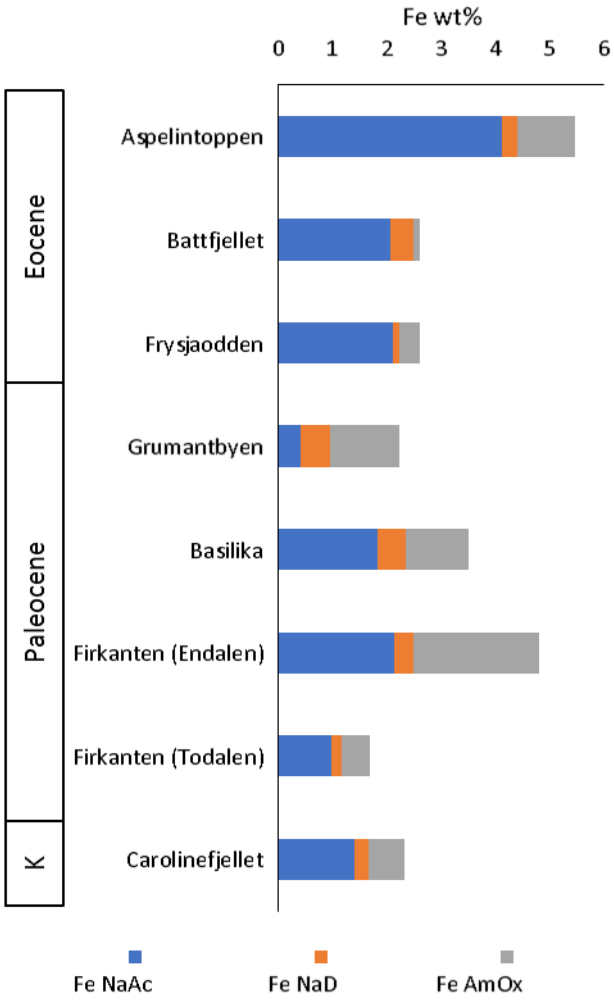

Figure 4.5 Average Fe compositions of each formation excluding pyrite bound iron

4.3.4 Sulphur and sulphide - iron

In this section, results of bulk sulphur and sulphide sulphur analysis are discussed. Bulk sulphur was analysed using LECO while Pyrite bound sulphur (iron sulphide) was extracted as per Chapter 2. Mass of pyrite iron was calculated assuming all extracted sulphide was derived from pyrite.

4.3.4.1 Results

Bulk sulphur and sulphur isotope data of pyrite extracted from bedrock are displayed in Figure 4.7 and Table 4.3. In the same table are isotope data of mm size pyrite crystals scraped from a sandstone boulder in the field. Pyrite was scraped from 3 separate boulders however only pyrite from one boulder yielded sufficient sulphur for isotope analysis perhaps due to low sulphur rock matrix incorporated in the sample. The successfully analysed pyrite had formed on a piece of fossilised plant occurring within siderite cemented sandstone. It was located in the proglacial moraine field of Møysalbreen and based on the rock description and catchment geology is likely sourced from the Firkanten Fm. Pyrite collected from the boulder had a $\delta^{34}S$ value of -22.56‰. Bedrock sulphide exhibited a wide range of $\delta^{34}S$ values which are generally more positive than the pyrite sample.

Pyrite is most abundant in shales of the Firkanten Fm and the Basilika Fm with pyrite – iron concentrations of up to 5.2 wt. % (Figure 4.7).

Table 4.3 Results of sulphur isotope analysis of bedrock sulphides and scrapings of pyrite from a boulder.

Formation	n	Mean sulphide S wt. %	Numerical mean sulphide $\delta^{34}S_{VCDT}$ (‰)	Mass weighted mean sulphide $\delta^{34}S_{VCDT}$ (‰)
Aspelintoppen	4	0.09	0.44	1.78
Battfjellet	3	0.06	1.56	1.49
Frysjaodden (Gilsenryggen Mb)	4	0.15	-4.98	1.34
Grumantbyen	3	0.10	-32.35	-40.60
Basilika	4	1.71	8.45	2.04
Firkanten (Endalen Mb)	3	0.24	-6.22	-7.88
Firkanten (Todalen Mb)	3	3.55	-0.76	-2.01
Carolinefjellet	3	0.15	-13.27	-13.79
All Samples	**27**	**0.74**	**-5.09**	**-1.48**
			$\delta^{34}S_{VCDT}$ (‰)	
Pyrite scrapings from rock in proglacial moraine field of Møysalbreen (1 SD, n=3)			-22.56 (±0.76)	

4.3.4.2 Discussion

The wide range of $\delta^{34}S$ values in sulphide is likely due to differences in sampling. Only 1 pyrite mineral separate was analysed and while its value falls within the range of bedrock sulphide, its deviation from the mass weighted mean of bedrock sulphide suggests that it is unlikely to represent bulk rock $\delta^{34}S$. Furthermore, the disseminated sulphide in bedrock samples represents an average of all the sulphide in the rock and is therefore a more representative depiction of catchment sulphide $\delta^{34}S$.

Whilst the sulphide sulphur has a range from -50‰ to +25‰, the more extreme values are found in rocks with lower sulphide concentrations (Figure 4.6). To see which isotope values are more representative of each rock formation, a mass weighted mean of sulphide was calculated (Table 4.3, Figure 4.6). The majority of sulphide sulphur falls within a range of -5‰ to +5‰ with a mass weighted mean of -1.48‰. Variations occur between formations, the Todalen member of the Firkanten Fm and the Basilka Fm have the highest average sulphide S wt. % (Figure 4.7, Table 4.3). These formations therefore have $\delta^{34}S$ close to the mass weighted mean. The Aspelintoppen, Battfjellet and Frysjaodden Fms also have similar values to the mean. Whereas the Carolinefjellet, Endalen member of the Firkanten Fm and the Grumantbyen Fm have more negative values.

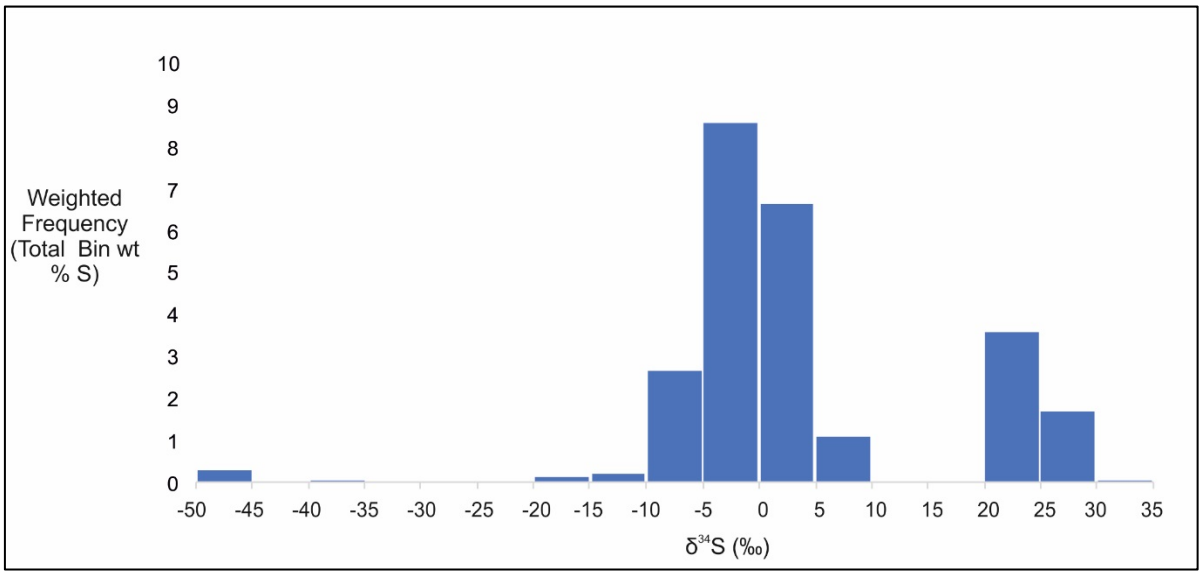

Figure 4.6 Mass weighted histogram of sulphide $\delta^{34}S$ extracted from a selection of core samples.

The methods employed here have considered sulphide sulphur only. The presence of coal seams within the catchments and abundance of TOC suggest that organosulfur compounds could contribute significant sulphur to overall bedrock S (which will also contribute to the meltwater sulfate $\delta^{34}S$). Organic sulphur is generally enriched in ^{34}S compared to pyrite sulphur (Raiswell et al.,

1993; Anderson, T.F. and Pratt, 1995), therefore any contribution of organic sulphur is likely to shift bedrock $\delta^{34}S$ to more positive values. However, sulphide sulphur represents at least 70% of total sulphur (determined by LECO) in 78% of samples analysed (Figure 4.8). Therefore, $\delta^{34}S$ of sulphide is likely to largely reflect total bedrock sulphur.

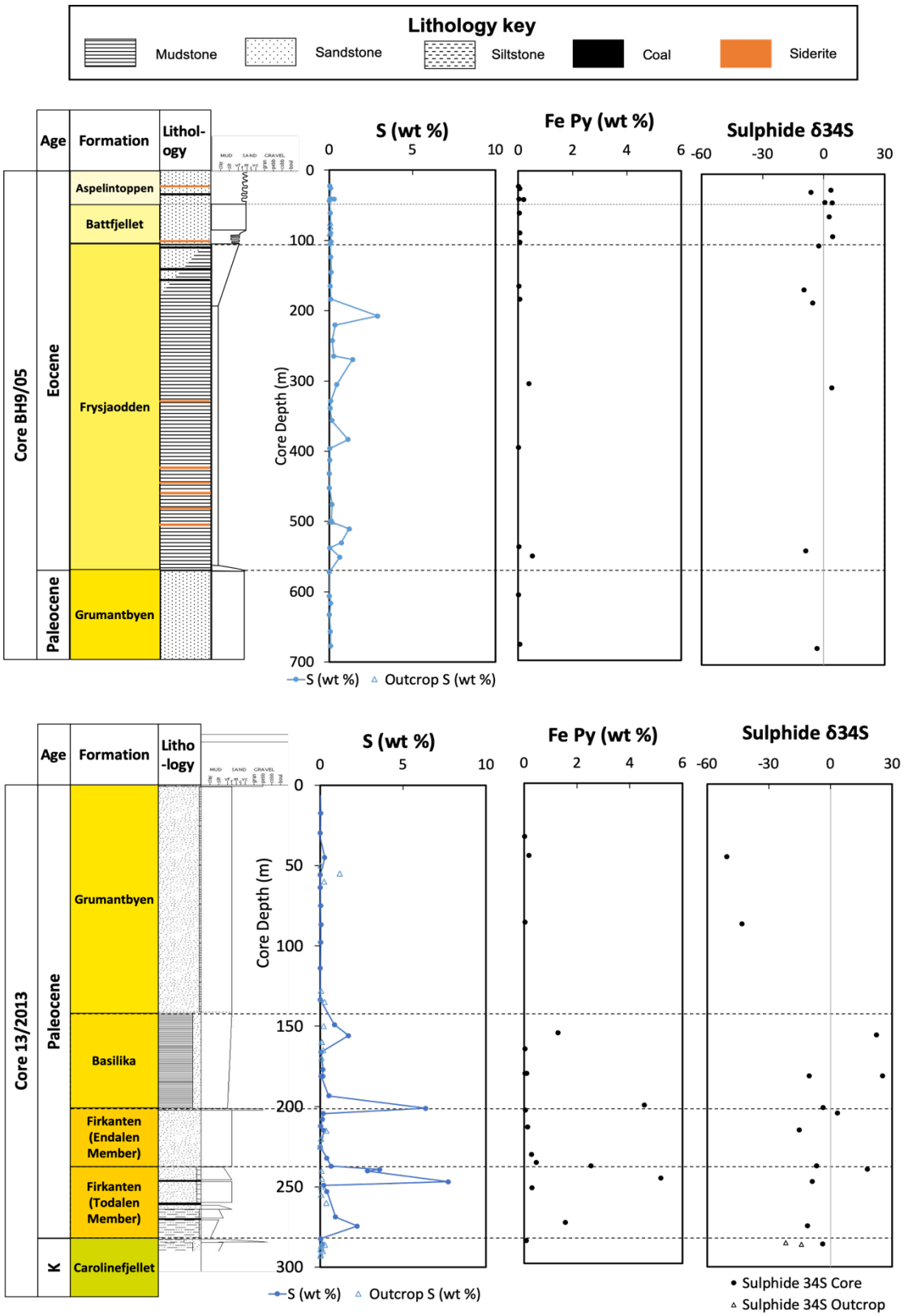

Figure 4.7 Bedrock Sulphur, Fe (pyrite) content and sulphide $\delta^{34}S$

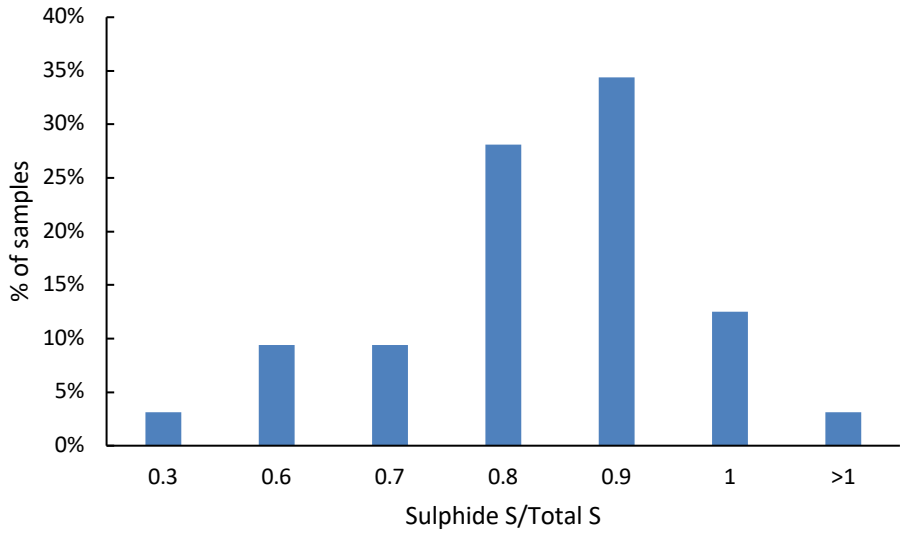

Figure 4.8 Histogram showing the proportion of sulphide S to total sulphur in bedrock samples. Y axis represents the proportion of samples in the X axis bins (width = 0.1). No samples have between 0.3 and 0.5 or < 0.2 sulphide S/total S.

4.3.5 Sedimentary geological interpretation

During the Paleocene, clastic sediments of the CTB were deposited in the foreland of the developing West Spitsbergen fold thrust belt. Sediment was largely derived from basalts located to the east of Svalbard. Later rifting of the North Atlantic accommodated the erosional products from the uplifting West Spitsbergen fold thrust belt located to the west of the depocentre. The sedimentary sequence of the CTB represents a deltaic environment experiencing marine regressions and transgressions. Climate fluctuations during Paleogene greenhouse conditions saw temperatures range from > 15°C to close to 0°C (Spielhagen and Tripati, 2009), while during the PETM, Arctic sea surface temperatures reached 23°C (Sluijs et al., 2006).

The delta plain consisted of broad leaf and coniferous trees within a raised bog/fen environment which would have experienced flooding (Firkanten Fm Todalen Mb). At the delta front, a high energy wave dominated environment formed sandstone units (Firkanten Fm Endalen Mb). Beyond the delta, siltstones and shales were deposited in suboxic conditions (Basilka Fm). Following the deposition of the Basilika Fm, regression resulted in a return to shallow water shelf deposits (Grumantbyen Fm). The Eocene sees a return to a deeper pro-delta environment, represented by shales (Frysjaodden Fm), but also accompanied by some shallow water sandstones (Hollenderdalen Fm). An increase in carbonate and sulphide minerals is indicative of a more marine but still brackish environment. Regression then sees a return to wave dominated

delta front sandstones (Battfjellet Fm) and a wooded delta plain (Aspelintoppen Fm).

Organic material (OM) derived from terrestrial plants on the delta plain and marine algae in prodelta environments was buried within sediments. The preservation of this organic matter is determined by the energy and redox conditions of the palaeaoenvironment. OM is well preserved in rocks deposited in low energy environments with fine grained sediments often undisturbed by bioturbation (prodelta, delta plain). These rocks typically feature reduced iron and manganese minerals such as pyrite and siderite. These are all characteristics of suboxic environments generated by lack of input of oxygenated water and a large supply of organic matter whose oxidation consumes dissolved oxygen. Conversely coarser sandstone units deposited in shallower, higher energy environments feature abundant bioturbation, limited sulphides and more oxidised iron. Such features are reflective of more oxygenated conditions in which organic matter is less well preserved (delta front, shoreface).

During diagenesis of the buried sediment, heating was sufficient to generate coal seams. The maturation of organic matter during this process would have liberated organically bound nitrogen into porewaters as ammonium. Within the temperature window of hydrocarbon generation, diagenetic clay minerals such as illite form (Williams, L.B. et al., 1995). Ammonium liberated from organics may be fixed into these clay minerals or substitute for potassium in pre-existing clays. The isotopic composition of fixed nitrogen likely reflects the signature of the original organic matter. Therefore, elevated nitrogen concentrations in rock are likely a function of an organic source, a low redox depositional environment and the presence of clay minerals to fix ammonium.

4.4 Summary

This chapter has provided an in-depth analysis of bedrock geochemistry in the Adventdalen area of Svalbard. This work underpins the work of the following chapters by providing an understanding of geochemical variations in different geological formations which affect the weathering reactions occurring in glacial catchments. It is clear from this analysis that the Frysjaodden Fm and the Firkanten Fm – Todalen Mb are significant crustal reservoirs of nitrogen and organic carbon. Furthermore, manganese is enriched in the Frysjaodden Fm where it substitutes into carbonate minerals. The distribution of iron varies with geological formation. Pyrite – iron is particularly abundant in the Firkanten Fm, while the Grumantbyen features mainly iron oxides and Eocene rocks (Frysjaodden Fm upwards) contain iron mainly within carbonate minerals.

The nitrogen and sulphur isotope signatures of bedrock have also been characterised here. This is an important step in considering rock as a source of S and N through stable isotope tracer studies. Bedrock has a fairly uniform $\delta^{15}N$ of ~3.7‰ while the majority of sulphur has $\delta^{34}S$ between +5‰ and -5‰.

Chapter 5 Nitrogen dynamics during simulated glacial rock weathering

5.1 Introduction

This chapter focusses on the weathering processes which occur in simulated glacial environments. Leaching experiments were carried out on crushed rock samples from glacial catchments in the study area of Svalbard. In this chapter, the experimental hypotheses are outlined, before an overview of rock geochemistry is provided and an assessment of crushed rock made through comparison with glacial sediment. This is followed by the experimental results, their interpretation and a discussion.

The aim of the experiment was to weather rocks from the glacial catchments in the study area in order to test the hypotheses in Table 5.1**Error! Reference source not found.**. The results of this experiment will provide insights into solute sources to glacial meltwater and how this varies between geological formations.

In Pilot Leaches 3 and 4 (Chapter 3), it was noted from a small sample suite that organic rich rocks liberated more nitrogen than organic poor rocks. It is hypothesised that this pattern will be true for all rocks in this study. This hypothesis is directly tested here using rocks of a variety of different organic contents.

Nitrogen within rocks may be released during weathering of silicate minerals as NH_4^+ but also from organic matter degradation (Lingle et al., 2017). Gill Olivas (2019), suggests that ·OH free radicals, likely produced during crushing of silicate minerals and pyrite, could break down organic matter producing alkenes and carboxylate ions such as acetate. Heat generated through crushing could also liberate ammonium from organic matter (Gill Olivas, 2019) since thermal degradation of organic matter was shown to liberate ammonium in geothermal springs (Holloway et al., 2011). Therefore, crushed samples with high TOC / organic N may release N as well as organic molecules such as acetate. Consequently, acetate in leachate could indicate organic matter degradation as a source of N. Acetate is therefore measured in this experiment to test the hypothesis that acetate concentrations are greatest in leachate of high TOC rocks.

This experiment also seeks to test the hypothesis that rocks containing abundant clay minerals have a greater capacity for ammonium adsorption than

clay-poor rocks. It is therefore anticipated that clay rich rocks such as shales will exhibit high K_D values for ammonium whereas clay-poor rocks such as sandstones will have lower K_D values for ammonium.

Analysis of glacial meltwater collected during fieldwork highlighted elevated iron (max 6.5 µmol/L) and manganese (max 61 µmol/L) concentrations in the Longyearbreen catchment (Chapter 6). The bedrock of this valley consists of upper Van Mijenfjorden Group rocks although the glacier is underlain predominantly by the Frysjaodden Fm and Grumantbyen Fm. During bedrock sampling, abundant iron bearing minerals (siderite and pyrite) were observed in the Frysjaodden Fm. Siderite forms a solid solution series with the manganese end member rhodocrosite, therefore these rocks may be rich in both iron and manganese. It is therefore hypothesised that Frysjaodden Fm rocks will leach significant iron and manganese during this leaching experiment.

5.2 Methods

The leaching experiment was carried out in duplicate with aliquots shaken at 6°C and 20°C. Water samples and KCl extractions were undertaken at days 1 and 11 of both experiments and day 49 for the 20°C experiment. The effect of temperature on solute acquisition and ammonium volatilisation at high pH will be compared. Full experiment methodology can be found in Chapter 3.

Table 5.1 Final leach details

Year	2019
Temperature	6°C & 20°C
Duration	49 days
Rock	Svalbard core samples
Liquid	Ultrapure water
Hypotheses	• Greater ammonia volatilisation and solute acquisition occur at warmer temperatures • Organic rich rocks liberate more nitrogen • K_D (NH_4^+) is greater in weathering of clay rich rocks • Elevated Fe^{2+} liberation from siderite in Frysjaodden Fm • TOC rich rocks release greater amounts of acetate

5.3 Rock Geochemistry

The geochemistry of rock samples from the study area were determined in Chapter 3. A summary of the geochemistry of rock samples specific to this experiment is displayed in Figure 5.1. Two - four representative samples from each formation/member where chosen for this experiment.

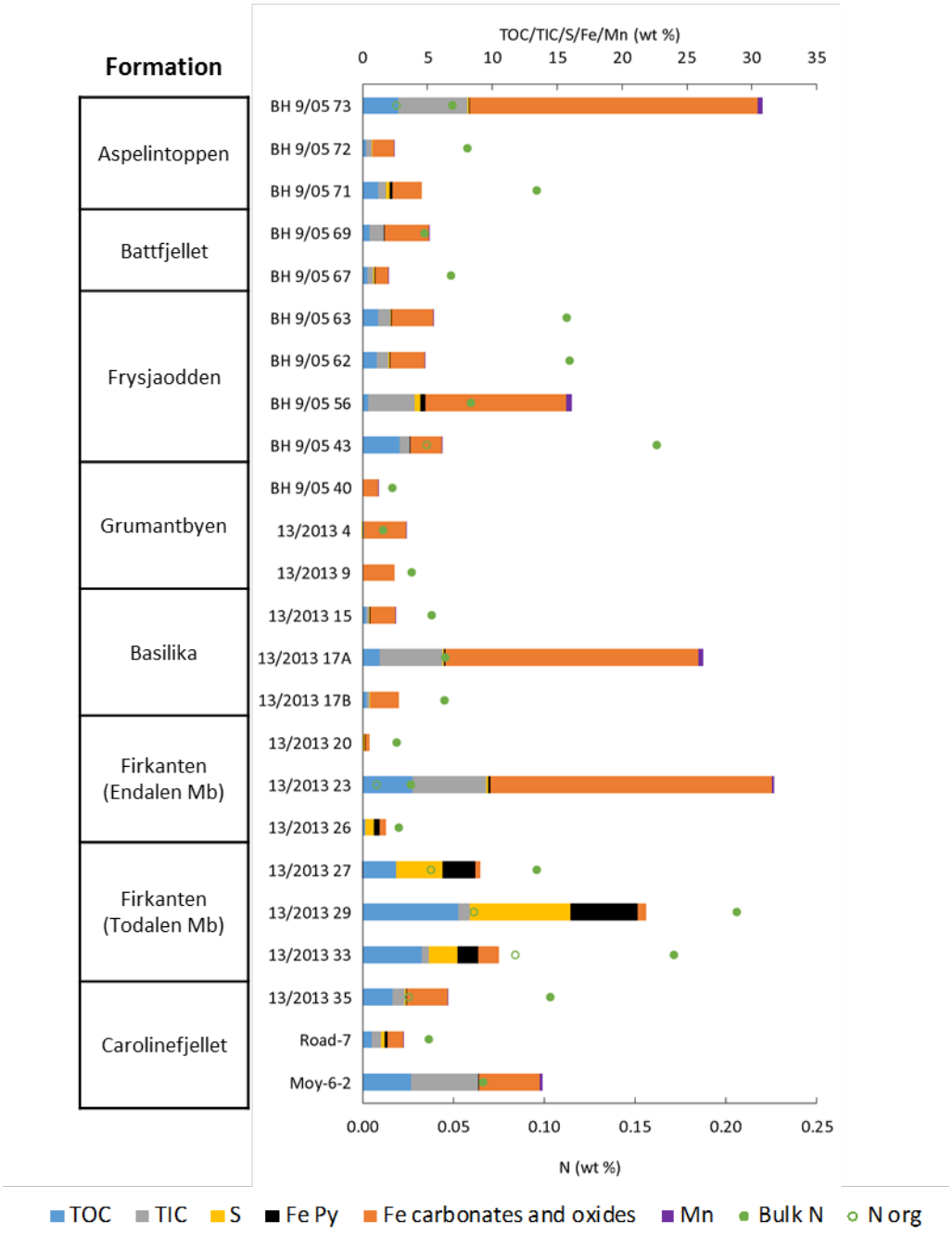

Figure 5.1 Geochemical analysis of each of the rocks used within the final leach experiment.

5.4 Results

5.4.1 Grain Size and Surface Area

The grain size distribution and surface area of a subset of crushed rock samples were compared to natural glacial sediment collected in proglacial streams (Chapter 2; Figure 5.2). The grain size distribution of suspended sediment is variable but this is related to suspended sediment concentration. At higher discharges, more energy is available to transport greater amounts of sediment in suspension. At higher suspended sediment concentration, there is a greater proportion of coarser grains. Therefore, the range of grain size distribution likely reflects variation in fluvial discharge.

The grain size distribution of experimentally crushed bedrock shows similar proportions of clay sized grains to glacial sediment. However, glacial sediment has a higher proportion of silt size grains and lower proportion of sand size grains. The surface area of crushed bedrock is negatively correlated with % sand size grains and positively correlated with % clay. The surface area of BH9/05 63 and 13/2013 15 are within the range of glacial sediments.

Finer grained sediment will likely have a greater impact on water chemistry as it has a larger surface area with which to react with water. The proportion of clay size grains is consistent with glacial samples while proportion of silt is close to that of glacial sediment. Therefore, the crushed rock represents glacially crushed material fairly well. The similarity of overall surface area to glacial sediment also supports this. It is therefore expected that the samples used in this experiment, accurately represent the products of glacial erosion.

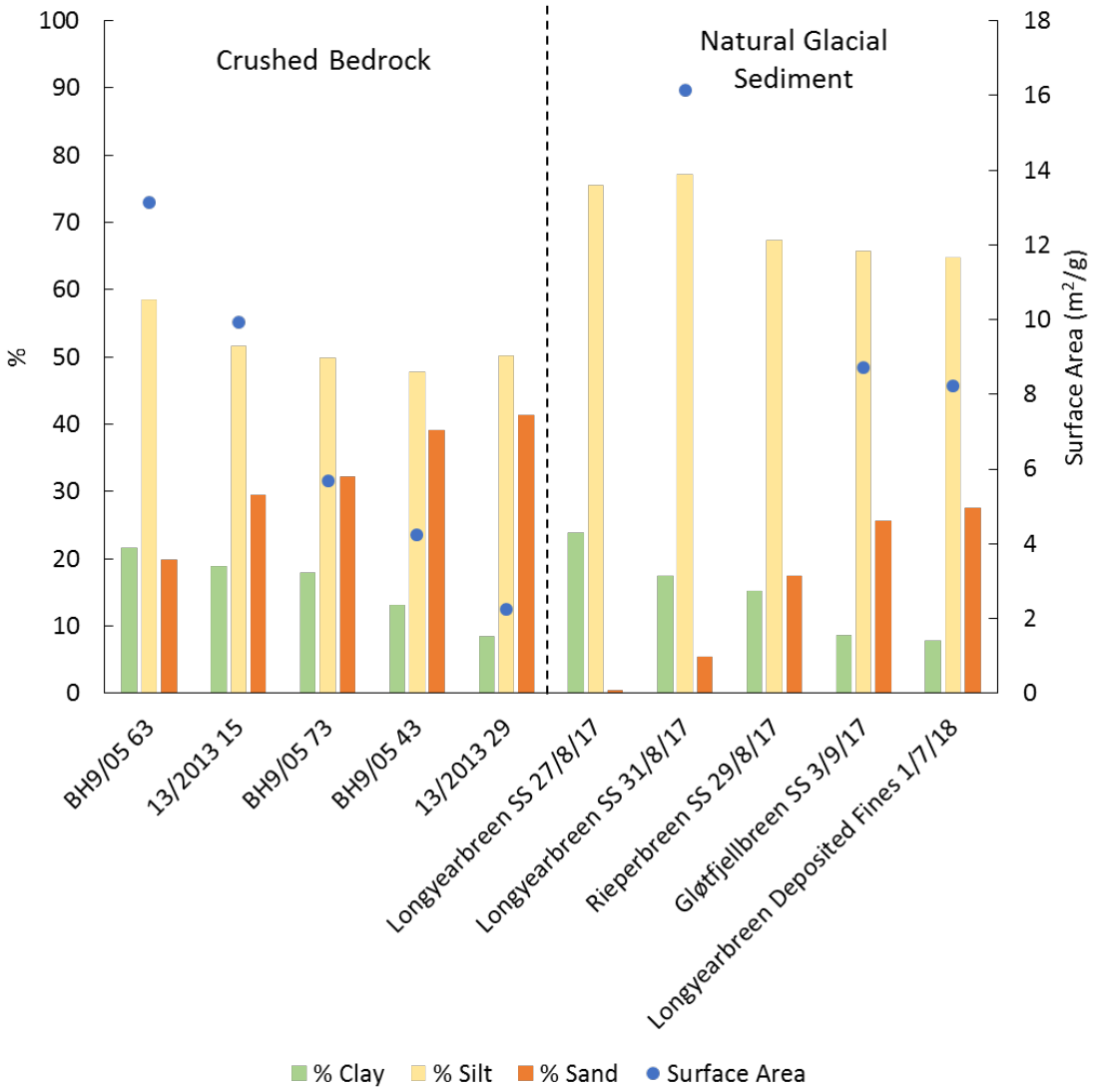

Figure 5.2 Grain size distribution and surface area of crushed bedrock and glacial sediment SS = suspended sediment

The measured surface area of crushed rock samples used in these experiments varied from 2.2 to 13.1 m^2/g. To explore the effect sediment surface area has on solute acquisition, scatter plots of surface area and solute release were constructed (Figure 5.3). There is no correlation between surface area and solute release of anions, acetate, cations or aqueous ammonium/nitrate. However, adsorbed ammonium correlates with surface area. This suggests that surface area is not a primary control on solute release, therefore solute concentrations are reported as µg/g. However, surface area does exert a control on ammonium adsorption and there appears to be two groups of $NH_4^+{}_{(ad)}$ data points which correlate positively with surface area. At higher surface areas, there are a greater number of sites for ammonium ions to adsorb to. Therefore, surface area is related to ammonium liberation rather than ammonium leaching (see definitions on page 3).

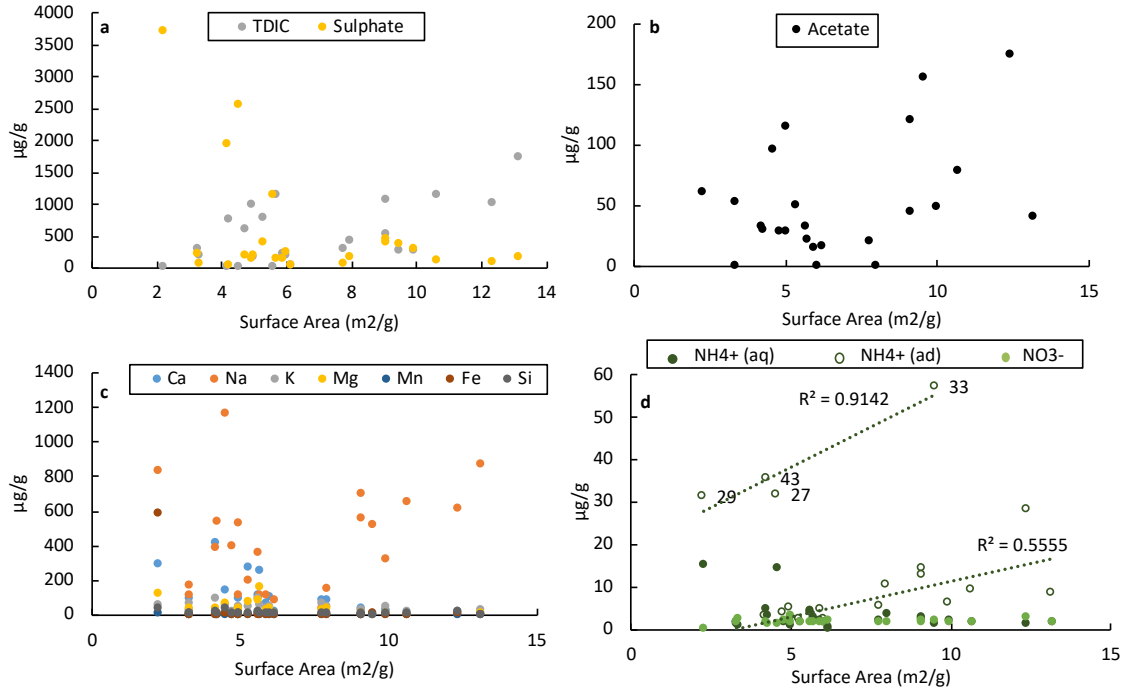

Figure 5.3 Surface area effect on solute acquisition. Panels show surface area of rock v release of a) anion b) acetate c) cations/metal and d) ammonium/nitrate concentration on day 11 of the 6°C experiment.

5.4.2 Anions

Anion concentrations (carbonate, sulphate, nitrate and acetate) were measured in the 6°C experiment only. Nitrate results are described alongside ammonium in Section 5.4.4. Carbonate and sulphate leachate concentrations are displayed in Figure 5.4. Acetate concentrations are displayed in Figure 5.5.

Figure 5.4 Major anions released during 6°C leach SMF values are displayed at end the end of bars

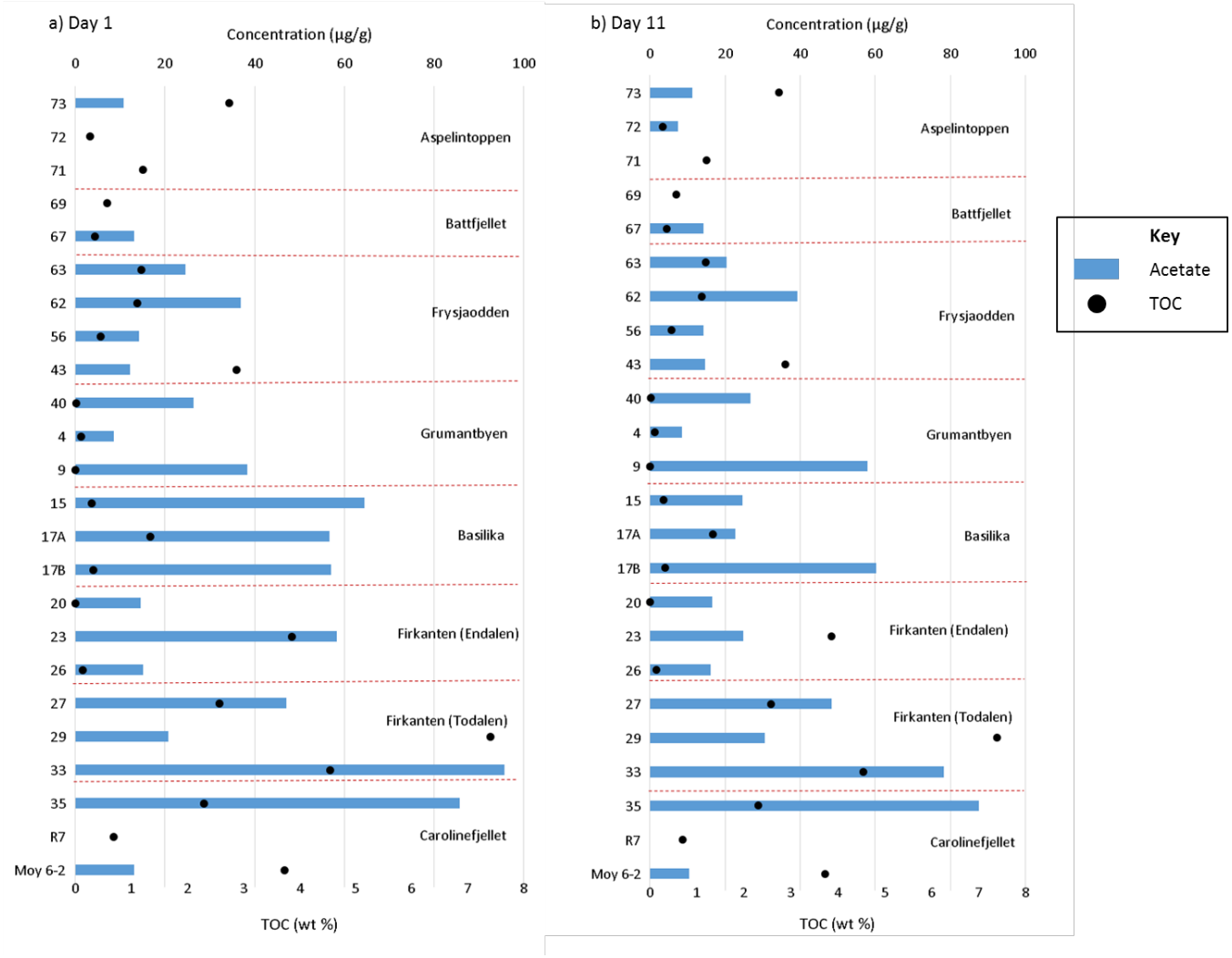

Figure 5.5 Acetate release during 6°C leach with TOC (wt. %) of bedrock

Total dissolved inorganic carbon in these leachate samples was measured by ion chromatography (Chapter 2). Given that the pH of most samples in these experiments are 8 - 9, inorganic carbon will mostly occur as bicarbonate. Bicarbonate concentrations are calculated from TDIC using pH and dissociation constants based on 0% salinity and 5°C (Chapter 2). The data displayed in Figure 5.5 show bicarbonate concentrations and sulphate concentrations in leachate in meq/L since this unit is useful in understanding weathering processes (see section 5.5.1).

In the majority of samples, bicarbonate was the dominant anion and pH was generally greater than 8. In these samples bicarbonate release varies from equal proportions to sulphate to 11 times sulphate release (equivalents). However pyrite-rich Firkanten Fm samples produced abundant sulphate with no detectable TDIC and were associated with low pH values (< 5). Samples can be split into 3 categories in terms of their proportions of sulphate and bicarbonate: bicarbonate dominant, mixed bicarbonate sulphate and sulphate only.

Acetate concentrations were 2 - 3 orders of magnitude lower than TDIC/sulphate and were greatest in the Firkanten Fm (Todalen Mb), Basilika Fm. and upper Carolinefjellet Fm (Figure 5.5). No acetate was detected in blanks. There is no statistically significant correlation between TOC and acetate release however (R^2 = 0.07: Figure 5.6). Between Day 1 and Day 11, acetate concentrations increased in most samples, although they decreased in samples 15, 17A and 23 (from core 13/2013) (Figure 5.7).

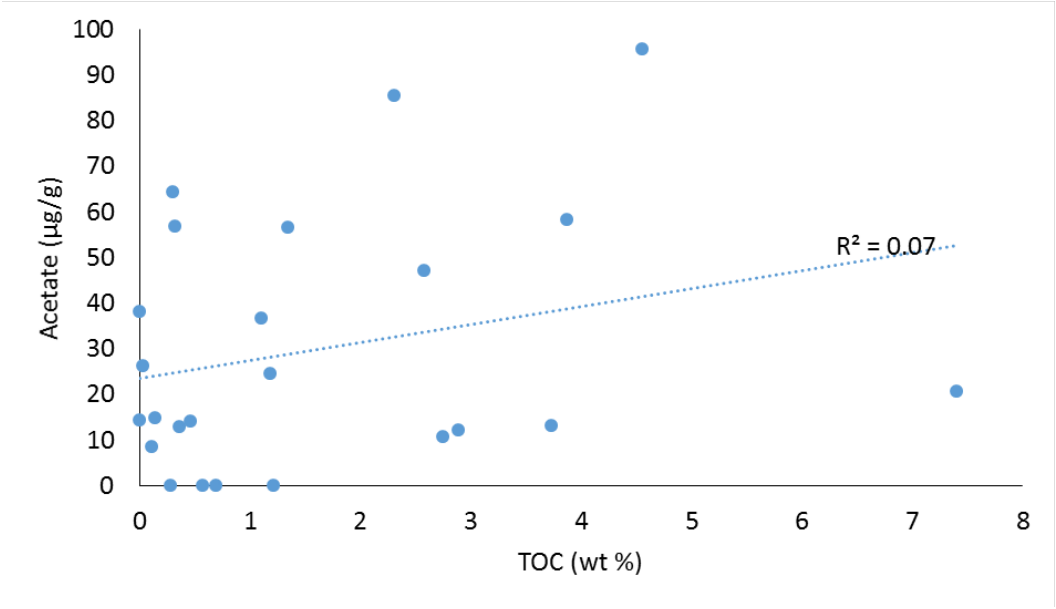

Figure 5.6 Bedrock TOC v Acetate in leachate

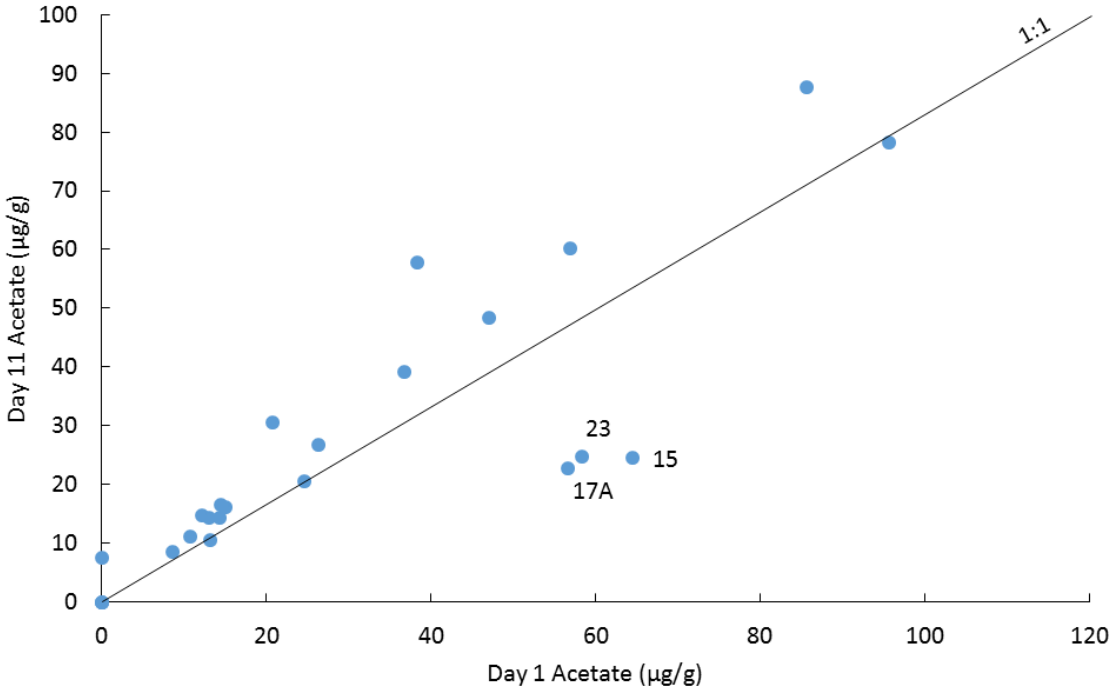

Figure 5.7 Acetate release in day 1 of experiment v day 11. The black line has slope 1:1, and so points above the line indicate that acetate concentrations increased during the experiment.

5.4.3 Cations

Sodium is the dominant cation in most leachates (Figure 5.8, Figure 5.9). Calcium is the second most common cation and dominates in a minority of samples. Concentrations of cations are greater in the 20°C leach compared to the 6°C leach.

Iron, manganese and silica concentrations are shown in Figure 5.10 and Figure 5.11. Iron and manganese concentrations are greatest in Firkanten Fm samples where pH is < 5 (samples 20, 26, 27, 29). Iron and manganese also weather from Grumantbyen, Frysjaodden and Aspelintoppen Fms.

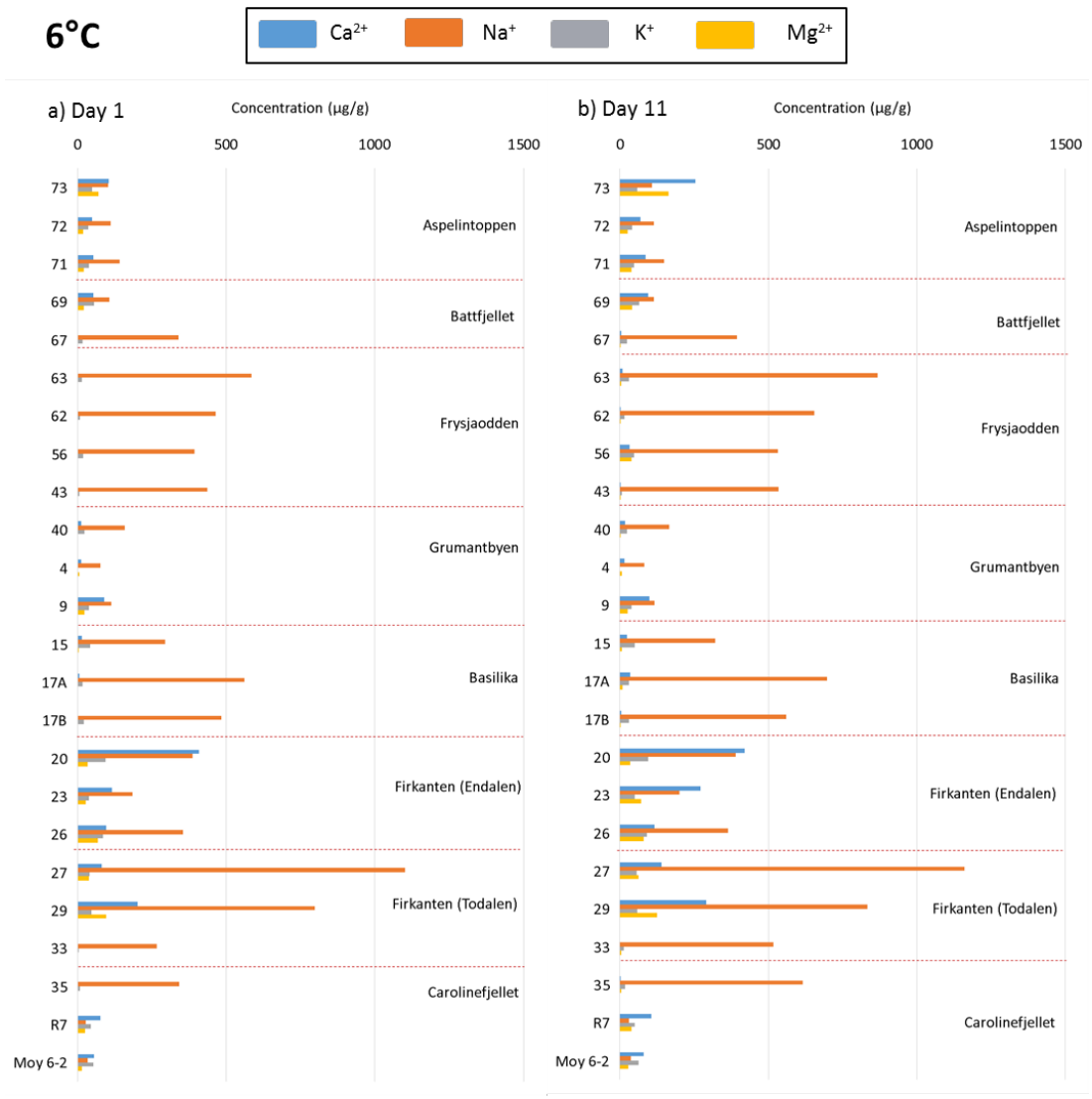

Figure 5.8 Major cations released during 6°C leach

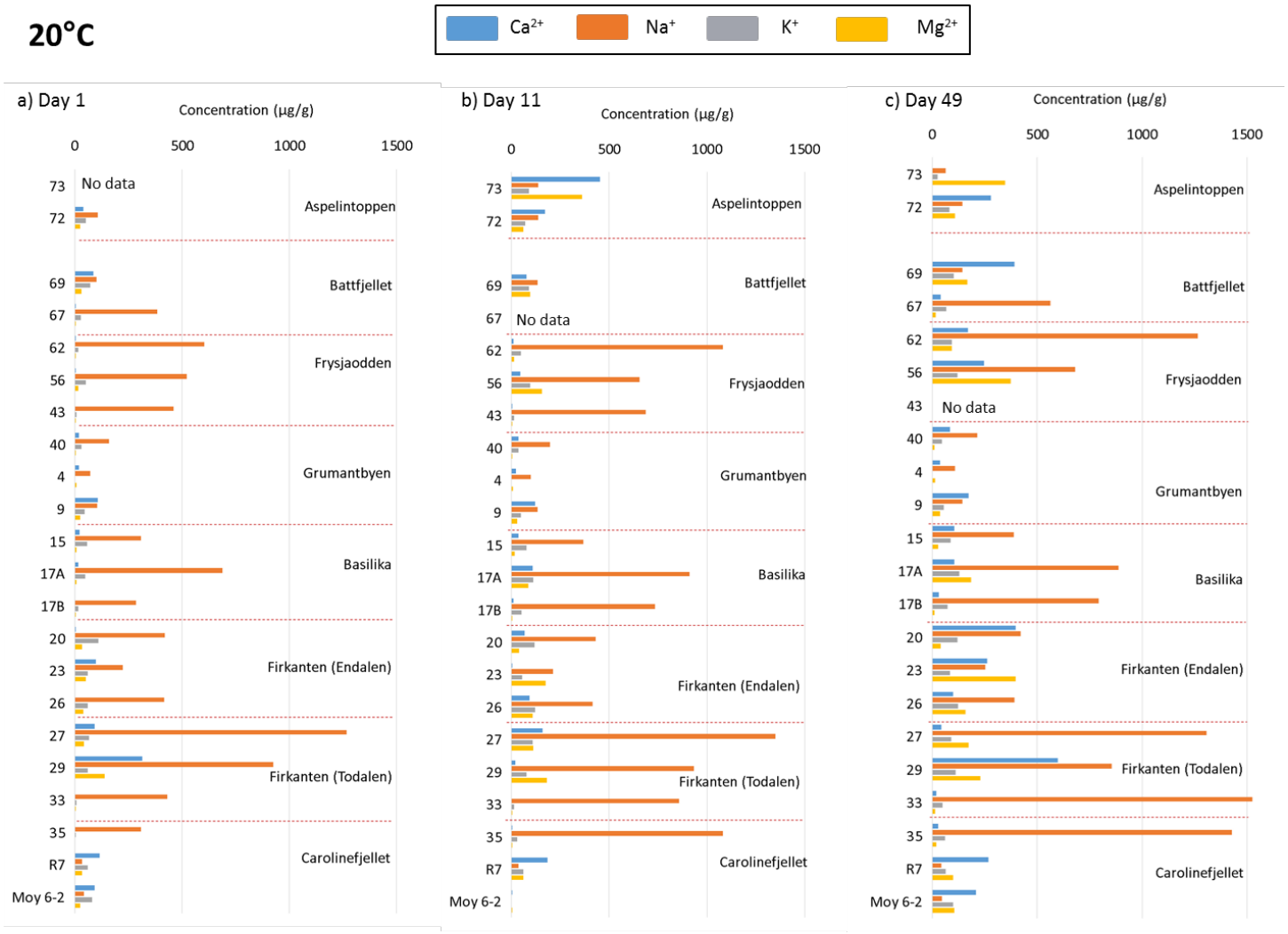

Figure 5.9 Major cations released during 20°C leach

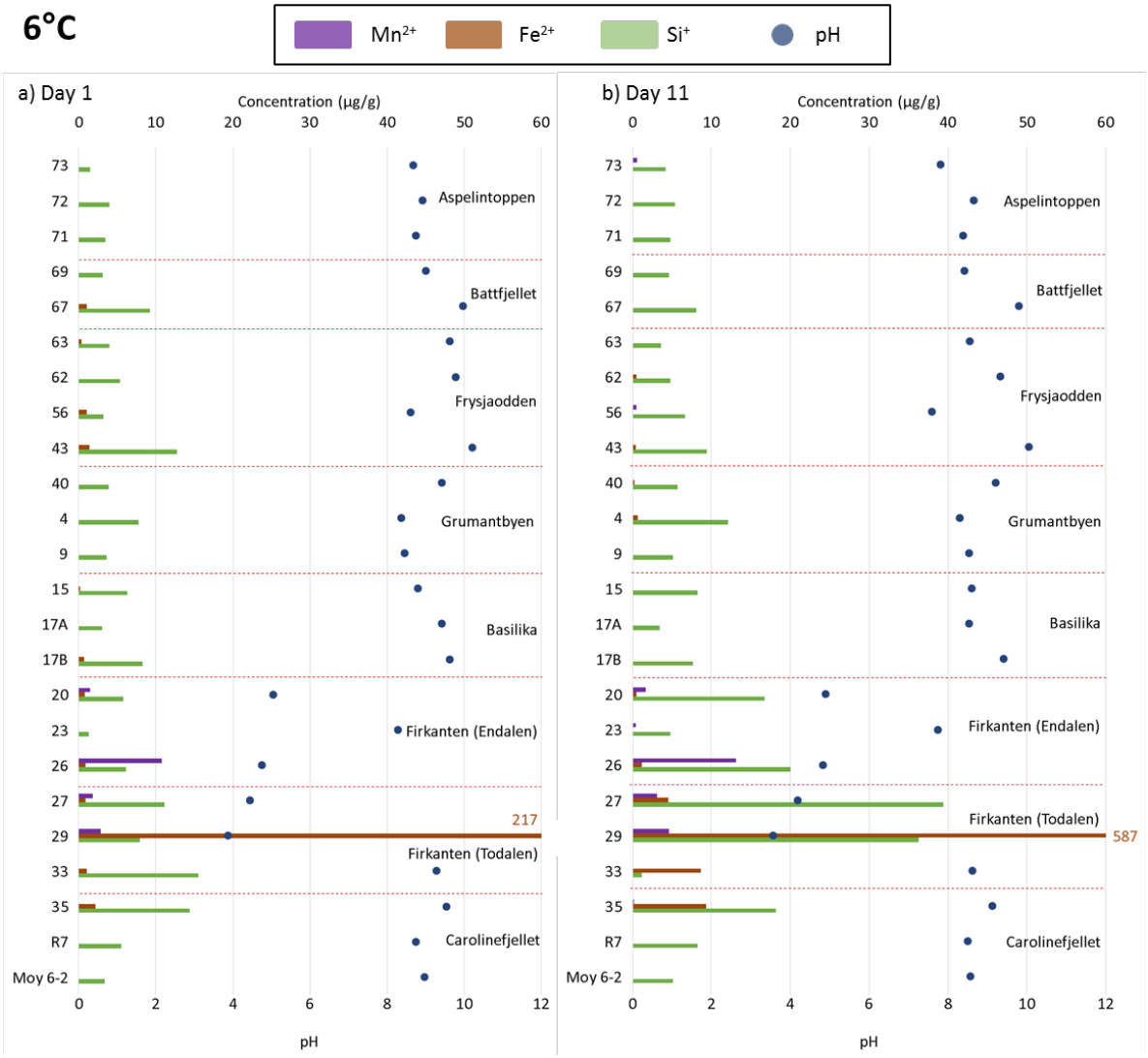

Figure 5.10 Minor cations released during 6°C leach. Concentration values exceeding scale are labelled on relevant bars.

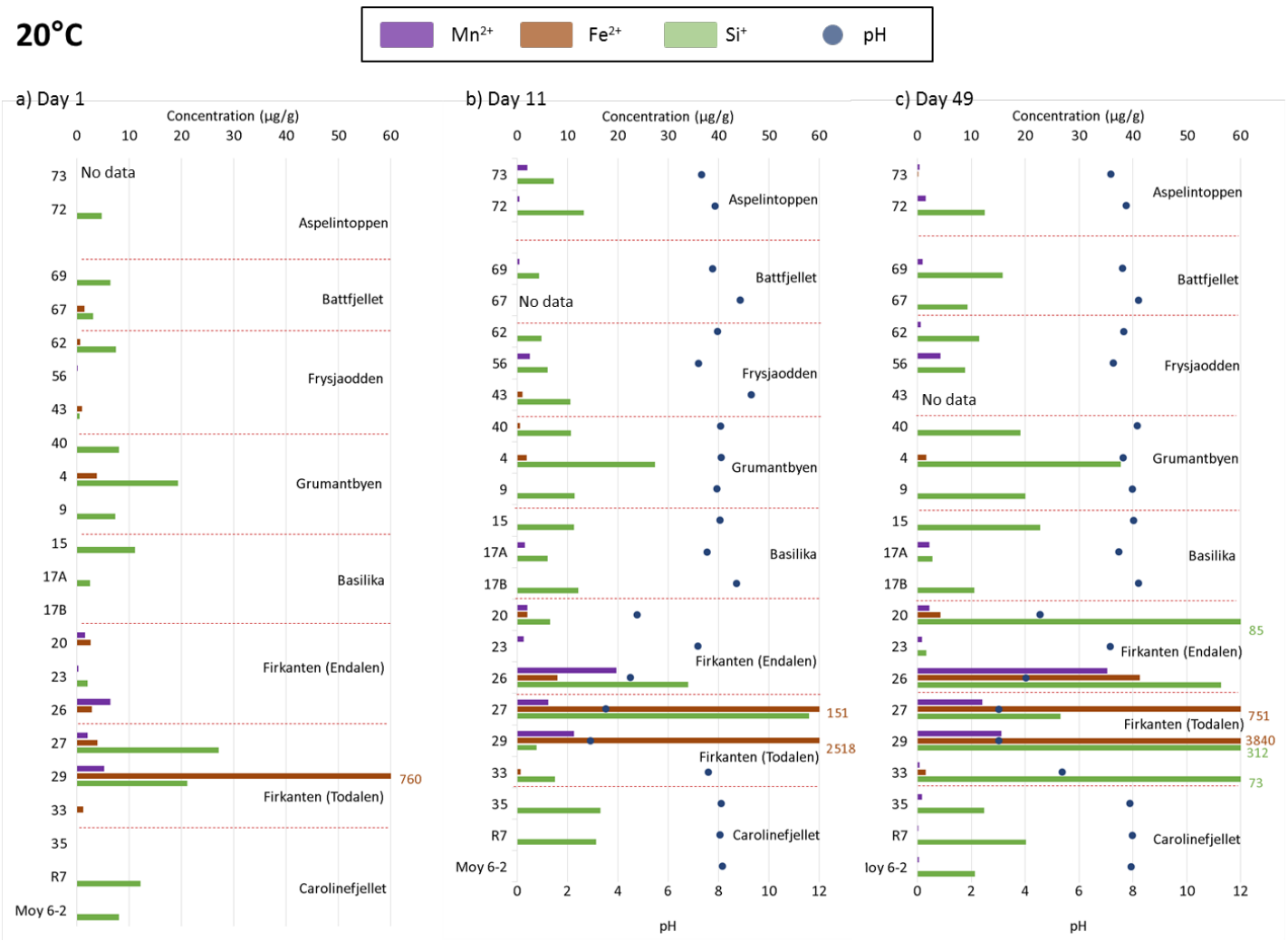

Figure 5.11 Minor cations released during 20°C leach. Concentration values exceeding scale are labelled on relevant bars

5.4.4 Nitrogen

The results of nitrogen release in the weathering experiments are displayed in Figure 5.12, Figure 5.14 and Figure 5.15. Both 6 and 20°C experiments exhibit similar NH_4^+ release. In the 6°C experiment, NH_4^+ tot is generally equal between days 1 and 11 with small decreases noted. However in the 20°C experiment, most samples show a decrease in NH_4^+ tot over days 1 to 49, while some samples show increases (samples 27, 29) (Figure 5.12). Samples from the Firkanten Fm and lowermost Frysjaodden Fm release the largest amount of nitrogen during weathering.

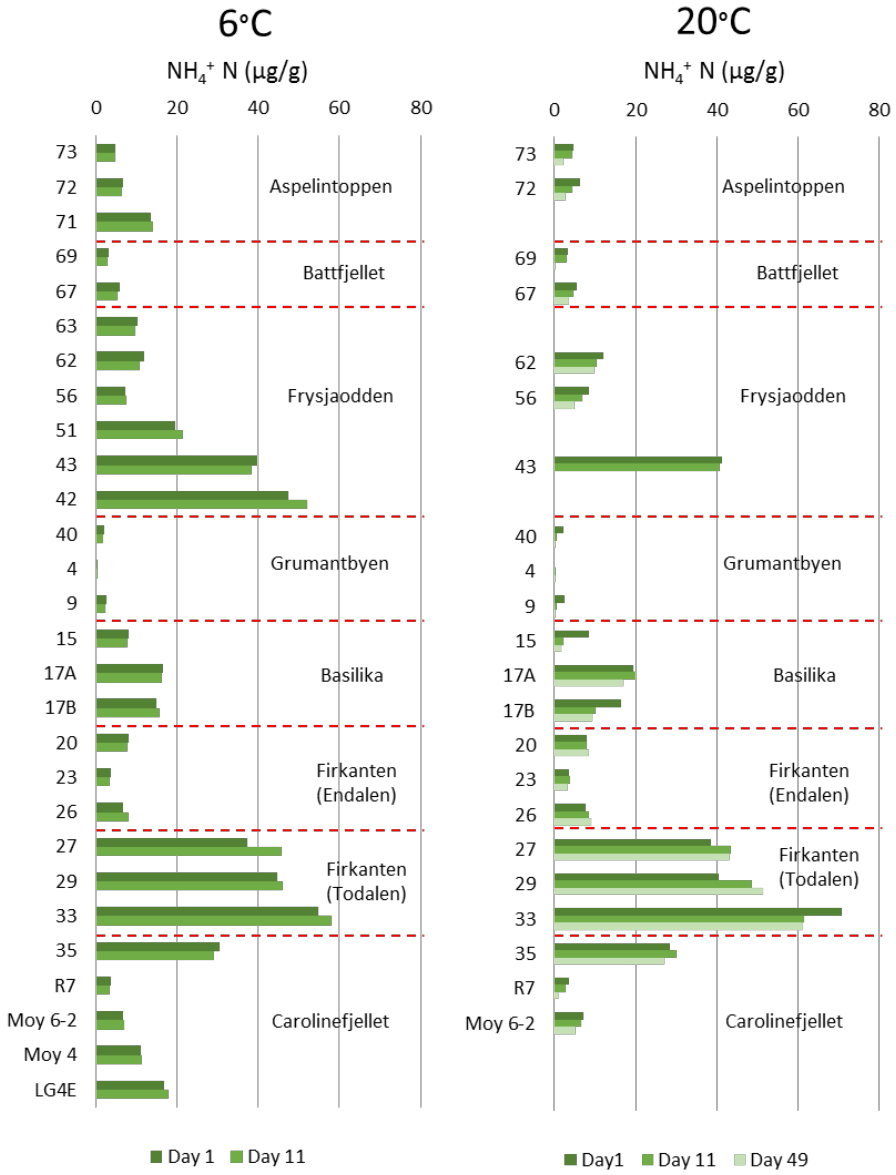

Figure 5.12 NH_4^+ (N) release over the course of a 11 or 49 day leach at 6°C and 20°C

The proportion of nitrogen released (as NO_3^-, NH_4^+ $_{(aq)}$ and NH_4^+ $_{(ad)}$) from overall mass of nitrogen in a rock sample is here termed liberation efficiency.

Between 0.5 and 5% of N in rock was liberated during weathering. Generally higher proportions of liberated nitrogen are associated with rocks containing more abundant nitrogen (Figure 5.13). However, some rocks have significantly higher N liberation efficiencies than other rocks (e.g. 17A, 17B, 20, 26, 27). These samples also released significant sulphate during weathering, likely via sulphide oxidation.

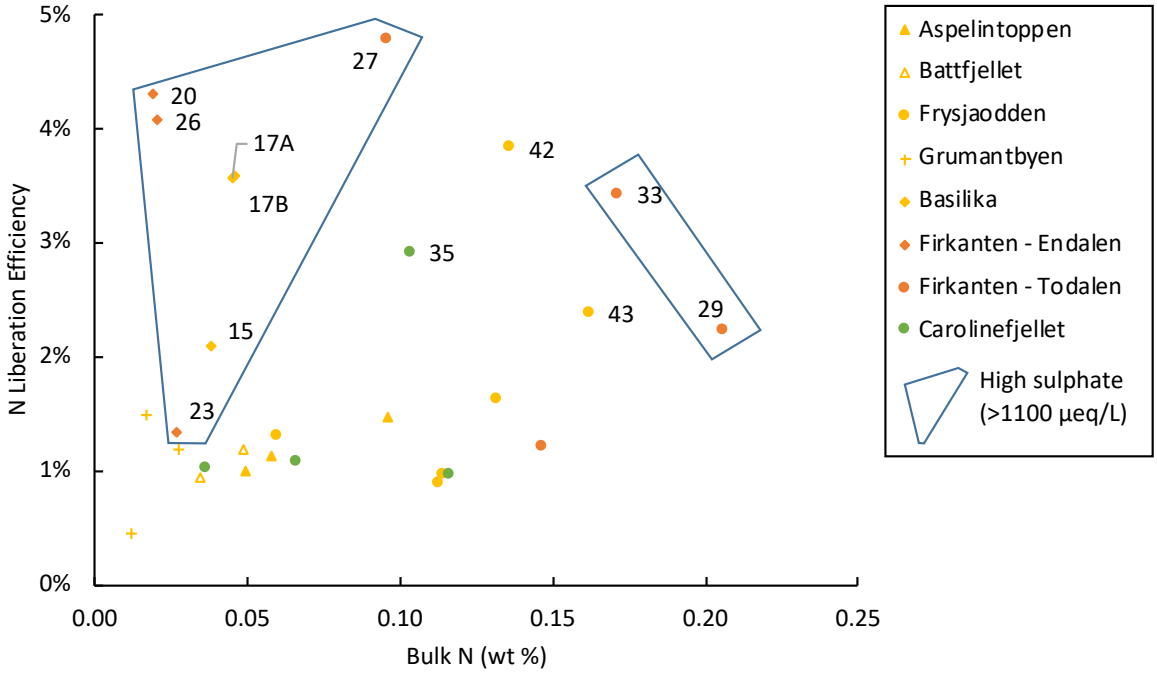

Figure 5.13 Bulk rock nitrogen v N liberation efficiency Data points labelled with sample ID

Nitrogen, liberated from rocks in this experiment was almost entirely in the form of ammonium with a minor amount of nitrate. Up to 55 µg/g and 70 µg/g of ammonium (N) were released from the 6 and 20°C experiments, respectively. Ammonium was distributed between dissolved ammonium and ammonium adsorbed to sediment. Ammonium is preferentially adsorbed in clay/siltstone samples (e.g. Basilika Fm, Frysjaodden Fm, Firkanten Fm (Todalen Mb)), while aqueous ammonium is dominant in the conglomerate only (sample 20) and proportions of aqueous and adsorbed ammonium are almost equal in sandstone samples (Grumantbyen, Battfjellet, Firkanten Fm - Endalen Mb). Decreases in NH_4^+ tot were almost always accompanied by decreases in adsorbed ammonium, while aqueous ammonium concentrations increased or decreased. Yet where pH was less than 5, total ammonium concentrations increased over the course of the experiments. In these samples, aqueous ammonium concentrations approached or even exceed adsorbed ammonium.

Nitrate was measured in the 6°C sample only with concentrations less than 1 µg/g over days 1 and 11.

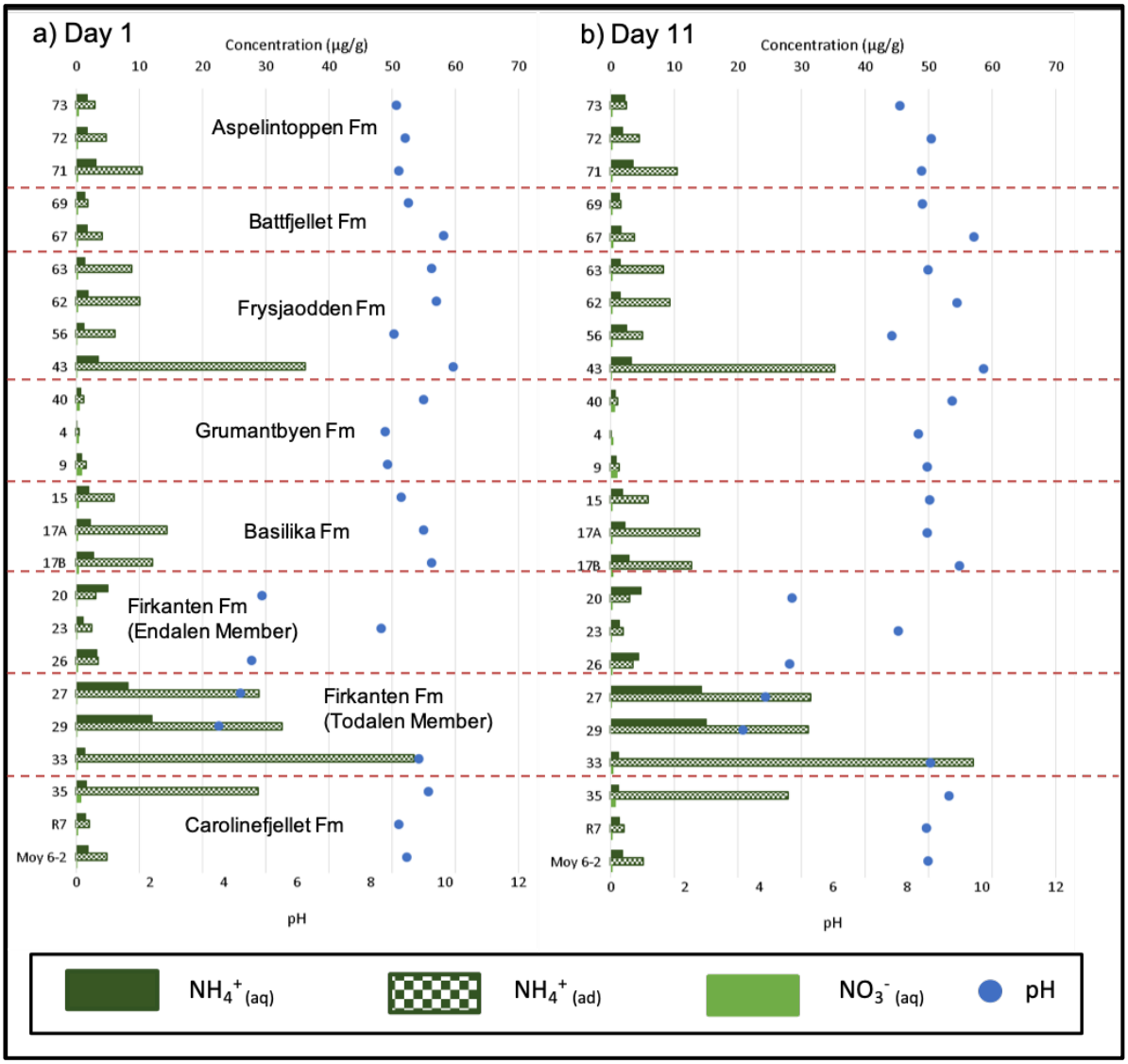

Figure 5.14 Ammonium (aqueous and adsorbed) and nitrate (N) released from bedrock during weathering experiment at 6°C on days a) 1, b) 11

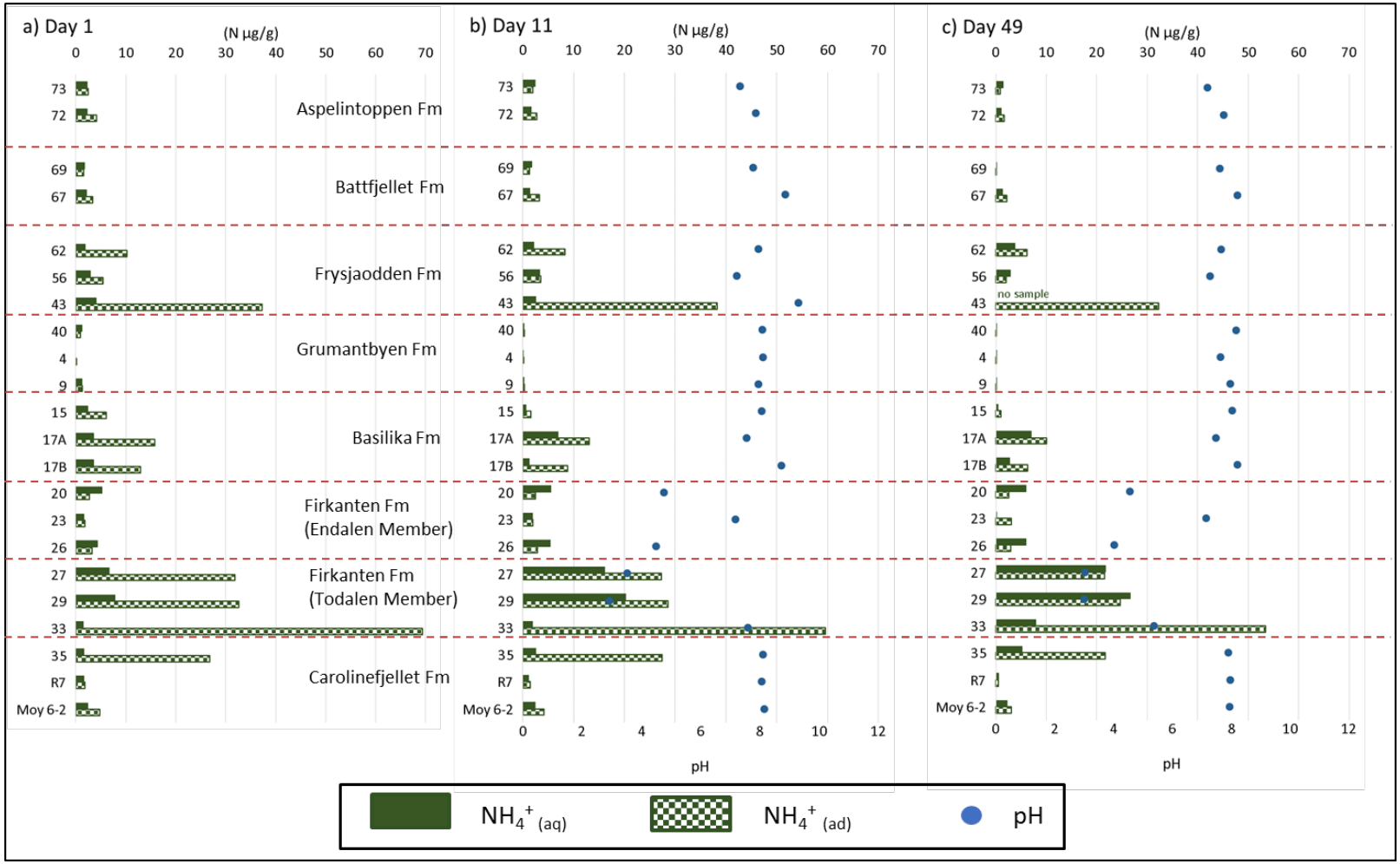

Figure 5.15 Ammonium (N) (aqueous and adsorbed) released from bedrock during weathering experiment at 20°C on days a) 1, b) 11, c) 49 (7 weeks)

5.5 Discussion

5.5.1 Weathering reactions

In these closed system experiments, solute was entirely derived from rock weathering, therefore water and rock chemistry can be used to infer weathering reactions. A limited amount of CO_2 may have dissolved from air during experiment set up, however once the experiment had begun, the tubes were sealed off from the atmosphere, inhibiting further CO_2 dissolution. The remainder of inorganic carbon was therefore assumed to be sourced from the dissolution of carbonate minerals.

There are either limited or no sulphate minerals in these rocks, but pyrite (iron sulphide) is present in variable concentrations. The oxidation of sulphide minerals typically couples with carbonate dissolution in subglacial environments, which liberates iron and sulphate (Equation 1.21).

High sulphate concentrations and low pH waters, in this experiment, are associated with rocks containing abundant pyrite and are therefore likely a product of sulphide oxidation. A useful tool for understanding geochemical weathering processes is the sulphate mass fraction (SMF). Assuming all other sources of sulphate are small, this index gives a crude estimate of whether coupled sulphide oxidation and carbonate dissolution are responsible for the major ionic chemistry of a given water. The equation for the SMF typically uses concentrations of sulphate and bicarbonate in equivalents (Equation 5.1) as derived from the SOCD equation. An SMF ratio of 0.5 would suggest water derives from this coupling (Tranter et al., 2002).

$$\mathrm{SMF} = \frac{[\mathrm{SO_4^{2-}}]}{([\mathrm{SO_4^{2-}}] + [\mathrm{HCO_3^-}])} \qquad \textbf{Equation 5.1}$$

Further insight into the weathering reactions involved can be gained using leachate element ratios of idealised reactions. Carbonates and silicates weather with carbonic and sulphuric acids to produce unique ratios of cations to sulphate and bicarbonate. These ratios are plotted as lines alongside leachate data points in Figure 5.16.

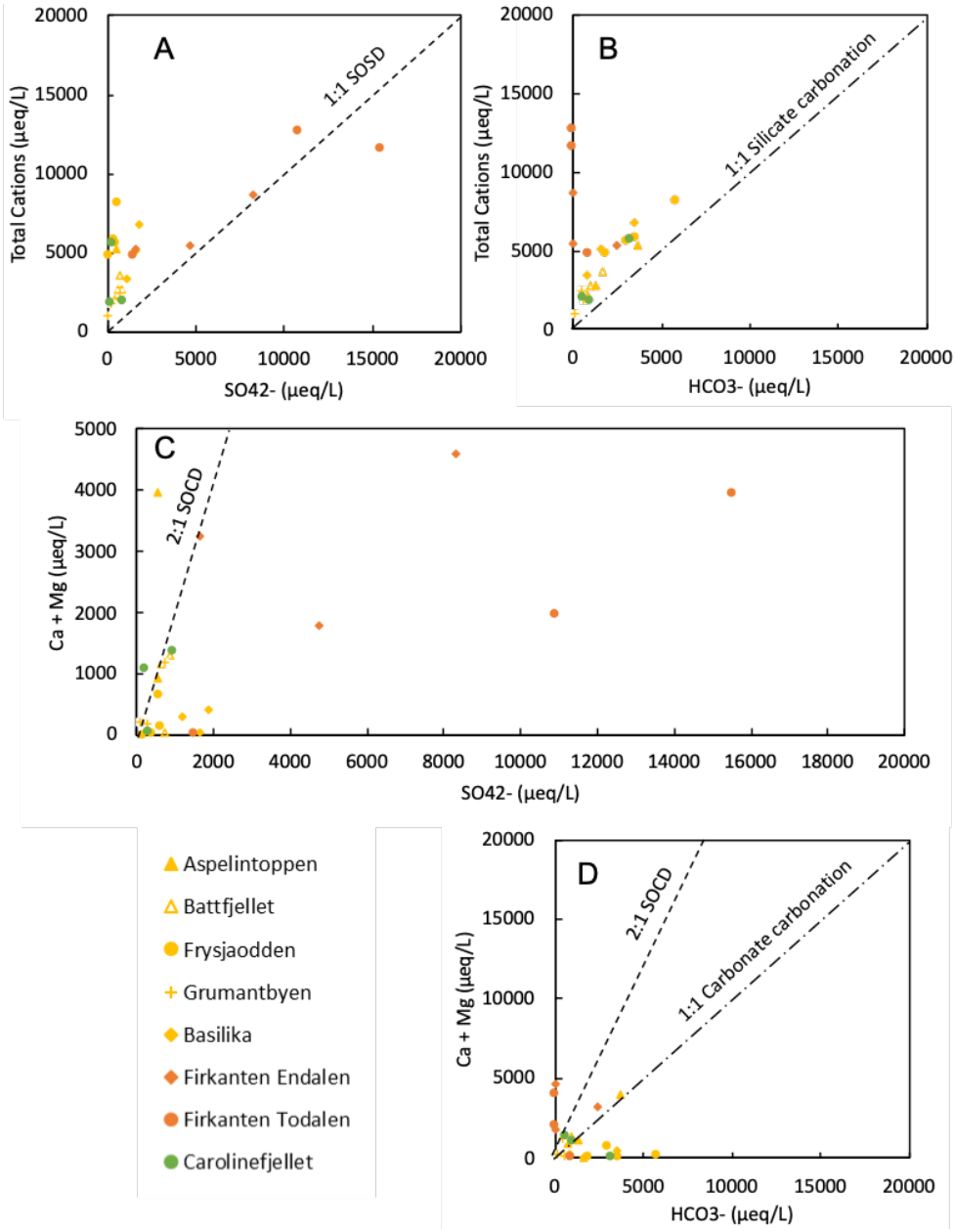

Figure 5.16 Graphs showing total cations (Ca, Mg, Na, K) in leachate from weathering experiment at 6°C after 11 days v a) sulphate and b) bicarbonate, as well as (Ca + Mg) v c) sulphate and d) bicarbonate. Figures a) and b) portray silicate weathering reactions, after assuming all cations are derived from silicates. The 1:1 line in a) depicts the idealised weathering products of coupled sulphide oxidation and silicate dissolution (SOSD). The 1:1 line in b) represents idealised silicate carbonation. Plots c) and d) portray carbonate weathering reactions assuming Ca and Mg are derived from carbonates only. The 2:1 line in c) represents the idealised weathering products of coupled sulphide oxidation and carbonate dissolution (SOCD). The 1:1 line in d) represents idealised carbonate carbonation

The SMF in the experiment varies between 0.1 and 0.6 in most samples (Figure 5.4). About a third of samples plot along the SOCD line in Figure 5.16c. These samples have SMF of 0.3-0.6.

Values < 0.5 may be associated with carbonation reactions in rocks lacking sulphide minerals or where anoxia promotes bacterial sulphide reduction (BSR) as this process consumes sulphate and yields bicarbonate (Wadham et al., 1998). The rocks associated with these samples have low pyrite contents therefore limited sulphide oxidation is possible. Dissolved oxygen was not measured in this experiment, so there is no direct way to assess the REDOX conditions. However, since these experiments were not inoculated with microbes, it is unlikely that BSR is responsible for low SMF values here. Inorganic carbon is therefore likely liberated via carbonate hydrolysis and carbonation (Equation 1.16 and 1.18) in addition to coupled sulphide oxidation and carbonate dissolution (Equation 1.21). The former reaction will be limited as the pH of solution rises, thereby lowering calcite solubility.

Sulphide oxidation coupled to silicate dissolution raises SMF above 0.5. Sulphate-rich samples with pH < 5 had a SMF of 1, i.e no detectable TDIC, and were associated with pyrite rich, carbonate poor sandstones/siltstones in the Firkanten Fm. Pyrite oxidation in these samples generated significant sulphuric acid thereby lowering the solution pH. The low pH in these experiments suggests that the acidity source exceeded the limited carbonate supply which was quickly exhausted. The solution therefore was unable to buffer the acidity and any inorganic carbon weathered, being stable as CO_2 at low pH, would have completely exsolved from solution. Three of the four samples with SMF of 1, plot along the idealised SOSD line in Figure 5.16a with the other sample having excess sulphate. This suggests that when carbonates are in limited supply and become exhausted, due to their rapid reaction kinetics, sulphide oxidation couples with silicate dissolution.

The 3 types of samples previously identified in section 5.4.1 can therefore be summarised in Table 5.2. The relative proportions of sulphide and carbonate minerals determines the dominant weathering processes and therefore the resultant water chemistry. Coupled carbonate dissolution and sulphide oxidation liberates carbonate and sulphate in a 2:1 ratio. Where pyrite is limited, carbonate is the major anion produced by carbonate hydrolysis. Yet where pyrite exceeds the buffering capacity of the rock, loss of carbonate results in sulphate becoming the dominant anion.

Table 5.2 A summary of 3 types of water chemistry produced in leaching experiment

Dominant Anions	Carbonate>> sulphate	Carbonate=> sulphate	Sulphate only
pH	>8	>8	<5
SMF	0.1-0.2	0.3-0.6	1
Source rock mineralogy	Pyrite poor (+ carbonate rich)	Trace/moderate carbonate and sulphide minerals	Pyrite rich (+ carbonate poor)

In both Figure 5.16 A and C, samples plot above the idealised SOCD and SOSD lines. This suggests that other more rapid processes are involved in solute acquisition. For example, Ca + Mg of samples 73 and Moy 6-2 plot above the SOCD line in Figure 5.16C. These are both carbonate rich rocks. Hydrolysis of carbonate minerals is thought to initially dominate subglacial weathering reactions since it is rapid and requires no acid source (Plummer and Wigley, 1976). Therefore excess Ca and Mg are likely sourced from early hydrolysis reactions occurring faster than sulphide oxidation.

Yet, sodium is the dominant cation in most samples which is not present in carbonate minerals and is therefore not produced from carbonate hydrolysis or SOCD. Cation exchange reactions, where divalent cations in solution preferentially substitute for monovalent cations on exchange sites in low ionic strength waters (Stumm and Morgan, 1996), may account for the lack of divalent cations relative to bicarbonate. Furthermore, many of the rocks in this study contain abundant iron carbonates which when weathered will contribute bicarbonate and only limited Ca and Mg. Iron has a low solubility in alkali water, therefore when iron carbonates are weathered, iron rapidly precipitates (hydr)oxide minerals.

However, while cation exchange may affect the distribution of ions in dissolved/adsorbed phases, sodium must ultimately be weathered from silicate minerals such as albite and clays. Silicate weathering does not produce bicarbonate and therefore generates elevated SMF values above 0.5. When there is abundant pyrite in bedrock relative to inorganic carbon, sulphuric acid production lowered pH to 3.5, facilitating the dissolution of silicate minerals. Rocks containing lower abundances of pyrite, had pH of 7 - 10, which yielded high total cations (mainly Na) relative to the SOSD line in Figure 5.16A . This suggests that this paired reaction cannot account for all the cations leached. Here, hydrolysis of silicate minerals (Equation 1.17) likely released sodium from

feldspar and clays as minerals are initially wetted, thereby raising solution pH through the release of hydroxide ions.

The abundance of sodium produced here demonstrates the importance of silicate weathering in these weathering experiments. This may have significant consequences for ammonium weathering which is also found within silicate minerals (see Section 5.5.4).

Enhanced weathering of cations in the higher temperature experiment suggests that the weathering reactions discussed above operate at faster rates when temperature is increased.

5.5.2 Iron and manganese

High iron concentrations are associated with elevated sulphate concentrations and likely represent the products of pyrite oxidation. Where pH is lowered significantly, iron released from pyrite is stable as Fe^{2+} in solution. However, in most cases, pH is buffered to ~ 8 - 9, where iron is insoluble and therefore likely precipitates oxides and hydroxides. Iron may also be derived from the weathering of siderite and clay minerals.

Manganese is also leached from rock under acidic conditions. Manganese concentrations in leachate relative to iron concentrations are high given the large iron: manganese ratio in the rocks. This is likely due to the greater solubility of manganese in slightly acidic to neutral water (Larsen and Mann, 2005).

In this sequence of rocks, manganese is relatively abundant, occurring in carbonate minerals. Manganese can substitute for iron in siderite, particularly in low salinity environments (Larsen and Mann, 2005) such as the depositional conditions associated with these rocks. However, samples 20, 26, 27, 29 yield significant Mn, yet no Mn carbonate or oxide was detected in these rocks during analysis of Mn speciation. Manganese may also be weathered from authigenic clay minerals, however growth rates of clay minerals are much slower than carbonates (Larsen and Mann, 2005). Therefore, it is more likely that abundant acidity allows for weathering of trace manganese in carbonates. Rocks that contain abundant manganese carbonates, do not efficiently release manganese due to their high buffering capacity. Insufficient acidity is generated in these samples to leach significant iron and manganese e.g. Sample 23 and Frysjaodden Fm samples. In a natural glacial system where rocks from different stratigraphic levels may be eroded simultaneously, acidity derived from pyrite rich rocks could enable the release of this manganese and iron.

5.5.3 Weathering as a source of organic carbon

Whilst there is no statistically significant correlation between TOC of rock and acetate in solution, acetate is present in almost all samples and not detected in blanks. Organic carbon may take multiple forms in rocks; therefore, the release of acetate may derive from acetate in organic material or the breakdown of more complex organic molecules. However, acetate is one of many possible degradation products and so a linear relationship with TOC is unlikely. Yet, the presence of acetate in these leachates and absence in blanks indicates that organic matter is weathered in these experiments.

Increases in acetate concentration from Day 1 to 11 indicate that sustained acetate production does occur during these experiments. In subglacial environments, many microbial REDOX reactions require a source of organic carbon. Acetate released from rock weathering may fuel microbial redox reactions, which oxidise acetate to CO_2 as oxidised species are reduced. It is unclear from these experiments why acetate concentrations decreased in samples 15, 17A and 23.

5.5.4 Nitrogen sources

Liberated ammonium correlates with bulk rock N content (Figure 5.17a) such that rocks containing greater amounts of nitrogen will release more nitrogen when weathered. The spread of data from the trendline in Figure 5.17a (R^2 = 0.7) suggests that some rocks liberate nitrogen more easily than others (see also Figure 5.13). Samples 20, 26, 27 (Firkanten Fm) are associated with low pH and sulphide oxidation coupled to silicate dissolution. Elevated sulphate concentrations in samples with low bulk N content and high N liberation efficiencies (Figure 5.13) suggests that acidic weathering (sulphuric acid) may more efficiently extract nitrogen from these rocks through dissolution of silicate minerals. Samples 27, 29, 33, 35 and 43 liberate significantly more ammonium per mass of rock than other samples (Figure 5.17a).

As previously discussed, these rocks contain both organic and inorganic forms of nitrogen, both of which may contribute to liberated N. One of the hypotheses of this experiment were that organic rich rocks would liberate more nitrogen than organic poor rocks. The 4 samples that liberate the most nitrogen all have TOC > 2.6 wt. % and C/N ratios less than 30. Ammonium release during weathering increases with TOC at given C/N ratios (Figure 5.17b). Ammonium release and C/N ratio have a hyperbolic relationship such that samples with low C/N ratios liberate more ammonium than those with higher ratios (Figure 5.17c). Therefore, TOC is not a direct indicator of releasable N, for example, rocks

containing abundant TOC with high C/N ratios liberate relatively little N e.g. 73 (2.75 wt. %), Moy 6-2 (3.73 wt. %), 23 (3.9 wt. %).

The non-linear relationship between nitrogen release and TOC may suggest nitrogen is principally derived from inorganic sources. Yet organic matter may be composed of a range of different molecules, with varying C/N ratios. A better test of organic matter as a source of releasable nitrogen is the organic nitrogen content. The amount of organic nitrogen within sediment is dependent on the amount of organic matter deposited and its C/N ratio. Although organic N has only been derived for a subset of samples, rocks with greater organic N content, liberate greater amounts of ammonium to solution (Figure 5.17d and f, R^2 = 0.72). For example, Sample 33, which liberates the greatest amount of ammonium, has the largest proportion of organic nitrogen (49%). By contrast, the correlation between inorganic N and liberated ammonium is much weaker (R^2 = 0.37). This suggests that the amount of organic nitrogen within rock exerts a primary control on the amount of releasable nitrogen. The majority of bulk nitrogen occurs as inorganic nitrogen, therefore labile organic forms of nitrogen may be more easily weathered than inorganic N. Organic matter is susceptible to oxidative weathering whereas silicate dissolution is limited by kinetic constraints associated with acid-hydrolysis reactions i.e. temperature, pH etc. (Houlton et al., 2018). Consequently, weathering of organic matter may proceed more quickly/completely than for silicate minerals.

Analysis of kerogen composition is beyond the scope of this study, however, consideration of organic matter in general may help to understand why organic nitrogen may be preferentially liberated from rock. Organic molecules may contain nitrogen within functional groups such as amines ($-NH_2$). These functional groups are polar and increase the solubility of organic molecules in water (Drever, 1997). Amines can also accept electrons to become $-NH_3^+$ (Drever, 1997). In natural systems, organic nitrogen may be oxidised to ammonium via ammonification. In these experiments not seeded with microorganisms, ammonification is unlikely. Alternatively, an abiotic pathway via crushing may liberate nitrogen from organic molecules. Free radicals produced during rock crushing could break down organic material releasing nitrogen. This pathway is consistent with the presence of acetate in leachate which may also be derived from organic material degradation.

Given that organic nitrogen is proportional to inorganic nitrogen in these rocks (Chapter 4) and both forms have similar isotope ratios, it is likely that inorganic N is derived from partitioning of the same organic matter during diagenesis. Consequently, sediment which receives greater organic nitrogen will likely retain

more nitrogen as kerogen following diagenesis, which may be released during later exposure and weathering.

The Firkanten Fm and the Frysjaodden Fm have the highest nitrogen concentrations and also liberate the largest amounts of nitrogen during weathering. Sediment from the Firkanten Fm contains abundant terrestrial organic matter with a high C/N ratio. In contrast, the Frysjaodden Fm contains lower amounts of organic matter of marine origin with low C/N ratios. Rocks from other formations generally have even lower organic contents and low C/N ratios such that N release during weathering is limited.

In Chapter 3, nitrate within fluid inclusions was considered as a source of nitrogen in rock. The release of only minor quantities of nitrate in this abiotic experiment demonstrate that this is not a significant source of nitrogen from Van Mijenfjorden Group rocks.

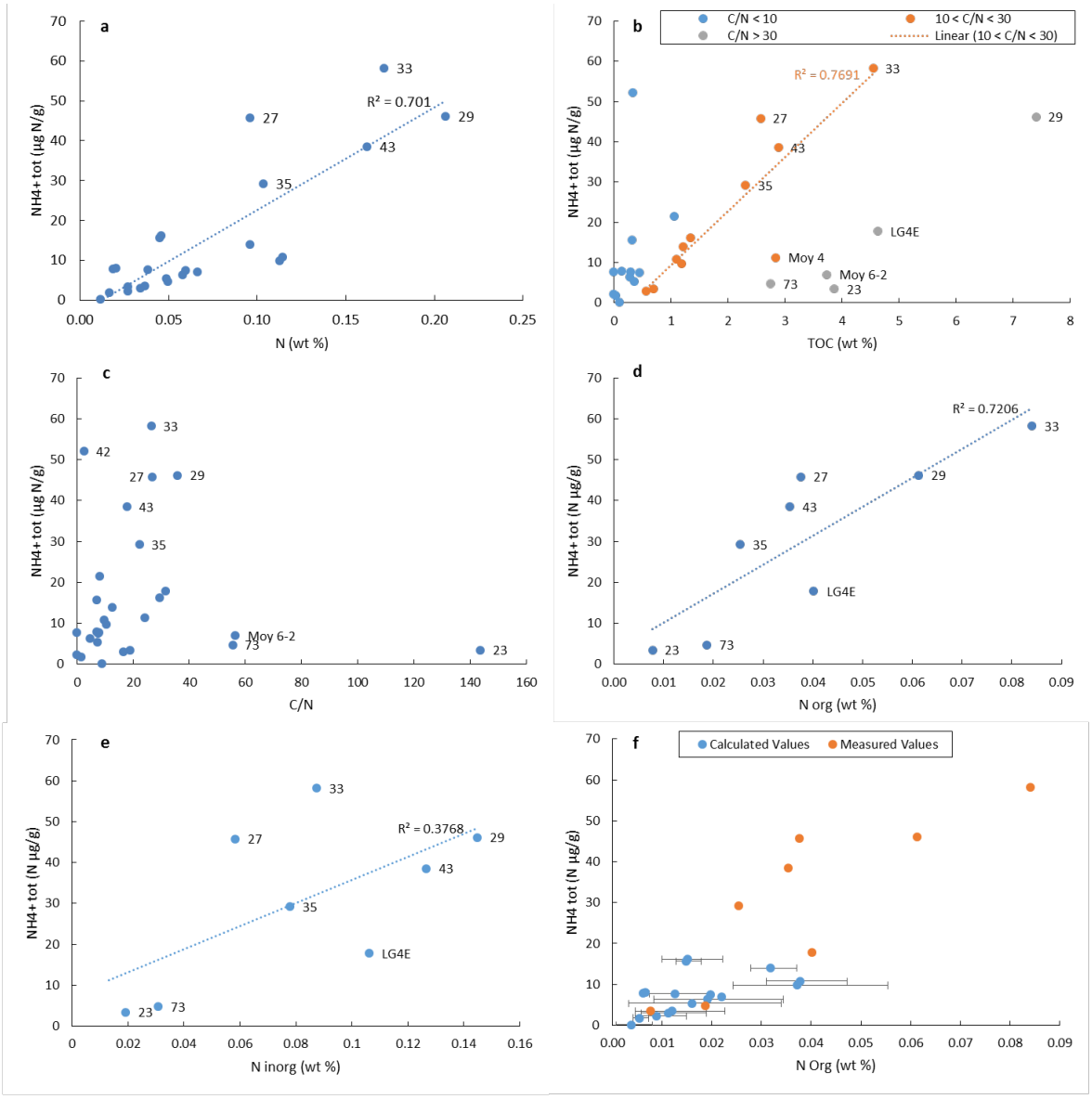

Figure 5.17 Ammonium liberated after 11 days at 6°C plotted against geochemical rock attributes: a) bulk N, b) total organic carbon, c) C/N d) organic N e) inorganic N f) same diagram as d but with calculated organic N of other samples also plotted. Organic N is calculated for rock samples using a calibration of TOC v bulk N using samples plotted in diagram d. Horizontal bars represent uncertainty on the calibration. Samples labelled with sample ID are discussed in the text

5.5.5 Nitrogen loss

5.5.5.1 pH Control

The pH of these experiments are typically > 8. At such pH values, significant ammonium deprotonation occurs resulting in free ammonia in solution, which forms an equilibrium with atmospheric NH_3. In these experiments, the headspace was assumed free of ammonia so ammonia would exsolve readily from solution, therefore reducing the aqueous ammonium concentration. Volatilisation was most likely enhanced by elevated temperatures, and while NH_3 (g) was not directly measured, N total loss was more significant in the 20°C experiment. This mechanism may therefore explain why total N seems to decrease, particularly in the 20°C experiment.

Samples with pH < 5 (Firkanten Fm) often showed increased ammonium concentrations over the course of the experiment (Figure 5.12). At lower pH, ammonium is more stable, > 99% of ammonia occurs as NH_4^+ when pH is less than 8 (Figure 3.9). Therefore, under such conditions ammonium equilibrates between aqueous and adsorbed phases. Continued weathering releases more ammonium which is not lost from the system. Whereas at pH > 8, ammonia can partition into a third (gaseous) phase (Figure 5.18). Given the rapid rise in pH in these experiments, it is likely that volatilisation of ammonia begins in the earliest stages of water – rock interaction. Glacial meltwater in the study area in Svalbard has pH of 7-9 (Chapter 6), therefore ammonium may be lost from solution via volatilisation. In glacial environments, where temperatures are closer to the 6°C experiment, loss of N via volatilisation is likely inhibited by lower temperatures. However, the 6°C experiment only ran for 11 days, therefore ammonia loss may become more significant at sustained elevated pH over the course of melt season.

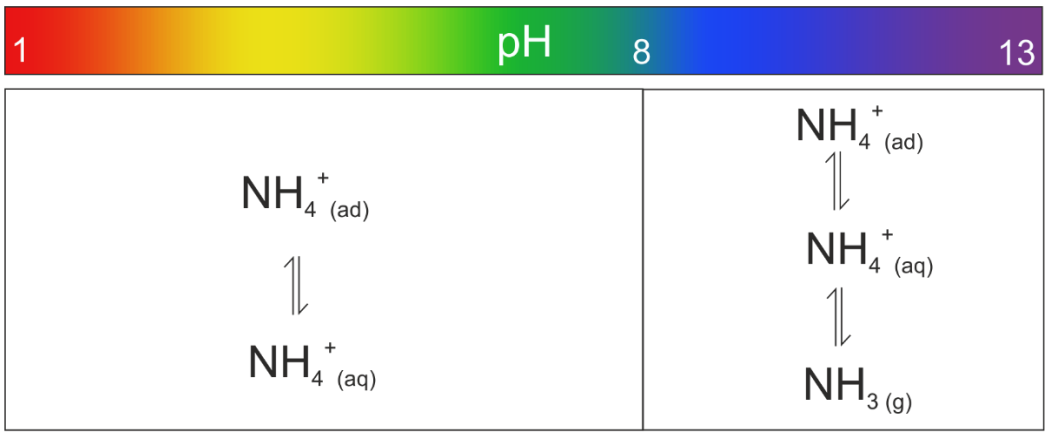

Figure 5.18 Ammonia speciation during weathering of rock

5.5.5.2 Lithological Control

An alternative mechanism of ammonium loss is via feammox (Equation 5.2, Equation 5.3). This reaction involves the direct oxidation of NH_4^+ by iron and manganese oxides to N_2 as documented in waste water treatment plants, wetlands and possibly marine environments (Barber et al., 2014). It has been observed in both abiotic and biotic environments, oxic/partially oxic conditions and where iron/manganese oxides are present (Barber et al., 2014). Large concentrations of iron and manganese occur in this sequence of bedrock mainly in reduced but reactive form but some in oxidised form. Weathering of these minerals in oxygenated waters will yield iron and manganese oxides that could promote feammox. These reactions likely take place on timescales longer than this experiment; therefore, they are unlikely to explain the results displayed here. However, in oxygenated glacial channels, over longer timescales, ammonium could be lost via this mechanism. Iron in Van Keulenfjorden sediments derived from glacial weathering of the same geological sequence as studied here have significant sodium acetate and sodium dithionite extractable iron concentrations of < 1.2 wt. % (Wehrmann et al., 2014). This suggests that abundant iron oxides derived from the subglacial environment could facilitate this reaction. Organic material often shields iron oxide surfaces, inhibiting this reaction. However, low organic material in glacial settings as well as continual supply of fresh mineral surfaces in oxygenated water could make this a viable pathway of N loss in glacial systems. However, since these environments are nutrient-limited, it is likely that biotic cycling of ammonium (nitrification) likely exceeds the rates of feammox.

$$FeOOH + 1/3NH_4^+ + 5/3H^+ \rightarrow 1/6N_2 + Fe^{2+} + 2H_2O$$ **Equation 5.2**

$$MnO_2 + 2/3NH_4^+ + 5/3H^+ \rightarrow 1/3N_2 + Mn^{2+} + 2H_2O$$ **Equation 5.3**

5.5.6 Nitrogen speciation

5.5.6.1 Lithological control

The majority of ammonium liberated from rock samples in these experiments adsorbs to mineral surfaces. The proportion of ammonium that is adsorbed relative to aqueous ammonium (K_D) is greater in clay/siltstones. These rocks typically have a greater abundance of clay minerals which have capacity for cation adsorption. Furthermore, these finer grained rocks also have larger surface areas which expose more clay minerals, thus enhancing their ability to facilitate cation exchange (Figure 5.19). Consequently, these rocks are able to effectively scavenge ammonium from solution through cation exchange reactions. Conversely, aqueous ammonium is elevated following reactions involving coarser grained rocks with larger surface areas such as sandstones and conglomerates. These rocks have fewer clay minerals and therefore fewer cation exchange sites. Consequently, a greater proportion of ammonium remains in solution.

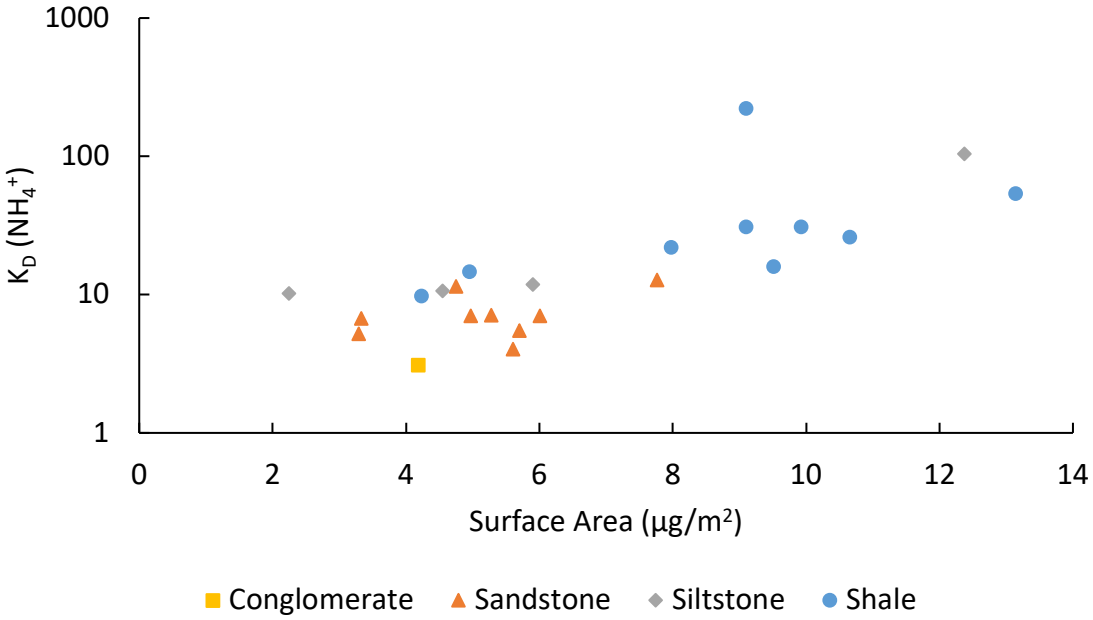

Figure 5.19 Surface area of crushed rock samples v K_D for ammonium. Data points are categorised by lithology. K_D is plotted on log scale.

5.5.6.2 pH control

Nitrogen loss via volatilisation as discussed above would decrease NH_4^+ (aq) concentrations thereby increasing K_D. This effect is shown in Figure 5.20, where K_D increases drastically above pH 8. As such pH can control the partitioning of ammonia between liquid and gaseous phases. However, pH may also indirectly affect the propensity for adsorption of ammonium. As previously discussed, clay minerals typically have negative electrostatic charges. At elevated pH, there are lower concentrations of protons in solution. As a result, the surface charge of minerals remains negative encouraging ammonium adsorption. Yet, even in the high pH samples, adsorbed ammonium concentrations decrease through both experiments, although more significantly in the 20°C experiment. Since volatilisation rates are greater at higher temperatures, loss of adsorbed ammonium may be associated with aqueous ammonium deprotonation. As ammonia volatilises and ammonium is lost from solution, desorption of ammonium may account for some of this loss (see high pH equilibrium in Figure 5.18)

At pH closer to mineral Point of Zero Charge (hereafter PZC), the concentration of protons at the mineral surface increases, therefore raising the surface charge, resulting in a reduced electrostatic charge to attract ammonium. As the pH falls below the PZC of a certain mineral, that mineral surface becomes positively charged thus repelling ammonium from mineral surfaces. Published values of the PZC of individual minerals are highly variable with much of the variation due to the method employed to quantify it. However, the PZC of a glacial till (consisting of 31% Quartz, 13% Feldspar, 35% carbonate, 21% clay minerals) was found to be ~ 7.0 ± 2.5 (Al-Hamdan and Reddy, 2006). Assuming a similar bulk rock PZC, the majority of these experiments have pH > PZC, therefore creating more negative electrostatic charges on mineral surfaces, thus promoting ammonium adsorption.

In these experiments, while all samples demonstrate ammonium desorption with time, K_D values for ammonium in acidic samples decrease most significantly. Ammonium desorbs over the course of the experiment until ammonium is almost equally distributed between dissolved and adsorbed phases. For example, in the 20°C experiment, on day 1 samples 27 and 29 have ~ 4x as much NH_4^+ (ad) as NH_4^+ (aq) but by day 49, the proportion of NH_4^+ (aq) and NH_4^+ (ad) is 1:1. This suggests that ammonium desorption is amplified at low pH. As acidity is continually produced from sulphide oxidation, protons may exchange for cations on ion exchange sites, moving ammonium from adsorbed to aqueous phase thereby lowering K_D.

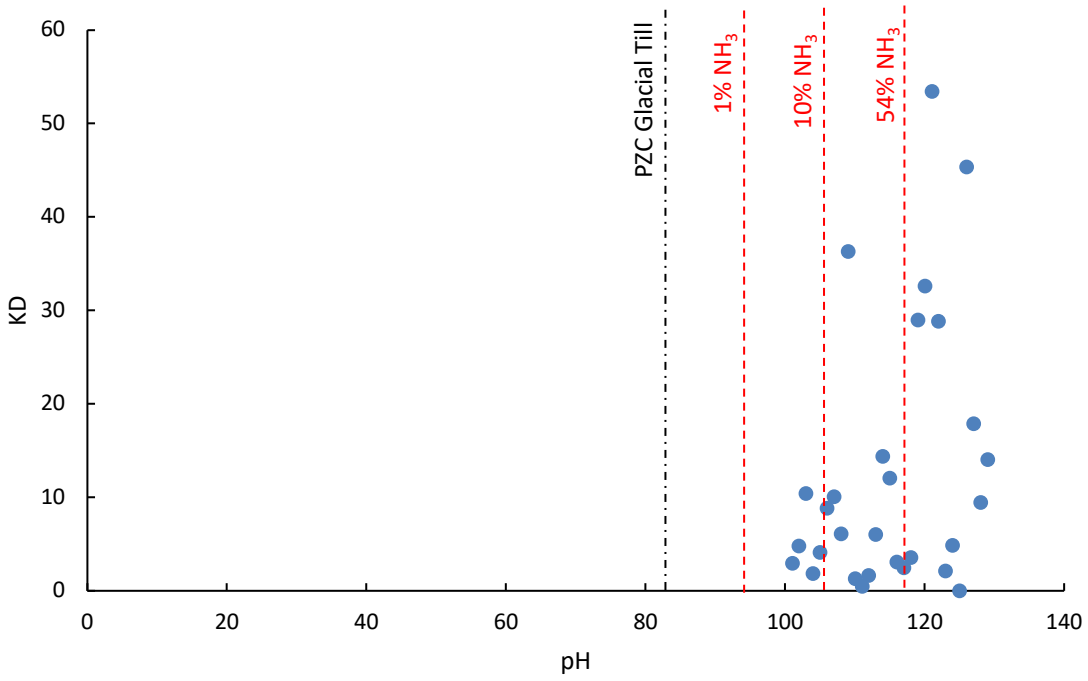

Figure 5.20 K_D and pH of samples measured on day 1 of 6°C leach. Black dot-dash line represents PZC of glacial till (Al-Hamdan and Reddy, 2006). Red dashed lines at pH = 8, 9, 10 represent proportion of ammonia to ammonium + ammonia at 4·C.

5.5.6.3 Implications

Adsorption of ammonium onto sediment surfaces is a significant sink for nitrogen yet adsorbed ammonium is not often considered in glacial N cycling studies e.g. (Wynn et al., 2007; Ansari, 2012). Therefore, glacial N output may be greater than previously thought. However, more recently, studies of Leverett Glacier in Greenland clearly show that the flux of ammonium adsorbed to suspended sediment is approximately equal to the dissolved inorganic nitrogen flux (Wadham et al., 2016; Hawkings et al., 2015). Furthermore, given that the crushed rocks used in these leaching experiments generally have a lower surface area than glacial sediment (Figure 5.2), it is likely that these experiments underestimate the amount of N adsorbed during weathering.

5.5.7 Weathering Model

Upon addition of water to rock, weathering reactions take place liberating solute from rock which are summarised in Figure 5.22. Initial weathering is dominated by rapid hydrolysis reactions which leach cations (including ammonium) and inorganic carbon into solution from carbonates and silicate minerals. In addition, soluble organic molecules in rocks containing kerogen likely contribute significant nitrogen and acetate to solution, possibly via interaction with free radicals produced during crushing. In natural systems, ammonium and acetate likely fuel biogeochemical reactions. Divalent cations exchange for monovalent cations on clay surfaces, such that sodium is the dominant cation in solution (Figure 5.21). Both of these reactions increase pH through release of OH^- and exchange of protons respectively.

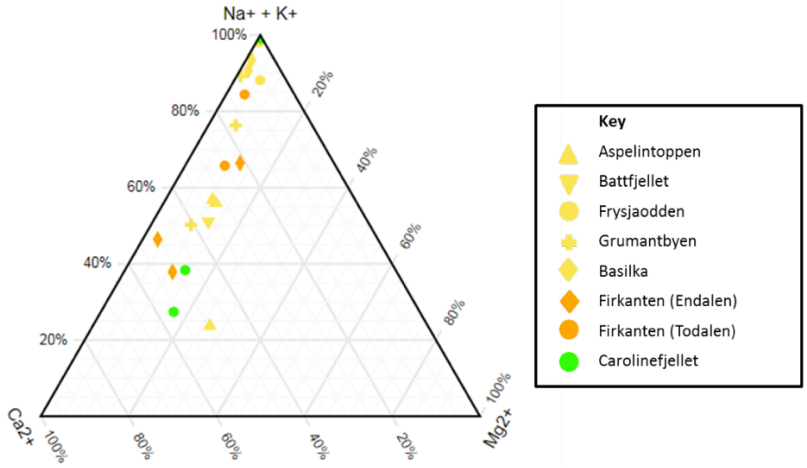

Figure 5.21 Ternary diagram showing major cations released after 11 days at 6°C. Values in equivalent units.

As the pH increases, clay mineral surfaces become more negatively charged, promoting the adsorbtion of ammonium. If abundant sulphide minerals are present, sulphide oxidation generates acidity which initially aids the dissolution of carbonate minerals. If the rock has limited buffering capacity, alkalinity may become exhausted resulting in acidic pH conditions and exsolution of CO_2 gas. Consequently, more positive mineral surface charges repel ammonium ions, partitioning ammonium from sediment into solution.

As sulphide oxidation continues, it couples with silicate dissolution, driving further release of ammonium from clay and feldspar minerals.

However, where there is limited acid generation potential e.g. in sulphide poor rocks, hydrolysis drives water pH to 9 - 10. Consequently, ammonium may be lost from the system as ammonia gas.

Iron (Fe^{2+}) is leached during sulphide oxidation and the weathering of carbonates (siderite). In oxygenated and neutral-alkali conditions, iron is oxidised and precipitates out of solution as iron oxyhydroxides. Manganese is also weathered from siderite in which it substitutes for iron. Efficient manganese extraction occurs under acidic conditions or when it is present in trace amounts in carbonate minerals. The greater solubility of manganese over iron in neutral-alkali water, means that manganese concentrations often exceed iron despite their lower abundance in bulk rock. However where acidic conditions are maintained, abundant iron may remain in solution as Fe^{2+}.

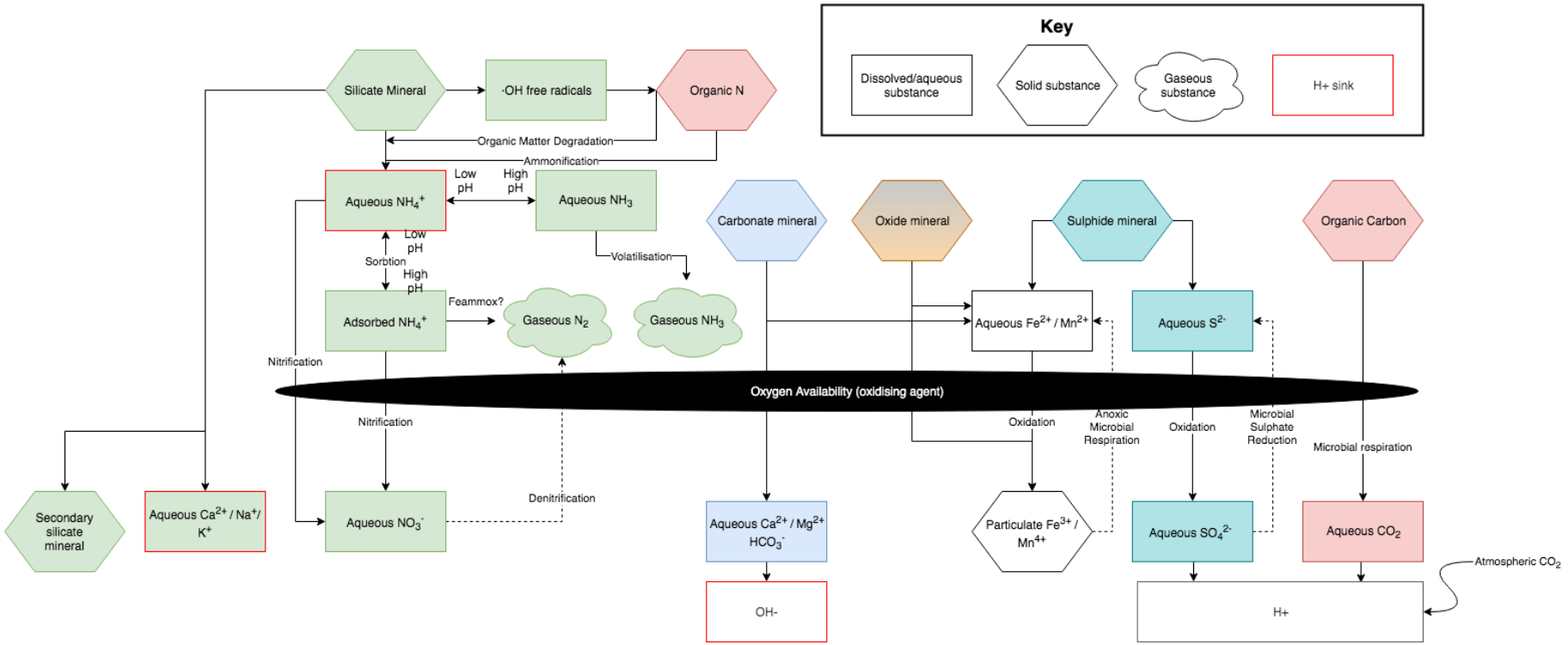

Figure 5.22 Model of weathering in subglacial systems. Lines represent processes, dashed lines are processes that occur under anoxic conditions.

5.6 Conclusions

Rock weathering experiments undertaken here show that sulphide oxidation and silicate weathering are key reaction in these rocks. Ammonium, present in silicate minerals such as feldspars and clays, was liberated from rock during silicate hydrolysis and coupled sulphide oxidation and silicate weathering. Nitrogen release was greater from rocks with higher nitrogen concentrations. Nitrogen was also liberated from organic matter within rocks, since rocks with more abundant organic nitrogen generally liberated the most nitrogen. Liberated ammonium exits solution at high pH through ammonia volatilisation, however this is more prevalent at warmer temperatures. During weathering, adsorption of ammonium onto sediment surfaces became a significant sink for nitrogen, particularly when clay minerals were in abundance. Thus, glacial N output may be greater than previously thought and may drive microbial nitrogen cycling in glacial environments.

Weathering of rock derived organic matter likely liberates acetate, a carbon source which could also fuel microbial processes. However, acetate release did not correlate with TOC due to the heterogeneous nature of kerogen.

The weathering of siderite was hypothesised to release significant iron into solution, particularly from siderite rich rocks of the Frysjaodden Fm. However low pH conditions are required for both efficient siderite weathering and iron solubility. Therefore, any Fe^{2+} weathered from Frysjaodden Fm rocks likely forms particulate oxyhydroxides. However, pyrite oxidation in samples of Firkanten Fm released abundant iron and generated low pH conditions where Fe^{2+} remained in solution.

The weathering experiments presented here were carried out under closed system conditions. The implications of these results to open systems such as glacial channels are discussed in a synthesis of field and experimental work in Chapter 8.

Chapter 6 Subglacial biogeochemical processes and nutrient dynamics

6.1 Introduction

This chapter details the results of chemical analyses from field work on glacial systems in Svalbard carried out in 2016 and 2017. Using the understanding of experimental 'glacial' weathering processes (Chapter 5), this chapter aims to constrain solute sources and biogeochemical reactions occurring within several glacial catchments. The detailed geochemical bedrock analysis undertaken in Chapter 4 provide a detailed insight into the bedrock as a source of N, Fe and Mn which allows for insights to be gained on solute acquisition by glacial run off (see diagram in Appendix D).

The aim of this fieldwork was to collect samples to test the hypotheses below. Snow samples were collected to constrain solute inputs via precipitation to glacial catchments. Bulk runoff was collected at the glacier termini to characterise catchment outputs. Geochemical and isotope analysis of these samples was carried out to constrain the weathering reactions occurring in glacial environments in order to better understand nitrogen liberation from rock.

It was predicted that significant nitrogen would be liberated by weathering as ammonium to glacial run off in catchments featuring nitrogen-rich bedrock. Therefore, catchments with elevated nitrate are anticipated to reflect microbial nitrification of geogenic ammonium. This chapter further seeks to explore geological control on glacial runoff composition in terms of iron and manganese geochemistry. The Firkanten Fm is a major source of N, Fe, sulphides and organic carbon. Leaching experiments suggest that weathering of Firkanten Fm would produce meltwater chemistry with the potential for high N, Fe and Mn. Foxfonna, Fleinsen and Møysalbreen glaciers erode this formation so it is anticipated that their meltwaters could be enriched in these elements.

6.2 Hypotheses

- Geological variation between different glacial catchments accounts for differing export of nutrients: nitrogen, iron and manganese.
- Anoxic sulphide oxidation generates acidity in subglacial environments which facilitates geogenic N liberation through silicate weathering.

6.3 Results

Meltwater collected from the termini of glaciers represents the bulk run off from the catchment. Water is therefore a combination of ice melt and precipitation (snow melt/rain). The solute in bulk run off therefore reflects both water sources and their pathways where additional solute may be acquired through weathering (Figure 6.1). Precipitation contains dissolved marine salts, particularly, sodium chloride, as well as nutrients such as nitrate and ammonium. Elution of solute from snow during melting and the rejection of solute from ice crystals during freezing result in a limited solute content of ice. Therefore, ice melt in this study is considered as an independent solute-free water source and is assumed not to contribute to the solute in bulk run off. As melt flows through crushed rock environments, weathering reactions release ions to meltwater. To establish solute acquisition from rock weathering, bulk run off is corrected for precipitation inputs.

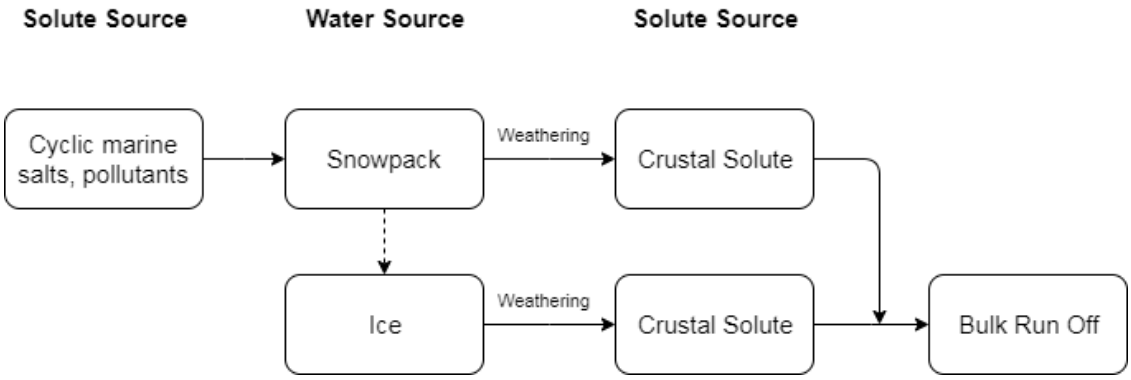

Figure 6.1 Flowchart of solute acquisition by water in glacial catchments. Dashed arrow indicates that the flux from snowpack to ice is relevant over long timescales, however, this study considers weathering over the timescale of a melt season, in which there is minimal incorporation of snow to ice.

6.3.1 Snow

6.3.1.1 Snow Chemistry

Nitrogen compounds in precipitation are dependent on atmospheric emissions of nitrogen oxides (NO_x), nitrous oxide (N_2O) and ammonia (NH_3). NO_x and N_2O are largely derived from fossil fuel combustion, biomass burning, lightning and soil emissions while domestic animal waste, soil emissions, sea surface emissions constitute the majority of ammonia emissions (Aneja et al., 2001). Ammonia is the most prevalent base gas in the atmosphere and when deposited through precipitation represents an ecologically significant nutrient source as reduced nitrogen species are believed to be the most biologically

available in N limited environments (Paerl, 1997). Ammonia has a short atmospheric lifetime (1 - 5 days (Warneck, 1999)) due to low source heights and high dry deposition velocity (Asman and van Jaarsveld, 1992) which mean that it generally deposits locally to its source. However, ammonia may react with acidic species such as H_2SO_4, HNO_3, HCl to form ammonium aerosols which can be transported longer distances in the atmosphere (Aneja et al., 2001).

Anion and ammonium concentrations of snow are outlined in Table 6.1. Sulphate is the dominant ion measured, followed by chloride. Solute concentrations are fairly dilute on the order of 10s of µeq/L likely derived from marine salts and anthropogenic emissions. Nitrate concentrations (up to 10 µeq/L) exceed ammonia (< 2 µeq/L).

Table 6.1 Chemistry of snow collected on Longyearbreen on 8/5/2017

Sample Name	Cl^- (µeq/L)	SO_4^{2-} (µeq/L)	NO_3^- (µeq/L)	NH_4^+ (µeq/L)
Snow 1	58.2	75.6	8.9	1.6
Snow 2	59.0	64.5	10.2	1.7
Snow 3	73.9	68.3	2.4	1.4
Snow 4	80.5	61.6	1.9	-

6.3.1.2 Snow Isotope Chemistry

Water oxygen isotopes of snow collected in May 2017 are outlined in Table 6.2. $\delta^{18}O$ values are negative and fall within the range of -13.6‰ to -15.3‰. Snow samples collected from higher elevations on the glacier are approximately 1.5‰ lighter ($\delta^{18}O$) than snow from around 130m lower on the glacier surface.

Table 6.2 Isotope chemistry of snow collected on Longyearbreen on 8/5/2017

Sample Name	Elevation (m ASL)	H_2O $\delta^{18}O_{VSMOW}$ (‰)
Snow 1	543	-15.08
Snow 2	510	-15.28
Snow 3	486	-13.71
Snow 4	410	-13.59

6.3.2 Meltwater

6.3.2.1 Precipitation Correction on Meltwater Data

Snow provides a source of sea salt, sulphate aerosols, and nitrate to glacial catchments (Tranter et al, 1996). In coastal environments, sea spray results in deposition of ions on land in their seawater molar proportions. These salts are dissolved by surface water and eventually return to the oceans. As such these are often termed cycling marine salts.

Chloride is derived from sea salt in the surrounding marine environment and precipitation as opposed to crustal sources. It is also a conservative ion with little involvement in biogeochemical reactions. Therefore, the ratio of chloride to other ions in snow can be used to calculate the proportion of bulk run off solute derived from snow pack and non-snowpack sources. Since snow samples were only collected from 2017 winter deposition, only 2017 summer melt is corrected for snowpack solute. Each corrected ion is discussed in the following text.

Sulphate concentrations in Longyearbreen snow (2017) were low (< 80 µeq/L) expressing a 1:1 ratio with chloride (Table 6.1). Sulphate in bulk glacial runoff may be derived from the snowpack and the oxidation of sulphide minerals originating from bedrock (Tranter, 1996); whereas snowpack sulphate is sourced from marine aerosols. Given the sulphate: chloride ratio of snow above, a value for non-snowpack sulphate (SO_4^{2-*}) can be derived via Equation 6.1.

$$^{\text{Non-snowpack}}SO_4^{2-*} = {}^{\text{total}}SO_4^{2-} - (1Cl^-) \qquad \textbf{Equation 6.1}$$

This assumes that all chloride is derived from snowmelt and the ratio of chloride to sulphate remains constant during snowmelt. During the late summer season, 90 - 99% of bulk sulphate in the samples presented here is derived from non-snowpack sources.

In addition to sulphate and chloride already addressed, sodium, calcium, magnesium and potassium may be sourced from cyclic salt spray. Whilst no data for cations is available for these snow samples, we can correct bulk run off data for salt spray using seawater molar ratios of these ions with chloride (Anthoni, 2006) (Equation 6.2 - Equation 6.5).

$$^{\text{Non-snowpack}}Na^{+*} = {}^{\text{total}}Na^{+} - (0.86Cl^-) \qquad \textbf{Equation 6.2}$$

$$^{\text{Non-snowpack}}Ca^{2+*} = {}^{\text{total}}Ca^{2+} - (0.019Cl^-) \qquad \textbf{Equation 6.3}$$

$$^{\text{Non-snowpack}}Mg^{2+*} = {}^{\text{total}}Mg^{2+} - (0.098Cl^-) \qquad \textbf{Equation 6.4}$$

$$^{\text{Non-snowpack}}K^{+*} = {}^{\text{total}}K^{+} - (0.018Cl^{-}) \qquad \textbf{Equation 6.5}$$

Snow also contains nitrate and ammonium because nitrogen oxides and ammonia gases interact with water in the atmosphere prior to falling as precipitation. Air pollutants including nitrogen oxides from Eurasia, accumulate in the Arctic during winter/spring and are then deposited on the snow/ground (Law and Stohl, 2007). Nitrate was the principal inorganic nitrogen form in these snow samples (up to 10 µeq/L), whereas ammonium concentrations were less than 2 µeq/L. Nitrate concentrations were greater at the two higher sampling sites. Since chloride acts as a tracer of snowmelt, we can determine the proportion of nitrate derived from snow. However, unlike chloride, nitrate is not a cyclic marine salt, therefore the relationship with chloride was not as robust as it was with the other corrected ions. The average ratio of nitrate: chloride in the snow samples was 0.1. In all samples except Foxfonna spring, the nitrate: chloride ratio of runoff exceeds this value. Calculating non-snowpack nitrate using the same approach as sulphate (Equation 6.6) implies that between 55 and 89% of nitrate is derived from non-meteoric sources. Using the same logic, between 34 and 96% of all aqueous ammonium comes from non-meteoric sources (Equation 6.7).

$$^{\text{Non-snowpack}}NO_3^{-*} = {}^{\text{total}}NO_3^{-} - (0.1Cl^{-}) \qquad \textbf{Equation 6.6}$$

$$^{\text{Non-snowpack}}NH_4^{+*} = {}^{\text{total}}NH_4^{+} - (0.03Cl^{-}) \qquad \textbf{Equation 6.7}$$

6.3.2.2 Catchment Meltwater Chemistry

The results of water chemical analysis from each catchment are outlined separately below. The full dataset can be found in Appendix C. Since sampling was limited in 2016, the majority of the results discussed below relate to fieldwork in 2017.

Ternary diagrams in Figure 6.2 provide an overview of bulk glacial runoff from each catchment. The major anion in all samples but one was sulphate which represented > 60% of all anions. The exception was Foxfonna Spring, whose anion budget consisted mainly of bicarbonate but also featured elevated chloride concentrations. Cation budgets of most samples were dominated by either calcium or magnesium, with the exception of Foxfonna Spring, where sodium and potassium comprised 79% of major cations (Na, K, Ca, Mg). Longyearbreen water was typically more sulphate and magnesium-rich, while Rieperbreen and Møysalbreen waters had a greater proportion of calcium and bicarbonate.

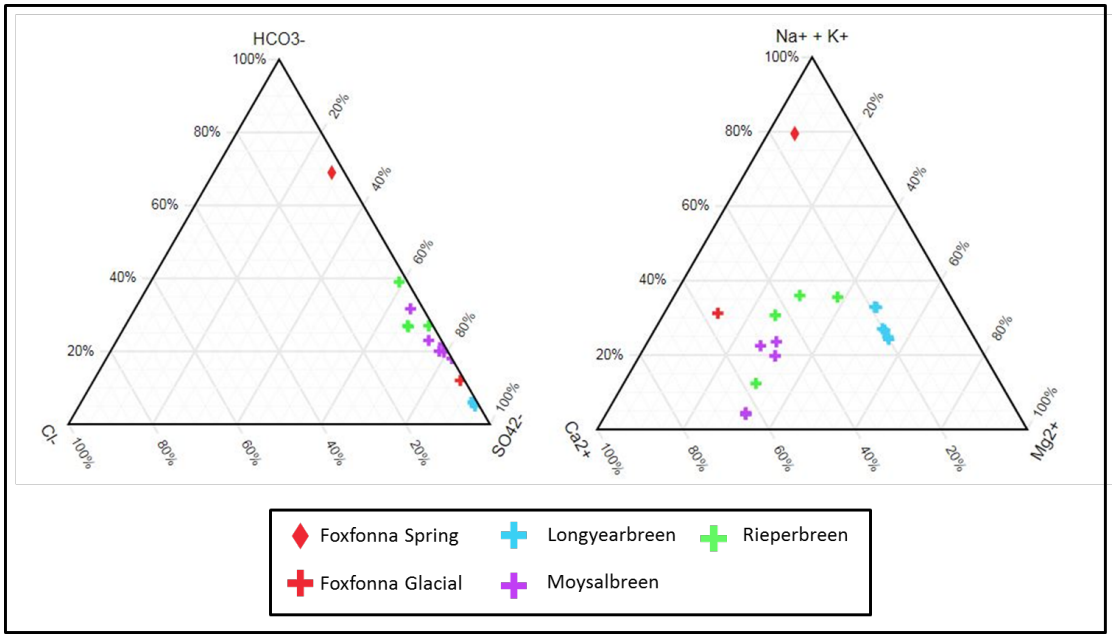

Figure 6.2 Major ion melt water chemistry (µeq) plotted in ternary diagrams. Meltwater collected in 2017 (Not Precipitation corrected).

Concentrations of chloride in glacial runoff can give an indication of water sources if it is assumed to be derived entirely from snowmelt. Electrical conductivity is a proxy of ionic strength and therefore combined with chloride can provide information on solute acquisition. The electrical conductivity of meltwater samples correlated positively with chloride concentrations (Figure 6.3). The trend line has a positive intercept, such that chloride concentrations were always > 0. Foxfonna Spring does not lie on the trend line since it is enriched with chloride.

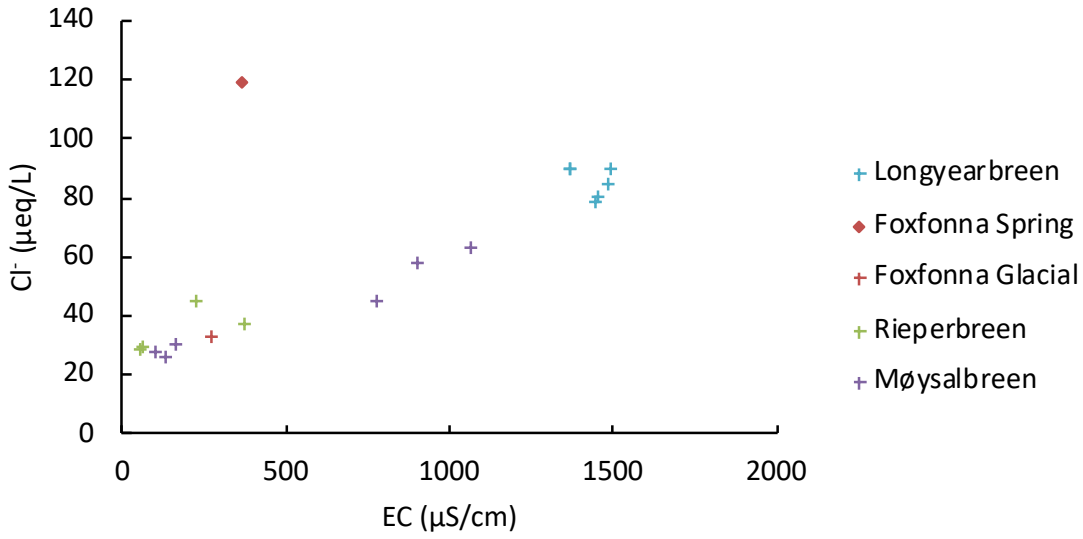

Figure 6.3 Electrical conductivity and chloride concentrations of 2017 meltwater samples.

6.3.2.2.1 Foxfonna (Appendix C)

Water sampling points at the spring at Foxfonna and at the glacial terminus are only metres apart but the chemistry of water samples from each were considerably different. Spring water had a dissolved oxygen saturation of only 8%. Unfortunately, the meter stopped working after this so no equivalent reading could be measured in the glacial water, but it is known to be highly oxygenated.

Chloride concentrations in the 2017 Foxfonna spring sample were the greatest of all samples analysed and four times greater than the glacial water. Sodium concentrations were also elevated relative to chloride in both samples (2017: Na/Cl = 22 - 23). Calcium was enriched relative to magnesium at both sampling points as indicated by the highest Ca/Mg ratios (> 2) in this dataset. The dominant anion in the spring water was bicarbonate, followed by sulphate, whereas glacial water was dominated by sulphate with only minor bicarbonate.

Furthermore, the glacial sample contained a significant amount of nitrate but little ammonium. Conversely, Foxfonna spring showed the opposite. The spring contained high concentrations of filterable iron (2017: 6.5 µM) while concentrations were below level of quantification in the glacial channel.

6.3.2.2.2 Longyearbreen (Appendix C)

Supraglacial, englacial and subglacial water were collected from Longyearbreen. Subglacial water and a moraine spring were sampled on three separate days. The water data of these two sites are highly similar and suggest that they are part of a common subglacial pathway, hence from here on these shall be grouped as "*subglacial*". However, it should be noted that subglacial drainage at Longyearbreen and other cold based glaciers actually represents channels formed by cut and closure which have reached the glacier bed (Figure 6.4; (Naegeli et al., 2014; Gulley et al., 2009)). Longyearbreen subglacial water had the highest ionic load of all the waters analysed and was well oxygenated. Electrical conductivity was high in all subglacial samples, typically around 1400 µS/cm, which is the highest of all sites visited. Sulphate was the dominant anion and concentrations exceed all other sites. High sulphate concentrations were accompanied by consistently high nitrate concentrations in the late melt season (maximum 134 µeq/l in 2016 and 82 µeq/l in 2017). The dominant cation was magnesium and the Ca/Mg ratio is ~0.4 (0.5 - 0.6 in 2016) whereas at other sites this ratio is > 1 (Figure 6.5). Sodium concentrations were particularly high compared to other sites (maximum 6996 µeq/l in 2016 and 4591 µeq/l in 2017). Supraglacial and englacial samples had lower nutrient concentrations than subglacial waters (Figure 6.6) in which nitrate was in the range 44 – 82 µeq/l, while ammonium was generally < 10 µeq/l. Filterable iron concentrations were

consistently significant (2 - 6 µM) but these were an order of magnitude lower than Mn concentrations (50 – 60 µM). Manganese concentrations were greater in Longyearbreen waters than any other catchment in this study.

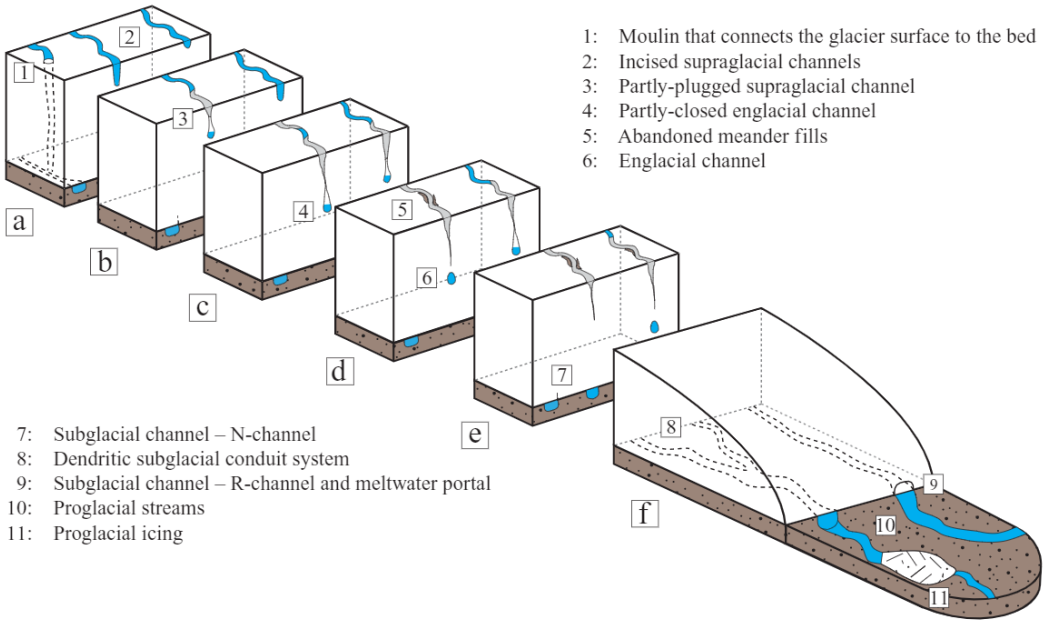

Figure 6.4 Schematic diagram of the temporal and spatial evolution of cold based glacier drainage systems (Naegeli et al., 2014)

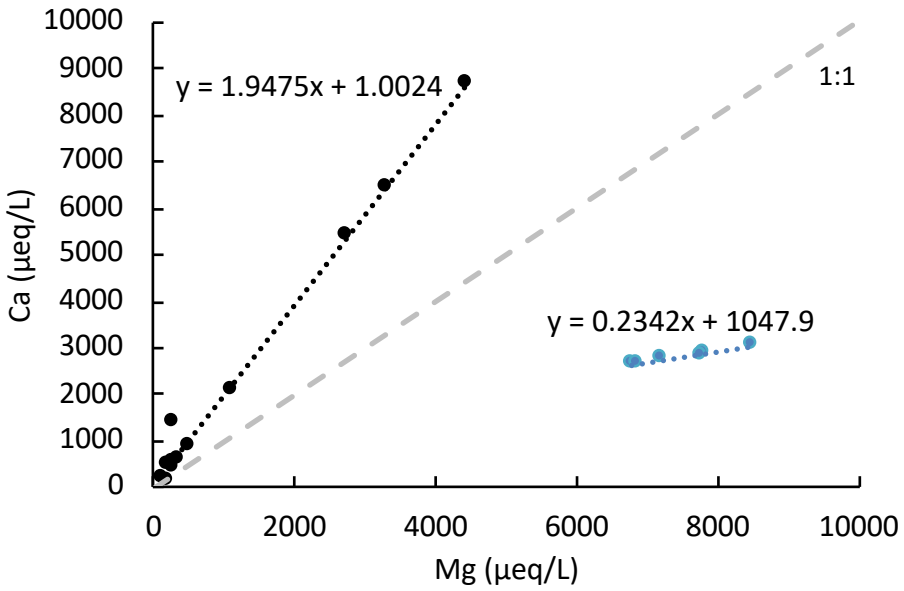

Figure 6.5 Calcium and Magnesium in meltwater samples (2017). Longyearbreen samples, plotted in blue, fall along a different trendline to the other catchments (black). Grey line is 1:1.

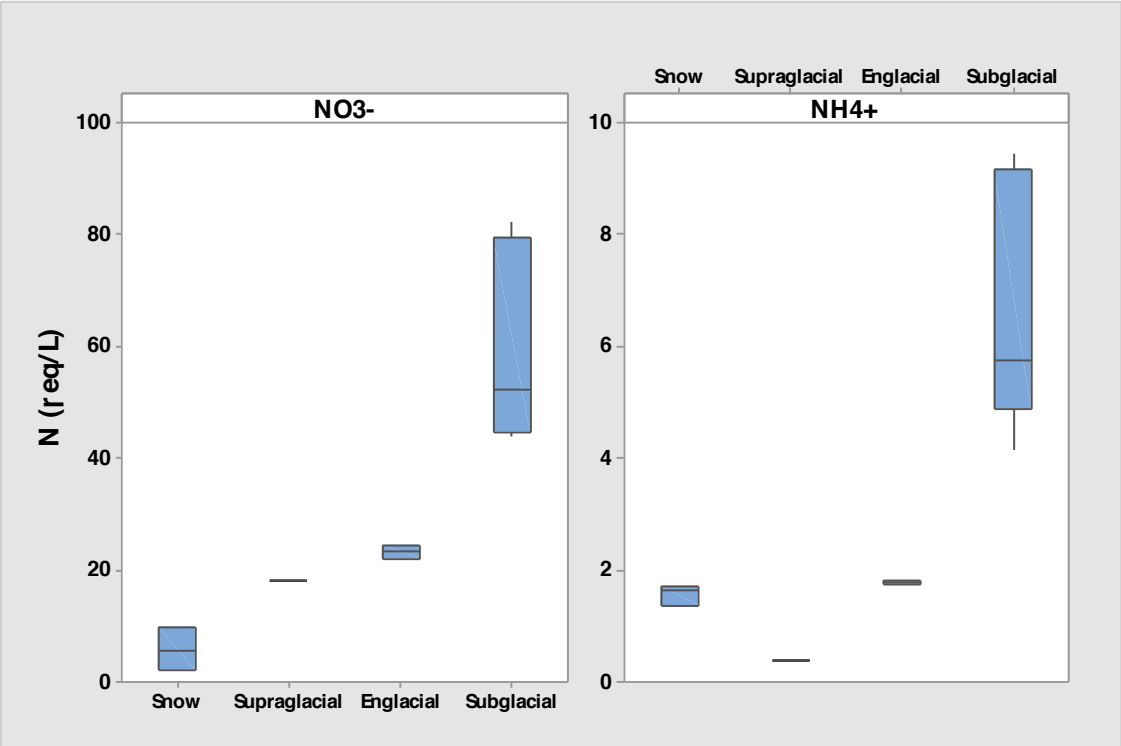

Figure 6.6 Box plots of nitrate and ammonium concentrations of snow and supraglacial, englacial and subglacial water at Longyearbreen in 2017. n = 4, 1, 2, 6 respectively

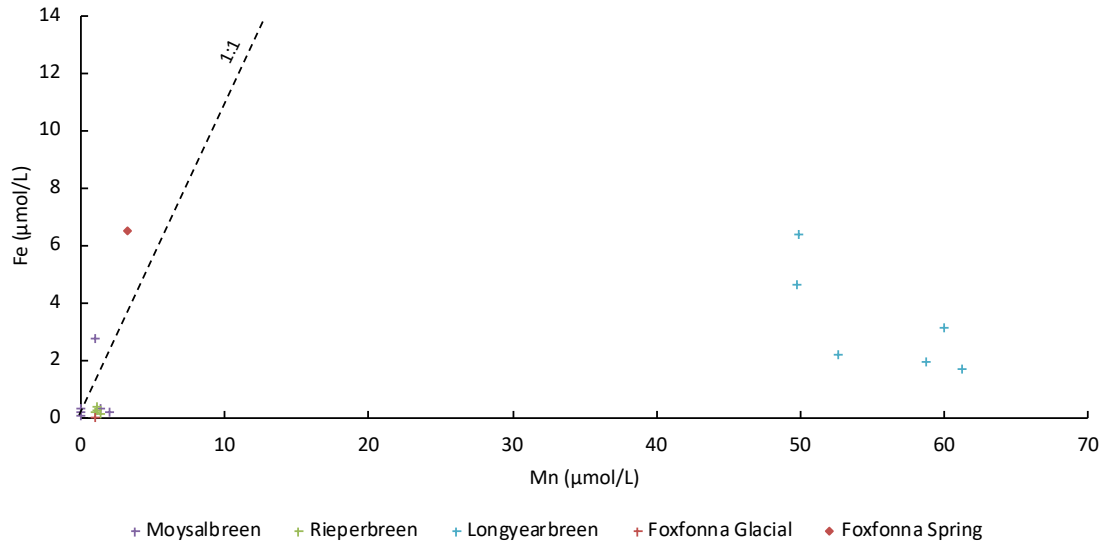

Figure 6.7 Manganese and Iron concentrations in glacial meltwater (2017)

6.3.2.2.3 Rieperbreen (Appendix C)

In 2017, two different glacial outflows were sampled at Rieperbreen. The first was a channel that flowed between the northern margin of the glacier and lateral moraine (named 'glacial'). The second was a spring (named 'ice spring') that emerged from beneath glacial ice ~10 m downstream of the channel. Samples were collected on two separate days, the first after a heavy rainfall event, when glacial and ice spring chemistry were identical. The second day of sampling

occurred during very cold weather when discharge was low. Electrical conductivity was greater at both sampling sites on the 2nd day as all solute was more concentrated, although the glacial water had higher concentrations. Unlike other ions, iron and manganese concentrations did not increase on the lower discharge day.

Nitrate concentrations were moderate (9 - 18 µeq/l) although they reached 28 µeq/l in 2016, while ammonium concentrations were < 6 µeq/l. Ca/Mg ratios were consistent with the other sites, being generally > 1.6. The Na/Cl ratio was 10 - 13 on the low discharge day, whereas on the day following heavy rainfall, the ratio was 5. This likely reflects a greater precipitation component in bulk runoff due to contribution of marine-derived chloride. Calcium is the major cation and sulphate the major anion. Fe concentrations were equal to blank samples of deionised water but Mn concentrations were 1 µM.

Water was suboxic (18% oxygen saturation in glacial, 45% in spring) under low flow conditions however the dissolved oxygen probe was not working on the high discharge day so no DO data exist for 29/8/17.

6.3.2.2.4 Møysalbreen and Gløtfjellbreen (Appendix C)

In 2016, water sampling was carried out at moraine springs on the glacial forefields of Gløttfjellbreen (Figure 6.8, stream E; Figure 6.19) and Møysalbreen (Figure 6.19). The moraines featured numerous different streams whose conductivity was measured. The springs with the highest conductivity were assumed to have been diluted to a lesser extent and were chosen to collect samples from. The stream at Gløttfjellbreen, was non-turbid and thought to be an artesian upwelling of groundwater. The moraine springs at Møysalbreen were turbid and flowed into a proglacial lake, which by the following summer had been completely drained by undercutting of channels beneath the lake bed. In 2017, the moraine springs had migrated downslope from their previous position onto the former lake bed. 2017 moraine spring samples were collected from here (Moy Loc 2 and 4) as well as from ice marginal channels at both Møysalbreen (Moy Loc 1) (Figure 6.9) and Gløttfjellbreen (H in Figure 6.8). A final sample was collected from the total Møysalbreen runoff (Møy Loc 3 = moraine spring + ice marginal channel). Water flowed at a high discharge in the channels (estimated > 200 l/second), much greater than at any other site. Water collected from the moraine spring was taken from where the water emerges (Møy Loc 4) and approximately 60 m downstream of here (Møy Loc 2). Electrical conductivity of the stream was highest where the spring emerged (1063 µS/cm) and decreased downstream as other water sources joined and diluted the flow. Ice marginal channels and larger rivers had lower conductivities than the moraine springs. The

water sampled in this catchment generally had a pH of around 9, which is 1 pH unit higher than the average of other catchments. All water samples were well oxygenated except Gløttfjellbreen which had 60% dissolved oxygen saturation.

The major anion in all but one sample was sulphate while the cation load was dominated by calcium and magnesium with a typical Ca/Mg ratio of 1.6-1.9. Moraine springs have low Na/Ca ratios whereas meltwater channels had much higher values. Nitrate concentrations were between 6 and 27 µeq/L. The higher discharge, low conductivity ice marginal channels (Møy Loc 1 and Glottfjellbreen 2017) had higher ammonium concentrations than nitrate, whereas the reverse was true in moraine springs where nitrate was the dominant inorganic form of nitrogen.

Gløtfjellbreen artesian spring (2016) exhibited a distinct chemical composition to the remainder of samples. Sulphate concentrations were an order of magnitude less than bicarbonate. This artesian spring was also characterised by elevated sodium 2608 µeq/l) and silica (70 µM) concentrations, while no nitrate was detected.

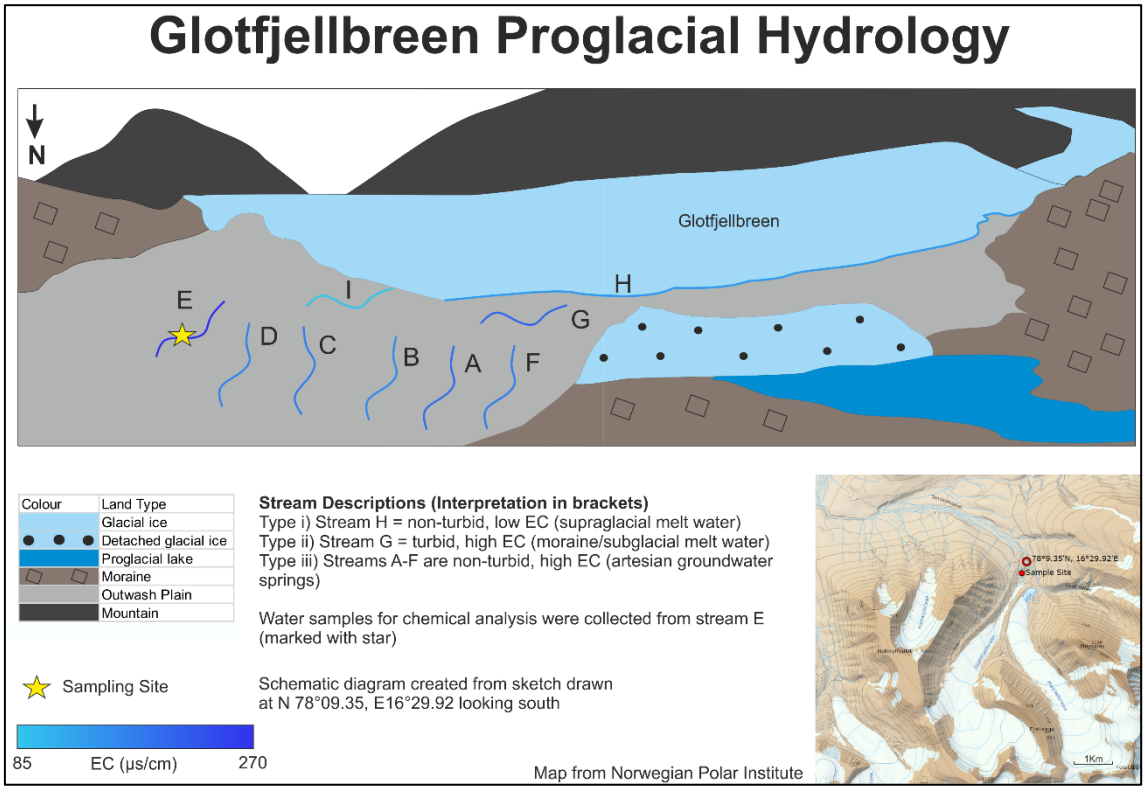

Figure 6.8 Sketch diagram of proglacial moraine springs at Glottfjellbreen in 2016.

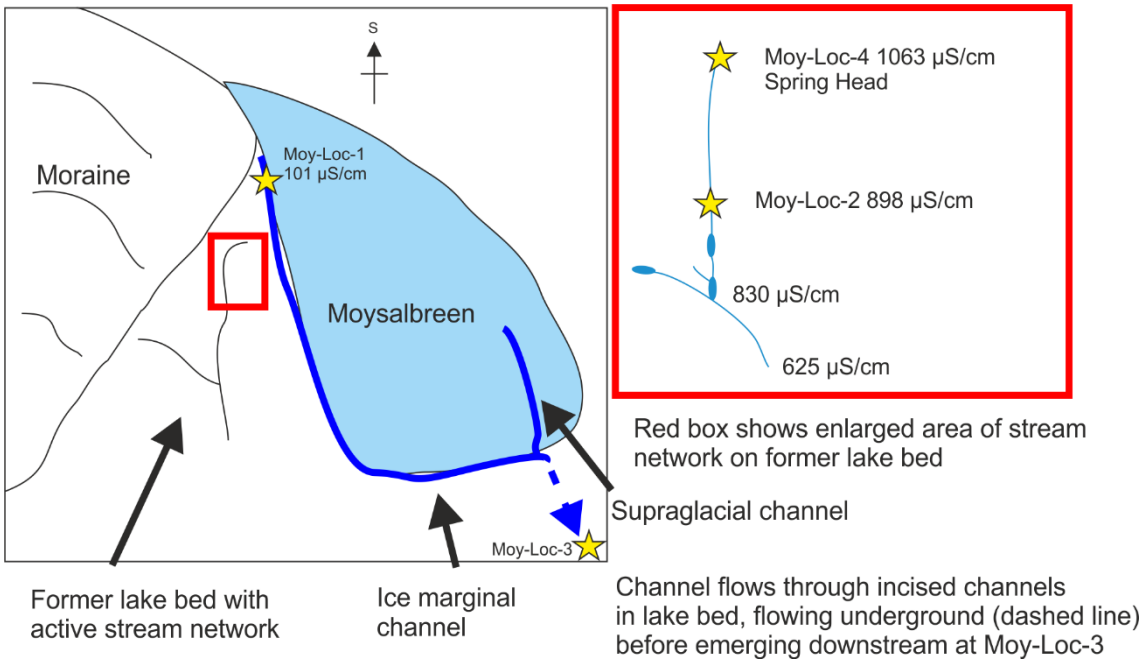

Figure 6.9 Sampling sites at Møysalbreen in 2017. Values are electrical conductivity recorded in situ.

6.3.2.2.5 Fleinisen (Appendix C)

Fleinisen was only visited during fieldwork in 2016. The meltwater, emanating from the glacier front, has dissolved oxygen saturation of 10% and likely represents an anoxic subglacial flowpath. Bicarbonate and sulphate have similar concentrations (2091 and 1466 µeq/L respectively) and represent the bulk of anions, while there were very low chloride concentrations. Calcium was the major cation, followed by sodium. Silica concentrations were 100 µmol/L, whilst nitrate concentrations were extremely low (1 µeq/L) and less than ammonium (9 µeq/L).

6.3.2.3 Meltwater Isotope Chemistry

The stable isotope geochemistry of water samples is outlined in Table 6.3. Oxygen ($\delta^{18}O$) and hydrogen (δD) isotopes of water, collected in 2016, are plotted in Figure 6.10 alongside the global meteoric water line (GMWL). As air masses move towards the poles, they become increasingly negative with respect to $\delta^{18}O$ and δD as precipitation is enriched with the heavier isotopes. During this process, hydrogen isotopes are fractionated in proportion to oxygen isotopes, giving the relationship first defined by Craig (1961):

$$\delta D = 8\ \delta^{18}O + 10$$

Equation 6.8

termed the GMWL. Deviation from this line may be caused by localised evaporation/freezing and mixing of different water bodies. The meltwater data

(Figure 6.10) fall along a trend line that is sub-parallel to the GMWL, and more similar to the local meteoric water line defined for Svalbard (Yde et al., 2012). Therefore, these meltwater samples likely reflect typical local evaporative conditions and are unlikely affected by unusual mixing with other water bodies.

The $\delta^{18}O\text{-}H_2O$ of snow ranges between -15.3 and -13.6‰, while that of water occupies a similar range with values between -14.7 and -12.3‰. The $\delta^{18}O\text{-}SO_4$ of water ranges between -10.4 and -1.0‰ and are all isotopically heavier than their equivalent $\delta^{18}O\text{-}H_2O$. $\delta^{18}O\text{-}SO_4$ at Foxfonna spring are the least negative of all samples (-1‰).

Sulphide extracted from rock samples exhibit a broad range of $\delta^{34}S$ values from -50 to +25‰ although the majority of values lie between -22 and +4‰. In Chapter 4 mass weighted means of $\delta^{34}S$ for each geological formation were calculated, here, the mass weighted mean of $\delta^{34}S$ from the bedrock sequence in each catchment is calculated (Table 6.4). Each catchment has distinctive $\delta^{34}S$ values. Meltwater sulphate $\delta^{34}S$ values vary with catchment and have values between -16.44 and +6.81 (Table 6.4). Meltwater sulphate $\delta^{34}S$ closely matches the average bedrock pyrite $\delta^{34}S$ in the Rieperbreen and Møysalbreen catchments, however Longyearbreen meltwater is isotopically lighter than bedrock, while Foxfonna spring water is isotopically heavier than bedrock with positive SO_4^{2-} $\delta^{34}S$.

Table 6.3 Isotope chemistry of meltwater collected in 2016 and 2017

Date	Site	H_2O $\delta^{18}O_{VSMOW}$ (‰)	SO_4^{2-} $\delta^{18}O_{VSMOW}$ (‰)	SO_4^{2-} $\delta^{34}S_{CDT}$ (‰)
2016				
27/08/2016	Foxfonna Spring	-14.56		3.24
28/08/2016	Longyearbreen	-14.87		-12.58
30/08/2016		-13.55	-6.53	-12.98
01/09/2016	Gløtfjellbreen spring	-14.62	-3.35	1.83
03/09/2016	Møysalbreen (moraine spring)	-13.44	-8.23	-0.26
07/09/2016	Rieperbreen	-14.49	-4.43	-10.67
10/09/2016	Fleinisen	-13.8		-2.94

Date	Site	H_2O $\delta^{18}O_{VSMOW}$ (‰)	SO_4^{2-} $\delta^{18}O_{VSMOW}$ (‰)	SO_4^{2-} $\delta^{34}S_{CDT}$ (‰)
2017				
01/09/2017	Foxfonna Spring	-14.31	-0.96	+6.81
27/08/2017	Longyearbreen	-12.59		-15.63
27/08/2017		-12.58		-16.03
28/08/2017		-12.97	-1.23	-15.99
28/08/2017		-12.58	-4.80	-16.44
01/09/2017		-12.31	-1.9	-13.86
01/09/2017		-12.84	-4.87	-13.97
04/09/2017	Møy-Loc-1	-12.81	-2.99	-1.99
04/09/2017	Møy-Loc-2	-14.06	-9.11	-2.59
04/09/2017	Gløttfjellbreen (ice marginal channel)	-13.00		-1.28
05/09/2017	Møy-Loc-2	-13.74		-2.69
05/09/2017	Møy-Loc-3	-13.25	-6.64	-2.38
05/09/2017	Møy-Loc-4	-13.85	-10.39	-2.78
29/08/2017	Rieperbreen	-14.64		
29/08/2017		-14.70		
14/09/2017		-13.90		-9.07
14/09/2017		-13.87	-7.05	-9.44

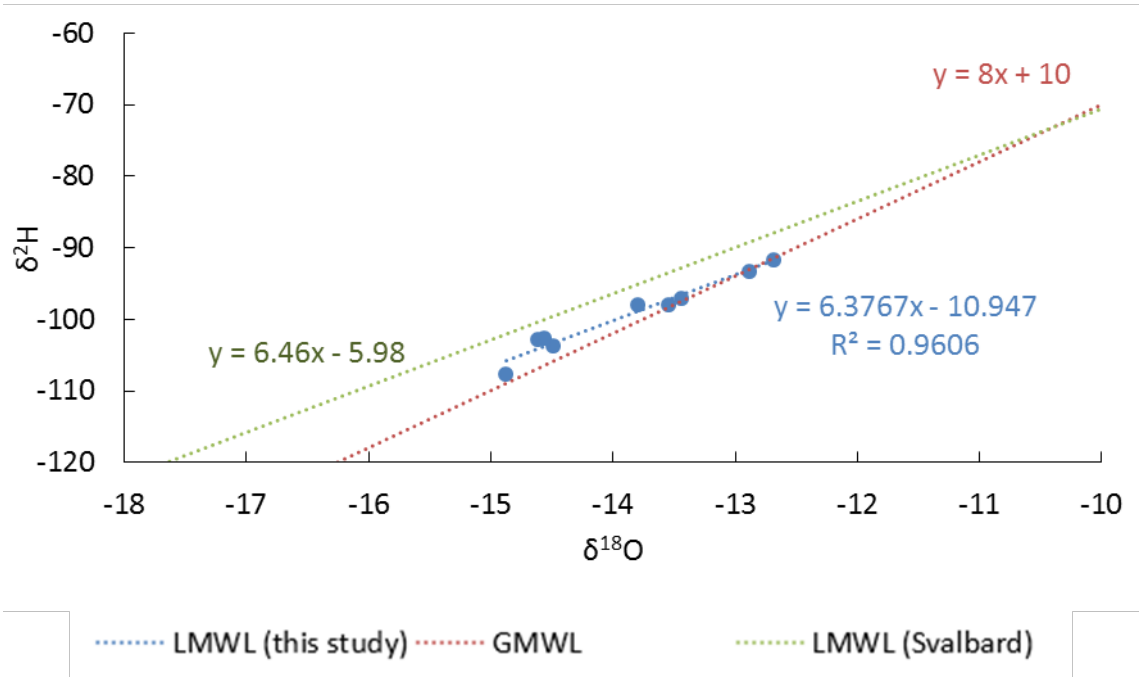

Figure 6.10 Oxygen and hydrogen isotope data (‰) of Svalbard glacial runoff collected in 2016 (blue points and blue best fit line). Red dotted line is global meteoric water line, green dotted line is local meteoric water line (Yde et al., 2012).

Table 6.4 Average sulphur isotope values of meltwater sulphate for 4 different glacial catchments. Value in parentheses is 1 standard deviation.

Catchment	Underlying bedrock		Meltwater
	Geological Fms	MWM Pyrite $\delta^{34}S_{CDT}$ (‰)	Mean SO_4 $\delta^{34}S_{CDT}$ (‰)
Longyearbreen	Aspelintoppen, Battfjellet, Frysjaodden, Grumantbyen, Basilika	0.45 n = 18	-15.32 (1.12) n = 6
Rieperbreen	Battfjellet, Frysjaodden, Grumantbyen,	-10.28 n = 10	-9.25 n = 2
Foxfonna Spring	Grumantbyen, Basilika, Firkanten	-1.36 n = 13	6.81 n = 1
Møysalbreen/Gløttfjellbreen	Basilika, Firkanten, Carolinefjellet	-2.63 n = 13	-2.26 (0.55) n = 6

6.3.3 Suspended Sediment

The results of suspended sediment concentration of water samples collected in August – September 2017 and in June – July 2018 are presented in Table 6.5 and Table 6.6 respectively. Adsorbed ammonium analysis of sediment sampled in 2018 is also shown in Table 6.6. Late melt season glacial runoff in 2017 featured suspended sediment concentrations of 0.4 - 2.4 g/l. The average suspended sediment concentration of these samples was 0.8 g/l whereas during the peak melt season in 2018, the suspended load was higher (1.6 g/l). Only 3 data points are available for the 2018 samples, therefore these data are not temporally representative over the melt season and are for indicative use only.

Between 2 and 12 µg of NH_4^+ (N) per g are adsorbed onto sediment samples collected from Longyearbeen in 2018. Whilst this dataset is limited, it gives an indication of the magnitude of sediment delivery and associated adsorbed ammonium in glacial runoff.

Table 6.5 Suspended sediment concentrations of glacial runoff in 2017

Sample Date	Locality	Suspended Sediment Concentration (g/l)	Surface Area (m^2/g)
29/08/2017	Rieperbreen	0.86	
27/08/2017	Longyearbreen	0.62	
28/08/2017	Longyearbreen	0.47	
29/08/2017	Rieperbreen	0.61	
31/08/2017	Longyearbreen	0.47	
31/08/2017	Longyearbreen	0.37	16.15
03/09/2017	Gløtfjellbreen	2.43	8.71
04/09/2017	Møysalbreen (Møy-Loc-1)	0.52	
04/09/2017	Møysalbreen (Møy-Loc-3)	1.01	
Average		**0.82**	
S		**0.60**	

Table 6.6 Adsorbed ammonium concentrations on sediment collected at Longyearbreen in 2018

Date	Sediment Type	Surface Area (m^2/g)	Suspended Sediment Concentration (g/l)	Adsorbed NH_4^+ (N µg/g)
29/06/2018	Suspended Sediment			5.92
29/06/2018	Suspended Sediment		1.64	12.11
30/06/2018	Suspended Sediment		1.56	4.43
30/06/2018	Suspended Sediment		1.53	5.64
01/07/2018	Suspended Sediment			1.97
01/07/2018	Suspended Sediment			2.19
01/07/2018	Deposited Fines	8.22		0.58

6.4 Discussion

6.4.1 Meltwater Sources and Weathering Reactions

Bulk glacial runoff at the portals likely represents a combination of ice melt and snow melt. Supraglacial melt likely moves through the glacial drainage system relatively quickly via crevasses whereas snowmelt from high altitude snow packs on the valley sides will have further to travel and are more prone to delayed transport via storage in talus/moraine (Rutter et al., 2011). Therefore, during late summer, any snowmelt in the bulk flow is likely to be derived from delayed flow paths where interaction with rock is more likely. Bulk discharge is lower in late summer as temperatures begin to cool and melting slows down. As a result, solute concentrations generally peak during late summer.

6.4.1.1 Flow paths

Whilst the majority of solute was calculated to derive from non-snowpack sources, the positive correlation between electrical conductivity and chloride concentrations (Figure 6.3) suggests that solute acquisition is related to a chloride-rich water source. However, the positive intercept suggests that chloride was derived from a different source to other solutes. EC does not discriminate between non-snowpack and snowpack solute, therefore non-snowpack sulphate and nitrate (acquired during weathering) are plotted against chloride in Figure 6.12 and Figure 6.13. These graphs show positive relationships between non-snowpack solute and chloride. They also show that when crustal solute concentrations are zero, chloride concentrations are always greater than zero. This suggests that solute acquisition is largely achieved through interaction of snowmelt with crushed rock. Foxfonna glacial and several Longyearbreen

samples are enriched with nitrate relative to chloride which is addressed in Section 6.4.1.6.

Furthermore, the positive slopes in Figure 6.12 and Figure 6.13 are likely achieved via mixing of solute-rich snowmelt with a more dilute water source containing low concentrations of chloride (most likely icemelt). Ice melt is largely routed through supraglacial and ice marginal channels where transit times are rapid and opportunity for interaction with crushed rock is limited. Therefore, this water source is unlikely to acquire much solute during its transit through the glacier. Snowmelt-fed moraine water was observed in springs on the valley sides, which feed into ice marginal channels containing lower ionic strength water. Therefore, bulk runoff solute concentrations are determined by mixing of solute poor ice-melt with solute rich snowmelt. This is consistent with other studies which demonstrate the importance of solute acquisition via ice marginal (moraine/talus) flow paths e.g. (Rutter et al., 2011; Hodson et al., 2010a). The resultant water composition derived from this 2 member mixing model is dependent on 1) the mixing ratio of solute rich and solute poor water and 2) the maximum amount of solute acquisition possible in each catchment. It is difficult to determine the maximum possible solute acquisition of each catchment without long term water chemistry data and a thorough understanding of the weathering reactions and redox conditions. However, abiotic weathering experiments carried out in Chapter 5 indicate that solute acquisition from different rock formations may vary by several orders of magnitude. While bedrock may exert a control on solute yield, a complex number of variables within the weathering environment mean that this is unlikely to be a sole factor.

Moraine springs at Møysalbreen have higher chloride and non-snowpack solute concentrations than higher discharge meltwater channels in the same catchment (Figure 6.12, Figure 6.13). This indicates that dilution with ice melt controls bulk runoff solute concentration. Water and solute sources in these glacial catchments are summarised in a revised flow diagram (Figure 6.11).

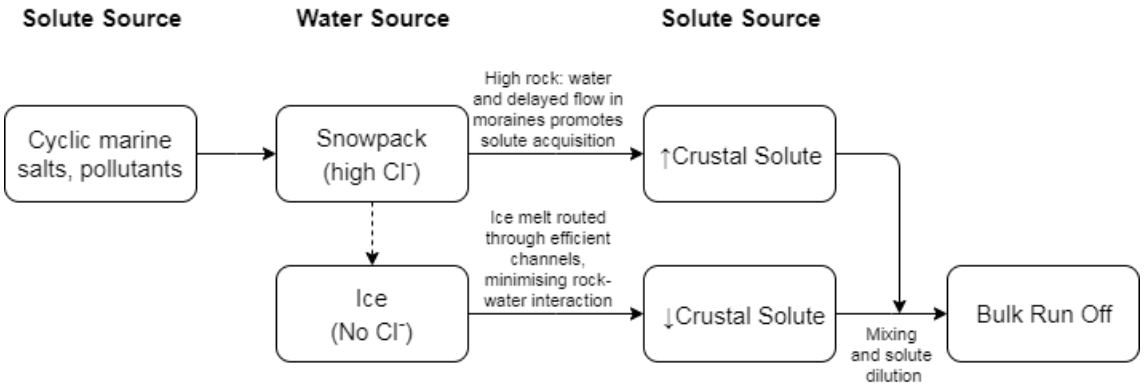

Figure 6.11 Revised flow diagram of water and solute sources in glacial catchments within the study area

By late summer, the only snow remaining could be found at high altitudes on the upper glacier surface and in gulleys on the lateral moraines. During melting, the former feeds supraglacial channels which either transfer water to the glacier terminus or divert water into ice marginal channels where it may combine with moraine water. The latter drains through moraine before ultimately joining the ice marginal channels. Thus, snowmelt throughout the summer was contributing water and solute, via high altitude flowpaths through moraines, to the glacial catchment.

Stable isotopes of water provide further insight into water sources. Typically winter precipitation is isotopically lighter than summer due to variations in temperature (Gat, 1996). In Svalbard, spring/summer precipitation may have $\delta^{18}O$ values of -10 to -5 ‰ while autumn/winter precipitation is isotopically lighter with values of -15 to -8‰ (Divine et al., 2011). Furthermore, throughout the melt season, the preferential evaporation of lighter ^{16}O isotope results in meltwater becoming isotopically heavier. $\delta^{18}O$ - H_2O of glacial runoff (collected in August/September 2016 & 2017) overlap with the $\delta^{18}O$ - H_2O range of snow samples collected in May 2017. Assuming minimal melting occurred since the previous summer, the snow samples therefore represent precipitation deposited from autumn 2016 - spring 2017. The isotopic signature of snow samples suggest that the bulk of the snowpack is derived from winter precipitation. Similar $\delta^{18}O$ - H_2O ratios of winter precipitation and late summer glacial runoff further suggests that snowmelt is stored throughout the summer in the catchment and drains through slow transit pathways.

Water sampled at Foxfonna spring and Gløtfjellbreen spring, have the highest chloride concentrations of all sites in 2017 and 2016 respectively. Yet sulphate and nitrate have concentrations close to zero. Anoxic conditions at Foxfonna spring are suggested by low dissolved oxygen (8%), elevated dissolved iron and manganese and the presence of ochrous deposits. The water pathway of

this spring is not known; however, the extremely high chloride concentrations suggest that it is fed by snowmelt/precipitation and concentrated through evaporation or freezing. Oxygen is consumed during weathering reactions, particularly during the oxidation of sulphide minerals and the low oxygen concentrations suggest that the pathway is isolated from the atmosphere. Observations of the spring over the last decade indicate that it flows all year without freezing (Hodson, 2019) and it may therefore be supplied by a large, deep aquifer in the bedrock.

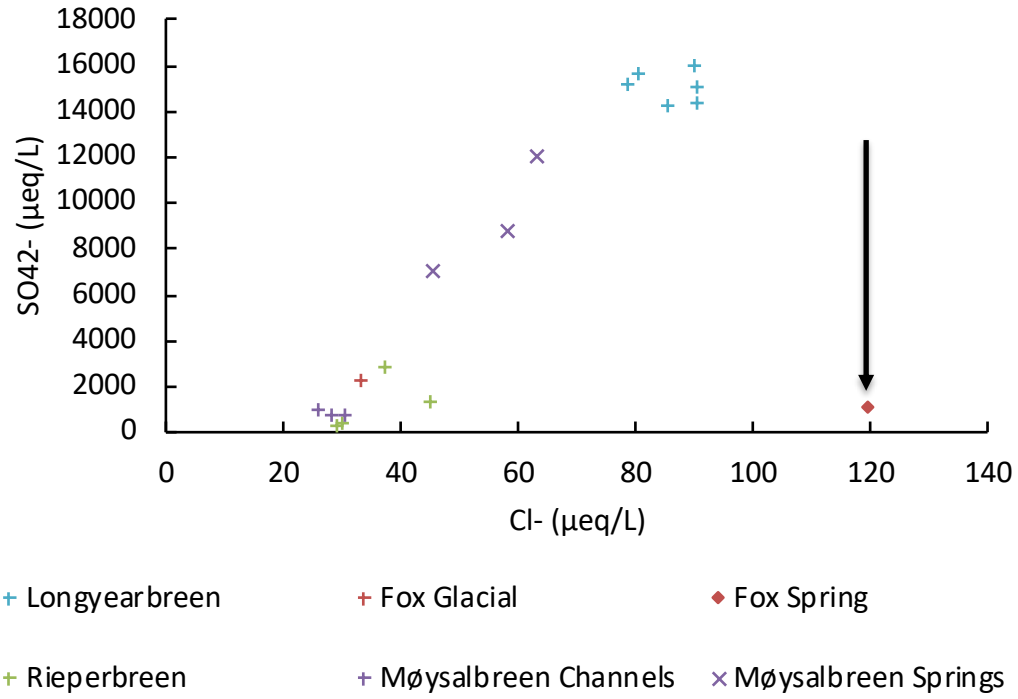

Figure 6.12 Meltwater chloride v non snowpack sulphate concentrations (2017). Arrow indicates depletion of sulphate with respect to chloride.

While Foxfonna spring and Gløtfjellbreen springs are depleted with repect to nitrate, Foxfonna glacial and several Longyearbreen samples are enriched with nitrate relative to chloride. This is discussed in section 6.4.1.6.

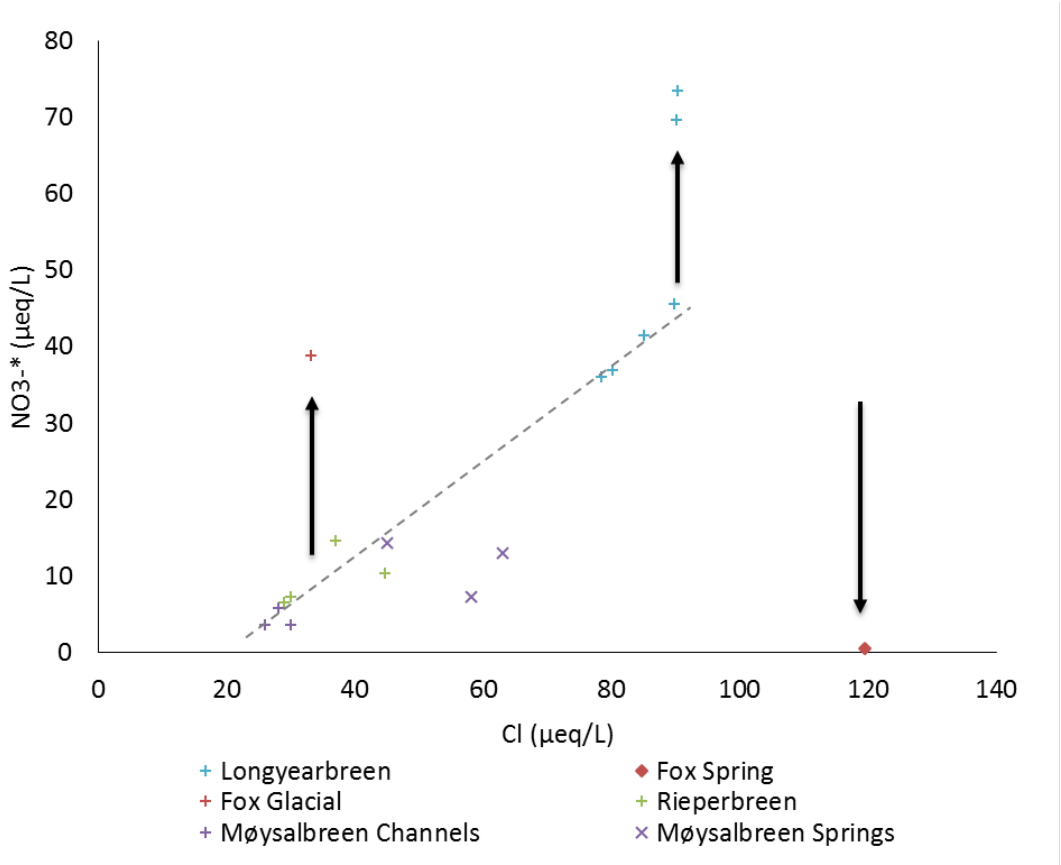

Figure 6.13 Meltwater chloride v non-snowpack nitrate concentrations (2017). Arrows indicate increases/decreases of nitrate with respect to chloride.

6.4.1.2 Sulphide oxidation dominates weathering reactions

Sulphate was the dominant anion in all but one sample. As previously discussed, practically all sulphate in bulk meltwater is derived from crustal sources. Sulphide minerals are abundant in the catchment bedrock and the oxidation of these minerals likely imparts a strong influence on the meltwater chemistry. Sulphide oxidation under fully oxic conditions (13 mg/l O_2 at 0°C) would yield approximately 464 µeq/l sulphate according to Equation 6.12.

$$FeS_2 + 3.5O_2 + H_2O \rightarrow 2SO_4^{2-} + Fe^{2+} + 2H^+$$ **Equation 6.9**

Almost all water samples collected have sulphate concentrations in excess of 464 µeq/l. Sulphate concentrations greater than this may occur by 4 different mechanisms (Tranter et al., 1996):

1. A subglacial source of oxygen, for example from gas bubbles in ice. This additional source of oxygen would enable the oxidation of more sulphide minerals.
2. Refreezing of meltwaters would increase sulphate concentrations as dissolved ions are incapable of entering the ice crystal lattice.
3. Alternative sources of sulphate e.g. gypsum
4. Alternative inorganic oxidising agents e.g. Fe^{3+}, NO_3^-, MnO_2

Oxygen sourced from ice melt is unlikely to provide adequate oxygen for sulphide oxidation (Tranter et al., 2002). Refreezing of meltwater is possible beneath cold based glaciers such as Rieperbreen and Longyearbreen. Yet a substantial volume of meltwater would need to freeze for this to occur. In the case of Longyearbreen, as much as 71% of meltwater would need to freeze to account for the additional sulphate. This seems unlikely, given the average temperature in Longyearbyen was 6°C during the sampling period. Regelation, the process of melting/freezing due to pressure changes can induce the precipitation of carbonate and gypsum which are readily dissolved in water yielding a $Ca+Mg:SO_4$ ratio of ~1 (Tranter et al., 2002). Abundant gypsum/anhydrite deposits have been identified at Rieperbreen (Rutter et al., 2011) and elsewhere on Svalbard (Wadham et al., 2001; Cooper et al., 2002) due to the evaporative concentration of weathering products linked to sulphide oxidation and calcite dissolution in the active layer of the moraines. $Ca+Mg:SO_4$ ratios in the Rieperbreen and Moysalbreen samples here have values ~1 which indicates that gypsum/anydrite dissolution likely contributes to bulk sulphate (Figure 6.16C). $Ca+Mg:SO_4$ ratios in the Foxfonna & Longyearbreen samples are < 0.75 which indicates that there is more sulphate than could be accounted for by secondary gypsum/anhydrite dissolution. Furthermore no gypsum has been observed at Longyearbreen in this study nor by others (Yde et al., 2008). Yde et al. (2008) also noted that sulphate was below saturation point at Longyearbreen, indicating that gypsum could only form when local conditions permit.

When oxygen becomes depleted, sulphide oxidation may continue through microbial mediation using alternative oxidising agents. Such reactions (e.g. Equation 1.13, Equation 6.10, Equation 6.11) stimulate more rapid acquisition of sulphate and iron (Sharp et al., 1999).

$$5FeS_2 + 14NO_3^- + 4H^+ \rightarrow 5Fe^{2+} + 10SO_4^{2-} + 7N_2 + 2H_2O$$ **Equation 6.10**

$$FeS_2 + 7.5MnO_2 + 11H^+ \rightarrow Fe(OH)_3 + 2SO_4^{2-} + 7.5Mn^{2+} + 4H_2O$$ **Equation 6.11**

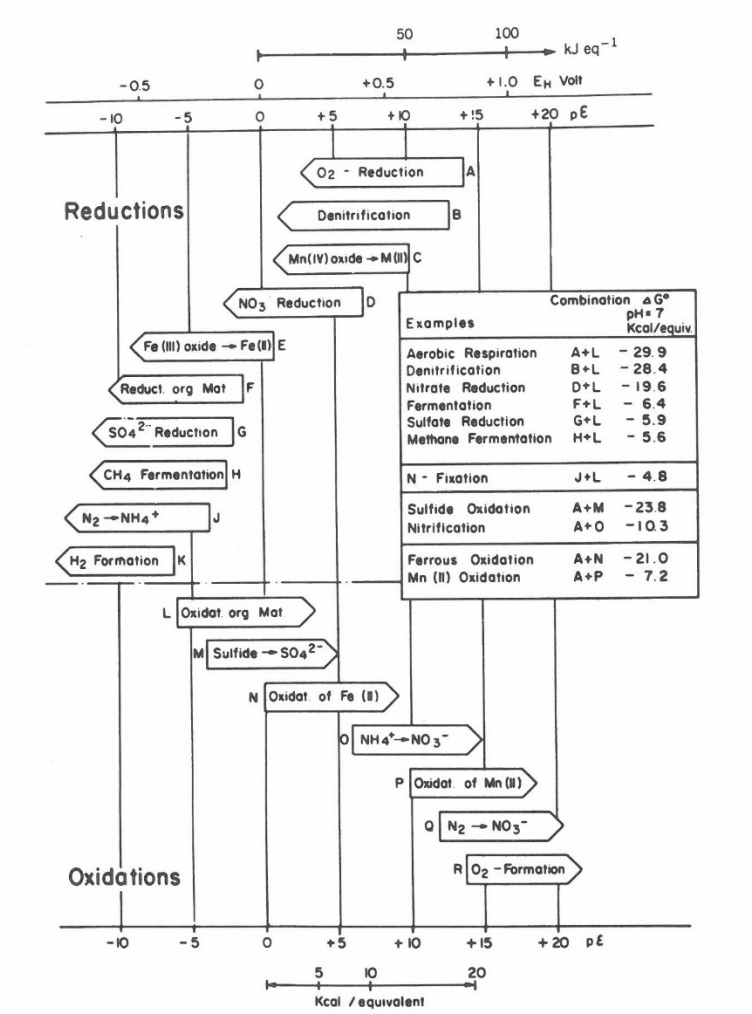

Figure 6.14 Sequence of microbially mediated redox processes (Stumm and Morgan, 1996)

Based on the availability of ions to donate/gain electrons, nitrate is the most efficient inorganic oxidising agent after oxygen (Figure 6.14). Nitrate may be reduced to N_2 via denitrification (Equation 6.10) or NH_4^+ via nitrate reduction. Atmospheric nitrate concentrations in snowmelt are too low to account for the amount of sulphate produced. Nitrate could also be produced in subglacial/ice marginal environments prior to denitrification, thus denitrification could drive sulphide oxidation. However, since the product of this reaction is N_2, it is not possible to quantify the extent to which this occurs. MnO_2 can also act as an electron acceptor in sulphide oxidation (Schippers and Jørgensen, 2001; Schippers and Jørgensen, 2002) producing dissolved Mn^{2+} (Equation 6.11). Manganese concentrations are elevated at Longyearbreen but not sufficiently so to account for the excess sulphate. Further down the REDOX ladder, microbial iron reduction can pair with sulphide oxidation. Iron concentrations of 2 – 6 µM at Longyearbreen and Foxfonna Spring suggest there is a source of reduced iron which may derive from this reaction. Anoxia at Foxfonna spring makes this a highly plausible mechanism for generating sulphate. Under anoxic conditions,

iron is stable in the reduced and soluble form, Fe^{2+}. When the water emerges at the spring, oxygen dissolves and the iron becomes oxidised forming ochre coloured deposits around the spring. Whilst the subglacial water at Longyearbreen portal is well oxygenated, it is unknown whether this is the case deep beneath the glacier. The channelised, open hydrological system would allow for subglacial oxygenation of meltwater (Yde et al., 2008) therefore MnO_2 and Fe^{3+} may facilitate sulphide oxidation in parts of the subglacial system where oxygen is depleted. Low iron concentrations could support anoxic sulphide oxidation due to continual recycling of iron according to the equation (Moses et al., 1987; Singer and Stumm, 1970):

$$14Fe^{2+} + \frac{7}{2}O_2 + 14H^+ \leftrightarrow 14Fe^{3+} + 7H_2O \qquad \textbf{Equation 6.12}$$

However, given that oxygen has previously been accounted for as an electron acceptor for sulphide oxidation, it is not possible to generate additional Fe^{3+} by this pathway. Instead, a continual supply of MnO_2 and Fe^{3+} may be derived from crushed rock debris, since this bedrock contains abundant iron and manganese (Chapter 4). Manganese and iron in bedrock largely occur in the reduced forms Fe^{2+} and Mn^{2+} (Chapter 4), which must be oxidised prior to fuelling sulphide oxidation. Thus, when oxygen becomes depleted, sulphide oxidation may be driven by denitrification of microbially produced nitrate, manganese reduction and iron reduction of previously oxidised bedrock iron and manganese.

6.4.1.3 Using sulphate - oxygen isotopes to determine the degree of oxygenation of the weathering environment

An insight into the oxygenation of weathering environments can be gained using $\delta^{18}O\text{-}SO_4^{2-}$ as originally demonstrated by Bottrell, S. and Tranter (2002). Differences in $\delta^{18}O$ values of different oxygen sources provides a framework to interpret $\delta^{18}O\text{-}SO_4^{2-}$ values and identify oxygen sources. Sulphate produced by sulphide oxidation which occurs under oxic conditions incorporates 3.5 oxygen atoms out of 4 from atmospheric O_2 (Equation 1.12), whereas oxygen in sulphate produced under anoxic conditions is derived entirely from water (Equation 1.13). Atmospheric oxygen and glacial runoff derived from ice melt/meteoric precipitation have distinctive $\delta^{18}O\text{-}H_2O$ values. Atmospheric oxygen has a well constrained $\delta^{18}O$ value of +23.5‰ (Hoefs, 2009) while glacial runoff is typically negative due to kinetic fractionation of oxygen isotopes during continued evaporation and precipitation during northward atmospheric transport. Both snow and glacial runoff collected in Svalbard have $\delta^{18}O\text{-}H_2O$ values of between -12 and -15.5‰. As oxygen is incorporated into sulphate molecules, kinetic isotope fractionation effects cause $\delta^{18}O\text{-}SO_4$ to differ from the

original $\delta^{18}O\text{-}H_2O$ (ε_w) or $\delta^{18}O\text{-}O_2$ (ε_o). These isotope effects have been constrained by previous experimental studies which found small fractionations between water and sulphate (ε_w between 0 and +4.1‰) (Balci et al., 2007; Taylor et al., 1984). Here, we adopt a fractionation value of +3.5‰ following Balci et al. (2007). Consequently, sulphate containing oxygen entirely from water would be expected to have a $\delta^{18}O\text{-}SO_4$ value between -12 and -8.5‰ (Equation 6.13).

$$H_2O \text{ derived sulphate} = H_2O\ \delta^{18}O + \varepsilon_w \quad \textbf{Equation 6.13}$$

$$(-8 \text{ to } -12‰) = (-12 \text{ to } -15.5‰) + (3.5‰)$$

Reported values of fractionation between O_2 and sulphate (ε_o) are larger, ranging between -10.0‰ and -11.4‰ for biological experiments and -4.3 to -9.8‰ for abiotic experiments (Balci et al., 2007; Taylor et al., 1984; Lloyd, 1968). Since sulphide oxidising microorganisms have been found in subglacial enevironments e.g. (Purcell et al., 2014; Achberger et al., 2016; Lanoil et al., 2009), a value representative of biological sulphide oxidation is used (-10.8‰) (Balci et al., 2007). Therefore sulphate derived from atmospheric oxygen would be expected to have an isotopic fingerprint of $\delta^{18}O\text{-}SO_4^{2-}$ = 12.7‰ (Equation 6.14).

$$O_2 \text{ derived sulphate} = \text{atmospheric oxygen}\ \delta^{18}O + \varepsilon_o \quad \textbf{Equation 6.14}$$

$$(12.7‰) = (23.5‰) + (-10.8‰)$$

A difference of ~ 30‰ between sulphate derived from atmospheric O_2 and water is therefore expected in runoff from Svalbard glaciers which allows for the discrimination of oxygen sources to sulphate.

However, the interpretation of sulphate oxygen isotopes is complicated by isotope exchange between water and oxygen atoms in sulfoxy ions of intermediate valency during sulphide oxidation to sulphate. In such an equilibrium process, O_2 derived oxygen is replaced by H_2O derived oxygen, causing the signal from atmospheric oxygen to become obscured. Such exchange is likely in sulphur IV species (e.g. SO_3^{2-}, HSO_3^-) therefore 3 of 4 oxygen atoms in sulphate are liable to exchange and could carry a water derived signal, regardless of their source. Once the final oxygen atom is incorporated, the product SO_4^{2-} is ‘locked’ and resistant to further isotopic exchange in low temperature and near neutral pH conditions (Bottrell, S. and Tranter, 2002). In their study of Glacier Haut d’Arolla, Bottrell, S. and Tranter (2002) adopted a conservative approach where only the final oxygen atom was assumed to have $\delta^{18}O$ representative of its source. Using this method, if sulphate contains less than 25% oxygen derived from O_2, part of the sulphate

must have formed in an anoxic environment. This implies that the weathering environment reaches anoxia but assessing the spatial extent to which the environment is anoxic is beyond the capabilities of this method. The proportion of oxygen derived from atmospheric O_2, X, is calculated using Equation 6.15, where $\delta^{18}O_{atm}$ and $\delta^{18}O_w$ are the O isotopic compositions of atmospheric and water derived O respectively. Equation 6.15 simplifies to Equation 6.16.

$$\delta^{18}O\ SO_4 = (\delta^{18}O_{atm} + \varepsilon_o)X + (\delta^{18}Ow + \varepsilon_w)(1\text{-}X) \quad \textbf{Equation 6.15}$$

$$\delta^{18}O\ SO_4 = 12.7X + (\delta^{18}Ow + 3.5)(1\text{-}X) \quad \textbf{Equation 6.16}$$

Measured glacial run off $\delta^{18}O\text{-}SO_4^{2-}$ values are displayed in Figure 6.15

Figure 6.15 alongside hypothesised $\delta^{18}O\text{-}SO_4^{2-}$ endmembers of O_2 and H_2O derived sulphate. All $\delta^{18}O\text{-}SO_4^{2-}$ values are negative and plot more closely to the water derived sulphate end-member. Eight samples contain less than 25% oxygen derived from atmospheric oxygen (and plot to the left of the red threshold line) which suggests that some of the sulphate in these samples was produced anoxically. The remaining 6 samples have between 25 and 42% oxygen derived from O_2 with the remainder sourced from water. All catchments feature points on both oxic and anoxic sides of the graph. This suggests that sulphide oxidation occurs under a range of redox conditions and that progressive consumption of oxygen by sulphide oxidation can cause anoxia whereby sulphide oxidation continues with alternative oxidation agents as previously discussed. While Foxfonna Spring and Glottfjellbreen spring plot on the oxic side of the graph, these samples are known to be anoxic as identified by low dissolved oxygen and nitrate concentrations as well as the presence of ochrous deposits. The reasons for this are discussed in the following section.

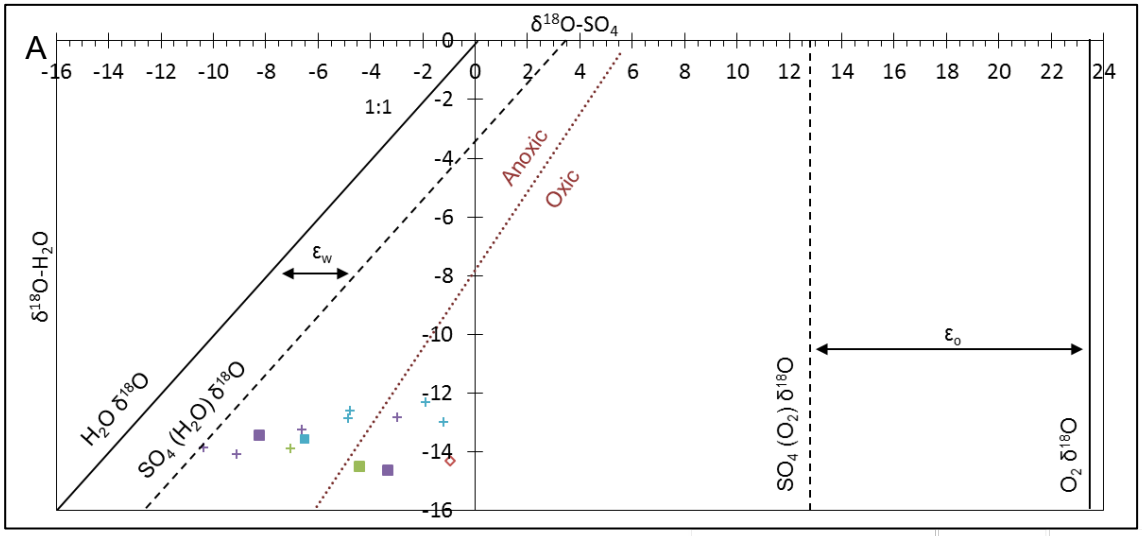

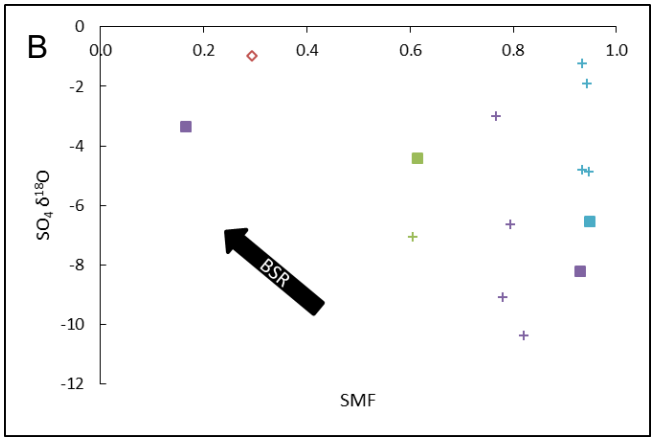

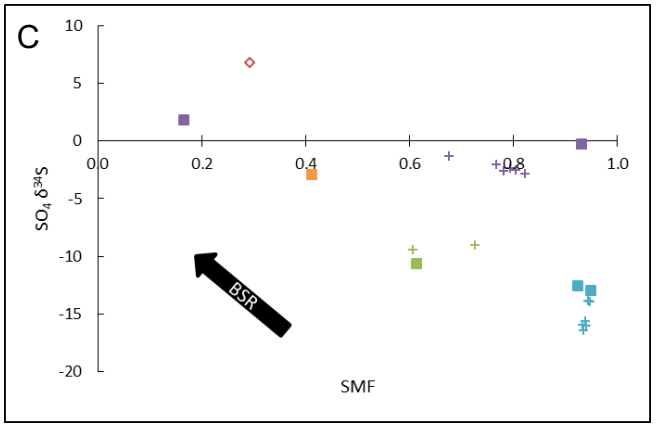

Glacier	2016	2017
Longyearbreen	■	+
Rieperbreen	■	+
Moysalbreen	■	+
Foxfonna Spring	◆	◇
Fleinisen	■	

Figure 6.15 (a-c) Sulphate-oxygen and sulphur isotope data from glacial run off.

A) Glacial runoff $\delta^{18}O\text{-}H_2O$ and $\delta^{18}O\text{-}SO_4$. Solid vertical line represents atmospheric oxygen $\delta^{18}O$. Dashed vertical line represents theoretical sulphate, containing oxygen entirely derived from atmospheric oxygen using ε_o = -10.8‰ (Balci et al., 2007). Solid diagonal 1:1 line represents sulphate containing oxygen derived entirely from water. Dashed 1:1 line represents theorised $\delta^{18}O\text{-}SO_4$ of water derived sulphate using ε_w = 3.5‰ (Balci et al., 2007). Dotted red line represents sulphate containing <25% oxygen derived from atmospheric O_2 i.e. threshold value of anoxic-oxic sulphide oxidation. B) $\delta^{18}O\text{-}SO_4$ v Sulphate mass fraction (SMF) C) $\delta^{34}S\text{-}SO_4$ v SMF. Block arrows indicate the approximate effect of bacterial sulphate reduction (BSR) on stable isotope values and SMF.

6.4.1.4 Stable isotopes as a tracer of sulfur biogeochemical cycling

Sulfur isotopes can be used as a tracer of sulfur sources to confirm the above assertions. Minimal fractionation is associated with sulphate release from sulphide oxidation, although $\delta^{34}S - SO_4^{2-}$ may be marginally depleted relevant to the sulphide (Toran and Harris, 1989; Clark and Fritz, 1997). Therefore, if meltwater sulphate is derived from sulphide minerals, it should have a $\delta^{34}S$ ratio that matches bedrock sulphur. Discrete values of meltwater $\delta^{34}S - SO_4^{2-}$ arise from each glacial catchment which match bedrock sulphide in the catchments of Rieperbreen and Møysalbreen. This supports bedrock as a source of sulphur (Table 6.4). However, differences between $\delta^{34}S\text{-}SO_4^{2-}$ and bedrock S in Longyearbreen and Foxfonna spring require further consideration.

Meltwater sulphate, enriched in ^{34}S and ^{18}O, at Foxfonna spring has low sulphate concentrations and low SMF (0.3), similar to Gløtfjellbreen spring (Figure 6.15). Anoxic conditions, present here, would facilitate bacterial sulphate reduction (Equation 1.14) which reduces sulphate to hydrogen sulphide (which was smelt during sampling) while oxidising organic carbon to inorganic CO_2. This would explain the elevated DIC concentrations (2780 µeq/L HCO_3^-) in a stream isolated from atmospheric CO_2, flowing through carbonate depleted rock. This reaction preferentially consumes light ^{32}S and ^{16}O leaving residual sulphate enriched in ^{34}S and ^{18}O. This process fits the observations, geochemical and isotope data above and explains the disparity of $\delta^{34}S$ between bedrock sulphide and meltwater sulphate. Organic carbon as an electron donor for this reaction may derive from dissolved organic carbon species such as acetate (Chapter 5) leached from bedrock kerogen.

Glacial runoff at Longyearbreen has $\delta^{34}S\text{-}SO_4^{2-}$ values more negative than mean weighted bedrock sulphide $\delta^{34}S$. This suggests that sulphide has a more variable $\delta^{34}S$ than suggested by the results of geochemical analyses presented here or there is a ^{34}S depleted source of sulphur to the catchment. Other potential sources of sulphur to the catchment could be organic sulphur compounds in coal bearing geological horizons or precipitation containing marine derived sulphate and/or anthropogenic emissions. Coal deposits generally have $\delta^{34}S$ values representative of source plant material, typically between 0 and 10‰ (Seal, 2006) therefore it is unlikely that weathering of coal would account for more negative runoff $\delta^{34}S\text{-}SO_4^{2-}$ A coal burning power plant is located in Longyearbyen, near to the glacier. Flue gas derived from the combustion of coal is often depleted in ^{34}S e.g. (Elswick et al., 2007), therefore wet deposition of local anthropogenic emissions may account for some of the sulphate in Longyearbreen run off. However the dominant annual wind direction

at Longyearbyen is ESE (Windfinder, 2019), which would transport most emissions offshore, reducing their influence on the Longyearbreen catchment. While sulphate isotope analysis was not undertaken on snow samples in this study, other research suggests that arctic snow generally has positive $\delta^{34}S\text{-}SO_4$ values, largely due to the contribution of sea salt aerosol in snow (Wynn, 2004). Furthermore, the low concentration of sulphate in snow on Longyearbreen (< 80 µeq/L) would not account for the mass of sulphate in Longyearbreen runoff. Glacial erosion may promote non-stoichometric reactions which may lead to the fractionation of S isotopes during initial stages of pyrite weathering (Hindshaw, Ruth S. et al., 2016). Such mechanisms include degassing of SO_2 and breaking of S-S bonds in the intermediate oxyanion thiosulphate (Brunner et al., 2008; Bottrell, S., 2007; Pisapia et al., 2007). However, such a process would result in sulphate becoming isotopically heavier than bedrock S. Strongly negative values are not unusual for sulphide minerals due to the fractionation associated with bacterial sulphate reduction inherent in their formation. In this study the $\delta^{34}S$ of bedrock at Longyearbreen is characterised using material from borehole BH9/05, located 35 Km south east of the glacier in question. Spatial variations in the degree of sulphide re-oxidation and the inherent microbial disproportionation of elemental sulfur during sedimentation can shift sulphide to more negative values (Bottrell, S. and Raiswell, 2000) and may result in variations of pyrite $\delta^{34}S$. Indeed, the limited dataset of bedrock $\delta^{34}S$ presented in Chapter 4 indicates the diverse values of pyrite sulphide which reach a minimum of -50‰. As such, it is plausible that these $\delta^{34}S\text{-}SO_4^{2-}$ values reflect weathering of bedrock sulphide with more negative average $\delta^{34}S$-sulphide.

Beneath polythermal and temperate glaciers, there is often an extensive source of freshly comminuted bedrock. However, since cold based glaciers are frozen to their substrates, active crushing is limited. Therefore, the oxidation of sulphide minerals beneath cold based glaciers such as Longyearbreen and Rieperbreen may be limited by access to freshly comminuted sulphide minerals. Yde et al. (2008) suggest that freeze-thaw & wet-dry cycling may account for the provision of fresh sulphide minerals. However, given that solute acquisition occurs in snowmelt fed moraine streams as previously discussed, high altitude marginal glacial environments such as talus slopes, gullies and moraines may represent the locus of sulphide oxidation.

6.4.1.5 Coupled weathering reactions

Sulphide oxidation provides a source of acidity which is able to drive further weathering reactions. Following the approach used in Chapter 5, an indication of the principal weathering reactions occurring in each catchment can be gained

through analysis of the ratios of major ions in run off. The leaching experiments in Chapter 5 demonstrated that weathering of this bedrock was dominated by rapid hydrolysis reactions and sulphide oxidation coupled to carbonate dissolution. When carbonates became exhausted, sulphide oxidation coupled with silicate dissolution. Major ion ratios of glacial runoff are plotted in Figure 6.16 to explore whether this experiment is representative of catchment scale processes.

In Figure 6.16, samples from each catchment tend to group together, which may reflect catchment scale variations in geology or hydrological processes. Longyearbreen and Møysalbreen spring samples are most solute rich and plot near to each other. Whereas Møysalbreen channels, Foxfonna (glacial) and Rieperbreen are more dilute and have similar chemistries. Since these glacial catchments contain different parts of the geological succession, variations in geology are unlikely to account for this trend.

The relative proportions of major ions are actually very similar in all samples, given that they generally all plot along the same slopes. Therefore, it seems that chemical weathering processes are similar in each catchment but waters are diluted to different degrees. This is evidenced by the concentration of chloride, which is not derived from weathering, because the most solute rich samples (Møysalbreen springs and Longyearbreen) also have greater chloride concentrations. Greater additions of low ionic strength ice melt to glacial runoff at Rieperbreen and Foxfonna, as well as to the ice marginal channels at Møysalbreen, most likely accounts for the lower solute concentrations in these catchments.

None of the water samples from Svalbard plot along the slopes indicative of SOCD (Figure 6.16c,d). The stoichiometry of meltwater chemistry suggests that sulphide oxidation couples with silicate weathering at all sites apart from Foxfonna spring (where BSR lowers the SMF) (Figure 6.16a). This is consistent with SMF > 0.5 at most sites since this coupling produces sulphate and not DIC. However, Yde et al. (2008) suggested that the principal weathering reaction in the Longyearbreen catchment was sulphide oxidation coupled to dolomite dissolution which leads to pCO_2 greater than atmospheric equilibrium. In open channels, such as the ice marginal channel at Longyearbreen, much of the produced HCO_3^- would diffuse out of solution as CO_2, resulting in relatively low HCO_3^- concentrations (high SMF). Values of glacial runoff pCO_2 were calculated by rearranging Equation 6.18 to determine H_2CO_3 and then substitution of this term into Equation 6.17 to give the overall equation for pCO_2 (Equation 6.19). These equations used values of pH, HCO_3^- and $K_0 = 10^{-1.11}$, $K_1 = 3.069.10^{-7}$ at 0% salinity and 0°C (Millero and Roy, 1997).

$$K_0 = \frac{[\mathrm{H_2CO_3}]}{pCO_2} \qquad \textbf{Equation 6.17}$$

$$\mathrm{K_1} = \frac{[\mathrm{H^+}][\mathrm{HCO_3^-}]}{[H_2CO_3]} \qquad \textbf{Equation 6.18}$$

$$\mathrm{pCO_2} = \log\left(\frac{10^{-pH}.[HCO_3^-]}{k_1.k_0}\right) \qquad \textbf{Equation 6.19}$$

Contrary to the findings of Yde et al. (2008), glacial runoff studied here, exhibits pCO_2 values approximately equal to atmospheric pCO_2 (Figure 6.17), which suggests that atmospheric CO_2 is in equilibrium with dissolved CO_2. This is likely maintained by open system conditions where the flow path undergoes gas exchange with the atmosphere. Some samples feature pCO_2 lower than atmospheric CO_2. Low pCO_2 values occur when the demand for protons i.e. the weathering rate exceeds the supply of protons causing dissolution of CO_2 into solution (Tranter et al., 1993). Therefore, such samples may reflect water derived from more isolated parts of the glacial drainage system. Significant sodium and silica concentrations in glacial runoff indicate that silicate weathering is an important weathering reaction in these catchments. It is likely that, despite low inorganic carbon concentration in bedrock, carbonate dissolution contributes solute due to its rapid dissolution kinetics, however, the proportion of calcite minerals in bedrock are low relative to other carbonates such as dolomite and siderite (Riber, 2009). These Mg and Fe rich carbonates have lower solubility products and slower dissolution rates than calcite (Nordstrom et al., 1990; Drever, 1997) which may also account for the lack of coupling between sulphide oxidation and carbonate dissolution (Figure 6.16). Instead, silicate weathering accounts for excess acidity created by sulphide oxidation that is not consumed by carbonate weathering. Sodium concentrations are elevated relative to calcium and chloride at Longyearbreen which may imply enhanced silicate (albite) weathering or greater adsorption of divalent cations through ion exchange reactions. Silica: chloride ratios are fairly consistent at all sites (~ 0.5) which suggests that Na-Ca exchange rather than enhanced silicate weathering may account for excess sodium. The rejection of sodium ions from ion exchange sites at the expense of calcium has been proposed by others to explain elevated sodium concentrations in glacial meltwaters (Wadham et al., 1998; Hodson et al., 2002). This process is consistent with low Ca/Mg ratios at Longyearbreen (Figure 6.5) where enhanced ion exchange may be accounted for by the abundance of clay minerals within the underlying Frysjaodden Fm.

Foxfonna spring and Gløttfjellbreen spring water are distinct from other sites due to their relative enrichment with bicarbonate and depletion of sulphate following sulphate reduction. Furthermore, charge balance is maintained almost entirely by sodium whereas other samples are dominated by calcium and magnesium. The lack of divalent cations in Foxfonna spring may be a result of calcite saturation promoted by high bicarbonate concentrations. This would result in the precipitation of calcium/magnesium carbonates, thereby reducing the dissolved load of calcium and magnesium. Under such conditions, carbonate dissolution would be inhibited, therefore acidity produced by sulphide oxidation would likely be buffered by silicate dissolution which releases more sodium into solution. However, PHREEQC modelling suggests that these springs are under saturated with respect to calcite. Perhaps, sulphide oxidation couples with silicate weathering in these springs, leaching sodium from feldspars and clays, while sulphate is reduced via BSR.

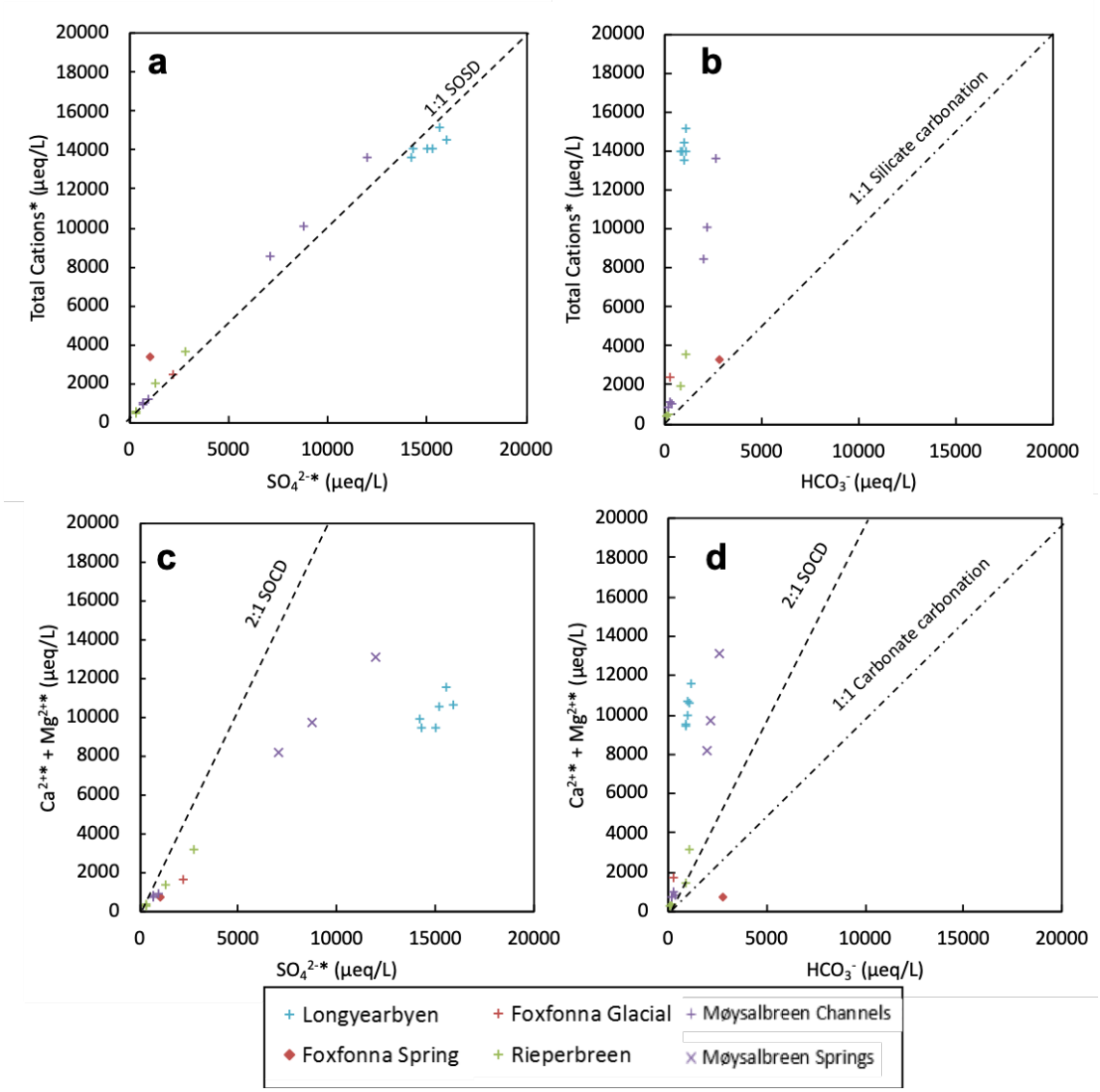

Figure 6.16 Graphs showing total cations (Ca, Mg, Na, K) in meltwater v a) sulphate and b) bicarbonate, as well as Ca + Mg v c) sulphate and d) bicarbonate. Figures a) and b) portray silicate weathering reactions assuming all cations are derived from silicates. The 1:1 line in a) depicts the idealised weathering products of coupled sulphide oxidation and silicate dissolution (SOSD). The 1:1 line in b) represents idealised silicate carbonation. Plots c) and d) portray carbonate weathering reactions assuming Ca and Mg are derived from carbonates only. The 2:1 line in c) represents the idealised weathering products of coupled sulphide oxidation and carbonate dissolution (SOCD). The 1:1 line in c) represents the products of secondary gypsum dissolution. The 1:1 line in d) represents idealised carbonate carbonation.

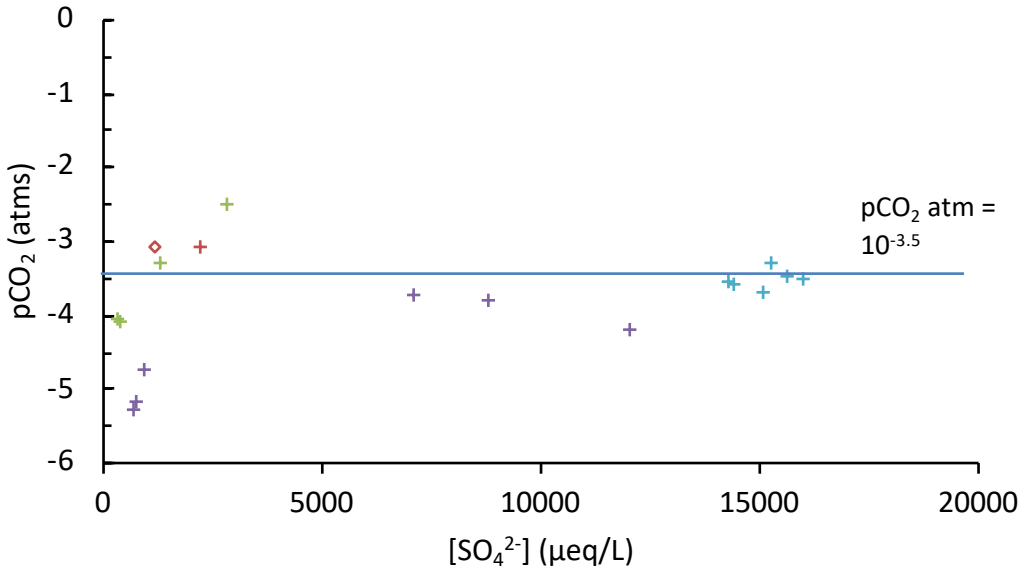

Figure 6.17 Sulphate concentrations v pCO_2 of glacial runoff. Solid line represents atmospheric pCO_2

6.4.1.6 Nitrogen Dynamics

Nitrogen species in glacial runoff differ drastically from abiotic weathering experiments (Chapter 5). In the glacial catchments, N is distributed as follows: NO_3^- > NH_4^+ $_{(aq)}$ > NH_4^+ $_{(ad)}$, conversely in the experiments, the order is reversed (Figure 6.18).

Nitrogen speciation broadly covaries with oxygen availability. Dissolved oxygen measurements generally agree with geochemical data in determining whether water is oxic or anoxic although several data points disagree. For example, Foxfonna spring and Gløttfjellbreen spring both recorded elevated dissolved oxygen in 2016 yet, contained limited nitrate and sulphate, which are indicative of anoxic conditions. This water may have become oxygenated close to re-emergence at the surface after anoxic processes such as denitrification and BSR had taken place deeper in the system. Nitrate is the dominant inorganic nitrogen compound in oxygenated waters with concentrations of up to 134 µeq/L (Longyearbeen 2016) while ammonium concentrations are commonly less than 10 µeq/L (Figure 6.19). Conversely, in anoxic streams where bacterial sulphate reduction occurs (such as Foxfonna and Gløtfjellbreen springs) total dissolved nitrogen (NO_3^- + NH_4^+) concentrations are lower, with nitrate concentrations close to zero or not detected and ammonium concentrations up to 21 µeq/L. Principal sources of N such as remineralised organic matter and rock minerals, contain N as ammonium. Although a small proportion of rock N may occur as nitrate within fluid inclusions (Chapter 3), this is not a significant source of nitrogen (Chapter 5). Therefore, the availability of oxygen seems to control processes involved in

the transformation of nitrogen. In oxygenated environments, nitrate is therefore produced and ammonium consumed while in anoxic environments nitrate is consumed.

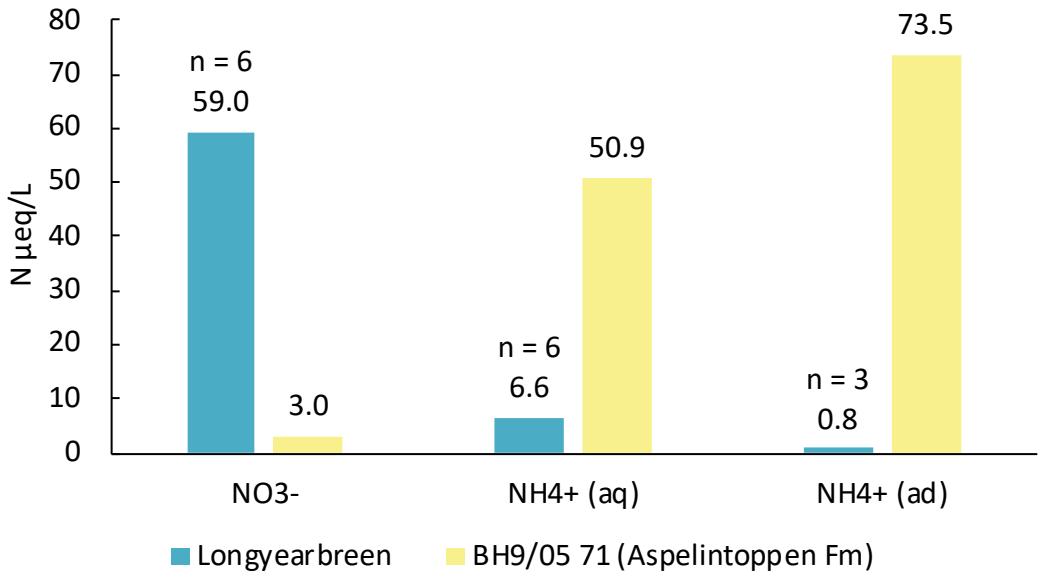

Figure 6.18 A comparison of nitrogen speciation in glacial runoff and an abiotic weathering experiment. Dissolved nitrate and ammonium concentrations in glacial runoff are an average of 6 samples collected from Longyearbreen in 2017. Adsorbed ammonium is an average of 6 suspended sediment samples collected from Longyearbreen in 2018. BH9/05 is a representative sample of bedrock within the Longyearbreen catchment which was weathered for 11 days at 6°C. Column labels are N concentrations.

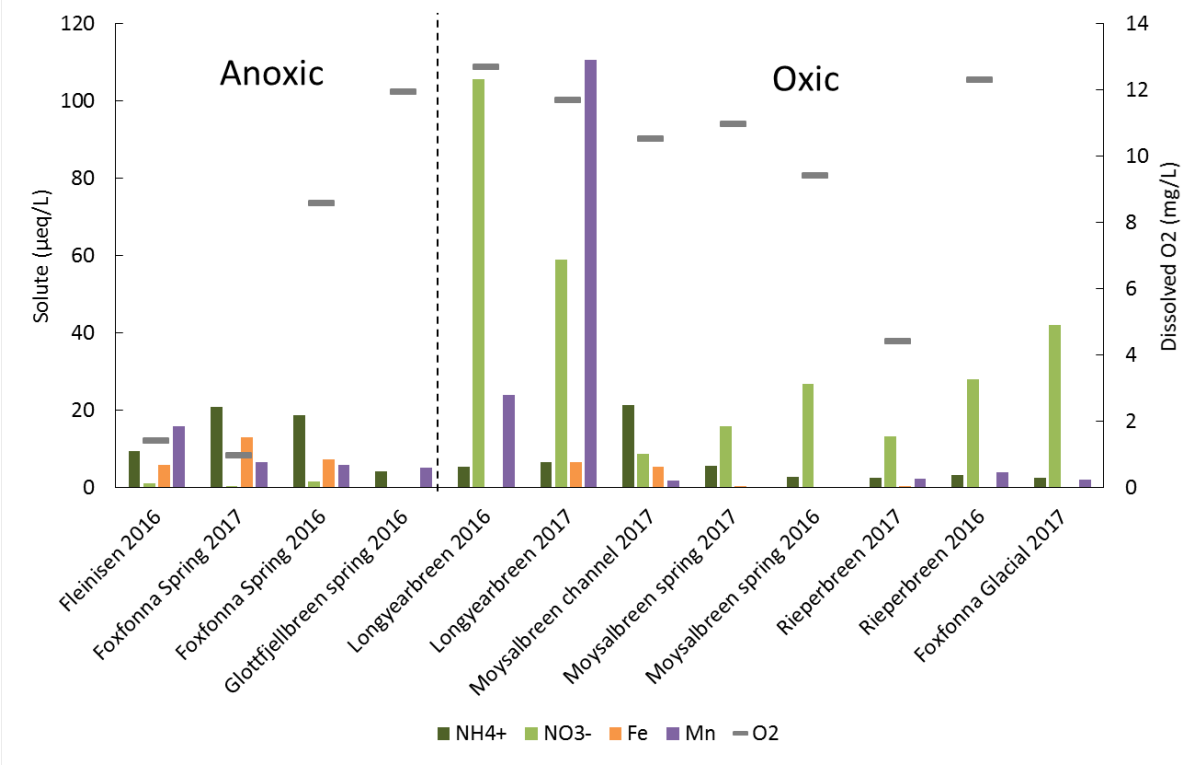

Figure 6.19 Average solute concentrations at various glacial basins in Adventdalen (2016 and 2017)

In nature, nitrate is produced largely by the biological process of nitrification of ammonium. This reaction requires the presence of oxygen and it is facilitated by microorganisms. Nitrate concentrations in glacial runoff presented here correlate strongly with rock derived ions sodium and silica (Figure 6.20) and snowpack derived chloride (Figure 6.13) but not where dissolved oxygen is unavailable. This suggests that nitrification occurs in oxygenated crushed rock environments where silicate weathering occurs in contact with water derived from snowmelt, which is consistent with other studies (Ansari et al., 2013; Wynn et al., 2007; Hodson et al., 2010a; Hodson, 2006). Sulphate - oxygen isotope data, presented above, indicate that weathering environments display a range of redox conditions from oxic to anoxic. In order for nitrification to take place in these environments, anoxia must be limited spatially/temporally. Crushed rock environments such as gullies on valley sides and moraines have low discharge throughflow with limited turbulent exchange of atmospheric gases, however, they receive oxygenated snowmelt and rainfall throughout the melt season. Temperature variations may therefore control the supply of dissolved oxygen via the magnitude of meltwater/rainfall to such environments facilitating nitrate production via nitrification, thereby limiting ammonium concentrations in oxic environments.

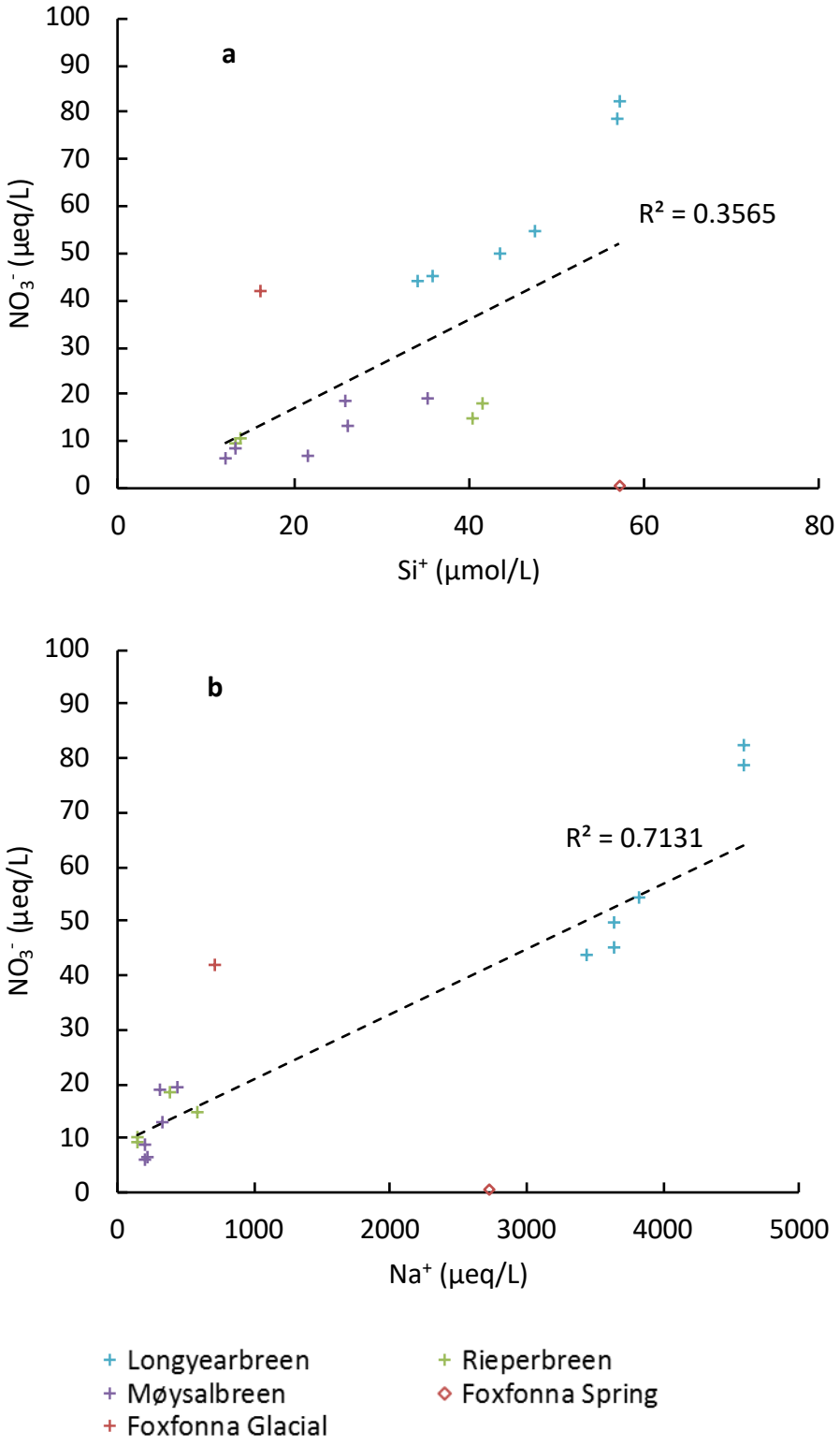

Figure 6.20 Concentrations of nitrate in meltwater vs a) silica, b) sodium

Sulphide and organic carbon oxidation deplete dissolved oxygen. Under anoxic or near-anoxic conditions, nitrification is not possible, and so ammonium remains in solution where it may be assimilated by microbes. However, should oxygenated snow melt containing nitrate become anoxic through extensive interaction with crushed rock, denitrification may occur. This process converts

nitrate to dinitrogen gas, lowering nitrate concentrations. This likely explains the low nitrate concentrations in anoxic water at Foxfonna and Gløtfjellbreen springs.

Adsorption of ammonium onto suspended sediment and ammonia volatilisation may further lower dissolved ammonium concentrations. Glacial runoff derived from subglacial/ice marginal channels contained significant suspended sediment (0.4 – 2.4 g/l). In June/July, during the peak melt season, meltwater discharge is higher and can transport a greater quantity of sediment than at the end of the melt season when ablation rates and the contribution of water by ground thaw to ice marginal streams are reduced. This entrained sediment provides a sink for ammonium which sorbs to mineral surfaces. Up to 12 µg/g of ammonium was found adsorbed to a limited suite of suspended sediment samples. These values fall at the low end of adsorbed ammonium measured in leaching experiments (Chapter 5), which had values up to 57 µg/g. However, the weathering experiments demonstrated a desorption of ammonium with time, therefore lower adsorbed ammonium concentrations in suspended sediment may reflect mature sediment that has lost ammonium through ion exchange processes or nitrification in the hyporheic zone of the river. Desorbed ammonium is more likely to become bioavailable and thus converted to nitrate by nitrification. Secondly, where pH is elevated, ammonium may be lost as ammonia gas. Volatilisation is associated with atmospheric gas exchange and is therefore unlikely to occur in environments with restricted atmospheric connectivity e.g. anoxic streams. Conversely, ammonium adsorption may occur regardless of whether the environment is a closed or open system and may therefore be a more spatially widespread reaction. pH values in glacial runoff in this study are typically 8-9 which permit volatilisation, however cold temperatures would mean that this may only be significant over long timescales. However, in nutrient limited environments, biological demand for N is high and it is likely that ammonium would be nitrified or assimilated faster than rates of volatilisation. The large disparity between nitrate and ammonium concentrations at Longyearbreen demonstrates the efficiency of this system in processing nitrogen from ammonium to nitrate.

6.4.2 Evidence for a geological control on glacial meltwater chemistry

6.4.2.1 Iron and Manganese

As previously discussed in Chapter 4, the bedrock in Adventdalen contains significant iron and manganese in various minerals. Iron and manganese carbonates are abundant in Eocene age rocks particularly within the Frysjaodden Fm (max. 9.7 wt. % Fe, 0.5 wt. % Mn) and Aspelintoppen siderite

layers (17 wt. % Fe). Magnetite type minerals featuring iron/manganese are significant in Palaeocene age rocks (Firkanten – Grumantbyen Fms). Iron pyrite is present in all formations but it is enriched in the Firkanten Fm (max 5.2 wt. % Fe). Furthermore, iron is also incorporated in silicate minerals such as glauconite (Chapter 4).

Variable iron and manganese concentrations were measured in different glacial catchments (Figure 6.7). Manganese was particularly concentrated in Longyearbreen glacial runoff (50 – 61 µmol/l). Iron was also abundant in runoff from Longyearbreen (2 – 6 µmol/l) and Møysalbreen (max. 3 µmol/l) but also in anoxic drainage from Fleinisen (3 µmol/l) and Foxfonna spring (6.5 µmol/l). Iron was below level of quantification/detection in other well oxygenated glacial runoff e.g. Rieperbreen, Foxfonna Glacial and Møysalbreen springs. Manganese concentrations exceed Fe concentrations in meltwater channels at Longyearbreen, Rieperbreen and Foxfonna Glacial whereas iron exceeds manganese in meltwater springs at Foxfonna and Moysalbreen.

Glacial solute is largely derived from crustal weathering and bedrock contains significant iron and manganese. Iron and manganese are therefore most likely derived from weathering of glacially comminuted bedrock. Møysalbreen, Fleinisen and Foxfonna were predicted to have highest concentrations of iron on account of their erosion of the Firkanten Fm and the data confirm this (Table 6.7). While the Firkanten Fm crops out at the head of the Møysalbreen valley and any interaction of meltwater with this unit would be shown in subglacial drainage, glacial runoff was sampled from an ice marginal channel which may not represent true subglacial drainage but more likely features leachate of moraines on the valley sides (Figure 6.9). This moraine is composed of Carolinefjellet Fm rocks only. Therefore, water samples collected at Møysalbreen likely reflect the leaching of Carolinefjellet Fm rocks. Pyrite weathering in the Firkanten Fm likely provides a significant source of Fe^{2+} to Fleinisen and Foxfonna Spring and the consumption of oxygen in this reaction likely explains anoxia at these sites. Iron is insoluble in oxygenated waters; therefore, anoxic conditions also facilitate the stability of dissolved iron.

Table 6.7 A comparison of iron within catchment bedrock and meltwater (Fe < 0.45 µm). Average bedrock iron concentrations from each catchment are calculated using iron from carbonate and oxide minerals ($Fe_{carb/oxide}$), pyrite (Fe_{pyrite}) and bulk rock (Fe_{total}).

Catchment	Underlying bedrock				Meltwater
	Geological Fms	$Fe_{carb/oxide}$ (average wt %)	Fe_{pyrite} (average wt %)	Fe_{total} (average wt %)	Mean Fe (µmol/L)
Møysalbreen/ Gløttfjellbreen	Basilika, Firkanten, Carolinefjellet	3.73	1.24	4.97	2.74 (2017 Channels) 0.19 (2017 Springs)
Foxfonna Spring	Grumantbyen, Basilika, Firkanten	3.00	0.91	3.90	3.70 (2016) 6.52 (2017)
Fleinisen	Grumantbyen, Basilika, Firkanten, Carolinefjellet	2.98	0.86	3.85	2.99 (2016)
Longyearbreen	Aspelintoppen, Battfjellet, Frysjaodden, Grumantbyen, Basilika	2.41	0.37	2.77	<LOQ (2016) 3.31 (2017)
Rieperbreen	Battfjellet, Frysjaodden, Grumantbyen,	2.34	0.20	2.54	<LOQ (2016) 0.24 (2017)

Water draining Longyearbreen is also enriched in iron and its meltwater chemistry closely matches the leachate from Firkanten Fm (Todalen Member) in weathering experiments (high SO_4^{2-}, Mn^{2+}, Fe^{2+}). Yet Longyearbreen does not overlie the Firkanten Fm (Todalen member) (Appendix D) where these elements are sourced in high concentrations. It is unlikely that the glacier has eroded to a depth where it reaches the Todalen member since the water sampling point is ~25 m above the top of the Firkanten Fm and the Todalen

member is ~30 m below this. The average depth of glacier was 53 m in 1990 (Etzelmüller et al., 2000) therefore ice may have eroded the Endalen Member but unlikely to have reached Todalen Member in its current position (also see Figure 6.21). The Grumantbyen Fm, which does underlie Longyearbreen, contains iron principally in the form of iron oxides (Fe^{3+}). This sequence of bedrock also contains significant TOC (e.g. Frysjaodden Fm), which may act as a reducing agent for Fe^{3+} to produce more soluble Fe^{2+}. However, the pH of runoff (8 - 9) would restrict iron solubility and therefore this mechanism is unlikely to explain the presence of dissolved iron here. The Frysjaodden Fm, which also underlies Longyearbreen, contains a significant concentration of iron carbonates and some pyrite which may supply significant iron to the catchment. During leaching experiments (Chapter 5), up to 1.4 µg/g of iron was liberated from Frysjaodden rocks after 1 day at 6°C. Although glacial runoff at Longyearbreen is oxic, sulphide oxidation likely occurs at least in part under anoxic conditions (section 6.4.1.3) which may have facilitated initially elevated iron concentrations. Therefore, iron in Longyearbreen runoff is likely sourced principally from the Frysjaodden Fm.

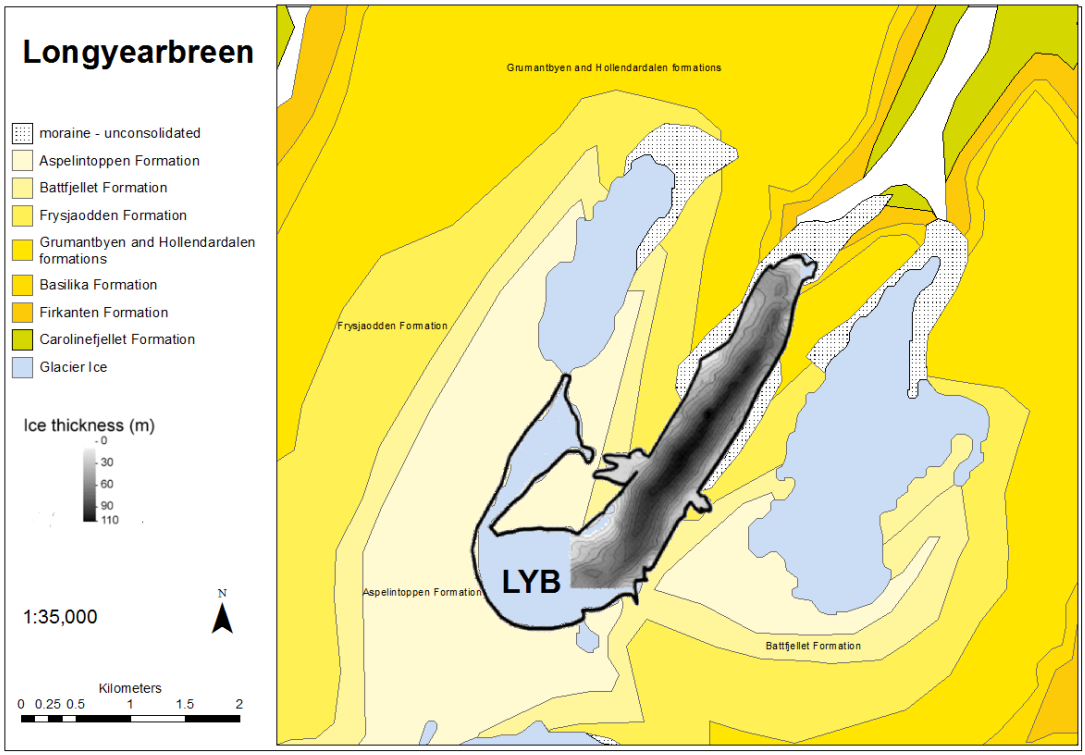

Figure 6.21 Outline of Longyearbreen glacier and surrounding geology. Interpolated ice thickness from Sevestre et al. (2015).

Elevated manganese concentrations at Longyearbreen are consistent with the underlying manganese rich Frysjaodden Fm. Since manganese occurs as Mn^{2+} in carbonate minerals within this unit, weathering will release Mn in a soluble form. Furthermore, the Frysjaodden formation consists of shales which are

always heavily weathered in outcrop, thus manganese may be easily liberated by weathering of this formation. Glacier ice is thickest in the central part of Longyearbreen which overlies the Frysjaodden Fm (Figure 6.22). While the glacier is now cold based, when it was more active, glacial erosion may have been more significant within units of softer rock such as the Frysjaodden shales, creating an abundance of exposed reactive minerals such as sulphides and Fe/Mn bearing carbonates. Whilst manganese concentrations of leachates of Frysjaodden Fm rocks were fairly low, variable redox conditions may permit a build-up of manganese in glacial meltwater as discussed below.

Iron concentration in the local bedrock are 1 - 2 orders of magnitude greater than manganese. Given that iron and manganese are both associated with carbonates (and magnetite), and iron is also associated with sulphide minerals, it is expected that iron would enter meltwater in a greater proportion to manganese during weathering. However, manganese concentrations exceed iron in waters draining most sites, in particular at Longyearbreen. As discussed previously sulphide oxidation likely occurs under anoxic conditions in moraine pore water. This water will likely drain downslope mixing with oxidised ice-marginal channels, where the availability of oxidising agents such as oxygen will control the solubility of iron and manganese. Manganese is more soluble than iron in neutral pH water, since iron oxidation is a more energetically favourable reaction (Figure 6.14). Therefore, the preferential oxidation of iron causes manganese to accumulate in runoff until Fe^{2+} becomes depleted. Glacial runoff at Longyearbreen featuring elevated sulphate, iron and manganese therefore likely reflects oxidation of pyrite particularly in Aspelintoppen and Frysjaodden Fms, producing Fe^{2+} and SO_4^{2-} and suboxic conditions, where iron is progressively oxidised. Acid weathering of manganese-rich carbonate minerals liberates manganese which remains in solution in preference to iron which is more readily precipitated on oxidation.

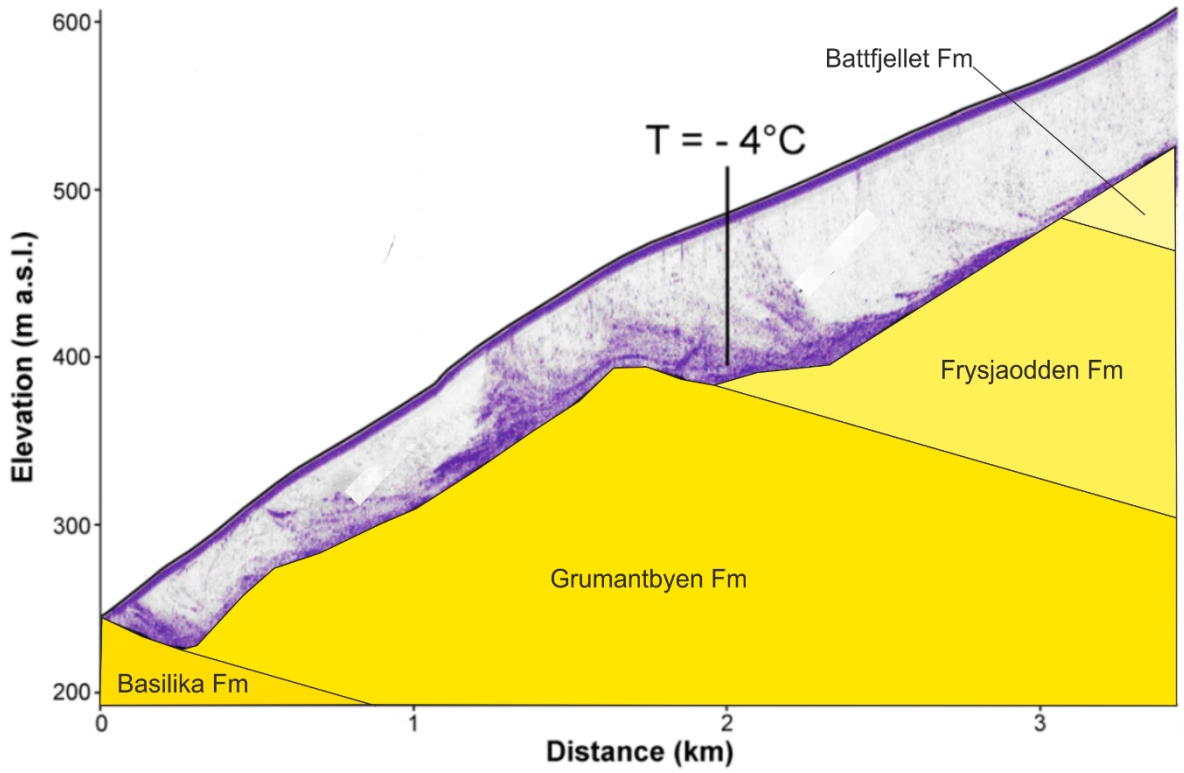

Figure 6.22 Ground penetrating radar data along centreline of Longyearbeen, modified from Sevestre et al. (2015). The top black line indicates glacier surface and bottom black lines follow the bottom reflector. X axis is distance from glacier terminus. Dip of geological units is 3° (Major and Nagy, 1972).

6.4.2.2 Nitrogen

Having established that the nitrate is likely of microbial origin (Section 6.4.1.6 and Chapter 7), a source of reduced nitrogen must be available in the catchments. Evaluation of sulphate oxygen isotopes has demonstrated that weathering takes place in both oxic and anoxic environments in each catchment. Leaching experiments described in Chapter 3, demonstrated no variation in speciation of rock derived nitrogen from oxygenated or anoxic inorganic weathering environments. Therefore, if nitrogen is sourced from bedrock, it will be released as ammonium. The positive correlation of nitrate and crustal derived elements such as silica and sodium in glacial runoff suggests these share a common origin (Figure 6.20). In chapter 5, an experimental approach demonstrated the release of ammonium during rock weathering. The concentration of aqueous ammonium leached from rock in those experiments (0 – 220 µeq/l) exhibit a similar range to nitrate concentrations in glacial runoff (0 – 106 µeq/l), which suggests that bedrock is a significant N source for microbial nitrification.

To explore the significance of this N source to glacial catchments, catchment scale comparisons of bedrock N and runoff nitrate are made and discussed below.

Bedrock nitrogen is enriched in the Frysjaodden shales and the Firkanten Fm. These units contain both inorganic and organic forms of nitrogen, with organic rich rocks found to preferentially release N (Chapter 5). Exposure of the Firkanten Fm is limited to Fleinisen, Foxfonna and the upper parts of Møysalbreen, where it is unlikely to be connected to the runoff sampled in that catchment. The Frysjaodden Fm is exposed beneath Longyearbreen and Rieperbreen.

Nitrate concentrations vary between the different catchments, with maximum values in Longyearbreen runoff. In order to compare catchment nitrate concentrations irrespective of discharge, runoff nitrate is plotted against chloride, a conservative non-crustal derived element (Figure 6.13). Nitrate: chloride ratios are elevated in runoff from Longyearbreen and Foxfonna glacial which demonstrates that nitrate is enriched relative to discharge. The occurrence of elevated nitrate production from glacial catchments featuring the most N-rich bedrock supports the hypothesis that bedrock is a source of nitrogen to microbial ecosystems and that geological variations of N content control the amount of N available through weathering. The association of nitrate rich meltwater from glaciers overlying rocks containing a greater proportion of organic nitrogen indicates that organic N is an important influence on nitrogen release during weathering.

Rieperbreen also lies above the Frysjaodden Fm, yet does not demonstrate such significant N/Cl ratios. Rieperbreen is a small valley glacier whose footprint on the Frysjaodden Fm is limited. Nitrate concentrations were higher at Rieperbreen in 2016, the variability of NO_3^- concentrations may reflect the exposure of different parts of the geological sequence.

Whilst meltwater from Fleinisen and Foxfonna spring likely interact with N rich bedrock, anoxic conditions at these sites facilitate the loss of nitrate via denitrification. Therefore, these catchments exhibit relatively depleted dissolved nitrate concentrations.

Whilst elevated bedrock nitrogen concentrations imply a significant source of N, particularly to the Longyearbreen catchment, these results by themselves cannot conclusively attribute nitrate production from geogenic ammonium. The use of stable isotopes ($\delta^{15}N$) of bedrock and meltwater nitrate may enable such a conclusion to be drawn (Chapter 7).

6.4.3 Export of glacial solute to fjords and the marine environment

Glacial runoff is ultimately transported into fjords and the marine environment where solute may affect primary productivity through the delivery of nutrients such as N, Fe, Mn. Variations in the bedrock geology are shown here to influence meltwater chemistry and therefore may be expected to have an influence on the composition of meltwater entering fjords. Mijenfjorden and Van Keulenfjorden are major fjords located south of Isfjorden that are surrounded by bedrock of the same geological sequence studied here. Fjord sediments collected in Van Keulenfjorden contain elevated iron and manganese concentrations compared to other fjord systems in Svalbard (Wehrmann et al., 2017). Furthermore, sediments from Mijenfjorden have a greater N content than other Svalbard fjord sediments where the regional bedrock differs (Knies et al., 2007). The nitrogen in Mijenfjorden sediments is largely inorganic and believed to be of terrestrial origin (Knies et al., 2007). This is consistent with the meltwater chemistry observed in Adventdalen and the bedrock geochemistry of the Van Mijenfjorden Group. Given its tendency to adsorb to mineral surfaces, inorganic ammonium is likely transported into fjords with suspended sediment. The salinity of marine waters could promote ion exchange and liberate fixed ammonium (Gardner et al., 1991) however this has not been tested experimentally in this study. Despite this, the contribution of nitrogen from glacial catchments to downstream environments may be greater than previously thought since adsorbed ammonium is not often considered in glacial nutrient cycling studies. Furthermore, inorganic nitrogen in Mijenfjorden sediments have $\delta^{15}N$ values of 3.3 - 3.9‰ (Knies et al., 2007) which are consistent with bedrock $\delta^{15}N$ reported in this study (Chapter 4; a thorough discussion of the use of $\delta^{15}N$ as a tracer for geogenic N is provided in Chapter 7). Therefore, bedrock geology likely exerts a strong control on both meltwater chemistry and nutrient dynamics in fjords.

The weathering processes involved in nutrient export discussed in this chapter are applicable to other glacial environments. Thus, the export of nitrogen as well as iron and manganese from glacial runoff is likely to contribute positively to primary production in the polar marine environment e.g. to the Arctic/Antarctic waters. Fjords and ocean ecosystems can become nutrient limited in the summer following phytoplankton blooms particularly with regard to nitrogen (Kulk et al., 2018; van De Poll et al., 2016; Popova et al., 2010). In addition, the Southern Ocean is believed to be iron limited e.g. (Martin, 1990; Jickells et al., 2005). As the average global temperature increases, reduced sea ice extent increases the amount of light that reaches fjord/marine water thereby encouraging primary productivity. However, this may be limited by nutrient

availability of nitrate (Vancoppenolle et al., 2013) or iron. Therefore, it is possible that nutrient fluxes of nitrate and iron from glacial runoff are becoming an increasingly important contributor to fjord and marine ecosystems.

6.5 Synthesis of field research

In the glacial systems studied here, delayed high altitude snowmelt flows through crushed rock environments within moraines, facilitating extensive rock-water interaction. The majority of solute in bulk run off is derived from weathering reactions which occur in these environments. The oxidation of sulphide minerals, within crushed bedrock, generates sulphuric acid which dominates glacial runoff chemistry. The acidity generated promotes coupled carbonate dissolution and the slower dissolution of silicate minerals which neutralises the acidity. Open system conditions cause loss of CO_2 in ice marginal channels and moraine streams. Interrelated REDOX processes control the oxygenation of the weathering environment. The transfer of electrons from oxygen/oxidised species to reduced species e.g. NH_4^+, Fe^{2+}, Mn^{2+} or sulphides and the oxidation of reduced forms of these elements creates competition for oxygen which will drive the environment towards anoxia where atmosphere connectivity is limited. This will therefore inhibit oxidation with oxygen causing other electron acceptors to be used. Under such conditions, microbes likely mediate continued sulphide oxidation using alternative oxidising agents such as NO_3^-, Fe^{3+} and Mn^{4+}. The bedrock in this area contains abundant siderite (Fe, Mn), pyrite (Fe) and other iron bearing minerals (Fe oxides, glauconite). Oxidation of this source of iron and manganese likely fuels anoxic sulphide oxidation.

Under low oxygen conditions, reduced forms of iron and manganese are more soluble, however as dissolved oxygen concentrations increase through turbulence or mixing with more oxygenated waters, iron solubility decreases resulting in the precipitation of iron oxyhydroxides. Manganese concentrations often exceed iron, due to its higher solubility at near neutral pH.

Elevated nitrate in glacial runoff exceeds concentrations of nitrogen in snow and correlates with chloride and non-snowpack ions such as sodium, silica and sulphate, suggesting that nitrate is produced in environments associated with sulphide oxidation and silicate weathering. Ammonium is likely weathered from silicate minerals and kerogen via acid and oxidative weathering respectively (as demonstrated in Chapter 5) within the moraines. Organic nitrogen appears to be a significant control on the amount of nitrogen released while acidity generated through sulphide oxidation accelerates nitrogen liberation. Ion exchange processes control the sorbtion/desorption of ammonium to/from clay minerals.

Redox conditions also affect the biogeochemical cycling of nitrogen. In oxygenated gullies/moraines, geogenic ammonium in snowmelt is nitrified by microbial activity. When snowmelt encounters closed system, anoxic environments featuring abundant reactive sulphides, microbial denitrification causes loss of nitrate to the atmosphere as dinitrogen gas. Such conditions also facilitate bacterial sulphate reduction, resulting in diminished sulphate and increased bicarbonate concentrations.

Efficient comminution of bedrock into fine material with large surface area, cause the most reactive minerals to dominate meltwater chemistry, even if they represent only trace amounts of bedrock. However, variations in bedrock geology between different catchments do exert some control over meltwater chemistry, particularly with regard to nitrogen and manganese supply as well as clay minerals which control the effectiveness of ion exchange reactions.

Chapter 7 Nitrogen isotope dynamics during glacial rock weathering

7.1 Introduction

Previous research has attempted to trace the source(s) of 'excess' nitrate in glacial systems using stable N-isotope ($\delta^{15}N$) values of meltwater. However, the insight that can be gained in this way is limited by a lack of a clear understanding of nitrogen speciation and isotope effects during weathering. In order to validate N-isotopes as a tracer for geogenic nitrogen, clarity is required on the chemical transformation of nitrogen between reduced ammonium in rock and oxidised nitrate in meltwater and any associated isotope fractionation(s). There is strong evidence that nitrate results from microbial nitrification of ammonium (Wynn et al., 2007; Ansari et al., 2013), which is assumed to impart a negligible fractionation on $\delta^{15}N$. Previous stable isotope studies have therefore assumed that nitrate $\delta^{15}N$ in meltwater directly represents the source material. Yet the potential for isotope fractionation during the weathering of ammonium from bedrock and during nitrification have not been adequately examined. This project has shown that $\delta^{15}N$ of organic N within rock is either isotopically lighter than inorganic N or indistinguishable from bulk rock N (Chapter 4). In addition, rocks containing abundant clay minerals promote absorption of ammonium (Chapter 5). This partitioning of ammonium into adsorbed and aqueous phases imparts an isotopic fractionation on nitrogen (Karamanos and Rennie, 1978; Delwiche and Steyn, 1970). Ammonium adsorbed to sediment surfaces is enriched in heavy ^{15}N. Given that adsorbed ammonium represents a significant proportion of liberated N (Chapter 5), aqueous ammonium, could as a result, be significantly isotopically lighter than bulk rock $\delta^{15}N$. The results from this chapter will explore such issues which may therefore require the reinterpretation of previous studies to account for potential fractionation affects during weathering.

7.2 A predictive model

Nitrate in glacial runoff that is derived from bedrock weathering is therefore likely to have an N isotope signature that reflects:

- Bedrock $\delta^{15}N$ (Chapter 4)
- Isotope effects associated with ammonium adsorption (ε = +1 to +11‰) (Karamanos and Rennie, 1978; Delwiche and Steyn, 1970)
- Isotope effects associated with nitrification (assumed ε = 0‰)

These factors are explained below and used to create hypotheses which are outlined in Figure 7.1.

Given that each glacier erodes a different section of the overall stratigraphic sequence, the parent material $\delta^{15}N$ will vary for each glacial catchment (**hypothesis 1**).

Isotope fractionation effects of ammonium adsorption have been previously discussed, however the potential for ammonium adsorption is dependent on the availability of absorption surfaces such as clay minerals. Lithological variations in the bedrock sequence feature rock formations both rich and poor in clay minerals. Therefore, catchment geology may determine the partitioning of ammonium such that the weathering of rocks containing abundant clay minerals will result in ^{15}N-depleted N in solution and ^{15}N-enriched N in suspended sediment. Because a large proportion of ammonium enters the adsorbed phase from such rocks, the isotope fractionation effect is likely to significantly deplete aqueous ammonium with ^{15}N. Conversely N from rocks containing few clay minerals will feature less adsorption and not be fractionated as much and therefore this N liberated to solution will more closely match source $\delta^{15}N$ (**hypothesis 2**).

Microbial nitrification, which converts ammonium to nitrate in meltwater channels, has been long assumed to have negligible fractionation on ^{15}N in oligotrophic glacial environments due to high levels of competition. Therefore, nitrate in glacial runoff is expected to have $\delta^{15}N$ which reflects bedrock $\delta^{15}N$ and adsorption isotope effects only (**hypothesis 3**). Microbially produced nitrate has $\delta^{18}O$ distinctive from atmospheric sources of nitrate, since it incorporates 2 oxygen atoms from water and 1 from the atmosphere. Nitrate of atmospheric oxygen will have $\delta^{18}O$ of close to atmospheric O_2 (+23.5‰ (Hoefs, 2009)), while biogenic nitrate will have values closer to the $\delta^{18}O$ of water (-14.7‰ and -12.3‰ see Chapter 6).

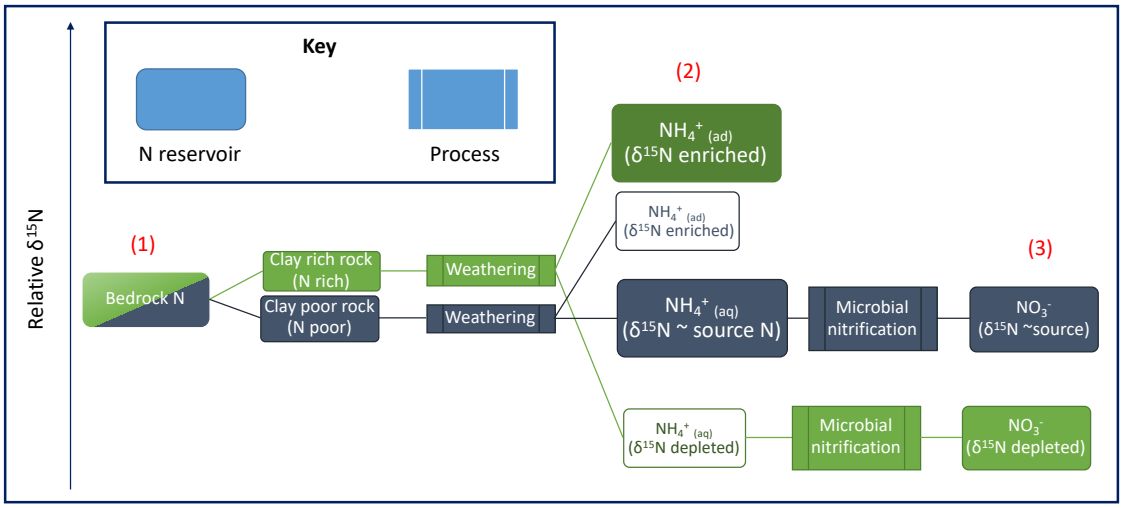

Figure 7.1 Schematic diagram of hypothesised isotope effects during rock weathering. Coloured boxes indicate whether source rock is clay rich or clay poor (same bedrock $\delta^{15}N$). Weathering products are divided into major (large, shaded) and minor (small, no shading) reservoirs of ammonium. (ad) = adsorbed; (aq) = aqueous. Red numbers in parentheses refer to hypotheses (see above).

7.3 Methods

Experiments were designed to test these hypotheses using the ammonium diffusion method (Chapter 2) to analyse $\delta^{15}N$ from 3 separate sample types:

- Rock weathering experiments – KCl extracts
- Glacial (Svalbard) suspended sediment – KCl extracts
- Glacial (Svalbard) meltwater

7.3.1 Rock weathering experiments

Experiments discussed in Chapter 5 address the significance of rock weathering as a source of N via quantification of the mass of N released from rocks during weathering. It was envisaged that these experiments would also be used to better understand the effects weathering has on $\delta^{15}N$ via isotope analysis of both aqueous NH_4^+ and adsorbed NH_4^+. However, because ammonium was preferentially adsorbed to mineral surfaces in these experiments, insufficient aqueous N was leached during weathering for isotope analysis via the diffusion method. Some N rich rocks such as shales and siltstones liberated sufficient adsorbed ammonium for isotope processing ($\delta^{15}N$). Therefore, it was only possible to study the effect on $\delta^{15}N$ upon the adsorbed phase relative to bulk rock N. According to hypothesis 2, clay poor rocks should liberate ammonium into aqueous and adsorbed phases with $\delta^{15}N$ values approximately equal to bedrock. In clay rich rocks, adsorbed ammonium

should be enriched in ^{15}N relative to aqueous and bedrock ammonium. Since only clay rich lithologies liberated enough ammonium, it was not possible to test the effect of lithology upon $\delta^{15}N$ (hypothesis 2). Therefore, catchments featuring clay poor rocks which would be expected to exhibit no fractionation of N are unlikely to yield much nitrogen. However, isotope effects associated with ammonium adsorption by rocks specific to the study area could be studied.

7.3.2 Suspended Sediment

A limited set of suspended sediment and deposited fines were collected from Longyearbreen portal in June 2018 and stored frozen. It was originally envisaged that a KCl extraction of these sediments would be carried out with subsequent processing for $\delta^{15}N$ analysis. It was anticipated that $\delta^{15}N$ of ammonium adsorbed to suspended sediment would be enriched in heavy ^{15}N relative to ammonium dissolved in meltwater (see Section 7.4.2) and bedrock N (hypothesis 2). However, following a 2 M KCl extraction, it was discovered that the sediment only contained between 2 and 12 µg/g adsorbed N (see Chapter 6). Unfortunately, this meant that there was insufficient sediment to liberate enough NH_4^+ (ad) for $\delta^{15}N$ analysis via the diffusion method. Therefore, it was not possible to use ammonium adsorbed to suspended sediment to test hypothesis 2. A discussion of adsorbed ammonium on suspended sediment can be found in Chapter 6.

7.3.3 Glacial meltwater

Glacial meltwater, collected in Svalbard, was loaded onto cation and anion resin columns in the field to concentrate ammonium and nitrate ions respectively for isotope analysis. Ammonium was eluted from the resin and then processed via ammonium diffusion method in order to measure $NH_4^+{}_{(ad)}$ $\delta^{15}N$ (Chapter 2). Nitrate was eluted from anion resins using HCl which was subsequently neutralised using silver oxide. Following processing via the acetone method, nitrate $\delta^{15}N$ and $\delta^{18}O$ were analysed by mass spectrometry (Chapter 2).

7.4 Results

7.4.1 Weathering experiment

Adsorbed ammonium $\delta^{15}N$ values from days 1 and 11 of the weathering experiment (see Section 3.5 and Chapter 5 for methods and geochemical results) are displayed in Figure 7.2 relative to their respective bedrock $\delta^{15}N$ (offset). Isotope offsets are plotted against K_D for ammonium, where higher K_D values indicate a greater proportion of ammonium is adsorbed than in aqueous form. Isotope offsets are similar for each sample on both days. The pH of most of the samples in this experiment rose to between 7 and 10. In this range of pH values, adsorption processes are enhanced by increasingly negative surface charge on minerals. However, at pH > 8, volatilisation may also occur causing loss of aqueous ammonium to ammonia gas.

Ammonium is present in both adsorbed and aqueous forms in all samples. While adsorption occurs in all samples, the isotope offset of adsorbed ammonium (N) relative to bedrock N is variable. Two trends are visible in Figure 7.2, firstly there is a positive linear correlation between K_D and offset for a small number of samples which have offsets < 5‰. Secondly there is a trend of decreasing offset with increasing K_D for a larger number of samples. In these samples, nitrogen in adsorbed ammonium is up to 10‰ isotopically heavier than bulk rock N. Sample Møy 4 (days 1 and 11) does not fall within either of these trends and unlike all other samples has a negative offset from bulk rock N (Figure 7.2). All offset values are at least 1.9‰ different from bulk rock. The smallest offsets occur in samples with low values of K_D and pH < 5 (Figure 7.2b).

Low values of K_D indicate that there is a more equal partitioning of ammonium between adsorbed and aqueous phases. Samples with K_D < 30 exert a slight positive correlation with pH up to ~ pH 8.5, whereas above pH 9 the proportion of ammonium adsorbed to sediment increases dramatically up to K_D values of 222 (Figure 7.3b). However, K_D values are also extremely varied at pH > 9 with values as low as 32 (Figure 7.3b). This group of samples with high pH and variable K_D are associated with larger $\delta^{15}N$ offsets from bedrock N (Figure 7.2b). While increased variability in K_D does not occur until ~ pH 9 (Figure 7.3b), $\delta^{15}N$ offsets become greater and more variable from pH 7 - 8 and there appears to be no systematic relationship between pH and $\delta^{15}N$ offset (Figure 7.3a).

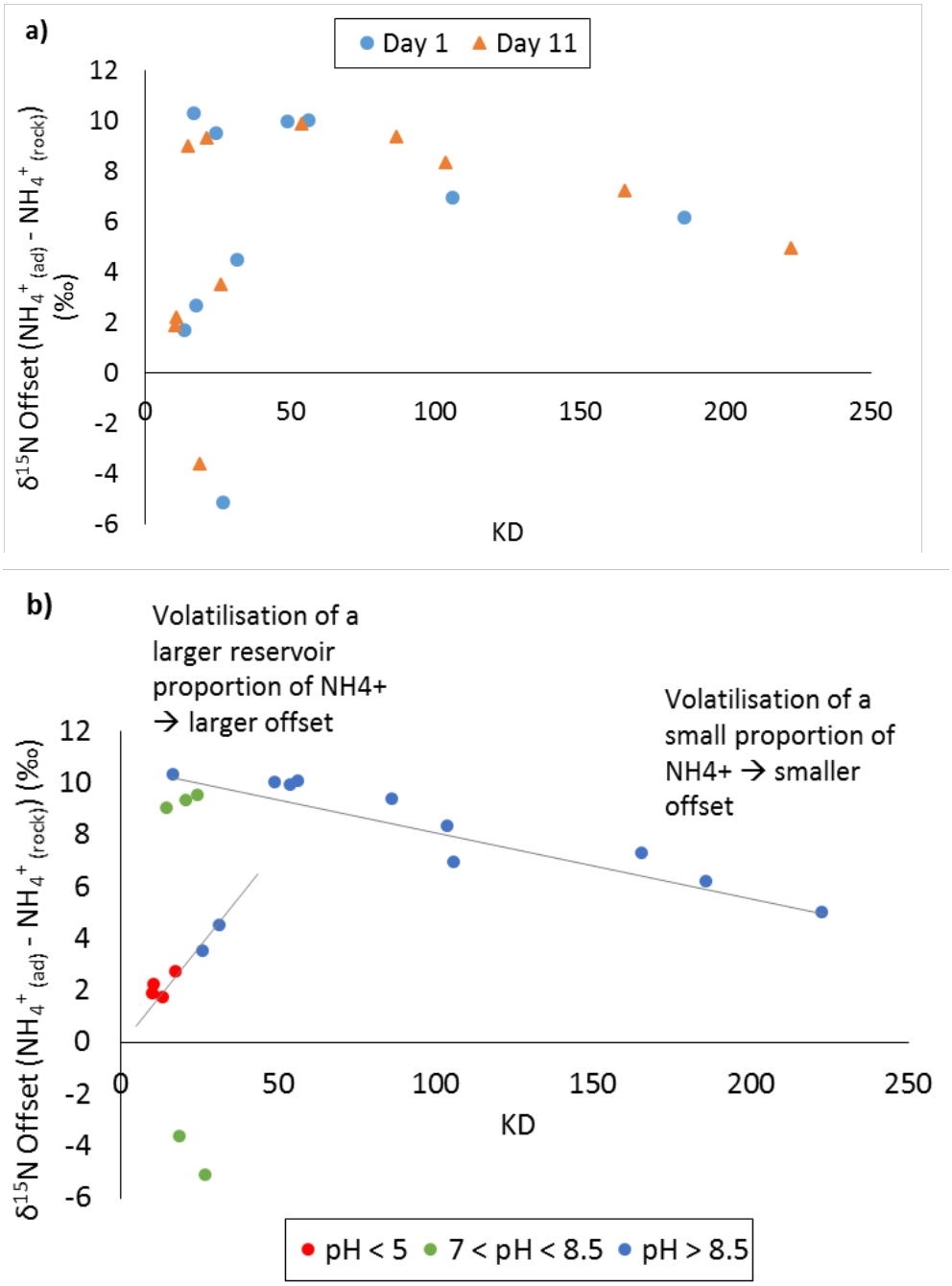

Figure 7.2 Proportion of ammonium adsorbed to mineral surfaces (K_D) v $\delta^{15}N$ of adsorbed ammonium, categorised by a) sampling day and b) pH. Two trends are observed: 1) a positive correlation between K_D and $\delta^{15}N$ offset where offsets between 0 and +5‰, 2) a negative correlation between K_D and $\delta^{15}N$ offset where offsets are > 5‰ and pH values tend to be > 8.5. In the second trend, where K_D is high, aqueous ammonium represents a smaller proportion of total ammonium pool (*cf* adsorbed ammonium), thus volatilisation of aqueous ammonium appears to have a small isotope fractionation on residual adsorbed ammonium. Low K_D samples have a greater proportion of ammonium that could be volatilised (aqueous ammonium) and thus a greater isotope fractionation effect.

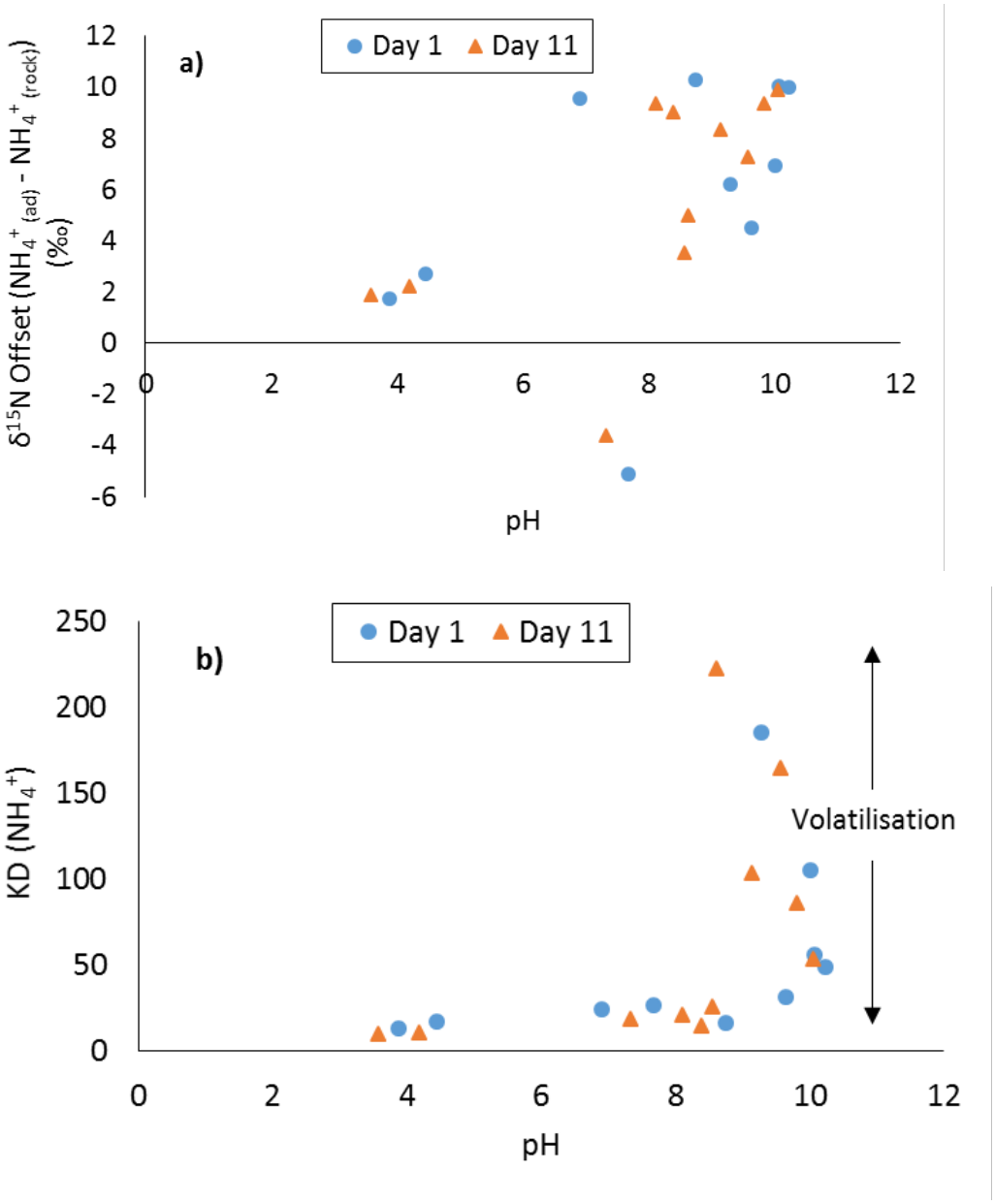

Figure 7.3 pH of water leach v a) $\delta^{15}N$ offset between adsorbed NH_4^+ and bedrock N (‰) and b) K_D for ammonium.

7.4.2 Glacial meltwater

Unfortunately, due to low natural concentrations of dissolved ammonium, very few samples were suitable for isotope analysis ($NH_4^+{}_{(aq)}$ $\delta^{15}N$) (Table 7.1). Ammonium in snow had negative NH_4^+ $\delta^{15}N$ values of -5 to -6‰, which are consistent with published snowmelt ammonium $\delta^{15}N$ values from Svalbard (Wynn et al., 2007). Only meltwater samples from Foxfonna spring were analysed for NH_4^+ $\delta^{15}N$ and these had values 12 - 13‰ heavier than snowpack ammonium (NH_4^+ $\delta^{15}N$ = +7‰).

Table 7.1 NH_4^+ $_{(aq)}$ $\delta^{15}N$ of snow and meltwater collected in 2017

Date	Site	NH_4^+ $\delta^{15}N_{AIR}$ (‰)
1/9/2017	Foxfonna Spring	+6.91 (n = 2)
8/5/2017	Longyearbreen Snow 1	-5.91 (n = 1)
8/5/2017	Longyearbreen Snow 2	-4.81 (n = 1)

Nitrate concentrations in neutralised resin effluents were measured to ensure that nitrate yields were close to 100%. The amount of nitrate loaded onto each column was calculated by multiplying the volume of meltwater sample loaded with the nitrate concentration of that water sample. The mass of nitrate in the resin effluent was found to be inconsistent with the mass of nitrate in meltwater previously loaded onto resin columns. The mass of nitrate within the effluent exceeded the expected amount of nitrate by up to 477 µmol (Table 7.2), while some samples demonstrate nitrate yields close to 100%. Variable yields may suggest that some of the samples have become contaminated during sample processing via the acetone method or during the elution/neutralisation step. The acetone method has previously been used in the lab without problems and is therefore unlikely a source of contamination. This suggests that contamination may have arisen from elution/neutralisation with silver oxide. Stable isotope values are therefore examined carefully to try to identify the source of any contamination in samples.

The amount of excess nitrate in each sample relative to the predicted amount of nitrate that should be present was plotted against nitrate $\delta^{15}N$ (Figure 7.4) and $\delta^{18}O$ (Figure 7.5). These graphs show that higher values of $\delta^{15}N$ and $\delta^{18}O$ are associated with excess nitrate. This is particularly clear for $\delta^{18}O$ which approaches approximately 25‰ as the sample becomes more contaminated. Contamination from an isotopically enriched oxygen and/or nitrogen source may cause elevated isotope values in samples. One possible source of contamination could be impurities within the lab reagents used such as HCl or AgO. Industrially produced chemicals may contain oxygen bearing impurities with isotope composition reflecting atmospheric oxygen (+23.5‰). Incorporation of such impurities during sample elution/neutralisation may explain this apparent trend towards more positive $\delta^{18}O$ values.

O and N isotope ratios are particularly enriched in samples with excess nitrate > 100 µmol. These samples are considered contaminated and are not considered during interpretation. Samples with excess nitrate close to zero are assumed to be unaffected by contaminant. These include glacial runoff from Rieperbreen and Møysalbreen as well as a single $\delta^{18}O$ value from Longyearbreen. These

samples have $\delta^{18}O$ between 0‰ and 11.3‰ and $\delta^{15}N$ between 2.7‰ and 6.8‰.

Table 7.2 Nitrate yield of anion resins and associated stable isotope ratios. * indicates peak height of sample was too small to derive a reliable isotope ratio. Red font indicates sample has elevated excess nitrate and is likely contaminated. Estimated % microbial NO_3^- is calculated using an isotope mass balance equation described in section 7.5.1.

Date	Expected NO_3^- (meltwater concentration * volume) (µmol)	NO_3^- in effluent (µmol)	Predicted excess NO_3^- (µmol)	NO_3^- $\delta^{15}N_{AIR}$ (‰)	NO_3^- $\delta^{18}O_{VSMOW}$ (‰)	Estimated % microbial NO_3^-
Longyearbreen						
27/08/2017	25	475.45	450.45	*	*	
27/08/2017	27.3	166.69	139.39	11.25	23.89	
28/08/2017	22.5	194.89	172.39	*	*	
28/08/2017	21.9	19.54	-2.36	*	11.29	82 ± 1
01/09/2017	39.3	160.4	121.1	12.51	18.70	
01/09/2017	41.2	80.91	39.71	*	*	
Rieperbreen						
29/08/2017	18.9	19.82	0.92	6.86	9.22	85 ± 1
29/08/2017	20.7	185.22	164.52	11.08	22.66	
14/09/2017	36.6	37.42	0.82	4.15	7.60	87 ± 1
14/09/2017	29.9	41.41	11.51	6.78	7.10	88 ± 1
Møysalbreen						
04/09/2017 (Moy-Loc-2)	37.6	29.39	-8.21	2.98	-0.01	98 ± 1
05/09/2017 (Moy-Loc-2)	6.6	17.99	11.39	2.67	0.95	97 ± 1
05/09/2017 (Moy-Loc-4)	9.6	17.13	7.53	2.89	4.32	92 ± 1
Snow						
08/05/2017	89.29	366.68	277.39	11.22	24.48	
08/05/2017	18.57	495.21	476.64	11.37	28.14	

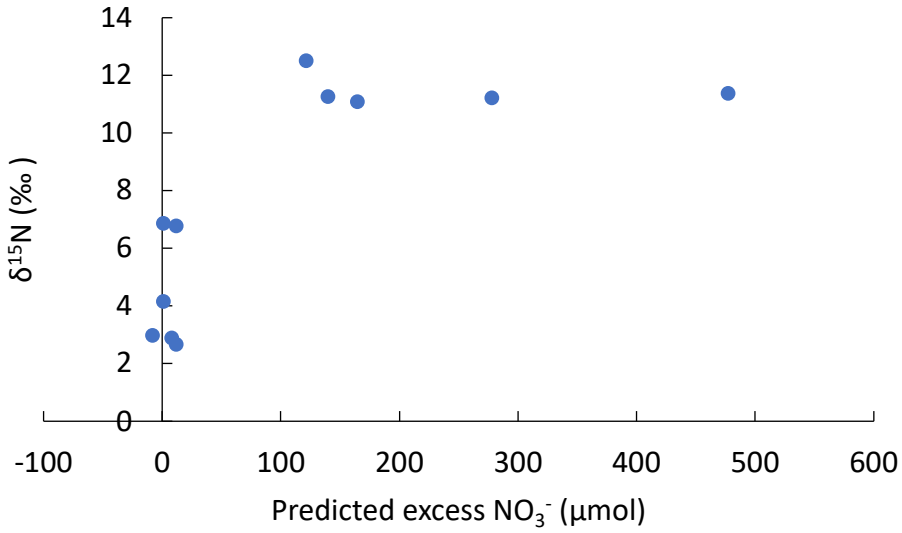

Figure 7.4 Predicted excess nitrate in anion resin effluent and nitrate $\delta^{15}N$

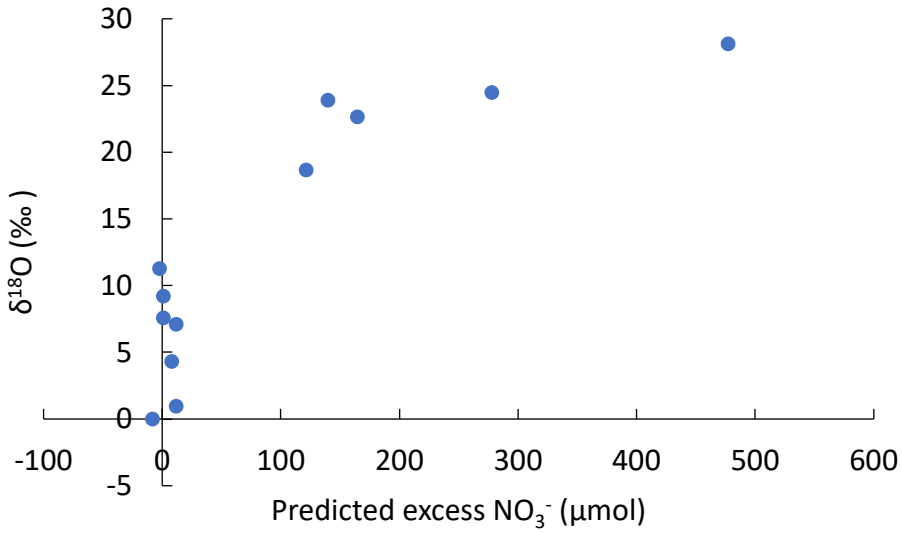

Figure 7.5 Predicted excess nitrate in anion resin effluent and nitrate $\delta^{18}O$

7.5 Discussion

7.5.1 Isotope fractionation ($\delta^{15}N$) associated with ammonium adsorption

An initial hypothesis (2) was that mineralogy would exert a dominant control on $\delta^{15}N$ of ammonium through increased potential for cation sorption. Whilst it is not possible to evaluate this directly from these results, broad insights into isotope fractionation during weathering can be gained.

Adsorbed ammonium generally has more positive $\delta^{15}N$ ratios than bulk rock N with offsets of up to 10‰. This isotope enrichment agrees with previous research which finds that N isotopes are fractionated during adsorption by +1 to

+11‰ (Karamanos and Rennie, 1978; Delwiche and Steyn, 1970. By virtue, it is assumed that aqueous ammonium is isotopically lighter than bulk rock N.

Larger $\delta^{15}N$ offsets are associated with high pH values. Ammonia volatilisation and adsorption processes are promoted at high pH, whose effects directly or indirectly both fractionate adsorbed ammonium to heavier values. Volatilisation would leave residual $NH_4^+{}_{(aq)}$ isotopically enriched as lighter ^{14}N preferentially partitions into NH_3. Adsorption fractionates heavier ^{15}N isotopes into adsorbed ammonium, leaving residual $NH_4^+{}_{(aq)}$ – N isotopically light. Therefore, adsorption and volatilisation cause fractionation of $NH_4^+{}_{(aq)}$ - N in opposite directions (Figure 7.6). Consequently, the measured $\delta^{15}N$ - $NH_4^+{}_{(ad)}$ reflects the net isotope ratio associated with these processes. Whether one of these processes dominates and therefore controls the product isotopic signal of adsorbed ammonium $\delta^{15}N$ is difficult to determine.

In order to consider this further, it is helpful to consider the different N reservoirs in the system (Figure 7.6). As discussed in Chapter 5, ammonium speciation is pH dependent due to surface charge and ammonium deprotonation. Where pH < 8, ammonium is distributed between aqueous and adsorbed phases. In this experiment, at pH < 4, ammonium is almost equally split between adsorbed and aqueous phases and N isotopes of rock and adsorbed ammonium are only ~2‰ apart (Figure 7.3a). However, as pH increases up to pH 8, there is a gradual increase in K_D (Figure 7.3b) which may reflect mineral surface charges becoming less positive/more negative and thus attracting more ammonium to sorption sites. As ammonium is increasingly partitioned into the adsorbed phase (increasing K_D), $NH_4^+{}_{(ad)}$ becomes more positive which suggests that isotope fractionation results in heavier ^{15}N preferentially entering the adsorbed phase (Figure 7.2).

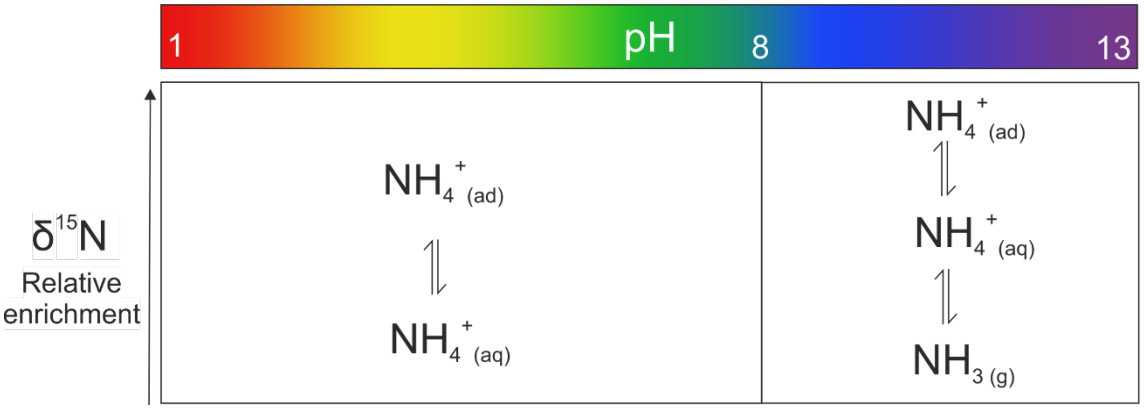

Figure 7.6 Ammonia/ammonium species during rock weathering and their relative nitrogen isotope ratios.

However, at pH > 8, aqueous ammonium begins to deprotonate forming ammonia, hence the system evolves from having 2 phases to 3 phases, where

ammonia is able to degas/volatilise and exit the aqueous system (Figure 7.6). The mass of gaseous ammonia produced in this experiment was not measured, therefore it cannot conclusively be stated whether this reaction occurred. However, elevated K_D values associated with high pH (Figure 7.3b) indicate that only a small proportion of ammonium occurs in the aqueous phase. This could be due to loss of $NH_4^+{}_{(aq)}$ by volatilisation. During volatilisation, light ^{14}N preferentially enters the gas phase leaving the residual $NH_4^+{}_{(aq)}$ and $NH_4^+{}_{(ad)}$ pool isotopically heavy. Only samples with pH ~ 9 - 10 have isotope offsets > 5‰ which may suggest that volatilisation occurred. Fractionation factors associated with this reaction are inversely proportional to temperature (Li, L. et al., 2012), therefore at low temperatures, high degrees of fractionation may occur. Yet since the rate of ammonia diffusion is influenced by temperature, the overall flux of isotopically light NH_3 may be limited. However, because pH is measured in a log scale, a small positive change in pH can have a large effect on ammonium speciation as NH_4^+ deprotonates. Diffusion of free ammonia out of solution is a function of the concentration of NH_3 in solution and NH_3 in the headspace. Since the initial headspace in the experiment was assumed to contain negligible ammonia, this is unlikely to be a rate limiting step. Therefore, pH change would be expected to have a direct effect on volatilisation. In this experiment, the lack of a systematic variation between pH and $\delta^{15}N$ offset in high pH samples (Figure 7.3a) suggests that the isotope affect possibly associated with volatilisation varies due to a factor other than pH. The isotope effect of a reaction is dependent on the enrichment factor and the reservoir size of the reactant. Therefore, assuming a constant isotope enrichment factor of volatilisation (at a fixed experiment temperature), variations in the overall isotope effect may reflect the amount of ammonium which is liable to volatilisation. Assuming volatilisation only affects aqueous ammonium and adsorbed ammonium which is held on mineral surfaces, the amount of volatilised ammonia is dependent on the mass of aqueous ammonium.

The proportion of aqueous ammonium initially in the system, following rock-water interaction, is dependent on the amount of adsorption which has occurred. At high pH values associated with volatilisation, more negative surface charges also promote adsorption. In this experiment, as K_D increased, the isotope offset between adsorbed ammonium and bulk rock N decreased (Figure 7.2). In other words, the largest offsets occurred where the proportion of $NH_4^+{}_{(aq)}$ were greatest while the smallest isotope offsets occurred where $NH_4^+{}_{(aq)}$ comprised a greater proportion of the aqueous – adsorbed ammonium pool. At very high K_D values the proportion of nitrogen adsorbed to sediment approaches 100%. Consequently, the isotopic signature of adsorbed

ammonium more closely represents bulk rock N. This may represent scenarios where efficient adsorption processes restrict aqueous ammonium to a small reservoir of N which is rapidly depleted by volatilisation, such that the overall isotope effect on adsorbed ammonium is minimal (Figure 7.2b). Conversely, a larger reservoir of $NH_4^+{}_{(aq)}$ would require a longer time to deplete it by volatilisation. During this time, kinetic fractionation associated with volatilisation would enrich aqueous ammonium with ^{15}N while isotope equilibration between aqueous and adsorbed ammonium would enrich adsorbed ammonium with ^{15}N, thus giving adsorbed ammonium the heaviest $\delta^{15}N$ of the 3 species. The combined effect would yield a larger offset of adsorbed N from bedrock N in lower K_D samples relative to higher K_D samples (Figure 7.2b).

The offset between adsorbed ammonium and rock N is not completely eliminated in these samples which suggests that either i) volatilisation has occurred causing loss of ^{14}N such that the offset will not be reduced further or ii) volatilisation has not occurred and longer than 11 days is required to reach equilibrium between $NH_4^+{}_{(ad)}$ and $NH_4^+{}_{(aq)}$. Given the high pH (Figure 7.3), it is highly likely that volatilisation has occurred to some degree. Decreases in total N over the course of the experiment (Chapter 5) further suggest loss of N from the system. Furthermore, equilibration of N isotopes between aqueous and adsorbed ammonium occurs within 24 hours at 23°C (Karamanos and Rennie, 1978), therefore it is likely that isotope equilibration would have been reached during the 11 days of this experiment. As previously discussed, the rate of volatilisation is dependent on the diffusive transfer of ammonia from the liquid to the gas phase which is in turn controlled by the concentration gradient of $NH_{3(g)}$. This experiment was carried out in a closed environment; therefore, the headspace would have had an initial $NH_{3\ (g)}$ concentration of zero. However, following the onset of NH_3 diffusion, the NH_3 concentration gradient would have dramatically reduced, reducing rates of volatilisation. Therefore, it is likely that rapid initial pH rise caused by hydrolysis reactions which liberate NH_4^+ (Chapter 5), quickly increased the solution pH, thereby promoting volatilisation during the early stages of rock – water interaction. As this reaction slows, ongoing isotope fractionation may be dominated by equilibration between aqueous and adsorbed ammonium.

However, not all samples fall in this trend of decreasing offset with increasing K_D. The positive linear trend of 6 samples in Figure 7.2 suggests that N isotope offset between rock and adsorbed N increases with larger K_D values, which contradicts the previous trend. Four of the six samples had pH < 5. Volatilisation would not have affected these samples; therefore, it is conceivable that as more ammonium is adsorbed, the isotope fractionation effect associated with this

process increases the offset between adsorbed ammonium and bedrock N. However, the other 2 samples in the trend had pH values of 8.5 and 9.6 (Figure 7.2b) which would suggest that they would be at risk of isotope effects caused by volatilisation. However, this seems to not be the case and it is unclear why they fall in this positive trend. Furthermore, the reasons for the negative isotope offsets demonstrated by sample Møy 4 are also not clear (Figure 7.2). Adsorption and volatilisation both cause adsorbed ammonium to become isotopically heavier then bulk rock N and it is thus unknown how adsorbed ammonium could become lighter than rock N.

The reasoning above assumes that liberated ammonium is derived from both organic and inorganic N in proportion to their ratio in rock and thus its $\delta^{15}N$ reflects bulk rock $\delta^{15}N$. However, if ammonium is preferentially derived from organic nitrogen, its $\delta^{15}N$ may be isotopically lighter than bulk rock N since organic N can be depleted in ^{15}N relative to inorganic N (Chapter 4). Analysis of organic/inorganic $\delta^{15}N$ was not carried out on Møy 4, therefore it is not possible to test this assertion. Møy 4 contains 2.8 wt. % organic carbon, therefore, it may contain significant organic N which may be more readily weathered than inorganic N, potentially yielding isotopically light ammonium.

During weathering the isotope signature of rock nitrogen is translated into liberated ammonium. However, subsequent volatilisation and speciation of ammonium between aqueous NH_4^+ and adsorbed NH_4^+ incurs an isotope fractionation causing the nitrogen isotope signature of adsorbed ammonium to differ from the parent rock by up to 10‰. Therefore, in glacial meltwater, the isotope composition of nitrogen derived from bedrock is unlikely to directly reflect the bedrock source. These results find that at pH values relevant to runoff from glaciers in this study (8-10), there is a net isotope enrichment factor (where $\varepsilon = NH_4^+{}_{(ad)} - NH_4^+{}_{(rock)}$) of between 3.5‰ and 10.3‰. More rigorous evaluation of isotope fractionation effects associated with adsorption and volatilisation at temperatures representative of glacial environments are required to further constrain isotope effects associated with these processes during rock weathering. Uncertainty regarding these effects therefore currently confound the use of stable isotopes to attribute nitrogen to bedrock weathering.

7.5.2 Isotope evidence for microbial nitrate production

According to hypothesis 3, nitrate is produced via microbial nitrification. As such biogenic nitrate should incorporate 2 oxygen atoms from water (-14.7 to -12.3‰ (Chapter 6)) and 1 oxygen atom from atmospheric O_2 (+23.5‰ (Hoefs, 2009)). Many studies that have measured this microbial endmember found that nitrate $\delta^{18}O$ was more positive than predicted via the ratio given above. However, the

magnitude and causes of this isotope enrichment factor are currently poorly constrained. As such this approach should be used with caution. Assuming no fractionation effect, the oxygen isotope composition of microbial nitrate $\delta^{18}O$ should have a value of between -0.4‰ and -1.9‰ (Equation 7.1).

$$\delta^{18}O_{NO3} = (0.33 \times \delta^{18}O_{Air}) + (0.66 \times \delta^{18}O_{Water})$$

$$-0.4‰ \text{ to } -1.9‰ = (0.33 \times +23.5‰) + (0.66 \times (-12.3‰ \text{ to } -14.7‰)) \quad \textbf{Equation 7.1}$$

A crude estimate of the proportion of nitrate in glacial runoff that was produced by microbial nitrification can be made by assuming a 2 member mixing model between snowpack nitrate $\delta^{18}O$ and microbial nitrate $\delta^{18}O$ (-0.4‰ and -1.9‰). Unfortunately, no snow samples were suitable for interpretation due to contamination, however studies from northern Svalbard report snowpack nitrate $\delta^{18}O$ values of +59‰ to +80‰ (Table 7.3). Assuming an average snowpack $\delta^{18}O$ of +67.2‰, between 82% and 92% of nitrate is likely produced microbially (Table 7.2). These values are at the upper end of the range of percentages of non-snowpack nitrate calculated in Chapter 6 (55% - 89%).

Table 7.3 Summary of published Svalbard snowpack nitrate $\delta^{18}O$ values

$\delta^{18}O$	Glacier	Year	Reference
+57.3±2.7‰	Midtre Lovénbreen	2002	Wynn et al. (2007)
+72‰	Midtre Lovénbreen	2003	Wynn et al. (2007)
+78±1.5‰	Midtre Lovénbreen	2009	Ansari et al. (2013)
+76±4‰	Lomonosovfonna	2011	Vega et al. (2015)
+66±5‰	Kongsvegen		
+59±3‰	Holtedahlfonna		
+62±5‰	Holtedahlfonna		
+67.2‰	Average		

As discussed previously in Chapter 6, non-snowpack nitrate is associated with water which has acquired crustal solute such as Na^+, Si^{4+} and SO_4^{2-} during interaction with rock debris in ice marginal moraines. Therefore, nitrate production may be occurring in these debris rich environments as also reported by others (Hodson, 2006; Wynn et al., 2007; Ansari et al., 2013).

7.5.3 Applying stable isotopes as a tracer of geogenic nitrogen to glacial water

Given that nitrate is likely biogenic, an ammonium substrate is required to drive nitrification. Ammonium may be derived from i) snowmelt and glacier ice, ii) mineralised organic matter or iii) geogenic NH_4^+ liberated during rock weathering (Wynn et al., 2007). Glacial environments are oligotrophic; therefore, it is assumed that there is negligible fractionation of nitrogen during nitrification. As such, $\delta^{15}N$ NO_3^- in glacial meltwater should match source $\delta^{15}N$ $NH_4^+{}_{(aq)}$. Only one isotope value for aqueous ammonium is available (Foxonna Spring) which has $\delta^{15}N$ similar to Rieperbreen NO_3^- but is ~4‰ heavier than Møysalbreen NO_3^- (Table 7.1 and Table 7.2).

Snow $\delta^{15}N$ NH_4^+ values (-5‰ to -6‰) are 8‰ to 13‰ lighter than meltwater ammonium/nitrate (Table 7.1 and Table 7.2). The divergence of $\delta^{15}N$ between snow and meltwater suggests that snow is unlikely a major source of ammonium for nitrification, unless the isotope signature has been modified by geochemical processes such as volatilisation and adsorption. Volatilisation would cause a positive shift in $\delta^{15}N$ as the lighter ^{14}N isotope is preferentially lost to NH_3 gas. Adsorption could become a significant process when snowmelt enters crushed rock environments. This would have an opposite isotope effect as ^{15}N is preferentially adsorbed to mineral surfaces leaving residual NH_4^+ enriched in the lighter ^{14}N isotope. Given the pH of 8.2, some volatilisation may occur but this is may be limited by atmospheric gas exchange depending on the atmospheric connectivity of the flow path. Whereas the abundance of negatively charged clay minerals at this pH is likely to make the isotopic effect of adsorption more important. Therefore, the difference in $\delta^{15}N$ between snow and meltwater is unlikely accounted for by isotope fractionation processes.

An evaluation of modern organic matter as a nutrient source is beyond the scope of this project. However, isotope analysis of supraglacial cryoconite on another Svalbard glacier, Midtre Lovenbreen, derived $\delta^{15}N$ values of -4.8‰ to -3.3‰ (Wynn et al., 2007). Whilst such values do not correspond with meltwater nitrogen observed in this study, catchment specific sampling would be required to investigate this as an isotope endmember.

Table 7.4 Average nitrogen concentration and $\delta^{15}N$ of different geological Formations in the bedrock sequence. Colour gradient (yellow – red) indicates low to high N concentrations.

Formation	n	Mean N wt %	Mass weighted mean $\delta^{15}N$ (‰)
Aspelintoppen	5	0.05	2.49
Battfjellet	4	0.04	3.04
Frysjaodden	24	0.12	3.80
Grumantbyen	18	0.02	1.82
Basilika	8	0.04	3.58
Firkanten (Endalen)	7	0.02	1.59
Firkanten (Todalen)	8	0.10	3.41
Carolinefjellet	1	0.10	4.13
All Samples	75	0.07	3.43

Bedrock Formations in these glacial catchments have average N concentrations of between 0.02 and 0.12 wt. % N (Table 7.4). The abundance of rock debris within the catchments makes rock a significant potential source of ammonium, liberated through weathering reactions (as discussed in chapter 5). Mass weighted $\delta^{15}N$ of geologic formations vary between 1.6‰ and 4.1‰, although N rich formations tend to have isotope signatures within the upper end of this range (Table 7.4). Mass weighted $\delta^{15}N$ values of bedrock N are derived for each glacial catchment using $\delta^{15}N$ data from the geological formations that appear in each catchment (Table 7.5). These catchment averages are highly similar (+3 to +3.5‰) and therefore N derived from rock weathering would be expected to have an isotope value within this range prior to isotope affects associated with adsorption/volatilisation.

Table 7.5 Mass weighted mean $\delta^{15}N$ of bedrock in different glacial catchments in Svalbard and corresponding meltwater nitrate/ammonium $\delta^{15}N$. Average pH of meltwater for each catchment is also provided. N.d. = no data

Catchment	Underlying bedrock		Meltwater	
	Geological Fms	MWM $\delta^{15}N_{AIR}$ (‰)	$\delta^{15}N$ (‰)	pH
Longyearbreen	Aspelintoppen, Battfjellet, Frysjaodden, Grumantbyen, Basilika	+3.48 (n = 59)	n.d.	8.2 (n = 5)
Rieperbreen	Battfjellet, Frysjaodden, Grumantbyen,	+3.54 (n = 46)	+5.93 (NO_3^-) (n = 3)	7.7 (n = 4)
Foxfonna Spring	Grumantbyen, Basilika, Firkanten	+2.96 (n = 41)	+6.91 (NH_4^+) (n = 2)	8.2 (n = 1)
Møysalbreen/ Gløttfjellbreen	Basilika, Firkanten, Carolinefjellet	+3.34 (n = 24)	+2.85 (NO_3^-) (n = 3)	9.1 (n = 6)

Meltwater ammonium and nitrate $\delta^{15}N$ at Rieperbreen and Foxfonna spring are both heavier than bedrock $\delta^{15}N$ whilst at Møysalbreen, nitrate $\delta^{15}N$ is only 0.5‰ lighter than bedrock $\delta^{15}N$.

Whilst the results from the small-scale weathering experiment demonstrated net isotope fractionation of up to +10‰ ($\varepsilon = NH_4^+{}_{(ad)} - NH_4^+{}_{(rock)}$), the effect on aqueous N species has not been constrained. Following the above discussion, meltwater nitrogen derived from bedrock would be expected to be depleted in ^{15}N due to adsorption. However, the small number of observed meltwater isotope ratios generally infer a positive shift in $\delta^{15}N$. Meltwater nitrogen was closest to bedrock at Møysalbreen, yet there, higher pH values of ~9 (Table 7.5) would make volatilisation more likely which would be expected to make aqueous ammonium/nitrate $\delta^{15}N$ more positive. Therefore, while small isotope differences between rock and meltwater N may hint at geogenic N as a nitrogen source, uncertainties of isotope effects of N during rock weathering do not allow this to be proven through isotope analysis. As such, it was not possible to test whether the nitrogen isotope composition of nitrate and ammonium in meltwater directly represent bedrock N (hypothesis 3). However, given that nitrogen is likely fractionated during weathering of ammonium from bedrock, nitrate $\delta^{15}N$ is unlikely to directly represent bedrock $\delta^{15}N$.

7.6 Conclusions

A microbial origin of nitrate in glacial runoff is supported by stable isotope data ($\delta^{18}O$) which shows that oxygen is incorporated into nitrate from an isotopically light source i.e. non-atmospheric origin. Isotope mass balance equations estimate that the biogenic nitrate represents the bulk of nitrate in late summer glacial discharge.

Geogenic ammonium was explored as an ammonium substrate for nitrification by researching nitrogen isotope dynamics during weathering. A weathering experiment undertaken in this study has demonstrated the occurrence of nitrogen isotope fractionation during rock weathering. pH controls ammonium speciation with the system evolving from a two member system (adsorbed and aqueous NH_4^+) to a 3 member system at pH 8, where free ammonia gas may volatilise. Ammonium adsorbed to mineral surfaces is up to 10‰ enriched compared to bulk rock $\delta^{15}N$ at pH > 8. The net isotope effect is likely a combination of adsorption and volatilisation.

Catchment scale isotope values for rock nitrogen have been defined which differ from meltwater ammonium/nitrate $\delta^{15}N$ by only a few per mille. However, the use of stable isotopes as tracer of geogenic N is currently inhibited by uncertainty over the specific isotope effects of adsorption and volatilisation during weathering. Further research into these processes and their isotope fractionation factors in glacial conditions are required in order to use stable isotopes as a tracer of geogenic N.

Chapter 8 Synthesis and conclusions

8.1 Introduction

This project consists of three strands:

1. Characterisation of rock geochemistry of glacial catchments in Adventdalen area of Svalbard
2. Rock weathering experiments using rocks from study area to understand solute acquisition processes particularly relating to N, Fe and Mn
3. Field work to sample and analyse glacial meltwater geochemistry to identify biogeochemical processes relating to N, Fe, Mn and S in subglacial environments

In this chapter, these elements are drawn together to synthesise the project findings. Geochemical characterisation of bedrock provides a new understanding of the reginal geology in which to interpret glacial runoff geochemistry. In addition, the results of rock weathering experiments, designed to simulate subglacial weathering environments, are used to interpret glacial runoff chemistry and infer geochemical processes which occur during the release of nutrients from rock.

8.2 Summary of rock geochemistry

The bedrock sequence in the study area was found to consist of carbonate poor siliciclastic units deposited in a deltaic environment during the Palaeocene and Eocene (Figure 8.1). This period featured fluctuations in sea level, uplift of the nearby West Spitsbergen mountain belt and a major climatic warming episode (the Paleocene - Eocene Thermal Maximum). A summary of bedrock geochemistry is provided in Appendix D alongside a stratigraphic log.

In the coastal palaeoenvironment, organic matter derived from both terrestrial plants and marine algae was incorporated and preserved within sediment where the environment was poorly oxygenated. Organic carbon is particularly enriched in the Firkanten Fm and Aspelintoppen Fm where coal seams are found. However organic carbon is also elevated in the black shales of the Frysjaodden Fm which do not contain coal. Bedrock nitrogen concentrations fluctuate within the sedimentary sequence and covary with organic carbon. The average N concentration is 0.07 wt. %, although the highest concentrations occur in siltstones and shales such as the Firkanten Fm – Todalen Mb (average 0.1 wt. %) and Frysjaodden Fm (average 0.12 wt. %) as opposed to coarser

sandstones. The majority of nitrogen occurred as inorganic N (N_{inorg}), within silicate minerals, while around a third of rock N is organic (N_{org}). Silicate N was likely sourced from the mineralisation of organic N as indicated by indistinguishable $\delta^{15}N$ ratios of N_{org} and N_{inorg}. The sedimentary sequence has a fairly uniform nitrogen isotope composition of 3 – 4 ‰ which reflects a mixed terrestrial and marine organic source.

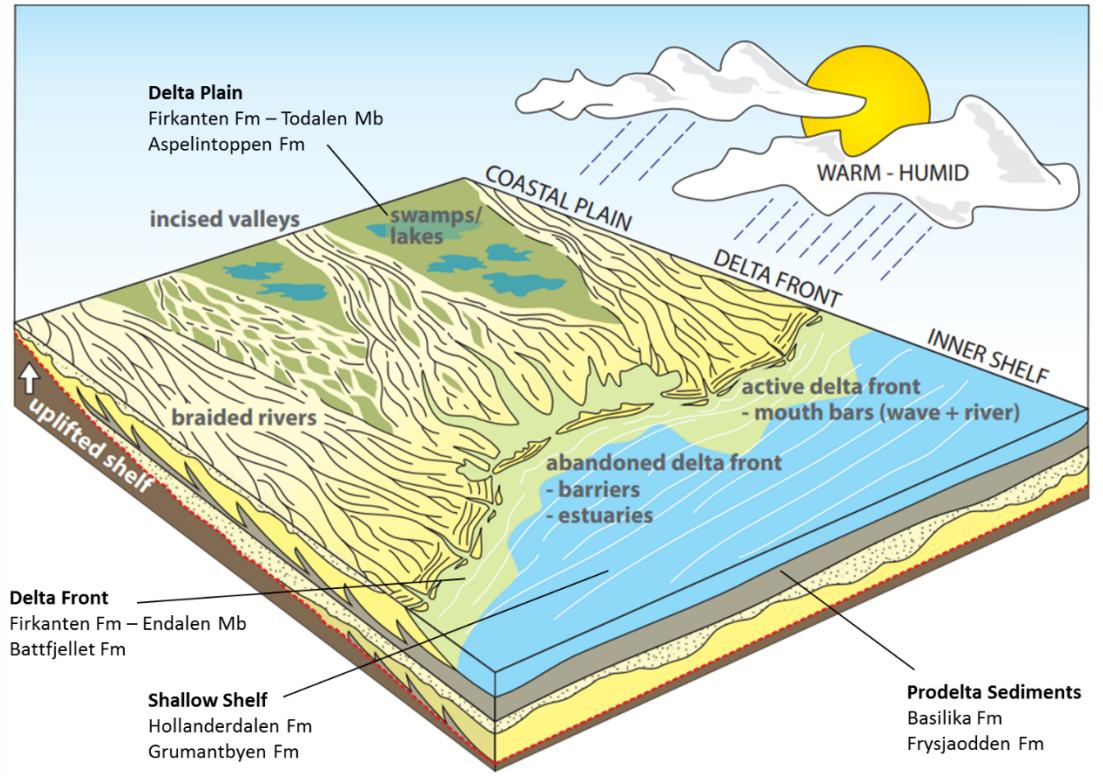

Figure 8.1 Schematic diagram of the palaeoenvironment during Paleocene/Eocene deposition of Central Tertiary Basin deposits in Svalbard. Adapted from (Dallman, 2015).

The mixing of terrestrial freshwater and marine saltwater at the delta front would have created brackish conditions characterised by low inorganic carbon and sulphate concentrations relative to normal marine conditions. Suspended sediment within rivers likely contributed iron derived from terrestrial weathering, which in oxygenated waters, was largely deposited as iron oxide minerals (e.g. Grumantbyen Fm). By contrast, in more reducing environments, iron formed diagenetic minerals such as siderite and pyrite depending on the availability of inorganic carbon and sulphate. Pyrite is more abundant in Palaeocene rocks, particularly within the coal bearing Firkanten Fm. Pyrite sulphur has a mass weighted mean of -1.5‰ $\delta^{34}S$, however a wide range of pyrite $\delta^{34}S$ in this sequence mean that bedrock $\delta^{34}S$ is spatially variable. The carbonate content of rock increases in Eocene age rocks which is coincident with an abundance of iron carbonates (siderite). Manganese substitution occurs within siderite, particularly within the Frysjaodden Fm.

The depositional history of this bedrock sequence thus reveals different palaeoenvironments which resulted in the formation of geochemically distinct rock formations. Their exposure in modern glacial environments likely contributes to differences in solute acquired in glacial runoff as discussed in the following section.

8.3 Synthesis of experimental and field work

In order to better understand the weathering processes involved in the release of nitrogen from rock, geochemical analysis was undertaken of both glacial meltwater and leachates from rock weathering experiments. In both lab-based experiments and glacial environments, sulphide oxidation was an important weathering reaction. However, sulphate generally represented a greater proportion of the anion budget in glacial runoff than in rock weathering leachate. In the weathering experiments the dominant anion was generally bicarbonate (>50%) whereas in glacial runoff, bicarbonate represented < 40% of the anion budget (SMF generally 0.6 - 1). Sulphide oxidation is accelerated by microbial activity; however, weathering experiments were carried out under abiotic conditions. Thus, the lack of microbial catalysis likely restricted sulphate production. As such, while coupled sulphide oxidation and silicate dissolution accounted for much of the solute in glacial catchments, faster silicate and carbonate hydrolysis liberated most solute in abiotic weathering experiments (Figure 8.2).

Furthermore, weathering experiments were carried out under closed system conditions whereas natural weathering environments in these catchments were open to atmospheric gas exchange, apart from more isolated parts of flow paths. Since many of the glacial water samples were oxygenated and dissolved CO_2 was in equilibrium with atmospheric CO_2 (Chapter 6), the flowpaths feature atmospheric gas exchange. In subglacial environments proton consumption by weathering reactions is balanced by proton supply largely from sulphuric acid and carbonic acid. Production of these acids are largely dependent on the dissolution of atmospheric oxygen (which fuels sulphide oxidation) and carbon dioxide (which forms carbonic acid) into meltwater respectively. However, in the closed system weathering experiments, protons are rapidly consumed in hydrolysis reactions yet acid sources are limited by a lack of gaseous diffusion as well as slow rates of abiotic sulphide oxidation. Thus, the demand for protons can exceed supply in closed systems inhibiting acid hydrolysis. Consequently, these experiments largely reflect the early stages of weathering characterised mainly by hydrolysis reactions. Over longer timescales and with microbially catalysed sulphide oxidation, weathering becomes dominated by acid hydrolysis of silicate minerals fuelled by pyrite oxidation (Figure 8.2).

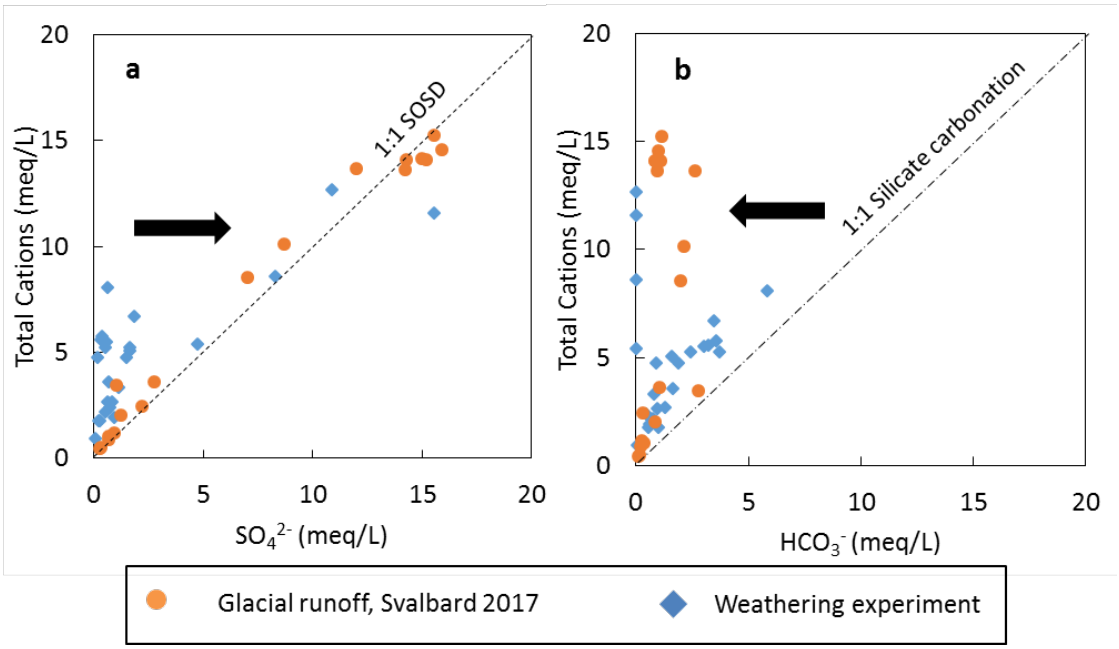

Figure 8.2 Graphs showing a) sulphate and b) bicarbonate v total cations
Blue diamonds indicate solute in weathering experiments after 11 days at 6°C (Chapter 5), while orange circles indicate solute in glacial runoff collected in Svalbard in 2017 (Chapter 6). Black arrows indicate evolution of weathering reactions and solute from silicate carbonation in short term weathering reactions to sulphide oxidation coupled to silicate dissolution over long term in glacial catchments.

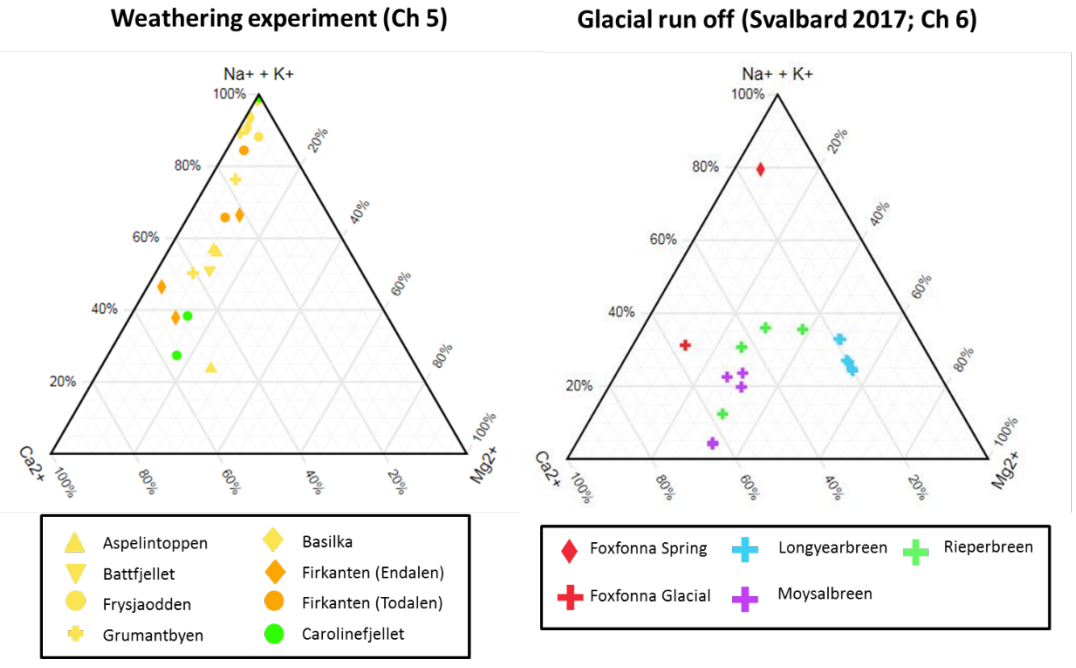

Figure 8.3 Comparison of proportions of cations in leachate from simulated glacial weathering as well as from glacial runoff.

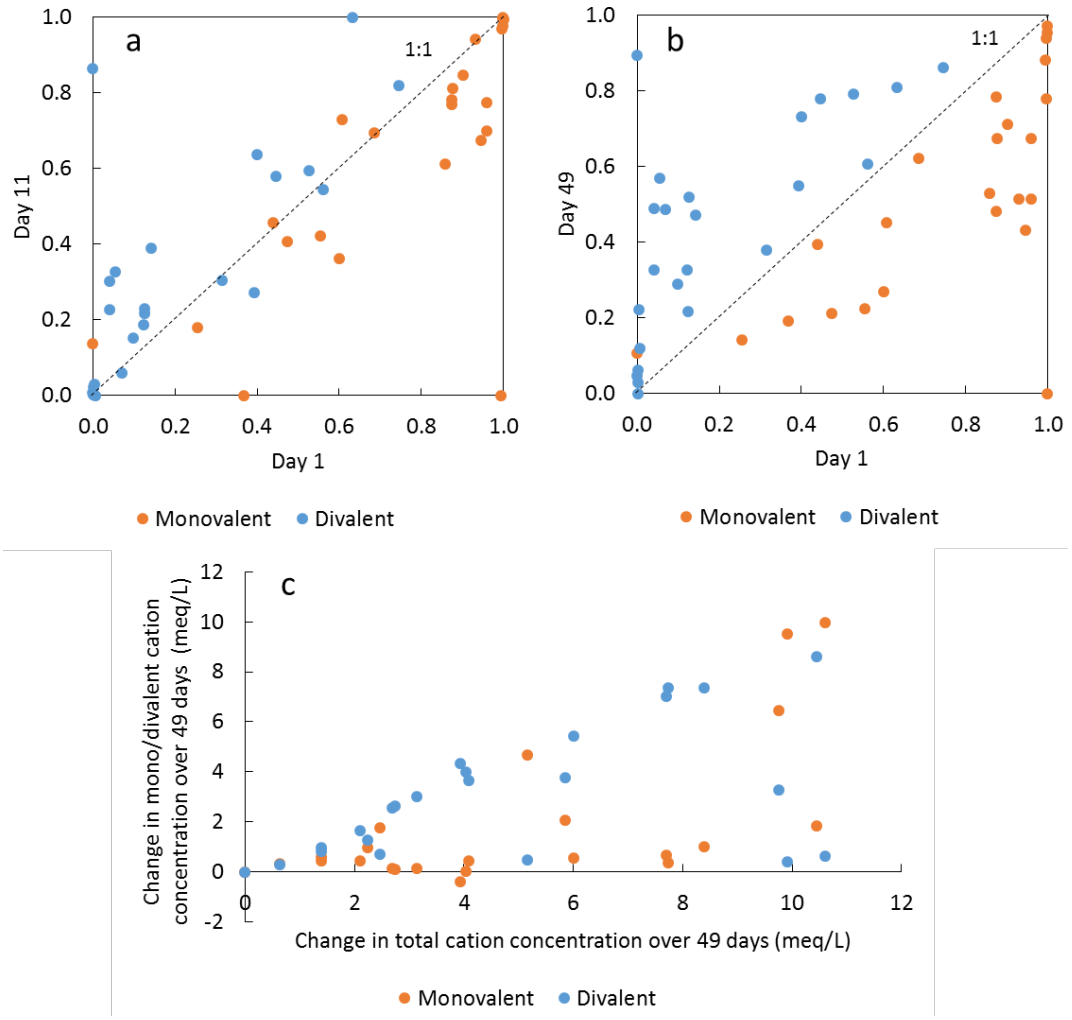

Figure 8.4 Changes in monovalent/divalent cation concentrations during 20°C leach (Chapter 5) a) proportion of total cations comprised by monovalent cations and divalent cations on days 1 and 11, b) proportion of total cations comprised by monovalent cations and divalent cations on days 1 and 49, c) change in monovalent and divalent cation concentration v change in total cation concentration over course of 49 day experiment

Nonetheless, changes in proportions of cations in leachate throughout the experiments may indicate a progression of weathering reactions. Leachates and meltwater have comparable cation concentrations (1-15 meq/L) (Figure 8.2). However, glacial runoff features proportionately less sodium and potassium but more magnesium than leachate with the exception of Foxfonna spring (Figure 8.3). The experiments in Chapter 5, highlighted in Figure 8.4, demonstrate that the proportion of divalent cations increases with time and initial solute release was driven largely by hydrolysis reactions and ion exchange. Changes in weathering process and ion exchange likely explain the divergence between in field and experimental data. Firstly, the high selectivity of divalent cations by clay minerals in dilute water (Stumm and Morgan, 1996) preferentially causes adsorption of calcium and magnesium, resulting in elevated sodium

concentrations. Over time, total cation concentration in leachate scales linearly with divalent ions while there is minimal change in monovalent ion concentration (Figure 8.4c). Therefore, the proportion of divalent cations increased as the experiment proceeded (Figure 8.4a, b). Since total cation concentration increases through the experiment, ion exchange processes alone cannot account for this shift in mono/divalent cation distribution. This suggests that after day 1 there is a shift in weathering reaction to liberate more Ca^{2+} and Mg^{2+} than Na^{+} and K^{+}. Secondly, the onset of coupled sulphide oxidation and carbonate dissolution liberates divalent cations after the initial rapid hydrolysis reactions. Consequently, elevated proportions of divalent cations in the glacial catchments relative to the weathering experiments likely reflects established carbonate dissolution through longer rock – water contact times. Elevated magnesium concentrations in glacial runoff may derive from magnesium rich carbonate minerals such as dolomite (Yde et al., 2008). However, it is thought that since dolomite and siderite constitute much of the carbonate content of bedrock (Riber, 2009) and are less reactive than calcite, sulphide oxidation largely couples with silicate dissolution in these glacial catchments.

These weathering dynamics have important considerations on N liberation. While initial release of NH_4^{+} by hydrolysis is rapid, this will slow down as pH increases. However, the onset of sulphide oxidation and the associated acid production then drives silicate dissolution, for example in the weathering experiment, N liberation was elevated when sulphide oxidation generated pH of < 5. The results from the weathering experiments demonstrate that ammonium is derived from weathering of both inorganic silicate minerals as well as organic matter. Nitrate occurs in negligible concentrations in the abiotic weathering experiments and is possibly derived from fluid inclusions. Low nitrate concentrations in the abiotic experiment are also consistent with a microbial origin of nitrate as opposed to oxidation of ammonium by mineral derived electron acceptors e.g. Fe^{3+}. Concentrations of ammonium (aq) leached from rock in weathering experiments were the same order of magnitude as aqueous nitrate in runoff from glaciers in this study (Figure 8.5). While the weathering experiments were carried out at a fixed rock: water ratio (0.2 g/l), solute rich water in glacial systems is diluted to varying degrees by low solute ice melt, so they are not directly comparable. Nonetheless, the significance of rock weathering as a nitrogen source is clear from the magnitude of adsorbed ammonium concentrations in the weathering experiment which are 1 - 2 orders of magnitude greater than nitrate concentrations in runoff (Figure 8.5).

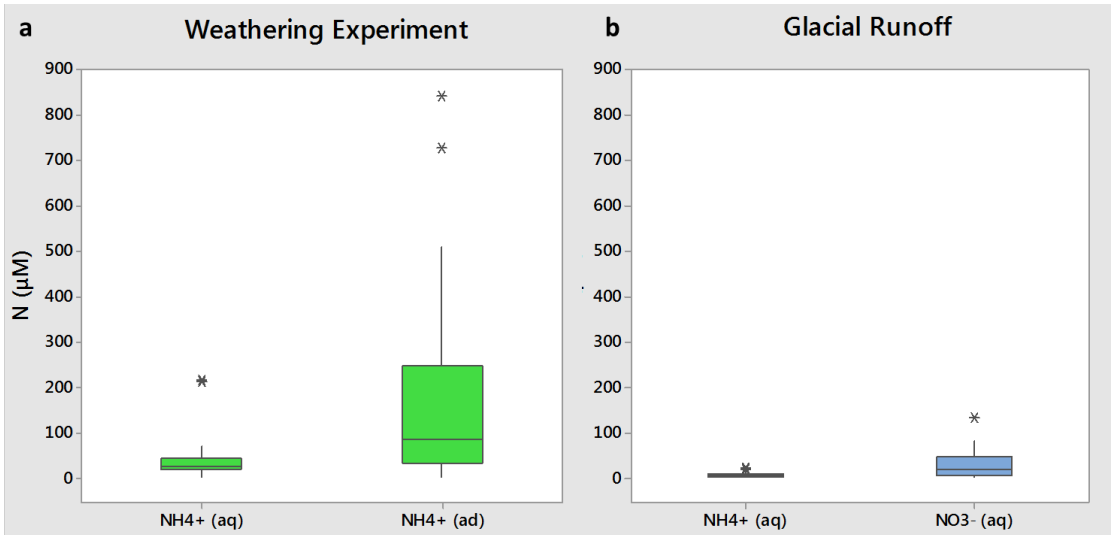

Figure 8.5 Boxplots of nitrogen species during a) 11 day 6°C weathering experiment (Chapter 5) and b) Svalbard glacial runoff from all sites during 2016 and 2017. Asterisks indicate outliers which are defined as values greater than 1.5 x the interquartile range.

In the weathering experiment, the largest yield of ammonium was liberated from Firkanten Fm and Frysjaodden Fm samples. These rocks are particularly enriched in organic forms of nitrogen, which suggests that organic N may be more effectively weathered than inorganic forms. This is corroborated by modelled N weathering fluxes which indicate that as much as 65% of the global N chemical flux is derived from organic N (Houlton et al., 2018). A large exposure of highly weathered Frysjaodden Fm rock in the Longyearbreen catchment likely contributes significant ammonium to meltwater (Figure 8.6). Longyearbreen consistently has the greatest nitrate concentrations in run off out of all the glaciers in this study. While geogenic ammonium likely fuels nitrification in each glacial catchment, the enhanced nitrogen liberation potential from the Frysjaodden Fm could well explain the elevated nitrate concentrations at Longyearbreen.

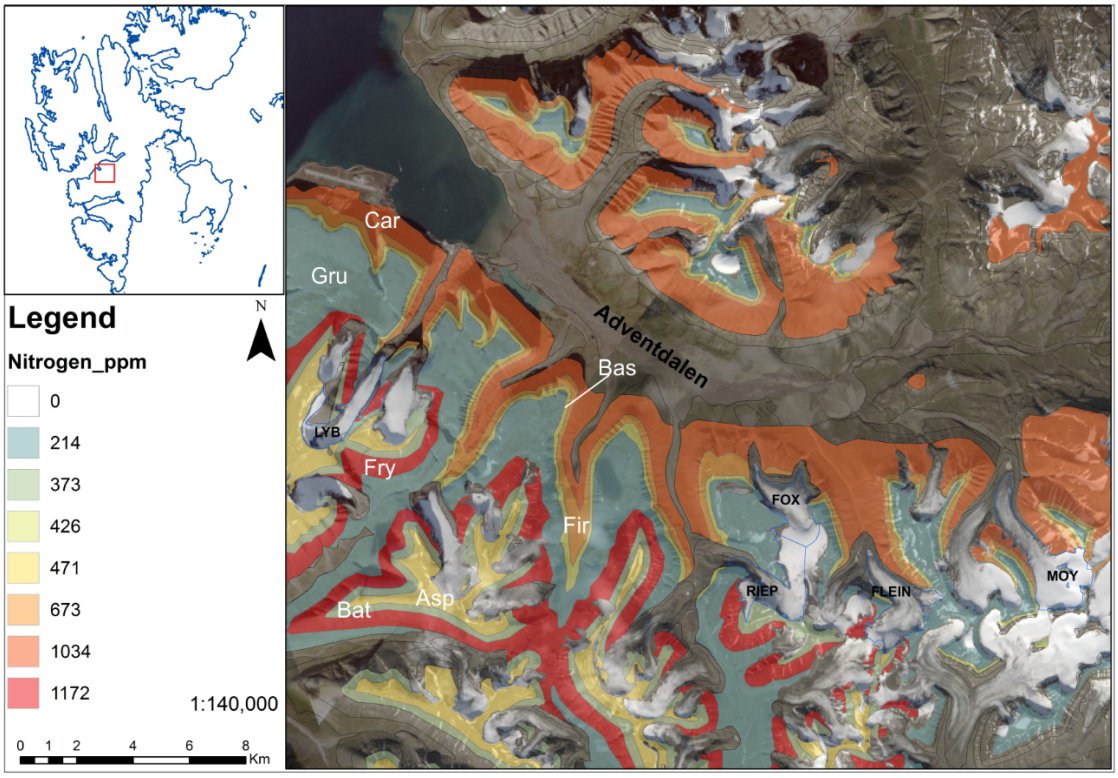

Figure 8.6 Average nitrogen concentration of bedrock formations (ppm) in Adventdalen

Nitrogen within sedimentary organic matter occurs mostly in the form of amido- and amine structures (proteins, peptides and amino acids), although in ancient kerogen (defined as “solvent-insoluble macromolecular organic matter found in sedimentary rocks” (Petsch, 2014)), nitrogen may be restricted to more chemically resistant and insoluble fractions (Baxby et al., 1994). While simple hydrolysis and acid hydrolysis of silicates have been suggested previously (Chapters 5 and 6) as drivers of geogenic N release, the chemical pathway of organic forms of N to ammonium is unclear. Acid hydrolysis may also liberate organic nitrogen, especially given that standard techniques to quantify soil organic carbon include treatment with acid e.g. (Leavitt et al., 1996). However, several additional mechanisms (see bullets below) have been considered previously in Chapter 5 to explain the apparent higher ‘weatherability’ of organic N. The relevance of these to glacial environments are discussed here.

- Interaction of organic matter with ·OH free radicals produced during crushing of silicate minerals (Gill Olivas, 2019).
- Deamination of proteins and subsequent protonation of amines.
- Oxidative weathering of organic matter

Glaciers in this study are cold based with low rates of active crushing and thus free radical production. Free radicals are highly reactive and are therefore unlikely to remain long after crushing which occurred during more dynamic

glacial regimes. Therefore, while this reaction may have occurred in weathering experiments, it is an unlikely pathway in these cold based glacier systems and is instead more likely to occur under bigger, more mobile ice masses. Soluble amines exposed through the disintegration and crushing of rock could be transformed to ammonium via protonation if there is a source of protons available. Given the abundance of sulphide oxidation that occurs in these catchments, this is a conceivable pathway for conversion of organic N to ammonium. However, nitrogen within ancient kerogen may be depleted in soluble amines therefore formal characterisation of the organic nitrogen compounds within bedrock would be required to explore this further as a weathering mechanism. Oxidative weathering of organic matter requires only an exposed organic surface and oxygen, therefore this reaction proceeds rapidly (although not as fast as pyrite oxidation (Chang, S. and Berner, 1999)). Oxidative weathering fluxes of organic carbon in sedimentary rocks are 2 - 3 times higher in watersheds dominated by glacier cover (Horan et al., 2017). This is driven in part by the effective physical mechanisms such as abrasion and frost shattering, which increase the surface area of rock, as well as increasing permeability permitting greater access of O_2 within air and water to exposed rock surfaces (Horan et al., 2017). Whilst rates of abrasion are likely to be small in these catchments, frost shattering in moraines, driven by freeze – thaw cycles and prolonged sub-zero temperatures will drive exposure of fresh rock surfaces.

However, the supply of organic nitrogen may be further elevated through biogeochemical factors. Microbial organisms are able to utilise ancient sedimentary carbon (Petsch, 2014) and the oxidation of kerogen has been reported in both subglacial environments (Tranter et al., 2002; Wadham et al., 2004) and recently deglaciated moraines (Bardgett et al., 2007). These processes may expose N bearing organic compounds which may be mineralised to produce more bioavailable forms of N i.e. ammonium.

8.4 Summary

The aim of this research was to explore the weathering processes involved in the supply of geogenic nitrogen as well as rock derived micronutrients (Fe and Mn) to subglacial environments. This project sought to achieve this aim using a combination of field work and laboratory experiments to achieve 3 objectives which are discussed below. A conceptual diagram in Figure 8.7 illustrates the findings presented here of geogenic N as a nutrient source to glacial environments.

The first objective was to characterise the geochemistry of a bedrock sequence that underlies glacial catchments in terms of carbon, nitrogen, sulphur, iron and manganese (Objective 1). Objective 1 also aimed to constrain isotopic fingerprints of bedrock nitrogen and sulphur. Therefore stable isotope analysis of $\delta^{15}N$ and $\delta^{34}S$ was also undertaken on rock samples.

The results of the geochemical analyses (Chapter 4) found that the rock type and depositional environment control the content and distribution of N, Fe and Mn within bedrock. Nitrogen concentrations are variable within the sedimentary succession and co-vary with organic content. N was particularly enriched in the Frysjaodden Fm and Firkanten Fm (Todalen Mb) shales which had a maximum concentration of 0.21 wt. % (2061 ppm) (Figure 8.6). Nitrogen in rock occurs primarily in inorganic minerals but also within organic matter (up to 49% of bulk N). Organic matter of both terrestrial and marine origin was deposited during sedimentation. Breakdown of this organic matter would have liberated nitrogen as ammonium into porewaters which was subsequently incorporated into clay minerals. The nitrogen isotope composition of bedrock is fairly uniform ~3.7‰ ($\delta^{15}N$) which likely represents the isotope signature of the source organic matter. Nitrogen and organic rich rocks were also associated with abundant pyrite (mass weighted mean $\delta^{34}S$ of all samples = -1.5‰), particularly in the coal bearing Firkanten Fm, reflecting reducing conditions in the sedimentary palaeoenvironment. Furthermore, sandstones and siltstones deposited in more oxygenated conditions feature low TOC and N concentrations due to enhanced breakdown of organic matter. In such rocks, iron oxides are more abundant while pyrite occurs in very low concentrations.

The second objective was to determine the magnitude of N liberation and associated geochemical weathering reactions through laboratory leaching experiments of different geological formations found in the glacial catchments (Objective 2). These experiments attempted to determine any nitrogen speciation and isotope fractionation processes inherent in nitrogen weathering.

Through a series of pilot experiments, a procedure was developed to simulate rock weathering under subglacial conditions (Chapter 3). These experiments found that nitrogen speciation during abiotic weathering appears to be unaffected by oxygen availability. Rocks from the field area in Svalbard were weathered experimentally (Chapter 5) which found that weathering reactions were dominated by carbonate and silicate hydrolysis as well as sulphide oxidation. Between 0.5 and 5% of rock nitrogen was liberated as ammonium during the experiment from both organic and inorganic phases. Organic N rich rocks liberated the most nitrogen (up to 58 µg N/g rock) which may reflect more efficient weathering of organic N phases than silicate bound N. For example via the protonation of soluble organic molecules such as amines to become $-NH_3^+$ or via interaction of organic N with ·OH free radicals produced during crushing (Gill Olivas, 2019). Acetate, which is produced during these experiments, may also derive from the interaction of organic matter with free radicals (Gill Olivas, 2019) which suggests that organic degradation may be a pathway for N liberation from bedrock. The majority of ammonium liberated from rock was adsorbed to mineral surfaces ($K_{D\ NH4+}$ >1), however this began to desorb over the course of the experiment. Finer grained, clay rich sedimentary rocks with a larger surface area had a greater amount of sorbtion sites and were thus more effective at adsorbing ammonium (and thus had higher values of $K_{D\ NH4+}$). Silicate and carbonate hydrolysis reactions raised solution pH to 8 - 10 which likely caused a partial loss of nitrogen via ammonia volatilisation.

Attempts to constrain the effect of weathering on nitrogen isotopes (Chapter 7) involved isotope analysis of adsorbed ammonium and bedrock N. Unfortunately, due to the preferential adsorption of ammonium, insufficient dissolved ammonium was available for isotope analysis. Therefore the insight that could be gained from such experiments was limited, however, adsorbed ammonium was isotopically enriched relative to bedrock N (up to 10‰ $\delta^{15}N$) which suggests that fractionation may be associated with adsorption having enrichment factors consistent with previous studies (Delwiche and Steyn, 1970; Karamanos and Rennie, 1978). However, ammonia volatilisation which likely occurred in solutions with pH > 8 may also have contributed to this isotope fractionation.

The third objective was to use glacial meltwater chemistry and stable isotopes of sulphur, nitrogen and oxygen to identify processes of biogeochemical weathering and nutrient cycling in the subglacial environment (Objective 3). Analysis of glacial meltwater derived from cold based glaciers in the high Arctic highlighted that chloride, which acts as a natural tracer for snowmelt positively correlated with non-snowpack ions such as sulphate and sodium. Since limited

snow remained during sampling in late summer, the majority of solute acquisition was derived from interaction of stored snowmelt and crushed rock within ice marginal moraines. Sulphide oxidation exerted a pivotal control on solute acquisition, with non-snowpack sulphate concentrations up to 15.9 meq/L (764 mg/l). Sulphate in glacial runoff had $\delta^{34}S$ representative of bedrock sulphide $\delta^{34}S$ from its respective catchment with the exception of Longyearbreen. The difference in $\delta^{34}S$ could not be explained easily but it is thought to be due to spatial variation of pyrite $\delta^{34}S$. Such high concentrations of sulphate are 2 orders of magnitude greater than can be derived from pyrite oxidation using oxygenated conditions. The oxidation of sulphides and other organic carbon likely drive localised anoxia. Therefore, sulphide oxidation is likely microbially mediated using alternative electron acceptors such as Fe^{3+} and Mn^{4+}. These reducing environments facilitate elevated concentrations of redox sensitive ions such as Fe^{2+} and Mn^{2+}. Manganese concentrations (up to 122 µeq/l) frequently exceed iron despite its low relative abundance in bedrock due to its enhanced solubility at near neutral pH.

Furthermore, high nitrate concentrations in glacial runoff (up to 134 µeq/l), are associated with snowmelt fed moraine water featuring sulphate and products of silicate weathering such as sodium and silica. Concentrations of nitrate in snow are too low to account for the nitrate in run off. Instead it is likely that nitrogen as ammonium is sourced from weathering of silicate minerals and kerogen. In oxygenated channels/gullies, nitrogen occurs as nitrate, likely produced by microbial nitrification of geogenic ammonium. Meltwater nitrate $\delta^{18}O$ values were consistent with a microbial origin as opposed to an atmospheric nitrate source. In addition, nitrate has a nitrogen isotope signature closer to bedrock N than snow. However, a more detailed understanding of N isotope fractionation during weathering is required to utilise stable isotopes to trace the provenance of nitrogen in environmental studies. When water encounters isolated anoxic environments, featuring abundant sulphides, nitrate becomes absent likely due to obligate anaerobic denitrifying bacteria reducing it to N_2. Under such conditions sulphate was also reduced to sulphide by sulphate reducing bacteria as evidenced by isotopically heavy sulphate – sulphur (+6.8‰ $\delta^{34}S$).

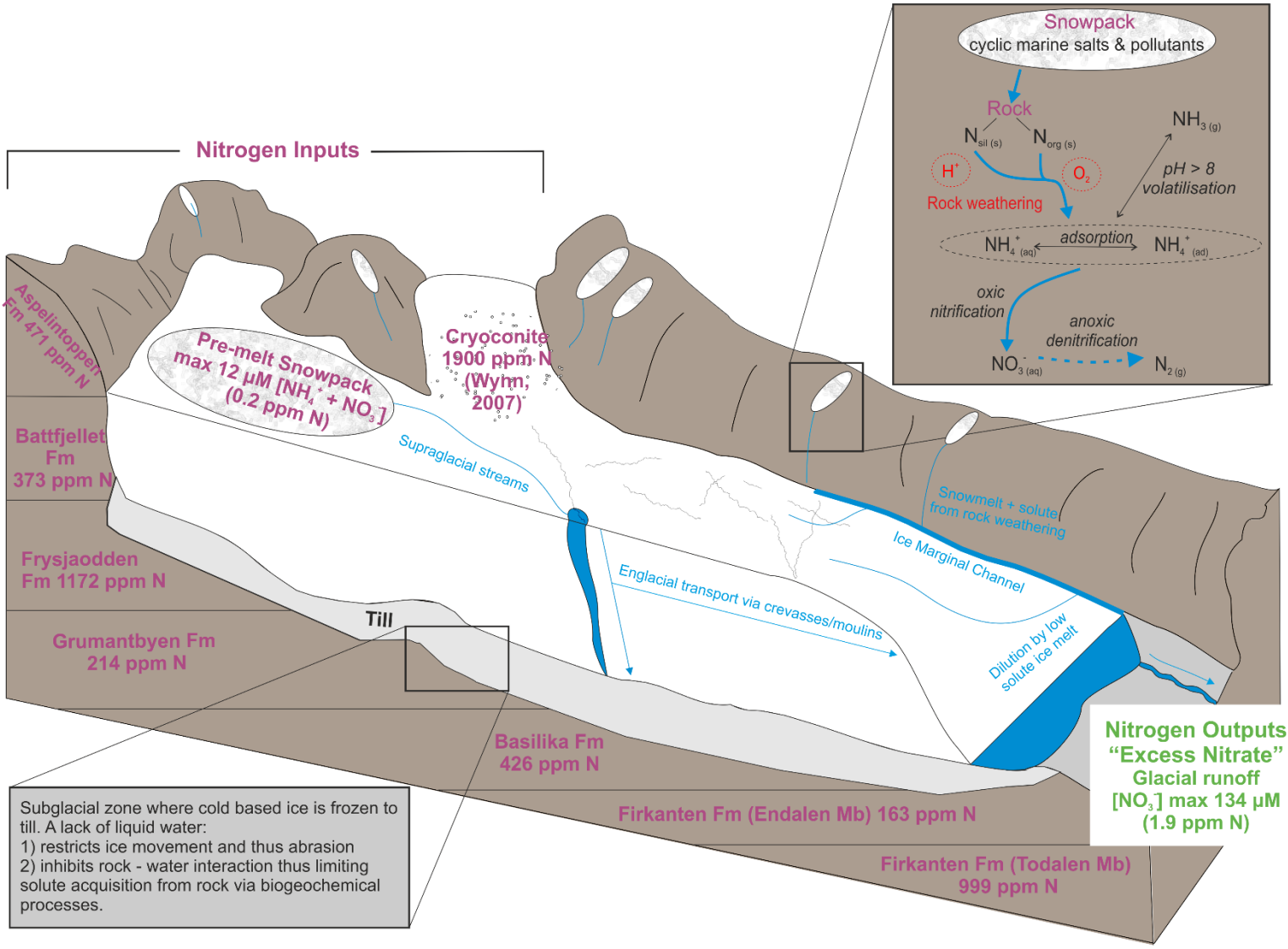

Figure 8.7 Conceptual diagram of geogenic N weathering in glacial environments in the study area N_{sil} and N_{org} represent silicate bound N and organic N respectively while $NH_4^+{}_{(ad)}$ and $NH_4^+{}_{(aq)}$ reflect adsorbed and aqueous ammonium respectively. All data derived from this project except indicative cryoconite values from Midtre Lovénbreen (Wynn et al., 2007).

8.5 Hypotheses

Three overarching hypotheses were developed at the start of this project:

1. Geological variation between different glacial catchments accounts for differing export of nutrients: nitrogen, iron and manganese.
2. The dissolution of geogenic nitrogen imparts a fractionation on N isotopes which accounts for the $\delta^{15}N$ difference between bedrock and glacial runoff.
3. Anoxic sulphide oxidation generates acidity in subglacial environments which facilitates geogenic N dissolution through silicate weathering.

These hypotheses are revisited in turn below to discuss whether the results presented here support them or not.

1. Ratios of major ions in glacial meltwater from different catchments are highly consistent which suggests that weathering processes and solute acquisition is similar in each catchment. The variable conductivity/total solute load of the glacial runoff seems to be controlled by catchment specific mixing ratios of solute poor ice melt and stored snowmelt in moraines which has acquired abundant solute from rock-water reactions. Consequently, hydrology exerts a key control on the solute acquisition from glacial catchments. In these catchments chloride acts as a conservative tracer of snowmelt, thus solute acquired from rock weathering positively correlates with chloride. However, nitrate is particularly enriched relative to chloride in some samples from Longyearbreen and Foxfonna Glacial. These glacial catchments contain Frysjaodden Fm and Firkanten Fm rocks which are rich in organic N. Such rocks are shown to more effectively liberate ammonium during weathering (Chapter 5) therefore, weathering of sedimentary horizons enriched with organic N may drive enhanced nitrogen weathering fuelling subsequent nitrate production. In addition, manganese is enriched in bedrock only in the Frysjaodden Fm where it occurs within carbonate minerals. Longyearbreen is the only glacier in this study to overly this geological unit and its runoff contains exceptionally high dissolved (< 0.45µm) manganese concentrations (max 122 µeq/L). In addition, sediment from Van Keulenfjorden, which is fed by glaciers eroding the same bedrock contain elevated manganese compared to other fjords in Svalbard with different bedrock (Wehrmann et al., 2014). Therefore, geological variations may account for differences in the export of nutrients such as nitrogen and manganese. Iron minerals are weathered in these catchments as indicated by the occurrence of pyrite oxidation and ochrous staining at glacial springs. However, the export of iron occurs largely as Fe^{3+} since most glacial runoff is oxygenated. Thus, iron

precipitates and forms particulates. This study did not measure particulate iron and because of its redox sensitivity, it was not possible to determine differences in iron export using dissolved iron alone.

2. As outlined in Chapter 7, attempts were made to constrain the isotope effects of nitrogen during weathering experiments. At the pH of most of the leachates (7 - 10), ammonium was present in aqueous and adsorbed forms and likely as free ammonia too. However, analytical limitations regarding the mass of nitrogen required for isotope analysis via the ammonium diffusion method restricted the number of suitable samples. For example, the tendency for ammonium to adsorb to mineral surfaces made it impossible to analyse the nitrogen isotope ratio of aqueous ammonium. An isotope enrichment in adsorbed ammonium of up to 10‰ was observed relative to bedrock N. However, any further understanding was confounded by the complexities inherent in a system containing multiple phases of ammonium/ammonia.
3. Laboratory weathering experiments demonstrated that silicate hydrolysis and sulphide oxidation coupled to silicate dissolution (as well as organic degradation) liberated ammonium from rock. In the glacial catchments of this study, the dominant weathering process was coupled sulphide oxidation and silicate weathering, therefore ammonium is expected to be liberated to these glacial environments as shown in the weathering experiments. High sulphate concentrations and sulphate – oxygen isotope ratios suggest that sulphide oxidation was mediated by microbes using alternative terminal electron acceptors such as Fe^{3+} when dissolved oxygen was limited. This suggests that parts of the flowpaths must be anoxic, likely where water enters closed system environments containing abundant crushed rock and sulphides whose oxidation consumes oxygen. Anoxic conditions are further evidenced by elevated dissolved concentrations of redox sensitive ions such as Fe^{2+} and Mn^{2+}. While N is derived from silicate weathering, experiments showed that N is more efficiently liberated as ammonium from organic matter during weathering. The exact chemical reactions involved in this process are not clear but may include acid hydrolysis, protonation of amines or organic degradation through interaction with free radicals. Thus while sulphide oxidation is an important process in liberating N from rock but other processes may be involved.

8.6 Implications

The research presented in this study contribute valuable quantitative experimental data regarding the liberation of nitrogen during weathering. Currently, experimental studies of nitrogen weathering in the literature are sparse. In abiotic weathering experiments carried out at 6°C, crushed sedimentary rocks leached significant aqueous ammonium (1 - 16 μg $NH_4^+{}_{(aq)}$ (N) per gram of rock) over 11 days and even greater amounts of ammonium liberated from rock were adsorbed to mineral surfaces (0.1 – 57 μg $NH_4^+{}_{(ad)}$ (N) per gram of rock). Given the large mass of comminuted rock in glacial catchments, weathering of rocks likely contributes significant nitrogen to glacial microbial ecosystems. This crustal source of nitrogen is likely ecologically significant, given that nitrogen sources in Arctic environments are limited. Furthermore, release of nitrogen by subglacial weathering may have sustained microbial life during glaciations on geological timescales such as Snowball Earth scenarios. While enhanced physical erosion in glacial systems increase rock surface area and thus N chemical weathering fluxes (Houlton et al., 2018), rock weathering is also likely to be an important nitrogen source to other terrestrial environments as suggested by others (Houlton et al., 2018; Morford et al., 2016a; Morford et al., 2011; Holloway and Dahlgren, 1999).

In the cold based glaciers studied here, the locus of solute acquisition by meltwater occurred in ice marginal moraines, since subglacial drainage was limited. As glaciers melt and thin in a warming climate, the proportion of ice above the pressure melting point reduces. As such, in thinning glaciers which become increasingly cold based, moraines and proglacial environments may become more important (nitrogen) weathering hubs in glacial catchments.

The majority of ammonium released from rock during weathering experiments adsorbed to mineral surfaces. Suspended sediment has been overlooked in several studies of nitrogen export from valley glaciers (Wynn et al., 2007; Ansari, 2012), therefore N output may be greater than previously thought. This is consistent with recent studies of Leverett Glacier, an outlet of the Greenland Ice Sheet which show that around half of N export occurs as adsorbed ammonium (Wadham et al., 2016; Hawkings et al., 2015). Glacial runoff is typically neutral - slightly alkaline; yet experiments in this study demonstrate that where pH is elevated above 8, via hydrolysis reactions for example, ammonia volatilisation may occur. This causes loss of N from solution as ammonia gas, however the extent to which this occurs in glacial environments may be limited by low temperatures and high biological demand for N.

Attempts to trace the provenance of nitrogen in glacial studies have assumed there is no fractionation during weathering of N. Yet, both adsorption and volatilisation can impart fractionation effects on N isotopes as discussed in this study. While the respective isotope enrichments caused by these processes remain poorly constrained, caution should be taken when using stable isotopes of N in tracer studies.

Weathering experiments carried out in this study also demonstrate that organic nitrogen is liberated from rock more efficiently than inorganic nitrogen. As deglaciation continues under a warming climate, exposure of more ancient organic matter to oxidative weathering may liberate more N. Enhanced rates of geogenic NH_4^+ production via increased oxidative weathering may amplify fluxes of ammonium adsorbed to suspended sediment as well as increase the supply of ammonium for microbial nitrification in moraine porewater. The export of increased nitrogen in glacial runoff may positively affect primary productivity in downstream environments such as Svalbard fjords (Kulk et al., 2018; van De Poll et al., 2016) and the Arctic Ocean (Popova et al., 2010) which can become nitrogen limited following phytoplankton blooms in summer. Nitrogen in glacial runoff will largely be in the form of dissolved NO_3^- as well as any dissolved/adsorbed ammonium that has not been nitrified. However, as glacially derived freshwater enters more saline fjord and ocean waters, the increased salinity may cause a salt effect causing ammonium release from sediment to ambient water (Gardner et al., 1991). This is because sea salt anions neutralise the polarity of the ammonium ion by forming non polar ion pairs while cations occupy sediment cation exchange sites, thus displacing ammonium (Gardner et al., 1991). In a warming global climate, reduced sea ice extent in the Arctic increases light levels in fjord/marine water which may therefore increase primary productivity, however this may be inhibited by nutrient supply, particularly nitrate (Vancoppenolle et al., 2013). Therefore, glacial runoff may become an increasingly important nitrogen supply to polar marine environments, where N_2 fixation has long been considered to be inhibited by low temperatures.

In addition, glacial export of iron produced largely through sulphide oxidation may be an important nutrient source where marine primary productivity is limited by iron. High nutrient low chlorophyll (HNLC) zones are regions of oceans where phytoplankton growth is limited despite the availability of macronutrients. In these zones, micronutrients, such as iron are believed to be limiting. The Southern Ocean is a HNLC, therefore iron delivery from Antarctic glaciers may play a significant role in marine ecosystems. In oxygenated meltwater, iron is stable as oxyhydroxide minerals, iron delivered to

downstream environments will largely be in particulate form, i.e. as suspended sediment or ice rafted debris from melting ice bergs.

8.7 Limitations of study

8.7.1 Experiments

Weathering experiments undertaken in this study attempted to simulate glacial weathering environments, however experimental conditions were highly simplified in contrast to complex natural systems. Such differences mean that the results from experiments do not perfectly replicate natural types and rates of weathering reactions. For example, laboratory experiments were carried out under closed system conditions in sealed centrifuge tubes. By contrast, natural systems are a mix of open systems featuring atmospheric gas exchange and isolated, closed system environments with limited atmospheric connectivity. Under open system conditions, dissolved CO_2 tends towards equilibrium with atmospheric CO_2. As protons are consumed during weathering reactions, dissolution of atmospheric CO_2 would seek to produce carbonic acid. This would facilitate further acid hydrolysis reactions, increase inorganic carbon concentrations and regulate pH. Furthermore, dissolution of atmospheric oxygen in open systems fuels efficient oxidation reactions thus maintaining oxygenated conditions. In addition, rock samples from individual formations were freshly crushed and therefore have abundant highly reactive mineral surfaces. By contrast, in natural settings, the rock weathered is a mix of different geological formations within the catchment, therefore solute represents an average of the rock geochemistry. Furthermore, the amount of reactive surface area is depleted over time as leached layers develop and secondary precipitates coat reaction surfaces (White and Brantley, 2003). Therefore, the exposure of fresh mineral surfaces is limited by rates of active crushing/frost cracking and the extent of previous weathering. In subglacial environments, rock is crushed in the presence of water whereas in the experimental procedure adopted here, rocks were ground in a dry environment which influences solute acquisition. Furthermore, microbial activity amplifies mineral weathering (Montross, S.N. et al., 2012; Sharp et al., 1999), yet weathering experiments were abiotic. These factors mean that the experiments demonstrate relative amounts of N liberated from different geological formations but further work is required to provide quantitative yields representative of natural conditions.

8.7.2 Using isotopes as a tracer of N.

This study attempted to advance the use of stable isotopes as a tracer for geogenic nitrogen. Success was gained from characterising bedrock $\delta^{15}N$ in the geological sequence underlying the study area. Since bedrock $\delta^{15}N$ was fairly uniform, an accurate isotope fingerprint for rock derived N was quantified. However, following attempts to investigate isotope fractionation affects during weathering, uncertainty remains regarding the isotope enrichments associated with ammonia volatilisation and adsorption. Furthermore, limited nitrate isotope data was available, therefore it was not possible to accurately constrain glacial run off and snow nitrate isotope ratios. As such the effectiveness of stable isotopes as a tracer of geogenic N was limited in this study.

8.8 Future Work

8.8.1 Experiments

Whilst rock weathering has been shown to liberate nitrogen, in order to determine well constrained nitrogen weathering rates representative of glacial environments, some of the limitations of weathering experiments previously discussed could be addressed. Future experiments could be designed in which wet rocks are crushed in an environment incubated with subglacial microbes. Such experiments run alongside abiotic controls would conclusively demonstrate whether microbes utilise rock derived nitrogen in nitrification.

Currently, research relating to the contribution of bedrock N to ecosystems are limited to a handful of experimental and modelling studies. While the global model (Houlton et al., 2018) provides estimates of total rock N fluxes to ecosystems, the equations rely on assumptions of numerous unknowns. For example, the relative fluxes of organic and inorganic N are still poorly constrained. While the research presented here, demonstrates the significance of organic N weathering, more work is required to provide a more detailed understanding of weathering rates of both inorganic and organic N fractions. Insights into the weathering reactions which liberate organic N and its pathway to NH_4^+ and the geochemical conditions in which they occur would improve the sensitivity of such models. This could be achieved through experimental work to investigate, for example, the impact on organic N by crushing induced free radicals, acid hydrolysis and oxidative weathering.

Rocks used in this study were largely fine grained siliciclastics which are generally the rock type most enriched in nitrogen (Morford et al., 2016b). Similar weathering experiments should be applied to different rocks underlying other

glaciers to quantify their efficacy of N liberation in order provide broader insights into geogenic N as a glacial nutrient source.

8.8.2 Methods

Further work is required to continue to develop the use of stable isotopes as a tracer for nitrogen. The acetone method (Huber et al., 2011) was adapted to prepare meltwater samples containing low nitrate concentrations for isotope analysis. Contamination, likely associated with elution of nitrate from anion exchange resins and subsequent effluent neutralisation, restricted the amount of useful nitrate isotope data produced in this study. Development of this method to eliminate the source of contamination would facilitate improved sample processing. Alternatively, other methods such as the denitrifier method (Sigman et al., 2001), which is suited to low nitrate freshwater samples, could be used to quantify the $\delta^{15}N$ and $\delta^{18}O$ ratios of glacial runoff.

In addition, optimisation of the ammonium diffusion method is required to measure aqueous ammonium $\delta^{15}N$ at low concentrations. This is required to better constrain the isotope effects of volatilisation and adsorption which should also be further investigated through experimental studies.

8.8.3 Field work

Field work could be improved through increased sampling frequency, particularly with regards to suspended sediment adsorbed ammonium concentrations. Measurements of glacial runoff discharge over the course of a melt season alongside geochemical data would enable dissolved and particulate nitrogen fluxes to be calculated. Whilst nitrogen yields from weathering experiments can be calculated, it is difficult to compare these to glacial catchments in order to quantify the significance of rock weathering as a source of N. This is due to the mixing of different water sources of varying concentrations which affect net runoff concentration. Conversely, $\delta^{15}N$ is not affected by dilution of solute concentrations. Thus, the isotope ratios of N in glacial runoff and suspended sediment reflect the mass weighted mean of N sources and any fractionation processes which occur within the glacial system. Therefore, improvements to our understanding of N isotope fractionation during weathering as well as in methods to quantify N isotope ratios in dilute waters could allow comparison of field and experimental data.

8.9 Concluding remarks

Weathering of crushed rock liberates significant nitrogen as ammonium from within silicate minerals and kerogen. In glacial environments, the oxidation of

pyrite minerals generates sulphuric acid which facilitates N release from rock as well as micronutrients Fe and Mn. The amount of geogenic N released appears to be dependent on intrinsic factors such as bedrock N concentration, the form of nitrogen (organic v inorganic) and availability of sulphide minerals as well as extrinsic factors such as pH. Following liberation, ammonium may adsorb to mineral surfaces, diffuse out of solution as NH_3 or be converted to nitrate by bacteria. Nitrification is associated with oxygenated debris rich environments, while in isolated drainage systems where intense rock weathering occurs, water may subsequently become anoxic where denitrifying bacteria likely convert nitrate to N_2. In the glacial catchments within this study, the association of biogenic nitrate with crustal derived solute in snowmelt fed moraine pore water suggests that nitrification of geogenic ammonium may explain the elevated nitrate concentrations frequently measured in late summer glacial runoff.

Bibliography

Achberger, A.M., Christner, B.C., Michaud, A.B., Priscu, J.C., Skidmore, M.L., Vick-Majors, T.J., , t.W.S.T., Adkins, W., Anandakrishnan, S., Barbante, C., Barcheck, G., Beem, L., Behar, A., Beitch, M., Bolsey, R., Branecky, C., Carter, S., Christianson, K., Edwards, R., Fisher, A., Fricker, H., Foley, N., Guthrie, B., Hodson, T., Jacobel, R., Kelley, S., Mankoff, K., McBryan, E., Mikucki, J., Mitchell, A., Powell, R., Purcell, A., Sampson, D., Scherer, R., Sherve, J., Siegfried, M. and Tulaczyk, S. 2016. Microbial Community Structure of Subglacial Lake Whillans, West Antarctica. **7**(1457).

Al-Hamdan, A.Z. and Reddy, K.R. 2006. Adsorption of heavy metals in glacial till soil. *Geotechnical & Geological Engineering.* **24**(6), pp.1679-1693.

Alshameri, A., He, H., Zhu, J., Xi, Y., Zhu, R., Ma, L. and Tao, Q. 2018. Adsorption of ammonium by different natural clay minerals: Characterization, kinetics and adsorption isotherms. *Applied Clay Science.* **159**, pp.83-93.

Anderson, S.P., Drever, J.I. and Humphrey, N.F. 1997. Chemical weathering in glacial environments. *Geology.* **25**(5), pp.399-402.

Anderson, T.F. and Pratt, L.M. 1995. Isotopic Evidence for the Origin of Organic Sulfur and Elemental Sulfur in Marine Sediments. *Geochemical Transformations of Sedimentary Sulfur.* American Chemical Society, pp.378-396.

Aneja, V.P., Roelle, P.A., Murray, G.C., Southerland, J., Erisman, J.W., Fowler, D., Asman, W.A.H. and Patni, N. 2001. Atmospheric nitrogen compounds II: emissions, transport, transformation, deposition and assessment. *Atmospheric Environment.* **35**(11), pp.1903-1911.

Ansari, A.H. 2012. *Nitrogen and Sulphur biogeochemistry in a High Arctic glacial watershed: an investigation with isotopic tracers and solute chemistry*. Ph.D. Thesis thesis, University of Sheffield.

Ansari, A.H., Hodson, A.J., Heaton, T.H.E., Kaiser, J. and Marca-Bell, A. 2013. Stable isotopic evidence for nitrification and denitrification in a High Arctic glacial ecosystem. *Biogeochemistry.* **113**(1-3), pp.341-357.

Anthoni, J.F. 2006. *The chemical composition of seawater.* [Online]. [Accessed 30 September]. Available from: http://seafriends.org.nz/oceano/seawater.htm

Asman, W.A.H. and van Jaarsveld, H.A. 1992. A variable-resolution transport model applied for NHχ in Europe. *Atmospheric Environment. Part A. General Topics.* **26**(3), pp.445-464.

Balci, N., Shanks Iii, W.C., Mayer, B. and Mandernack, K.W. 2007. Oxygen and sulfur isotope systematics of sulfate produced by bacterial and abiotic oxidation of pyrite. *Geochimica et Cosmochimica Acta.* **71**(15), pp.3796-3811.

Barber, A., Lalonde, K., Mucci, A. and Gélinas, Y. 2014. The role of iron in the diagenesis of organic carbon and nitrogen in sediments: A long-term incubation experiment. *Marine Chemistry.* **162**, pp.1-9.

Bardgett, R.D., Richter, A., Bol, R., Garnett, M.H., Bäumler, R., Xu, X., Lopez-Capel, E., Manning, D.A.C., Hobbs, P.J., Hartley, I.R. and Wanek, W. 2007. Heterotrophic microbial communities use ancient carbon following glacial retreat. *Biological Letters.* **3**, pp.487-490.

Baxby, M., Patience, R.L. and Bartle, K.D. 1994. The origin and diagenesis of sedimentary organic nitrogen. *Journal of Petroleum Geology.* **17**(2), pp.211-230.

Bebout, G.E., Cooper, D.C., Bradley, A.D. and Sadofsky, S.J. 1999. Nitrogen-isotope record of fluid-rock interactions in the Skiddaw aureole and granite, English Lake District. *American Mineralogist.* **84**(10), pp.1495-1505.

Bebout, G.E., Fogel, M.L. and Cartigny, P. 2013. Nitrogen: Highly Volatile yet Surprisingly Compatible. *Elements.* **9**(5), pp.333-338.

Benn, D.I. and Evans, D.J.A. 2010. *Glaciers and Glaciation.* 2nd ed.

Bhatia, M., Sharp, M. and Foght, J. 2006. Distinct Bacterial Communities Exist beneath a High Arctic Polythermal Glacier. **72**(9), pp.5838-5845.

Björnsson, H., Gjessing, Y., Hamran, S.-E., Hagen, J.O., LiestøL, O., Pálsson, F. and Erlingsson, B. 1996. The thermal regime of sub-polar glaciers mapped by multi-frequency radio-echo sounding. *Journal of Glaciology.* **42**(140), pp.23-32.

Böhlke, J.K., Smith, R.L. and Miller, D.N. 2006. Ammonium transport and reaction in contaminated groundwater: Application of isotope tracers and isotope fractionation studies. *Water Resources Research.* **42**(5).

Bottrell, S. 2007. Stable isotopes in aqueous sulphate as tracers of natural and contaminant sulphate sources: a reconnaissance study of the Xingwen karst aquifer, Sichuan, China. **279**(1), pp.123-135.

Bottrell, S. and Raiswell, R. 2000. Sulphur Isotopes and Microbial Sulphur Cycling in Sediments. In: R.E., R. and S.M., A. eds. *Microbial Sediments.* Berlin, Heidelberg: Springer.

Bottrell, S. and Tranter, M. 2002. Sulphide oxidation under partially anoxic conditions at the bed of the Haut Glacier d'Arolla, Switzerland. *Hydrological Processes.* **16**(12), pp.2363-2368.

Bottrell, S.H. and Newton, R.J. 2006. Reconstruction of changes in global sulfur cycling from marine sulfate isotopes. *Earth-Science Reviews.* **75**(1), pp.59-83.

Boyd, E.S., Hamilton, T.L., Havig, J.R., Skidmore, M.L. and Shock, E.L. 2014. Chemolithotrophic Primary Production in a Subglacial Ecosystem. *Applied and Environmental Microbiology.* **80**(19), pp.6146-6153.

Boyd, E.S., Lange, R.K., Mitchell, A.C., Havig, J.R., Hamilton, T.L., Lafrenière, M.J., Shock, E.L., Peters, J.W. and Skidmore, M. 2011. Diversity, Abundance, and Potential Activity of Nitrifying and Nitrate-Reducing Microbial Assemblages in a Subglacial Ecosystem. *Applied and Environmental Microbiology.* **77**(14), pp.4778-4787.

Boyd, E.S., Skidmore, M., Mitchell, A.C., Bakermans, C. and Peters, J.W. 2010. Methanogenesis in subglacial sediments. **2**(5), pp.685-692.

Boyd, S.R., Hall, A. and Pillinger, C.T. 1993. The measurement of δ15N in crustal rocks by static vacuum mass spectrometry: Application to the origin of the ammonium in the Cornubian batholith, southwest England. *Geochimica et Cosmochimica Acta.* **57**(6), pp.1339-1347.

Brooks, P.D., Stark, J.M., McInteer, B.B. and Preston, T. 1989. Diffusion Method To Prepare Soil Extracts For Automated Nitrogen-15 Analysis. **53**(6), pp.1707-1711.

Brunner, B., Contreras, S., Lehmann, M.F., Matantseva, O., Rollog, M., Kalvelage, T., Klockgether, G., Lavik, G., Jetten, M.S.M., Kartal, B. and Kuypers, M.M.M. 2013. Nitrogen isotope effects induced by anammox bacteria. **110**(47), pp.18994-18999.

Brunner, B., Yu, J.-Y., Mielke, R.E., MacAskill, J.A., Madzunkov, S., McGenity, T.J. and Coleman, M. 2008. Different isotope and chemical patterns of pyrite oxidation related to lag and exponential growth phases of Acidithiobacillus ferrooxidans reveal a microbial growth strategy. *Earth and Planetary Science Letters.* **270**(1–2), pp.63-72.

Burcă, F. 2008. *Palaeogene depositional environments of the Frysjaodden and Hollendardalen formations in central Spitsbergen*. Petroleum Geology and Geophysics thesis, University of Oslo.

Burnell, J.N. 1988. The Biochemistry of Manganese in Plants. In: Graham, R.D., et al. eds. *Manganese in Soils and Plants: Proceedings of the International Symposium on 'Manganese in Soils and Plants' held at the Waite Agricultural Research Institute, The University of Adelaide, Glen Osmond, South Australia, August 22–26, 1988 as an Australian Bicentennial Event.* Dordrecht: Springer Netherlands, pp.125-137.

Canfield, D.E., Raiswell, R., Westrich, J.T., Reaves, C.M. and Berner, R.A. 1986. The use of chromium reduction in the analysis of reduced inorganic sulfur in sediments and shales. *Chemical Geology.* **54**(1), pp.149-155.

Canfield, D.E. and Teske, A. 1996. Late Proterozoic rise in atmospheric oxygen concentration inferred from phylogenetic and sulphur-isotope studies. *Nature.* **382**(6587), pp.127-132.

Casciotti, K.L., McIlvin, M. and Buchwald, C. 2010. Oxygen isotopic exchange and fractionation during bacterial ammonia oxidation. **55**(2), pp.753-762.

Casciotti, K.L., Sigman, D.M., Hastings, M.G., Böhlke, J.K. and Hilkert, A. 2002. Measurement of the Oxygen Isotopic Composition of Nitrate in Seawater and Freshwater Using the Denitrifier Method. *Analytical Chemistry.* **74**(19), pp.4905-4912.

Caulkett, A.P. and Ellis-Evans, J.C. 1997. Chemistry of streams of Signy Island, maritime Antarctic: sources of major ions. *Antarctic Science.* **9**(1), pp.3-11.

Chandra, A.P. and Gerson, A.R. 2011. Pyrite (FeS2) oxidation: A sub-micron synchrotron investigation of the initial steps. *Geochimica et Cosmochimica Acta.* **75**(20), pp.6239-6254.

Chang, C.C.Y., Langston, J., Riggs, M., Campbell, D.H., Silva, S.R. and Kendall, C. 1999. A method for nitrate collection for δ15N and δ18O analysis from waters with low nitrate concentrations. *Canadian Journal of Fisheries and Aquatic Sciences.* **56**(10), pp.1856-1864.

Chang, S. and Berner, R.A. 1999. Coal weathering and the geochemical carbon cycle. *Geochimica et Cosmochimica Acta.* **63**(19), pp.3301-3310.

Chen, R.R. and Dittert, K. 2008. Diffusion technique for 15N and inorganic N analysis of low-N aqueous solutions and Kjeldahl digests. **22**(11), pp.1727-1734.

Christiansen, H.H., French, H.M. and Humlum, O. 2005. Permafrost in the Gruve-7 mine, Adventdalen, Svalbard. *Norsk Geografisk Tidsskrift - Norwegian Journal of Geography.* **59**(2), pp.109-115.

Christner, B.C., Priscu, J.C., Achberger, A.M., Barbante, C., Carter, S.P., Christianson, K., Michaud, A.B., Mikucki, J.A., Mitchell, A.C., Skidmore, M.L., Vick-Majors, T.J., the, W.S.T., Adkins, W.P., Anandakrishnan, S., Barcheck, G., Beem, L., Behar, A., Beitch, M., Bolsey, R., Branecky, C., Edwards, R., Fisher, A., Fricker, H.A., Foley, N., Guthrie, B., Hodson, T., Horgan, H., Jacobel, R., Kelley, S., Mankoff, K.D., McBryan, E., Powell, R., Purcell, A., Sampson, D., Scherer, R., Sherve, J., Siegfried, M. and Tulaczyk, S. 2014. A microbial ecosystem beneath the West Antarctic ice sheet. *Nature.* **512**, p310.

Clark, I. and Fritz, P. 1997. *Environmental isotopes in hydrogeology.* Boca Raton, FL: CRC Press/Lewis Publishers.

Cooper, R.J., Wadham, J.L., Tranter, M., Hodgkins, R. and Peters, N.E. 2002. Groundwater hydrochemistry in the active layer of the proglacial zone, Finsterwalderbreen, Svalbard. *Journal of Hydrology.* **269**(3), pp.208-223.

Craig, H. 1961. Isotopic Variations in Meteoric Waters. **133**(3465), pp.1702-1703.

Crichton, R. 2016. The Essential Role of Iron in Biology. In: Crichton, R. ed. *Iron Metabolism.* pp.22-70.

Crompton, J.W., Flowers, G.E., Kirste, D., Hagedorn, B. and Sharp, M.J. 2015. Clay mineral precipitation and low silica in glacier meltwaters explored through reaction-path modelling. *Journal of Glaciology.* **61**(230), pp.1061-1078.

Cui, Y., Kump, L.R., Ridgwell, A.J., Charles, A.J., Junium, C.K., Diefendorf, A.F., Freeman, K.H., Urban, N.M. and Harding, I.C. 2011. Slow release of fossil carbon during the Palaeocene–Eocene Thermal Maximum. *Nature Geoscience.* **4**, p481.

Dahlgren, R.A. 1994. Soil acidification and nitrogen saturation from weathering of ammonium-bearing rock. *Nature.* **368**(6474), pp.838-841.

Dahlgren, R.A. 2005. Geologic Nitrogen as a Source of Soil Acidity. **51**(5), pp.719-723.

Dallman, W.K. 1999. *Lithostratigraphic Lexicon of Svalbard.* [Online]. [Accessed 04/07].

Dallman, W.K. 2015. *Geoscience Atlas of Svalbard.* Norsk Polarinstitutt.

Dalsgaard, T., Thamdrup, B. and Canfield, D.E. 2005. Anaerobic ammonium oxidation (anammox) in the marine environment. *Research in Microbiology.* **156**(4), pp.457-464.

Delwiche, C.C. and Steyn, P.L. 1970. Nitrogen isotope fractionation in soils and microbial reactions. *Environmental Science & Technology.* **4**(11), pp.929-935.

Denk, T.R.A., Mohn, J., Decock, C., Lewicka-Szczebak, D., Harris, E., Butterbach-Bahl, K., Kiese, R. and Wolf, B. 2017. The nitrogen cycle: A review of isotope effects and isotope modeling approaches. *Soil Biology and Biochemistry.* **105**, pp.121-137.

Divine, D.V., Sjolte, J., Isaksson, E., Meijer, H.A.J., van de Wal, R.S.W., Martma, T., Pohjola, V., Sturm, C. and Godtliebsen, F. 2011. Modelling the regional climate and isotopic composition of Svalbard precipitation using REMOiso: a comparison with available GNIP and ice core data. **25**(24), pp.3748-3759.

Dixon, J.C., Campbell, S.W. and Durham, B. 2012. Geologic nitrogen and climate change in the geochemical budget of Kärkevagge, Swedish Lapland. *Geomorphology.* **167–168**, pp.70-76.

Doane, T.A. 2017. The Abiotic Nitrogen Cycle. *ACS Earth and Space Chemistry.* **1**(7), pp.411-421.

Doxsey-Whitfield, E.L. 2012. *Magnitude and controls of microbial nitrate production in the streams and till of a glaciated alpine catchment, Canadian Rocky Mountains, Alberta*. thesis, Queen's University.

Doyle, K. 2018. *The chemical evolution of the Proterozoic biosphere*. thesis, University of Leeds.

Drever, J.I. 1997. *The geochemistry of natural waters.* 3rd edition ed. NJ, USA: Prentice-Hall, Inc.

Drits, V.A., Lindgreen, H. and Salyn, A.L. 1997. Determination of the content and distribution of fixed ammonium in illite-smectite by X-ray diffraction: Application to North Sea illite-smectite. *American Mineralogist.* **82**(1-2), pp.79-87.

Dypvik, H., Riber, L., Burca, F., Rüther, D., Jargvoll, D., Nagy, J. and Jochmann, M. 2011. The Paleocene–Eocene thermal maximum (PETM) in Svalbard — clay mineral and geochemical signals. *Palaeogeography, Palaeoclimatology, Palaeoecology.* **302**(3), pp.156-169.

Edmond, J.M., Measures, C., McDuff, R.E., Chan, L.H., Collier, R., Grant, B., Gordon, L.I. and Corliss, J.B. 1979. Ridge crest hydrothermal activity and the balances of the major and minor elements in the ocean: The Galapagos data. *Earth and Planetary Science Letters.* **46**(1), pp.1-18.

Ehrlich, H.L. 1982. Enhanced removal of Mn2+ from seawater by marine sediments and clay minerals in the presence of bacteria. *Canadian Journal of Microbiology.* **28**(12), pp.1389-1395.

Elling, F.J., Spiegel, C., Estrada, S., Davis, D.W., Reinhardt, L., Henjes-Kunst, F., Allroggen, N., Dohrmann, R., Piepjohn, K. and Lisker, F. 2016. Origin of Bentonites and Detrital Zircons of the Paleocene Basilika Formation, Svalbard. **4**(73).

Elswick, E.R., Hower, J.C., Carmo, A.M., Sun, T. and Mardon, S.M. 2007. Sulfur and carbon isotope geochemistry of coal and derived coal-combustion by-products: An example from an Eastern Kentucky mine and power plant. *Applied Geochemistry.* **22**(9), pp.2065-2077.

Etzelmüller, B., Ødegård, R.S., Vatne, G., Mysterud, R.S., Tonning, T. and Sollid, J.L. 2000. Glacier characteristics and sediment transfer system of Longyearbreen and Larsbreen, western Spitsbergen. *Norsk Geografisk Tidsskrift - Norwegian Journal of Geography.* **54**(4), pp.157-168.

Fisher, S. and Brown, T. 1994. An overview of sample collection analytical methodologies interpretative framework for acid-base characterisation on earthern materials for planning reclamation of drastically disturbed lands. In: *Association Abandoned Mined Lands Programs, 16th Annual Conference, Park City, Utah*. Abandoned Mined Lands Program, Office of Surface Mining, Washington DC, pp.202-221.

Fogel, M.L. and Cifuentes, L.A. 1993. Isotope Fractionation during Primary Production. In: Engel, M.H. and Macko, S.A. eds. *Organic Geochemistry: Principles and Applications.* Boston, MA: Springer US, pp.73-98.

Foght, J., Aislabie, J., Turner, S., Brown, C.E., Ryburn, J., Saul, D.J. and Lawson, W.J.M.E. 2004. Culturable Bacteria in Subglacial Sediments and Ice from Two Southern Hemisphere Glaciers. **47**(4), pp.329-340.

Fowler, D., Coyle, M., Skiba, U., Sutton, M.A., Cape, J.N., Reis, S., Sheppard, L.J., Jenkins, A., Grizzetti, B., Galloway, J.N., Vitousek, P., Leach, A., Bouwman, A.F., Butterbach-Bahl, K., Dentener, F., Stevenson, D., Amann, M. and Voss, M. 2013. The global nitrogen cycle in the twenty-first century. **368**(1621), p20130164.

Frimmel, H.E. and Hallbauer, D.K. 1999. Gold mobilizing fluids in the Witwatersrand Basin: composition and possible sources. *Mineralogy and Petrology.* **66**(1), pp.55-81.

Fritz, P., Basharmal, G.M., Drimmie, R.J., Ibsen, J. and Qureshi, R.M. 1989. Oxygen isotope exchange between sulphate and water during bacterial reduction of sulphate. *Chemical Geology: Isotope Geoscience section.* **79**(2), pp.99-105.

Galloway, J.N. 2003. 8.12 - The Global Nitrogen Cycle. In: Holland, H.D. and Turekian, K.K. eds. *Treatise on Geochemistry.* Oxford: Pergamon, pp.557-583.

Gardner, W.S., Seitzinger, S.P. and Malczyk, J.M. 1991. The effects of sea salts on the forms of nitrogen released from estuarine and freshwater sediments: Does ion pairing affect ammonium flux? *Estuaries.* **14**(2), pp.157-166.

Gat, J.R. 1996. OXYGEN AND HYDROGEN ISOTOPES IN THE HYDROLOGIC CYCLE. **24**(1), pp.225-262.

Gill Olivas, B. 2019. *Rock comminution of subglacial lake sediments as a potential source of energy and nutrients to the Subglacial Lake Whillans microbial ecosystem*. thesis, University of Bristol.

Goldhaber, M.B. 2003. 7.10 - Sulfur-rich Sediments. In: Holland, H.D. and Turekian, K.K. eds. *Treatise on Geochemistry.* Oxford: Pergamon, pp.257-288.

Graham, T. 1827. XXXVII An account of M. Longchamp's theory of nitrification; with an extension of it. *The Philosophical Magazine.* **1:3**, pp.172-180.

Gulley, J.D., Benn, D.I., Müller, D. and Luckman, A. 2009. A cut-and-closure origin for englacial conduits in uncrevassed regions of polythermal glaciers. *Journal of Glaciology.* **55**(189), pp.66-80.

Gulley, J.D., Walthard, P., Martin, J., Banwell, A.F., Benn, D.I. and Catania, G. 2012. Conduit roughness and dye-trace breakthrough curves: why slow velocity and

high dispersivity may not reflect flow in distributed systems. *Journal of Glaciology.* **58**(211), pp.915-925.
Hagen, J.O., Kohler, J., Melvold, K. and Winther, J.-G. 2003. Glaciers in Svalbard: mass balance, runoff and freshwater flux. *Polar Research.* **22**(2), pp.145-159.
Hall, P.J. and Aller, R.C. 1992. Rapid, small-volume, flow injection analysis for SCO2, and NH4+ in marine and freshwaters. **37**(5), pp.1113-1119.
Hallet, B. 1976. Deposits formed by subglacial precipitation of CaCO3. *GSA Bulletin.* **87**(7), pp.1003-1015.
Hallet, B., Hunter, L. and Bogen, J. 1996. Rates of erosion and sediment evacuation by glaciers: A review of field data and their implications. *Global and Planetary Change.* **12**(1), pp.213-235.
Harrold, Z.R., Skidmore, M.L., Hamilton, T.L., Desch, L., Amada, K., van Gelder, W., Glover, K., Roden, E.E. and Boyd, E.S. 2016. Aerobic and Anaerobic Thiosulfate Oxidation by a Cold-Adapted, Subglacial Chemoautotroph. **82**(5), pp.1486-1495.
Hawkings, J.R., Wadham, J.L., Tranter, M., Lawson, E., Sole, A., Cowton, T., Tedstone, A.J., Bartholomew, I., Nienow, P., Chandler, D. and Telling, J. 2015. The effect of warming climate on nutrient and solute export from the Greenland Ice Sheet. *Geochemical Perspectives Letters.* **1**(0), pp.94-104.
Heaton, T.H.E. 1986. Isotopic studies of nitrogen pollution in the hydrosphere and atmosphere: A review. *Chemical Geology: Isotope Geoscience section.* **59**, pp.87-102.
Heaton, T.H.E. 2001. Procedure and notes of the 'diffuison' method for 15N/14N analysis of nitrate and ammonium. *NIGL Report Series.* **176**.
Heaton, T.H.E., Baruch, S. and Robertson, S.M.C. 1997. Potential Canopy Influences on the Isotopic Composition of Nitrogen and Sulphur in Atmospheric Deposition. *Oecologia.* **109**(4), pp.600-607.
Helland-Hansen, W. 1990. Sedimentation in Paleogene foreland basin, Spitsbergen. pp.260-272.
Hindshaw, R.S., Heaton, T.H.E., Boyd, E.S., Lindsay, M.R. and Tipper, E.T. 2016. Influence of glaciation on mechanisms of mineral weathering in two high Arctic catchments. *Chemical Geology.* **420**, pp.37-50.
Hindshaw, R.S., Tosca, N.J., Piotrowski, A.M. and Tipper, E.T. 2018. Clay mineralogy, strontium and neodymium isotope ratios in the sediments of two High Arctic catchments (Svalbard). *Earth Surf. Dynam.* **6**(1), pp.141-161.
Hodgkins, R. 1997. Glacier hydrology in Svalbard, Norwegian high arctic. *Quaternary Science Reviews.* **16**(9), pp.957-973.
Hodgkins, R., Tranter, M. and Dowdeswell, J.A. 1998. The hydrochemistry of runoff from a ‘cold-based’ glacier in the High Arctic (Scott Turnerbreen, Svalbard). **12**(1), pp.87-103.
Hodson, A. 2006. Biogeochemistry of snowmelt in an Antarctic glacial ecosystem. *Water Resources Research.* **42**(11), pp.n/a-n/a.
Hodson, A. 2019. *Conversation,* 23 October.
Hodson, A., Anesio, A.M., Tranter, M., Fountain, A., Osborn, M., Priscu, J., Laybourn-Parry, J. and Sattler, B. 2008. Glacial ecosystems. *Ecological monographs.* **78**(1), pp.41-67.
Hodson, A., Heaton, T., Langford, H. and Newsham, K. 2010a. Chemical weathering and solute export by meltwater in a maritime Antarctic glacier basin. *Biogeochemistry.* **98**(1-3), pp.9-27.
Hodson, A., Mumford, P.N., Kohler, J. and Wynn, P.M. 2005. The High Arctic glacial ecosystem: new insights from nutrient budgets. *Biogeochemistry.* **72**(2), pp.233-256.
Hodson, A., Roberts, T.J., Engvall, A.-C., Holmén, K. and Mumford, P.J.B. 2010b. Glacier ecosystem response to episodic nitrogen enrichment in Svalbard, European High Arctic. **98**(1), pp.171-184.

Hodson, A., Tranter, M., Gurnell, A., Clark, M. and Hagen, J.O. 2002. The hydrochemistry of Bayelva, a high Arctic proglacial stream in Svalbard. *Journal of Hydrology.* **257**(1), pp.91-114.

Hoefs, J. 2009. *Stable Isotope Geochemistry.* Berlin: Springer.

Holdren, G.R. and Berner, R.A. 1979. Mechanism of feldspar weathering—I. Experimental studies. *Geochimica et Cosmochimica Acta.* **43**(8), pp.1161-1171.

Holloway, J.M. and Dahlgren, R.A. 1999. Geologic nitrogen in terrestrial biogeochemical cycling. *Geology.* **27**(6), pp.567-570.

Holloway, J.M. and Dahlgren, R.A. 2002. Nitrogen in rock: Occurrences and biogeochemical implications. *Global Biogeochemical Cycles.* **16**(4), pp.65-61-65-17.

Holloway, J.M., Dahlgren, R.A. and Casey, W.H. 2001. Nitrogen release from rock and soil under simulated field conditions. *Chemical Geology.* **174**(4), pp.403-414.

Holloway, J.M., Dahlgren, R.A., Hansen, B. and Casey, W.H. 1998. Contribution of bedrock nitrogen to high nitrate concentrations in stream water. *Nature.* **395**(6704), pp.785-788.

Holloway, J.M., Nordstrom, D.K., Böhlke, J.K., McCleskey, R.B. and Ball, J.W. 2011. Ammonium in thermal waters of Yellowstone National Park: Processes affecting speciation and isotope fractionation. *Geochimica et Cosmochimica Acta.* **75**(16), pp.4611-4636.

Holmes, R.M., McClelland, J.W., Sigman, D.M., Fry, B. and Peterson, B.J. 1998. Measuring 15N–NH4+ in marine, estuarine and fresh waters: An adaptation of the ammonia diffusion method for samples with low ammonium concentrations. *Marine Chemistry.* **60**(3), pp.235-243.

Horan, K., Hilton, R.G., Selby, D., Ottley, C.J., Gröcke, D.R., Hicks, M. and Burton, K.W. 2017. Mountain glaciation drives rapid oxidation of rock-bound organic carbon. **3**(10), pe1701107.

Houlton, B.Z., Morford, S.L. and Dahlgren, R.A. 2018. Convergent evidence for widespread rock nitrogen sources in Earth's surface environment. **360**(6384), pp.58-62.

Huber, B., Bernasconi, S.M., Luster, J. and Pannatier, E.G. 2011. A new isolation procedure of nitrate from freshwater for nitrogen and oxygen isotope analysis. *Rapid Communications in Mass Spectrometry.* **25**(20), pp.3056-3062.

Hulth, S., Aller, R.C. and Gilbert, F. 1999. Coupled anoxic nitrification/manganese reduction in marine sediments. *Geochimica et Cosmochimica Acta.* **63**(1), pp.49-66.

Humlum, O., Elberling, B., Hormes, A., Fjordheim, K., Hansen, O.H. and Heinemeier, J. 2005. Late-Holocene glacier growth in Svalbard, documented by subglacial relict vegetation and living soil microbes. **15**(3), pp.396-407.

Jennings, S.R., Dollhopf, D.J. and Inskeep, W.P. 2000. Acid production from sulfide minerals using hydrogen peroxide weathering. *Applied Geochemistry.* **15**(2), pp.235-243.

Jickells, T.D., An, Z.S., Andersen, K.K., Baker, A.R., Bergametti, G., Brooks, N., Cao, J.J., Boyd, P.W., Duce, R.A., Hunter, K.A., Kawahata, H., Kubilay, N., laRoche, J., Liss, P.S., Mahowald, N., Prospero, J.M., Ridgwell, A.J., Tegen, I. and Torres, R. 2005. Global Iron Connections Between Desert Dust, Ocean Biogeochemistry, and Climate. *Science.* **308**(5718), pp.67-71.

Johnson, B. and Goldblatt, C. 2015. The nitrogen budget of Earth. *Earth-Science Reviews.* **148**, pp.150-173.

Jones, M.T., Eliassen, G.T., Shephard, G.E., Svensen, H.H., Jochmann, M., Friis, B., Augland, L.E., Jerram, D.A. and Planke, S. 2016. Provenance of bentonite layers in the Palaeocene strata of the Central Basin, Svalbard: implications for magmatism and rifting events around the onset of the North Atlantic Igneous Province. *Journal of Volcanology and Geothermal Research.* **327**, pp.571-584.

Karamanos, R.E. and Rennie, D.A. 1978. Nitrogen isotope fractionation during ammonium exchange reactions with soil clay. *Canadian Journal of Soil Science.* **58**(1), pp.53-60.

Kendall, C. 1998. Chapter 16 - Tracing Nitrogen Sources and Cycling in Catchments. In: Kendall, C. and McDonnell, J.J. eds. *Isotope Tracers in Catchment Hydrology.* Amsterdam: Elsevier, pp.519-576.

Kendall, C. and Caldwell, E.A. 1998. Chapter 2 - Fundamentals of Isotope Geochemistry. In: Kendall, C. and McDonnell, J.J. eds. *Isotope Tracers in Catchment Hydrology.* Amsterdam: Elsevier, pp.519-576.

Kirshenbaum, I., Smith, J.S., Crowell, T., Graff, J. and McKee, R. 1947. Separation of the Nitrogen Isotopes by the Exchange Reaction between Ammonia and Solutions of Ammonium Nitrate. **15**(7), pp.440-446.

Kivimaki, A.-L. 2005. Presence and activity of microbial populations in glaciers and their impact on rock weathering at glacial beds. *Ph.D. Thesis, University of Bristol.*

Knauer, G.A., Martin, J.H. and Gordon, R.M. 1982. Cobalt in north-east Pacific waters. *Nature.* **297**(5861), pp.49-51.

Knies, J., Brookes, S. and Schubert, C.J. 2007. Re-assessing the nitrogen signal in continental margin sediments: New insights from the high northern latitudes. *Earth and Planetary Science Letters.* **253**(3), pp.471-484.

König, M., Nuth, C., Kohler, J., Moholdt, G. and Pettersen, R. 2014. A digital glacier database for svalbard. In: Kargel, J.S., et al. eds. *Global Land Ice Measurements from Space.* Berlin, Heidelberg: Springer Berlin Heidelberg, pp.229-239.

Kosmulski, M. 2011. The pH-dependent surface charging and points of zero charge: V. Update. *Journal of Colloid and Interface Science.* **353**(1), pp.1-15.

Kulk, G., van de Poll, W.H. and Buma, A.G.J. 2018. Photophysiology of nitrate limited phytoplankton communities in Kongsfjorden, Spitsbergen. **63**(6), pp.2606-2617.

Lanoil, B., Skidmore, M., Priscu, J.C., Han, S., Foo, W., Vogel, S.W., Tulaczyk, S. and Engelhardt, H. 2009. Bacteria beneath the West Antarctic Ice Sheet. **11**(3), pp.609-615.

Larsen, D. and Mann, R. 2005. Origin of high manganese concentrations in coal mine drainage, eastern Tennessee. *Journal of Geochemical Exploration.* **86**(3), pp.143-163.

Law, K.S. and Stohl, A. 2007. Arctic Air Pollution: Origins and Impacts. *Science.* **315**(5818), pp.1537-1540.

Laybourn-Parry, J., Hodson, A. and Tranter, M. 2012. *The Ecology of Snow and Ice Environments.* Oxford: OUP.

Leavitt, S.W., Follett, R.F. and Paul, E.A. 1996. Estimation of Slow- and Fast-Cycling Soil Organic Carbon Pools from 6N HCl Hydrolysis. *Radiocarbon.* **38**(2), pp.231-239.

Li, L., Lollar, B.S., Li, H., Wortmann, U.G. and Lacrampe-Couloume, G. 2012. Ammonium stability and nitrogen isotope fractionations for NH4+–NH3(aq)–NH3(gas) systems at 20–70°C and pH of 2–13: Applications to habitability and nitrogen cycling in low-temperature hydrothermal systems. *Geochimica et Cosmochimica Acta.* **84**, pp.280-296.

Li, W.-B., Song, Y.-B., Xu, H.-K., Chen, L.-Y., Dai, W.-H., Dong, M.J.E.S. and Research, P. 2015. Ion-exchange method in the collection of nitrate from freshwater ecosystems for nitrogen and oxygen isotope analysis: a review. **22**(13), pp.9575-9588.

Lingle, D.A., Kehew, A.E. and Krishnamurthy, R.V. 2017. Use of nitrogen isotopes and other geochemical tools to evaluate the source of ammonium in a confined glacial drift aquifer, Ottawa County, Michigan, USA. *Applied Geochemistry.* **78**, pp.334-342.

Lloyd, R.M. 1968. Oxygen isotope behavior in the Sulfate-Water System. **73**(18), pp.6099-6110.

Luther, G.W., Sundby, B., Lewis, B.L., Brendel, P.J. and Silverberg, N. 1997. Interactions of manganese with the nitrogen cycle: Alternative pathways to dinitrogen. *Geochimica et Cosmochimica Acta.* **61**(19), pp.4043-4052.

Lysså, A. and Lønne, I. 2001. Moraine development at a small High-Arctic valley glacier: Rieperbreen, Svalbard. *Journal of Quaternary Science.* **16**(6), pp.519-529.
Macdonald, M.L., Wadham, J.L., Telling, J. and Skidmore, M.L. 2018. Glacial Erosion Liberates Lithologic Energy Sources for Microbes and Acidity for Chemical Weathering Beneath Glaciers and Ice Sheets. **6**(212).
Major, H. and Nagy, J. 1972. Geology of the Adventdalen map area. *NORSK POLARINSTITUTT.* **138**.
Mariotti, A., Leclerc, A. and Germon, J.C. 1982. Nitrogen isotope fractionation associated with the NO2− → N2O step of denitrification in soils. *Canadian Journal of Soil Science.* **62**(2), pp.227-241.
Marshall, C., Large, D.J., Meredith, W., Snape, C.E., Uguna, C., Spiro, B.F., Orheim, A., Jochmann, M., Mokogwu, I., Wang, Y. and Friis, B. 2015. Geochemistry and petrology of Palaeocene coals from Spitsbergen — Part 1: Oil potential and depositional environment. *International Journal of Coal Geology.* **143**, pp.22-33.
Martin, J.H. 1990. Glacial-interglacial CO2 change: The Iron Hypothesis. **5**(1), pp.1-13.
Mayer, B., Bollwerk, S.M., Mansfeldt, T., Hütter, B. and Veizer, J. 2001. The oxygen isotope composition of nitrate generated by nitrification in acid forest floors. *Geochimica et Cosmochimica Acta.* **65**(16), pp.2743-2756.
Maynard, D.G., Kalra, Y.P. and Crumbaugh, J.A. 2007. Nitrate and exchangeable ammonium nitrogen. In: Carter, M.R. ed. *Soil Sampling and Methods of Analysis.* 2nd ed. CRC Press, p.1262.
McCready, R.G.L., Gould, W.D. and Barendregt, R.W. 1983. Nitrogen isotope fractionation during the reduction of NO3− to NH4+ by Desulfovibrio sp. *Canadian Journal of Microbiology.* **29**(2), pp.231-234.
McIlvin, M.R. and Altabet, M.A. 2005. Chemical Conversion of Nitrate and Nitrite to Nitrous Oxide for Nitrogen and Oxygen Isotopic Analysis in Freshwater and Seawater. *Analytical Chemistry.* **77**(17), pp.5589-5595.
Melle, C., Wallenstein, M., Darrouzet-Nardi, A. and Weintraub, M.N. 2015. Microbial activity is not always limited by nitrogen in Arctic tundra soils. *Soil Biology and Biochemistry.* **90**, pp.52-61.
Meyers, P.A. and Doose, H. 1999. Sources, preservation, and thermal maturity of organic matter in Pliocene–Pleistocene organic-carbon–rich sediments of the Western Mediterranean Sea. In: Zahn, R., Comas, M.C., and Klaus, A. ed. *Proceedings of the Ocean Drilling Program, Scientific Results.*
Michalski, G., Meixner, T., Fenn, M., Hernandez, L., Sirulnik, A., Allen, E. and Thiemens, M. 2004. Tracing Atmospheric Nitrate Deposition in a Complex Semiarid Ecosystem Using Δ17O. *Environmental Science & Technology.* **38**(7), pp.2175-2181.
Mikucki, J.A. and Priscu, J.C. 2007. Bacterial Diversity Associated with Blood Falls, a Subglacial Outflow from the Taylor Glacier, Antarctica. **73**(12), pp.4029-4039.
Millero, F.J. and Roy, R.N. 1997. A Chemical Equilibrium Model for the Carbonate System in Natural Waters. *Croatica Chemica Acta.* **70**(1), pp.1-38.
Minoura, K., Hoshino, K., Nakamura, T. and Wada, E. 1997. Late Pleistocene-Holocene paleoproductivity circulation in the Japan Sea: sea-level control on δ13C and δ15N records of sediment organic material. *Palaeogeography, Palaeoclimatology, Palaeoecology.* **135**(1), pp.41-50.
Mizutani, Y. and Rafter, T.A. 1973. Isotopic behaviour of sulphate oxygen in the bacterial reduction of sulphate. *GEOCHEMICAL JOURNAL.* **6**(4), pp.183-191.
Montross, G.G., McGlynn, B.L., Montross, S.N. and Gardner, K.K. 2013. Nitrogen production from geochemical weathering of rocks in southwest Montana, USA. *Journal of Geophysical Research: Biogeosciences.* **118**(3), pp.1068-1078.
Montross, S.N., Skidmore, M., Tranter, M., Kivimäki, A.-L. and Parkes, R.J. 2012. A microbial driver of chemical weathering in glaciated systems. *Geology.*
Morel, F.M.M. and Price, N.M. 2003. The Biogeochemical Cycles of Trace Metals in the Oceans. **300**(5621), pp.944-947.

Morford, S.L., Houlton, B.Z. and Dahlgren, R.A. 2011. Increased forest ecosystem carbon and nitrogen storage from nitrogen rich bedrock. *Nature.* **477**(7362), pp.78-81.
Morford, S.L., Houlton, B.Z. and Dahlgren, R.A. 2016a. Direct quantification of long-term rock nitrogen inputs to temperate forest ecosystems. **97**(1), pp.54-64.
Morford, S.L., Houlton, B.Z. and Dahlgren, R.A. 2016b. Geochemical and tectonic uplift controls on rock nitrogen inputs across terrestrial ecosystems. *Global Biogeochemical Cycles.* **30**(2), pp.333-349.
Moses, C.O., Kirk Nordstrom, D., Herman, J.S. and Mills, A.L. 1987. Aqueous pyrite oxidation by dissolved oxygen and by ferric iron. *Geochimica et Cosmochimica Acta.* **51**(6), pp.1561-1571.
Müller, R.D. and Spielhagen, R.F. 1990. Evolution of the Central Tertiary Basin of Spitsbergen: towards a synthesis of sediment and plate tectonic history. *Palaeogeography, Palaeoclimatology, Palaeoecology.* **80**(2), pp.153-172.
Naegeli, K., Lovell, H., Zemp, M. and Benn, D.I. 2014. Dendritic Subglacial Drainage Systems in Cold Glaciers Formed by Cut-and-Closure Processes. *Geografiska Annaler: Series A, Physical Geography.* **96**(4), pp.591-608.
Nagy, J., Jargvoll, D., Dypvik, H., Jochmann, M. and Riber, L. 2013. Environmental changes during the Paleocene–Eocene Thermal Maximum in Spitsbergen as reflected by benthic foraminifera. *Polar Research.* **32**(1), p19737.
Nixon, S.L., Telling, J.P., Wadham, J.L. and Cockell, C.S. 2017. Viable cold-tolerant iron-reducing microorganisms in geographically diverse subglacial environments. *Biogeosciences.* **14**(6), pp.1445-1455.
Nordstrom, D.K., Plummer, L.N., Langmuir, D., Busenberg, E., May, H.M., Jones, B.F. and Parkhurst, D.L. 1990. Revised Chemical Equilibrium Data for Major Water—Mineral Reactions and Their Limitations. *Chemical Modeling of Aqueous Systems II.* American Chemical Society, pp.398-413.
NPI, N.P.I. 2016. *Geological map of Svalbard (1:250000) [Data set].*
NPI, N.P.I. not released. NP_Satellitt_Svalbard_WMTS_25833 [Data set]. [Online]. Available from: https://data.npolar.no/dataset/71528149-b8e0-4646-9e5d-f7202acaee6e
Paerl, H.W. 1997. Coastal eutrophication and harmful algal blooms: Importance of atmospheric deposition and groundwater as “new” nitrogen and other nutrient sources. **42**(5part2), pp.1154-1165.
Palya, A.P., Buick, I.S. and Bebout, G.E. 2011. Storage and mobility of nitrogen in the continental crust: Evidence from partially melted metasedimentary rocks, Mt. Stafford, Australia. *Chemical Geology.* **281**(3), pp.211-226.
Patrick, W.H. and Jugsujinda, A. 1992. Sequential Reduction and Oxidation of Inorganic Nitrogen, Manganese, and Iron in Flooded Soil. **56**(4), pp.1071-1073.
Peters, K.E., Sweeney, R.E. and Kaplan, I.R. 1978. Correlation of carbon and nitrogen stable isotope ratios in sedimentary organic matter 1. **23**(4), pp.598-604.
Petrovich, R. 1981. Kinetics of dissolution of mechanically comminuted rock-forming oxides and silicates—I. Deformation and dissolution of quartz under laboratory conditions. *Geochimica et Cosmochimica Acta.* **45**(10), pp.1665-1674.
Petsch, S.T. 2014. 12.8 - Weathering of Organic Carbon. In: Holland, H.D. and Turekian, K.K. eds. *Treatise on Geochemistry (Second Edition).* Oxford: Elsevier, pp.217-238.
Pisapia, C., Chaussidon, M., Mustin, C. and Humbert, B. 2007. O and S isotopic composition of dissolved and attached oxidation products of pyrite by Acidithiobacillus ferrooxidans: Comparison with abiotic oxidations. *Geochimica et Cosmochimica Acta.* **71**(10), pp.2474-2490.
Plummer, L.N. and Wigley, T.M.L. 1976. The dissolution of calcite in CO2-saturated solutions at 25°C and 1 atmosphere total pressure. *Geochimica et Cosmochimica Acta.* **40**(2), pp.191-202.
Popova, E., Yool, A., Coward, A., Aksenov, Y., Alderson, S., De Cuevas, B. and Anderson, T.J.B. 2010. Control of primary production in the Arctic by nutrients

and light: insights from a high resolution ocean general circulation model. **7**(11), pp.3569-3591.

Poulton, S.W. and Canfield, D.E. 2005. Development of a sequential extraction procedure for iron: implications for iron partitioning in continentally derived particulates. *Chemical Geology.* **214**(3), pp.209-221.

Purcell, A.M., Mikucki, J.A., Achberger, A.M., Alekhina, I.A., Barbante, C., Christner, B.C., Ghosh, D., Michaud, A.B., Mitchell, A.C., Priscu, J.C., Scherer, R., Skidmore, M.L., Vick-Majors, T.J. and the WISSARD Science Team. 2014. Microbial sulfur transformations in sediments from Subglacial Lake Whillans. **5**(594).

Raiswell, R., Benning, L.G., Davidson, L., Tranter, M. and Tulaczyk, S. 2009. Schwertmannite in wet, acid, and oxic microenvironments beneath polar and polythermal glaciers. *Geology.* **37**(5), pp.431-434.

Raiswell, R., Benning, L.G., Tranter, M. and Tulaczyk, S. 2008. Bioavailable iron in the Southern Ocean: the significance of the iceberg conveyor belt. *Geochemical Transactions.* **9**(1), p7.

Raiswell, R., Bottrell, S., Al-Biatty, H.J. and Tan, M.M. 1993. The influence of bottom water oxygenation and reactive iron content on sulfur incorporation into bitumens from Jurassic marine shales. **293**(6), pp.569-596.

Raiswell, R., Tranter, M., Benning, L.G., Siegert, M., De'ath, R., Huybrechts, P. and Payne, T. 2006. Contributions from glacially derived sediment to the global iron (oxyhydr)oxide cycle: Implications for iron delivery to the oceans. *Geochimica et Cosmochimica Acta.* **70**(11), pp.2765-2780.

Riber, L. 2009. *Paleogene Depositional Conditions and Climatic Changes of the Frysjaodden Formation in Central Spitsbergen (Sedimentology and Mineralogy)*. thesis, University of Oslo.

Risgaard-Petersen, N., Revsbech, N.P. and Rysgaard, S. 1995. Combined Microdiffusion-Hypobromite Oxidation Method for Determining Nitrogen-15 Isotope in Ammonium. **59**(4), pp.1077-1080.

Rosman, K.J.R. and Taylor, P.D.P. 1998. *Isotopic compositions of the elements 1997 (Technical Report)*. Pure and Applied Chemistry. 70. p.217. [Accessed 2019-11-13t14:58:01.864+01:00]. Available from: https://www.degruyter.com/view/j/pac.1998.70.issue-1/pac199870010217/pac199870010217.xml

Rudnick, R.L. and Gao, S. 2003. 3.01 - Composition of the Continental Crust A2 - Holland, Heinrich D. In: Turekian, K.K. ed. *Treatise on Geochemistry.* Oxford: Pergamon, pp.1-64.

Rutter, N., Hodson, A., Irvine-Fynn, T. and Solås, M.K. 2011. Hydrology and hydrochemistry of a deglaciating high-Arctic catchment, Svalbard. *Journal of Hydrology.* **410**(1–2), pp.39-50.

Ryba, S.A. and Burgess, R.M. 2002. Effects of sample preparation on the measurement of organic carbon, hydrogen, nitrogen, sulfur, and oxygen concentrations in marine sediments. *Chemosphere.* **48**(1), pp.139-147.

Schimel, J.P. and Bennett, J. 2004. NITROGEN MINERALIZATION: CHALLENGES OF A CHANGING PARADIGM. **85**(3), pp.591-602.

Schippers, A. and Jørgensen, B.B. 2001. Oxidation of pyrite and iron sulfide by manganese dioxide in marine sediments. *Geochimica et Cosmochimica Acta.* **65**(6), pp.915-922.

Schippers, A. and Jørgensen, B.B. 2002. Biogeochemistry of pyrite and iron sulfide oxidation in marine sediments. *Geochimica et Cosmochimica Acta.* **66**(1), pp.85-92.

Schlegel, A., Lisker, F., Dörr, N., Jochmann, M., Schubert, K. and Spiegel, C. 2013. Petrography and geochemistry of siliciclastic rocks from the Central Tertiary Basin of Svalbard & implications for provenance, tectonic setting and climate [Petrografie und Geochemie siliziklastischer Gesteine aus dem Zentralen Tertiärbecken auf Spitzbergen & Folgerungen fär das Liefergebiet, seine

tektonische Stellung und das Klima.]. *Zeitschrift der Deutschen Gesellschaft für Geowissenschaften.* **164**(1), pp.173-186.
Schlesinger, W.H.B., E. S. 2013. *Biogeochemistry: An Analysis of Global Change.* 3rd Edition ed. Academic Press.
Scholten, S.O. 1991. The distribution of nitrogen isotopes in sediments. *Geologica Ultraiectina.* **81**, p101.
Schubert, C.J. and Calvert, S.E. 2001. Nitrogen and carbon isotopic composition of marine and terrestrial organic matter in Arctic Ocean sediments:: implications for nutrient utilization and organic matter composition. *Deep Sea Research Part I: Oceanographic Research Papers.* **48**(3), pp.789-810.
Schweitzer, H.-J. 1980. Environment and climate in the early tertiary of spitsbergen. *Palaeogeography, Palaeoclimatology, Palaeoecology.* **30**, pp.297-311.
Seal, R.R., II. 2006. Sulfur Isotope Geochemistry of Sulfide Minerals. *Reviews in Mineralogy and Geochemistry.* **61**(1), pp.633-677.
Sebilo, M., Mayer, B., Grably, M., Billiou, D. and Mariotti, A. 2004. The Use of the Ammonium Diffusion Method for 15N-NH4+ and 15N-NO3<sup/> Measurements: Comparison with Other Techniques %J Environmental Chemistry. **1**(2), pp.99-103.
Sevestre, H., Benn, D.I., Hulton, N.R.J. and Bælum, K. 2015. Thermal structure of Svalbard glaciers and implications for thermal switch models of glacier surging. **120**(10), pp.2220-2236.
Sharp, M., Parkes, J., Cragg, B., Fairchild, I.J., Lamb, H. and Tranter, M. 1999. Widespread bacterial populations at glacier beds and their relationship to rock weathering and carbon cycling. *Geology.* **27**(2), pp.107-110.
Sharp, M. and Tranter, M. 2017. Glacier Biogeochemistry. *Geochemical Perspectives.* **6**(2), pp.173-174.
Shaw, T.J., Gieskes, J.M. and Jahnke, R.A. 1990. Early diagenesis in differing depositional environments: The response of transition metals in pore water. *Geochimica et Cosmochimica Acta.* **54**(5), pp.1233-1246.
Sheridan, P.P., Miteva, V.I. and Brenchley, J.E. 2003. Phylogenetic Analysis of Anaerobic Psychrophilic Enrichment Cultures Obtained from a Greenland Glacier Ice Core. **69**(4), pp.2153-2160.
Sigman, D.M., Casciotti, K.L., Andreani, M., Barford, C., Galanter, M. and Böhlke, J.K. 2001. A Bacterial Method for the Nitrogen Isotopic Analysis of Nitrate in Seawater and Freshwater. *Analytical Chemistry.* **73**(17), pp.4145-4153.
Silva, J.A. and Bremner, J.M. 1966. Determination and Isotope-Ratio Analysis of Different Forms of Nitrogen in Soils: 5. Fixed Ammonium. *Soil Science Society of America Journal.* **30**(5), pp.587-594.
Silva, S.R., Kendall, C., Wilkison, D.H., Ziegler, A.C., Chang, C.C.Y. and Avanzino, R.J. 2000. A new method for collection of nitrate from fresh water and the analysis of nitrogen and oxygen isotope ratios. *Journal of Hydrology.* **228**(1–2), pp.22-36.
Silver, B.J., Raymond, R., Sigman, D.M., Prokopeko, M., Sherwood Lollar, B., Lacrampe-Couloume, G., Fogel, M.L., Pratt, L.M., Lefticariu, L. and Onstott, T.C. 2012. The origin of NO3− and N2 in deep subsurface fracture water of South Africa. *Chemical Geology.* **294-295**, pp.51-62.
Sim, M.S., Bosak, T. and Ono, S. 2011. Large Sulfur Isotope Fractionation Does Not Require Disproportionation. **333**(6038), pp.74-77.
Singer, P.C. and Stumm, W. 1970. Acidic Mine Drainage: The Rate-Determining Step. *Science.* **167**(3921), pp.1121-1123.
Skidmore, M., Anderson, S.P., Sharp, M., Foght, J. and Lanoil, B.D. 2005. Comparison of Microbial Community Compositions of Two Subglacial Environments Reveals a Possible Role for Microbes in Chemical Weathering Processes. *Applied and Environmental Microbiology.* **71**(11), pp.6986-6997.
Skidmore, M., Foght, J.M. and Sharp, M.J. 2000. Microbial Life beneath a High Arctic Glacier. *Applied and Environmental Microbiology.* **66**(8), pp.3214-3220.

Sluijs, A., Schouten, S., Pagani, M., Woltering, M., Brinkhuis, H., Damsté, J.S.S., Dickens, G.R., Huber, M., Reichart, G.-J., Stein, R., Matthiessen, J., Lourens, L.J., Pedentchouk, N., Backman, J., Moran, K. and the Expedition, S. 2006. Subtropical Arctic Ocean temperatures during the Palaeocene/Eocene thermal maximum. *Nature.* **441**(7093), pp.610-613.

Snider, D.M., Spoelstra, J., Schiff, S.L. and Venkiteswaran, J.J. 2010. Stable Oxygen Isotope Ratios of Nitrate Produced from Nitrification: 18O-Labeled Water Incubations of Agricultural and Temperate Forest Soils. *Environmental Science & Technology.* **44**(14), pp.5358-5364.

SNSK, S.N.S.K. 2013. *Core Description - Core 13/2013*. Unpublished.

Sobek, A., Schuller, W. and Inskeep, W.P. 1978. *Field and Laboratory Methods Applicable to Overburdens and Minesoils.* Cincinnati OH: Environmental Protection Agency.

Spielhagen, R.F. and Tripati, A. 2009. Evidence from Svalbard for near-freezing temperatures and climate oscillations in the Arctic during the Paleocene and Eocene. *Palaeogeography, Palaeoclimatology, Palaeoecology.* **278**(1), pp.48-56.

Spoelstra, J., Schiff, S.L., Hazlett, P.W., Jeffries, D.S. and Semkin, R.G. 2007. The isotopic composition of nitrate produced from nitrification in a hardwood forest floor. *Geochimica et Cosmochimica Acta.* **71**(15), pp.3757-3771.

Statham, P.J., Skidmore, M. and Tranter, M. 2008. Inputs of glacially derived dissolved and colloidal iron to the coastal ocean and implications for primary productivity. **22**(3).

Steel, R.J., Dalland, A., Kalgraff, K. and Larsen, V. 1981. The Central Tertiary Basin of Spitsbergen: Sedimentary Development of a Sheared-Margin Basin. *Geology of the North Atlantic Borderlands.* **Memoir 7**, pp.647-664.

Stevenson, F.J. 1959. On the Presence of Fixed Ammonium in Rocks. **130**(3369), pp.221-222.

Stibal, M., Wadham, J.L., Lis, G.P., Telling, J., Pancost, R.D., Dubnick, A., Sharp, M.J., Lawson, E.C., Butler, C.E.H., Hasan, F., Tranter, M. and Anesio, A.M. 2012. Methanogenic potential of Arctic and Antarctic subglacial environments with contrasting organic carbon sources. **18**(11), pp.3332-3345.

Strathouse, S.M., Sposito, G., Sullivan, P.J. and Lund, L.J. 1980. Geologic Nitrogen: A Potential Geochemical Hazard in the San Joaquin Valley, California1. **9**(1), pp.54-60.

Strebel, O., Böttcher, J. and Fritz, P. 1990. Use of isotope fractionation of sulfate-sulfur and sulfate-oxygen to assess bacterial desulfurication in a sandy aquifer. *Journal of Hydrology.* **121**(1), pp.155-172.

Stumm, W. and Morgan, J.J. 1996. *Aquatic Chemistry, Chemical Equilibria and Rates in Natural Waters.* 3rd Edition ed. New York.: John Wiley & Sons, Inc.

Sykes, G. 1969. Methods and Equipment for Sterilisation of Laboratory Apparatus and Media. In: Norris, J.R. and Ribbons, D.W. eds. *Methods in Microbiology.* Academic Press, pp.77-121.

Taylor, B.E., Wheeler, M.C. and Nordstrom, D.K. 1984. Stable isotope geochemistry of acid mine drainage: Experimental oxidation of pyrite. *Geochimica et Cosmochimica Acta.* **48**(12), pp.2669-2678.

Telling, J., Anesio, A.M., Tranter, M., Irvine-Fynn, T., Hodson, A., Butler, C. and Wadham, J. 2011. Nitrogen fixation on Arctic glaciers, Svalbard. *Journal of Geophysical Research: Biogeosciences.* **116**(G3), pp.n/a-n/a.

Telling, J., Boyd, E.S., Bone, N., Jones, E.L., Tranter, M., MacFarlane, J.W., Martin, P.G., Wadham, J.L., Lamarche-Gagnon, G., Skidmore, M.L., Hamilton, T.L., Hill, E., Jackson, M. and Hodgson, D.A. 2015. Rock comminution as a source of hydrogen for subglacial ecosystems. *Nature Geosci.* **8**(11), pp.851-855.

Tiedje, J.M. 1988. Ecology of denitrification and dissimilatory nitrate reduction to ammonium. In: Zehnder, A.J.B. ed. *Environmental Microbiology of Anaerobes.* New York: John Wiley and Sons, pp.179-244.

Tockner, K., Malard, F., Uehlinger, U. and Ward, J.V. 2002. Nutrients and organic matter in a glacial river—floodplain system (Val Roseg, Switzerland). **47**(1), pp.266-277.

Toran, L. and Harris, R.F. 1989. Interpretation of sulfur and oxygen isotopes in biological and abiological sulfide oxidation. *Geochimica et Cosmochimica Acta.* **53**(9), pp.2341-2348.

Tranter, M. 1991. Controls on the Composition of Snowmelt. In: *Berlin, Heidelberg*. Springer Berlin Heidelberg, pp.241-271.

Tranter, M. 2003. 5.07 - Geochemical Weathering in Glacial and Proglacial Environments. In: Holland, H.D. and Turekian, K.K. eds. *Treatise on Geochemistry.* Oxford: Pergamon, pp.189-205.

Tranter, M., Brown, G., Raiswell, R., Sharp, M. and Gurnell, A. 1993. A conceptual model of solute acquisition by Alpine glacial meltwaters. *Journal of Glaciology, .* **133**, pp.573 - 581.

Tranter, M., Brown, G.H., Hodson, A.J. and Gurnell, A.M. 1996. HYDROCHEMISTRY AS AN INDICATOR OF SUBGLACIAL DRAINAGE SYSTEM STRUCTURE: A COMPARISON OF ALPINE AND SUB-POLAR ENVIRONMENTS. *Hydrological Processes.* **10**, pp.541–556.

Tranter, M., Sharp, M.J., Lamb, H.R., Brown, G.H., Hubbard, B.P. and Willis, I.C. 2002. Geochemical weathering at the bed of Haut Glacier d'Arolla, Switzerland—a new model. *Hydrological Processes.* **16**(5), pp.959-993.

Tye, A.M. and Heaton, T.H.E. 2007. Chemical and isotopic characteristics of weathering and nitrogen release in non-glacial drainage waters on Arctic tundra. *Geochimica et Cosmochimica Acta.* **71**(17), pp.4188-4205.

Usher, C.R., Cleveland, C.A., Strongin, D.R. and Schoonen, M.A. 2004. Origin of Oxygen in Sulfate during Pyrite Oxidation with Water and Dissolved Oxygen: An In Situ Horizontal Attenuated Total Reflectance Infrared Spectroscopy Isotope Study. *Environmental Science & Technology.* **38**(21), pp.5604-5606.

van De Poll, W.H., Maat, D.S., Fischer, P., Rozema, P.D., Daly, O.B., Koppelle, S., Visser, R.J.W. and Buma, A.G.J. 2016. Atlantic Advection Driven Changes in Glacial Meltwater: Effects on Phytoplankton Chlorophyll-a and Taxonomic Composition in Kongsfjorden, Spitsbergen. **3**(200).

Vancoppenolle, M., Bopp, L., Madec, G., Dunne, J., Ilyina, T., Halloran, P.R. and Steiner, N. 2013. Future Arctic Ocean primary productivity from CMIP5 simulations: Uncertain outcome, but consistent mechanisms. **27**(3), pp.605-619.

Vega, C.P., Björkman, M.P., Pohjola, V.A., Isaksson, E., Pettersson, R., Martma, T., Marca, A. and Kaiser, J. 2015. Nitrate stable isotopes and major ions in snow and ice samples from four Svalbard sites. *Polar Research.* **34**(1), p23246.

Vitousek, P.M., Menge, D.N.L., Reed, S.C. and Cleveland, C.C. 2013. Biological nitrogen fixation: rates, patterns and ecological controls in terrestrial ecosystems. **368**(1621), p20130119.

Voicu, G. and Hallbauer, D.K. 2005. Determination of the physico-chemical characteristics of hydrothermal fluids from the post-metamorphic Omai gold deposit, Guiana Shield, using analysis of ionic species by crush-leach technique and capillary electrophoresis. *Mineralogy and Petrology.* **83**(3), pp.243-270.

Wada, E., Minagawa, M., Mizutani, H., Tsuji, T., Imaizumi, R. and Karasawa, K. 1987. Biogeochemical studies on the transport of organic matter along the Otsuchi River watershed, Japan. *Estuarine, Coastal and Shelf Science.* **25**(3), pp.321-336.

Wadham, J.L., Bottrell, S., Tranter, M. and Raiswell, R. 2004. Stable isotope evidence for microbial sulphate reduction at the bed of a polythermal high Arctic glacier. *Earth and Planetary Science Letters.* **219**(3–4), pp.341-355.

Wadham, J.L., Cooper, R.J., Tranter, M. and Bottrell, S. 2007. Evidence for widespread anoxia in the proglacial zone of an Arctic glacier. *Chemical Geology.* **243**(1), pp.1-15.

Wadham, J.L., Cooper, R.J., Tranter, M. and Hodgkins, R. 2001. Enhancement of glacial solute fluxes in the proglacial zone of a polythermal glacier. *Journal of Glaciology.* **47**(158), pp.378-386.

Wadham, J.L., Hawkings, J., Telling, J., Chandler, D., Alcock, J., Lawson, E., Kaur, P., Bagshaw, E.A., Tranter, M., Tedstone, A. and Nienow, P. 2016. Sources, cycling and export of nitrogen on the Greenland Ice Sheet. *Biogeosciences Discuss.* **2016**, pp.1-30.

Wadham, J.L., Hodson, A.J., Tranter, M. and Dowdeswell, J.A. 1998. The hydrochemistry of meltwaters draining a polythermal-based, high Arctic glacier, south Svalbard: I. The ablation season. *Hydrological Processes.* **12**(12), pp.1825-1849.

Wadham, J.L., Tranter, M., Skidmore, M., Hodson, A.J., Priscu, J., Lyons, W.B., Sharp, M., Wynn, P. and Jackson, M. 2010. Biogeochemical weathering under ice: Size matters. *Global Biogeochemical Cycles.* **24**(3), pp.n/a-n/a.

Warneck, P. 1999. *Chemistry of the natural atmosphere.* Academic Press.

Wehrmann, L.M., Formolo, M.J., Owens, J.D., Raiswell, R., Ferdelman, T.G., Riedinger, N. and Lyons, T.W. 2014. Iron and manganese speciation and cycling in glacially influenced high-latitude fjord sediments (West Spitsbergen, Svalbard): Evidence for a benthic recycling-transport mechanism. *Geochimica et Cosmochimica Acta.* **141**, pp.628-655.

Wehrmann, L.M., Riedinger, N., Brunner, B., Kamyshny, A., Hubert, C.R.J., Herbert, L.C., Brüchert, V., Jørgensen, B.B., Ferdelman, T.G. and Formolo, M.J. 2017. Iron-controlled oxidative sulfur cycling recorded in the distribution and isotopic composition of sulfur species in glacially influenced fjord sediments of west Svalbard. *Chemical Geology.* **466**, pp.678-695.

Wentworth, C.K. 1922. A Scale of Grade and Class Terms for Clastic Sediments. *The Journal of Geology.* **30**(5), pp.377-392.

White, A.F. and Brantley, S.L. 2003. The effect of time on the weathering of silicate minerals: why do weathering rates differ in the laboratory and field? *Chemical Geology.* **202**(3), pp.479-506.

Williams, L.B., Ferrell, R.E., Hutcheon, I., Bakel, A.J., Walsh, M.M. and Krouse, H.R. 1995. Nitrogen isotope geochemistry of organic matter and minerals during diagenesis and hydrocarbon migration. *Geochimica et Cosmochimica Acta.* **59**(4), pp.765-779.

Williams, M.W., Brooks, P.D., Mosier, A. and Tonnessen, K.A. 1996. Mineral nitrogen transformations in and under seasonal snow in a high-elevation catchment in the Rocky Mountains, United States. **32**(10), pp.3161-3171.

Williams, M.W., Knauf, M., Cory, R., Caine, N. and Liu, F. 2007. Nitrate content and potential microbial signature of rock glacier outflow, Colorado Front Range. **32**(7), pp.1032-1047.

Windfinder. 2019. *Windfinder.* [Online]. [Accessed 10th October]. Available from: www.windfinder.com/windstatistics/longyearbyen_spitsbergen

Wynn, P.M. 2004. *The provenance and fate of nitrogen in arctic glacial melt waters: an isotopic approach*. thesis, University of Sheffield.

Wynn, P.M., Hodson, A. and Heaton, T. 2006. Chemical and Isotopic Switching within the Subglacial Environment of a High Arctic Glacier. *Biogeochemistry.* **78**(2), pp.173-193.

Wynn, P.M., Hodson, A.J., Heaton, T.H.E. and Chenery, S.R. 2007. Nitrate production beneath a High Arctic glacier, Svalbard. *Chemical Geology.* **244**(1–2), pp.88-102.

Yde, J.C., Bárcena, T.G. and Finster, K.W. 2011. Subglacial and Proglacial Ecosystem Responses to Climate Change,. In: (Ed.), D.J.B. ed. *Climate Change - Geophysical Foundations and Ecological Effects.*

Yde, J.C., Hodson, A.J., Solovjanova, I., Steffensen, J.P., Nørnberg, P., Heinemeier, J. and Olsen, J. 2012. Chemical and isotopic characteristics of a glacier-derived naled in front of Austre Grønfjordbreen, Svalbard. *Polar Research.* **31**(1), p17628.

Yde, J.C., Riger-Kusk, M., Christiansen, H.H., Knudsen, N.T. and Humlum, O. 2008. Hydrochemical characteristics of bulk meltwater from an entire ablation season, Longyearbreen, Svalbard. *Journal of Glaciology.* **54**(185), pp.259-272.

Zachos, J., Pagani, M., Sloan, L., Thomas, E. and Billups, K. 2001. Trends, Rhythms, and Aberrations in Global Climate 65 Ma to Present. **292**(5517), pp.686-693.

Zachos, J., Röhl, U., Schellenberg, S.A., Sluijs, A., Hodell, D.A., Kelly, D.C., Thomas, E., Nicolo, M., Raffi, I., Lourens, L.J., McCarren, H. and Kroon, D. 2005. Rapid Acidification of the Ocean During the Paleocene-Eocene Thermal Maximum. **308**(5728), pp.1611-1615.

Zhang, G., Dong, H., Xu, Z., Zhao, D. and Zhang, C. 2005. Microbial Diversity in Ultra-High-Pressure Rocks and Fluids from the Chinese Continental Scientific Drilling Project in China. *Applied and Environmental Microbiology.* **71**(6), pp.3213-3227.

Zhang, R., John, S.G., Zhang, J., Ren, J., Wu, Y., Zhu, Z., Liu, S., Zhu, X., Marsay, C.M. and Wenger, F. 2015. Transport and reaction of iron and iron stable isotopes in glacial meltwaters on Svalbard near Kongsfjorden: From rivers to estuary to ocean. *Earth and Planetary Science Letters.* **424**, pp.201-211.

Appendices

Appendix A Rock data

A.1 Basic sample information including sample location, lithology and formation

A.2 Geochemical data including carbon, sulphur, nitrogen, iron speciation

A.3 Geochemical data including manganese speciation and isotopes

A.1 Basic rock sample information

N.B. for grain size: vf = very fine grained sand, f = fine grained sand, m = medium grained sand

Core BH9/05

Sample	Core Depth min (m)	Core Depth max (m)	Formation	Lithology	Grain Size
BH 9/05 74	22.43	22.59	Aspelintoppen	Sandstone	M
BH 9/05 73	25.69	25.83	Aspelintoppen	Siderite	Clay
BH 9/05 72	40.43	40.54	Aspelintoppen	Shale	Clay
BH 9/05 71	41	41.14	Aspelintoppen	Shale	Clay
BH 9/05 70	43.25	43.35	Aspelintoppen	Sandstone	M
BH 9/05 69	60.81	60.94	Battfjellet	Sandstone	M
BH 9/05 68	89	89.12	Battfjellet	Sandstone	F
BH 9/05 67	102	102.13	Battfjellet	Sandstone	F
BH 9/05 66	105	105.15	Battfjellet	Sandstone	F
BH 9/05 65	123.66	123.75	Frysjaodden	Siltstone	Silt
BH 9/05 64	145.2	145.33	Frysjaodden	Shale	Clay
BH 9/05 63	165.22	165.33	Frysjaodden	Siderite	Clay
BH 9/05 62	183.6	183.71	Frysjaodden	Shale	Silt
BH 9/05 61	207.6	207.71	Frysjaodden	Shale	Clay
BH 9/05 60	220.49	220.6	Frysjaodden	Shale	Clay
BH 9/05 59	242.39	242.49	Frysjaodden	Shale	Clay

Sample	Core Depth min (m)	Core Depth max (m)	Formation	Lithology	Grain Size
BH 9/05 58	264.63	264.73	Frysjaodden	Shale	Clay
BH 9/05 57	284.35	254.47	Frysjaodden	Shale	Clay
BH 9/05 56	304.79	304.89	Frysjaodden	Shale	Clay
BH 9/05 55	328.56	328.63	Frysjaodden	Shale	Clay
BH 9/05 54	338.41	338.53	Frysjaodden	Shale	Clay
BH 9/05 53	356.18	356.28	Frysjaodden	Shale	Clay
BH 9/05 52	383.23	383.38	Frysjaodden	Shale	Clay
BH 9/05 51	395.84	395.93	Frysjaodden	Shale	Clay
BH 9/05 50	412.67	412.78	Frysjaodden	Shale	Clay
BH 9/05 49	431.84	431.95	Frysjaodden	Shale	Clay
BH 9/05 48	452.21	452.32	Frysjaodden	Shale	Clay
BH 9/05 47	475.47	475.6	Frysjaodden	Shale	Clay
BH 9/05 46	500.48	500.59	Frysjaodden	Shale	Clay
BH 9/05 45	510.5	510.58	Frysjaodden	Shale	Clay
BH 9/05 44	530.26	530.36	Frysjaodden	Shale	Clay
BH 9/05 43	537.38	537.55	Frysjaodden	Shale	Clay
BH 9/05 42	550.85	551	Frysjaodden	Siltstone	Silt
BH 9/05 41	571.9	572	Grumantbyen	Sandstone	F
BH 9/05 40	616.16	596.33	Grumantbyen	Sandstone	F
BH 9/05 39	616.58	616.73	Grumantbyen	Sandstone	F
BH 9/05 38	632.55	632.74	Grumantbyen	Sandstone	F
BH 9/05 37	656.9	657.02	Grumantbyen	Sandstone	F
BH 9/05 36	676.89	677.01	Grumantbyen	Sandstone	F

Core 13/2013

Sample	Core Depth min (m)	Core Depth max (m)	Formation	Lithology	Grain Size
13/2013 1	6.38	6.56	Grumantbyen	Sandstone	F
13/2013 2	17.46	17.66	Grumantbyen	Sandstone	F
13/2013 3	29.75	30	Grumantbyen	Sandstone	F
13/2013 4	33.09	33.31	Grumantbyen	Sandstone	F
13/2013 5	45	45.26	Grumantbyen	Sandstone	F
13/2013 6	55.67	55.87	Grumantbyen	Sandstone	F
13/2013 7	63.73	63.96	Grumantbyen	Sandstone	F
13/2013 8	75	75.25	Grumantbyen	Sandstone	F
13/2013 9	86.78	87	Grumantbyen	Sandstone	F
13/2013 10	97.79	98	Grumantbyen	Sandstone	F
13/2013 11	113.79	114	Grumantbyen	Sandstone	F
13/2013 12	133.54	133.78	Grumantbyen	Sandstone	F
13/2013 13	149	149.21	Basilika	Shale	F
13/2013 14	155.74	155.95	Basilika	Shale	F
13/2013 15	166	166.21	Basilika	Shale	F
13/2013 16	177	177.2	Basilika	Shale	Vf
13/2013 17A	181.23	181.39	Basilika	Shale	F
13/2013 17B	181.23	181.39	Basilika	Shale	M
13/2013 18	193.25	193.35	Basilika	Shale	Vf
13/2013 19	201	201.14	Basilika	Shale	Vf
13/2013 20	204	204.8	Firkanten (Endalen)	Conglomerate	Pebbles
13/2013 21	207.89	208.03	Firkanten (Endalen)	Sandstone	F
13/2013 22	212.26	212.3	Firkanten (Endalen)	Shale	Clay
13/2013 23	214.83	214.98	Firkanten (Endalen)	Sandstone	F
13/2013 24	225.15	225.3	Firkanten (Endalen)	Siltstone	Silt

Sample	Core Depth min (m)	Core Depth max (m)	Formation	Lithology	Grain Size
13/2013 25	232.03	232.13	Firkanten (Endalen)	Sandstone	M
13/2013 26	237	237.14	Firkanten (Endalen)	Sandstone	F
13/2013 27	239.14	239.28	Firkanten (Todalen)	Siltstone	Silt
13/2013 28	240.1	240.2	Firkanten (Todalen)	Siltstone	Silt
13/2013 29	246.74	246.87	Firkanten (Todalen)	Siltstone	Silt
13/2013 30	249	249.18	Firkanten (Todalen)	Sandstone	F
13/2013 31	252.82	252.95	Firkanten (Todalen)	Siltstone	Silt
13/2013 32	268.66	268.86	Firkanten (Todalen)	Shale	Clay
13/2013 33	274.3	274.48	Firkanten (Todalen)	Shale	Clay
13/2013 34	282.19	282.39	Firkanten (Todalen)	Siltstone	Silt
13/2013 35	285.76	285.9	Carolinefjellet	Siltstone	Silt

Outcrop

N.B. Outcrop site numbers refer to map in Section 2.1.2

Sample	Outcrop Site	Formation	Lithology	Grain Size
Longgeo_3c	8	Battfjellet?	Sandstone	F
Longgeo_3b	8	Battfjellet?	Sandstone	F
Longgeo_3a_2	8	Battfjellet?	Sandstone	F
Longgeo_3a	8	Battfjellet?	Sandstone	F
Longgeo_1e	7	Grumantbyen	Sandstone	F
Longgeo_1b_upper	7	Grumantbyen	Siltstone	Silt
Longgeo_1b	7	Grumantbyen	Siltstone	Silt
Longgeo_1a	7	Grumantbyen	Sandstone	F
Longgeo_2c	6	Basilika?	Shale	Silt
Longgeo_2b	6	Basilika?	Sandstone	F
Longgeo_2a	6	Basilika?	Sandstone	F

Sample	Outcrop Site	Formation	Lithology	Grain Size
Longgeo_1d	7	Firkanten - Endalen?	Sandstone	F
Longgeo_1c	7	Firkanten - Endalen?	Sandstone	M
Longgeo_4a	5	Firkanten - Todalen	Sandstone	M
Longgeo_4b	5	Firkanten - Todalen	Siltstone	Silt
Longgeo_4c	5	Firkanten - Todalen	Siltstone	Silt
Longgeo_4d	5	Firkanten - Todalen	Siltstone	Silt
Longgeo_4e	5	Firkanten - Todalen	Shale	Clay
Road-8	1	Carolinefjellet	Siltstone	Silt
Road-7	1	Carolinefjellet	Sandstone	F
Road-6	2	Carolinefjellet	Sandstone	F
Road-5	2	Carolinefjellet	Siltstone	Silt
Road-4	3	Carolinefjellet	Sandstone	M
Road-3	3	Carolinefjellet	Sandstone	F
Road-2	4	Carolinefjellet	Sandstone	F
Road 1A	4	Carolinefjellet	Sandstone	M
Road-1B	4	Carolinefjellet	Sandstone	M
Møy-6-5	12	Carolinefjellet	Sandstone	F
Møy-6-4	12	Carolinefjellet	Sandstone	M
Møy-6-3	12	Carolinefjellet	Sandstone	M
Møy-6-2	12	Carolinefjellet	Sandstone	F
Møy-6-1	12	Carolinefjellet	Sandstone	F
Møy-5	12	Carolinefjellet	Sandstone	M
Møy-4	12	Carolinefjellet	Sandstone	Vf
Møy-3	12	Carolinefjellet	Sandstone	F
Møy-2	12	Carolinefjellet	Sandstone	F
Møy-1	12	Carolinefjellet	Sandstone	F

Sample	Outcrop Site	Formation	Lithology	Grain Size
Møy_Moraine_4	Møysalbreen moraine	Unknown	Siltstone	Silt
G1	Gløtfjellbreen moraine	Unknown	Sandstone	F
Riep Mor 1	Rieperbreen moraine	Unknown	Conglomerate	Pebbles
75	9	Hollanderdalen	Sandstone	M
76	9	Hollanderdalen	Sandstone	M
77	14	Grumantbyen	Sandstone	F
78	14	Grumantbyen	Sandstone	F
79	14	Basilika	Shale	Clay
80	13	Basilika	Siltstone	Silt
81	13	Basilika	Siltstone	Silt
82	12	Firkanten - Endalen	Sandstone	M
83	12	Firkanten - Endalen	Sandstone	M
84	12	Firkanten - Endalen	Sandstone	F
85	11	Carolinefjellet	Shale	Clay
86	11	Carolinefjellet	Sandstone	F

A.2 Rock geochemical data (1/2)

BH9/05

Sample	TOC (wt. %)	TIC (wt. %)	S (wt. %)	Sulphide S (wt. %)	N (wt. %)	Fe NaAc (wt. %)	Fe NaD (wt. %)	Fe AmOx (wt. %)	Fe Py (wt. %)
BH 9/05 74	0.478	0.133	0.025	0.014	0.024	0.039	0.855	0.026	0.012
BH 9/05 73	2.746	5.370	0.075	0.065	0.050	17.261	0.000	4.951	0.057
BH 9/05 72	0.274	0.445	0.040	0.038	0.058	1.218	0.259	0.152	0.033
BH 9/05 71	1.215	0.598	0.276	0.239	0.096	1.990	0.113	0.170	0.208
BH 9/05 70	0.000	<LOD	<LOD		0.008	0.046	0.268	0.029	
BH 9/05 69	0.566	1.057	0.051	0.041	0.034	3.011	0.147	0.230	0.036
BH 9/05 68	0.455	0.360	0.075	0.069	0.052	1.023	0.151	0.149	0.060
BH 9/05 67	0.357	0.468	0.089	0.064	0.049	0.776	0.062	0.176	0.056
BH 9/05 66	0.000	0.208	0.042		0.015	0.185	0.245	0.060	
BH 9/05 65	0.873	0.675	0.078		0.075	1.672	0.161	0.252	

Sample	TOC (wt. %)	TIC (wt. %)	S (wt. %)	Sulphide S (wt. %)	N (wt. %)	Fe NaAc (wt. %)	Fe NaD (wt. %)	Fe AmOx (wt. %)	Fe Py (wt. %)
BH 9/05 64	1.142	0.567	0.109		0.097	1.337	0.128	0.226	
BH 9/05 63	1.184	0.973	0.056	0.035	0.112	2.806	0.096	0.281	0.031
BH 9/05 62	1.101	0.890	0.081	0.071	0.114	2.274	0.148	0.257	0.062
BH 9/05 61	1.270	0.820	2.899		0.112	2.156	0.098	0.235	
BH 9/05 60	1.291	0.731	0.341		0.117	1.991	0.096	0.240	
BH 9/05 59	1.145	0.367	0.170		0.125	1.056	0.070	0.230	
BH 9/05 58	0.890	0.267	0.264		0.118	0.898	0.080	0.237	
BH 9/05 57	1.177	0.353	1.403		0.125	1.571	0.112	0.319	
BH 9/05 56	0.454	3.559	0.443	0.447	0.060	9.649	0.020	1.187	0.389
BH 9/05 55	0.833	0.816	0.076		0.109	2.278	0.145	0.365	
BH 9/05 54	0.823	0.496	0.045		0.122	1.505	0.075	0.337	
BH 9/05 53	0.987	0.321	0.143		0.129	1.210	0.439	0.308	

Sample	TOC (wt. %)	TIC (wt. %)	S (wt. %)	Sulphide S (wt. %)	N (wt. %)	Fe NaAc (wt. %)	Fe NaD (wt. %)	Fe AmOx (wt. %)	Fe Py (wt. %)
BH 9/05 52	1.036	0.580	1.127		0.126	1.685	0.107	0.468	
BH 9/05 51	1.058	0.473	0.029	0.017	0.132	1.587	0.122	0.354	0.015
BH 9/05 50	0.851	0.524	0.027		0.116	1.758	0.194	0.385	
BH 9/05 49	0.918	0.113	<LOQ		0.126	0.432	0.111	0.280	
BH 9/05 48	0.887	0.234	<LOQ		0.118	1.058	0.108	0.378	
BH 9/05 47	1.114	0.262	0.164		0.126		0.106	0.395	
BH 9/05 46	1.228	0.329	0.124		0.124	1.109	0.074	0.298	
BH 9/05 45	0.789	0.697	1.186		0.118	2.356	0.105	0.226	
BH 9/05 44	0.938	2.217	0.717		0.113	5.958	0.199	0.708	
BH 9/05 43	2.883	0.740	0.028	0.038	0.162	1.799	0.096	0.555	0.033
BH 9/05 42	0.337	1.022	0.633	0.591	0.136	0.413	0.096	0.524	0.515
BH 9/05 41	0.010	<LOD	<LOQ		0.021	0.201	0.083	0.548	

Sample	TOC (wt. %)	TIC (wt. %)	S (wt. %)	Sulphide S (wt. %)	N (wt. %)	Fe NaAc (wt. %)	Fe NaD (wt. %)	Fe AmOx (wt. %)	Fe Py (wt. %)
BH 9/05 40	0.027	<LOD	<LOQ	0.010	0.017	0.393	0.098	0.663	0.009
BH 9/05 39	0.406	0.060	0.084		0.035	0.199	0.089	0.667	
BH 9/05 38	0.000	0.297	<LOQ		0.022	0.348	0.118	0.868	
BH 9/05 37	0.126	0.071	0.050		0.029	0.549	0.141	0.954	
BH 9/05 36	0.353	0.237	0.070	0.057	0.048	0.904	0.150	0.901	0.050

13/2013

Sample	TOC (wt. %)	TIC (wt. %)	S (wt. %)	Sulphide S (wt. %)	N (wt. %)	Fe NaAc (wt. %)	Fe NaD (wt. %)	Fe AmOx (wt. %)	Fe Py (wt. %)
13/2013 1	0.097	0.020	<LOD		0.013	0.090	0.525	0.229	
13/2013 2	0.211	-0.005	0.021		0.017	0.326	0.163	1.191	
13/2013 3	0.123	0.001	<LOQ		0.010	0.064	1.707	1.097	
13/2013 4	0.103	0.027	<LOD	0.005	0.012	0.086	2.044	1.110	0.005
13/2013 5	0.352	-0.034	0.266	0.209	0.028	0.264	0.231	0.974	0.182
13/2013 6	<LOD	<LOD	<LOQ		0.021	0.077	1.640	0.888	
13/2013 7	<LOD	<LOD	<LOQ		0.010	1.161	0.869	2.800	
13/2013 8	<LOD	<LOD	<LOQ		0.017	0.428	0.343	2.245	
13/2013 9	<LOD	<LOD	0.041	0.028	0.027	0.361	0.271	1.781	0.024
13/2013 10	0.000	0.228	0.023		0.026	0.413	0.276	1.902	
13/2013 11	0.179	0.161	<LOQ		0.018	0.853	0.538	3.051	

Sample	TOC (wt. %)	TIC (wt. %)	S (wt. %)	Sulphide S (wt. %)	N (wt. %)	Fe NaAc (wt. %)	Fe NaD (wt. %)	Fe AmOx (wt. %)	Fe Py (wt. %)
13/2013 12	0.156	0.393	<LOQ		0.015	0.931	1.802	2.316	
13/2013 13	0.305	0.103	0.852		0.034	0.179	0.217	0.456	
13/2013 14	0.343	0.001	1.699	1.462	0.035	0.241	0.152	0.449	1.273
13/2013 15	0.295	0.214	0.054	0.032	0.038	0.697	0.432	0.789	0.028
13/2013 16	0.207	0.261	0.161		0.044	0.964	0.121	0.501	
13/2013 17A	1.346	4.800	0.142	0.110	0.046	10.447	2.072	6.977	0.096
13/2013 17B	0.320	0.237	0.047	0.031	0.045	0.806	0.799	0.561	0.027
13/2013 18	0.353	-0.030	0.515		0.074	0.046	0.939	0.093	
13/2013 19	0.135	0.007	6.364	5.232	0.025	0.489	0.172	0.210	4.557
13/2013 20	<LOD	<LOD	0.178	0.053	0.019	0.059	0.187	0.090	0.046
13/2013 21	<LOD	<LOD	0.123		0.007	0.055	0.018	0.030	
13/2013 22	<LOD	<LOD	0.025		0.014	0.241	0.020	0.075	

Sample	TOC (wt. %)	TIC (wt. %)	S (wt. %)	Sulphide S (wt. %)	N (wt. %)	Fe NaAc (wt. %)	Fe NaD (wt. %)	Fe AmOx (wt. %)	Fe Py (wt. %)
13/2013 23	3.864	5.636	0.203	0.151	0.027	8.396	2.198	11.142	0.132
13/2013 24	0.202	5.225	<LOD		0.016	9.314	0.320	4.562	
13/2013 25	<LOD	<LOD	0.391	0.315	0.012	0.304	0.077	0.077	0.274
13/2013 26	0.140	0.074	0.641	0.521	0.020	0.248	0.118	0.119	0.454
13/2013 27	2.574	-0.004	3.578	2.910	0.096	0.199	0.123	0.070	2.535
13/2013 28	3.229	0.109	2.855		0.112	0.174	0.041	0.087	
13/2013 29	7.399	0.883	7.716	5.949	0.206	0.578	0.058	0.060	5.182
13/2013 30	<LOQ	0.367	0.191		0.010	0.130	0.058	0.051	
13/2013 31	3.786	1.751	0.397	0.334	0.124	4.434	0.168	1.948	0.291
13/2013 32	2.588	0.813	0.924		0.114	1.727	0.092	0.893	
13/2013 33	4.546	0.566	2.223	1.787	0.172	1.003	0.064	0.532	1.557
13/2013 34	0.758	0.024	<LOQ		0.061	0.136	0.024	0.062	

Outcrop

Sample	TOC (wt. %)	TIC (wt. %)	S (wt. %)	Sulphide S (wt. %)	N (wt. %)	Fe NaAc (wt. %)	Fe NaD (wt. %)	Fe AmOx (wt. %)	Fe Py (wt. %)
Longgeo_3c	0.397	1.262	0.037		0.042	3.312	0.543	0.074	
Longgeo_3b	0.436	1.198	0.037		0.044	4.534	0.571	0.084	
Longgeo_3a_2	0.213	0.147	0.017		0.028	3.531	0.717	0.113	
Longgeo_3a	0.241	0.119	0.022		0.032	0.057	0.945	0.126	
Longgeo_1e	0.288	<LOD	0.021		0.025	0.120	0.538	0.994	
Longgeo_1b_upper	0.403	<LOD	1.181		0.044	0.473	0.264		
Longgeo_1b	0.411	0.430	0.229		0.042	0.213	0.106	0.459	
Longgeo_1a	0.150	<LOD	<LOD		0.017	0.244	0.184	1.384	
Longgeo_2c	0.512	0.021	0.087		0.050	0.293	0.224		
Longgeo_2b	0.570	0.022	0.175		0.047	5.634	0.314	0.579	

Sample	TOC (wt. %)	TIC (wt. %)	S (wt. %)	Sulphide S (wt. %)	N (wt. %)	Fe NaAc (wt. %)	Fe NaD (wt. %)	Fe AmOx (wt. %)	Fe Py (wt. %)
Longgeo_2a	0.429	0.022	0.079		0.040	0.208	0.462	0.769	
Longgeo_1d	0.692	0.248	0.041		0.035	0.221	0.193		
Longgeo_1c	0.142	0.305	<LOQ		0.015	0.338	0.176		
Longgeo_4a	0.258	0.315	0.076		0.018				
Longgeo_4b	0.998	0.702	0.111		0.038	1.187	1.101	1.021	
Longgeo_4c	0.892	0.530	0.045		0.056	1.083	0.108	0.805	
Longgeo_4d	0.844	0.537	0.041		0.053				
Longgeo_4e	4.623	0.120	0.369		0.146	0.161	0.152	0.198	
Road-8	1.800	0.030	0.137	0.109	0.076	0.144	0.312	0.221	0.095
Road-7	0.691	0.725	0.277	0.242	0.037	0.613	0.150	0.490	0.211
Road-6	0.560	<LOD	0.035		0.042	0.068	1.055	0.206	
Road-5					0.095				

Sample	TOC (wt. %)	TIC (wt. %)	S (wt. %)	Sulphide S (wt. %)	N (wt. %)	Fe NaAc (wt. %)	Fe NaD (wt. %)	Fe AmOx (wt. %)	Fe Py (wt. %)
Road-4	0.247	0.803	0.036		0.026	0.789	0.500	0.512	
Road-3	0.398	0.025	0.146		0.041	0.296	0.171	0.323	
Road-2					0.043				
Road 1A	0.244	0.132	0.018		0.023	0.267	0.323	0.403	
Road-1B	0.415	0.038	0.024		0.022	0.287	0.307	0.354	
Moy-6-5			<LOQ		0.059				
Moy-6-4	1.006	5.926	0.271		0.046	2.680	0.133	0.571	
Moy-6-3	2.374	4.859	<LOQ		0.046	3.120	0.132	0.851	
Moy-6-2	3.732	5.202	<LOQ	0.028	0.066	3.765	0.119	0.833	0.020
Moy-6-1	4.030	5.327	<LOQ		0.051	3.388	0.109	0.158	
Moy-5	0.323	0.790	<LOD		0.025	0.150	0.064	0.746	
Moy-4	2.830	0.071	0.319		0.116	0.590	0.158	0.879	

Sample	TOC (wt. %)	TIC (wt. %)	S (wt. %)	Sulphide S (wt. %)	N (wt. %)	Fe NaAc (wt. %)	Fe NaD (wt. %)	Fe AmOx (wt. %)	Fe Py (wt. %)
Moy-3	0.648	2.204	0.030		0.019	4.553	0.556	3.554	
Moy-2	0.225	0.071	<LOD		0.022	0.170	0.073	0.338	
Moy-1	0.237	0.071	<LOD			0.147	0.123	0.368	
Moy_Moraine_4	0.401	0.180	0.047		0.028	0.270	0.137	1.028	
G1	2.297	0.348	0.116		0.042	0.005	0.066	0.000	
Riep Mor 1					0.007	0.132	0.410	0.377	
75	<LOQ	<LOQ	0.167		0.034	0.303	0.469	0.094	
76	0.127	0.107	0.027		0.024				
77	0.185	0.072	0.034		0.034				
78	0.293	0.083	0.039		0.042				
79	0.579	0.070	0.244		0.049				
80	0.315	0.046	0.198		0.043				

Sample	TOC (wt. %)	TIC (wt. %)	S (wt. %)	Sulphide S (wt. %)	N (wt. %)	Fe NaAc (wt. %)	Fe NaD (wt. %)	Fe AmOx (wt. %)	Fe Py (wt. %)
81	0.367	0.091	0.077		0.048				
82	<LOD	<LOQ	<LOD		0.012				
83	3.042	5.201	0.349		0.019				
84	<LOD	<LOQ	<LOD		0.013				
85	1.280	0.225	0.066		0.083				
86	0.239	0.235	0.033		0.041				

A.3 Rock geochemical data (2/2)

BH9/05

Sample	Mn NaAc (wt. %)	Mn NaD (wt. %)	Mn AmOx (wt. %)	Pyrite $\delta^{34}S$ (‰)	$\delta^{15}N$ (‰)
BH 9/05 74	<LOD	0.006	<LOD	3.46	
BH 9/05 73	0.271	0.015	0.073	-6.26	2.27
BH 9/05 72	0.040	0.006	<LOD	0.48	3.45
BH 9/05 71	<LOD	<LOD	<LOD	4.07	2.87
BH 9/05 70	<LOD	<LOD	<LOD		
BH 9/05 69	0.038	<LOD	<LOD	2.67	3.42
BH 9/05 68	0.028	<LOD	<LOD	4.41	3.39
BH 9/05 67	0.019	<LOD	<LOD	-2.41	3.31
BH 9/05 66	0.009	0.006	<LOD		
BH 9/05 65	0.027	0.011	<LOD		3.04
BH 9/05 64	0.022	<LOD	<LOD		2.93
BH 9/05 63	0.043	<LOD	<LOD	-9.75	2.81
BH 9/05 62	0.039	<LOD	<LOD	-5.42	3.33
BH 9/05 61	0.026	<LOD	<LOD		3.21
BH 9/05 60	0.030	<LOD	<LOD		3.23
BH 9/05 59	0.026	<LOD	<LOD		3.54
BH 9/05 58	0.038	<LOD	<LOD		3.77
BH 9/05 57	0.031	<LOD	<LOD		3.87
BH 9/05 56	0.389	<LOD	0.042	4.17	4.51
BH 9/05 55	0.452	<LOD	0.043		3.91
BH 9/05 54	0.133	<LOD	<LOD		3.95
BH 9/05 53	0.074	<LOD	<LOD		4.12
BH 9/05 52	0.162	<LOD	0.021		4.01
BH 9/05 51	0.068	<LOD	<LOD		4.22
BH 9/05 50	0.104	<LOD	<LOD		4.12

BH 9/05 49	0.017	<LOD	<LOD		4.15
BH 9/05 48	0.039	<LOD	<LOD		4.13
BH 9/05 47	0.043	<LOD	<LOD		4.06
BH 9/05 46	0.035	<LOD	<LOD		3.95
BH 9/05 45	0.084	<LOD	<LOD		3.97
BH 9/05 44	0.187	<LOD	0.019		3.80
BH 9/05 43	0.019	<LOD	<LOD	-8.90	3.93
BH 9/05 42	<LOD	<LOD	<LOD		4.30
BH 9/05 41	<LOD	<LOD	<LOD		
BH 9/05 40	0.016	<LOD	<LOD		
BH 9/05 39	<LOD	<LOD	<LOD		4.79
BH 9/05 38	0.031	<LOD	<LOD		
BH 9/05 37	0.021	<LOD	<LOD		4.67
BH 9/05 36	0.024	<LOD	<LOD	-3.29	4.71

13/2013

Sample	Mn NaAc (wt. %)	Mn NaD (wt. %)	Mn AmOx (wt. %)	Pyrite $\delta^{34}S$ (‰)	$\delta^{15}N$ (‰)
13/2013 1	<LOD	<LOD	<LOD		
13/2013 2	<LOD	<LOD	<LOD		
13/2013 3	<LOD	0.003	<LOD		
13/2013 4	<LOD	0.005	<LOD		
13/2013 5	<LOD	<LOD	<LOD	-50.51	2.99
13/2013 6	<LOD	<LOD	<LOD		
13/2013 7	<LOD	<LOD	<LOD		
13/2013 8	<LOD	<LOD	<LOD		
13/2013 9	<LOD	<LOD	<LOD	-43.24	3.08
13/2013 10	<LOD	<LOD	<LOD		
13/2013 11	0.016	<LOD	<LOD		
13/2013 12	0.248	0.007	0.074		

13/2013 13	<LOD	<LOD	<LOD		3.50
13/2013 14	<LOD	<LOD	<LOD	22.42	3.18
13/2013 15	0.014	<LOD	<LOD		3.71
13/2013 16	0.022	<LOD	<LOD		3.58
13/2013 17A	0.270	0.016	0.116	-10.39	3.59
13/2013 17B	<LOD	<LOD	<LOD	25.30	3.58
13/2013 18	0.127	<LOD	<LOD		3.52
13/2013 19	<LOD	<LOD	<LOD	-3.53	4.16
13/2013 20	<LOD	<LOD	<LOD	3.47	
13/2013 21	<LOD	<LOD	<LOD		
13/2013 22	<LOD	<LOD	<LOD		
13/2013 23	0.085	0.013	0.060	-15.24	3.77
13/2013 24	0.102	<LOD	0.037		
13/2013 25	0.077	<LOD	<LOD		
13/2013 26	<LOD	<LOD	<LOD	-6.89	3.97
13/2013 27	<LOD	<LOD	<LOD	17.87	3.18
13/2013 28	<LOD	<LOD	<LOD		3.09
13/2013 29	<LOD	<LOD	<LOD	-8.99	2.99
13/2013 30	<LOD	<LOD	<LOD		
13/2013 31	0.020	<LOD	<LOD		3.22
13/2013 32	<LOD	<LOD	<LOD		3.64
13/2013 33	<LOD	<LOD	<LOD	-11.16	4.01
13/2013 34	<LOD	<LOD	<LOD		4.28
13/2013 35	0.063	<LOD	<LOD	-3.81	4.13

Outcrop

Sample	Mn NaAc (wt. %)	Mn NaD (wt. %)	Mn AmOx (wt. %)	Pyrite $\delta^{34}S$ (‰)	$\delta^{15}N$ (‰)
Longgeo_3c	0.025	0.002	0.004		3.94
Longgeo_3b	0.028	0.003	0.005		3.98

Sample	Mn NaAc (wt. %)	Mn NaD (wt. %)	Mn AmOx (wt. %)	Pyrite $\delta^{34}S$ (‰)	$\delta^{15}N$ (‰)
Longgeo_3a_2	0.003	0.006	0.004		4.31
Longgeo_3a	0.001	0.004	0.004		3.84
Longgeo_1e	0.000	<LOD	0.005		
Longgeo_1b_upper	0.000	<LOD	0.002		4.78
Longgeo_1b	0.055	<LOD	0.003		4.59
Longgeo_1a	0.020	<LOD	0.004		
Longgeo_2c	<LOD	<LOD	0.004		4.19
Longgeo_2b	<LOD	<LOD	0.003		3.84
Longgeo_2a	0.001	<LOD	0.003		4.03
Longgeo_1d	0.007	<LOD	0.004		3.27
Longgeo_1c	0.010	<LOD	0.003		
Longgeo_4a					
Longgeo_4b	0.001	0.002	0.009		5.10
Longgeo_4c	<LOD	<LOD	0.015		4.43
Longgeo_4d					4.55
Longgeo_4e	0.001	<LOD	0.007		3.99
Road-8	0.001	<LOD	0.007	-21.87	4.07
Road-7	0.018	<LOD	0.009	-14.14	4.61
Road-6	0.018	0.002	0.005		4.61
Road-5					4.10
Road-4	0.029	0.003	0.013		5.43
Road-3	0.005	<LOD	0.008		4.48
Road-2					4.24
Road 1A	0.010	<LOD	0.009		5.21
Road-1B	0.012	0.002	0.008		
Moy-6-5					4.31
Moy-6-4	0.174	<LOD	0.011		4.41

Sample	Mn NaAc (wt. %)	Mn NaD (wt. %)	Mn AmOx (wt. %)	Pyrite $\delta^{34}S$ (‰)	$\delta^{15}N$ (‰)
Moy-6-3	0.169	<LOD	0.015		4.30
Moy-6-2	0.196	<LOD	0.015		4.26
Moy-6-1	0.202	<LOD	0.013		4.43
Moy-5	0.019	<LOD	0.006		
Moy-4	0.008	<LOD	0.008		3.58
Moy-3	0.089	0.001	0.053		
Moy-2	0.001	<LOD	0.004		
Moy-1	0.002	<LOD	0.005		
Moy_Moraine_4	0.015	<LOD	0.007		4.78
G1	<LOD	<LOD	0.005		
Riep Mor 1	<LOD	<LOD	0.005		
75	<LOD	<LOD	<LOD		3.36
76					4.75
77					3.82
78					3.68
79					3.74
80					3.94
81					3.93
82					
83					
84					
85					3.65
86					4.38

Appendix B Weathering experiment leachate geochemical data

B.1 Final leaching experiment 6°C

N.B. n.d. = no data

Aqueous concentration

Day 1

Sample	pH	NH_4^+ aq (N µg/L)	Acetate (mg/L)	NO_3^- (µg/L)	TDIC (mg/L)	SO_4^{2-} (mg/L)	Ca^{2+} (mg/L)	Na^+ (mg/L)	K^+ (mg/L)	Mg^{2+} (mg/L)	Mn (mg/L)	Fe (mg/L)	Si (mg/L)
BH9/05 73	8.7	368.6	2.23	68.48	55.39	22.30	20.3	19.9	9.4	13.6	<LOQ	<LOD	0.28
BH9/05 72	8.9	368.9	<LOQ	41.56	32.12	24.71	10.2	23.0	7.6	3.8	<LOD	<LOD	0.81
BH9/05 71	8.8	627.8	<LOQ	40.16	36.86	25.78	10.5	28.1	7.8	4.3	<LOD	<LOD	0.68
BH9/05 69	9.0	277.3	<LOQ	59.79	28.42	36.90	10.9	21.9	11.4	4.3	<LOD	<LOD	0.64
BH9/05 67	10.0	362.8	2.69	65.59	94.51	24.61	0.4	70.1	3.7	0.2	<LOD	0.22	1.90
BH9/05 63	9.6	280.8	4.88	61.84	215.08	25.94	0.3	115.9	2.9	0.2	<LOD	0.06	0.78
BH9/05 62	9.8	369.7	7.34	61.98	143.40	14.78	0.1	92.5	1.9	0.0	<LOD	<LOQ	1.07
BH9/05 56	8.6	253.7	2.89	32.39	85.73	22.27	0.2	79.4	3.8	0.3	<LOD	0.20	0.65

Sample	pH	NH_4^+ aq (N µg/L)	Acetate (mg/L)	NO_3^- (µg/L)	TDIC (mg/L)	SO_4^{2-} (mg/L)	Ca^{2+} (mg/L)	Na^+ (mg/L)	K^+ (mg/L)	Mg^{2+} (mg/L)	Mn (mg/L)	Fe (mg/L)	Si (mg/L)
BH9/05 43	10.2	740.9	2.49	20.78	152.09	5.39	0.1	89.5	1.2	0.1	<LOD	0.28	2.62
BH9/05 40	9.4	167.8	5.32	112.12	22.73	12.54	2.7	32.3	4.6	0.3	<LOD	<LOD	0.79
13/2013 4	8.4	5.5	1.78	79.47	<LOQ	2.03	2.6	15.9	<LOD	1.1	<LOD	<LOQ	1.61
13/2013 9	8.5	189.5	7.74	172.80	25.17	31.47	18.2	22.8	7.9	4.7	<LOD	<LOD	0.73
13/2013 15	8.8	406.9	12.91	74.85	40.85	50.80	2.8	59.2	8.5	0.9	<LOD	0.04	1.27
13/2013 17A	9.4	450.7	11.29	41.62	130.34	73.29	1.4	112.1	3.6	0.3	<LOD	<LOQ	0.60
13/2013 17B	9.6	558.6	11.31	71.25	100.66	66.67	0.4	96.0	4.3	0.1	<LOD	0.13	1.65
13/2013 20	5.0	1028.5	2.98	38.09	<LOQ	382.66	83.7	79.5	19.4	6.8	0.31	0.17	1.18
13/2013 23	8.3	244.6	12.14	33.84	43.05	72.36	23.9	38.3	8.1	5.7	<LOD	<LOD	0.27
13/2013 26	4.8	655.0	3.03	46.31	<LOQ	192.58	19.7	71.5	17.2	13.7	2.17	0.17	1.23
13/2013 27	4.5	1647.3	9.39	25.00	<LOQ	424.58	16.3	219.5	8.0	7.6	0.36	0.17	2.22
13/2013 29	3.9	2387.4	4.12	5.95	<LOQ	596.71	40.1	158.1	9.2	19.1	0.57	42.96	1.57
13/2013 33	9.3	287.6	18.95	59.58	23.50	36.85	<LOD	52.7	0.9	0.1	<LOD	0.21	3.07

Sample	pH	NH_4^+ aq (N µg/L)	Acetate (mg/L)	NO_3^- (µg/L)	TDIC (mg/L)	SO_4^{2-} (mg/L)	Ca^{2+} (mg/L)	Na^+ (mg/L)	K^+ (mg/L)	Mg^{2+} (mg/L)	Mn (mg/L)	Fe (mg/L)	Si (mg/L)
13/2013 35	9.6	314.5	16.91	156.23	98.34	11.37	<LOQ	67.4	1.6	0.2	<LOD	0.43	2.84
Road 7	8.8	308.2	<LOQ	54.36	25.98	42.88	15.9	5.8	9.3	5.4	<LOD	<LOD	1.12
Moy 6-2	9.0	369.9	2.61	32.22	44.94	8.54	11.1	6.9	10.4	3.1	<LOD	<LOD	0.66
Blank	n.d.	<LOQ	<LOQ	0.00	0.00	0.00	<LOD	<LOD	14.7	<LOD	<LOD	<LOD	<LOD
BH9/05 42	10.0	429.1											
BH9/05 51	10.1	316.7											
Moy 4	7.7	349.7											
LG4E	6.9	576.7											

Day 11

Sample	pH	NH_4^+ aq (N µg/L)	Acetate (mg/L)	NO_3^- (µg/L)	TDIC (mg/L)	SO_4^{2-} (mg/L)	Ca^{2+} (mg/L)	Na^+ (mg/L)	K^+ (mg/L)	Mg^{2+} (mg/L)	Mn (mg/L)	Fe (mg/L)	Si (mg/L)
BH9/05 73	7.8	454.8	2.3	51.37	233.4	26.1	52.0	22.3	11.8	33.7	0.11	<LOD	0.87
BH9/05 72	8.7	381.9	1.5	51.16	44.8	25.8	14.1	23.8	8.6	5.6	<LOQ	<LOD	1.11
BH9/05 71	8.4	712.2	<LOQ	42.26	79.7	29.8	17.2	29.4	9.5	7.6	<LOQ	<LOD	0.95
BH9/05 69	8.4	294.5	<LOQ	46.06	58.9	40.2	19.5	23.3	13.2	8.4	<LOD	<LOD	0.93
BH9/05 67	9.8	325.2	2.9	87.18	117.4	33.8	0.8	79.0	4.6	0.2	<LOD	<LOQ	1.62
BH9/05 63	8.6	315.6	4.2	41.85	355.6	29.8	1.9	178.8	6.2	1.2	<LOD	<LOD	0.74
BH9/05 62	9.3	301.9	7.8	62.26	226.1	18.5	0.5	130.3	3.2	0.2	<LOD	0.11	0.96
BH9/05 56	7.6	508.9	2.9	47.98	197.3	27.1	6.6	106.2	9.6	7.9	0.10	<LOD	1.33
BH9/05 43	10.1	656.1	3.0	28.20	150.4	8.0	0.3	108.4	1.4	0.0	<LOD	0.08	1.91
BH9/05 40	9.2	154.1	5.4	139.39	34.8	12.8	3.5	33.5	4.9	0.4	<LOD	0.05	1.15
13/2013 4	8.3	<LOQ	1.7	85.90	5.1	2.9	3.3	16.7	<LOD	1.5	<LOD	0.14	2.48
13/2013 9	8.5	187.8	11.6	193.55	28.8	34.0	19.7	23.3	7.9	5.3	<LOD	<LOD	1.03

Sample	pH	NH_4^+ aq (N µg/L)	Acetate (mg/L)	NO_3^- (µg/L)	TDIC (mg/L)	SO_4^{2-} (mg/L)	Ca^{2+} (mg/L)	Na^+ (mg/L)	K^+ (mg/L)	Mg^{2+} (mg/L)	Mn (mg/L)	Fe (mg/L)	Si (mg/L)
13/2013 15	8.6	368.6	4.9	63.08	49.9	55.6	5.0	63.8	10.1	1.5	<LOD	<LOD	1.64
13/2013 17A	8.5	451.9	4.6	46.24	212.6	88.3	7.1	141.1	6.2	2.0	<LOQ	<LOD	0.70
13/2013 17B	9.4	580.3	12.0	82.85	101.7	78.7	1.0	111.4	6.0	0.2	<LOD	<LOD	1.53
13/2013 20	4.9	985.0	3.4	50.87	<LOQ	398.7	86.6	80.6	19.5	7.2	0.34	0.11	3.45
13/2013 23	7.8	282.9	4.9	30.47	154.2	78.6	53.8	40.0	9.8	14.1	0.09	<LOD	0.95
13/2013 26	4.8	880.8	3.2	46.91	<LOQ	227.0	23.2	72.1	17.8	16.0	2.61	0.23	3.97
13/2013 27	4.2	2949.5	10.0	25.40	<LOQ	522.9	28.9	239.3	11.4	13.0	0.64	0.94	8.13
13/2013 29	3.6	3042.2	6.2	<LOQ	<LOQ	745.3	58.5	168.0	11.8	25.4	0.93	118.39	7.32
13/2013 33	8.6	256.2	16.2	84.34	55.2	72.4	<LOD	106.8	2.7	0.7	<LOD	1.78	0.25
13/2013 35	9.1	269.4	17.9	163.21	202.3	14.6	0.3	125.6	3.5	0.9	0.04	1.91	3.70
Road 7	8.5	289.3	<LOQ	53.75	36.8	45.6	21.5	6.2	9.9	7.7	<LOD	<LOQ	1.65
Moy 6-2	8.6	399.7	2.2	40.21	61.8	10.7	16.9	7.9	12.9	5.9	<LOD	<LOD	1.08
Blank	n.d.	8.7	<LOQ	<LOQ	<LOQ	<LOQ	0.0	<LOD	<LOD	<LOD	<LOD	<LOD	<LOD

Sample	pH	NH_4^+ aq (N µg/L)	Acetate (mg/L)	NO_3^- (µg/L)	TDIC (mg/L)	SO_4^{2-} (mg/L)	Ca^{2+} (mg/L)	Na^+ (mg/L)	K^+ (mg/L)	Mg^{2+} (mg/L)	Mn (mg/L)	Fe (mg/L)	Si (mg/L)
BH9/05 42	9.6	306.3	3.98	32.43	28.22	33.68							
BH9/05 51	9.8	235.8	<LOQ	29.22	70.18	9.62							
Moy 4	7.3	481.3	5.66	53.53	7.10	44.45							
LG4E	8.1	683.6	1.93	110.80	1.72	51.60							

Data normalised by mass of rock (µg/g)

Day 1

Sample	pH	NH_4^+ (aq) (N) (µg/g)	NH_4^+ (ad) (N) (µg/g)	K_D (NH_4^+)	Acetate (µg/g)	NO_3^- (µg/g)	TDIC (µg/g)	SO_4^{2-} (µg/g)	Ca^{2+} (µg/g)	Na^+ (µg/g)	K^+ (µg/g)	Mg^{2+} (µg/g)	Mn (µg/g)	Fe (µg/g)	Si (µg/g)
BH9/05 73	8.7	1.8	3.0	8	10.8	0.33	268.2	108.0	105.4	103.8	48.8	70.7	<LOQ	<LOD	1.43
BH9/05 72	8.9	1.8	4.8	13	<LOQ	0.20	156.4	120.3	49.5	111.8	36.9	18.4	<LOD	<LOD	3.93
BH9/05 71	8.8	3.2	10.4	17	<LOQ	0.20	185.4	129.7	52.8	141.1	39.2	21.7	<LOD	<LOD	3.43
BH9/05 69	9.0	1.4	1.8	7	<LOQ	0.29	139.3	180.9	53.4	107.3	56.1	21.0	<LOD	<LOD	3.13
BH9/05 67	10.0	1.8	4.1	11	13.1	0.32	459.2	119.6	1.8	340.7	17.9	0.7	<LOD	1.07	9.21
BH9/05 63	9.6	1.4	8.8	31	24.6	0.31	1085.0	130.8	1.5	584.7	14.5	0.9	<LOD	0.31	3.95
BH9/05 62	9.8	1.9	10.1	27	36.8	0.31	718.9	74.1	0.4	463.7	9.4	0.2	<LOD	<LOQ	5.35
BH9/05 56	8.6	1.3	6.1	24	14.3	0.16	424.2	110.2	0.9	393.1	19.0	1.4	<LOD	1.00	3.23
BH9/05 43	10.2	3.6	36.3	49	12.1	0.10	741.5	26.3	0.4	436.2	5.8	0.4	<LOD	1.39	12.78
BH9/05 40	9.4	0.8	1.3	8	26.3	0.55	112.5	62.0	13.3	159.8	22.9	1.3	<LOD	<LOD	3.93
13/2013 4	8.4	<LOQ	0.4	79	8.6	0.38	<LOQ	9.8	12.6	76.6	<LOD	5.5	<LOD	<LOQ	7.76

Sample	pH	NH_4^+ (aq) (N) (µg/g)	NH_4^+ (ad) (N) (µg/g)	K_D (NH_4^+)	Acetate (µg/g)	NO_3^- (µg/g)	TDIC (µg/g)	SO_4^{2-} (µg/g)	Ca^{2+} (µg/g)	Na^+ (µg/g)	K^+ (µg/g)	Mg^{2+} (µg/g)	Mn (µg/g)	Fe (µg/g)	Si (µg/g)
13/2013 9	8.5	0.9	1.6	9	38.3	0.85	124.5	155.7	90.1	113.0	39.1	23.2	<LOD	<LOD	3.59
13/2013 15	8.8	2.0	6.0	15	64.4	0.37	203.8	253.4	14.2	295.5	42.5	4.4	<LOD	0.19	6.34
13/2013 17A	9.4	2.3	14.4	32	56.6	0.21	652.9	367.1	7.2	561.5	18.0	1.5	<LOD	<LOQ	3.03
13/2013 17B	9.6	2.8	12.1	22	57.0	0.36	507.2	335.9	1.9	483.8	21.7	0.5	<LOD	0.66	8.32
13/2013 20	5.0	5.0	3.1	3	14.5	0.19	<LOQ	1864.2	407.8	387.3	94.4	33.2	1.51	0.82	5.74
13/2013 23	8.3	1.2	2.4	10	58.3	0.16	206.8	347.6	115.0	184.0	38.8	27.3	<LOD	<LOD	1.31
13/2013 26	4.8	3.2	3.6	5	15.0	0.23	<LOQ	955.3	97.5	354.4	85.1	68.1	10.78	0.85	6.09
13/2013 27	4.5	8.3	28.9	18	47.1	0.13	<LOQ	2129.7	81.8	1101.2	40.3	38.1	1.82	0.88	11.13
13/2013 29	3.9	12.0	32.6	14	20.8	0.03	<LOQ	3011.7	202.3	797.7	46.6	96.5	2.85	216.84	7.90
13/2013 33	9.3	1.5	53.4	186	95.7	0.30	118.7	186.1	<LOD	266.2	4.5	0.5	<LOD	1.07	15.50
13/2013 35	9.6	1.6	28.8	92	85.6	0.79	498.1	57.6	<LOQ	341.5	7.9	1.0	<LOD	2.16	14.39

Sample	pH	NH_4^+ (aq) (N) (µg/g)	NH_4^+ (ad) (N) (µg/g)	K_D (NH_4^+)	Acetate (µg/g)	NO_3^- (µg/g)	TDIC (µg/g)	SO_4^{2-} (µg/g)	Ca^{2+} (µg/g)	Na^+ (µg/g)	K^+ (µg/g)	Mg^{2+} (µg/g)	Mn (µg/g)	Fe (µg/g)	Si (µg/g)
Road 7	8.8	1.5	2.1	7	<LOQ	0.27	127.4	210.3	78.1	28.6	45.6	26.7	<LOD	<LOD	5.49
Moy 6-2	9.0	1.9	4.9	13	13.2	0.16	227.5	43.2	56.0	35.0	52.8	15.9	<LOD	<LOD	3.36
BH9/05 42	10.0	2.1	45.4	106											
BH9/05 51	10.1	1.6	17.9	56											
Moy 4	7.7	1.7	9.4	27											
LG4E	6.9	2.8	14.0	24											

Day 11

Sample	pH	NH_4^+ (aq) (N) (µg/g)	NH_4^+ (ad) (N) (µg/g)	K_D (NH_4^+)	Acetate (µg/g)	NO_3^- (µg/g)	TDIC (µg/g)	SO_4^{2-} (µg/g)	Ca^{2+} (µg/g)	Na^+ (µg/g)	K^+ (µg/g)	Mg^{2+} (µg/g)	Mn (µg/g)	Fe (µg/g)	Si (µg/g)
BH9/05 73	7.8	2.2	2.5	5	11.2	0.25	1140.9	127.4	254.2	108.8	57.6	164.6	0.54	<LOD	4.24
BH9/05 72	8.7	1.9	4.5	12	7.4	0.25	217.4	124.8	68.6	115.5	41.6	27.0	<LOQ	<LOD	5.38
BH9/05 71	8.4	3.6	10.4	15	<LOQ	0.21	402.2	150.1	86.8	148.2	48.1	38.4	<LOQ	<LOD	4.78
BH9/05 69	8.4	1.4	1.5	5	<LOQ	0.23	289.8	197.7	96.1	114.5	64.7	41.1	<LOD	<LOD	4.59
BH9/05 67	9.8	1.6	3.7	11	14.3	0.43	585.1	168.6	4.0	393.5	23.0	0.9	<LOD	<LOQ	8.08
BH9/05 63	8.6	1.5	8.3	26	20.5	0.20	1726.2	144.4	9.4	867.9	30.1	5.7	<LOD	<LOD	3.59
BH9/05 62	9.3	1.5	9.3	31	39.2	0.31	1135.1	93.1	2.7	654.0	16.2	0.9	<LOD	0.53	4.83
BH9/05 56	7.6	2.6	5.0	10	14.3	0.24	988.8	136.0	32.9	532.0	48.3	39.6	0.52	<LOD	6.68
BH9/05 43	10.1	3.2	35.3	54	14.7	0.14	742.1	39.4	1.4	535.1	6.9	0.2	<LOD	0.37	9.41
BH9/05 40	9.2	0.8	1.0	7	26.7	0.69	172.0	63.2	17.3	165.6	24.4	1.9	<LOD	0.25	5.68
13/2013 4	8.3		0.1		8.5	0.42	25.1	14.2	16.3	82.0	<LOD	7.1	<LOD	0.68	12.15

Sample	pH	NH_4^+ (aq) (N) (µg/g)	NH_4^+ (ad) (N) (µg/g)	K_D (NH_4^+)	Acetate (µg/g)	NO_3^- (µg/g)	TDIC (µg/g)	SO_4^{2-} (µg/g)	Ca^{2+} (µg/g)	Na^+ (µg/g)	K^+ (µg/g)	Mg^{2+} (µg/g)	Mn (µg/g)	Fe (µg/g)	Si (µg/g)
13/2013 9	8.5	0.9	1.3	7	57.8	0.97	144.0	170.0	98.4	116.5	39.3	26.6	<LOD	<LOD	5.15
13/2013 15	8.6	1.9	5.9	16	24.6	0.32	250.5	279.2	25.0	320.4	50.5	7.7	<LOD	<LOD	8.22
13/2013 17A	8.5	2.2	14.0	31	22.7	0.23	1050.2	436.3	35.1	696.7	30.9	9.8	<LOQ	<LOD	3.48
13/2013 17B	9.4	2.9	12.8	22	60.2	0.42	510.3	395.0	5.1	559.1	29.9	0.9	<LOD	<LOD	7.67
13/2013 20	4.9	4.8	3.0	3	16.6	0.25	<LOQ	1930.9	419.3	390.2	94.4	34.7	1.63	0.53	16.71
13/2013 23	7.8	1.4	2.0	7	24.8	0.15	776.2	396.0	270.9	201.5	49.3	71.2	0.43	<LOD	4.78
13/2013 26	4.8	4.4	3.5	4	16.2	0.24	<LOQ	1145.0	117.1	363.9	89.7	80.7	13.16	1.15	20.01
13/2013 27	4.2	14.3	31.5	11	48.3	0.12	<LOQ	2536.9	140.1	1161.0	55.4	62.8	3.13	4.54	39.42
13/2013 29	3.6	15.1	31.1	10	30.6	<LOQ	<LOQ	3696.3	290.0	833.0	58.7	126.0	4.59	587.14	36.30
13/2013 33	8.6	1.2	57.0	222	78.2	0.41	266.8	350.2	<LOD	516.7	13.3	3.6	<LOD	8.62	1.21
13/2013 35	9.1	1.3	27.9	104	87.7	0.80	993.2	71.6	1.5	616.6	17.0	4.2	0.17	9.37	18.18

Sample	pH	NH_4^+ (aq) (N) (µg/g)	NH_4^+ (ad) (N) (µg/g)	K_D (NH_4^+)	Acetate (µg/g)	NO_3^- (µg/g)	TDIC (µg/g)	SO_4^{2-} (µg/g)	Ca^{2+} (µg/g)	Na^+ (µg/g)	K^+ (µg/g)	Mg^{2+} (µg/g)	Mn (µg/g)	Fe (µg/g)	Si (µg/g)
Road 7	8.5	1.4	2.0	7	<LOQ	0.27	183.1	226.9	106.8	30.9	49.3	38.3	<LOD	<LOQ	8.22
Moy 6-2	8.6	1.9	5.1	13	10.4	0.19	294.5	51.0	80.7	37.8	61.7	28.0	<LOD	<LOD	5.14
BH9/05 42	9.6	1.5	50.6	165											
BH9/05 51	9.8	1.2	20.4	86											
Moy 4	7.3	2.3	8.9	19											
LG4E	8.1	3.5	14.4	21											

B.2 Final leaching experiment 20°C

Aqueous concentration

Day 1

Sample	pH	NH_4^+ aq (N µg/L)	Ca^{2+} (mg/L)	Na^+ (mg/L)	K^+ (mg/L)	Mg^{2+} (mg/L)	Mn (mg/L)	Fe (mg/L)	Si (mg/L)
BH9/05 73		469.3	<LOD	<LOQ	<LOD	<LOQ	<LOQ	<LOQ	<LOD
BH9/05 72		463.0	7.9	21.0	10.0	4.6	<LOQ	<LOD	0.9
BH9/05 69		363.6	17.4	20.4	14.1	6.3	<LOD	<LOD	1.3
BH9/05 67		440.6	0.1	79.1	5.3	0.2	<LOD	0.30	0.6
BH9/05 62		367.3	0.2	118.4	3.1	0.1	<LOD	0.13	1.5
BH9/05 56		595.3	0.1	106.0	10.3	3.3	0.04	<LOD	<LOQ
BH9/05 43		843.6	<LOD	93.8	1.5	0.1	<LOD	0.21	0.1
BH9/05 40		240.7	3.8	32.2	5.9	0.3	<LOD	<LOQ	1.7
13/2013 4		<LD	3.6	14.6	<LOD	1.3	<LOQ	0.77	3.9
13/2013 9		243.3	20.9	20.4	8.8	4.6	<LOD	<LOD	1.5

13/2013 15		474.7	4.4	61.1	11.3	1.2	<LOD	<LOD	2.2
13/2013 17A		708.0	2.9	137.4	9.6	1.4	<LOD	<LOD	0.5
13/2013 17B		712.8	<LOD	57.4	3.1	0.1	<LOD	<LOQ	<LOD
13/2013 20		1071.1	1.0	84.8	22.1	6.8	0.33	0.54	<LOQ
13/2013 23		329.5	19.4	44.8	12.1	10.4	0.05	<LOD	0.4
13/2013 26		882.8	<LOD	83.8	12.0	7.9	1.29	0.59	<LOD
13/2013 27		1366.1	18.8	257.6	13.3	8.6	0.42	0.80	5.5
13/2013 29		1598.4	64.0	188.0	12.2	27.9	1.07	154.51	4.3
13/2013 33		293.0	<LOD	88.1	1.4	0.1	<LOD	0.26	<LOQ
13/2013 35		335.1	<LOD	61.7	0.8	<LOQ	<LOD	<LOQ	<LOD
Road 7		340.5	23.3	6.4	12.2	6.9	<LOD	<LOD	2.5
Moy 6-2		485.9	18.7	8.3	16.0	4.8	<LOQ	<LOD	1.7
17A		753.5	8.1	160.7	11.8	1.7	<LOQ	<LOD	1.2
17A		628.2	3.5	156.3	8.8	1.4	<LOD	<LOD	0.6
Blank		8.9	<LOD	<LOD	<LOD	<LOD	<LOD	<LOD	<LOD

Day 11

	pH	NH_4^+ aq (N µg/L)	Ca^{2+} (mg/L)	Na^+ (mg/L)	K^+ (mg/L)	Mg^{2+} (mg/L)	Mn (mg/L)	Fe (mg/L)	Si (mg/L)
BH9/05 73	7.344	513.41	93.5	28.5	18.4	74.7	0.41	<LOQ	1.5
BH9/05 72	7.878	322.02	33.1	26.7	13.4	12.1	0.08	<LOD	2.6
BH9/05 69	7.775	350.30	15.3	26.5	18.2	19.5	0.09	<LOD	0.9
BH9/05 67	8.858	289.76	sample lost						
BH9/05 62	7.966	435.20	2.1	221.6	9.8	2.5	<LOQ	<LOD	1.0
BH9/05 56	7.22	693.70	9.0	134.3	19.7	31.9	0.52	<LOD	1.2
BH9/05 43	9.311	501.58	0.2	137.5	2.5	0.1	<LOD	0.21	2.1
BH9/05 40	8.095	43.76	7.5	40.1	7.6	0.9	<LOD	0.11	2.2
13/2013 4	8.119	25.64	4.8	19.9	<LOD	1.7	<LOQ	0.40	5.6
13/2013 9	7.952	49.94	24.0	27.0	10.02	6.1	<LOD	<LOD	2.3
13/2013 15	8.059	138.86	7.6	76.1	15.6	3.5	<LOD	<LOD	2.3
13/2013 17A	7.562	1394.49	21.6	182.1	22.5	17.1	0.29	<LOD	1.2

13/2013 17B	8.728	254.82	2.4	149.2	10.4	0.5	<LOD	<LOQ	2.5
13/2013 20	4.769	1110.64	13.7	87.6	24.1	7.7	0.40	0.42	1.3
13/2013 23	7.175	398.74	0.6	43.6	11.4	36.2	0.27	<LOD	<LOQ
13/2013 26	4.502	1100.57	18.6	83.5	24.2	21.6	3.96	1.61	6.8
13/2013 27	3.532	3270.66	32.2	273.0	21.6	22.5	1.25	30.61	11.7
13/2013 29	2.924	4109.93	3.9	190.3	15.6	36.9	2.28	512.47	0.8
13/2013 33	7.602	395.36	<LOD	175.2	2.9	0.1	<LOD	0.12	1.5
13/2013 35	8.111	504.00	0.63	214.6	5.6	0.5	<LOQ	<LOQ	3.3
Road 7	8.057	231.69	36.5	7.1	12.1	11.8	<LOQ	<LOD	3.1
Moy 6-2	8.157	499.6	0.2	<LOD	<LOD	0.1	<LOD	<LOD	<LOQ
17A	8.491	664.6	1.4	177.30	14.63	5.4	<LOQ	<LOD	0.1
17A	7.686	816.296	47.9	181.4	16.1	14.6	0.28	<LOD	2.7
Blank	5.762	22.695	<LOD	<LOD	<LOD	<LOQ	<LOD	0.12	<LOQ

Day 49

Sample	pH	NH_4^+ aq (N µg/L)	Ca^{2+} (mg/L)	Na^+ (mg/L)	K^+ (mg/L)	Mg^{2+} (mg/L)	Mn (mg/L)	Fe (mg/L)	Si (mg/L)
BH9/05 73	7.194	296.42	0.1	12.9	5.4	71.8	0.08	0.0	<LOD
BH9/05 72	7.744	214.31	54.1	27.9	16.1	20.9	0.29	<LOD	2.4
BH9/05 69	7.612	22.40	80.3	29.4	21.2	34.2	0.20	<LOD	3.2
BH9/05 67	8.21	266.30	8.3	114.9	13.7	3.7	<LOQ	<LOD	1.9
BH9/05 62	7.66	775.46	34.8	257.4	19.1	19.1	0.13	<LOD	2.3
BH9/05 56	7.284	600.56	51.0	139.9	24.8	77.1	0.87	<LOD	1.8
BH9/05 43	no sample								
BH9/05 40	8.159	25.78	17.4	43.7	9.2	2.0	<LOQ	<LOD	3.9
13/2013 4	7.643	6.81	7.5	22.2	<LOD	2.6	<LOD	0.3	7.8
13/2013 9	7.98	11.91	35.0	29.2	10.9	7.7	<LOQ	<LOD	4.0
13/2013 15	8.037	96.12	21.7	79.7	18.0	6.1	<LOQ	<LOD	4.7
13/2013 17A	7.48	1405.23	20.7	175.6	25.8	36.4	0.45	<LOD	0.5

13/2013 17B	8.214	566.22	6.1	158.4	14.8	2.0	<LOD	<LOD	2.1
13/2013 20	4.561	1195.86	79.4	84.3	24.0	8.0	0.45	0.86	16.9
13/2013 23	7.153	30.09	52.8	50.7	16.8	79.6	0.16	<LOD	0.3
13/2013 26	4.033	1213.72	20.1	79.3	25.3	32.1	7.16	8.39	11.5
13/2013 27	3.034	4399.70	8.5	264.7	18.1	35.1	2.44	151.99	5.4
13/2013 29	3.017	5281.58	120.6	172.9	22.6	46.2	3.14	775.6	63.2
13/2013 33	5.387	1579.94	4.0	301.7	9.5	2.7	0.08	0.3	14.5
13/2013 35	7.896	1062.204	5.7	284.3	12.1	4.2	0.17	<LOQ	2.5
Road 7	7.978	108.562	54.0	8.6	13.1	20.2	0.04	<LOD	4.1
Moy 6-2	7.942	446.714	42.2	9.1	20.3	21.5	0.05	<LOD	2.2
17A	7.435	1026.828	92.22947	170.4597	21.78787	35.99071	0.437885	<LOD	2.30434
17A	7.547	1111.304	94.59678	172.1965	21.77613	35.71521	0.453255	<LOD	2.28045
Blank	5.369	27.382	0.07366	<LOQ	<LOD	<LOQ	<LOD	<LOD	<LOD

Data normalised by mass of rock (µg/g)

Day 1

Sample	pH	NH_4^+ (aq) (N) (µg/g)	NH_4^+ (ad) (N) (µg/g)	K_D (NH_4^+)	Ca^{2+} (µg/g)	Na^+ (µg/g)	K^+ (µg/g)	Mg^{2+} (µg/g)	Mn (µg/g)	Fe (µg/g)	Si (µg/g)
BH9/05 73	n.d.	2.3	2.5	5	<LOD	<LOQ	<LOD	<LOQ	<LOQ	<LOQ	<LOD
BH9/05 72	n.d.	2.3	4.1	9	39.6	105.0	49.8	23.2	<LOQ	<LOD	4.7
BH9/05 69	n.d.	1.8	1.5	4	86.4	101.2	69.9	31.3	<LOD	<LOD	6.4
BH9/05 67	n.d.	2.1	3.4	8	0.3	384.7	25.8	1.1	<LOD	1.46	3.1
BH9/05 62	n.d.	1.9	10.3	28	1.2	603.1	15.6	0.6	<LOD	0.69	7.5
BH9/05 56	n.d.	2.9	5.5	9	0.4	521.0	50.8	16.4	0.19	<LOD	<LOQ
BH9/05 43	n.d.	4.1	37.3	44	<LOD	458.6	7.4	0.3	<LOD	1.02	0.5
BH9/05 40	n.d.	1.2	0.9	4	18.5	158.0	29.0	1.7	<LOD	<LOQ	8.1
13/2013 4	n.d.	<LOD	0.1		17.8	71.9	<LOD	6.6	<LOQ	3.81	19.4
13/2013 9	n.d.	1.2	1.3	5	105.0	102.3	44.3	23.2	<LOD	<LOD	7.4
13/2013 15	n.d.	2.4	6.1	13	22.0	306.3	56.5	6.2	<LOD	<LOD	11.1

Sample	pH	NH_4^+ (aq) (N) (µg/g)	NH_4^+ (ad) (N) (µg/g)	K_D (NH_4^+)	Ca^{2+} (µg/g)	Na^+ (µg/g)	K^+ (µg/g)	Mg^{2+} (µg/g)	Mn (µg/g)	Fe (µg/g)	Si (µg/g)
13/2013 17A	n.d.	3.5	15.9	22	14.7	688.9	48.2	6.8	<LOD	<LOD	2.5
13/2013 17B	n.d.	3.5	12.9	18	<LOD	284.3	15.2	0.3	<LOD	<LOQ	<LOD
13/2013 20	n.d.	5.3	2.8	3	5.0	419.8	109.4	33.8	1.64	2.69	<LOQ
13/2013 23	n.d.	1.6	1.8	6	96.3	222.7	60.4	51.7	0.26	<LOD	2.1
13/2013 26	n.d.	4.4	3.2	4	<LOD	416.6	59.6	39.3	6.40	2.93	<LOD
13/2013 27	n.d.	6.7	31.8	23	92.3	1265.2	65.1	42.2	2.07	3.92	27.1
13/2013 29	n.d.	7.9	32.6	20	314.8	924.1	60.0	137.3	5.24	759.70	21.1
13/2013 33	n.d.	1.4	69.3	237	<LOD	431.5	6.7	0.4	<LOD	1.25	<LOQ
13/2013 35	n.d.	1.7	26.8	80	<LOD	306.4	4.2	<LOQ	<LOD	<LOQ	<LOD
Road 7	n.d.	1.7	1.9	5	114.6	31.5	60.1	33.9	<LOD	<LOD	12.2
Moy 6-2	n.d.	2.4	4.9	10	91.1	40.5	78.2	23.6	<LOQ	<LOD	8.1
17A	n.d.	3.7	15.2	20	39.3	780.8	57.1	8.3	<LOQ	<LOD	6.0
17A	n.d.	3.1	16.3	26	17.0	759.1	42.9	7.0	<LOD	<LOD	2.8

Day 11

Sample	pH	NH_4^+ (aq) (N) (µg/g)	NH_4^+ (ad) (N) (µg/g)	K_D (NH_4^+)	Ca^{2+} (µg/g)	Na^+ (µg/g)	K^+ (µg/g)	Mg^{2+} (µg/g)	Mn (µg/g)	Fe (µg/g)	Si (µg/g)
BH9/05 73	7.344	2.48	1.93	4	452.7	138.0	89.0	361.7	2.00	<LOQ	7.2
BH9/05 72	7.878	1.66	2.73	8	170.3	137.5	69.1	62.5	0.42	<LOD	13.3
BH9/05 69	7.775	1.75	1.34	4	76.5	132.3	91.0	97.4	0.44	<LOD	4.3
BH9/05 67	8.858	1.46	3.23	11	sample lost						
BH9/05 62	7.966	2.13	8.26	19	10.1	1082.9	47.8	12.1	<LOQ	<LOD	4.8
BH9/05 56	7.22	3.38	3.48	5	43.8	654.8	95.9	155.7	2.53	<LOD	6.0
BH9/05 43	9.311	2.51	38.24	76	1.2	688.5	12.4	0.4	<LOD	1.04	10.5
BH9/05 40	8.095	0.21	0.33	8	36.6	197.1	37.1	4.5	<LOD	0.53	10.7
13/2013 4	8.119	0.13	0.17	6	23.7	97.6	<LOD	8.3	<LOQ	1.95	27.3
13/2013 9	7.952	0.25	0.26	5	119.8	134.5	50.0	30.5	<LOD	<LOD	11.4
13/2013 15	8.059	0.67	1.60	12	37.0	369.3	75.8	17.0	<LOD	<LOD	11.2

Sample	pH	NH_4^+ (aq) (N) (µg/g)	NH_4^+ (ad) (N) (µg/g)	K_D (NH_4^+)	Ca^{2+} (µg/g)	Na^+ (µg/g)	K^+ (µg/g)	Mg^{2+} (µg/g)	Mn (µg/g)	Fe (µg/g)	Si (µg/g)
13/2013 17A	7.562	6.99	13.10	9	108.5	912.6	112.7	85.7	1.47	<LOD	6.1
13/2013 17B	8.728	1.25	8.83	35	11.9	733.9	51.1	2.6	<LOD	<LOQ	12.1
13/2013 20	4.769	5.48	2.53	2	67.8	432.5	119.0	38.2	1.97	2.06	6.5
13/2013 23	7.175	1.94	1.96	5	2.8	212.5	55.8	176.3	1.31	<LOD	<LOQ
13/2013 26	4.502	5.46	2.95	3	92.5	414.4	120.3	107.0	19.67	8.01	33.9
13/2013 27	3.532	16.17	27.25	8	159.4	1349.9	107.0	111.2	6.18	151.36	58.0
13/2013 29	2.924	20.20	28.61	7	19.4	935.1	76.5	181.3	11.23	2518.44	3.9
13/2013 33	7.602	1.94	59.53	151	<LOD	858.4	14.0	0.6	<LOD	0.61	7.5
13/2013 35	8.111	2.54	27.46	54	3.2	1083.0	28.1	2.3	<LOQ	<LOQ	16.6
Road 7	8.057	1.18	1.52	7	185.6	35.9	61.6	60.2	<LOQ	<LOD	15.7
Moy 6-2	8.157	2.47	4.18	8	1.0	<LOD	<LOD	0.4	<LOD	<LOD	<LOQ

Sample	pH	NH_4^+ (aq) (N) (µg/g)	NH_4^+ (ad) (N) (µg/g)	K_D (NH_4^+)	Ca^{2+} (µg/g)	Na^+ (µg/g)	K^+ (µg/g)	Mg^{2+} (µg/g)	Mn (µg/g)	Fe (µg/g)	Si (µg/g)
17A	8.491	3.25	10.24	15	7.1	867.7	71.6	26.3	<LOQ	<LOD	0.7
17A	7.686	4.03	9.34	11	236.6	895.7	79.3	72.0	1.37	<LOD	13.5

Day 49

Sample	pH	NH_4^+ (aq) (N) (µg/g)	NH_4^+ (ad) (N) (µg/g)	K_D (NH_4^+)	Ca^{2+} (µg/g)	Na^+ (µg/g)	K^+ (µg/g)	Mg^{2+} (µg/g)	Mn (µg/g)	Fe (µg/g)	Si (µg/g)
BH9/05 73	7.194	1.43	0.90	3	0.6	62.6	26.3	347.4	0.40	0.21	<LOD
BH9/05 72	7.744	1.10	1.64	8	279.0	144.0	82.8	107.7	1.51	<LOD	12.5
BH9/05 69	7.612	0.11	0.08	4	390.2	142.7	102.9	166.2	0.96	<LOD	15.8
BH9/05 67	8.21	1.30	2.22	8	40.6	562.2	66.9	18.0	<LOQ	<LOD	9.3
BH9/05 62	7.66	3.81	6.16	8	171.3	1266.0	94.1	94.1	0.66	<LOD	11.5
BH9/05 56	7.284	2.92	2.12	4	248.0	680.3	120.4	375.1	4.25	<LOD	8.9
BH9/05 43	sample lost		32.31		sample lost						
BH9/05 40	8.159	0.13	0.14	5	85.2	213.5	45.0	9.9	<LOQ	<LOD	19.1
13/2013 4	7.643	0.03	0.15	22	36.5	108.0	<LOD	12.7	<LOD	1.69	37.7
13/2013 9	7.98	0.06	0.10	9	174.1	144.9	54.2	38.5	<LOQ	<LOD	20.0
13/2013 15	8.037	0.49	1.04	11	105.7	388.0	87.6	29.9	<LOQ	<LOD	22.8

Sample	pH	NH_4^+ (aq) (N) (µg/g)	NH_4^+ (ad) (N) (µg/g)	K_D (NH_4^+)	Ca^{2+} (µg/g)	Na^+ (µg/g)	K^+ (µg/g)	Mg^{2+} (µg/g)	Mn (µg/g)	Fe (µg/g)	Si (µg/g)
13/2013 17A	7.48	7.03	10.03	7	104.5	886.3	130.1	183.8	2.27	<LOD	2.8
13/2013 17B	8.214	2.83	6.35	11	30.7	792.1	74.2	10.0	<LOD	<LOD	10.6
13/2013 20	4.561	5.95	2.64	2	396.7	421.2	120.0	39.9	2.23	4.28	84.6
13/2013 23	7.153	0.15	3.07	102	262.7	252.4	83.5	396.3	0.82	<LOD	1.6
13/2013 26	4.033	6.00	3.00	2	98.9	390.0	124.3	157.8	35.21	41.24	56.4
13/2013 27	3.034	21.78	21.57	5	42.0	1307.5	89.4	173.2	12.05	750.87	26.5
13/2013 29	3.017	26.70	24.70	5	597.1	856.1	111.8	228.5	15.54	3839.67	313.0
13/2013 33	5.387	7.92	53.46	34	20.0	1525.1	47.8	13.4	0.40	1.56	73.1
13/2013 35	7.896	5.23	21.73	20	28.7	1425.5	60.9	20.9	0.83	<LOQ	12.4
Road 7	7.978	0.53	0.46	4	266.2	42.5	64.7	99.5	0.21	<LOD	20.1
Moy 6-2	7.942	2.22	3.09	7	207.9	44.9	99.7	106.0	0.25	<LOD	10.7

Sample	pH	NH_4^+ (aq) (N) (µg/g)	NH_4^+ (ad) (N) (µg/g)	K_D (NH_4^+)	Ca^{2+} (µg/g)	Na^+ (µg/g)	K^+ (µg/g)	Mg^{2+} (µg/g)	Mn (µg/g)	Fe (µg/g)	Si (µg/g)
17A	7.435	5.14	8.53	8	459.2	848.8	108.5	179.2	2.18	<LOD	11.5
17A	7.547	5.50	9.06	8	473.3	861.5	108.9	178.7	2.27	<LOD	11.4

Appendix C Svalbard meltwater geochemical data

C.1 2016 Glacial runoff – major ion data

1/2

Date	Location	Cl^- µeq/L	NO_3^- µeq/L	SO_4^{2-} µeq/L	HCO_3^- µeq/L	NH_4^+ µeq/L	Na^+ µeq/L	K^+ µeq/L	Mg^{2+} µeq/L	Ca^{2+} µeq/L	ΔZ µeq/L	CBE %
27/08/2016	Foxfonna spring	12.7	1.7	909	n.d.	18.8	2423	24.4	191	514	n.d.	n.d.
28/08/2016	Longyearbreen	12.5	77.0	11302	925	3.9	3359	54.7	5598	3317	15	0.1%
30/08/2016	Longyearbreen	19.7	134.3	24316	1329	6.9	6996	83.3	13210	6910	1407	2.7%
01/09/2016	Gløttfjellbreen artesian spring E	36.8	<LOQ	674	3387	4.3	2608	38.4	543	1294	390	4.5%
03/09/2016	Møysalbreen moraine spring	9.2	26.9	10349	772	2.7	331	42.1	3876	6559	-346	-1.6%
07/09/2016	Rieperbreen	14.3	28.2	4024	2537	3.3	2920	58.3	1464	2199	41	0.3%
10/09/2016	Fleinisen	7.5	1.2	1466	2091	9.4	1138	38.9	726	1587	-66	-0.9%

2/2

Date	Location	pH	EC	DO_2	DO_2	Mn	Fe	Al	Si
			µs/cm	%	mg/L	µmol/L	µmol/L	µmol/L	µmol/L
27/08/2016	Foxfonna spring	7.9	183.7	62	8.58	3.0	3.7	<LOD	0.06
28/08/2016	Longyearbreen	7.94	755	91.4	12.61	8.1	0.2	<LOQ	0.03
30/08/2016	Longyearbreen	8	1420	92.2	12.76	15.9	<LOQ	<LOQ	0.04
01/09/2016	Gløttfjellbreen artesian spring E	8.4	270	89.8	11.93	2.6	<LOQ	<LOQ	0.07
03/09/2016	Møysalbreen moraine spring	8.44	619	68.3	9.41	<LOQ	<LOQ	<LOQ	0.05
07/09/2016	Rieperbreen	8.82	402	88.1	12.3	1.9	<LOQ	<LOQ	0.05
10/09/2016	Fleinisen	7.6	214	10	1.42	7.9	3.0	2.125	0.10

C.2 2017 Glacial runoff – major ion data

1/2

Date	Sample Type	pH	EC µs/cm	DO_2 %	DO_2 mg/L	Mn µmol/L	Fe µmol/L	Al µmol/L	Si µmol/L	log pCO_2
Longyearbreen										
27/08/2017	Englacial	n.d.	336	78.3	11.66					
27/08/2017	Subglacial	n.d.	1479	85.1	11.69	52.65	2.18	<LOQ	43.52	-3.54
27/08/2017	Moraine spring	n.d.	1493	86.5	11.11	60.01	3.11	<LOQ	47.58	-3.50
28/08/2017	Subglacial	8.2	1451	96.8	13.47	61.18	1.66	<LOQ	35.85	-3.46
28/08/2017	Englacial	8	486	86.6	11.91	n.d.	n.d.	n.d.	n.d.	n.d.
28/08/2017	Supraglacial	n.d.	n.d.	n.d.	n.d.	n.d.	n.d.	n.d.	n.d.	n.d.
28/08/2017	Moraine spring	8	1441	83.6	11.05	58.71	1.93	<LOQ	34.17	-3.28
01/09/2017	Subglacial	8.2	1363	82.4	11.4	49.72	4.60	<LOQ	56.75	-3.58
01/09/2017	Moraine spring	8.3	1363	80	11.5	49.90	6.39	<LOQ	57.20	-3.69

Date	Sample Type	pH	EC µs/cm	DO_2 %	DO_2 mg/L	Mn µmol/L	Fe µmol/L	Al µmol/L	Si µmol/L	log pCO_2
Foxfonna										
01/09/2017	Foxfonna Spring	8.2	361	8	0.96	3.29	6.52	<LOD	57.06	-3.07
01/09/2017	Foxfonna Glacial	7.23	273	n.d.	n.d.	1.01	<LOQ	<LOD	16.01	-3.07
Møysalbreen/Gløttfjellbreen										
04/09/2017	Møy-Loc-1 (Ice marginal channel)	9.3	100.7	96	12.69	0.97	2.74	<LOQ	13.29	-5.29
04/09/2017	Møy-Loc-2 (Moraine spring)	8.7	773	81	10.89	0.02	0.06	<LOQ	25.93	-3.72
04/09/2017	Gløttfjellbreen (Ice marginal channel)	9.4	161	59.8	7.8	1.96	0.21	<LOQ	21.45	-5.17
05/09/2017	Møy-Loc-2 (Moraine spring)	8.8	898	81.6	11.03	0.04	0.32	<LOQ	26.22	-3.78

Date	Sample Type	pH	EC µs/cm	DO_2 %	DO_2 mg/L	Mn µmol/L	Fe µmol/L	Al µmol/L	Si µmol/L	log pCO_2
05/09/2017	Møy-Loc-3 (Bulk runoff)	8.8	131.4	81	11.09	1.41	0.29	<LOQ	12.25	-4.73
05/09/2017	Møy-Loc-4 (Moraine spring)	9.3	1063	71.5	10.98	<LOQ	0.17	<LOQ	35.08	-4.20
Rieperbreen										
29/08/2017	Rieperbreen Glacial	7.8	53.4	n.d.	n.d.	1.14	0.25	<LOQ	13.30	-4.03
29/08/2017	Rieperbreen Ice Spring	7.9	57.4	n.d.	n.d.	1.16	0.39	<LOQ	13.74	-4.07
14/09/2017	Rieperbreen Glacial	7.2	367	18	2.62	0.95	0.19	<LOD	41.42	-2.49
14/09/2017	Rieperbreen Ice Spring	7.9	218.8	44.5	6.2	1.35	0.13	<LOD	40.27	-3.29

2/2

Date	Sample Type	Cl^- µeq/L	NO_3^- µeq/L	SO_4^{2-} µeq/L	HCO_3^- µeq/L	NH_4^+ µeq/L	Na^+ µeq/L	K^+ µeq/L	Mg^{2+} µeq/L	Ca^{2+} µeq/L	ΔZ µeq/L	CBE %
Longyearbreen												
27/08/2017	Englacial	58.3	22.1	2696		1.7						
27/08/2017	Subglacial	85.1	49.9	14289	951	9.5	3637	52.5	7205	2742	-1729	-6%
27/08/2017	Moraine spring	89.8	54.6	15998	1022	4.2	3828	54.2	7803	2887	-2588	-8%
28/08/2017	Subglacial	80.1	44.9	15634	1125	5.7	3639	58.1	8488	3063	-1630	-5%
28/08/2017	Englacial	59.7	24.4	4503	n.d.	1.8	n.d.	n.d.	n.d.	n.d.	n.d.	n.d.
28/08/2017	Supraglacial	36.2	18.2	14	n.d.	0.4	n.d.	n.d.	n.d.	n.d.	n.d.	n.d.
28/08/2017	Moraine spring	78.4	43.9	15268	1081	9.1	3446	53.0	7779	2809	-2376	-8%
01/09/2017	Subglacial	90.1	78.6	14385	862	5.9	4591	55.3	6787	2678	-1297	-4%
01/09/2017	Moraine spring	90.3	82.4	15074	851	5.1	4584	52.4	6861	2627	-1968	-7%
Foxfonna												
01/09/2017	Foxfonna Spring	119.5	0.5	1150	2780	21.0	2721	24.7	215	494	-575	-8%

Date	Sample Type	Cl^- µeq/L	NO_3^- µeq/L	SO_4^{2-} µeq/L	HCO_3^- µeq/L	NH_4^+ µeq/L	Na^+ µeq/L	K^+ µeq/L	Mg^{2+} µeq/L	Ca^{2+} µeq/L	ΔZ µeq/L	CBE %
01/09/2017	Foxfonna Glacial	33.2	42.1	2232	297	2.7	722	39.4	303	1374	-162	-3%
Møysalbreen/Gløttfjellbreen												
04/09/2017	Møy-Loc-1 (Ice marginal channel)	28.1	8.7	704	214	21.4	192	20.2	270	419	-32	-2%
04/09/2017	Møy-Loc-2 (Moraine spring)	45.1	18.8	7068	1981	2.9	309	75.3	2758	5394	-573	-3%
04/09/2017	Gløttfjellbreen (Ice marginal channel)	30.1	6.7	725	348	20.1	213	21.2	279	528	-49	-2%
05/09/2017	Møy-Loc-2 (Moraine spring)	58.1	13.1	8761	2145	8.6	329	82.8	3294	6423	-841	-4%
05/09/2017	Møy-Loc-3 (Bulk runoff)	26.0	6.2	945	245	12.0	201	33.4	374	578	-24	-1%

Date	Sample Type	Cl^- µeq/L	NO_3^- µeq/L	SO_4^{2-} µeq/L	HCO_3^- µeq/L	NH_4^+ µeq/L	Na^+ µeq/L	K^+ µeq/L	Mg^{2+} µeq/L	Ca^{2+} µeq/L	ΔZ µeq/L	CBE %
05/09/2017	Møy-Loc-4 (Moraine spring)	63.2	19.3	12028	2622	<LOQ	447	121.1	4441	8656	-1067	-4%
Rieperbreen												
29/08/2017	Rieperbreen Glacial	28.9	9.4	302	121	1.3	146	16.9	132	158	-9	-1%
29/08/2017	Rieperbreen Ice Spring	30.0	10.4	361	141	1.5	146	37.8	197	136	-24	-2%
14/09/2017	Rieperbreen Glacial	37.0	18.3	2790	1057	5.2	392	57.1	1117	2064	-267	-4%
14/09/2017	Rieperbreen Ice Spring	44.7	14.9	1302	849	2.8	586	32.1	526	871	-192	-5%

C.3 2017 Glacial runoff – major ion data (precipitation corrected)

Date	Sample Type	NO_3^-* µeq/L	SO_4^{2-}* µeq/L	NH_4^+* µeq/L	Na^+* µeq/L	K^+* µeq/L	Mg^{2+}* µeq/L	Ca^{2+}* µeq/L
Longyearbreen								
27/08/2017	Englacial	16.2	2638					
27/08/2017	Subglacial	41.4	14204	6.9	3564	51.0	7196	2741
27/08/2017	Moraine spring	45.6	15909	1.5	3751	52.6	7794	2886
28/08/2017	Subglacial	36.9	15554	3.3	3570	56.7	8480	3061
28/08/2017	Englacial	18.5	4444	n.d.	n.d.	n.d.	n.d.	n.d.
28/08/2017	Supraglacial	14.6	-22	n.d.	n.d.	n.d.	n.d.	n.d.
28/08/2017	Moraine spring	36.0	15189	6.8	3379	51.6	7771	2807
01/09/2017	Subglacial	69.6	14295	3.2	4514	53.7	6778	2677
01/09/2017	Moraine spring	73.4	14984	2.4	4506	50.7	6852	2625
Foxfonna								
01/09/2017	Foxfonna Spring	-11.4	1030	17.4	2618	22.5	203	491

Date	Sample Type	NO_3^-* µeq/L	SO_4^{2-}* µeq/L	NH_4^+* µeq/L	Na^+* µeq/L	K^+* µeq/L	Mg^{2+}* µeq/L	Ca^{2+}* µeq/L
01/09/2017	Foxfonna Glacial	38.8	2199	1.7	693	38.8	300	1374
Møysalbreen/Gløttfjellbreen								
04/09/2017	Møy-Loc-1 (Ice marginal channel)	5.9	676	20.5	168	19.7	267	419
04/09/2017	Møy-Loc-2 (Moraine spring)	14.3	7023	1.5	271	74.5	2754	5394
04/09/2017	Gløttfjellbreen (Ice marginal channel)	3.7	695	19.1	187	20.7	276	528
05/09/2017	Møy-Loc-2 (Moraine spring)	7.3	8703	6.8	279	81.7	3288	6422
05/09/2017	Møy-Loc-3 (Bulk runoff)	3.6	919	11.2	179	32.9	371	578
05/09/2017	Møy-Loc-4 (Moraine spring)	13.0	11965	<LOQ	392	120	4435	8655
Rieperbreen								
29/08/2017	Rieperbreen Glacial	6.5	273	0.5	121	16.4	129	157
29/08/2017	Rieperbreen Ice Spring	7.4	331	0.6	120	37.2	194	135
14/09/2017	Rieperbreen Glacial	14.6	2753	4.1	360	56.5	1113	2063
14/09/2017	Rieperbreen Ice Spring	10.5	1257	1.4	548	31.3	522	870

C.4 2017 Snow – major ion data

Sample	Date	Glacier	Cl^- (µeq/L)	NO_3^- (µeq/L)	SO_4^{2-} (µeq/L)	NH_4^+ (µeq/L)
Snow 1	08/05/2017	Longyearbreen	58.2	8.9	76	1.6
Snow 2	08/05/2017	Longyearbreen	59.0	10.2	65	1.7
Snow 3	08/05/2017	Longyearbreen	73.9	2.4	68	1.4
Snow 4	08/05/2017	Longyearbreen	80.5	1.9	62	-

Appendix D Summary sedimentary log and geochemistry diagram

Sedimentary log and geochemical composition of bedrock samples from cores 13/2013 and BH9/05 and outcrop(Overleaf). Dashed lines represent geological boundaries. Solid circles with line are core samples and open triangles are outcrop samples. Rectangles on left of diagram indicate erosional depth of glaciers in the study area. Solid dark blue rectangles indicate geological formations where the surface area of glacier coverage is greatest. Dashed, grey rectangles indicate formations where there is a small amount of glacial coverage.

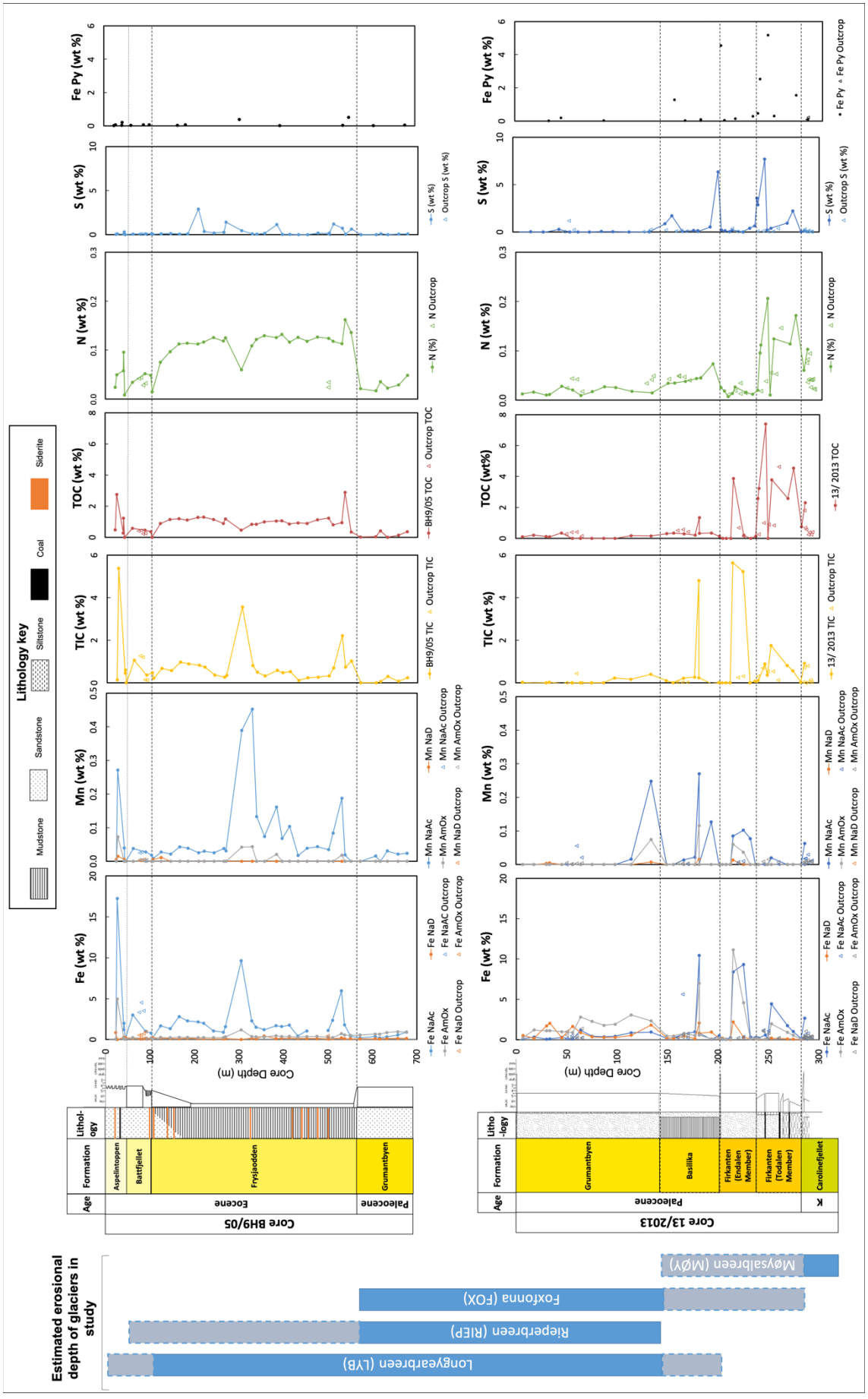
Lithology key
Mudstone
Sandstone
Siltstone
Coal
Siderite
Core BH9/05
Core 13/2013
Age
Formation
Litho-logy
Paleocene
Eocene
Aspelintoppen
Battfjellet
Frysjaodden
Grumantbyen
K
Basilika
Firkanten (Endalen Member)
Firkanten (Todalen Member)
Carolinefjellet
Core Depth (m)
Fe (wt %)
Mn (wt %)
TIC (wt %)
TOC (wt %)
N (wt %)
S (wt %)
Fe Py (wt %)
Fe NaAc
Fe NaD
Fe AmOx
Fe NaAC Outcrop
Fe AmOx Outcrop
Fe NaD Outcrop
Mn NaAc
Mn NaD
Mn AmOx
Mn NaAc Outcrop
Mn AmOx Outcrop
Mn NaD Outcrop
BH9/05 TIC
Outcrop TIC
13/ 2013 TIC
BH9/05 TOC
Outcrop TOC
13/ 2013 TOC
N (%)
N Outcrop
S (wt %)
Outcrop S (wt %)
Fe Py
Fe Py Outcrop
Estimated erosional depth of glaciers in study
Longyearbreen (LYB)
Riepebreen (RIEP)
Foxfonna (FOX)
Møysalbreen (MØY)